HELLENIC REPUBLIC
National and Kapodistrian University of Athens
EST. 1837

SCHOOL OF HEALTH SCIENCES
DEPARTMENT OF PHARMACY
SECTION OF PHARMACOGNOSY AND CHEMISTRY OF NATURAL PRODUCTS

ISOLATION AND STRUCTURE ELUCIDATION OF SECONDARY METABOLITES FROM MARINE ORGANISMS OF THE RED SEA

DOCTORAL THESIS

MOHAMED TAMMAM

ATHENS
DECEMBER 2020

THREE-MEMBERED ADVISORY COMMITTEE

Vassilios Roussis (Supervisor)
Professor, Department of Pharmacy, National and Kapodistrian University of Athens

Efstathia Ioannou
Assistant Professor, Department of Pharmacy, National and Kapodistrian University of Athens

Olga Tzakou
Professor, Department of Pharmacy, National and Kapodistrian University of Athens

SEVEN-MEMBERED EXAMINATION COMMITTEE

Vassilios Roussis
Professor, Department of Pharmacy, National and Kapodistrian University of Athens

Efstathia Ioannou
Assistant Professor, Department of Pharmacy, National and Kapodistrian University of Athens

Olga Tzakou
Professor, Department of Pharmacy, National and Kapodistrian University of Athens

Maria-Marina Couladis
Professor, Department of Pharmacy, National and Kapodistrian University of Athens

Nikolaos Thomaidis
Professor, Department of Chemistry, National and Kapodistrian University of Athens

Maria Zervou
Researcher B, Institute of Chemical Biology, National Hellenic Research Foundation

Carlos Duarte
Professor, Red Sea Research Center, King Abdullah University of Science and Technology, Saudi Arabia

ABSTRACT

Despite the continuous efforts of many research groups to develop new therapeutic treatments for various health problems, current medicines yield low cure rates and undesirable side effects. In the ongoing search for more effective anticancer and antibiotic agents, marine organisms have emerged as a promising new resource yielding unusual chemical structures with potent biological activities. The vast diversity and relatively unexplored nature of these unique sources of chemodiversity is expected to open a new era to drug discovery. Natural products have been the predominant source of new pharmaceuticals in the last fifty years. Between 1981 and 2002, 60% of the anticancer drugs and 75% of the anti-infectious disease drugs could be traced to or were inspired by natural products. Humankind has explored and exploited the terrestrial environment for more than 3,000 years, but only relatively recently turned its attention to the oceans as a possible source for natural medicines. From the early investigations in the 1970s until now marine organisms have yielded more than 32,000 natural products. Already a number of them are available in the pharmaceutical market, such as ziconotide (strong analgesic for severe pain relief by the brand name Prialt®) and ecteinascidin 743 (potent antitumor for the treatment of soft tissue sarcoma by the brand name Yondelis®), while many compounds are in advanced clinical trials for the treatment of numerous diseases.

In the framework of the present PhD thesis, the chemical composition of organic extracts obtained after the exhaustive extraction of three marine organisms, namely the red alga *Laurencia majuscula*, a sponge of the genus *Lamellodysidea* and the soft coral *Sinularia polydactyla*, collected from Hurghada and Thuwal, in the Red Sea (Egypt and Saudi Arabia) was investigated. To isolate the secondary metabolites of these marine organisms, the extracts were submitted to a series of chromatographic separations with various solvents and different types of chromatography. The isolated metabolites were identified on the basis of their spectroscopic data (NMR, MS, IR, UV-Vis) and comparison with literature data. In total 64 secondary metabolites have been isolated from these marine organisms, among which 59 have been structurally characterized, including 18 new natural products and one previously reported as a synthetic derivative.

Twenty-two secondary metabolites (**1-22**) were isolated and identified on the basis of their spectroscopic characteristics from the red alga *L. majuscula* collected from Hurghada, Egypt. These included seven laurane sesquiterpenes (**1-7**), one cuparane sesquiterpene (**8**), one seco-laurane derivative (**9**), one snyderane derivative (**10**), two chamigranes (**11** and **12**) and two rearranged chamigranes (**13** and **14**), one aristolane sesquiterpene (**15**), one tricyclic diterpene (**16**), one five-membered C_{15} acetogenin (**17**), four tricyclic C_{15} acetogenins of the maneonene type (**18-21**) and a chlorinated fatty acid derivative (**22**). Compounds **2**, **3**, **5**, **6**, **9**, **17** and **19-21** are new natural products.

From the marine sponge *Lamellodysidea* sp. collected from the coral reef off Thuwal in Saudi Arabia, 11 sesquiterpenes (**23-31**), mostly containing furan or γ-lactone in their structures, were isolated, three of which are new natural products (**25**, **30** and **31**) and one (**33**) is reported for the first time from a natural source.

Twenty six steroids (**34-59**) have been isolated and structurally characterized from the soft coral *S. polydactyla* collected from Hurghada, Egypt, including 15 4*α*-methylated derivatives. Compounds **34**, **35**, **39**, **41**, **46** and **53** are new natural products. Among them, metabolites **34** and **35** feature the rare 4-methyl-8,9-seco-cholastane steroidal nucleus.

The cytotoxic, anti-inflammatory, anti-angiogenic, and neuroprotective activity of compounds **36**–**40**, **42**–**45**, **47**–**53** and **55**–**59**, as well as their effect on androgen receptor-regulated transcription was evaluated in vitro in human tumor and non-cancerous cells.

ΠΕΡΙΛΗΨΗ

Παρά τις συνεχείς προσπάθειες πολλών ερευνητικών ομάδων για την ανάπτυξη νέων θεραπευτικών αγωγών για διάφορες ασθένειες, τα υπάρχοντα φάρμακα παρέχουν σχετικά χαμηλά ποσοστά θεραπείας συχνά συνοδευόμενα με ανεπιθύμητες παρενέργειες. Στην αναζήτηση νέων και πιο αποτελεσματικών φαρμάκων με αντικαρκινική και αντιβιοτική δράση, οι θαλάσσιοι οργανισμοί έχουν αναδειχθεί ως μία πολλά υποσχόμενη πηγή νέων μορίων με ασυνήθιστες χημικές δομές και υψηλή βιολογική δράση.

Η τεράστια ποικιλία αυτών των σχετικά ανεξερεύνητων οργανισμών ως πηγή χημειοποικιλότητας αναμένεται να ανοίξει μια νέα εποχή στην εξέλιξη νέων φαρμάκων. Τα φυσικά προϊόντα έχουν αποτελέσει την βασική πηγή νέων φαρμακευτικών προϊόντων τα τελευταία πενήντα χρόνια. Μεταξύ του 1981 και του 2002, το 60% των αντικαρκινικών φαρμάκων και το 75% των φαρμάκων κατά των λοιμωδών νόσων προέρχονταν ή είχαν εμπνευστεί από φυσικά προϊόντα. Η ανθρωπότητα έχει εξερευνήσει και εκμεταλλευτεί το χερσαίο περιβάλλον για περισσότερα από 3.000 χρόνια, αλλά μόνο σχετικά πρόσφατα στράφηκε στους ωκεανούς αναζητώντας νέες πηγές βιοδραστικών μορίων. Από τις πρώτες έρευνες, που ξεκίνησαν στη δεκαετία του 1970 έως τώρα οι θαλάσσιοι οργανισμοί έχουν αποδώσει περισσότερα από 32.000 φυσικά προϊόντα. Ήδη ορισμένα από αυτά είναι εμπορικά διαθέσιμα φάρμακα, όπως π.χ. το ziconotide (ισχυρό αναλγητικό για ανακούφιση από έντονους πόνους, με το εμπορικό σήμα Prialt) και η ecteinascidin 743 (ισχυρό αντικαρκινικό για τη θεραπεία σαρκώματος μαλακών ιστών με το εμπορικό σήμα Yondelis), ενώ πολλοί άλλοι μεταβολίτες από θαλάσσιους οργανισμούς βρίσκονται σε προχωρημένα στάδια κλινικών δοκιμών για τη θεραπεία πολλών ασθενειών.

Στο πλαίσιο της παρούσας διδακτορικής διατριβής μελετήθηκε η χημική σύσταση των οργανικών εκχυλισμάτων που παρελήφθησαν κατόπιν εξαντλητικής εκχύλισης τριών θαλάσσιων οργανισμών που συλλέχθηκαν στην Ερυθρά Θάλασσα. Συγκεκριμένα η μελέτη εστιάσθηκε στο ροδοφύκος *Laurencia majuscula*, ενός σπόγγου του γένους *Lamellodysidea* και του μαλακού κοραλλιού *Sinularia polydactyla* που συλλέχθηκαν από τις περιοχές της Hurghada και του Thuwal, στην Ερυθρά Θάλασσα (Αίγυπτος και Σαουδική Αραβία). Για την απομόνωση των δευτερογενών μεταβολιτών αυτών των θαλάσσιων οργανισμών, τα οργανικά τους εκχυλίσματα υποβλήθηκαν σε σειρά χρωματογραφικών διαχωρισμών με ποικίλους διαλύτες και τύπους χρωματογραφίας.

Οι απομονωμένοι μεταβολίτες ταυτοποιήθηκαν κατόπιν ανάλυσης των φασματοσκοπικών τους δεδομένων (NMR, MS, IR, UV-Vis) και σύγκρισης με δεδομένα βιβλιογραφίας όπου υπήρχαν διαθέσιμα. Συνολικά από τους ανωτέρω θαλάσσιους οργανισμούς απομονώθηκαν 64 δευτερογενείς μεταβολίτες, εκ των οποίων οι 59 έχουν χαρακτηριστεί πλήρως ως προς την χημική τους δομή και μεταξύ αυτών περιλαμβάνονται 18 μεταβολίτες με νέες χημικές δομές καθώς και 1 μόριο που απομονώνεται για πρώτη φορά ως φυσικό προϊόν.

Από το ροδοφύκος *L. majuscula* που συλλέχθηκε από την περιοχή της Hurghada της Αιγύπτου απομονώθηκαν και ταυτοποιήθηκαν με βάση τα φασματοσκοπικά χαρακτηριστικά τους είκοσι δύο δευτερογενείς μεταβολίτες (**1**-**22**) Μεταξύ αυτών συμπεριλαμβάνονται επτά σεσκιτερπένια με σκελετό λαουράνιου (**1**-**7**), ένα σεσκιτερπένιο με σκελετό κουπαράνιου (**8**), ένας μεταβολίτης με σκελετό σεκο-λαυρανίου (**9**), ένα παράγωγο σνυδερανίου (**10**), δύο μεταβολίτες με τσαμιγκρανικό σκελετό (**11** και **12**), δύο αναδιαταγμένα τσαμιγκράνια (**13** και **14**) , ένα σεσκιτερπένιο με σκελετό αριστολανίου (**15**), ένα τρικυκλικό διτερπένιο (**16**), μία C_{15} ακετογενίνη με πενταμελή δακτύλιο (**17**), τέσσερεις τρικυκλικές C_{15} ακετογενίνες τύπου μανεονένης (**18**-**21**) και ένα χλωριωμένο παράγωγο λιπαρού οξέος (**22**). Οι ενώσεις **2**, **3**, **5**, **6**, **9**, **17** και **19**-**21** αποτελούν νέα φυσικά προϊόντα.

Από τον θαλάσσιο σπόγγο *Lamellodysidea* sp. που συλλέχθηκε από τη περιοχή του Thuwal στη Σαουδική Αραβία, απομονώθηκαν 11 σεσκιτερπένια (**23**-3**1**) που περιέχουν στις δομές τους φουράνιο ή γ-λακτόνη, τρία εκ των οποίων αποτελούν νέα φυσικά προϊόντα (**25**, **30** και **31**) και ένα (**33**) που αναφέρεται για πρώτη φορά από φυσική πηγή.

Από το μαλακό κοράλλι *S. polydactyla* που συλλέχθηκε από την Ερυθρά θάλασσα στην περιοχή της Hurghada στην Αίγυπτο απομονώθηκαν και χαρακτηρίσθηκαν ως προς την χημική δομή τους είκοσι έξι στεροειδή (**34**-**59**) μεταξύ των οποίων περιλαμβάνονται 15 4α-μεθυλιωμένα στεροειδή. Οι ενώσεις **34**, **35**, **39**, **41**, **46** και **53** αποτελούν νέα φυσικά προϊόντα. Μεταξύ αυτών, οι μεταβολίτες **34** και **35** παρουσιάζουν τον σπάνιο σκελετό 4-μεθυλο-8,9-σεκο-χολαστανίου.

Η κυτταροτοξική, η αντιφλεγμονώδης, η αντι-αγγειογενετική και η νευροπροστατευτική δράση των μεταβολιτών **36**–**40**, **42**–**45**, **47**–**53** και **55**–**59**, καθώς και η επίδρασή τους στη μεταγραφή που ρυθμίζεται από τον ανδρογόνο υποδοχέα αξιολογήθηκε *in vitro* σε ανθρώπινες καρκινικές και φυσιολογικές κυτταρικές σειρές.

ACKNOWLEDGEMENTS

Above all, all praise belongs to Allah, the Lord of the worlds, for His most Bounteous guidance throughout the various stages of this research.

I would like to express my extreme gratitude to my esteemed Professors, Professor Vassilios Roussis, Assistant Professor Efstathia Ioannou and Professor Olga Tzakou. They have offered me the best academic guidance and the warmest family care in the course of this study and my life in my second home Greece. It has been a great privilege and joy to work under their guidance and their encouragement.

I also owe special thanks to the other members of the examination committee Professor Carlos Duarte, Dr. Maria Zervou, Professor Nikolaos Thomaidis and Professor Maria-Marina Couladis, for reading and evaluating my PhD thesis.

Special thanks should go to my professors in the Department of Biochemistry, Faculty of Agriculture, Fayoum University, Egypt for their kind and endless support and inspiring me to deal with these scientific fields.

I would like to thank Professor Carlos Duarte (Red Sea Research Center, King Abdullah University for Science and Technology, Saudi Arabia) for enabling the collection of the marine sponge studied, as well as for the acquisition of a number of NMR spectra.

Furthermore, I would like to thank Professor Miroslav Strnad and Dr. Lucie Rarova (Laboratory of Growth Regulators, Institute of Experimental Botany of the Czech Academy of Sciences, and Faculty of Science, Palacky University, Olomouc, Czech Republic) for the evaluation of the biological activity of a number of the isolated metabolites.

I would also like to acknowledge with gratitude all dear colleagues, postgraduate students, candidate PhD students, postdoctoral researchers and technicians of our laboratory who have always advised and supported me at different stages of the current research.

Special thanks should go to the mission sector of the Ministry of High Education of the Arab Republic of Egypt (Egyptian cultural bureau in Athens) for funding me during my joint supervision.

I would also like to acknowledge the Directorate of Education and Cultural Affairs, Ministry of Foreign Affairs E1 Greece, for funding me during my PhD thesis.

I would like to extend my sincere thanks to the non-profit organization “Kleon Tsetis” for their kind support during my PhD thesis.

I also owe special thanks to everyone in my family. In particular, many thanks must go to my father and my mother, who have always enlightened my life. I thank them for their generous advice and passionate care. Without their prayers, support and encouragement, this research would not have come to light. It is my pleasure to dedicate this research to them.

I am also deeply indebted to my wife Hanaa, whose lots of love and support have meant so much to me. I thank her for her patience, sympathy and always-generous support to a husband whose mind was always occupied with his research.

TABLE OF CONTENTS

LIST OF FIGURES

LIST OF TABLES

ABBREVIATIONS

1D-NMR	One-dimensional NMR experiment
2D-NMR	Two-dimensional NMR experiment
^{1}H NMR	1D-NMR experiment of hydrogen nuclei (proton)
^{13}C NMR	1D-NMR carbon core experiment, with broad-spectrum decoupling (proton-noise decoupled)
$[\alpha]_D$	Optical rotation
Ac	Acetyl
APCIMS	Atmospheric Pressure Chemical Ionization Mass Spectrometry
br	Broad (NMR)
C_6D_6	Deuterated benzene
CD_3OD	Deuterated methanol
$CDCl_3$	Deuterated chloroform
CH_2Cl_2	Dichloromethane
$CHCl_3$	Chloroform
cHex	Cyclohexane
COSY	2D-NMR homonuclear correlation experiment ^{1}H-^{1}H for ^{2}J and ^{3}J (Correlated Spectroscopy)
d	doublet (NMR)
EIMS	Electron Impact Mass Spectrometry
ESIMS	ElectroSpray Ionization Mass Spectrometry
EtOAc	Ethyl acetate
GC	Gas Chromatography
H_2O	Water
HMBC	2D-NMR ^{1}H-^{13}C heterologous correlation experiment for ^{2}J and ^{3}J (Heteronuclear Multiple-Bond Correlation)
*n*Hex	Normal hexane
HPLC	High Pressure Liquid Chromatography
HR-MS	High Resolution Mass Spectrometry
HSQC	2D-NMR 1H-13C heterologous correlation experiment for ^{1}J (Heteronuclear Single Quantum Coherence)
IR	Infrared Spectroscopy
J	Coupling constant (in Hz) (NMR)
m	Multiplet (NMR)
Me	Methyl
MeOH	Methanol
MS	Mass Spectrometry
m/z	Mass to charge ratio
NMR	Nuclear Magnetic Resonance Spectroscopy
NOE, nOe	Nuclear Overhauser Effect
NOESY	2D-NMR Nuclear Overhauser Effect SpectroscopY (Nuclear Overlapping Effect Spectroscopy)
q	quaternary (NMR)
RI	Refractive Index
s	singlet (NMR)
t	triplet (NMR)

TLC	Thin Layer Chromatography
tR	Retention time
UV-Vis	UV-visible Spectroscopy
δ	Chemical shift in the absorbance of a core relative to tetramethylsilane (in ppm) (NMR)

1. INTRODUCTION

1.1 Pharmacognosy - Natural products chemistry

Since ancient times, nature has been proven to be the most prolific source of biological and chemical diversity. It continues to be the most promising source of bioactive metabolites used for modern drug development (Harizani et al., 2016).

People have been using different natural sources for food and medicinal purposes for thousands of years, acquiring extensive knowledge of their properties (Brouwer et al., 2005).

The term "natural products" is usually associated with the secondary metabolites produced by an organism, which in many cases function as a defense mechanism against herbivores, microorganisms, insects and competing plants (Majeed et al., 2012).

Natural products are usually complex molecules with defined stereochemistry which grants them a specific relation with their biological targets. Furthermore, they are often used as lead molecules for the development of new drugs and hold an important place in the interests of the pharmaceutical industry (Montaser & Luesch, 2011). In the 1990s the focus was primarily on combinatorial chemistry and rapid evaluation methods for the identification of new active molecules (Kong et al., 2010).

These nature-based medicines have generated a rich source of structurally diverse substances with a wide range of biological activities, which could be useful for the development of alternative or adjunctive therapies.

Finding new bioactive compounds with new modes of action has become an urgent target for scientists due to the fast increase of diseases, such as cancer, diabetes, hepatitis, hypertension, chronic pains and microbial infections (El-Demerdash et al., 2018).

A large number of molecules from different natural sources have been approved for clinical use or used as the starting points for optimization programs (Medina-Franco, 2019). Figure 1 shows the contribution of natural products to drug development from 1981 until 2016 (Newman & Cragg, 2016).

Morphine (**1**) was the first natural product introduced commercially for therapeutic use in 1826 (Veeresham, 2012) and approved by FDA in 1827. In 1973, pilocarpine (**2**), an alkaloid extracted from the leaves of the tropical plant *Pilocarpus jaborandi*, was approved for the treatment of glaucoma. Cabazitaxel (**3**) which is a semisynthetic analog of the natural product taxol®, isolated from the bark of the yew tree, was approved in 2010, exhibiting cytotoxic activity against a broad range of cancer cell lines and tumor models with greater potency than docetaxel (Patridge et al., 2016).

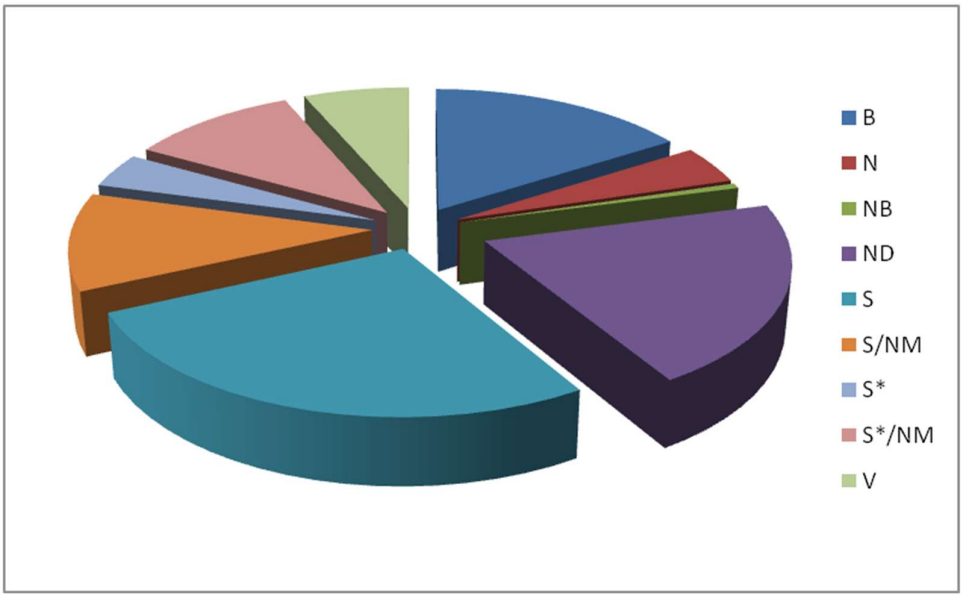

Figure 1. Approved drugs from 1981 until 2014.
(B: Biological macromolecule; N: Unaltered natural product; NB: Botanical drug (defined mixture); ND: Natural product derivative; S: Synthetic drug; S*: Synthetic drug (NP pharmacophore); V: Vaccine; /NM: Mimic of nature)

1 **2**

3

1.2 Marine natural products

Almost 70% of the Earth's surface is covered with water, showing extraordinary biological and chemical diversity. A significant number of novel drugs have been isolated from marine organisms, especially from sponges, corals and tunicates (El-Demerdash et al., 2019).

Marine natural products (MNPs) continue to be in the spotlight in the global drug discovery endeavor. More than 34,000 structurally diverse secondary metabolites

have been isolated from marine sources according to MarinLit database (MarinLit, 2020), making MNPs a profound source of novel compounds for pharmaceuticals, food, cosmeceutical, chemical, and agrochemical applications.

Up to now, a significant number of MNPs and their derivatives were released in the market, e.g. ω-3 acid ethyl esters (**4**) (Lovaza®, approved by FDA in 2004 for lowering blood triglycerides levels in adults with severe hypertriglyceridemia), cytarabine (**5**) (Cytosar-U®, DepoCyst®', FDA approval in 1969 for cancer treatment), trabectedin (**6**) (Yondelis®, ET- 743, EU approval in 2011 for cancer treatment), and vidarabine (**7**) (Vira-A®, approved by FDA in 1976 as an antiviral drug) (El-Demerdash et al., 2019).

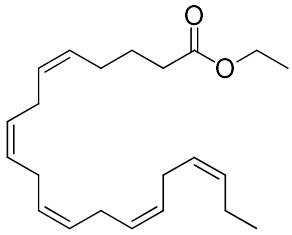

4

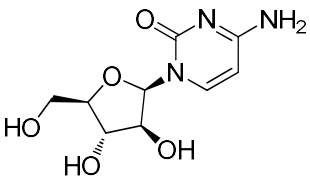

5

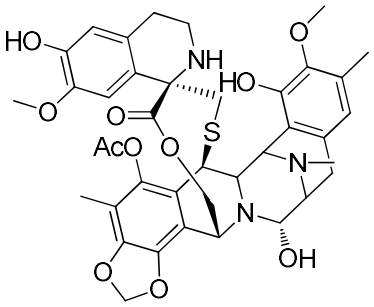

6

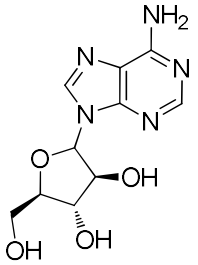

7

1.3 Red algae of the genus *Laurencia*

Algae were one of the first groups of marine organisms to be studied as sources for food, nutrition supplements, soil fertilizers, and bioactive metabolites (Harizani et al., 2016).

Macroalgae are classified into three classes, namely green (Chlorophyceae), brown (Phaeophyceae), and red (Rhodophyceae). Red algae are commonly found in subtropical and tropical waters and their populations in deeper waters are more dense in comparison with green and brown algae (Darley, 1982).

The red algal genus *Laurencia* has a wide distribution all over the world (Figure 2), with the southern hemisphere hosting the majority of the species (McDermid, 1988).

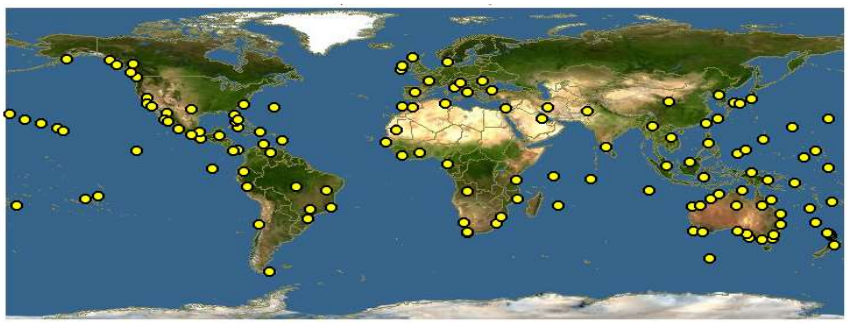

Figure 2. Global distribution map for the genus *Laurencia*.

The genus *Laurencia* is one of the richest sources of new secondary metabolites among red algae (Blunt et al., 2015). The plasticity of the morphoanatomical characters of *Laurencia* species has resulted in frequent taxonomic revisions of the genus that along with the genera *Chondrophycus*, *Osmundea*, *Palisada*, *Yuzurua*, and *Laurenciella*, are now included in the so called "*Laurencia* complex" (Harper & Garbary, 1997; Nam & Choi, 2000; Serio et al., 1999; Yoneshigue-Valentin et al., 2003). The cosmopolitan distribution, along with the chemical variation influenced to a significant degree by environmental and genetic factors, have resulted in an almost endless array of metabolites, often featuring multiple halogenation sites (Harizani et al., 2016).

Currently, 146 species are included in the genus *Laurencia* (order Ceramiales, family Rhodomelaceae, tribe Laurencieae) and are mainly found in tropical, subtropical, and temperate coastal waters (Guiry & Guiry, 2015).

Sesquiterpenes, diterpenes, triterpenes and C_{15} acetogenins are the major classes of secondary metabolites isolated from the genus *Laurencia*, while indoles, aromatic compounds and steroids have also been reported (Figure 3) (Harizani et al., 2016).

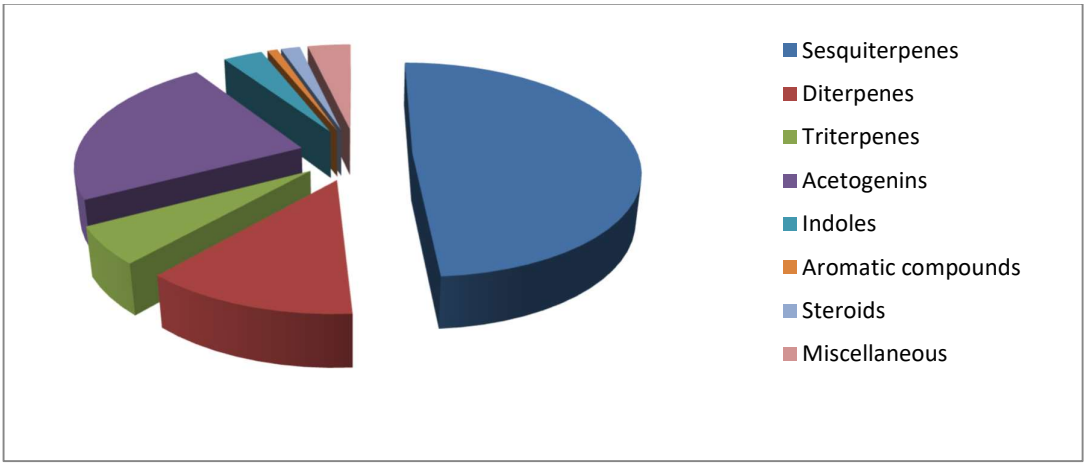

Figure 3. Contribution of the different chemical classes to the total number of metabolites isolated from *Laurencia* species.

1.3.1 Sesquiterpenes

More than 500 sesquiterpenes, comprising the largest group of secondary metabolites isolated from the genus *Laurencia* until now, have been reported from *Laurencia* species, featuring mono-, bi-, or tri-carbocyclic skeletons, often with fused- or spiro-ring systems (Harizani et al., 2016).

Sesquiterpenes from the genus *Laurencia* can be classified according to the their carbon framework in chamigranes, lauranes, cyclolauranes, snyderanes, bisabolanes, perforanes, cycloperforanes, brasilanes, cuparanes, eudesmanes, cycloeudesmanes, aristolanes, among others (Harizani et al., 2016).

More than 150 chamigranes have been isolated from the genus *Laurencia*, e.g. (10*R*)-10-bromo-*α*-chamigrene (**8**) isolated from *Laurencia nipponica* (Suzuki et al., 1985), 2,10-dibromo-3-chloro-*α*-chamigrene (**9**) isolated from *Laurencia nidifica* (Kimura et al., 1999) showing moderate toxicity against brine shrimps (Li et al., 2012a), 2,10-dibromo-3-chloro-chamigra-7,9-diene-5-ol (**10**) isolated from *Laurencia composita* (Ji et al., 2008), obtusol (**11**) isolated from *Laurencia dendroidea* showing *in-vitro* and *in-vivo* leishmanicidal activity and very low cytotoxicity (da Silva Machado et al., 2011), dendroidone (**12**) isolated from *L. dendroidea* (da Silva Machado et al., 2014), tristichones A and B (**13** and **14**), tristichols A-D (**15-18**) and tristichones C and D (**19** and **20**) isolated from *Laurencia tristicha* (Chen et al., 2016), compositacins A-K (**21-31**) isolated from *L. composita*, with compositacin G (**27**) showing significant antifungal activity against *Microsporum gypseum* (Yu et al., 2017).

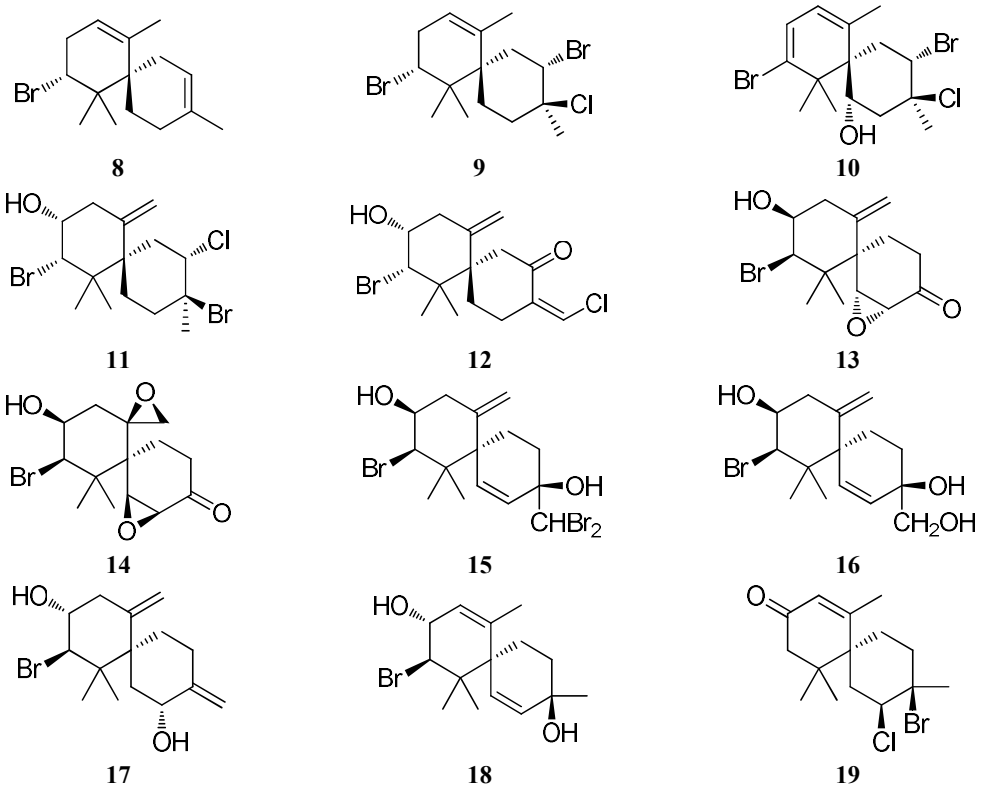

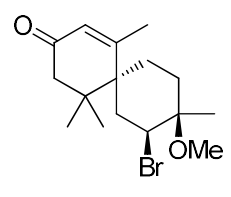

20

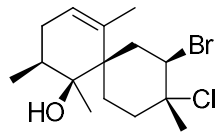

21

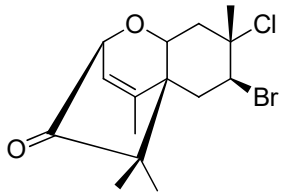

22

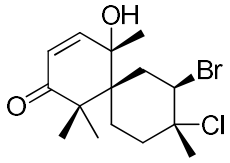

23

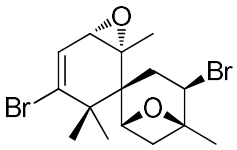

24

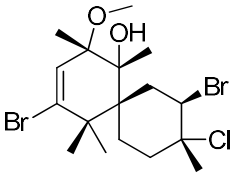

25

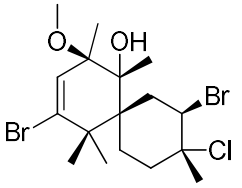

26

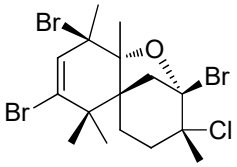

27

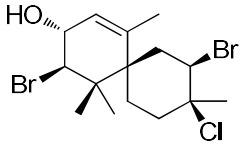

28

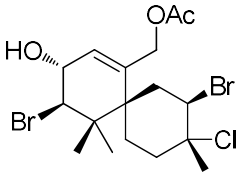

29

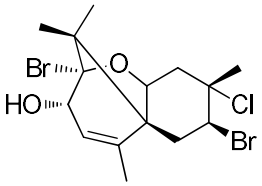

30

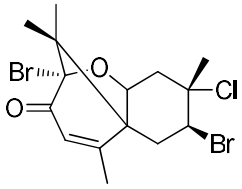

31

About 100 lauranes and cyclolauranes have been isolated from the genus *Laurencia*, e.g. laurene (**32**) isolated from *Laurencia elata* (Hall & Reiss, 1986) and found to be a moderate antibacterial agent against *Escherichia coli* and *Staphylococcus aureus* (Li et al., 2012b), 10,11-dibromo-7-hydroxylaurene (**33**) isolated from *Laurencia majuscula* (Masuda et al., 2002), isolaurinterol acetate (**34**) isolated from *Laurencia okamurai* (Mao & Guo, 2005), debromofiliformin (**35**) isolated from *Laurencia caduciramulosa* (Cassano et al., 2008) and found to be moderately toxic towards brine shrimps (Liang et al., 2012), debromoallolaurinterol acetate (**36**) and allolaurinterol acetate (**37**) isolated from *L. okamurai*, both showing strong antibacterial activity against *E. coli* and *S. aureus* (Li et al., 2012b), laurokamurene D (**38**) isolated from *L. okamurai* (Yu et al., 2014), 8,11-dihydro-1-methoxy-laurokamuren-12-ol (**39**) obtained from *Laurencia obtusa* (Angawi et al., 2014), debromo-3α-hydroperoxy-3-epiaplysin (**40**) and debromo-3β-hydroperoxyaplysin (**41**) isolated from *L. okamurai* (Li et al., 2015), debromoaplysinal (**42**) isolated from *Laurencia* sp. showing weak antifouling activity against larvae of the barnacle *Amphibalanus amphitrite* (Oguri et al., 2017), 3α-hydroperoxy-3-epiaplysin (**43**) and 3β-hydroperoxyaplysin (**44**) isolated from *L. okamurai* (Yang et al., 2018).

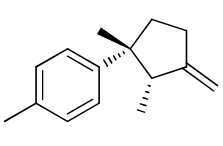

32

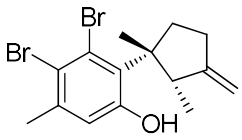

33

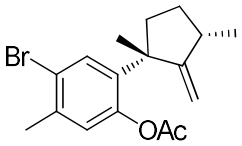

34

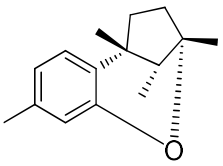

35

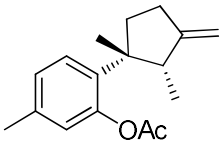

36

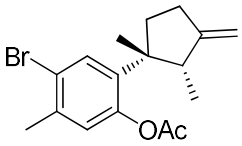

37

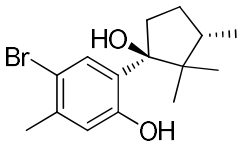

38

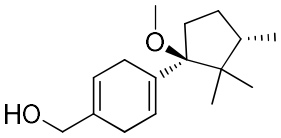

39

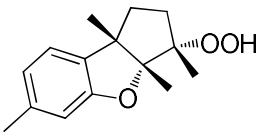

40

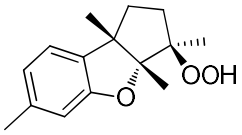

41

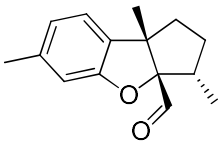

42

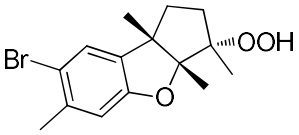

43

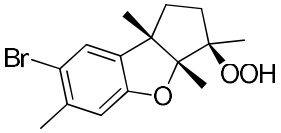

44

Examples of snyderanes isolated from the genus *Laurencia* include (8*R**)-8-bromo-10-epi-*β*-snyderol (**45**) isolated from *L. obtusa* and showing antimalarial activity with IC_{50} values of 2.7 and 4 mg/mL against the D6 and W2 clones of *Plasmodium falciparum*, respectively (Topcu et al., 2003), luzondiol (**46**) isolated from *Laurencia luzonensis* (Makhanu et al., 2006), 4-hydroxy-palisadin C (**47**) isolated from *Laurencia saitoi* (Su et al., 2009a), dactyloxene A (**48**) isolated from *Laurencia nangii* (Vairappan et al., 2014).

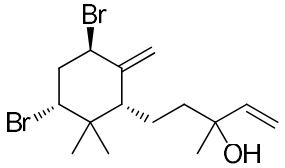

45

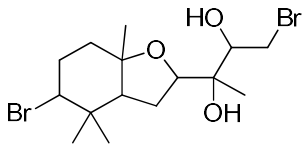

46

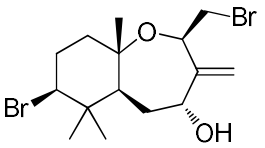

47

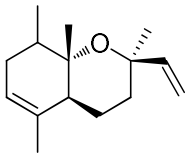

48

Another group of sesquiterpenes isolated from the genus *Laurencia* is the bisabolanes, including gossonorol (**49**) isolated from *L. tristicha* (Sun et al., 2005), (5*S*)-5-acetoxy-acetylcaespitol (**50**) isolated from *Laurencia catarinensis* (Lhullier et al., 2010), (5*S*)-5-acetoxy-*β*-bisabolene (**51**) isolated from *L. okamurai* (Yu et al., 2014).

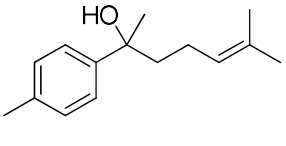

49

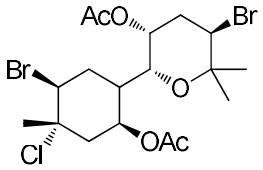

50

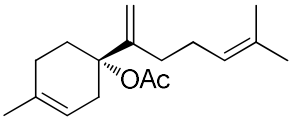

51

9-Hydroxy-3-epi-perforenone A (**52**) isolated from *Laurencia perforata* (Wright et al., 2003) and perforenol B (**53**) isolated from *L. obtusa* showing weak cytotoxicity towards K562 and CHO cell lines (Kladi et al., 2006) are examples of the perforanes and cycloperforanes.

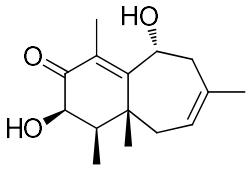

52

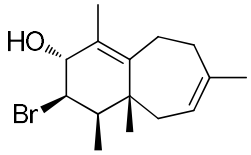

53

Additionally, brasilanes, such as 4-hydroxy-5-brasilene (**54**) isolated from *L. obtusa* (Amico et al., 1991), and cuparanes, such as 10-bromo-3-chloro-cupar-5-en-2-ol (**55**) isolated from *L. okamurai* (Li et al., 2012c) and 4*α*-hydroxy-bromo-cuparene (**56**) isolated from *L. tristicha* (Chen et al., 2016) are examples of sesquiterpenes commonly isolated from the genus of *Laurencia*.

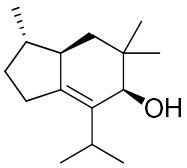

54

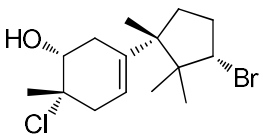

55

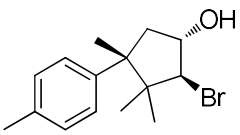

56

Eudesmanes and cycloeudesmanes are also isolated from the genus *Laurencia*, e.g. 1-bromo-selin-4(14),11-diene (**57**) isolated from *L. composita* (Li et al., 2012b) and 1*β*-bromo-6,8-cycloselin-4(15)-ene (**58**) isolated from *L. composita* (Ji et al., 2016).

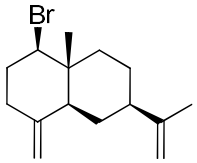

57

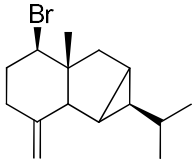

58

Aristolan-1α-bromo-9β,10β-epoxide (**59**) isolated from *Laurencia similis* (Li et al., 2010) and debilone (**60**) isolated from *Laurencia complanata* (Rahelivao et al., 2015) are examples of aristolanes isolated from the genus *Laurencia.*

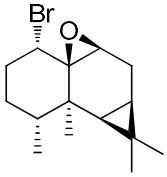

59

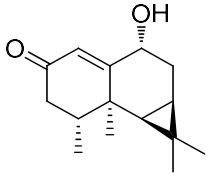

60

1.3.2 Diterpenes

Diterpenes are one of the biggest classes of secondary metabolites isolated from the genus *Laurencia* until now (Harizani et al., 2016). They can be classified into pargueranes and isopargueranes, e.g. 15-bromo-parguer-9(11)-en-16-ol (**61**) isolated from *L. nipponica* (Lyakhova et al., 2004) and parguerol 7,19-diacetate (**62**) isolated from *L. saitoi* (Ji et al., 2008), labdanes and pimaranes, e.g. 3-bromobarekoxide (**63**) isolated from *L. luzonensis* (Kuniyoshi et al., 2000) and compound **64** isolated from *L. obtusa* (Esselin et al., 2018), irieanes and neoirieanes, e.g. 11-deacetyl-pinnaterpene C (**65**) isolated from *Laurencia decumbens* (Ji et al., 2007a) and neoirietriol (**66**) isolated from *Laurencia yonaguniensis* (Takahashi et al., 2010), dactylomelanes, e.g. punctatene (**67**) isolated from *Laurencia* sp. (Fernández et al., 2005) and laurendecumtriol (**68**) isolated from *L. decumbens* (Ji et al., 2007a), obtusanes and 15,14-friedoobtusanes, e.g. rogioldiol A (**69**) isolated from *L. microladia* (Guella et al., 1997) and laurenditerpenol (**70**) isolated from *Laurencia intricata* showing inhibitory effect on HIF-1-mediated hypoxic signaling in breast tumor cells (Mohammed et al., 2004), prevezanes and neorogiolanes, e.g. prevezol C (**71**) and neorogioldiol B (**72**) isolated from *L. obtusa* with both compounds showing potent cytotoxicity (Iliopoulou et al., 2003), and diterpenes featuring prenylated sesquiterpene skeletons, e.g. compound **73** isolated from *Laurencia* sp. and found to exhibit antifouling activity against larvae of the barnacle *A. amphitrite* (Oguri et al., 2017).

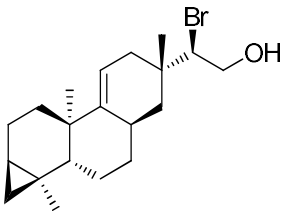

61

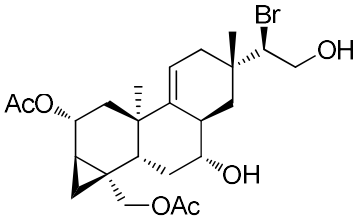

62

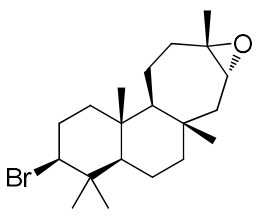

63

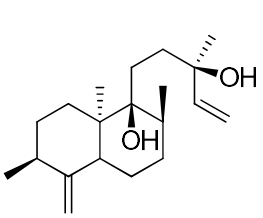

64

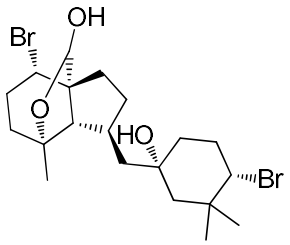

65

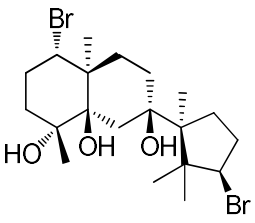

66

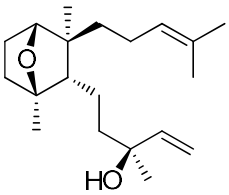

67

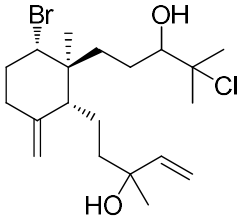

68

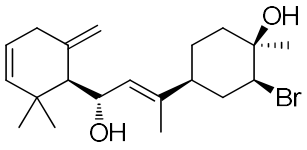

69

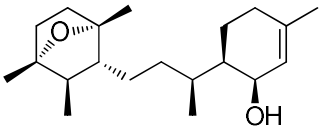

70

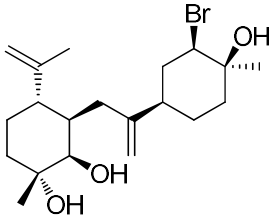

71

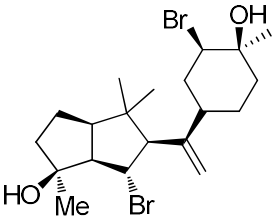

72

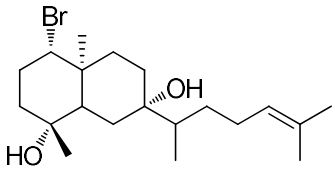

73

1.3.3 Triterpenes

Triterpenes isolated from the genus *Laurencia* can be classified (Harizani et al., 2016) into three classes: triterpenes possessing a 2,7-dioxabicyclo[4.4.0]decane ring system e.g. alfredensinol A (**74**) isolated from *Laurencia alfredensis* (Dziwornu et al., 2017), triterpenes possessing a 2,8-dioxabicyclo[5.4.0]undecane ring system e.g. dioxepandehydrothyrsiferol (**75**) isolated from *Laurencia viridis* (Manríquez et al., 2001) and triterpenes possessing symmetry elements e.g. intricatriol (**76**) isolated from *Laurencia* sp. (Oguri et al., 2017).

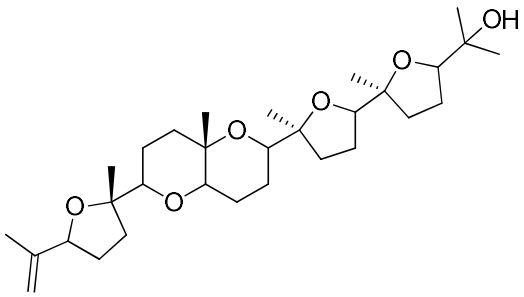

74

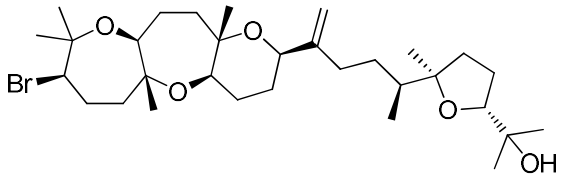

75

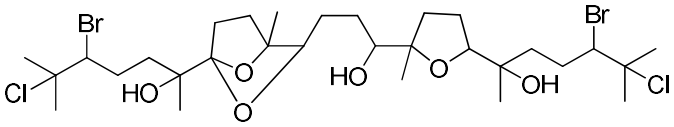

76

1.3.4 Acetogenins

Acetogenins isolated from the genus *Laurencia* can be classified (Harizani et al., 2016) into:

- Acetogenins containing a five-membered cyclic ether (tetrahydrofuran) ring which can be divided into four subgroups, namely: (1) those containing one tetrahydrofuran ring e.g. omazallene (**77**) isolated from *Laurencia* sp. showing promising antifouling activity (Umezawa et al., 2014); (2) those containing two isolated tetrahydrofuran rings e.g. laurefurenyne B (**78**) isolated from *Laurencia* sp. (Abdel-Mageed et al., 2010); (3) those containing two fused tetrahydrofuran rings e.g. laurentusenin (**79**) isolated from *L. obtusa* which may play a role in apoptosis induction, initiation and propagation of inflammatory responses (Ghandourah et al., 2019); and (4) maneonenes and isomaneonenes containing three tetrahydrofuran rings e.g. the three rare C_{12} acetogenins **80–82** isolated from the Red Sea *L. obtusa* showing promising anti-inflammatory effects (Alarif et al., 2019).

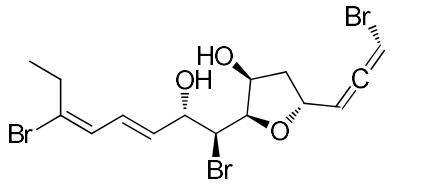

77

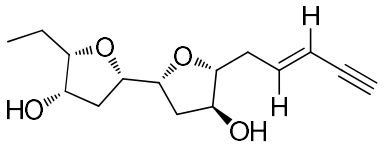

78

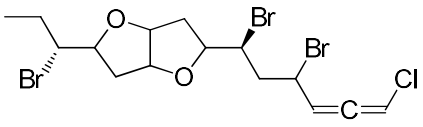

79

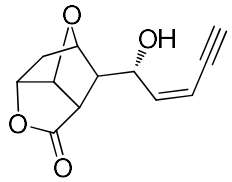

80

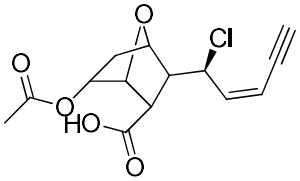

81

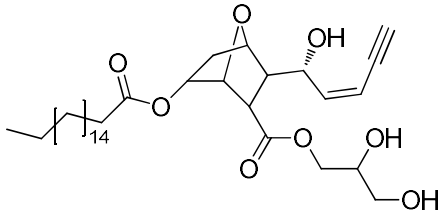

82

- Acetogenins containing a six-membered cyclic ether (tetrahydropyran) ring which can be divided into four subgroups, namely: (1) those containing one tetrahydropyran ring e.g. sagonenyne (**83**) isolated from *L. obtusa* (Esselin et al., 2018); (2) those containing isolated tetrahydrofuran and tetrahydropyran rings e.g. compound **84** isolated from *L. obtusa* (Esselin et al., 2018); (3) those containing fused tetrahydrofuran and tetrahydropyran rings e.g. japonenyne C (**85**) isolated from *Laurencia japonensis* (Takahashi et al., 1999); and (4) those containing two fused tetrahydropyran rings e.g. vagiallene (**86**) isolated from *L. obtusa* (Perdikaris et al., 2019).

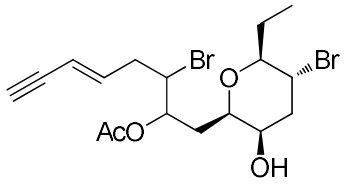

83

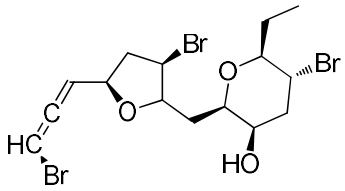

84

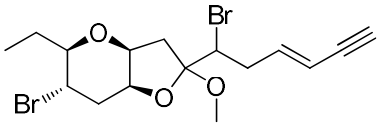

85

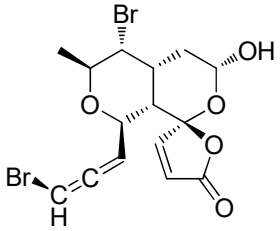

86

- Acetogenins containing a seven-membered cyclic ether (oxepane) ring which can be divided into three subgroups: (1) monocyclic acetogenins with a 1-bromopropanyl side chain attached to C-12 e.g. neonipponallene (**87**) isolated from *L. nipponica* (Lyakhova et al., 2006); (2) branched monocyclic acetogenins with bromomethyl and ethyl side chains attached to C-11 and C-12, respectively e.g. rogiolenyne A (**88**) isolated from *L. microcladia* (Guella & Pietra, 1991); and (3) acetogenins with a 1-bromopropanyl side chain attached to C-12 featuring a second ether ring formed between C-6 and C-9 e.g. (3*E*)-neoisoprelaurefucin (**89**) isolated from *L. obtusa* (Aydoğmuş et al., 2004).

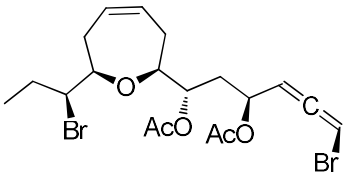

87

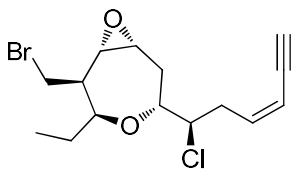

88

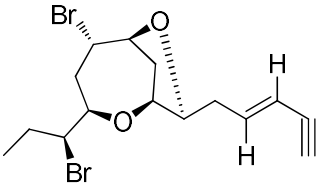

89

- Acetogenins containing an eight-membered cyclic ether (oxocane) ring which can be divided into six subgroups, namely: (1) those with a 6,12-epoxy, also known as laurenan-type acetogenins e.g. marilzallene B (**90**) isolated from *Laurencia chondrioides* (Kokkotou et al., 2014); (2) those with a 7,13-epoxy, also known as lauthisan-type acetogenins e.g. bermudenynol acetate (**91**) isolated from *L. intricata* (Grode & Cardellina, 1984); (3) those with a 4,7:6,12-bisepoxy e.g. desepilaurallene (**92**) isolated from *L. okamurai* (Li et al., 2012c); (4) those with a 6,12-epoxy and a second epoxy system between C-7 and either C-9, C-10 or C-11 e.g. okamuragenin (**93**) isolated from *L. okamurai* (Liang et al., 2012); (5) those with a 7,13-epoxy and a second epoxy system between C-6 and either C-9 or C-10 e.g. laurefurenyne F (**94**) isolated from *Laurencia* sp. showing moderate cytotoxicity towards three solid tumours (Abdel-Mageed et al., 2010); and (6) those with a 4,10:9,13-bisepoxy e.g. microcladallene C (**95**) isolated from *L. obtusa* (Kennedy et al., 1984).

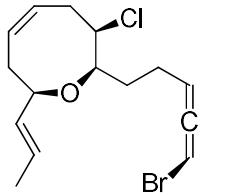

90

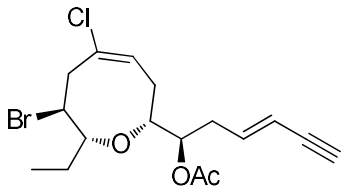

91

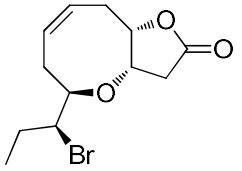

92

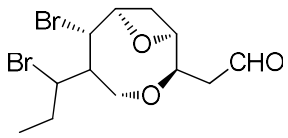

93

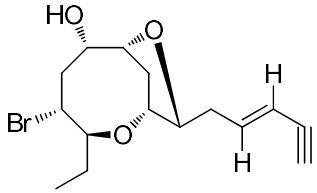

94

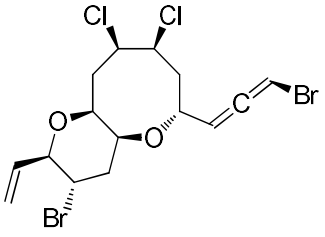

95

- Acetogenins containing a nine- or ten-membered cyclic ether ring. Among the nine-membered acetogenins, three subgroups can be discriminated, namely: (1) those containing a 5,12-epoxy ring e.g. compound **96** isolated from *Laurencia implicata* (Coll & Wright, 1989); (2) those containing a 6,13-epoxy ring e.g. (3*E*,12*R*,13*R*)-

obtusenyne (**97**) isolated from *L. chondrioides* (Kokkotou et al., 2014); and (3) those containing a 4,7:6,13-bisepoxy system e.g. laurendecumallene A (**98**) isolated from *L. decumbens* (Ji et al., 2007b). An example of an acetogenin containing a ten-membered cyclic ether is compound **99** isolated from *L. implicata* (Coll & Wright, 1989).

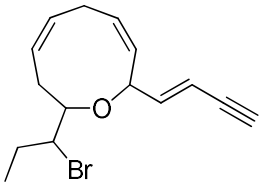

96

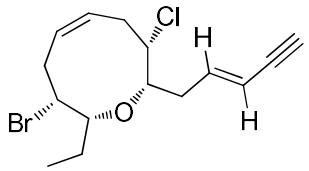

97

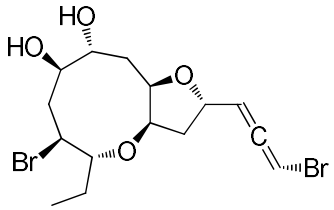

98

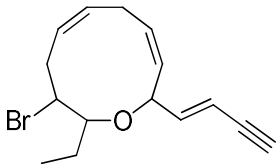

99

- Acetogenins containing a twelve-membered cyclic ether ring e.g. marilzanin (**100**) isolated from *Laurencia marilzae* (Gutiérrez-Cepeda et al., 2016).
- Linear acetogenins e.g. (3*Z*,9*Z*,12*E*)-7-acetoxy-6-chloropentadeca-3,9,12-trien-1-yne (**101**) isolated from *Laurencia glandulifera* (Kladi et al., 2009).

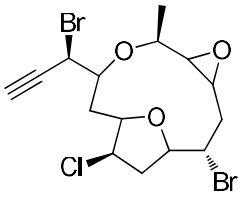

100

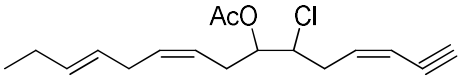

101

1.3.5 Indoles

Indoles isolated from the genus *Laurencia* can be divided into three subclasses (Harizani et al., 2016), namely: (1) monoindoles, e.g. 2,5,6-tri-bromo-3[(3^{-}-bromo-4^{-}-hydroxyl-phenyl)-methyl]-1*H*-indole (**102**) isolated from *L. similis* exhibiting promising antimicrobial activity (Li et al., 2016); (2) bisindoles, e.g. 3,3^{-}-bis-(2,5,6-tribromo)indole (**103**) isolated from *L. similis* (Su et al., 2009b); and (3) spiro-trisindoles, e.g. similisine A (**104**) isolated from *L. similis* (Sun et al., 2013).

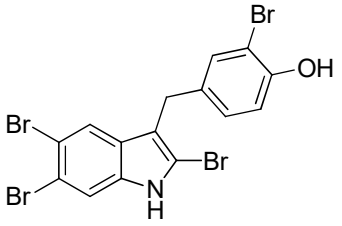

102

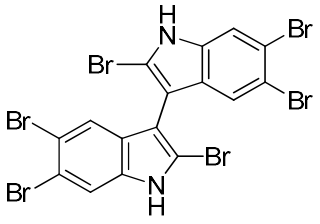

103

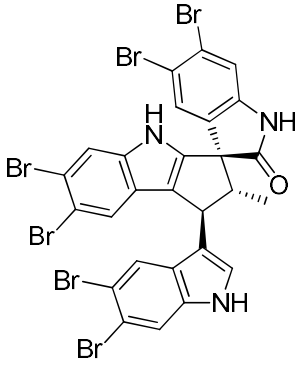

104

1.3.6 Aromatic compounds

A low number of aromatic compounds has been isolated from the genus *Laurencia* e.g. 3,5,6,6-tetrabromo-2,4-dimethyldiphenyl ether (**105**) isolated from *L. similis* showing strong inhibition effect against protein tyrosine phosphatase 1B (Qin et al., 2010).

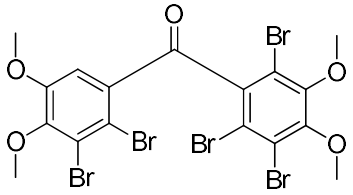

105

1.3.7 Steroids

Steroids isolated from the genus *Laurencia* are very few in comparison with the other classes of secondary metabolites isolated. A recently isolated example is alfredensterol (**106**) obtained from *L. alfredensis* and showing cytotoxicity towards HeLa cervical cancer cell line (Dziwornu et al., 2017).

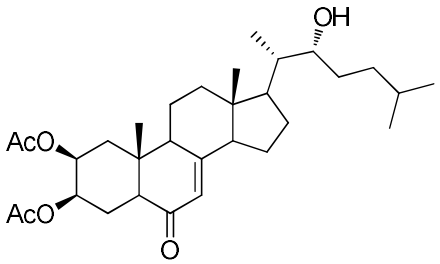

106

1.3.8 Miscellaneous metabolites

Other metabolites have been isolated from the genus *Laurencia* that cannot be assigned to one of the previous groups. One of the most recent examples is the glycolipid 1,2-di-*O*-palmitoyl-3-*O*-(6-sulfo-*α*-D-quinovopyranosyl)-glycerol (**107**) isolated from *L. alfredensis* (Dziwornu et al., 2017).

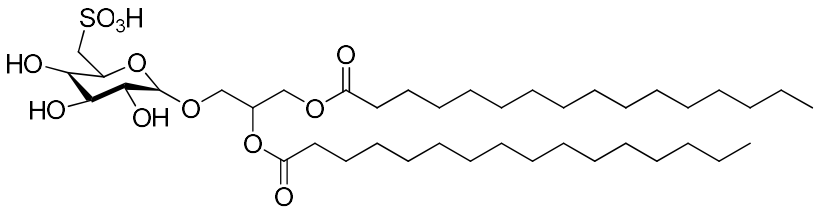

107

1.4 Sponges of the genus *Lamellodysidea*

Marine sponges (phylum Porifera) are a large phylum within the Kingdom Animalia. They are considered to be prolific factories of bioactive natural products (El-Demerdash et al., 2018).

Recently a reclassification of the genus *Dysidea* resulted in its splitting and creation of the new genus *Lamellodysidea*, including three species up to now i.e. *Lamellodysidea herbacea*, *Lamellodysidea chlorea* and *Lamellodysidea fragilis* (Kapojos et al., 2018; Sauleau & Bourguet-Kondracki, 2005). Among them, the most extensively studied is the species *L. herbacea* (Hanif et al., 2007).

The symbiotic relation with the filamentous cyanobacterium *Oscillatoria spongeliae* was found to be a biological characteristic for the genus *Lamellodysidea* (Hanif et al., 2007).

Up to now, only a low number of compounds has been isolated from the genus *Lamellodysidea* (MarinLit, 2020), including sesquiterpenes (Torii et al., 2017) polyhydroxysterols (Sauleau & Bourguet-Kondracki, 2005), polychlorinated pyrrolidinones (Sauleau et al., 2005), dysinosins (Carroll et al., 2004), and polyhalogenated diphenyl ethers (Kapojos et al., 2018).

1.4.1 Sesquiterpenes

Lamellodysidines A and B, *O,O*-dimethyl-lingshuiolide A, 11-*epi*-*O,O*-dimethyl-lingshuiolide A and *O*-methyl-nakafuran-8 lactone (**108-112**) were isolated from the organic extract of an Indonesian *L. herbacea* (Torii et al., 2017).

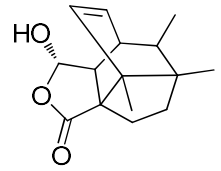

108

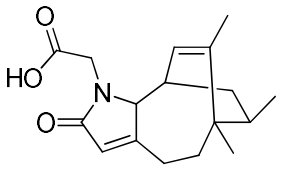

109

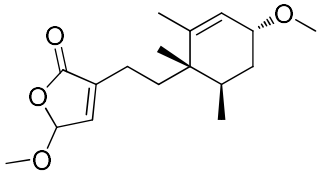

110

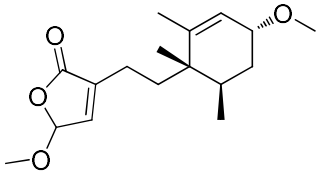

111

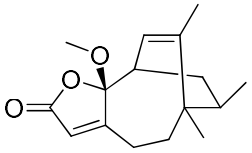

112

Two monocyclofarnesol-derived sesquiterpenes, namely lamellolactones A and B (**113** and **114**) have been isolated from *Lamellodysidea* sp. (Kapojos et al., 2018).

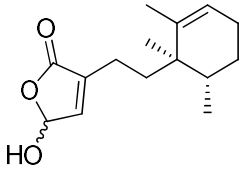

113

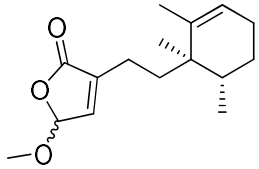

114

1.4.2 Steroids

Up to now only four steroids have been isolated from the genus *Lamellodysidea*, namely cholesta-8(9)-en-3*β*,5*α*,6*α*,25-tetraol (**115**), cholesta-8(14)-en-3*β*,5*α*,6*α*,25-tetraol (**116**), cholesta-8(9),24-dien-3*β*,5*α*,6*α*-triol (**117**) and cholesta-8(14),24-dien-3*β*,5*α*,6*α*-triol (**118**) isolated from *L. herbacea*, with **117** and **118** showing antifungal activity against *Candida tropicalis* (Sauleau & Bourguet-Kondracki, 2005).

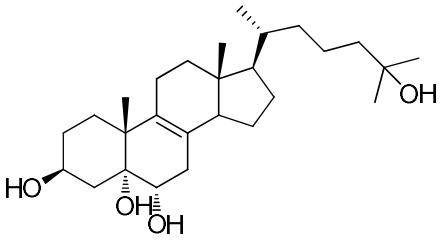

115

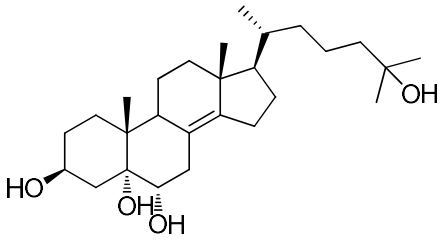

116

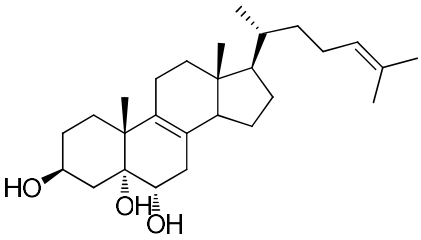

117

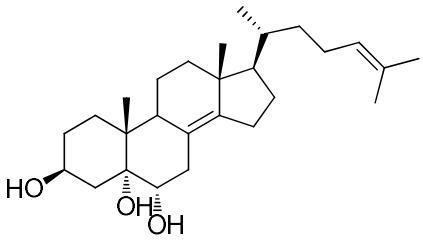

118

1.4.3 Polychlorinated pyrrolidinones

Eleven polychlorinated pyrrolidinones analogs dysidamide (**119**), dysidamide D (**120**), dysidamide E (**121**), dysidamide B (**122**), dysidamide H (**123**), 7,7,7-tricholoro-3-hydroxy-2,2,6 trimethyl-4-(4,4,4-trichloro-3-methyl-1-oxobutyl-amino)-heptanoic acid methyl ester (**124**), 7,7,7-tricholoro-2,2,6 trimethyl-3-oxo-4-(4,4,4-trichloro-3-methyl-1-oxobutyl-amino)-heptanoic acid methyl ester (**125**), dysidamide F (**126**), dysidamide C (**127**), dysidamide G (**128**) and 5-*epi*-dysidamide G (**129**) have been isolated from *L. herbacea* collected in the Red Sea. Among them, dysidamide (**119**) was found to be neurotoxic towards mesencephalic and cortical murine neurons with concentration 0.8 μg/ml (Sauleau et al., 2005).

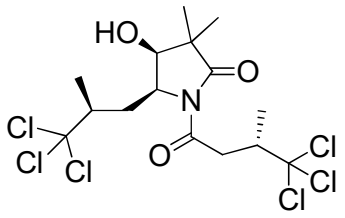

119

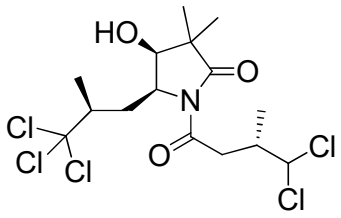

120

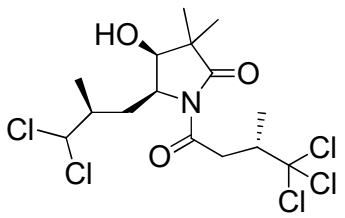

121

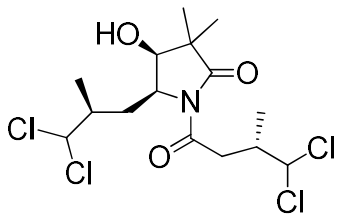

122

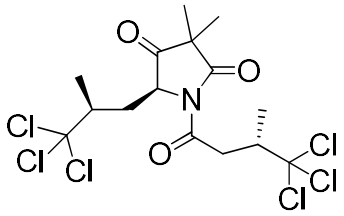

123

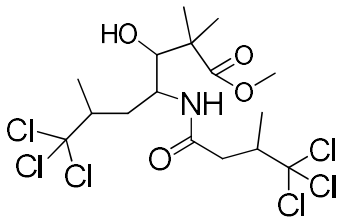

124

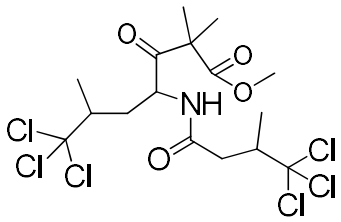

125

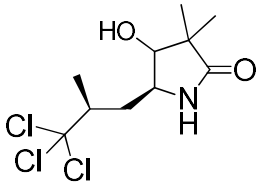

126

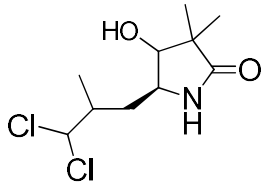

127

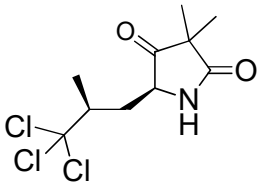

128

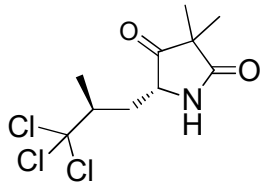

129

1.4.4 Dysinosins

Three dysinosin analogs, namely dysinosins B-D (**130-132**) have been isolated from *L. chlorea* and were found to be blood coagulation cascade serine proteases factor VIIa and thrombin inhibitors (Carroll et al., 2004).

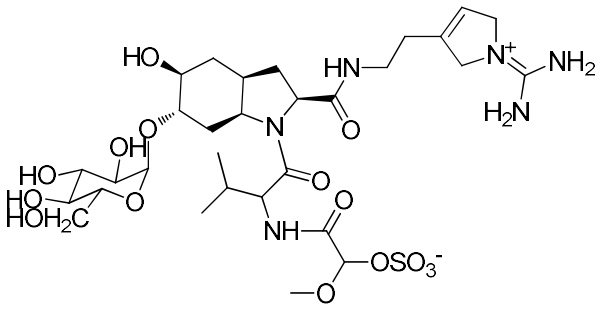

130

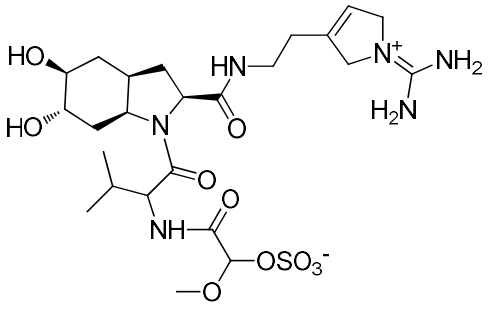

131

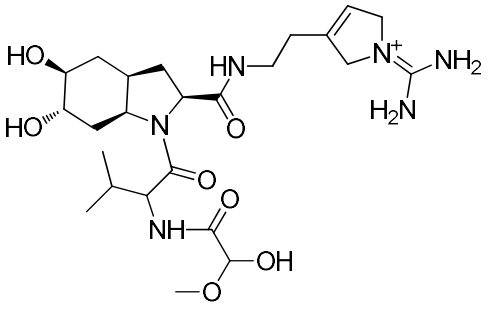

132

1.4.5 Polyhalogenated diphenyl ethers

Fourteen polybrominated diphenyl ethers (**133-146**) have been isolated from the organic extract of an Indonesian *L. herbacea*. These compounds were found to have strong antibacterial activity against *Bacillus subtilis* (Hanif et al., 2007).

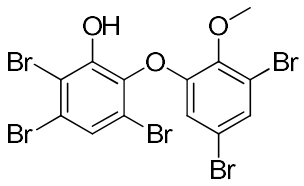

133

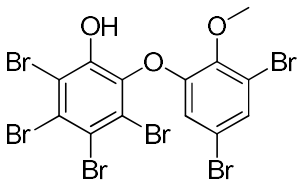

134

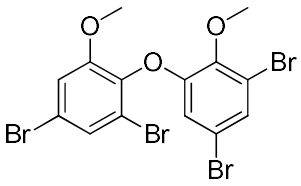

135

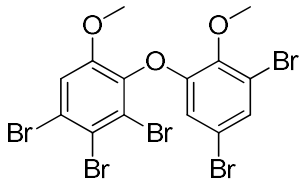

136

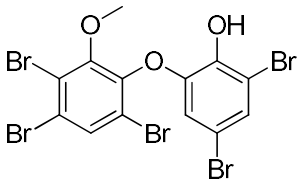

137

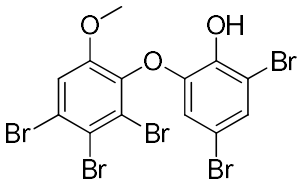

138

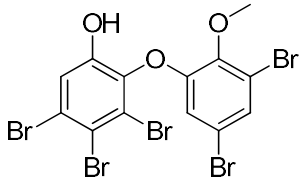

139

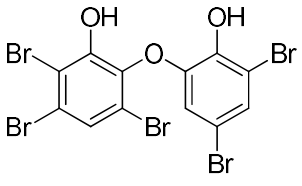

140

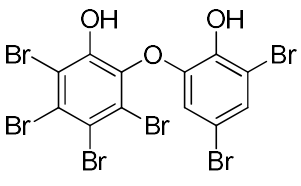

141

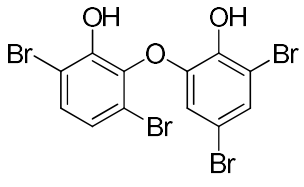

142

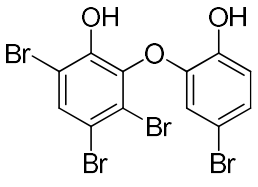

143

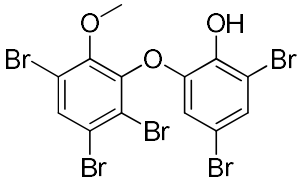

144

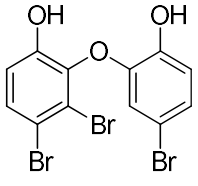

145

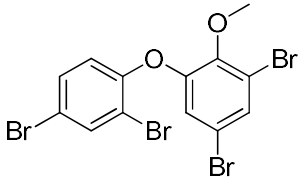

146

2-(2′,4′-Dibromophenoxy)-3,5-dibromophenol (**147**), 2-(2′,4′dibromophenoxy)-4,6-dibromophenol (**148**) and 2-(2′-dibromophenoxy)-3,4,5,6-tetrabromophenol (**149**), three polybromobiphenyl ethers have been isolated from *L. cf. herbacea*, showing inhibitory effects towards protein tyrosine phosphatase 1B (PTP1B) with IC_{50} values of 5.3, 7.8, and 5.3 μM, respectively (Kapojos et al., 2018).

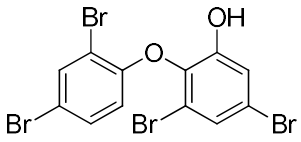

147

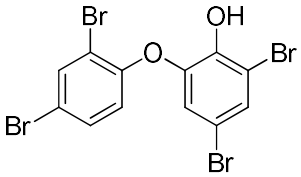

148

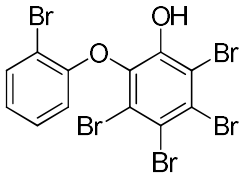

149

1.5 Soft corals of the genus *Sinularia*

Sinularia is a genus of soft corals that belongs to the phylum Cnidaria, the class Alcyonaria and the family Alcyoniidae. The taxonomy is based on the spicules' examination and a fairly reliable taxonomic key is available to guide species' identification (Kamel & Slattery, 2005; Verseveldt, 1980).

The genus *Sinularia* is widely distributed from western Pacific to the east of Africa (Figure 4) and consists of approximately 90 species, among which more than 50 have been chemically investigated (Chen et al., 2012).

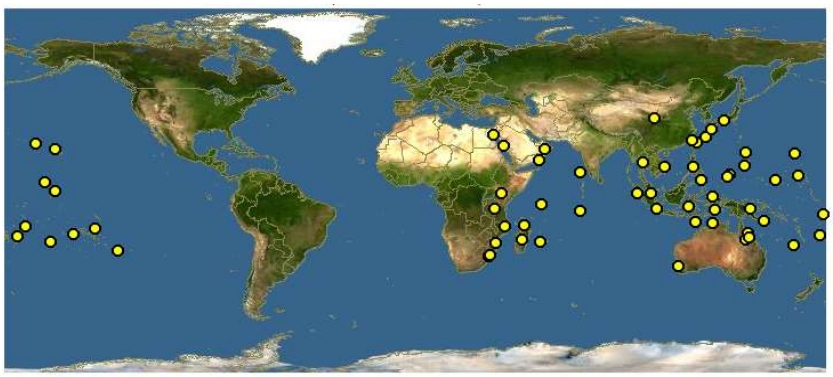

Figure 4. Global distribution map for the genus *Sinularia*.

Over 500 metabolites have been isolated from soft corals of the genus *Sinularia*, including sesquiterpenes, diterpenes, polyhydroxylated steroids, alkaloids and polyamines (Hegazy et al., 2016).

1.5.1 Sesquiterpenes

A furano-sesquiterpenoid acid, namely furanoic acid (**150**), was the first reported sesquiterpene obtained from *Sinularia gonatodes* (Coll et al., 1977). Later, in 1994 its *in vitro* anti-inflammatory activity against bee venom phospholipase A2 (bvPLA2) with an IC_{50} value of 0.5µM was reported (Grace et al., 1994).

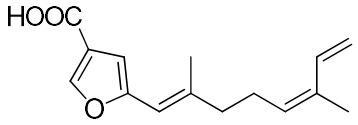

150

Africanene (**151**), the most commonly reported sesquiterpene from species of the genus *Sinularia*, was first reported from *Sinularia polydactyla* (Braekman et al., 1980). Africanene (**151**) has mild CNS depressant activity and dose-dependent hypotensive activity. Furthermore, it acts as an anti-inflammatory agent against carrageenan-induced rat edema with a 60% reduction at a dose of 10 mg/kg body weight as compared to ibuprofen (Reddy et al., 1999).

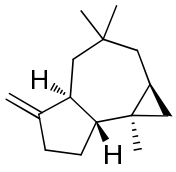

151

Sesquiterpenes **152** and **153**, along with 9*α*,15-dihydroxyafricanane (**154**) have been isolated from *Sinularia dissecta* (Ramesh & Venkateswarlu, 1999).

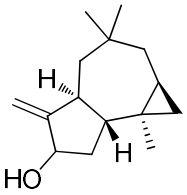

152

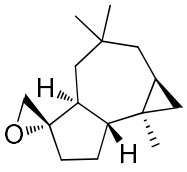

153

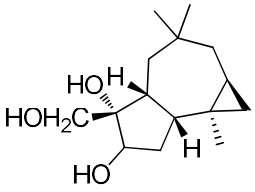

154

A sesquiterpene featuring the aromadendrane skeleton, namely spathulenol (**155**), has been isolated from *Sinularia kavarattiensis* (Goud et al., 2002).

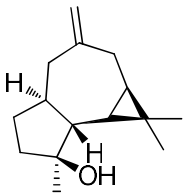

155

Capillobenzopyranol (**156**), capillobenzofuranol (**157**) and capillofuranocarboxylate (**158**) have been isolated from *Sinularia capillosa* (Cheng et al., 2010). Capillobenzopyranol (**156**) was weakly cytotoxic against P-388 with an ED_{50} value of 12.7 µM, while capillobenzofuranol (**158**) showed antiviral activity (IC_{50} = 13.5 µM) (Arepalli et al., 2009).

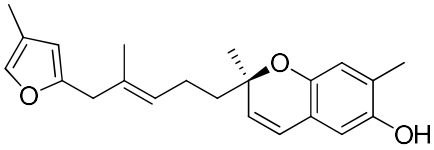

156

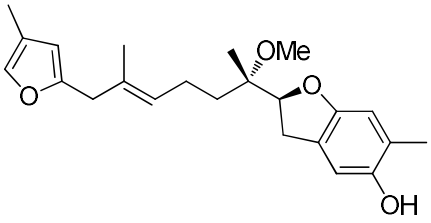

157

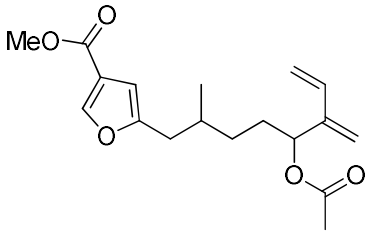

158

Peroxygibberol (**159**), gibberodione (**160**) and sinugibberodiol (**161**) were isolated from *Sinularia gibberosa* (Ahmed et al., 2005). Peroxygibberol (**159**) exhibited mild cytotoxic activity against human liver carcinoma cell line.

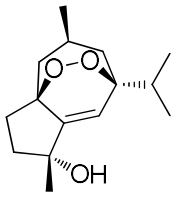

159

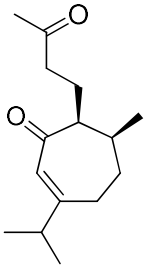

160

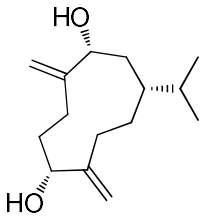

161

Polydactins A (**162**) and B (**163**), along with 10*α*-hydroxy-cadin-4-en-15-al (**164**), have been isolated from *S. polydactyla*. Polydactin B (**163**) was weakly cytotoxic against KB and MCF cell lines, while polydactin A (**162**) showed moderate cytotoxic effects against KB and MCF cell lines with IC_{50} values 13.0 and 14.0 µg/ml, respectively (Zhang et al., 2008).

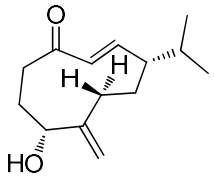

162

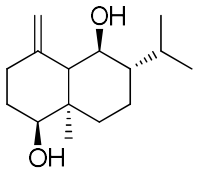

163

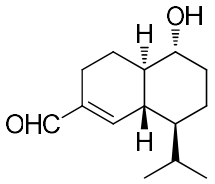

164

Extraction of *Sinularia nanolobata* with *n*Hex yielded nanolobatol A (**165**), nanolobatol B (**166**), sinularianin B (**167**) and sinularianin D (**168**) (Ngoc et al., 2017).

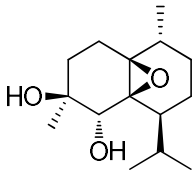

165

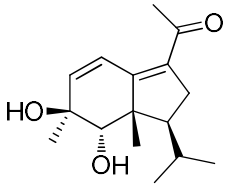

166

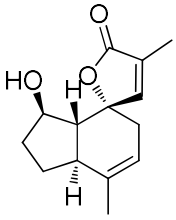

167

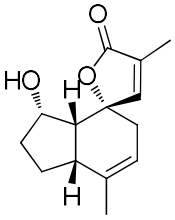

168

The seco-guaiane-type sesquiterpenes molestin A (**169**), epi-gibberodione (**170**) and its *S*-isomer at position 1 (**171**) and three guaiane-type sesquiterpenes molestin B (**172**), molestin C (**173**) and molestin D (**174**) have been isolated from *Sinularia* cf. *molesta*. Molestin C (**173**) and molestin D (**174**) exhibited strong inhibitory effect against PTP1B with IC_{50} values 218 and 344 μM, respectively (Chu et al., 2018).

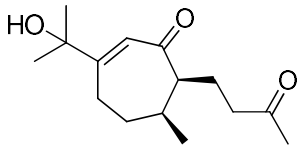

169

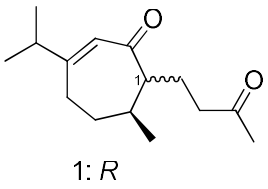

170

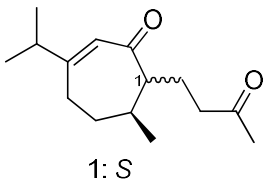

171

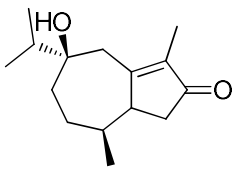

172

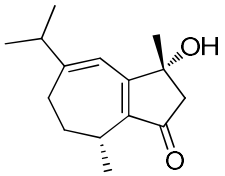

173

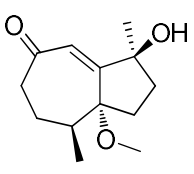

174

3*β*,5*α*-Dihydroxy-eudesma-4(15),11-diene (**175**), 4(15)-eudesmene-1*β*,6*α*-diol (**176**), 6*α*-hydroxy-eudesm-4(15)-ene-1-one (**177**) and 4*β*,15-epoxy-eudesmene-1*β*,6*α*-

diol (**178**) have been isolated from the methanolic extract of *Sinularia erecta*. 3*β*,5*α*-Dihydroxy-eudesma-4(15),11-diene (**175**) showed selective cytotoxicity against A549 cell line (IC_{50} = 14.8±0.91 μM) (Huong et al., 2018).

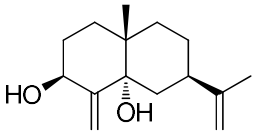

175

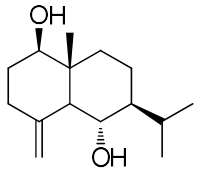

176

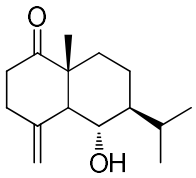

177

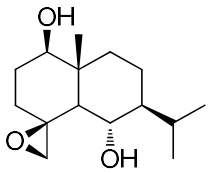

178

1.5.2 Diterpenes

Two cembrene diterpenes, namely (1*R*,4*R*,2*E*,7*E*,11*E*)-cembra-2,7,11-trien-4-ol (**179**) and (1*R*,3*S*,4*S*,7*E*,11*E*)-3,4-epoxy-cembra-7,11,15-triene (**180**) have been isolated from *Sinularia facile* (Bowden et al., 1981).

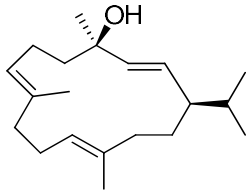

179

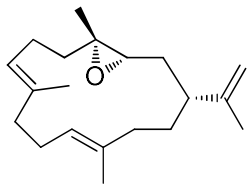

180

The ethyl acetate extract of *Sinularia flexibilis* afforded flexibiloide (**181**) and dihydroflexibilolide (**182**) (Anjaneyulu & Sagar, 1996).

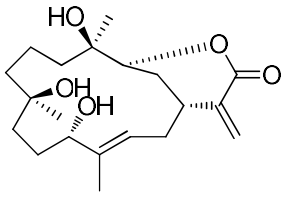

181

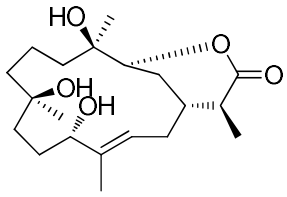

182

Chromatographic separation of the organic extract of *S. capillosa* allowed for the isolation of capillolide (**183**), sinulariolide (**184**), flexibilide (**185**) and (1*R*,4*R*,5*S*,8*R*,9*S*,12*S*,13*S*)-9-acetoxy-5,8:12,13-diepoxy-cembr-15(17)-en-16,4-olide (**186**). All of them were found to be moderately to strongly cytotoxic against P-388 and L1210 cancer cell lines (Su et al., 2000).

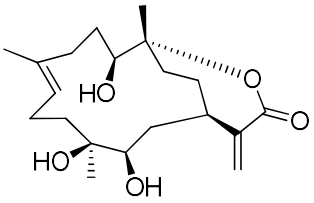

183

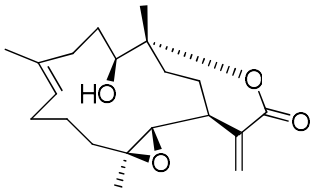

184

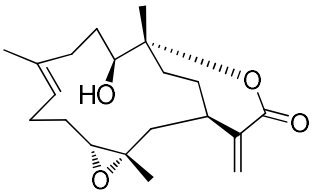

185

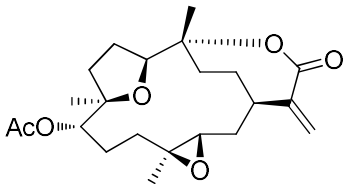

186

Microclavatin (**187**), a diterpene obtained from the EtOAc extract of the soft coral *Sinularia microclavata*, was found to be cytotoxic against KB and MCF with IC_{50} values of 5.0 and 20.0 µg/mL, respectively (Zhang et al., 2005).

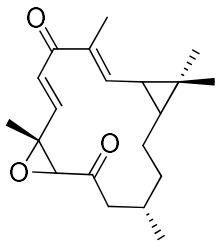

187

Grandilobatins A-E (**188-192**) have been isolated from *Sinularia grandilobata*. Grandilobatin D (**191**) was found to be pro-inflammatory for iNOS protein of LPS-stimulated RAW264.7 macrophage cells at 50 µM (Ahmed et al., 2008).

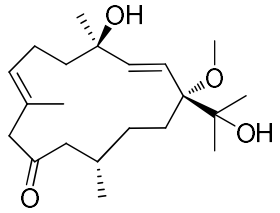

188

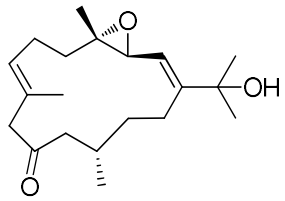

189

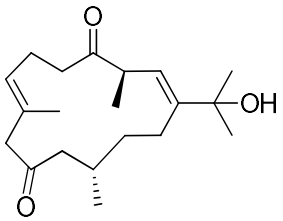

190

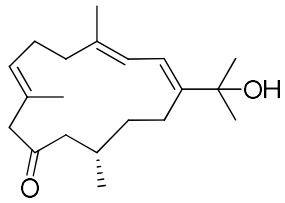

191

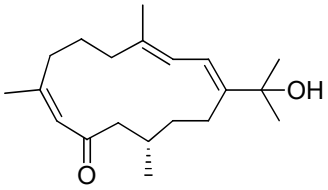

192

Pavidolides A-E (**193-197**), sarchophytin (**198**) and chatancin (**199**) have been obtained from *Sinularia pavida*. Their cytotoxicity was tested against HL-60, HCT-8, HePG2, BGC-823, A549 and A375 cancer cell lines. Pavidolides B (**194**) and C (**195**) exhibited activity against HL-60 with IC_{50} values of 2.7 and 5.3 μg/mL, respectively. Furthermore, pavidolides C (**195**) and D (**196**) showed mild antifouling activity against *A. amphitrite* (ED_{50} 4.32 and 2.12 μg/mL, respectively) with low cytotoxicity (LD_{50}> 50 μg/mL) (Shen et al., 2012).

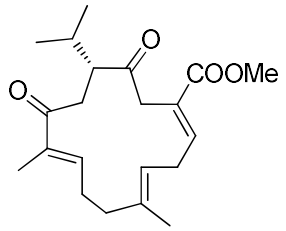

193

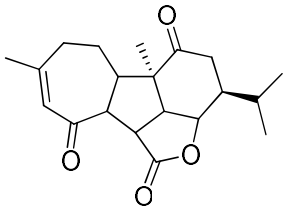

194

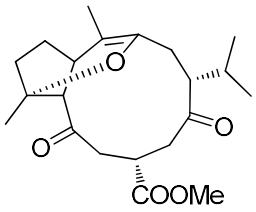

195

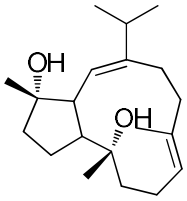

196

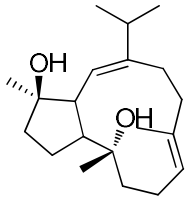

197

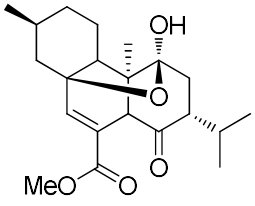

198

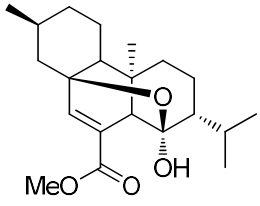

199

Sinulariaoids A-D (**200-203**), dihydrosinularin (**204**), sinularin (**205**) and dihydrosinflexoide (**206**) have been isolated from a South China Sea *Sinularia* sp. and their cytotoxicity was evaluated against HPG2, HPG2/ADM, MCF-7 and MCF-7/ADM

human cancer cell lines. While sinulariaoids B-D (**201-203**), dihydrosinularin (**204**) and dihydrosinflexoide (**206**) were found to be inactive, sinulariaoid A (**200**) and sinularin (**205**) showed moderate cytotoxicity (Lei et al., 2014).

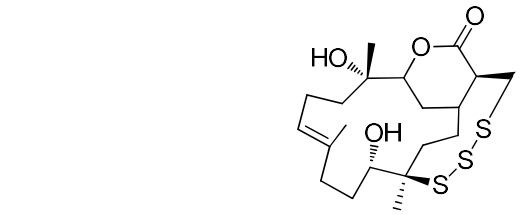

200

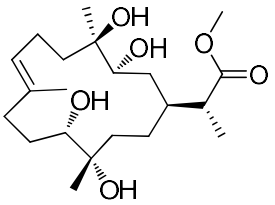

201

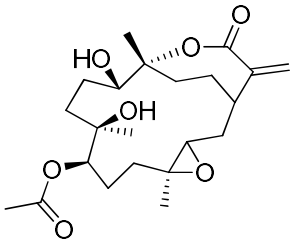

202

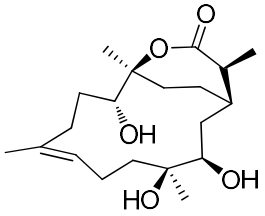

203

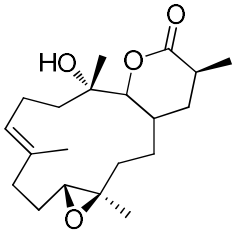

204

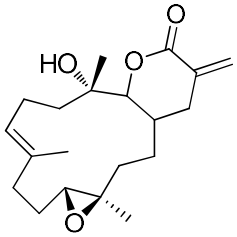

205

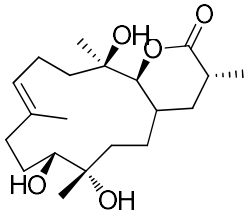

206

Chemical examination of the organic extract of *S. flexibilis* yielded nine *α*-methylene-*δ*-lactone-bearing cembranoids, namely 9*α*-hydroxy-flexibilide (**207**), 15(17)-dehydro-manaarenolide E (**208**), 8-dehydroxy-15(17)-dehydro-manaarenolide E (**209**), 15(17)-dehydro-manaarenolide (**210**), 15(17)-dehydro-manaarenolide C (**211**), *epi*-flexilarin A (**212**), flexibilide (**213**), sinuflexolide (**214**), 11-acetyl-sinuflexolide (**215**), the 15-membered macrocyclic epoxyflexibilene (**216**) and the two cembrane dimers sinulaflexiolide L (**217**) and sinulaflexiolide A (**218**). Flexibilide (**213**) exhibited anti-tumor activity against the inositol-requiring 1/X-box-binding protein 1 (IRE1/XBP1) signaling pathway (IC_{50} = 4.1 μg/mL) (Chen et al., 2015).

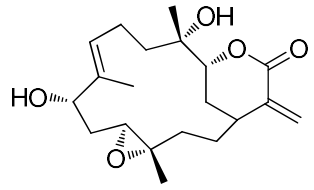

207

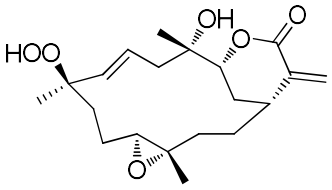

208

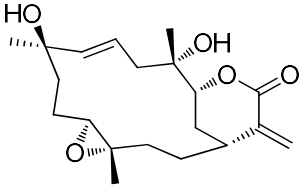

209

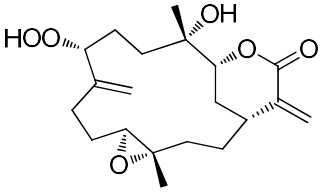

210

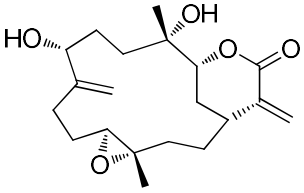

211

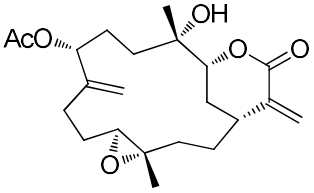

212

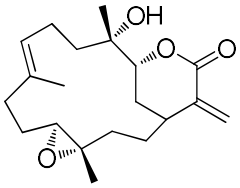

213

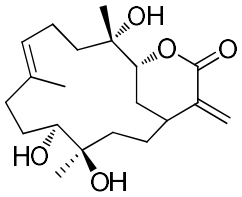

214

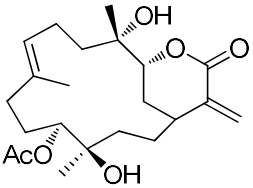

215

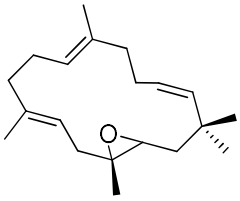

216

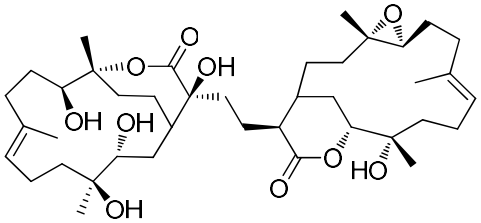

217

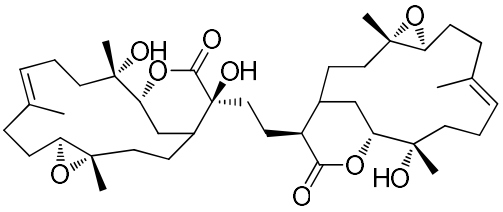

218

Chemical investigation of *S. nanolobata* afforded sinulariols A, C, D, H and J (**219-223**), nanolobols A-C (**224-226**), calyculone I (**227**) and nanoculones A and B (**228** and **229**). Sinulariol C (**220**) was found to be a promising anti-inflammatory agent (Chao et al., 2016).

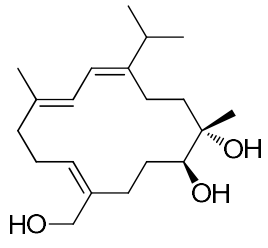

219

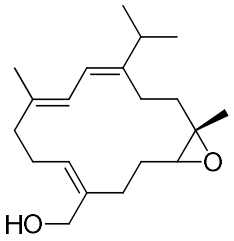

220

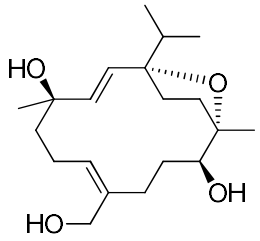

221

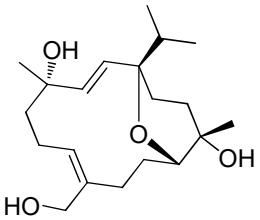

222

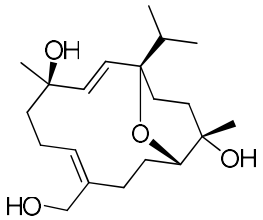

223

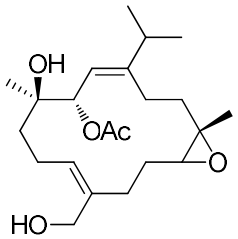

224

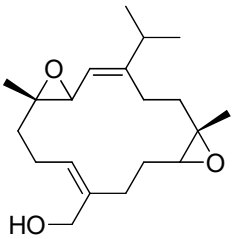

225

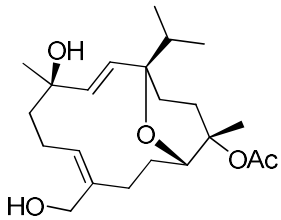

226

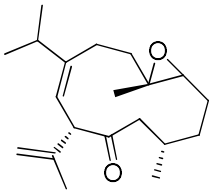

227

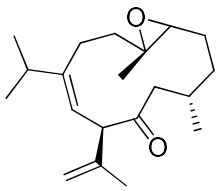

228

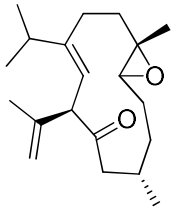

229

Sinularcasbanes M, N and O (**230-232**), scabrolide F (**233**) and ineleganolide (**234**) were isolated from the Egyptian Red Sea *S. polydactyala* (Hegazy et al., 2016).

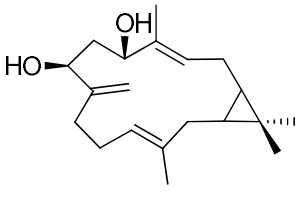

230

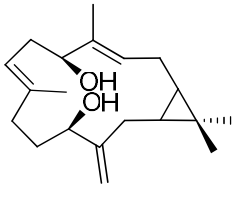

231

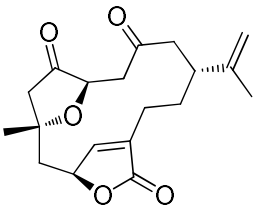

232

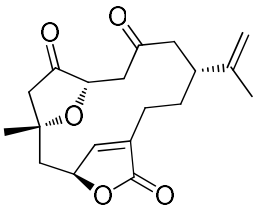

233

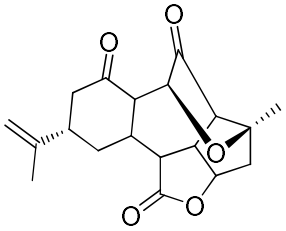

234

Xishacorenes A-C (**235-237**) and fuscol (**238**) were isolated from a Chinese *S. polydactyala* (Ye et al., 2017).

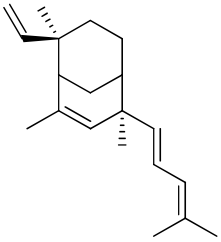

235

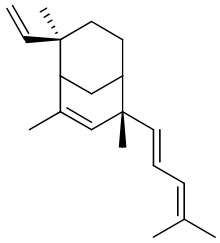

236

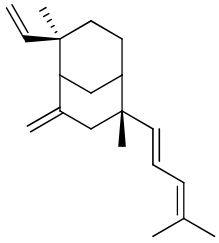

237

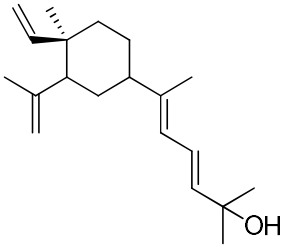

238

The methanolic extract of *S. flexibilis* afforded sinulaflexiolides L, M, N and O (**239-242**), ent-sinuflexibilin D (**243**), enolide I (**244**), sinularin (**245**), dihydrosinularin (**246**), 11-dehydrosinulariolide (**247**), 14-deoxycrassin (**248**), thioflexibilolide A (**249**), epoxycembrane A (**250**), diepoxyceane A (**251**) and flexilarin B (**252**). Compounds **239-245**, **248**, **249** and **252** were tested for their inhibitory effect against lipopolysaccharide (LPS)-induced nitric oxide (NO) production and the levels of TNF-α in RAW 264.7 macrophages. Among them, compound **245** exhibited the highest inhibitory effect with 88.6 and 94.2%, respectively, at a 10 μM concentration (Zhao et al., 2018).

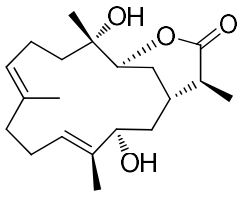

239

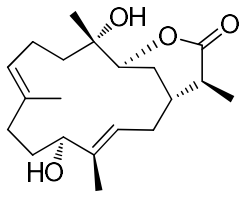

240

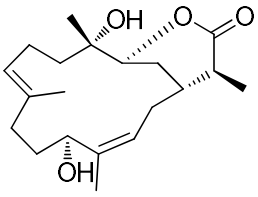

241

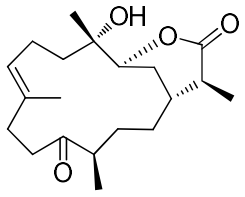

242

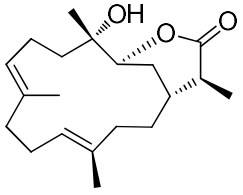

243

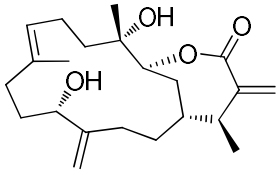

244

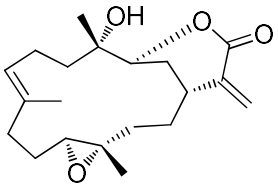

245

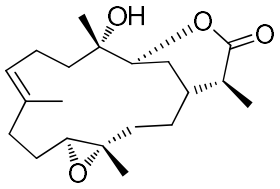

246

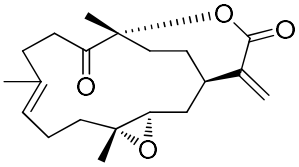

247

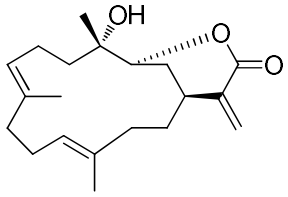

248

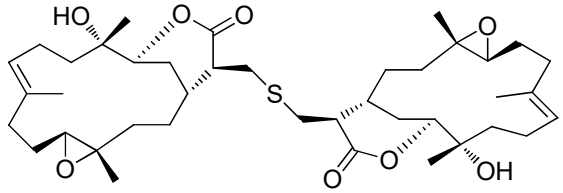

249

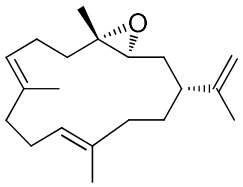

250

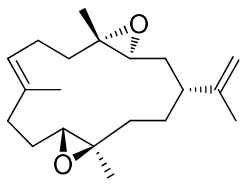

251

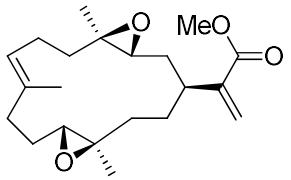

252

Chemical examination of *S. flexibilis* led to the isolation of xidaosinularides A-C (**253-255**), sinuladiterpene I (**256**), 5-dehydrosinulariolide (**257**), 11-epi-sinulariolide acetate (**258**) and diepoxycembrene A (**259**), along with sinulariolide (**184**) and flexilarin B (**252**). Among them, compounds **258**, **184** and **252** were found to be strong anti-inflammatory agents with IC_{50} values of 2.7, 4.7 and 4.2 μM, respectively. Moreover compound **257** showed cytotoxicity against several cancer cell line (Wu et al., 2019).

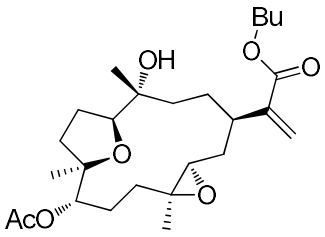

253

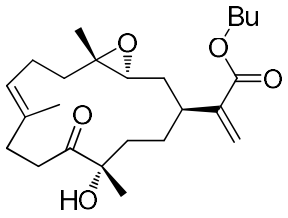

254

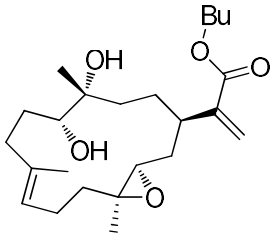

255

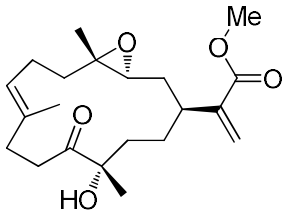

256

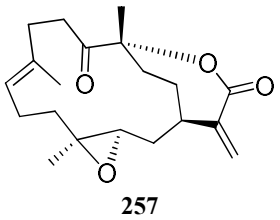

257

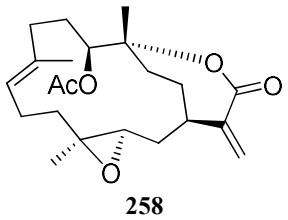

258

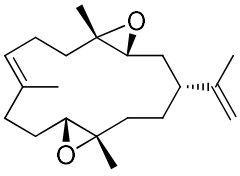

259

1.5.3 Steroids

Approximately 50 steroids have been reported from the genus *Sinularia* (MarinLit, 2020). Five polyoxygenated steroids, namely 24(*S*)-methyl-cholest-

3*β*,5*α*,6*β*,25-tetraol (**260**), cholest-1*β*,3*β*,5*α*,6*β*,11*α*-pentaol (**261**), 24(28)-methyl-cholesten-1*β*,3*β*,5*α*,6*β*,11*α*-pentaol (**262**), 24(28)-methyl-cholesten-1*β*,3*β*,5*α*,6*α*,11*α*-pentaol (**263**) and 24(*S*)-methyl-cholest-11*α*,12*α*-epoxy-1*β*,3*β*,6*β*-triol (**264**) were isolated from the soft coral *S. dissecta* (Ramesh & Venkateswarlu, 1999).

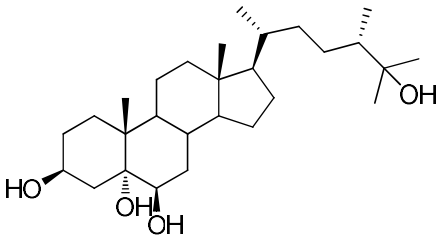

260

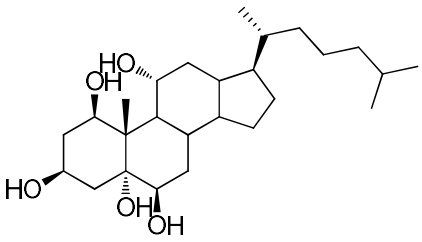

261

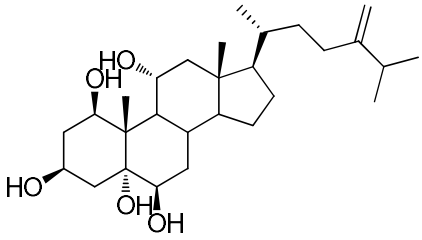

262

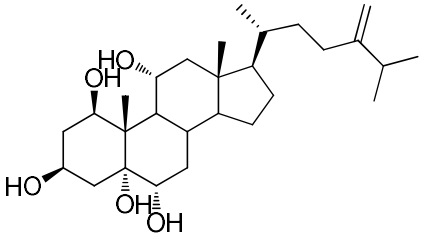

263

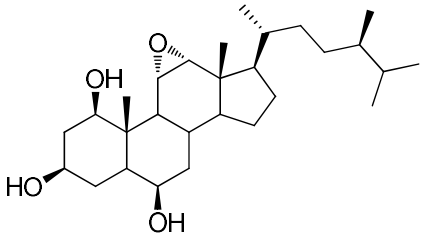

264

Chemical investigation of *S. grandilobata* led to the isolation of four steroids, namely sinugrandisterols A-D (**265-268**) (Ahmed et al., 2007).

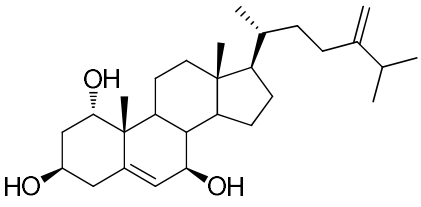

265

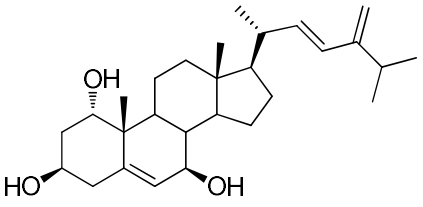

266

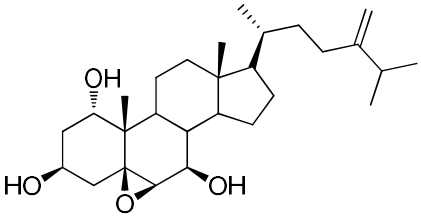

267

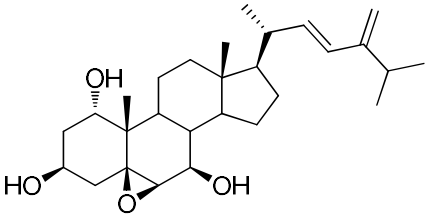

268

24-Methylene-cholesterol (**269**), 24(*S*)-methyl-cholesterol (**270**), 24(*S*)-methyl-cholestan-1*α*,3*β*-diol (**271**), 24(*S*)-methyl-cholestan-1*α*,3*β*,25-triol (**272**), 11α-acetoxy-24(*S*)-methyl-cholestan-1*α*,3*β*,5*α*,6*β*-tetraol (**273**), 6-oxo-24(*S*)-methyl-cholestan-3*β*,5*α*-diol (**274**), gorgosterol (**275**) and 6-oxo-grogostan-3*α*,5*β*-diol (**276**) were isolated from an Indonesian *Sinularia* sp. Among them, compounds **271** and **275** were found to have a consistently antagonistic activity with the farnesoid X-activated receptor (FXR) which is useful for the cholestasis treatment (Putra et al., 2012).

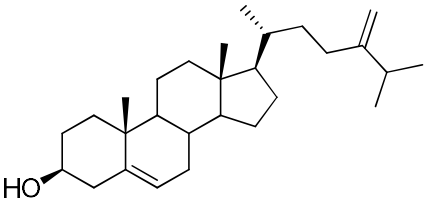

269

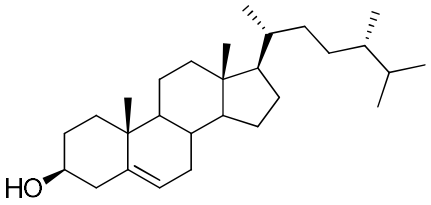

270

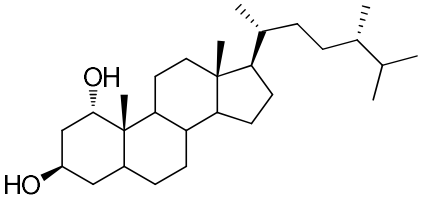

271

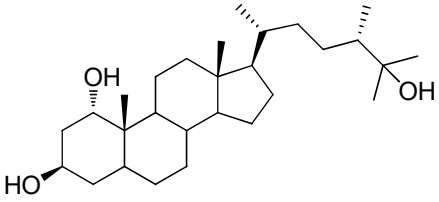

272

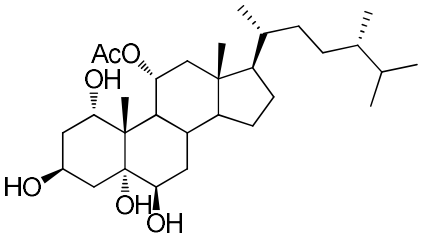

273

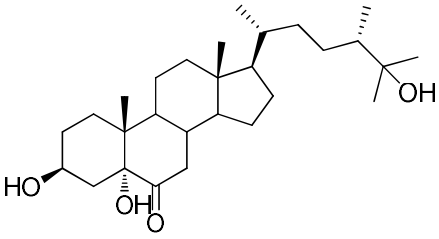

274

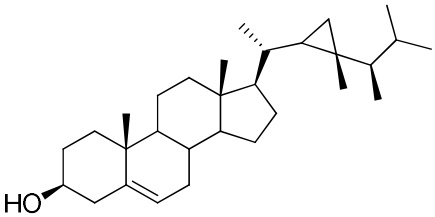

275

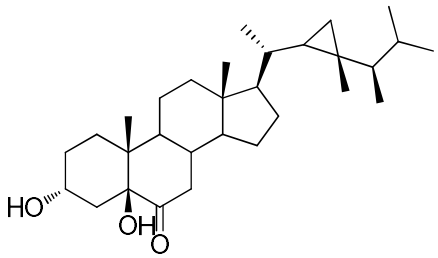

276

Chemical examination of *Sinularia acuta* led to the isolation of 24-oxo-6*β*-acetoxy,22(*E*)-cholest-22(23)-ene-3*β*,5*α*-diol (**277**), 28,6*β*-diacetoxy-ergost-24(25)-ene-3*β*,5*α*-diol (**278**), 6*β*-acetoxy-24-methyl-cholest-24(28)-ene-3*β*,5*α*-diol (**279**), 6*β*-acetoxy-24(*S*)-methyl-cholesta-3*β*,5*α*-diol (**280**), 6*β*-acetoxy-16*β*-methoxy-23,24-dimethyl-ergost-17(20)-ene-3*β*,5*α*-diol (**281**), 16*β*-methoxy-23,24-dimethyl-ergost-5(6),17(20)-diene-3*β*-ol (**282**), 6*β*-acetoxy-20-oxo-pregn-16(17)-en-3*β*-ol (**283**) and 20-oxo-pregn-5(6),16(17)-dien-3*β*-ol (**284**) (Zhang et al., 2015).

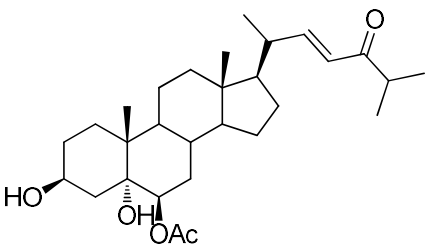

277

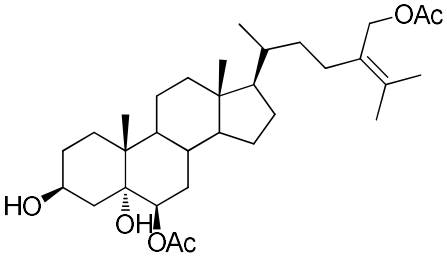

278

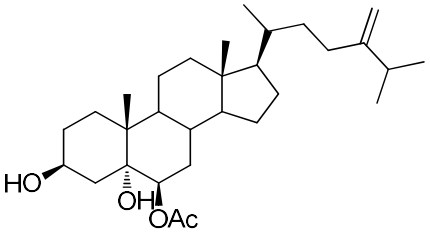

279

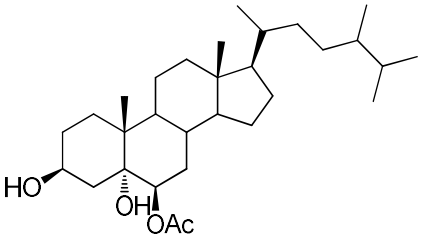

280

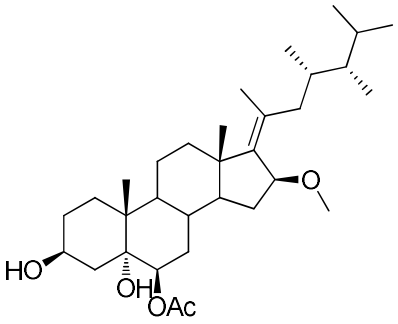

281

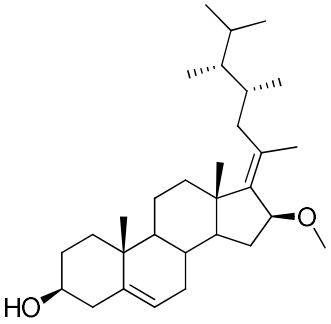

282

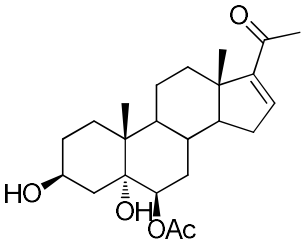

283

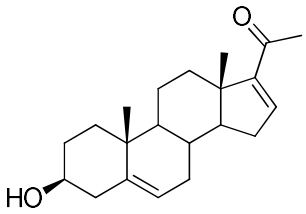

284

Five polyhydroxylated sterols, namely (22*E*)-24-methyl-cholesta-22,24(28)-dien-3*β*,5*α*,6*β*-triol (**285**), 24-methyl-cholest-24(28)-en-3*β*,5*α*,6*β*-triol (**286**), (22*E*)-24-methyl-cholest-22(23)-en-3*β*,5*α*,6*β*-triol (**287**), 24-methyl-cholest-3*β*,5*α*,6*β*-triol (**288**) and cholest-3*β*,5*α*,6*β*-triol (**289**) were obtained from a Chinese *Sinularia* sp., with all of them being cytotoxic against HepG2 and HeLa cell lines with IC_{50} values between 8.36 to 37.30 μM (Sun et al., 2016).

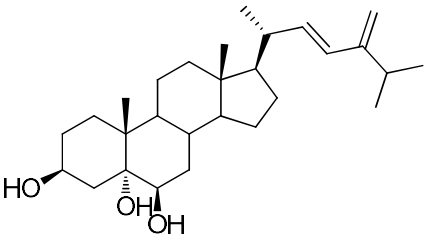

285

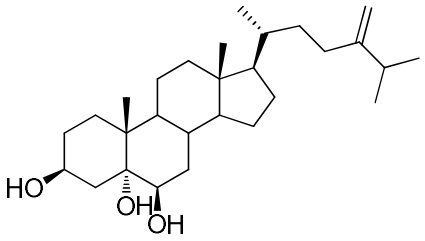

286

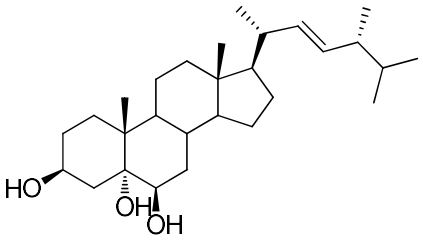

287

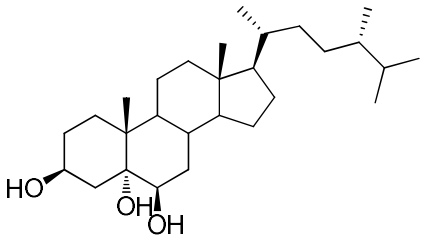

288

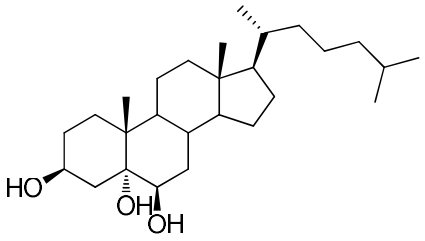

289

Sinubrassione (**290**), ergosta-1*α*,3*β*,5*α*,6*β*,11*α*-pentaol (**291**), sarcoaldesterol B (**292**), ergosta-1*β*,3*β*,5*α*,6*β*-tetraol (**293**), ergosta-3*β*,5*α*,6*β*-triol (**294**), sarcoaldesterol A (**295**), sinubrassioside (**296**) and pregnedioside A (**297**) were isolated from a Vietnamese *Sinularia brassica* (Tran et al., 2017).

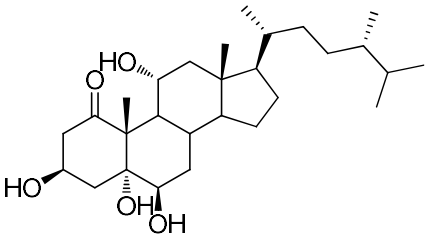

290

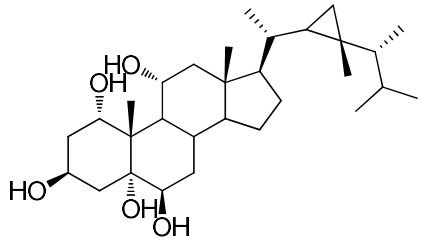

291

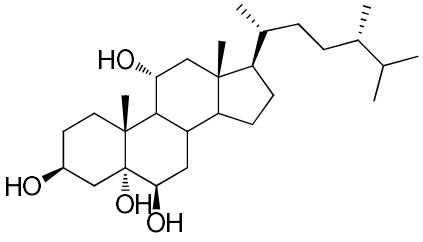

292

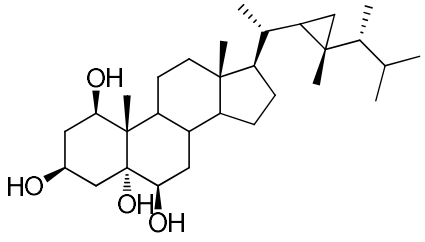

293

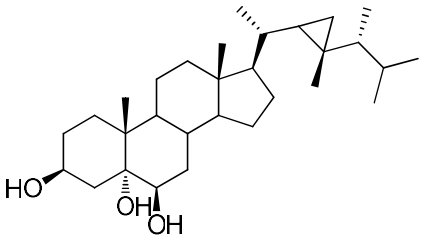

294

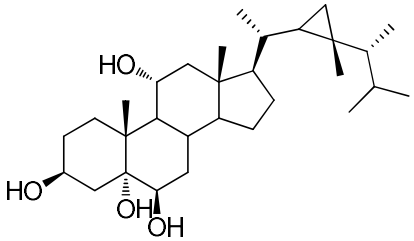

295

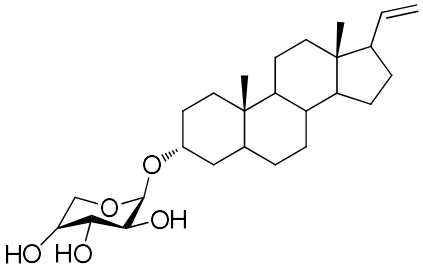

296

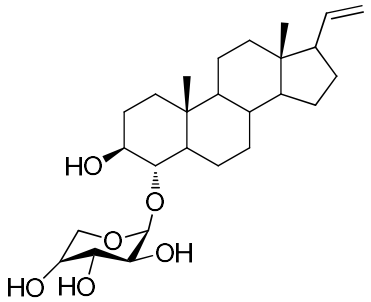

297

Chemical examination of a Chinese *Sinularia* sp. led to the isolation of ximaosteroids E and F (**298** and **299**), astrogorgol N (**300**) and 20(*S*)-20-hydroxycholest-1-ene-3,16-dione (**301**). Ximaosteroids E and F (**298** and **299**) and 20(*S*)-20-hydroxycholest-1-ene-3,16-dione (**301**) exhibited potent cytotoxicity against HL-60 (Li et al., 2018).

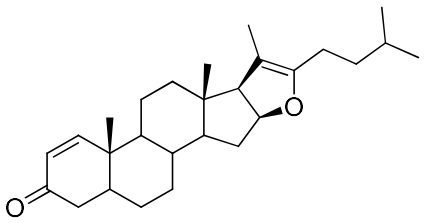

298

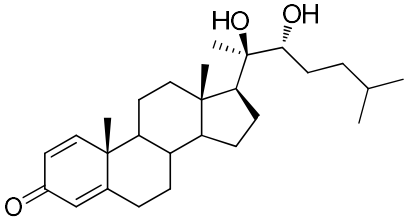

299

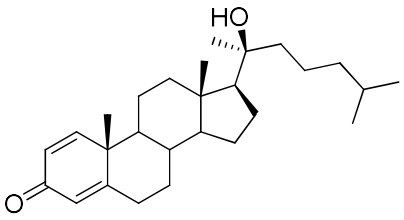

300

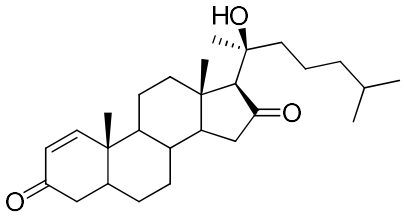

301

1.5.4 Nitrogen-containing compounds

A series of acylspermidines, namely compounds **302-309**, were obtained from *Sinularia* sp. Acylspermidines **304-306**, **308** and **309** exhibited potent cytotoxicity against A431 cells derived from vulval squamous cell carcinoma (SCC) and NAKATA cells derived from oral SCC (Ojika et al., 2003).

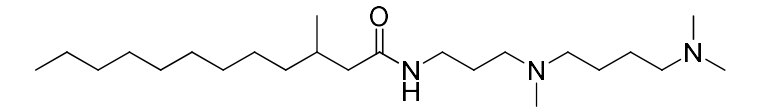

302

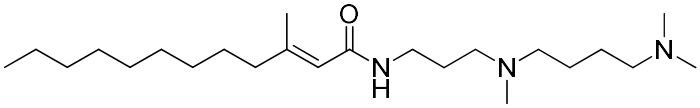

303

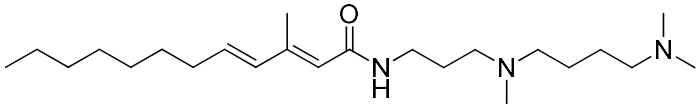

304

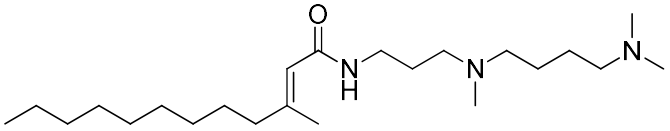

305

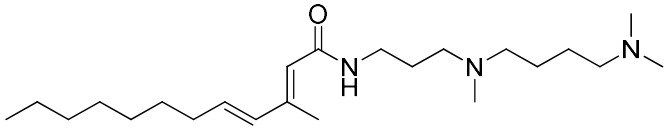

306

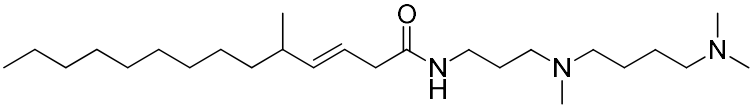

307

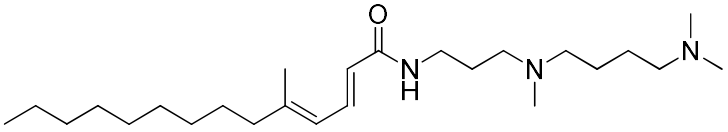

308

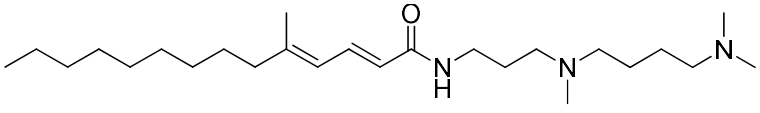

309

Three ceramides, namely *N*-[(2*S*,3*R*,*E*)-1,3-dihydroxyhexacos-4-en-2-yl]icosanamide, *N*-[(2*S*,3*S*,4*R*)-1,3,4-trihydroxyhexacosan-2-yl]icosanamide and (*R*)-2[-]-hydroxy-*N*-[(2*S*,3*S*,4*R*)-1,3,4-trihydroxypentacosan-2-yl]nonadecanamide (**310-312**), were isolated from the Egyptian Red Sea *Sinularia candidula*, with all three showing

reduction of virus H5N1 titer by 48.8, 10.4 and 15.8, respectively, at a concentration of 1 ng/mL (Ahmed et al., 2013).

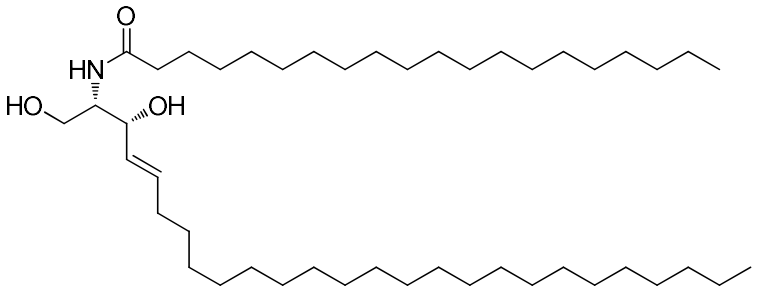

310

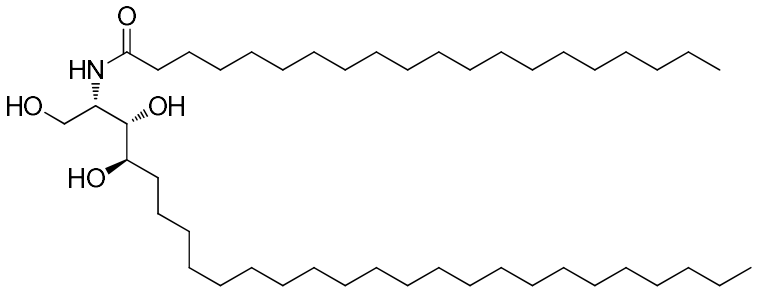

311

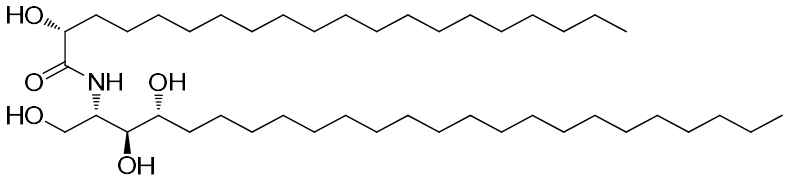

312

1.6 Aim of the study

In view of the immense but underexplored potential of marine organisms from the Red Sea as sources of metabolites with potent bioactivities, the aim of the present PhD thesis was the chemical investigation of a number of marine organisms collected from the Red Sea towards the isolation and structure elucidation of new natural products, as well as the evaluation of their biological activity.

2. MATERIALS AND METHODS

2.1 General experimental procedures

NMR spectra were obtained on Bruker AC 200, Bruker DRX 400, Avance NEO 700 and Avance NEO 950 (Bruker BioSpin GmbH, Rheinstetten, Germany) and Varian 600 (Varian, Inc., Palo Alto, CA, USA) spectrometers. The 2D NMR experiments (HSQC, HMBC, COSY, NOESY) were performed using standard Bruker or Varian pulse sequences. Chemical shifts are given on the δ (ppm) scale with reference to the solvent signals.

Low-resolution EI mass spectra were measured on a Thermo Electron Corporation DSQ mass spectrometer (Thermo Fisher Scientific, Bremen, Germany) or Hewlett Packard 5973 mass spectrometer. High-resolution APCI or ESI mass spectra were measured on a LTQ Orbitrap Velos mass spectrometer (Thermo Fisher Scientific, Bremen, Germany).

Optical rotations were measured on a Krüss polarimeter (A. KRÜSS Optronic GmbH, Hamburg, Germany) equipped with a 0.5 dm cell. UV spectra were recorded on a Lambda 40 UV/Vis spectrophotometer (Perkin Elmer Ltd., Beaconsfield, UK). IR spectra were obtained on an Alpha II FTIR spectrometer (Bruker Optik GmbH, Ettlingen, Germany).

High pressure liquid chromatography (HPLC) separations were conducted on a Waters 600 liquid chromatography pump equipped with a Waters 410 differential refractometer (Waters Corporation, Milford, MA, USA) or an Agilent 1100 series liquid chromatography pump equipped with an Agilent 1100 series refractive index detector, using (a) a Kromasil 100 C_{18} (MZ-Analysentechnik GmbH, 5 µm, 25 cm × 8 mm i.d.), (b) an Econosphere C_{18} (Grace, 25 cm × 10 mm i.d.), (c) a Supelcosil Si (Supelco, 25 cm × 10 mm i.d) or (d) an Econosphere Silica 10µ (Grace, 25 cm × 10 mm i.d) column.

Evaporation of the solvents was performed under vacuum using a BÜCHI Rotavapor R-200 rotary evaporator at temperatures up to 40 °C.

The minimal energy structure steric configurations were designed with the computational molecular modeling program HyperChem 8.0 (Hypercube, Inc.).

2.2 Solvents and chemical reagents

Normal- or reversed-phase vacuum column chromatography separations were performed with Silica 60, 0.015-0.04 mm (Macherey-Nagel) or Kieselgel 60 RP-18, 40-63 µm (Merck), respectively.

Normal-phase gravity column chromatography separations were performed with Silica 60, 0.04-0.063 mm (Macherey-Nagel).

Solid phase extractions were performed using normal (SiOH) or reversed (C18) phase cartridges (Waters Associates or Macherey-Nagel).

Normal- or reversed-phase thin layer chromatography (TLC) separations were performed using ALUGRAM SIL G/UV_{254} (Macherey-Nagel, thickness of layer 0.2

mm) or ALUGRAM RP-18 W/UV_{254} (Macherey-Nagel, thickness of layer 0.15 mm) aluminium sheets, respectively, and spots were detected under a UV lamp at 254 and 365 nm and after spraying with 25% H_2SO_4 in MeOH reagent and heating at 100 °C for 1-2 min.

All solvents used in extractions and chromatographic separations, with the exception of H_2O, were purchased from LAB-SCAN Analytical Sciences. Me_2CO was of A.R. grade, cHex, EtOAc, CH_2Cl_2 and MeOH were of A.R. grade that were distilled prior to use and MeCN was of HPLC grade. H_2O used in chromatographic separations was initially distilled and further purified through a reverse osmosis membrane and filtered through a deionization resin. All solvents prior to use in HPLC separations were filtered under vacuum and sonicated.

NMR spectra were measured in deuterated solvents ($CDCl_3$, CD_3OD or C_6D_6) without TMS as internal standard, obtained from Deutero GmbH.

2.3 Collection of organisms

Specimens of the investigated marine organisms (Figure 5) were hand-picked by SCUBA diving either at Hurghada, Egypt or in Thuwal, Saudi Arabia (Table 1) and transported to the laboratory in ice chests, where they were stored at −20 °C until analyzed. Voucher specimens have been deposited at the animal collection of the Section of Pharmacognosy and Chemistry of Natural Products, Department of Pharmacy, National and Kapodistrian University of Athens.

Laurencia majuscula ***Lamellodysidea* sp.** ***Sinularia polydactyla***

Figure 5. The marine organisms investigated in the present PhD thesis.

Table 1. Collection data for the marine organisms investigated in the present PhD thesis.

Herbarium code	Organism	Type	Depth	Location	Date
ATPH/ MP0548	*Laurencia majuscula*	Alga	10 m	Hurghada, Egypt	07/2016
ATPH/ MP0649	*Lamellodysidea* sp.	Sponge	1-2 m	KAEC lagoon, Saudi Arabia	01/2018
ATPH/ MP0533	*Sinularia polydactyla*	Soft coral	10 m	Hurghada, Egypt	10/2015

2.4 Extraction and isolation of metabolites from the alga *Laurencia majuscula*

Specimens of the alga *L. majuscula* were extensively extracted with mixtures of CH_2Cl_2 and MeOH to afford after evaporation of the solvents in vacuo a crude extract that was subjected to a series of chromatographic separations (Figure 6, Figure 7, Figure 8, Figure 9), including normal- and reversed-phase vacuum column chromatography, gravity column chromatography and HPLC, to allow for the isolation of a number of metabolites in pure form. After each chromatographic step, the fractions were analyzed by ^{1}H NMR spectroscopy.

Initially, the organic extract LMH (9.0 g) was subjected to normal-phase vacuum column chromatography, using cHex with increasing amounts of EtOAc, followed by EtOAc with increasing amounts of MeOH as the mobile phase, to afford 16 fractions, which after an initial screening with TLC were combined into 14 fractions (Table 2).

Table 2. Experimental details for the separation of the crude extract LMH.

Fraction	**Mobile phase**			**Volume (mL)**
	cHex %	**EtOAc %**	**MeOH %**	
LMH1	100	-	-	450
	95	5	-	250
LMH2	90	10	-	250
LMH3	85	15	-	250
LMH4	80	20	-	250
LMH5	70	30	-	250
LMH6	60	40	-	250
LMH7	50	50	-	250
LMH8	40	60	-	250
LMH9	30	70	-	250
LMH10	20	80	-	250
LMH11	10	90	-	250
LMH12	-	100	-	250
	-	80	20	250
LMH13	-	50	50	250
LMH14	-	-	100	250

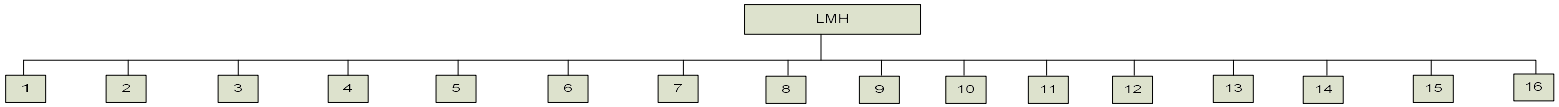

Figure 6. Fractionation scheme for the isolation of metabolites from the crude extract LMH (part 1).

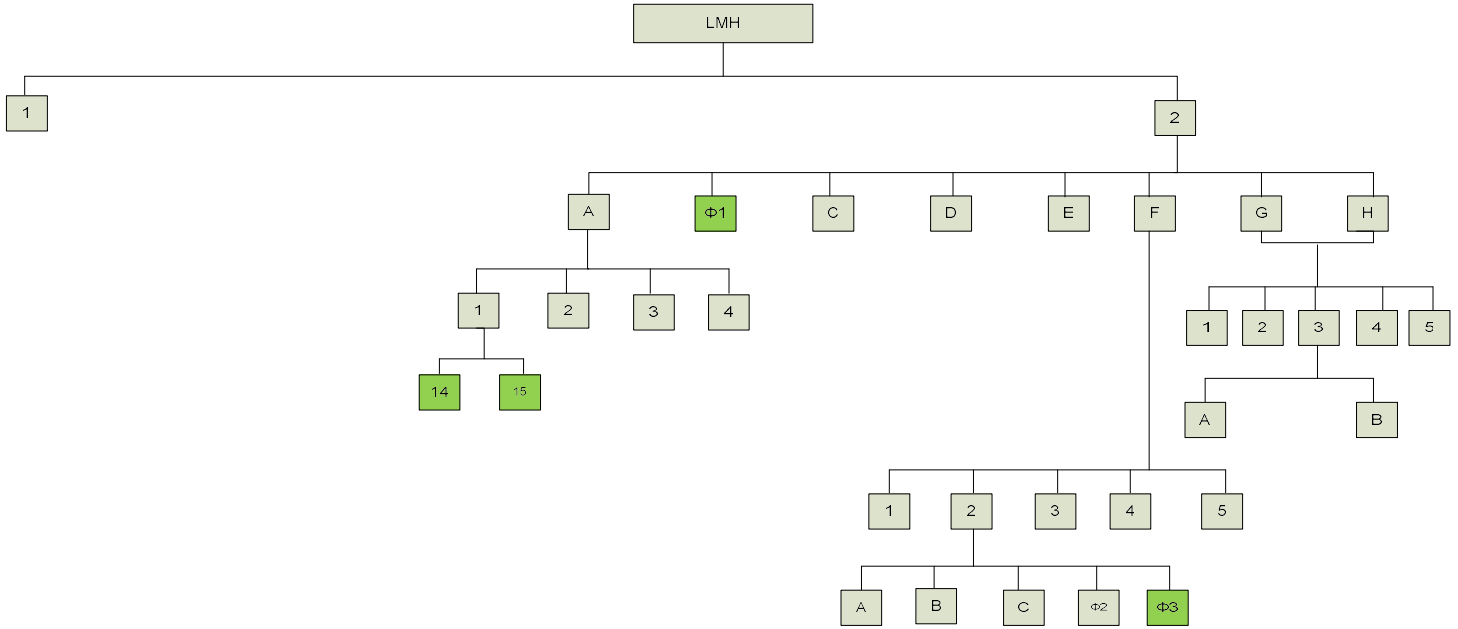

Figure 7. Fractionation scheme for the isolation of metabolites from the crude extract LMH (part 2).

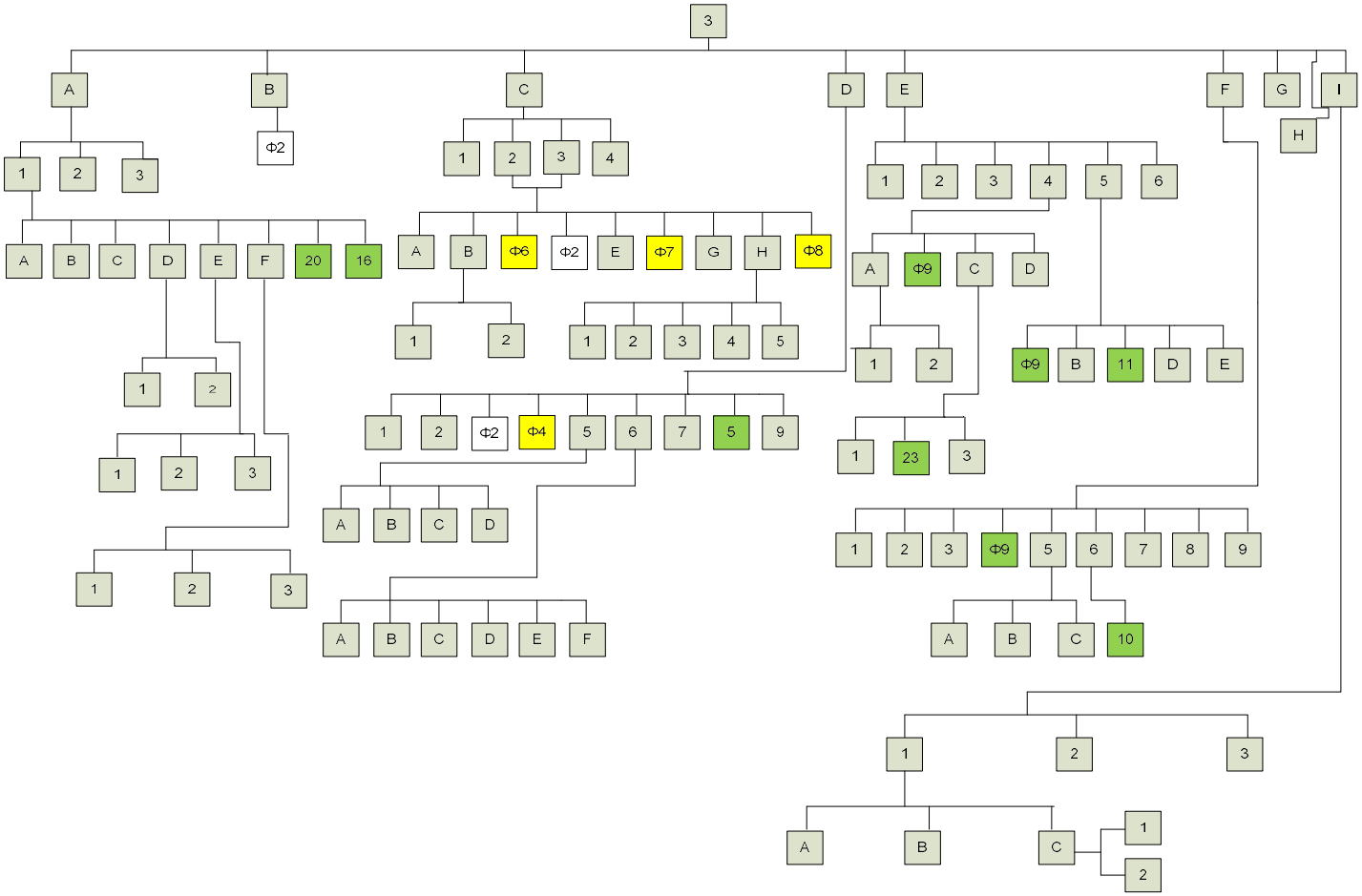

Figure 8. Fractionation scheme for the isolation of metabolites from the crude extract LMH (part 3).

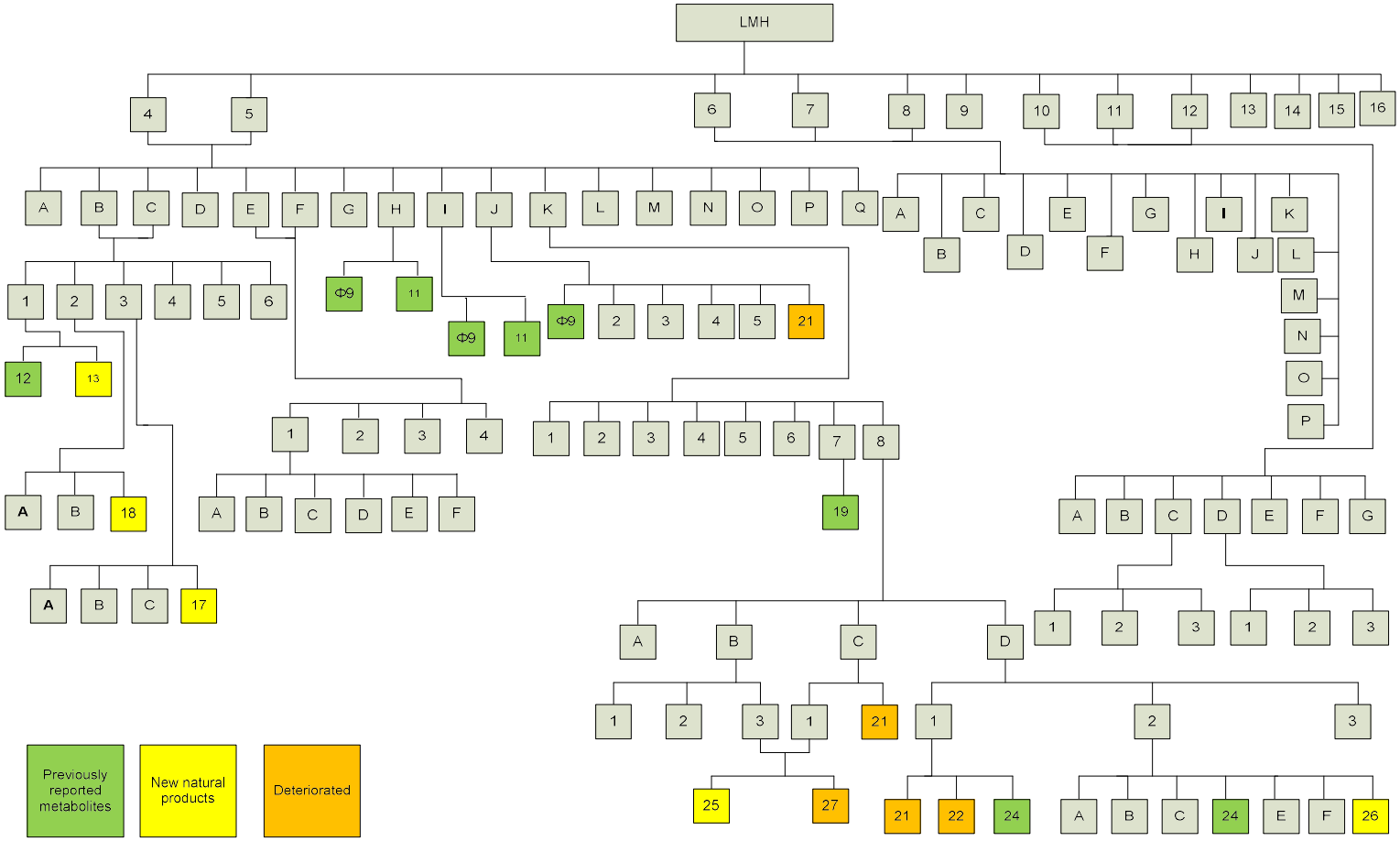

Figure 9. Fractionation scheme for the isolation of metabolites from the crude extract LMH (part 4).

Fraction LMH2 (222.4 mg) was further fractionated by normal-phase gravity column chromatography, using cHex with increasing amounts of EtOAc as the mobile phase, to afford 55 fractions of approx. 20 mL each, which after an initial screening with TLC were combined into 8 fractions (Table 3), among which fraction LMH2b was identified as metabolite **LMH01**.

Table 3. Experimental details for the separation of fraction LMH2.

Fraction	Mobile phase		Volume (mL)
	cHex %	EtOAc %	
LMH2a	99	1	120
LMH2b	99	1	140
LMH2c	98	2	60
LMH2d	98	2	80
LMH2e	98	2	100
LMH2f	97	3	200
LMH2g	95	5	100
	90	10	100
	80	20	50
LMH2h	80	20	50
	-	100	100

Fraction LMH2a (9.7 mg) was further fractionated by normal-phase SPE chromatography, using *n*Hex and cHex with increasing amounts of EtOAc as the mobile phase, to afford four fractions (Table 4).

Table 4. Experimental details for the separation of fraction LMH2a.

Fraction	Mobile phase			Volume (mL)
	*n*Hex %	cHex %	EtOAc %	
LMH2a1	100	-	-	6
LMH2a2	-	98	2	4
LMH2a3	-	95	5	4
LMH2a4	-	-	100	4

Fraction LMH2a1 (3.5 mg) was subjected to normal-phase HPLC to yield two fractions LMH2a1a and LMH2a1b (Table 5) which were identified as metabolites **LMH14** and **LMH15**, respectively.

Table 5. Experimental details for the separation of fraction LMH2a1.

Chromatographic conditions	
Column	Econosphere Silica 10µ (250 mm × 10 mm i.d.)
Mobile phase	*n*Hex 100%, 1.5 mL/min

Fraction	Retention time (min)	Weight (mg)
LMH2a1a	11.9	2.1
LMH2a1b	13.0	0.7

Fraction LMH2f (60.6 mg) was further fractionated by normal-phase SPE chromatography, using cHex with increasing amounts of EtOAc as the mobile phase, to afford five fractions (Table 6).

Table 6. Experimental details for the separation of fraction LMH2f.

Fraction	Mobile phase		Volume (mL)
	cHex %	EtOAc %	
LMH2f1	95	5	20
LMH2f2	90	10	10
LMH2f3	80	20	10
LMH2f4	-	100	10
LMH2f5	-	100	10

Fraction LMH2f2 (23.3 mg) was subjected to normal-phase HPLC to yield five fractions (Table 7), among which fraction LMH2f2e was identified as metabolite **LMH03**.

Table 7. Experimental details for the separation of fraction LMH2f2.

Chromatographic conditions	
Column	Econosphere Silica 10µ (250 mm × 10 mm i.d.)
Mobile phase	cHex/EtOAc 96:4%, 1.5 mL/min

Fraction	Retention time (min)	Weight (mg)
LMH2f2a	10.0	12.0
LMH2f2b	13.7	2.0
LMH2f2c	15.6	1.9
LMH2f2d	17.8	2.6
LMH 2f2e	19.0	2.1

Fraction LMH3 (1.0 g) was further fractionated by normal-phase gravity column chromatography, using cHex with increasing amounts of EtOAc as the mobile phase, to afford 116 fractions of approx. 25 mL each, which after an initial screening with TLC were combined into 9 fractions (Table 8).

Table 8. Experimental details for the separation of fraction LMH3.

Fraction	Mobile phase		Volume (mL)
	cHex %	EtOAc %	
LMH3a	100	-	250
	99	1	200
	98	2	200
	97	3	200
	96	4	200
	95	5	50
LMH3b	95	5	250
	94	6	50
LMH3c	94	6	150
LMH3d	94	6	50
	93	7	100
LMH3e	93	7	250
LMH3f	92	8	250
LMH3g	90	10	200
	85	15	100
LMH2h	75	25	200
LMH3i	-	100	200

Fraction LMH3a (354.2 mg) was further fractionated by normal-phase SPE chromatography, using *n*Hex with increasing amounts of EtOAc as the mobile phase, to afford three fractions (Table 9).

Table 9. Experimental details for the separation of fraction LMH3a.

Fraction	Mobile phase		Volume (mL)
	***n*Hex %**	**EtOAc %**	
LMH3a1	99	1	60
LMH3a2	99	1	10
LMH3a3	-	100	50

Fraction LMH3a1 (74.8 mg) was subjected to normal-phase HPLC to yield eight fractions (Table 10), among which fractions LMH3a1g and LMH3a1h were identified as metabolites **LMH20** and **LMH16**, respectively.

Table 10. Experimental details for the separation of fraction LMH3a1.

Chromatographic conditions	
Column	Econosphere Silica 10µ (250 mm × 10 mm i.d.)
Mobile phase	*n*Hex/EtOAc 92:8%, 1.5 mL/min

Fraction	Retention time (min)	Weight (mg)
LMH3a1a	10.0	4.5
LMH3a1b	10.7	2.1
LMH3a1c	14.8	6.7
LMH3a1d	17.1	4.6
LMH3a1e	18.2	4.2
LMH3a1f	19.1	11.9
LMH3a1g	22.1	3.3
LMH3a1h	24.3	3.8

Fraction LMH3b (41.6 mg) was subjected to normal-phase HPLC to yield one fraction (Table 11) which was identified as metabolite **LMH02**.

Table 11. Experimental details for the separation of fraction LMH3b.

Chromatographic conditions	
Column	Econosphere Silica 10μ (250 mm × 10 mm i.d.)
Mobile phase	cHex/EtOAc 96:4%, 1.5 mL/min

Fraction	Retention time (min)	Weight (mg)
LMH3b1	21.9	30.0

Fraction LMH3c (124.4 mg) was further fractionated by normal-phase SPE chromatography, using cHex with increasing amounts of EtOAc as the mobile phase, to afford 6 fractions which after an initial screening with TLC were combined into 4 fractions (Table 12).

Table 12. Experimental details for the separation of fraction LMH3c.

Fraction	Mobile phase		Volume (mL)
	cHex %	EtOAc %	
LMH3c1	100	-	30
LMH3c2	95	5	20
LMH3c3	90	10	20
LMH3c4	80	20	20
	-	100	20
	-	100	20

Fractions LMH3c2 and LMH3c3, pooled together in one fraction thereafter designated as LMH3c2 (85 mg), were subjected to normal-phase HPLC to yield nine fractions (Table 13), among which fractions LMH3c2c, LMH3c2d, LMH3c2f and LMH3c2i were identified as metabolites **LMH06**, **LMH02**, **LMH07** and **LMH08**, respectively.

Table 13. Experimental details for the separation of fraction LMH3c2.

Chromatographic conditions	
Column	Econosphere Silica 10µ (250 mm × 10 mm i.d.)
Mobile phase	cHex/EtOAc 96:4%, 1.5 mL/min

Fraction	**Retention time (min)**	**Weight (mg)**
LMH3c2a	10.9	3.8
LMH3c2b	16.1	2.9
LMH3c2c	17.9	7.6
LMH3c2d	22.4	12.3
LMH3c2e	26.2	0.9
LMH3c2f	27.5	8.2
LMH3c2g	30.1	1.2
LMH3c2h	31.5	7.6
LMH3c2i	34.1	19.5

Fraction LMH3d (108.6 mg) was subjected to normal-phase HPLC to yield nine fractions (Table 14), among which fractions LMH3d3, LMH3d4 and LMH3d8 were identified as metabolites **LMH02**, **LMH04** and **LMH05**, respectively.

Table 14. Experimental details for the separation of fraction LMH3d.

Chromatographic conditions	
Column	Econosphere Silica 10µ (250 mm × 10 mm i.d.)
Mobile phase	cHex/EtOAc 96:4%, 1.5 mL/min

Fraction	**Retention time (min)**	**Weight (mg)**
LMH3d1	10.9	2.1
LMH3d2	15.8	1.9
LMH3d3	21.8	13.9
LMH3d4	25.5	3.6
LMH3d5	27.2	4.1
LMH3d6	28.9	36.9
LMH3d7	33.2	2.7
LMH3d8	35.5	8.8
LMH3d9	41.5	3.3

Fraction LMH3e (62.3 mg) was further fractionated by normal-phase SPE chromatography, using cHex with increasing amounts of EtOAc as the mobile phase, to afford 8 fractions which after an initial screening with TLC were combined into 6 fractions (Table 15).

Table 15. Experimental details for the separation of fraction LMH3e.

Fraction	Mobile phase		Volume (mL)
	cHex %	EtOAc %	
LMH3e1	100	-	30
LMH3e2	97	3	15
	95	5	15
LMH3e3	92	8	15
LMH3e4	90	10	15
LMH3e5	88	12	15
LMH3e6	85	15	15
	80	20	15
	-	100	15

Fraction LMH3e4 (20.4 mg) was subjected to normal-phase HPLC to yield four fractions (Table 16).

Table 16. Experimental details for the separation of fraction LMH3e4.

Chromatographic conditions	
Column	Econosphere Silica 10µ (250 mm × 10 mm i.d.)
Mobile phase	cHex/EtOAc 90:10%, 1.5 mL/min

Fraction	Retention time (min)	Weight (mg)
LMH3e4a	16.2	2.2
LMH3e4b	16.7	6.9
LMH3e4c	18.3	2.6
LMH3e4d	21.8	0.7

Fraction LMH3e4c (2.6 mg) was subjected to normal-phase HPLC to yield three fractions (Table 17), among which fraction LMH3e4c2 was identified as metabolite **LMH23**.

Table 17. Experimental details for the separation of fraction LMH3e4c.

Chromatographic conditions	
Column	Econosphere Silica 10µ (250 mm × 10 mm i.d.)
Mobile phase	cHex/Acetone 93:7%, 1.5 mL/min

Fraction	Retention time (min)	Weight (mg)
LMH3e4c1	14.6	0.6
LMH3e4c2	23.4	0.2
LMH3e4c3	36.9	0.7

Fraction LMH3e5 (5.5 mg) was subjected to normal-phase HPLC to yield five fractions (Table 18), among which fraction LMH3e5c was identified as metabolite **LMH11**.

Table 18. Experimental details for the separation of fraction LMH3e5.

Chromatographic conditions	
Column	Econosphere Silica 10µ (250 mm × 10 mm i.d.)
Mobile phase	cHex/EtOAc 90:10%, 1.5 mL/min

Fraction	**Retention time (min)**	**Weight (mg)**
LMH3e5a	16.7	1.3
LMH3e5b	18.2	0.6
LMH3e5c	19.0	0.8
LMH3e5d	22.1	0.6
LMH3e5e	27.3	0.5

Fractions LMH4 and LMH5, pooled together in one fraction thereafter designated as LMH4 (1.2 g), were further fractionated by normal-phase gravity column chromatography, using cHex with increasing amounts of EtOAc and EtOAc with increasing amounts of MeOH as the mobile phase, to afford 116 fractions of approx. 25 mL each, which after an initial screening with TLC were combined into 17 fractions (Table 19).

Table 19. Experimental details for the separation of fraction LMH4.

Fraction	**Mobile phase**			**Volume (mL)**
	cHex %	**EtOAc %**	**MeOH %**	
LMH4a	95	5	-	125
LMH4b	95	5	-	75
LMH4c	94	6	-	100
LMH4d	94	6	-	50
LMH4e	93	7	-	75
LMH4f	93	7	-	125
LMH4g	91	9	-	75
LMH4h	91	9	-	100
LMH4i	90	10	-	100
LMH4j	90	10	-	50
LMH4k	88	12	-	225
LMH4l	85	15	-	100
LMH4m	85	15	-	75
	80	20	-	150
LMH4n	80	20	-	75
	70	30	-	250
LMH4o	60	40	-	200

LMH4p	50	50	-	200
LMH4q	-	100	-	250
	-	97	3	100
	-	90	10	100
	-	50	50	300

Fraction LMH4b and LMH4c, pooled together in one fraction thereafter designated as LMH4b (73.6 mg), were further fractionated by normal-phase SPE chromatography, using cHex with increasing amounts of EtOAc as the mobile phase, to afford 9 fractions which after an initial screening with TLC were combined into 6 fractions (Table 20).

Table 20 . Experimental details for the separation of fraction LMH4b.

Fraction	**Mobile phase**		**Volume (mL)**
	cHex %	**EtOAc %**	
LMH4b1	100	-	30
	98	2	20
LMH4b2	96	4	20
	94	6	20
LMH4b3	92	8	20
	90	10	20
LMH4b4	88	12	20
LMH4b5	80	20	20
LMH4b6	-	100	20

Fraction LMH4b1 (21.9 mg) was subjected to normal-phase HPLC to yield two fractions (Table 21) which were identified as metabolites **LMH12** and **LMH13**, respectively.

Table 21. Experimental details for the separation of fraction LMH4b1.

Chromatographic conditions	
Column	Econosphere Silica 10μ (250 mm × 10 mm i.d.)
Mobile phase	*n*Hex 100%, 1.0 mL/min

Fraction	**Retention time (min)**	**Weight (mg)**
LMH4b1a	17.4	5.2
LMH4b1b	21.3	3.4

Fraction LMH4b2 (14.6 mg) was subjected to normal-phase HPLC to yield three fractions (Table 22), among which fraction LMH4b2c was identified as metabolite **LMH18**.

Table 22. Experimental details for the separation of fraction LMH4b2.

Chromatographic conditions	
Column	Econosphere Silica 10µ (250 mm × 10 mm i.d.)
Mobile phase	cHex/EtOAc 96:4%, 1.5 mL/min

Fraction	Retention time (min)	Weight (mg)
LMH4b2a	12.9	1.4
LMH4b2b	14.0	0.7
LMH4b2c	15.2	0.8

Fraction LMH4b3 (10.4 mg) was subjected to normal-phase HPLC to yield four fractions (Table 23), among which fraction LMH4b3d was identified as metabolite **LMH17**.

Table 23. Experimental details for the separation of fraction LMH4b3.

Chromatographic conditions	
Column	Econosphere Silica 10µ (250 mm × 10 mm i.d.)
Mobile phase	cHex/EtOAc 90:10%, 1.5 mL/min

Fraction	Retention time (min)	Weight (mg)
LMH4b3a	14.5	0.7
LMH4b3b	15.8	1.4
LMH4b3c	18.8	0.6
LMH4b3d	19.6	3.3

Fraction LMH4h (15.8 mg) was subjected to normal-phase HPLC to yield two fractions (Table 24), among which fraction LMH4h2 was identified as metabolite **LMH11**.

Table 24. Experimental details for the separation of fraction LMH4h.

Chromatographic conditions	
Column	Econosphere Silica 10µ (250 mm × 10 mm i.d.)
Mobile phase	cHex/EtOAc 90:10%, 1.5 mL/min

Fraction	Retention time (min)	Weight (mg)
LMH4h1	17.1	3.8
LMH4h2	19.5	3.3

Fraction LMH4i (26.1 mg) was subjected to normal-phase HPLC to yield two fractions (Table 25), among which fraction LMH4i2 was identified as metabolite **LMH11**.

Table 25. Experimental details for the separation of fraction LMH4i.

Chromatographic conditions	
Column	Econosphere Silica 10µ (250 mm × 10 mm i.d.)
Mobile phase	cHex/EtOAc 90:10%, 1.5 mL/min

Fraction	**Retention time (min)**	**Weight (mg)**
LMH4i1	16.7	4.5
LMH4i2	20.2	1.6

Fraction LMH4j (15.8 mg) was subjected to normal-phase HPLC to yield six fractions (Table 26), among which fraction LMH4j6 was identified as metabolite **LMH21**.

Table 26. Experimental details for the separation of fraction LMH4j.

Chromatographic conditions	
Column	Econosphere Silica 10µ (250 mm × 10 mm i.d.)
Mobile phase	cHex/EtOAc 80:20%, 1.5 mL/min

Fraction	**Retention time (min)**	**Weight (mg)**
LMH4j1	11.4	1.0
LMH4j2	12.0	0.5
LMH4j3	13.3	0.6
LMH4j4	14.3	0.9
LMH4j5	16.6	0.3
LMH4j6	17.1	1.0

Fractions LMH4k and LMH4l, pooled together in one fraction thereafter designated as LMH4k (334.2 mg), were further fractionated by normal-phase gravity column chromatography, using cHex with increasing amounts of EtOAc as the mobile phase, to afford 46 fractions of approx. 15 mL each, which after an initial screening with TLC were combined into 8 fractions (Table 27).

Table 27. Experimental details for the separation of fraction LMH4k.

Fraction	**Mobile phase**		**Volume (mL)**
	cHex %	**EtOAc %**	
LMH4k1	92	8	150
	90	10	45
LMH4k2	90	10	45
LMH4k3	90	10	30
	88	12	30
LMH4k4	88	12	45
LMH4k5	85	15	60
LMH4k6	85	15	60

	80	20	75
LMH4k7	80	20	60
LMH4k8	-	100	100

Fraction LMH4k7 (9.9 mg) was subjected to normal-phase HPLC to yield one fraction (Table 28) which was identified as metabolite **LMH19**.

Table 28. Experimental details for the separation of fraction LMH4k7.

Chromatographic conditions	
Column	Econosphere Silica 10µ (250 mm × 10 mm i.d.)
Mobile phase	cHex/EtOAc 80:20%, 1.5 mL/min

Fraction	**Retention time (min)**	**Weight (mg)**
LMH4k7a	19.2	3.0

Fraction LMH4k8 (78.0 mg) was further fractionated by normal-phase SPE chromatography, using cHex with increasing amounts of EtOAc as the mobile phase, to afford 4 fractions (Table 29).

Table 29. Experimental details for the separation of fraction LMH4k8.

Fraction	**Mobile phase**		**Volume (mL)**
	cHex %	**EtOAc %**	
LMH4k8a	80	20	25
LMH4k8b	80	20	15
LMH4k8c	80	20	15
LMH4k8d	-	100	20

Fraction LMH4k8b (12.7 mg) was subjected to normal-phase HPLC to yield three fractions (Table 30).

Table 30. Experimental details for the separation of fraction LMH4k8b.

Chromatographic conditions	
Column	Econosphere Silica 10µ (250 mm × 10 mm i.d.)
Mobile phase	cHex/EtOAc 75:25%, 1.5 mL/min

Fraction	**Retention time (min)**	**Weight (mg)**
LMH4k8b1	9.3	0.6
LMH4k8b2	17.8	2.9
LMH4k8b3	22.1	1.6

Fraction LMH4k8b3 (1.6 mg) was subjected to normal-phase HPLC to yield two fractions (Table 31) which were identified as metabolites **LMH25** and **LMH27**, respectively.

Table 31. Experimental details for the separation of fraction LMH4k8b3.

Chromatographic conditions	
Column	Econosphere Silica 10µ (250 mm × 10 mm i.d.)
Mobile phase	cHex/EtOAc 82:18%, 1.5 mL/min

Fraction	Retention time (min)	Weight (mg)
LMH4k8b3a	16.3	1.5
LMH4k8b3b	17.5	0.7

Fraction LMH4k8c (10.0 mg) was subjected to normal-phase HPLC to yield two fractions (Table 32) which were identified as metabolites **LMH25** and **LMH21**, respectively.

Table 32. Experimental details for the separation of fraction LMH4k8c.

Chromatographic conditions	
Column	Econosphere Silica 10µ (250 mm × 10 mm i.d.)
Mobile phase	cHex/EtOAc 75:25%, 1.5 mL/min

Fraction	Retention time (min)	Weight (mg)
LMH4k8c1	22.1	1.2
LMH4k8c2	23.9	3.6

Fraction LMH4k8d, (33.0 mg) was further fractionated by normal-phase SPE chromatography, using cHex with increasing amounts of EtOAc as the mobile phase, to afford 3 fractions (Table 33).

Table 33. Experimental details for the separation of fraction LMH4k8d.

Fraction	Mobile phase		Volume (mL)
	cHex %	EtOAc %	
LMH4k8d1	60	40	20
LMH4k8d2	60	40	30
LMH4k8d3	-	100	15

Fraction LMH4k8d1 (17.4 mg) was subjected to normal-phase HPLC to yield three fractions (Table 34), which were identified as metabolites **LMH21**, **LMH22** and **LMH24**, respectively.

Table 34. Experimental details for the separation of fraction LMH4k8d1.

Chromatographic conditions	
Column	Econosphere Silica 10µ (250 mm × 10 mm i.d.)
Mobile phase	cHex/EtOAc 65:35%, 1.5 mL/min

Fraction	Retention time (min)	Weight (mg)
LMH4k8d1a	16.9	6.5
LMH4k8d1b	19.8	2.3
LMH4k8d1c	25.0	0.6

Fraction LMH4k8d2 (17.4 mg) was subjected to normal-phase HPLC to yield seven fractions (Table 35), among which fractions LMH4k8d2d and LMH4k8d2g were identified as metabolites **LMH24** and **LMH26**, respectively.

Table 35. Experimental details for the separation of fraction LMH4k8d2.

Chromatographic conditions	
Column	Econosphere Silica 10µ (250 mm × 10 mm i.d.)
Mobile phase	cHex/EtOAc 60:40%, 1.5 mL/min

Fraction	Retention time (min)	Weight (mg)
LMH4k8d2a	15.0	0.5
LMH4k8d2b	17.0	1.0
LMH4k8d2c	17.8	0.5
LMH4k8d2d	20.8	1.1
LMH4k8d2e	23.4	3.4
LMH4k8d2f	25.9	0.7
LMH4k8d2g	34.7	0.8

In total, from the chemical investigation of the organic extract of the red alga *L. majuscula*, 25 metabolites were isolated in pure form (Table 36).

Table 36. Isolated metabolites from the red alga *L. majuscula*.

Metabolite	Code	Fraction	Weight (mg)
1	LMH12	LMH4b1a	5.2
2	LMH17	LMH4b3d	3.3
3	LMH13	LMH4b1b	3.4
4	LMH20	LMH3a1g	2.0
5	LMH18	LMH4b2c	0.8
6	LMH25	LMH4k8b3a, LMH4k8c1	2.7
7	LMH24	LMH4k8d1c, LMH4k8d2d	1.7
8	LMH19	LMH4k7a	3.0
9	LMH26	LMH4k8d2g	0.8
10	LMH23	LMH3e4c2	0.2
11	LMH01	LMH2b	76.6
12	LMH15	LMH2a1b	0.7
13	LMH03	LMH2f2e	2.0
14	LMH14	LMH2a1a	2.1
15	LMH05	LMH3d8	8.8

16	LMH11	LMH3e5c, LMH4h2, LMH4i2	5.7
17	LMH04	LMH3d4	3.6
18	LMH02	LMH3b1, LMH3c2d, LMH3d3	56.2
19	LMH06	LMH3c2c	7.6
20	LMH07	LMH3c2f	8.2
21	LMH08	LMH3c2i	19.5
22	LMH16	LMH3a1h	3.8
	LMH21	LMH4j6, LMH4k8c2, LMH4k8d1a	11.1
	LMH22	LMH4k8d1b	2.3
	LMH27	LMH4k8b3b	0.7

2.5 Extraction and isolation of metabolites from the sponge *Lamellodysidea* sp.

Initially, a small quantity of the sponge *Lamellodysidea* sp. was extensively extracted with mixtures of CH_2Cl_2 and MeOH to afford after evaporation of the solvents in vacuo a crude extract (small-scale) that was subjected to a series of chromatographic separations (Figure 10), including normal- and reversed-phase vacuum column chromatography, gravity column chromatography and HPLC, to allow for the isolation of a number of metabolites in pure form. After each chromatographic step, the fractions were analyzed by ^{1}H NMR spectroscopy.

The organic extract k649 (905.5 mg) was subjected to normal-phase gravity column chromatography, using cHex with increasing amounts of EtOAc, followed by EtOAc with increasing amounts of MeOH as the mobile phase, to afford 95 fractions, of approx. 25 mL each, which after an initial screening with TLC were combined into 11 fractions (Table 37).

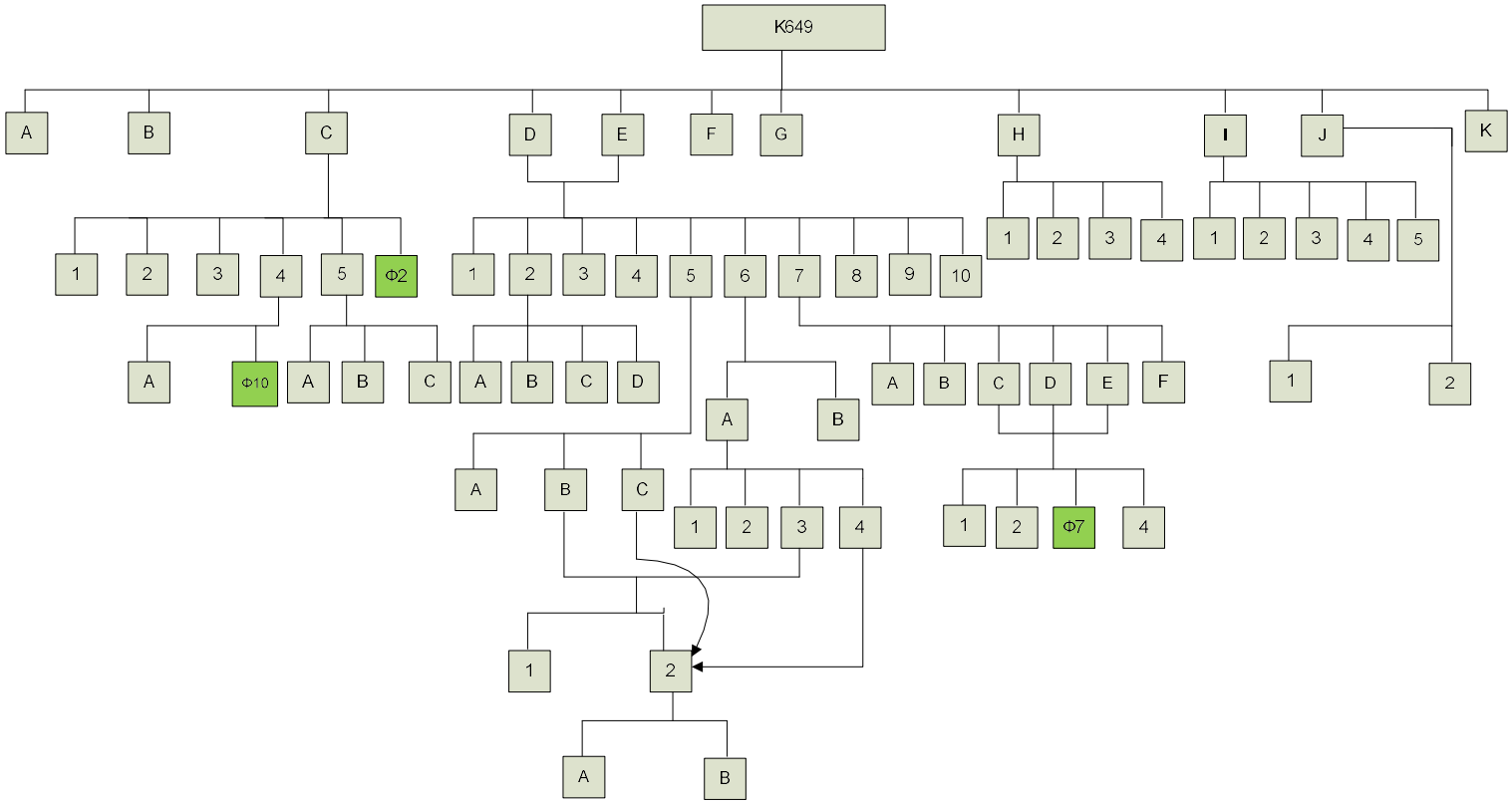

Figure 10. Fractionation scheme for the isolation of metabolites from the crude extract k649 (small-scale).

Table 37. Experimental details for the separation of the crude extract k649 (small-scale).

Fraction	Mobile phase			Volume (mL)
	cHex %	EtOAc %	MeOH %	
k649a	95	5	-	200
k649b	90	10	-	50
k649c	90	10	-	75
	85	15	-	75
k649d	85	15	-	150
k649e	80	20	-	200
	75	25	-	100
	70	30	-	75
k649f	70	30	-	75
	60	40	-	150
	50	50	-	75
k649g	50	50	-	125
	45	55	-	100
k649h	45	55	-	50
	40	60	-	125
	35	65	-	100
	30	70	-	100
k649i	25	75	-	100
	20	80	-	100
	10	90	-	100
	-	100	-	50
k649j	-	100	-	100
k649k	-	50	50	100

Fraction k649c (28.0 mg) was subjected to normal-phase HPLC to yield six fractions (Table 38), among which fraction k649c6 was identified as metabolite **K649-02**.

Table 38. Experimental details for the separation of fraction k649c.

Chromatographic conditions	
Column	Econosphere Silica 10µ (250 mm × 10 mm i.d.)
Mobile phase	cHex/EtOAc 90:10%, 1.5 mL/min

Fraction	Retention time (min)	Weight (mg)
k649c1	10.4	0.1
k649c2	12.8	1.3
k649c3	14.9	0.8
k649c4	15.8	4.3
k649c5	17.8	4.2
k649c6	19.2	10.7

Fraction k649c4 (4.3 mg) was subjected to normal-phase HPLC to yield two fractions (Table 39), among which fraction k649c4b was identified as metabolite **K649-10**.

Table 39. Experimental details for the separation of fraction k649c4.

Chromatographic conditions	
Column	Econosphere Silica 10µ (250 mm × 10 mm i.d.)
Mobile phase	cHex/Acetone 93:7%, 1.5 mL/min

Fraction	**Retention time (min)**	**Weight (mg)**
k649c4a	14.6	2.6
k649c4b	15.2	3.8

Fractions k649d and k649e, pooled together in one fraction thereafter designated as k649d (192.7 mg), were further fractionated by normal-phase gravity column chromatography, using cHex with increasing amounts of EtOAc as the mobile phase, to afford 57 fractions of approx. 15 mL each, which after an initial screening with TLC were combined into 10 fractions (Table 40).

Table 40. Experimental details for the separation of fraction k649d.

Fraction	**Mobile phase**		**Volume (mL)**
	cHex %	**EtOAc %**	
k649d1	90	10	120
k649d2	90	10	45
k649d3	90	10	45
k649d4	90	10	75
k649d5	90	10	45
k649d6	90	10	30
k649d7	90	10	165
k649d8	90	10	120
k649d9	90	10	75
	80	20	60
k649d10	-	100	75

Fraction k649d7 (18.9 mg) was further fractionated by normal-phase SPE chromatography, using cHex with increasing amounts of EtOAc as the mobile phase, to afford 10 fractions which after an initial screening with TLC were combined into 6 fractions (Table 41).

Table 41. Experimental details for the separation of fraction k649d7.

Fraction	Mobile phase		Volume (mL)
	cHex %	EtOAc %	
k649d7a	95	5	7
	90	10	5
	90	10	5
	88	12	5
k649d7b	88	12	5
k649d7c	88	12	5
	85	15	7
k649d7d	85	15	7
k649d7e	85	15	7
k649d7f	50	50	7

Fractions k649d7c, k649d7d and k649d7e, pooled together in one fraction thereafter designated as k649d7c (15.1 mg), were subjected to normal-phase HPLC to yield four fractions (Table 42), among which fraction k649d7c3 was identified as metabolite **K649-07**.

Table 42. Experimental details for the separation of fraction k649d7c.

Chromatographic conditions	
Column	Econosphere Silica 10µ (250 mm × 10 mm i.d.)
Mobile phase	cHex/EtOAc 80:20%, 1.5 mL/min

Fraction	Retention time (min)	Weight (mg)
k649d7c1	16.1	4.3
k649d7c2	18.7	0.2
k649d7c3	22.0	9.2
k649d7c4	24.5	0.5

Subsequently, a larger quantity of the sponge *Lamellodysidea* sp. was extensively extracted with mixtures of CH_2Cl_2 and MeOH to afford after evaporation of the solvents in vacuo a crude extract (large-scale) that was subjected to a series of chromatographic separations (Figure 11), including normal- and reversed-phase vacuum column chromatography, gravity column chromatography and HPLC, to allow for the isolation of a number of metabolites in pure form. After each chromatographic step, the fractions were analyzed by ^{1}H NMR spectroscopy.

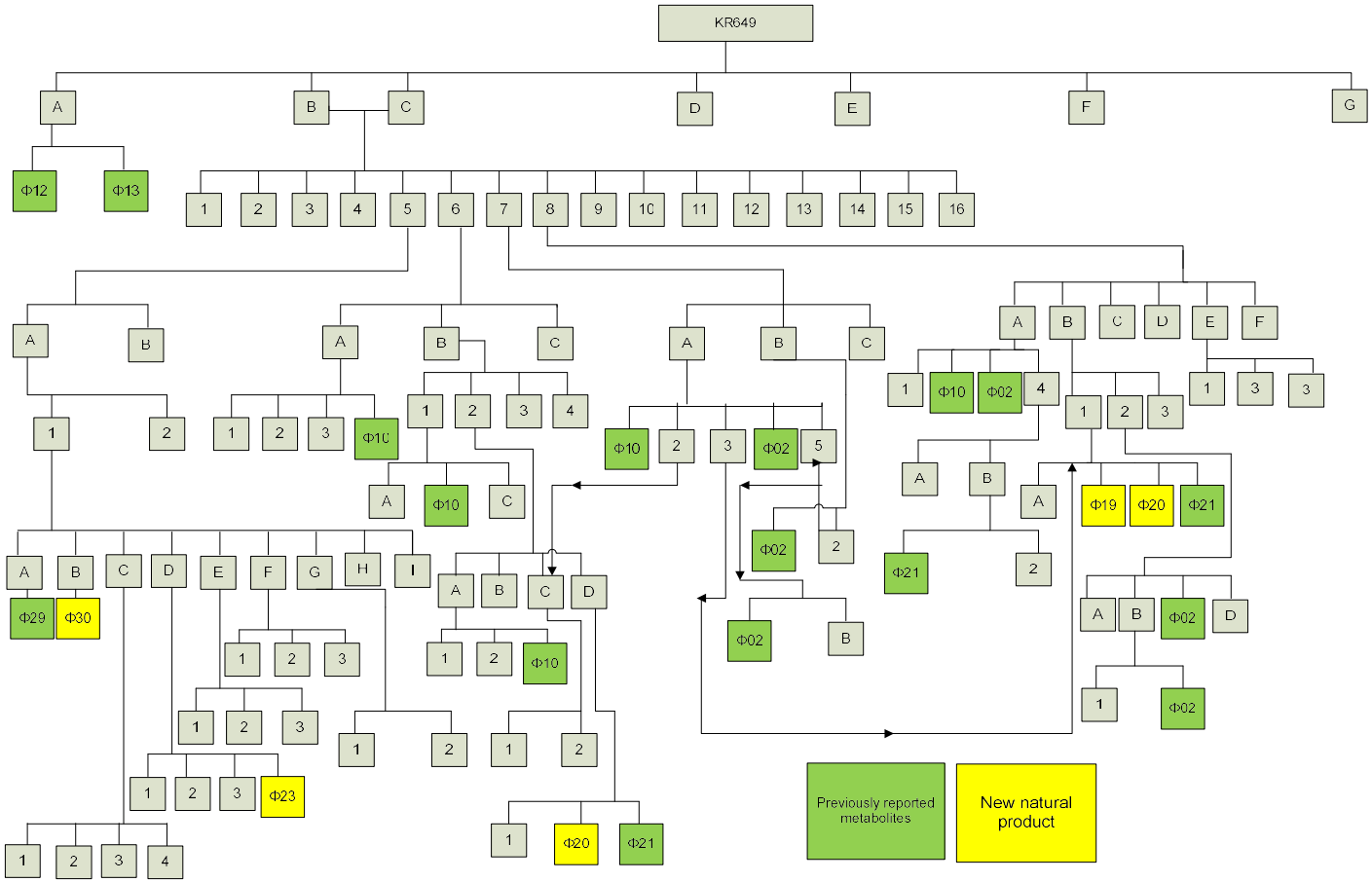

Figure 11. Fractionation scheme for the isolation of metabolites from the crude extract kr649 (large-scale).

The organic extract kr649 (15.5 g) was subjected to normal-phase vacuum column chromatography, using cHex with increasing amounts of EtOAc, followed by EtOAc with increasing amounts of MeOH as the mobile phase, to afford 18 fractions, which after an initial screening with TLC were combined into 7 fractions (Table 43).

Table 43. Experimental details for the separation of the crude extract kr649 (large-scale).

Fraction	Mobile phase			Volume (mL)
	cHex %	EtOAc %	MeOH %	
kr649a	100	-	-	700
	95	5	-	250
	90	10	-	250
	85	15	-	250
kr649b	80	20	-	250
	75	25	-	250
	70	30	-	250
	60	40	-	250
kr649c	50	50	-	250
	40	60	-	250
kr649d	30	70	-	250
	20	80	-	250
kr649e	10	90	-	250
	-	100	-	250
	-	90	10	250
kr649f	-	75	25	250
	-	-	100	250
kr649g	-	-	100	250

Fraction kr649a (107.0 mg) was subjected to reverse-phase HPLC to yield two fractions (Table 44) which were identified as metabolites **KR649-12** and **KR649-13**, respectively.

Table 44. Experimental details for the separation of fraction kr649a.

Chromatographic conditions	
Column	Kromasil 100-7-C_{18} (250 mm × 10 mm i.d.)
Mobile phase	MeCN 100%, 1.5 mL/min

Fraction	Retention time (min)	Weight (mg)
kr649a1	18.5	76.3
kr649a2	20.0	15.6

Fractions kr649b and kr649c, pooled together in one fraction thereafter designated as kr649b (4.9 g), were further fractionated by normal-phase gravity column chromatography, using cHex with increasing amounts of EtOAc and EtOAC with

increasing amounts of MeOH as the mobile phase, to afford 175 fractions of approx. 35 mL each, which after an initial screening with TLC were combined into 16 fractions (Table 45).

Table 45. Experimental details for the separation of fraction kr649b.

Fraction	Mobile phase			Volume (mL)
	cHex %	EtOAc %	MeOH %	
kr649b1	90	10	-	315
kr649b2	90	10	-	280
kr649b3	90	10	-	105
kr649b4	90	10	-	105
kr649b5	90	10	-	245
kr649b6	90	10	-	105
	88	12	-	175
kr649b7	88	12	-	140
kr649b8	88	12	-	245
	84	16	-	420
kr649b9	84	16	-	140
kr649b10	84	16	-	350
	82	18	-	105
kr649b11	82	18	-	280
kr649b12	82	18	-	70
	80	20	-	350
kr649b13	80	20	-	175
	70	30	-	210
	60	40	-	385
kr649b14	60	40	-	105
	40	60	-	315
kr649b15	20	80	-	315
	-	100	-	315
kr649b16	-	100	-	285
	-	95	5	595

Fraction kr649b5 (75.1 mg) was further fractionated by normal-phase SPE chromatography, using cHex with increasing amounts of Acetone as the mobile phase, to afford 4 fractions which after an initial screening with TLC were combined into 2 fractions (Table 46).

Table 46. Experimental details for the separation of fraction kr649b5.

Fraction	Mobile phase		Volume (mL)
	cHex %	Acetone %	
kr649b5a	95	5	34
	93	7	20
kr649b5b	90	10	20
	-	100	40

Fraction kr649b5a (67.5 mg) was further fractionated by normal-phase SPE chromatography, using cHex with increasing amounts of EtOAc as the mobile phase, to afford 4 fractions which after an initial screening with TLC were combined into 2 fractions (Table 47).

Table 47. Experimental details for the separation of fraction kr649b5a.

Fraction	Mobile phase		Volume (mL)
	cHex %	EtOAc %	
kr649b5a1	95	5	35
	93	7	20
	90	10	20
kr649b5a2	90	10	20

Fraction kr649b5a1 (57.5 mg) was subjected to normal-phase HPLC to yield nine fractions (Table 48).

Table 48. Experimental details for the separation of fraction kr649b5a1.

Chromatographic conditions	
Column	Econosphere Silica 10μ (250 mm × 10 mm i.d.)
Mobile phase	cHex/Acetone 94:6%, 1.5 mL/min

Fraction	Retention time (min)	Weight (mg)
kr649b5a1a	12.7	4.1
kr649b5a1b	13.6	2.3
kr649b5a1c	14.3	2.3
kr649b5a1d	15.1	3.3
kr649b5a1e	15.6	3.9
kr649b5a1f	16.4	2.9
kr649b5a1g	17.5	3.4
kr649b5a1h	18.7	10.0
kr649b5a1i	20.4	2.6

Fraction kr649b5a1a (4.1 mg) was subjected to normal-phase HPLC to yield one fraction (Table 49) which was identified as metabolite **KR649-29**.

Table 49. Experimental details for the separation of fraction kr649b5a1a.

Chromatographic conditions	
Column	Econosphere Silica 10µ (250 mm × 10 mm i.d.)
Mobile phase	*n*Hex/EtOAc 92:8%, 1.5 mL/min

Fraction	**Retention time (min)**	**Weight (mg)**
kr649b5a1a1	12.8	3.3

Fraction kr649b5a1b (3.0 mg) was subjected to normal-phase HPLC to yield one fraction (Table 50) which was identified as metabolite **KR649-30**.

Table 50. Experimental details for the separation of fraction kr649b5a1b.

Chromatographic conditions	
Column	Econosphere Silica 10µ (250 mm × 10 mm i.d.)
Mobile phase	*n*Hex/EtOAc 92:8%, 1.5 mL/min

Fraction	**Retention time (min)**	**Weight (mg)**
kr649b5a1b1	13.5	2.4

Fraction kr649b5a1d (3.3 mg) was subjected to normal-phase HPLC to yield four fractions (Table 51), among which fraction kr649b5a1d4 was identified as metabolite **KR649-23**.

Table 51. Experimental details for the separation of fraction kr649b5a1d.

Chromatographic conditions	
Column	Econosphere Silica 10µ (250 mm × 10 mm i.d.)
Mobile phase	cHex/Acetone 98:2%, 1.5 mL/min

Fraction	**Retention time (min)**	**Weight (mg)**
kr649b5a1d1	14.7	0.1
kr649b5a1d2	15.4	0.1
kr649b5a1d3	16.8	0.1
kr649b5a1d4	17.5	1.0

Fraction kr649b6 (60.8 mg) was further fractionated by normal-phase SPE chromatography, using cHex with increasing amounts of EtOAc as the mobile phase, to afford 4 fractions which after an initial screening with TLC were combined into 3 fractions (Table 52).

Table 52. Experimental details for the separation of fraction kr649b6.

Fraction	Mobile phase		Volume (mL)
	cHex %	EtOAc %	
kr649b6a	94	6	30
	92	8	15
kr649b6b	90	10	15
kr649b6c	-	100	15

Fraction kr649b6a (18.7 mg) was subjected to normal-phase HPLC to yield four fractions (Table 53), among which fraction kr649b6a4 was identified as metabolite **KR649-10**.

Table 53. Experimental details for the separation of fraction kr649b6a.

Chromatographic conditions	
Column	Econosphere Silica 10µ (250 mm × 10 mm i.d.)
Mobile phase	cHex/EtOAc 93:7%, 1.5 mL/min

Fraction	Retention time (min)	Weight (mg)
b6a1	14.3	2.4
b6a2	15.8	1.4
b6a3	16.6	6.9
b6a4	20.0	3.6

Fraction kr649b6b (34.6 mg) was further fractionated by normal-phase SPE chromatography, using cHex with increasing amounts of EtOAc as the mobile phase, to afford five fractions which after an initial screening with TLC were combined into 4 fractions (Table 54).

Table 54. Experimental details for the separation of fraction kr649b6b.

Fraction	Mobile phase		Volume (mL)
	cHex %	EtOAc %	
kr649b6b1	96	4	20
	94	6	10
kr649b6b2	94	6	10
kr649b6b3	93	7	10
kr649b6b4	92	8	10

Fraction kr649b6b1 (17.5 mg) was subjected to normal-phase HPLC to yield three fractions (Table 55), among which fraction kr649b6b1b was identified as metabolite **KR649-10**.

Table 55. Experimental details for the separation of fraction kr649b6b1.

Chromatographic conditions	
Column	Econosphere Silica 10µ (250 mm × 10 mm i.d.)
Mobile phase	cHex/EtOAc 93:7%, 1.5 mL/min

Fraction	Retention time (min)	Weight (mg)
kr649b6b1a	15.6	2.4
kr649b6b1b	18.8	1.4
kr649b6b1c	19.8	6.9

Fraction kr649b6b2 (13.3 mg) was subjected to normal-phase HPLC to yield four fractions (Table 56).

Table 56. Experimental details for the separation of fraction kr649b6b2.

Chromatographic conditions	
Column	Econosphere Silica 10µ (250 mm × 10 mm i.d.)
Mobile phase	cHex/EtOAc 93:7%, 1.5 mL/min

Fraction	Retention time (min)	Weight (mg)
kr649b6b2a	19.4	3.8
kr649b6b2b	20.5	1.9
kr649b6b2c	22.5	2.4
kr649b6b2d	24.0	1.3

Fraction kr649b6b2a (3.8 mg) was subjected to normal-phase HPLC to yield three fraction (Table 57), among which fraction kr649b6b2a3 was identified as metabolite **KR649-10**.

Table 57. Experimental details for the separation of fraction kr649b6b2a.

Chromatographic conditions	
Column	Econosphere Silica 10µ (250 mm × 10 mm i.d.)
Mobile phase	cHex/Acetone 96:4%, 1.5 mL/min

Fraction	Retention time (min)	Weight (mg)
kr649b6b2a1	12.8	0.6
kr649b6b2a2	19.4	2.4
kr649b6b2a3	20.2	2.1

Fraction kr649b6b2d (1.3 mg) was subjected to normal-phase HPLC to yield three fractions (Table 58), among which fractions kr649b6b2d2 and kr649b6b2d3 were identified as metabolites **KR649-20** and **KR649-21**, respectively.

Table 58. Experimental details for the separation of fraction kr649b6b2d.

Chromatographic conditions	
Column	Econosphere Silica 10µ (250 mm × 10 mm i.d.)
Mobile phase	cHex/Acetone 96:4%, 1.5 mL/min

Fraction	**Retention time (min)**	**Weight (mg)**
kr649b6b2d1	12.6	0.1
kr649b6b2d2	21.0	0.1
kr649b6b2d3	23.3	0.2

Fraction kr649b7 (39.5 mg) was further fractionated by normal-phase SPE chromatography, using cHex with increasing amounts of EtOAc as the mobile phase, to afford six fractions which after an initial screening with TLC were combined into 3 fractions (Table 59).

Table 59. Experimental details for the separation of fraction kr649b7.

Fraction	**Mobile phase**		**Volume (mL)**
	cHex %	**EtOAc %**	
kr649b7a	96	4	20
	94	6	10
	94	6	10
kr649b7b	93	7	10
	92	8	10
kr649b7c	-	100	10

Fraction kr649b7a (21.4 mg) was subjected to normal-phase HPLC to yield five fractions (Table 60), among which fractions kr649b7a1 and kr649b7a4 were identified as metabolites **KR649-10** and **KR649-02**, respectively.

Table 60. Experimental details for the separation of fraction kr649b7a.

Chromatographic conditions	
Column	Econosphere Silica 10µ (250 mm × 10 mm i.d.)
Mobile phase	cHex/EtOAc 93:7%, 1.5 mL/min

Fraction	**Retention time (min)**	**Weight (mg)**
kr649b7a1	19.5	6.4
kr649b7a2	22.9	2.1
kr649b7a3	24.2	2.3
kr649b7a4	26.4	3.3
kr649b7a5	27.9	1.4

Fraction kr649b7b (11.0 mg) was subjected to normal-phase HPLC to yield two fractions (Table 61), among which fraction kr649b7b1 was identified as metabolites **KR649-02**.

Table 61. Experimental details for the separation of fraction kr649b7b.

Chromatographic conditions	
Column	Econosphere Silica 10µ (250 mm × 10 mm i.d.)
Mobile phase	cHex/EtOAc 93:7%, 1.5 mL/min

Fraction	**Retention time (min)**	**Weight (mg)**
kr649b7b1	26.5	5.8
kr649b7b2	28.0	1.1

Fractions kr649b7a5 and kr649b7b2, pooled together in one fraction thereafter designated as kr649b7a5 (2.5 mg), were subjected to normal-phase HPLC to yield two fractions (Table 62), among which fraction kr649b7a5a was identified as metabolites **KR649-02**.

Table 62. Experimental details for the separation of fraction kr649b7a5.

Chromatographic conditions	
Column	Econosphere Silica 10µ (250 mm × 10 mm i.d.)
Mobile phase	cHex/Acetone 96:4%, 1.5 mL/min

Fraction	**Retention time (min)**	**Weight (mg)**
kr649b7a5a	21.7	1.1
kr649b7a5b	23.6	1

Fraction kr649b8 (181.7 mg) was further fractionated by normal-phase SPE chromatography, using cHex with increasing amounts of EtOAc as the mobile phase, to afford six fractions (Table 63).

Table 63. Experimental details for the separation of fraction kr649b8.

Fraction	**Mobile phase**		**Volume (mL)**
	cHex %	**EtOAc %**	
kr649b8a	96	4	46
kr649b8b	94	6	30
kr649b8c	94	6	30
kr649b8d	93	7	30
kr649b8e	92	8	30
kr649b8f	-	100	30

Fraction kr649b8a (15.5 mg) was subjected to normal-phase HPLC to yield four fractions (Table 64), among which fractions kr649b8a2 and kr649b8a3 were identified as metabolites **KR649-10** and **KR649-02**, respectively.

Table 64. Experimental details for the separation of fraction kr649b8a.

Chromatographic conditions	
Column	Econosphere Silica 10µ (250 mm × 10 mm i.d.)
Mobile phase	cHex/Acetone 96:4%, 1.5 mL/min

Fraction	**Retention time (min)**	**Weight (mg)**
kr649b8a1	12.9	2.5
kr649b8a2	19.9	2.7
kr649b8a3	21.9	3.8
kr649b8a4	23.6	1.7

Fraction kr649b8a4 (1.7 mg) was subjected to normal-phase HPLC to yield two fractions (Table 65).

Table 65. Experimental details for the separation of fraction kr649b8a4.

Chromatographic conditions	
Column	Econosphere Silica 10µ (250 mm × 10 mm i.d.)
Mobile phase	*n*Hex/Acetone 94:6%, 1.5 mL/min

Fraction	**Retention time (min)**	**Weight (mg)**
kr649b8a4a	19.5	0.1
kr649b8a4b	22.4	0.9

Fraction kr649b8a4b (0.9 mg) was subjected to normal-phase HPLC to yield two fractions (Table 66), among which fraction kr649b8a4b1 was identified as metabolite **KR649-21**.

Table 66. Experimental details for the separation of fraction kr649b8a4b.

Chromatographic conditions	
Column	Econosphere Silica 10µ (250 mm × 10 mm i.d.)
Mobile phase	*n*Hex/EtOAc 92:8%, 2.0 mL/min

Fraction	**Retention time (min)**	**Weight (mg)**
kr649b8a4b1	21.0	0.1
kr649b8a4b2	24.8	0.5

Fraction kr649b8b (86.5 mg) was subjected to normal-phase HPLC to yield three fractions (Table 67).

Table 67. Experimental details for the separation of fraction kr649b8b.

Chromatographic conditions	
Column	Econosphere Silica 10µ (250 mm × 10 mm i.d.)
Mobile phase	cHex/EtOAc 93:7%, 1.5 mL/min

Fraction	Retention time (min)	Weight (mg)
kr649b8b1	23.5	3.7
kr649b8b2	25.6	42.9
kr649b8b3	32.3	19.4

Fractions kr649b7a3 and kr649b8b1, pooled together in one fraction thereafter designated as kr649b8b1 (6.0. mg), were subjected to normal-phase HPLC to yield four fractions (Table 68), among which fractions kr649b8b1b, kr649b8b1c and kr649b8b1d were identified as metabolites **KR649-19**, **KR649-20** and **KR649-21**, respectively.

Table 68. Experimental details for the separation of fraction kr649b8b1.

Chromatographic conditions	
Column	Econosphere Silica 10µ (250 mm × 10 mm i.d.)
Mobile phase	cHex/Acetone 96:4%, 1.5 mL/min

Fraction	Retention time (min)	Weight (mg)
kr649b8b1a	13.6	0.4
kr649b8b1b	22.8	1.5
kr649b8b1c	24.5	1.0
kr649b8b1d	26.1	0.7

Fraction kr649b8b2 (42.9 mg) was subjected to normal-phase HPLC to yield four fractions (Table 69), among which fraction kr649b8b2c was identified as metabolite **KR649-02**.

Table 69. Experimental details for the separation of fraction kr649b8b2.

Chromatographic conditions	
Column	Econosphere Silica 10µ (250 mm × 10 mm i.d.)
Mobile phase	cHex/Acetone 96:4%, 1.5 mL/min

Fraction	Retention time (min)	Weight (mg)
kr649b8b2a	14.0	0.9
kr649b8b2b	19.6	1.9
kr649b8b2c	21.6	27.7
kr649b8b2d	23.5	9.0

Fraction kr649b8b2b (1.9 mg) was subjected to normal-phase HPLC to yield two fractions (Table 70), among which fraction kr649b8b2b2 was identified as metabolite **KR649-02**.

Table 70. Experimental details for the separation of fraction kr649b8b2b.

Chromatographic conditions	
Column	Econosphere Silica 10µ (250 mm × 10 mm i.d.)
Mobile phase	*n*Hex/Acetone 94:6%, 1.5 mL/min

Fraction	**Retention time (min)**	**Weight (mg)**
kr649b8b2b1	17.7	0.2
kr649b8b2b2	19.3	0.4

In total, from the chemical investigation of the organic extracts (small- and large-scale) of the sponge *Lamellodysidea* sp., 11 metabolites were isolated in pure form (Table 71).

Table 71. Isolated metabolites from the sponge *Lamellodysidea* sp.

Metabolite	**Code**	**Fraction**	**Weight (mg)**
23	KR649-13	kr649a2	15.6
24	KR649-12	kr649a1	76.3
25	KR649-23	kr649B5a1d4	1.0
26	K649-10	k649c4b	24.0
	KR649-10	kr649b6a4, kr649b6b1b, kr649b6b2a3, kr649b7a1, kr649b8a2	
27	KR649-21	kr649b6b2d3, kr649b8a4b1, kr649b8b1d	1.7
28	KR649-07	K649d7c3	9.2
29	K649-02	K649c6	58.2
	KR649-02	kr649b7a4, kr649b7b1, kr649b7a5a, kr649b8a3, kr649b8b2b2, kr649b8b2c	
30	KR649-20	kr649b6b2d2, kr649b8b1c	1.3
31	KR649-19	kr649b8b1b	2.1
32	KR649-29	kr649b5a1a1	3.3
33	KR649-30	kr649b5a1b1	2.4

2.6 Extraction and isolation of metabolites from the soft coral *Sinularia polydactyla*

Specimens of the soft coral *S. polydactyla* were extensively extracted with mixtures of CH_2Cl_2 and MeOH to afford after evaporation of the solvents in vacuo a crude extract that was subjected to a series of chromatographic separations (Figure 12, Figure 13, Figure 14), including normal- and reversed-phase vacuum column chromatography, gravity column chromatography and HPLC, to allow for the isolation of a number of metabolites in pure form. After each chromatographic step, the fractions were analyzed by ^{1}H NMR spectroscopy.

Initially, the organic extract sp (18.5 g) was subjected to normal-phase vacuum column chromatography, using cHex with increasing amounts of EtOAc, followed by EtOAc with increasing amounts of MeOH as the mobile phase, to afford 20 fractions, which after an initial screening with TLC were combined into 10 fractions (Table 72).

Table 72. Experimental details for the separation of the crude extract sp.

Fraction	Mobile phase			Volume (mL)
	cHex %	EtOAc %	MeOH %	
sp1	100	-	-	500
	90	10	-	250
	80	20	-	250
sp2	70	30	-	250
	60	40	-	250
	50	50	-	250
			-	250
sp3	40	60	-	250
	30	70	-	250
sp4	20	80	-	250
	10	90	-	250
sp5	-	100	-	250
sp6	-	90	10	250
	-	75	25	250
	-	50	50	250
sp7	-	50	50	250
sp8	-	-	100	250
sp9	-	-	100	250
sp10	-	-	100	250
	-	-	100	250

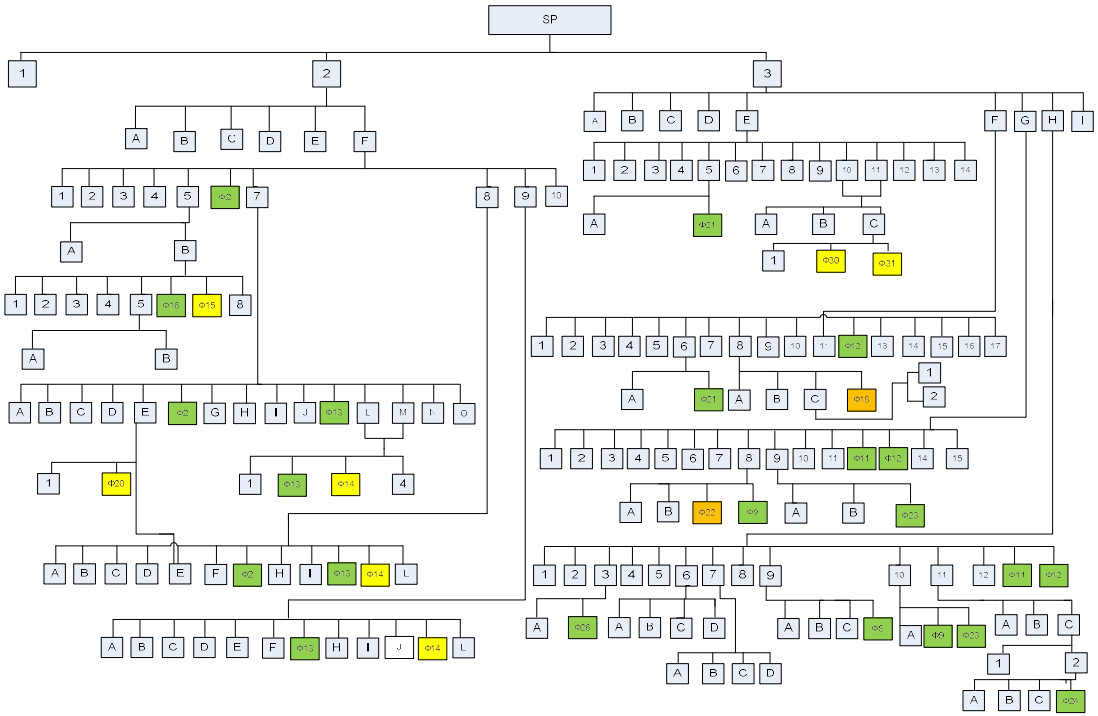

Figure 12. Fractionation scheme for the isolation of metabolites from the crude extract sp (part 1).

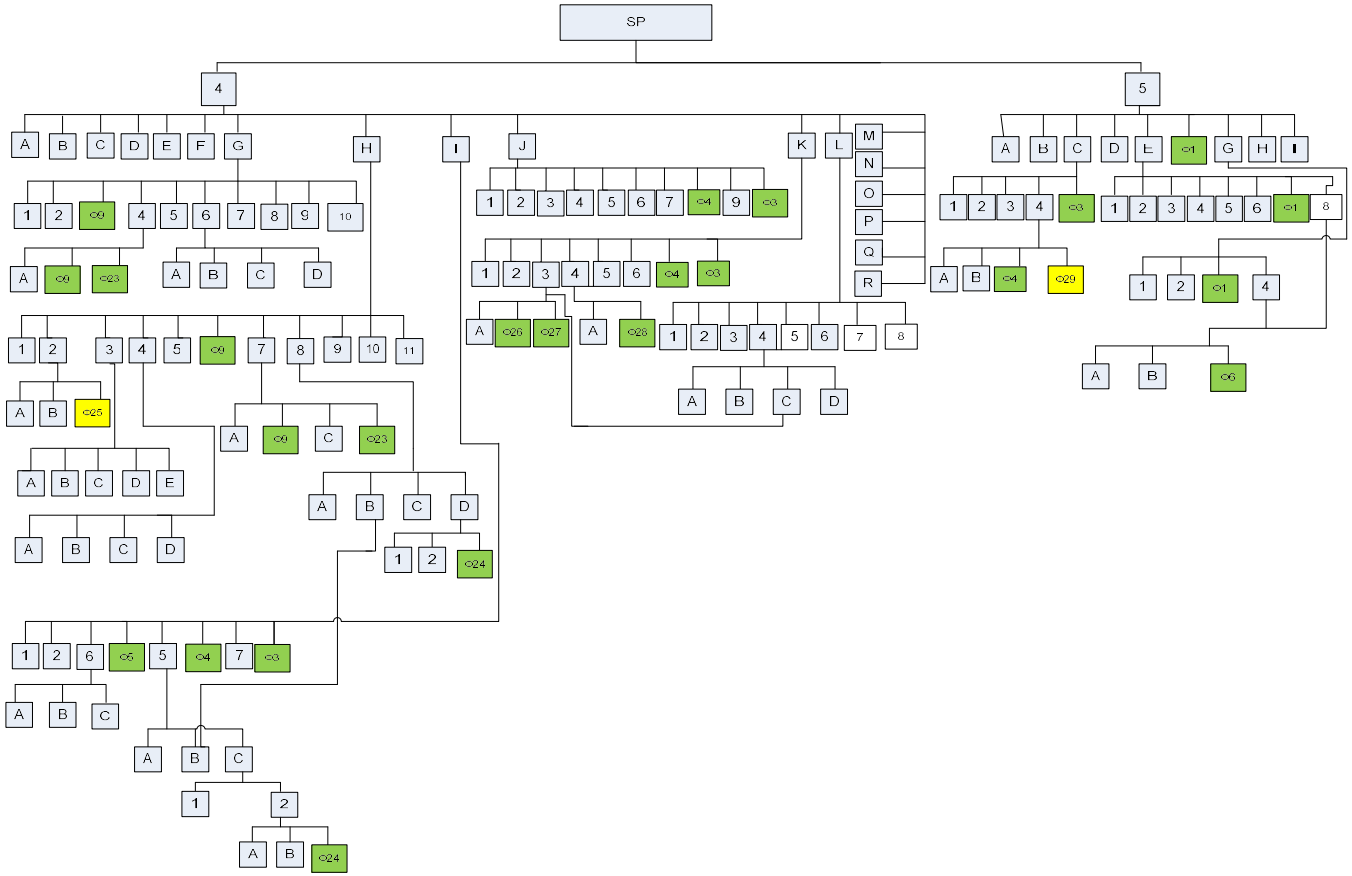

Figure 13. Fractionation scheme for the isolation of metabolites from the crude extract sp (part 2).

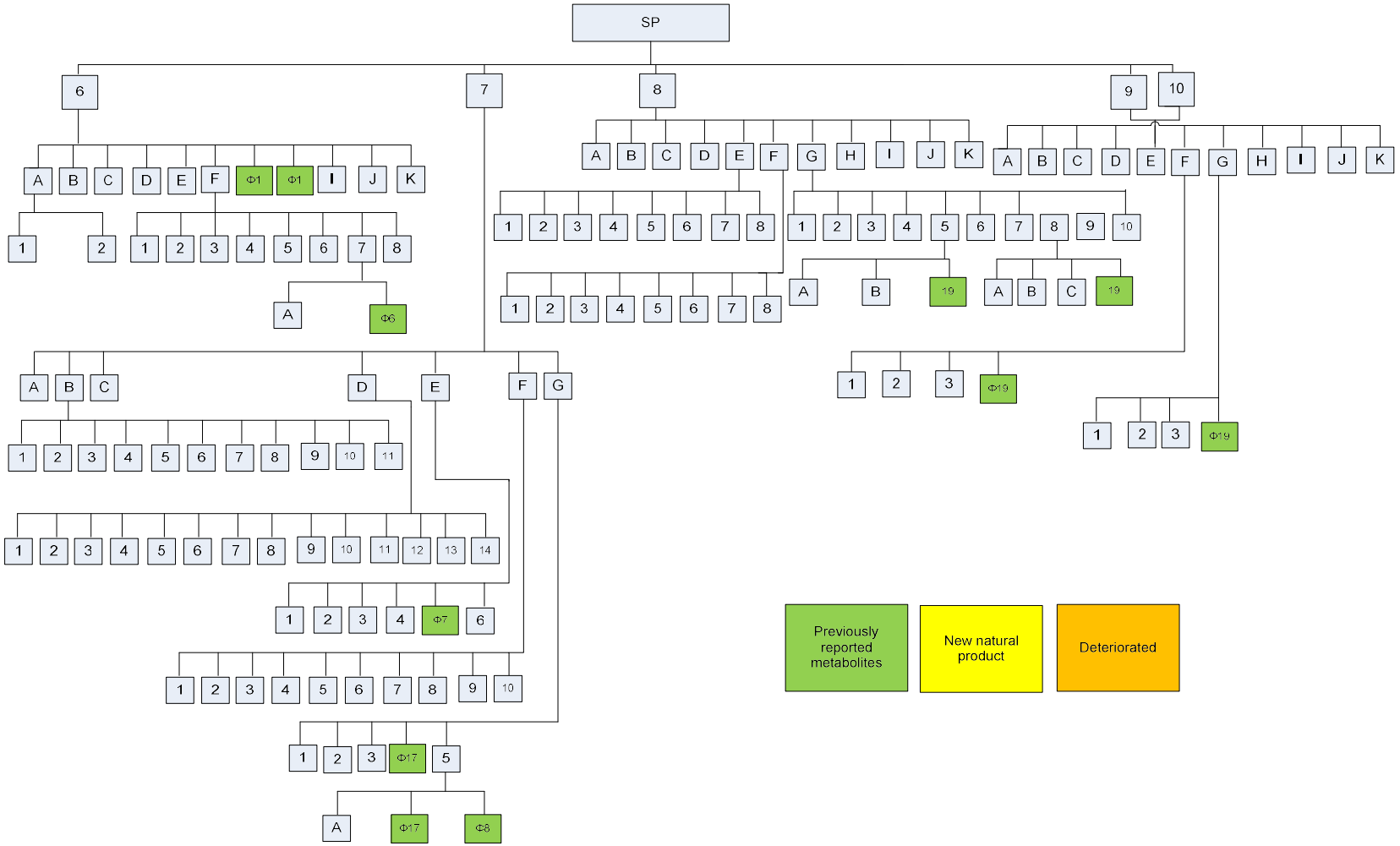

Figure 14. Fractionation scheme for the isolation of metabolites from the crude extract sp (part 3).

Fraction sp2 (2.373 g) was subjected to normal-phase vacuum column chromatography, using cHex with increasing amounts of EtOAc as the mobile phase, to afford 11 fractions, which after an initial screening with TLC were combined into 6 fractions (Table 73).

Table 73. Experimental details for the separation of fraction sp2.

Fraction	Mobile phase		Volume (mL)
	cHex %	EtOAc %	
sp2a	100	-	300
	98	2	150
sp2b	98	2	150
	96	4	150
sp2c	94	6	150
	92	8	150
sp2d	90	10	150
sp2e	88	12	150
	85	15	150
sp2f	80	20	150
	70	30	150

Fraction sp2f (494 mg) was further fractionated by normal-phase gravity column chromatography, using cHex with increasing amounts of EtOAc as the mobile phase, to afford 55 fractions of approx. 20 mL each, which after an initial screening with TLC were combined into 10 fractions, among which fraction sp2f6 was identified as metabolite **SP-02** (Table 74).

Table 74. Experimental details for the separation of fraction sp2f.

Fraction	Mobile phase		Volume (mL)
	cHex %	EtOAc %	
sp2f1	90	10	200
sp2f2	90	10	
sp2f3	88	12	200
sp2f4			
sp2f5			
sp2f6			
sp2f7	85	15	200
	80	20	200
	60	40	50
sp2f8	60	40	100
sp2f9	60	40	50
	-	100	50
sp2f10	-	100	50

Fraction sp2f5 (118.8 mg) was fractionated into two parts according to the solubility in MeOH, namely sp2f5a and sp2f5b. Fraction sp2f5b (92.6 mg) which was soluble in MeOH was subjected to reversed-phase HPLC to yield eight fractions (Table 75), among which fractions sp2f5b6 and sp2f5b7 were identified as metabolites **SP-16** and **SP-15**, respectively.

Table 75. Experimental details for the separation of fraction sp2f5b.

Chromatographic conditions	
Column	Kromasil 100 C_{18} (250 mm × 8 mm i.d.)
Mobile phase	MeOH 100%, 2.5 mL/min

Fraction	**Retention time (min)**	**Weight (mg)**
sp2f5b1	4.8	1.7
sp2f5b2	8.3	0.6
sp2f5b3	17.3	0.6
sp2f5b4	31.2	0.9
sp2f5b5	36.7	1.4
sp2f5b6	41.9	9.1
sp2f5b7	47.1	8.8
sp2f5b8	54.8	14.5

Fraction sp2f7 (78.0 mg) was subjected to reversed-phase HPLC to yield fifteen fractions (Table 76), among which fractions sp2f7f and sp2f7k were identified as metabolites **SP-02** and **SP-13**, respectively.

Table 76. Experimental details for the separation of fraction sp2f7.

Chromatographic conditions	
Column	Kromasil 100 C_{18} (250 mm × 8 mm i.d.)
Mobile phase	MeOH 100%, 1.5 mL/min

Fraction	**Retention time (min)**	**Weight (mg)**
sp2f7a	7.2	1.9
sp2f7b	9.6	1
sp2f7c	11.9	0.9
sp2f7d	13.0	2.5
sp2f7e	13.6	0.5
sp2f7f	15.9	14
sp2f7g	19.1	1
sp2f7h	21.5	2.4
sp2f7i	23.9	1.7
sp2f7j	24.6	1
sp2f7k	25.3	6.4
sp2f7l	27.4	8.9

sp2f7m	28.6	4.6
sp2f7n	30.8	1.5
sp2f7o	32.1	1.1

Fractions sp2f7l and sp2f7m, pooled together in one fraction thereafter designated as sp2f7l (13.5 mg), were further subjected to reversed-phase HPLC to yield four fractions (Table 77), among which fractions sp2f7l2 and sp2f7l3 was identified as metabolites **SP-13** and **SP-14**, respectively.

Table 77. Experimental details for the separation of fraction sp2f7l.

Chromatographic conditions	
Column	Kromasil 100 C_{18} (250 mm × 8 mm i.d.)
Mobile phase	MeOH/H_2O 98:2%, 2 mL/min

Fraction	**Retention time (min)**	**Weight (mg)**
sp2f7l1	6.5	3.4
sp2f7l2	30.6	1.8
sp2f7l3	33.8	5.7
sp2f7l4	34.9	2.6

Fraction sp2f8 (25.8 mg) was subjected to reversed-phase HPLC to yield twelve fractions (Table 78), among which fractions sp2f8g, sp2f8j and sp2f8k were identified as metabolites **SP-02, SP-13** and **SP-14**, respectively.

Table 78. Experimental details for the separation of fraction sp2f8.

Chromatographic conditions	
Column	Kromasil 100 C_{18} (250 mm × 8 mm i.d.)
Mobile phase	MeOH 100%, 1.5 mL/min

Fraction	**Retention time (min)**	**Weight (mg)**
sp2f8a	7.2	0.8
sp2f8b	8.1	0.3
sp2f8c	9.8	1.3
sp2f8d	11.6	1.4
sp2f8e	13.6	0.6
sp2f8f	17.8	0.2
sp2f8g	19.8	4.9
sp2f8h	22.2	0.1
sp2f8i	24.5	1.0
sp2f8j	25.7	2.4
sp2f8k	28.0	1.8
sp2f8l	29.0	0.6

Fractions sp2f7e and sp2f8e, pooled together in one fraction thereafter designated as sp2f8e (1.1 mg), were further subjected to reversed-phase HPLC to yield two fractions (Table 79), among which fraction sp2f8e2 was identified as metabolite **SP-20**.

Table 79. Experimental details for the separation of fraction sp2f8e.

Chromatographic conditions	
Column	Kromasil 100 C_{18} (250 mm × 8 mm i.d.)
Mobile phase	MeOH/H_2O 98:2%, 2 mL/min

Fraction	**Retention time (min)**	**Weight (mg)**
sp2f8e1	6.5	0.6
sp2f8e2	13.8	0.5

Fraction sp2f9 (15.5 mg) was subjected to reversed-phase HPLC to yield twelve fractions (Table 80), among which fractions sp2f9g and sp2f9k were identified as metabolites **SP-13** and **SP-14**, respectively.

Table 80. Experimental details for the separation of fraction sp2f9.

Chromatographic conditions	
Column	Kromasil 100 C_{18} (250 mm × 8 mm i.d.)
Mobile phase	MeOH 100%, 1.0 mL/min

Fraction	**Retention time (min)**	**Weight (mg)**
sp2f9a	7.9	2.6
sp2f9b	9.6	1.0
sp2f9c	11.0	1.3
sp2f9d	12.9	0.6
sp2f9e	14.3	1.3
sp2f9f	15.2	0.9
sp2f9g	18.8	0.8
sp2f9h	19.9	0.2
sp2f9i	21.9	0.7
sp2f9j	23.6	0.4
sp2f9k	28.7	1.6
sp2f9l	31.2	0.5

Fraction sp3 (2.486 g) was subjected to normal-phase vacuum column chromatography, using cHex with increasing amounts of EtOAc as the mobile phase, to afford 21 fractions, which after an initial screening with TLC were combined into 9 fractions (Table 81).

Table 81. Experimental details for the separation of fraction sp3.

Fraction	Mobile phase		Volume (mL)
	cHex %	EtOAc %	
sp3a	100	-	400
	98	2	150
	96	4	150
	94	6	150
	92	8	150
sp3b	90	10	150
	88	12	150
sp3c	85	15	150
	80	20	150
sp3d	80	20	150
	80	20	150
	75	25	150
sp3e	70	30	150
sp3f	65	35	150
	60	40	150
sp3g	60	40	150
sp3h	60	40	150
	50	50	150
	50	50	150
sp3i	50	50	150
	50	50	150

Fraction sp3e (138.6 mg) was subjected to reversed-phase HPLC to yield fourteen fractions (Table 82).

Table 82. Experimental details for the separation of fraction sp3e.

Chromatographic conditions	
Column	Kromasil 100 C_{18} (250 mm × 8 mm i.d.)
Mobile phase	MeOH 100%, 1.5 mL/min

Fraction	Retention time (min)	Weight (mg)
sp3e1	8.1	10.2
sp3e2	10.8	2
sp3e3	11.6	2.1
sp3e4	12.2	1.6
sp3e5	12.8	11.9
sp3e6	13.5	21.0
sp3e7	15.3	3.3
sp3e8	16.1	2.1
sp3e9	16.8	34.8

sp3e10	19.5	2.1
sp3e11	21.0	1.9
sp3e12	22.4	2.7
sp3e13	25.2	5.7
sp3e14	26.1	1.1

Fraction sp3e5 (11.9 mg) was subjected to reversed-phase HPLC to yield two fractions (Table 83), among which fraction sp3e5b was identified as metabolite **SP-21**.

Table 83. Experimental details for the separation of fraction sp3e5.

Chromatographic conditions	
Column	Kromasil 100 C_{18} (250 mm × 8 mm i.d.)
Mobile phase	MeOH/H_2O 98:2%, 1.5 mL/min

Fraction	**Retention time (min)**	**Weight (mg)**
sp3e5a	7.9	2.0
sp3e5b	16.9	6.3

Fractions sp3e510 and sp3e511, pooled together in one fraction thereafter designated as sp3e10 (4.0 mg), were subjected to reversed-phase HPLC to yield three fractions (Table 84).

Table 84. Experimental details for the separation of fraction sp3e10.

Chromatographic conditions	
Column	Kromasil 100 C_{18} (250 mm × 8 mm i.d.)
Mobile phase	MeOH/H_2O 98:2%, 2 mL/min

Fraction	**Retention time (min)**	**Weight (mg)**
sp3e10a	6.0	0.1
sp3e10b	10.2	0.1
sp3e10c	21.3	1.3

Fraction sp3e10c (1.3 mg) was subjected to reversed-phase HPLC to yield three fractions (Table 85), among which fractions sp3e10c2 and sp3e10c3 were identified as metabolites **SP-30** and **SP-31**, respectively.

Table 85. Experimental details for the separation of fraction sp3e10c.

Chromatographic conditions	
Column	Kromasil 100 C_{18} (250 mm × 8 mm i.d.)
Mobile phase	MeOH/H_2O 97:3%, 1.5 mL/min

Fraction	Retention time (min)	Weight (mg)
sp3e10c1	7.8	0.1
sp3e10c2	32.2	0.3
sp3e10c3	35.7	0.7

Fraction sp3f (254.7 mg) was subjected to reversed-phase HPLC to yield seventeen fractions (Table 86).

Table 86. Experimental details for the separation of fraction sp3f.

Chromatographic conditions	
Column	Kromasil 100 C_{18} (250 mm × 8 mm i.d.)
Mobile phase	MeOH 100%, 1.5 mL/min

Fraction	Retention time (min)	Weight (mg)
sp3f1	7.2	6.9
sp3f2	9.3	7.3
sp3f3	10.8	3.7
sp3f4	11.5	5.1
sp3f5	12.1	6.2
sp3f6	12.8	11.5
sp3f7	13.4	53.7
sp3f8	15.2	10
sp3f9	16.8	58.2
sp3f10	18.0	6.3
sp3f11	19.2	3.4
sp3f12	21.0	2.5
sp3f13	22.2	4.2
sp3f14	23.1	4.1
sp3f15	24.0	3.3
sp3f16	25.0	3
sp3f17	27.9	1.7

Fraction sp3f6 (11.5 mg) was subjected to reversed-phase HPLC to yield two fractions (Table 87), among which fraction sp3f6b was identified as metabolite **SP-21**.

Table 87. Experimental details for the separation of fraction sp3f6.

Chromatographic conditions	
Column	Kromasil 100 C_{18} (250 mm × 8 mm i.d.)
Mobile phase	MeOH/H_2O 98:2%, 1.5 mL/min

Fraction	Retention time (min)	Weight (mg)
sp3f6a	7.9	2.2
sp3f6b	16.9	1.9

Fraction sp3f8 (10.0 mg) was subjected to reversed-phase HPLC to yield four fractions (Table 88), among which fraction sp3f8d was identified as metabolite **SP-18**.

Table 88. Experimental details for the separation of fraction sp3f8.

Chromatographic conditions	
Column	Kromasil 100 C_{18} (250 mm × 8 mm i.d.)
Mobile phase	MeOH/H_2O 98:2%, 1.5 mL/min

Fraction	**Retention time (min)**	**Weight (mg)**
sp3f8a	6.2	2.0
sp3f8b	11.5	0.2
sp3f8c	15.5	3.3
sp3f8d	44.6	2.2

Fraction sp3g (136.7 mg) was subjected to reversed-phase HPLC to yield fifteen fractions (Table 89).

Table 89. Experimental details for the separation of fraction sp3g.

Chromatographic conditions	
Column	Kromasil 100 C_{18} (250 mm × 8 mm i.d.)
Mobile phase	MeOH 100%, 1.5 mL/min

Fraction	**Retention time (min)**	**Weight (mg)**
sp3g1	7.6	5.6
sp3g2	10.3	3.6
sp3g3	11.2	2.6
sp3g4	11.9	4
sp3g5	12.7	3.6
sp3g6	13.2	20.08
sp3g7	14.4	2.8
sp3g8	14.8	7.6
sp3g9	15.6	7.2
sp3g10	16.6	20.1
sp3g11	18.0	6.6
sp3g12	19.0	3.7
sp3g13	20.5	3.6
sp3g14	22.1	2.1
sp3g15	23.6	2.1

Fraction sp3g8 (7.6 mg) was subjected to reversed-phase HPLC to yield four fractions (Table 90), among which fractions sp3g8c and sp3g8d were identified as metabolites **SP-22** and **SP-09**, respectively.

Table 90. Experimental details for the separation of fraction sp3g8.

Chromatographic conditions	
Column	Kromasil 100 C_{18} (250 mm × 8 mm i.d.)
Mobile phase	MeOH/H_2O 98:2%, 1.5 mL/min

Fraction	Retention time (min)	Weight (mg)
sp3g8a	7.9	0.5
sp3g8b	12.8	0.3
sp3g8c	20.9	0.8
sp3g8d	21.6	2.4

Fraction sp3g9 (7.2 mg) was subjected to reversed-phase HPLC to yield three fractions (Table 91), among which fraction sp3g9c was identified as metabolite **SP-23**.

Table 91. Experimental details for the separation of fraction sp3g9.

Chromatographic conditions	
Column	Kromasil 100 C_{18} (250 mm × 8 mm i.d.)
Mobile phase	MeOH/H_2O 98:2%, 1.5 mL/min

Fraction	Retention time (min)	Weight (mg)
sp3g9a	7.9	0.3
sp3g9b	21.2	0.5
sp3g9c	22.8	2.2

Fraction sp3h (156.6 mg) was subjected to reversed-phase HPLC to yield fourteen fractions (Table 92).

Table 92. Experimental details for the separation of fraction sp3h.

Chromatographic conditions	
Column	Kromasil 100 C_{18} (250 mm × 8 mm i.d.)
Mobile phase	MeOH 100%, 1.5 mL/min

Fraction	Retention time (min)	Weight (mg)
sp3h1	7.1	5.2
sp3h2	9.1	2.4
sp3h3	9.7	3.9
sp3h4	11.3	6.4
sp3h5	12.0	4.6
sp3h6	12.9	10.7
sp3h7	13.4	23.1
sp3h8	14.1	3.9
sp3h9	14.9	15.9
sp3h10	15.9	11.6

sp3h11	16.9	14.6
sp3h12	18.1	4.7
sp3h13	19.4	5
sp3h14	21.0	2.4

Fraction sp3h3 (3.9 mg) was subjected to reversed-phase HPLC to yield two fractions (Table 93), among which fraction sp3h3b was identified as metabolite **SP-26**.

Table 93. Experimental details for the separation of fraction sp3h3.

Chromatographic conditions	
Column	Kromasil 100 C_{18} (250 mm × 8 mm i.d.)
Mobile phase	MeOH/H_2O 96:4%, 1.2 mL/min

Fraction	**Retention time (min)**	**Weight (mg)**
sp3h3a	9.5	1.0
sp3h3b	16.8	0.6

Fraction sp3h9 (15.9 mg) was subjected to reversed-phase HPLC to yield four fractions (Table 94), among which fraction sp3h9d was identified as metabolite **SP-09**.

Table 94. Experimental details for the separation of fraction sp3h9.

Chromatographic conditions	
Column	Kromasil 100 C_{18} (250 mm × 8 mm i.d.)
Mobile phase	MeOH/H_2O 98:2%, 1.5 mL/min

Fraction	**Retention time (min)**	**Weight (mg)**
sp3h9a	7.9	0.5
sp3h9b	12.7	0.1
sp3h9c	20.2	0.3
sp3h9d	21.0	5.7

Fraction sp3h10 (11.6 mg) was subjected to reversed-phase HPLC to yield three fractions (Table 95), among which fractions sp3h10b and sp3h10c were identified as metabolites **SP-09** and **SP-23**, respectively.

Table 95. Experimental details for the separation of fraction sp3h10.

Chromatographic conditions	
Column	Kromasil 100 C_{18} (250 mm × 8 mm i.d.)
Mobile phase	MeOH/H_2O 98:2%, 1.5 mL/min

Fraction	**Retention time (min)**	**Weight (mg)**
sp3h10a	7.9	0.3
sp3h10b	21.4	1.2

sp3h10c	22.9	5.7

Fraction sp3h11 (14.6 mg) was subjected to reversed-phase HPLC to yield three fractions (Table 96).

Table 96. Experimental details for the separation of fraction sp3h11.

Chromatographic conditions	
Column	Kromasil 100 C_{18} (250 mm × 8 mm i.d.)
Mobile phase	MeOH/H_2O 98:2%, 1.5 mL/min

Fraction	**Retention time (min)**	**Weight (mg)**
sp3h11a	7.9	0.9
sp3h11b	23.2	0.8
sp3h11c	24.4	6.5

Fraction sp3h11c (6.5 mg) was subjected to reversed-phase HPLC to yield two fractions (Table 97).

Table 97. Experimental details for the separation of fraction sp3h11c.

Chromatographic conditions	
Column	Kromasil 100 C_{18} (250 mm × 8 mm i.d.)
Mobile phase	MeOH/H_2O 97:3%, 1.5 mL/min

Fraction	**Retention time (min)**	**Weight (mg)**
sp3h11c1	8.0	1.0
sp3h11c2	28.2	5.5

Fraction sp3h11c2 (5.5 mg) was subjected to reversed-phase HPLC to yield four fractions (Table 98), among which fraction sp3h11c2d was identified as metabolite **SP-24**.

Table 98. Experimental details for the separation of fraction sp3h11c2.

Chromatographic conditions	
Column	Kromasil 100 C_{18} (250 mm × 8 mm i.d.)
Mobile phase	AC-N/H_2O 98:2%, 2.0 mL/min

Fraction	**Retention time (min)**	**Weight (mg)**
sp3h11c2a	6.1	0.5
sp3h11c2b	25.5	0.7
sp3h11c2c	27.2	0.7
sp3h11c2d	38.7	0.3

Fraction sp4 (863 mg) was subjected to normal-phase gravity column chromatography, using cHex with increasing amounts of Acetone as the mobile phase, to afford 132 fractions of approx. 25 mL each, which after an initial screening with TLC were combined into 18 fractions (Table 99).

Table 99. Experimental details for the separation of fraction sp4.

Fraction	Mobile phase			Volume (mL)
	cHex %	Acetone %	EtOAc %	
sp4a	90	10	-	120
sp4b	90	10	-	80
sp4c	90	10	-	100
	87	13	-	180
sp4d	87	13	-	120
sp4e	85	15	-	300
sp4f	85	15	-	240
sp4g	85	15	-	60
	82	18	-	200
sp4h	80	20	-	180
sp4i	80	20	-	100
sp4j	80	20	-	100
sp4k	80	20	-	60
	77	23	-	100
sp4l	77	23	-	100
	75	25	-	100
	72	28	-	120
sp4m	72	28	-	180
	70	30	-	60
sp4n	70	30	-	80
sp4o	70	30	-	80
sp4p	65	35	-	240
sp4q	60	40	-	100
sp4r	60	40	-	100
	-	-	100	200

Fraction sp4g (150.7 mg) was subjected to reversed-phase HPLC to yield ten fractions (Table 100), among which fraction sp4g3 was identified as metabolite **SP-09**.

Table 100. Experimental details for the separation of fraction sp4g.

Chromatographic conditions	
Column	Kromasil 100 C_{18} (250 mm × 8 mm i.d.)
Mobile phase	MeOH 100%, 1.5 mL/min

Fraction	Retention time (min)	Weight (mg)
sp4g1	7.2	19.5
sp4g2	12.6	3.1
sp4g3	15.1	6.3
sp4g4	16.0	11.1
sp4g5	16.9	13.6
sp4g6	17.5	4.2
sp4g7	19.5	3.3
sp4g8	21.8	45.3
sp4g9	25.4	1.8
sp4g10	29.4	1.1

Fraction sp4g4 (11.1 mg) was subjected to reversed-phase HPLC to yield three fractions (Table 101), among which fractions sp4g4b and sp4g4c were identified as metabolites **SP-09** and **SP-23**, respectively.

Table 101. Experimental details for the separation of fraction sp4g4.

Chromatographic conditions	
Column	Kromasil 100 C_{18} (250 mm × 8 mm i.d.)
Mobile phase	MeOH/H_2O 97:3%, 1.5 mL/min

Fraction	Retention time (min)	Weight (mg)
sp4g4a	8.0	1
sp4g4b	24.4	1.5
sp4g4c	26.5	8.2

Fraction sp4h (130.4 mg) was subjected to reversed-phase HPLC to yield eleven fractions (Table 102), among which fraction sp4h6 was identified as metabolite **SP-09**.

Table 102. Experimental details for the separation of fraction sp4h.

Chromatographic conditions	
Column	Kromasil 100 C_{18} (250 mm × 8 mm i.d.)
Mobile phase	MeOH 100%, 1.5 mL/min

Fraction	Retention time (min)	Weight (mg)
sp4h1	7.2	14.7
sp4h2	9.8	4.7
sp4h3	13.0	2.7
sp4h4	13.4	2.9
sp4h5	14.4	0.9
sp4h6	14.9	8.7
sp4h7	15.8	3.2
sp4h8	16.8	16.2

sp4h9	19.1	2
sp4h10	21.6	22.1
sp4h11	22.7	4.3

Fraction sp4h2 (4.7 mg) was subjected to reversed-phase HPLC to yield three fractions (Table 103), among which fraction sp4h2c was identified as metabolite **SP-25**.

Table 103. Experimental details for the separation of fraction sp4h2.

Chromatographic conditions	
Column	Kromasil 100 C_{18} (250 mm × 8 mm i.d.)
Mobile phase	MeOH/H_2O 98:2%, 1.5.0 mL/min

Fraction	**Retention time (min)**	**Weight (mg)**
sp4h2a	7.9	1.0
sp4h2b	11.8	0.3
sp4h2c	12.6	1.3

Fraction sp4h7 (3.2 mg) was subjected to reversed-phase HPLC to yield four fractions (Table 104), among which fractions sp4h7b and sp4h7d were identified as metabolite **SP-09** and **SP-23**, respectively.

Table 104. Experimental details for the separation of fraction sp4h7.

Chromatographic conditions	
Column	Kromasil 100 C_{18} (250 mm × 8 mm i.d.)
Mobile phase	MeOH/H_2O 98:2%, 1.5 mL/min

Fraction	**Retention time (min)**	**Weight (mg)**
sp4h7a	7.9	0.1
sp4h7b	21.2	1.1
sp4h7c	22.3	1
sp4h7d	23.4	0.9

Fraction sp4h8 (16.2 mg) was subjected to reversed-phase HPLC to yield four fractions (Table 105).

Table 105. Experimental details for the separation of fraction sp4h8.

Chromatographic conditions	
Column	Kromasil 100 C_{18} (250 mm × 8 mm i.d.)
Mobile phase	MeOH/H_2O 98:2%, 1.5 mL/min

Fraction	**Retention time (min)**	**Weight (mg)**
sp4h8a	7.9	0.6
sp4h8b	11.5	1.1

sp4h8c	23.5	0.7
sp4h8d	24.7	11.9

Fraction sp4h8d (11.9 mg) was subjected to reversed-phase HPLC to yield three fractions (Table 106), among which fraction sp4h8d3 was identified as metabolite **SP-24**.

Table 106. Experimental details for the separation of fraction sp4h8d3.

Chromatographic conditions	
Column	Kromasil 100 C_{18} (250 mm × 8 mm i.d.)
Mobile phase	AC-N/H_2O 98:2%, 2.0 mL/min

Fraction	**Retention time (min)**	**Weight (mg)**
sp4h8d1	6.1	1.5
sp4h8d2	33.2	7.2
sp4h8d3	38.2	2.3

Fraction sp4i (50.1 mg) was subjected to reversed-phase HPLC to yield eight fractions (Table 107), among which fractions sp4i4, sp4i6 and sp4i8 were identified as metabolites **SP-05**, **SP-04** and **SP-03**, respectively.

Table 107. Experimental details for the separation of fraction sp4i.

Chromatographic conditions	
Column	Kromasil 100 C_{18} (250 mm × 8 mm i.d.)
Mobile phase	MeOH 100%, 1.5 mL/min

Fraction	**Retention time (min)**	**Weight (mg)**
sp4i1	7.2	3.1
sp4i2	12.8	1.1
sp4i3	13.2	3.7
sp4i4	15.3	9.4
sp4i5	16.4	5.4
sp4i6	17.9	3.9
sp4i7	21.3	2.1
sp4i8	22.2	10.5

Fraction sp4j (53.1 mg) was subjected to reversed-phase HPLC to yield ten fractions (

Table **108**), among which fractions sp4j8 and sp4j10 were identified as metabolites **SP-04** and **SP-03**, respectively.

Table 108. Experimental details for the separation of fraction sp4j.

Chromatographic conditions	
Column	Kromasil 100 C_{18} (250 mm × 8 mm i.d.)
Mobile phase	MeOH 100%, 1.5 mL/min

Fraction	Retention time (min)	Weight (mg)
sp4j1	8.7	3.7
sp4j2	12.3	1.6
sp4j3	13.1	1.5
sp4j4	13.5	3.3
sp4j5	14.5	2.8
sp4j6	15.8	1.4
sp4j7	16.9	2.1
sp4j8	18.4	5.2
sp4j9	22.0	1
sp4j10	23.0	10.4

Fraction sp4k (56.6 mg) was subjected to reversed-phase HPLC to yield eight fractions (Table 109), among which fractions sp4k7 and sp4k8 were identified as metabolites **SP-04** and **SP-03**, respectively.

Table 109. Experimental details for the separation of fraction sp4k.

Chromatographic conditions	
Column	Kromasil 100 C_{18} (250 mm × 8 mm i.d.)
Mobile phase	MeOH 100%, 1.5 mL/min

Fraction	Retention time (min)	Weight (mg)
sp4k1	7.2	1.8
sp4k2	7.9	11.5
sp4k3	9.7	6.6
sp4k4	12.3	3.2
sp4k5	13.3	2.7
sp4k6	14.0	4.5
sp4k7	18.6	1.1
sp4k8	23.2	3.9

Fraction sp4k4 (3.2 mg) was subjected to reversed-phase HPLC to yield two fractions (

Table **110**), among which fraction sp4k4b was identified as metabolite **SP-28**.

Table 110. Experimental details for the separation of fraction sp4k4.

Chromatographic conditions	
Column	Kromasil 100 C_{18} (250 mm × 8 mm i.d.)
Mobile phase	MeOH/H_2O 97:3%, 1.5 mL/min

Fraction	Retention time (min)	Weight (mg)
sp4k4a	8.0	1.0
sp4k4b	18.2	1.1

Fraction sp4l (25.5 mg) was subjected to reversed-phase HPLC to yield eight fractions (Table 111).

Table 111. Experimental details for the separation of fraction sp 4l.

Chromatographic conditions	
Column	Kromasil 100 C_{18} (250 mm × 8 mm i.d.)
Mobile phase	MeOH 100%, 1.5 mL/min

Fraction	Retention time (min)	Weight (mg)
sp4l1	7.5	1.3
sp4l2	8.5	2.1
sp4l3	9.6	1.0
sp4l4	9.8	3.1
sp4l5	10.9	1.0
sp4l6	12.5	0.8
sp4l7	12.9	0.7
sp4l8	13.7	0.7

Fraction sp4l4 (3.1 mg) was subjected to reversed-phase HPLC to yield four fractions (Table 112).

Table 112. Experimental details for the separation of fraction sp4l4.

Chromatographic conditions	
Column	Kromasil 100 C_{18} (250 mm × 8 mm i.d.)
Mobile phase	MeOH/H_2O 98:2%, 1.5 mL/min

Fraction	Retention time (min)	Weight (mg)
sp4l4a	7.9	1.5
sp4l4b	12.1	0.1
sp4l4c	12.5	0.6
sp4l4d	13.1	0.2

Fractions sp4k3 and sp4l4c, pooled together in one fraction thereafter designated as sp4k3 (7.2 mg), were further subjected to reversed-phase HPLC to yield three

fractions (Table 113), among which fractions sp4k3b and sp4k3c were identified as metabolites **SP-26** and **SP-27**, respectively.

Table 113. Experimental details for the separation of fraction sp4k3.

Chromatographic conditions	
Column	Kromasil 100 C_{18} (250 mm × 8 mm i.d.)
Mobile phase	MeOH/H_2O 97:3%, 1 mL/min

Fraction	**Retention time (min)**	**Weight (mg)**
sp4k3a	11.6	1.0
sp4k3b	19.0	4.0
sp4k3c	19.9	2.2

Fraction sp5 (251.6 mg) was further fractionated by normal-phase gravity column chromatography, using cHex with increasing amounts of Acetone as the mobile phase, to afford 56 fractions of approx. 25 mL each, which after an initial screening with TLC were combined into 9 fractions (Table 114), among which fraction sp5f was identified as metabolite **SP-01**.

Table 114. Experimental details for the separation of fraction sp5.

Fraction	**Mobile phase**			**Volume (mL)**
	cHex %	**Acetone %**	**EtOAc %**	
sp5a	85	15	-	200
sp5b	80	20	-	150
sp5c	80	20	-	75
sp5d	80	20	-	100
sp5e	80	20	-	150
	78	22	-	50
sp5f	78	22	-	25
sp5g	78	22	-	200
sp5h	78	22	-	100
	75	25	-	100
sp5i	70	30	-	100
	-	-	100	150

Fraction sp5c (55.1 mg) was subjected to reversed-phase HPLC to yield five fractions (Table 115), among which fraction sp5c5 was identified as metabolite **SP-03**.

Table 115. Experimental details for the separation of fraction sp5c.

Chromatographic conditions	
Column	Kromasil 100 C_{18} (250 mm × 8 mm i.d.)
Mobile phase	MeOH 100%, 1.5 mL/min

Fraction	Retention time (min)	Weight (mg)
sp5c1	7.2	1.2
sp5c2	14.4	4.4
sp5c3	17.7	2.4
sp5c4	19.2	7.4
sp5c5	24.0	17.5

Fraction sp5c4 (7.4 mg) was subjected to reversed-phase HPLC to yield four fractions (Table 116), among which fractions sp5c4c and sp5c4d were identified as metabolites **SP-04** and **SP-29**, respectively.

Table 116. Experimental details for the separation of fraction sp5c4.

Chromatographic conditions	
Column	Kromasil 100 C_{18} (250 mm × 8 mm i.d.)
Mobile phase	MeOH/H_2O 97:3%, 1.5 mL/min

Fraction	Retention time (min)	Weight (mg)
sp5c4a	8.0	0.5
sp5c4b	30.2	0.9
sp5c4c	31.1	1.7
sp5c4d	32.3	2

Fraction sp5e (23.5 mg) was subjected to reversed-phase HPLC to yield eight fractions (Table 117), among which fraction sp5e7 was identified as metabolite **SP-01**.

Table 117. Experimental details for the separation of fraction sp5e.

Chromatographic conditions	
Column	Kromasil 100 C_{18} (250 mm × 8 mm i.d.)
Mobile phase	MeOH 100%, 1.5 mL/min

Fraction	Retention time (min)	Weight (mg)
sp5e1	7.9	0.7
sp5e2	8.6	0.8
sp5e3	9.3	1.2
sp5e4	10.6	0.2
sp5e5	10.9	1.6
sp5e6	13.8	1.4
sp5e7	15.2	5.3
sp5e8	16.7	1.4

Fraction sp5g (36.1 mg) was subjected to reversed-phase HPLC to yield four fractions (Table 118), among which fraction sp5g3 was identified as metabolite **SP-01**.

Table 118. Experimental details for the separation of fraction sp5g.

Chromatographic conditions	
Column	Kromasil 100 C_{18} (250 mm × 8 mm i.d.)
Mobile phase	MeOH 100%, 1.5 mL/min

Fraction	Retention time (min)	Weight (mg)
sp5g1	8.2	5.6
sp5g2	12.9	3.4
sp5g3	14.5	21.2
sp5g4	16.3	0.9

Fractions sp5e8 and sp5g4, pooled together in one fraction thereafter designated as sp5e8 (2.3 mg), were further subjected to reversed-phase HPLC to yield three fractions (Table 119), among which fraction sp5e8c was identified as metabolite **SP-06**.

Table 119. Experimental details for the separation of fraction sp5e8.

Chromatographic conditions	
Column	Kromasil 100 C_{18} (250 mm × 8 mm i.d.)
Mobile phase	MeOH 100%, 1.5 mL/min

Fraction	Retention time (min)	Weight (mg)
sp5e8a	7.9	0.5
sp5e8b	14.8	0.4
sp5e8c	16.2	1.0

Fraction sp6 (434.0 mg) was further fractionated by normal-phase gravity column chromatography, using cHex with increasing amounts of Acetone as the mobile phase, to afford 81 fractions of approx. 25 mL each, which after an initial screening with TLC were combined into 11 fractions (Table 120), among which fractions sp6g and sp6h were identified as metabolite **SP-01**.

Table 120. Experimental details for the separation of fraction sp6.

Fraction	Mobile phase		Volume (mL)
	cHex %	Acetone %	
sp6a	90	10	250
sp6b	90	10	275
sp6c	85	15	500
sp6d	80	20	100
sp6e	75	25	150
sp6f	75	25	125

sp6g	70	30	50
sp6h	70	30	125
sp6i	70	30	50
	65	35	50
sp6j	65	35	50
	60	40	100
sp6k	50	50	100
	0	100	100

Fraction sp6f (24.9 mg) was subjected to reversed-phase HPLC to yield eight fractions (Table 121).

Table 121. Experimental details for the separation of fraction sp6f.

Chromatographic conditions	
Column	Kromasil 100 C_{18} (250 mm × 8 mm i.d.)
Mobile phase	MeOH 100%, 1.5 mL/min

Fraction	**Retention time (min)**	**Weight (mg)**
sp6f1	8.0	1.4
sp6f2	11.9	4.4
sp6f3	13.8	1.2
sp6f4	14.7	1.1
sp6f5	15.2	3.8
sp6f6	15.9	1.3
sp6f7	16.8	1.9
sp6f8	17.5	1.2

Fraction sp6f7 (1.9 mg) was subjected to reversed-phase HPLC to yield two fractions (Table 122), among which fraction sp6f7b was identified as metabolite **SP-06**.

Table 122. Experimental details for the separation of fraction sp6f7.

Chromatographic conditions	
Column	Kromasil 100 C_{18} (250 mm × 8 mm i.d.)
Mobile phase	MeOH/H_2O 97:3%, 1.5 mL/min

Fraction	**Retention time (min)**	**Weight (mg)**
sp6f7a	8.0	0.5
sp6f7b	27.5	0.9

Fraction sp7 (144.4 mg) was further fractionated by normal-phase vacuum column chromatography, using cHex with increasing amounts of EtOAc, followed by EtOAc with increasing amounts of MeOH as the mobile phase, to afford 12 fractions, which after an initial screening with TLC were combined into 7 fractions (Table 123).

Table 123. Experimental details for the separation of fraction sp7.

Fraction	Mobile phase			Volume (mL)
	cHex %	EtOAc %	MeOH %	
sp7a	50	50	-	400
	40	60	-	200
sp7b	30	70	-	200
	20	80	-	200
sp7c	15	85	-	200
	10	90	-	200
sp7d	5	95	-	200
	0	100	-	200
sp7e	-	99	1	200
	-	98	2	200
sp7f	-	98	2	200
sp7g	-	95	5	200

Fraction sp7e (33.6 mg) was subjected to reversed-phase HPLC to yield six fractions (Table 124), among which fraction sp7e5 was identified as metabolite **SP-07**.

Table 124. Experimental details for the separation of fraction sp7e.

Chromatographic conditions	
Column	Kromasil 100 C_{18} (250 mm × 8 mm i.d.)
Mobile phase	MeOH 100%, 1.5 mL/min

Fraction	Retention time (min)	Weight (mg)
sp7e1	6.9	2.4
sp7e2	9.9	8.9
sp7e3	12.6	2.3
sp7e4	13.4	1.1
sp7e5	14.5	6.9
sp7e6	17.1	0.9

Fraction sp7g (39.7 mg) was subjected to reversed-phase HPLC to yield five fractions (Table 125), among which fraction sp7g4 was identified as metabolite **SP-17**.

Table 125. Experimental details for the separation of fraction sp7g.

Chromatographic conditions	
Column	Kromasil 100 C_{18} (250 mm × 8 mm i.d.)
Mobile phase	MeOH 100%, 1.5 mL/min

Fraction	Retention time (min)	Weight (mg)
sp7g1	6.9	6.0
sp7g2	10.7	1.5
sp7g3	11.6	0.8
sp7g4	13.4	3.1
sp7g5	14.2	3.3

Fraction sp7g5 (3.3 mg) was subjected to reversed-phase HPLC to yield three fractions (Table 126), among which fractions sp7g5b and sp7g5c were identified as metabolites **SP-17** and **SP-08**, respectively.

Table 126. Experimental details for the separation of fraction sp7g5.

Chromatographic conditions	
Column	Kromasil 100 C_{18} (250 mm × 8 mm i.d.)
Mobile phase	MeOH/H_2O 97:3%, 1.5 mL/min

Fraction	Retention time (min)	Weight (mg)
sp7g5a	8.0	0.5
sp7g5b	21.3	0.6
sp7g5c	23.1	2.0

Fraction sp8 (1.0 g) was further fractionated by normal-phase vacuum column chromatography, using cHex with increasing amounts of EtOAc, followed by EtOAc with increasing amounts of MeOH as the mobile phase, to afford 19 fractions, which after an initial screening with TLC were combined into 11 fractions (Table 127).

Table 127. Experimental details for the separation of fraction sp8.

Fraction	Mobile phase			Volume (mL)
	cHex %	EtOAc %	MeOH %	
sp8a	50	50	-	400
	40	60	-	200
	30	70	-	200
sp8b	20	80	-	200
	15	85	-	200
sp8c	10	90	-	200
sp8d	5	95	-	200
sp8e	-	100	-	200
	-	99	1	200
sp8f	-	98	2	200
sp8g	-	98	2	200
sp8h	-	95	5	200
	-	90	10	200
sp8i	-	80	20	200

sp8j	-	70	30	200
sp8k	-	60	40	200
	-	50	50	200
	-	-	100	200
	-	-	100	200

Fraction sp8g (34.0 mg) was subjected to reversed-phase HPLC to yield ten fractions (Table 128).

Table 128. Experimental details for the separation of fraction sp8g.

Chromatographic conditions	
Column	Kromasil 100 C_{18} (250 mm × 8 mm i.d.)
Mobile phase	MeOH 100%, 1.5 mL/min

Fraction	**Retention time (min)**	**Weight (mg)**
sp8g1	7.7	0.4
sp8g2	8.8	1.4
sp8g3	10.0	0.8
sp8g4	12.0	1.4
sp8g5	12.8	1.8
sp8g6	13.1	1.6
sp8g7	15.5	0.6
sp8g8	16.3	7.0
sp8g9	18.5	1.9
sp8g10	20.1	1.3

Fraction sp8g5 (1.8 mg) was subjected to reversed-phase HPLC to yield three fractions (Table 129), among which fraction sp8g5c was identified as metabolite **SP-19**.

Table 129. Experimental details for the separation of fraction sp8g5.

Chromatographic conditions	
Column	Kromasil 100 C_{18} (250 mm × 8 mm i.d.)
Mobile phase	MeOH/H_2O 97:3%, 1.5 mL/min

Fraction	**Retention time (min)**	**Weight (mg)**
sp8g5a	8.0	0.6
sp8g5b	16.6	0.4
sp8g5c	23.0	0.5

Fraction sp8g8 (7.0 mg) was subjected to reversed-phase HPLC to yield four fractions (

Table **130**), among which fraction sp8g8d was identified as metabolite **SP-19**.

Table 130. Experimental details for the separation of fraction sp8g8.

Chromatographic conditions	
Column	Kromasil 100 C_{18} (250 mm × 8 mm i.d.)
Mobile phase	MeOH/H_2O 97:3%, 1.5 mL/min

Fraction	Retention time (min)	Weight (mg)
sp8g8a	8.0	0.6
sp8g8b	16.3	0.6
sp8g8c	21.6	2.3
sp8g8d	24.0	0.2

Fractions sp9 and sp10, pooled together in one fraction thereafter designated as sp9 (200 mg), were further fractionated by normal-phase vacuum column chromatography, using cHex with increasing amounts of EtOAc, followed by EtOAc with increasing amounts of MeOH as the mobile phase, to afford 12 fractions, which after an initial screening with TLC were combined into 11 fractions (Table 131).

Table 131. Experimental details for the separation of fraction sp9.

Fraction	Mobile phase			Volume (mL)
	cHex %	EtOAc %	MeOH %	
sp9a	10	90	-	400
sp9b	5	95	-	200
sp9c	-	100	-	200
sp9d	-	99	1	200
sp9e	-	98	2	200
sp9f	-	98	2	200
sp9g	-	95	5	200
sp9h	-	90	10	200
	-	50	50	200
sp9i	-	-	100	200
sp9j	-	-	100	200
sp9k	-	-	100	200

Fraction sp9f (15.8 mg) was subjected to reversed-phase HPLC to yield four fractions (Table 132), among which fraction sp9f4 was identified as metabolite **SP-19**.

Table 132. Experimental details for the separation of fraction sp9f.

Chromatographic conditions	
Column	Kromasil 100 C_{18} (250 mm × 8 mm i.d.)
Mobile phase	MeOH 100%, 1.5 mL/min

Fraction	Retention time (min)	Weight (mg)
sp9f1	7.7	1.0
sp9f2	8.4	3.1
sp9f3	9.4	2.8
sp9f4	16.3	1.4

Fraction sp9g (10.5 mg) was subjected to reversed-phase HPLC to yield four fractions (Table 133), among which fraction sp9g4 was identified as metabolite **SP-19**.

Table 133. Experimental details for the separation of fraction sp9g.

Chromatographic conditions	
Column	Kromasil 100 C_{18} (250 mm × 8 mm i.d.)
Mobile phase	MeOH 100%, 1.5 mL/min

Fraction	Retention time (min)	Weight (mg)
sp9g1	7.9	2.7
sp9g2	9.9	0.6
sp9g3	14.5	0.1
sp9g4	16.4	2.0

In total, from the chemical investigation of the organic extract of the soft coral *S. polydactyla*, 28 metabolites were isolated in pure form (Table 134).

Table 134. Isolated metabolites from the soft coral *S. polydactyla*.

Metabolite	Code	Fraction	Weight (mg)
34	SP-31	sp3e10c3	0.7
35	SP-30	sp3e10c2	0.3
36	SP-16	sp2f5b6	9.1
37	SP-15	sp2f5b7	8.8
38	SP-13	sp2f7k, sp2f7l2, sp2f8j, sp2f9g	11.4
39	SP-14	sp2f7l3, sp2f8k, sp2f9k	9.1
40	SP-21	sp3e5b, sp3f6b	8.2
41	SP-20	sp2f8e2	0.5
42	SP-09	sp3g8d, sp3h9d, sp3h10b, sp4g3, sp4g4b, sp4h6, sp4h7b	26.9
43	SP-23	sp3g9c, sp3h10c, sp4g4c, sp4h7d	17.0
44	SP-26	sp3h3b, sp4k3b	4.6
45	SP-27	sp4k3c	2.2
46	SP-25	sp4h2c	1.3
47	SP-28	sp4k4b	1.1
48	SP-05	sp4i4	9.4
49	SP-24	sp3h11c2d, sp4h8d3	2.6

50	SP-02	sp2f6, sp2f7f, sp2f8g	232.9
51	SP-04	sp4i6, sp4j8, sp4k7, sp5c4c	11.9
52	SP-03	sp4i8, sp4j10, sp4k8, sp5c5	42.3
53	SP-29	sp5c4d	2.0
54	SP-19	sp8g5c, sp8g8d, sp9f4, sp9g4	4.1
55	SP-01	sp5f, sp5e7, sp5g3, sp6g, sp6h	155.4
56	SP-06	sp5e8c, sp6f7b	1.9
57	SP-07	sp7e5	6.9
58	SP-17	sp7g4, sp7g5b	3.7
59	SP-08	sp7g5c	2.0
	SP-18	sp3f8d	2.2
	SP-22	sp3g8d	0.8

2.7 Evaluation of the biological activity of some of the isolated compounds

2.7.1 Cell Culture

The tested compounds were dissolved in DMSO to afford 10 mM stock solutions. Human cervical carcinoma (HeLa) and human breast adenocarcinoma (MCF7) cell lines were purchased from European Collection of Authenticated Cell Cultures (ECACC, Salisbury, UK) and cultivated in Dulbecco's Modified Eagle Medium (DMEM) (Merck, Darmstadt, Germany), as previously reported (Rárová et al., 2016). Human umbilical vein endothelial cells (HUVECs) were a kind gift of Prof. Jitka Ulrichová (Faculty of Medicine and Dentistry, Palacky University, Olomouc). The cultivation and assay was performed in Endothelial Cell Proliferation Medium (ECPM, Provitro, Berlin, Germany) (Rárová et al., 2018). The 22Rv1-ARE14 reporter cell line (Bartonkova et al., 2015) was a generous gift of Prof. Zdeněk Dvořák (Department of Cell Biology and Genetics, Palacký University). The 22Rv1-ARE14 cell line was grown in Roswell Park Memorial Institute 1640 Medium (RPMI 1640) (Jorda et al., 2019). All cells were maintained in a humidified CO_2 incubator at 37 °C using the standard trypsinization procedure twice or three times a week. The SH-SY5Y human neuroblastoma cell line (ECACC, Salisbury, UK) was cultivated in DMEM and Ham's F12 Nutrient Mixture (DMEM:F12, 1:1), as previously described (Colle et al., 2016). Cells were used up to twenty passages. All trans-retinoic acid (10 μM) in 1% FBS DMEM/F12 medium was added to SH-SY5Y cells to achieve differentiation conditions (Cheung et al., 2009; Dwane et al., 2013) to reach longer neurites and reduced proliferation (48 h). All cells were maintained in a humidified CO_2 incubator at 37 °C using the standard trypsinization procedure twice or three times a week.

2.7.2 Evaluation of cytotoxicity

In cytotoxicity assays, cancer cells were treated with six different concentrations of each tested compound for 72 h. Cells were stained with resazurin and IC_{50} values

were calculated as previously reported (Dengler et al., 1995). Triplicates from at least three independent experiments were used. For the ELAM assay, the Calcein AM (Molecular Probes, Invitrogen, Karlsruhe, Germany) cytotoxicity assay, which assessed HUVEC viability after 4 h treatment, was used as previously described (Morrogh-Bernard et al., 2017).

2.7.3 Cell-surface ELISA CD62E (E-Selectin, ELAM)

An enzyme-linked immunosorbent assay (ELISA) was used to detect the levels of the cell adhesion molecule ELAM in HUVEC cells after 30 min of incubation with the tested compounds and 4 h of stimulation with TNFα, as previously described (Morrogh-Bernard et al., 2017).

2.7.4 Migration scratch assay

The scratch test was performed with HUVEC cells and evaluated after 20 h of treatment, as previously reported (Rárová et al., 2018).

2.7.5 AR-Transcriptional reporter aAssay

AR-transcriptional reporter assays were performed on 22Rv1-ARE14 cells after 24 h of incubation, as previously described (Jorda et al., 2019).

2.7.6 SH-SY5Y cell treatments and evaluation of cell viability/cytotoxicity

Cell viability of neuron-like SH-SY5Y cells growing in 96-well plates (7,000 cells/well) 24 h after treatment was evaluated using the Calcein AM assay (Rárová et al., 2016), with minor modification of Calcein AM concentration (0.75 μM). Cell death of SH-SY5Y cells (20,000 cells/well) was determined using the propidium iodide (PI) assay according to Stone et al. with a slight modification (Stone et al., 2003). Briefly, PI solution in PBS is added to cell medium to reach concentration 1 μg/mL, incubated for 15 min. at room temperature and quantified at 535/617 nm (excitation/emission) by Infinite M200 Pro reader (Tecan, Austria). The resulting fluorescence of 3-NPA toxin was considered as 100% cell death. In the assays, neuron-like cells were treated with the tested compounds in 0.1–10 μM concentration range for 48 h. DMSO treated cells (≤0.1% v/v) were used as healthy controls.

2.7.7 Statistical analysis

All data are expressed as mean ± SD or SEM. Data were evaluated by non-parametric Kruskal–Wallis test followed by post-hoc Mann–Whitney test with sequential Bonferroni correction of *p*-values or ANOVA followed by Tukey's multiple

comparison test (Figure 5) using the PAST (version 1.97) software package (Hammer et al., 2001). *P*-values < 0.05 were considered statistically significant.

3. RESULTS AND DISCUSSION

The aim of the present PhD thesis was to investigate the chemical profile of marine organisms from the Red Sea. Following an initial screening, the organic extracts of the red alga *Laurencia majuscula*, of a sponge belong to the genus *Lamellodysidea* and of the soft coral *Sinularia polydactyla* exhibited interesting chemical profiles and were selected for in depth chemical analysis.

Fresh algal tissues of the red alga *L. majuscula* collected by SCUBA diving from the coastline of Hurghada at the Egyptian Red Sea at a depth of 4-6 m in June 2015 were extracted with mixtures of organic solvents. The obtained organic extract was subjected to a series of chromatographic separations that led to the isolation of 25 secondary metabolites, among which **1**-**22** were identified on the basis of their spectroscopic data.

The chemical investigation of the organic extract of the marine sponge *Lamellodysidea* sp. collected from the coral reef of Thuwal in the Saudi Arabian Red Sea afforded 11 compounds (**23**-**33**).

A series of normal and reversed-phase chromatographic separations of the organic extract of the soft coral *S. polydactyla* collected from the Egyptian Red Sea coastline at Hurghada at a depth of 10 m allowed for the isolation of 28 compounds, 26 of which (**34**-**59**) were identified after extensive analysis of their NMR and MS data.

The identification of isolated metabolites was based on the analysis of their spectroscopic data (mainly NMR and MS) and their comparison with data from similar preciously reported structures.

3.1 Identification and structure elucidation of isolated metabolites from the red alga *Laurencia majuscula*

3.1.1 Metabolite 1

Metabolite **1** (LMH12) was isolated after a series of chromatographic separations as a colorless oil (5.2 mg).

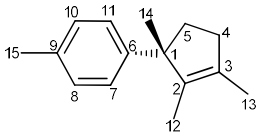

The mass spectrum of metabolite **1** (Figure 15) exhibited a molecular ion peak $[M]^+$ at *m/z* 200, as well as fragment ion peaks at *m/z* 185 and 170, corresponding to $[M\text{-}CH_3]^+$ and $[M\text{-}2CH_3]^+$, respectively.

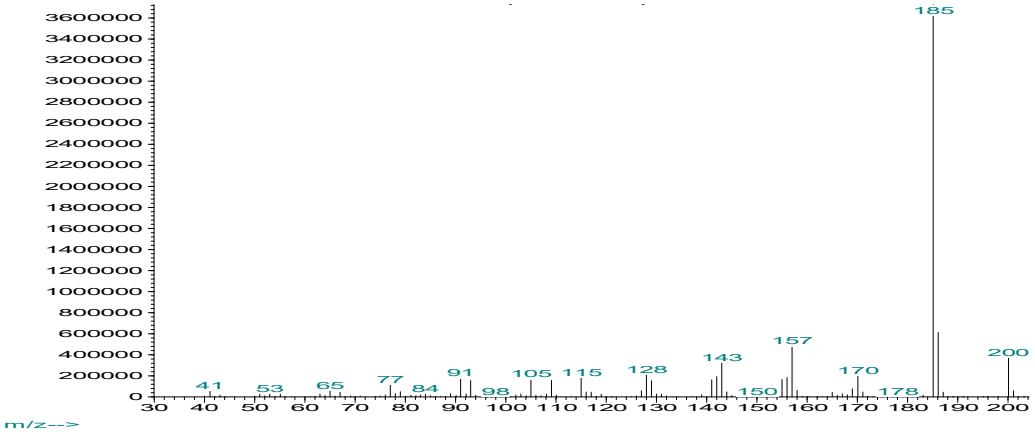

Figure 15. Mass spectrum (EIMS) of metabolite **1**.

In the ^{1}H NMR spectrum of metabolite **1** (Figure 16) obvious were:

- One aliphatic methyl on a non-protonated carbon at δ 1.35,
- Two olefinic methyls at δ 1.38 and 1.70,
- One aromatic methyl at δ 2.30, and
- Two doublets at δ 7.08 and 7.11 integrating for two protons each and attributed to four aromatic protons.

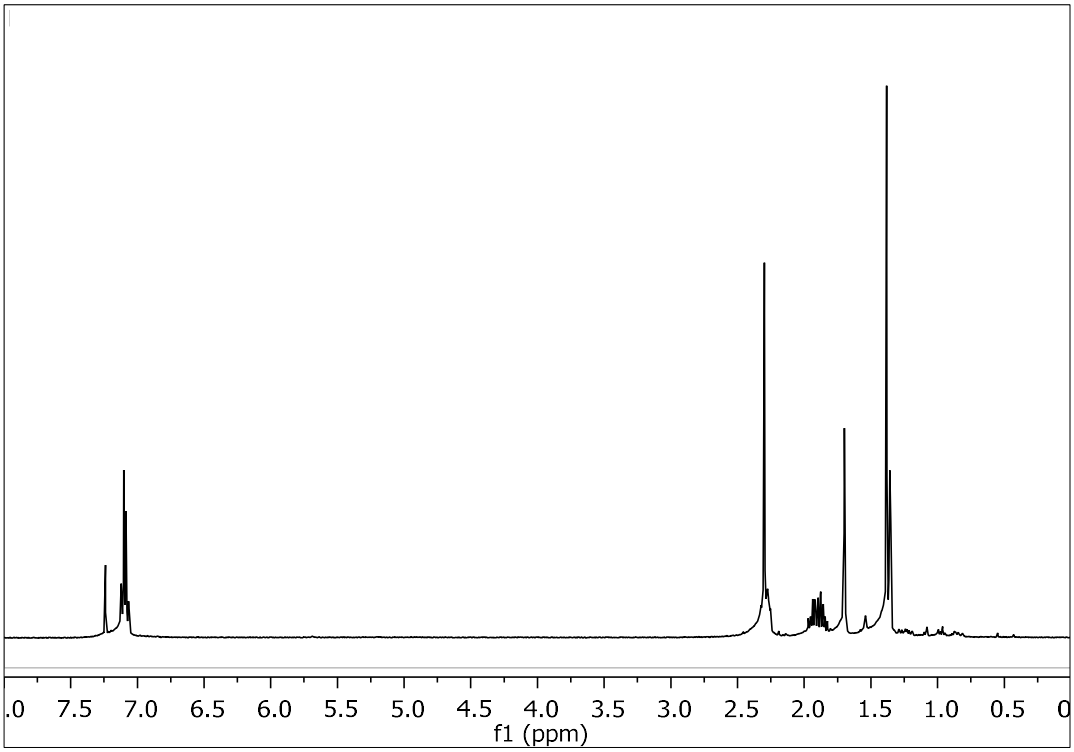

Figure 16. ^{1}H NMR spectrum of metabolite **1**.

Analysis of the NMR and MS data of **1** led to the molecular formula $C_{15}H_{20}$. Taking into account the four carbon-carbon double bonds as four of the six degrees of unsaturation, the molecular structure of **1** was determined as bicyclic.

Comparison of the spectroscopic and physical characteristics of metabolite **1** with those reported in the literature led to its identification as isolaurene, previously isolated from the alga *L. okamurai* (Suzuki & Kurosawa, 1979) and synthetically prepared (Takeshita et al., 1984). The ^{1}H NMR data of metabolite **1** are reported in Table 135.

Table 135. ^{1}H NMR data of metabolite **1** in $CDCl_3$ (δ in ppm, J in Hz).

Position	$\boldsymbol{\delta_{H,exp}}$	$\boldsymbol{\delta_{H,lit}}$
7	7.08 (d, 8.2)	7.07 (s)
8	7.11 (d, 8.2)	7.07 (s)
10	7.11 (d, 8.2)	7.07 (s)
11	7.08 (d, 8.2)	7.07 (s)
12	1.38 (s)	1.39 (s)
13	1.70 (s)	1.71 (s)
14	1.35 (s)	1.37 (s)
15	2.30 (s)	2.30(s)

3.1.2 Metabolite 2

Metabolite **2** (LMH-17) was isolated after a series of chromatographic separations as a colorless oil (3.3 mg).

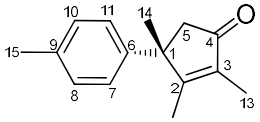

The mass spectrum of metabolite **2** (Figure 17) exhibited a molecular ion peak $[M]^+$ at *m/z* 214, as well as a fragment ion peak at *m/z* 199 corresponding to $[M\text{-}CH_3]^+$.

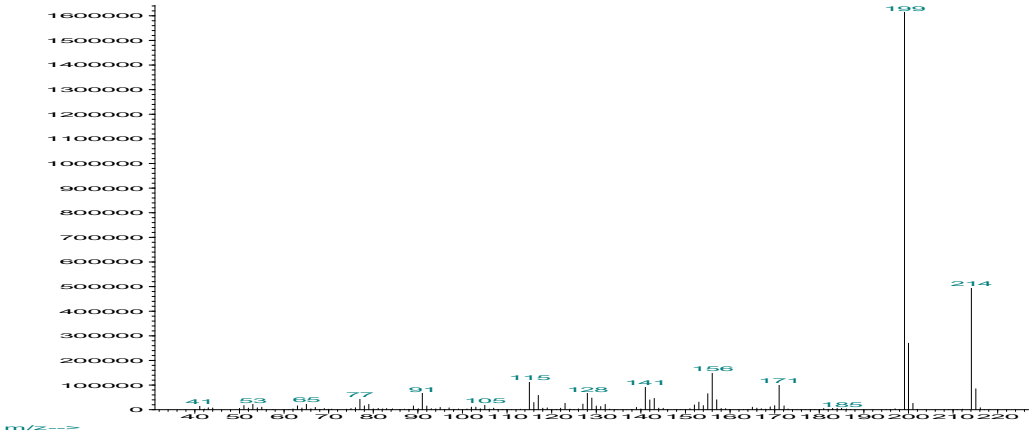

Figure 17. Mass spectrum (EIMS) of metabolite **2**.

In the ^{1}H NMR spectrum of metabolite **2** (Figure 18) obvious were:

- One aliphatic methyl on a non-protonated carbon at δ 1.56,
- Two olefinic methyls at δ 1.71 and 1.76,
- One aromatic methyl at δ 2.30, and
- Two doublets at δ 7.04 and 7.10 integrating for two protons each and attributed to four aromatic protons.

Analysis of the NMR and MS data of **2** led to the molecular formula $C_{15}H_{18}O$. Taking into account the four carbon-carbon double bonds and the carbonyl moiety as five of the seven degrees of unsaturation, the molecular structure of **2** was determined as bicyclic.

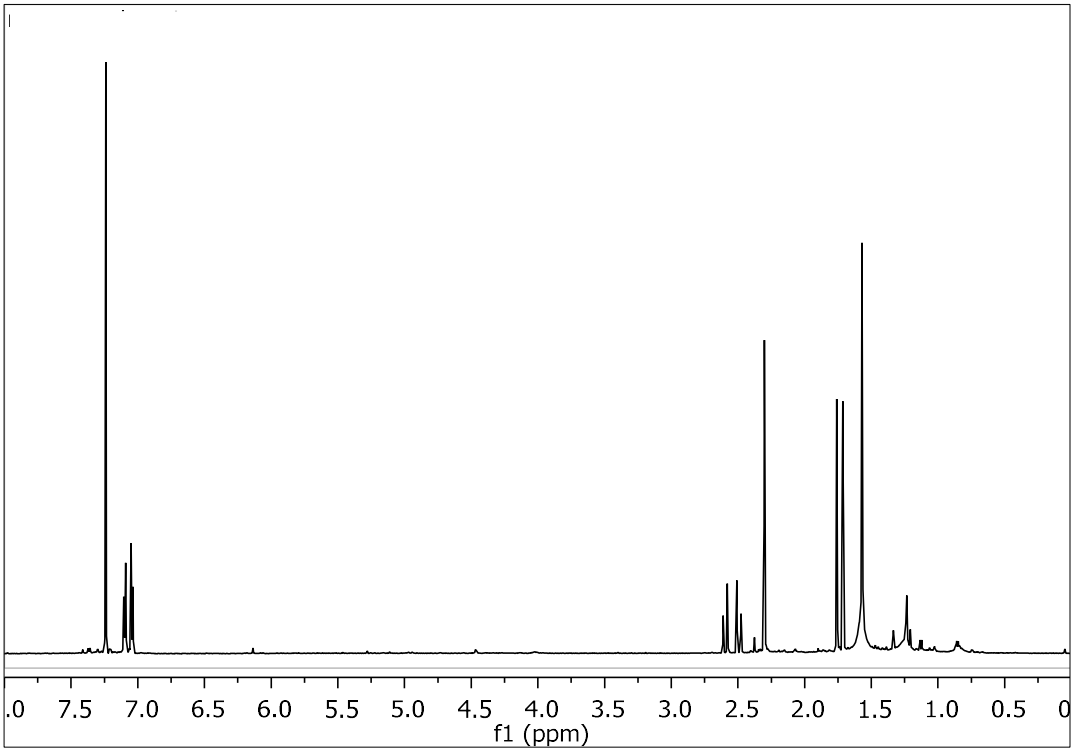

Figure 18. ^{1}H NMR spectrum of metabolite **2**.

The planar structure of metabolite **2** was determined on the basis of the homonuclear and heteronuclear correlations (Figure 19) observed in the HSQC-DEPT (Figure 20), HMBC (Figure 21) and COSY (Figure 22) spectra. In particular, the position of Me-14 on C-1 was confirmed by the HMBC correlations of Me-14 (δ_H 1.56) with C-1 (δ_C 47.8), C-5 (δ_C 53.3) and the aromatic carbon C-6 (δ_C 142.0). The correlations of Me-12 (δ_H 1.71) with C-1, C-2 (δ_C 176.2) and C-3 (δ_C 135.5) and of Me-13 (δ_H 1.76) with C-2, C-3 and C-4 (δ_C 208.6) secured the position of Me-12 on C-2 and Me-13 on C-3. Additionally, the presence of the two doublets at δ 7.04 and 7.10 integrating for two protons each indicated a *para*-substituted aromatic ring.

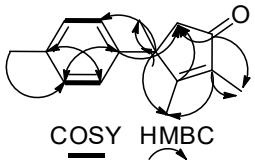

Figure 19. COSY and important HMBC correlations observed for metabolite **2**.

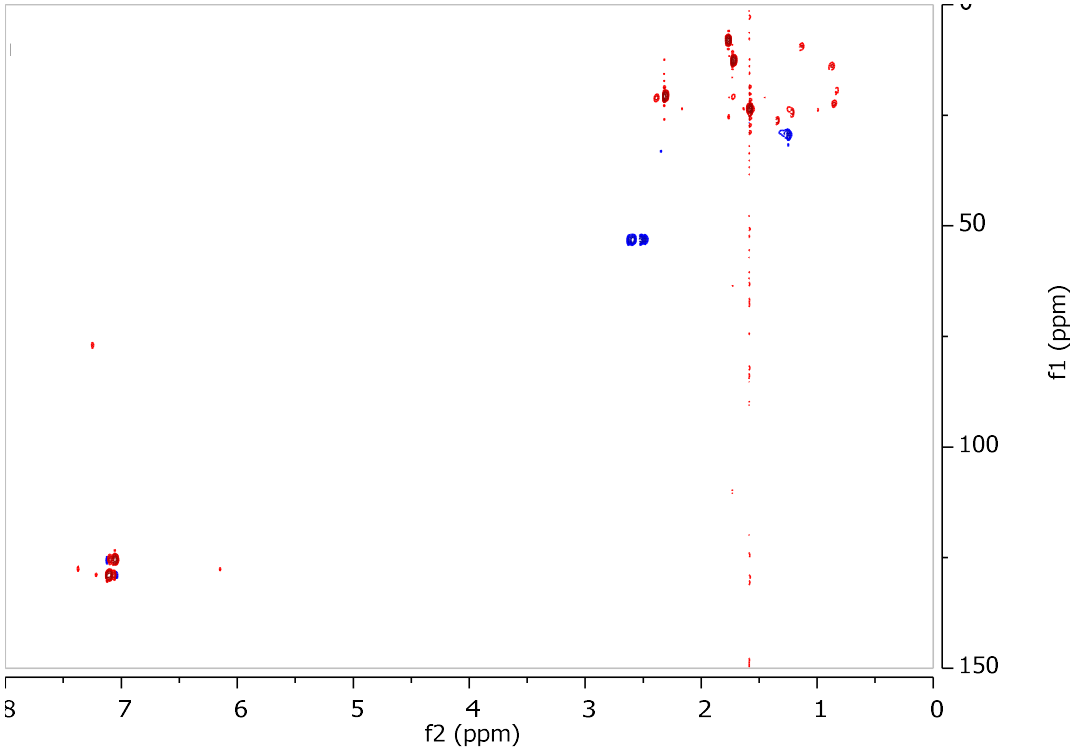

Figure 20. HSQC-DEPT spectrum of metabolite **2**.

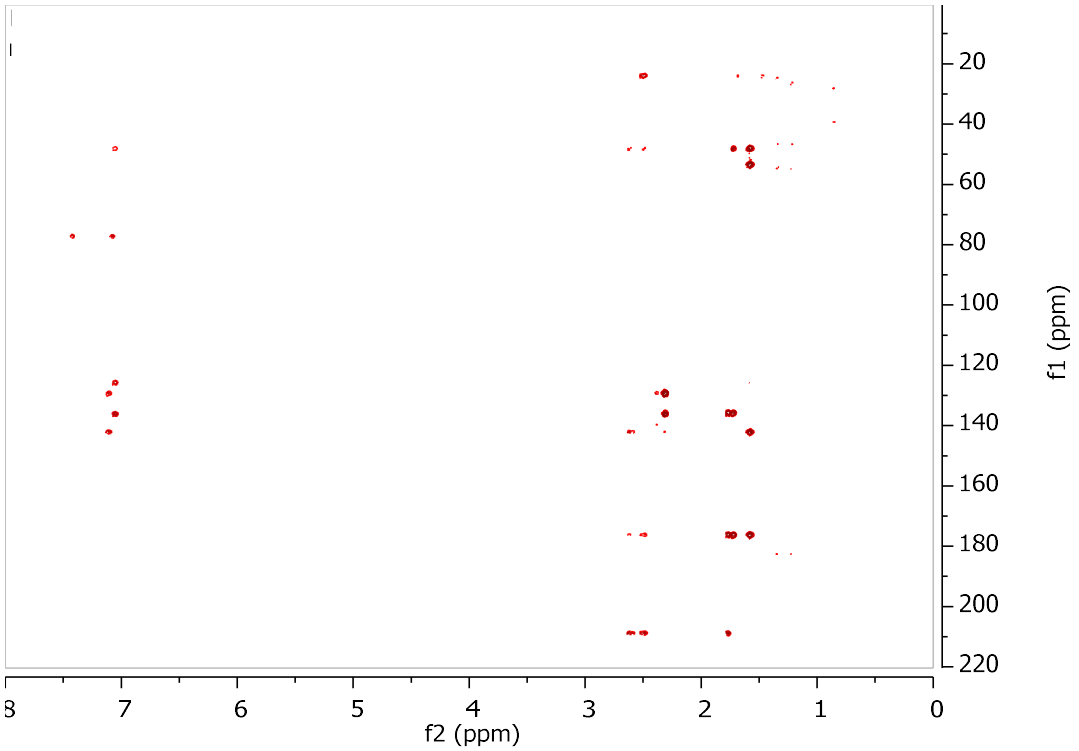

Figure 21. HMBC spectrum of metabolite **2**.

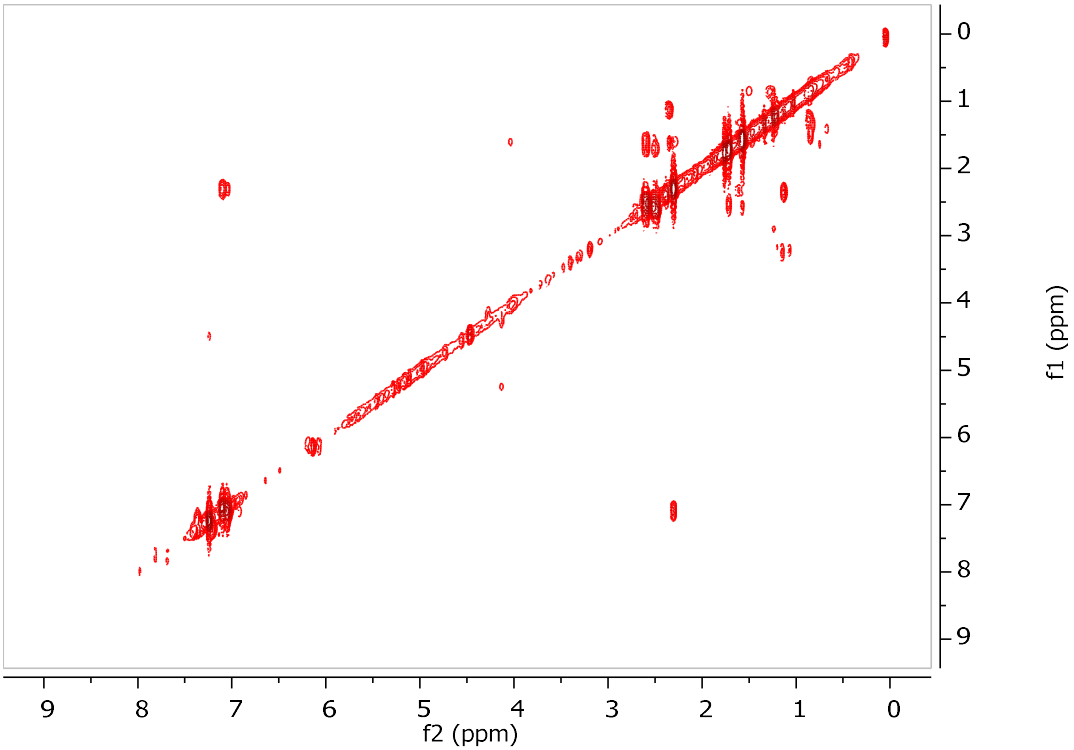

Figure 22. COSY spectrum of metabolite **2**.

Comparison of the spectroscopic and physical characteristics of metabolite **2** with those reported in the literature led to its identification as a new natural product, which was designated as 4-oxo-isolaurene. The NMR data of metabolite **2** are reported in Table 136.

Table 136. ^{1}H and ^{13}C NMR data of metabolite **2** in $CDCl_3$ (δ in ppm, J in Hz).

Position	δ_C	δ_H
1	48.3	-
2	176.2	-
3	135.5	-
4	208.6	-
5	53.5	2.60 (d, 18.7), 2.49 (d, 18.7)
6	142.0	-
7	129.3	7.04 (d, 8.1)
8	129.3	7.10 (d, 8.1)
9	135.9	-
10	125.5	7.10 (d, 8.1)
11	125.5	7.04 (d, 8.1)
12	12.7	1.71 (s)
13	8.2	1.76 (s)
14	23.8	1.56 (s)
15	20.9	2.30 (s)

3.1.3 Metabolite 3

Metabolite **3** (LMH13) was isolated after a series of chromatographic separations as a colorless oil (3.4 mg).

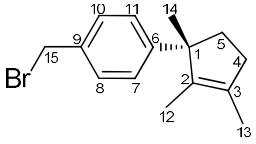

The mass spectrum of metabolite **3** (Figure 23) exhibited a molecular ion peak $[M]^+$ at *m/z* 278 with an isotopic ion peak at *m/z* 280 in a 1:1 ion intensity, indicating the presence of a bromine atom in the molecule, as well as fragment ion peaks at *m/z* 263 and 265, corresponding to $[M\text{-}CH_3]^+$.

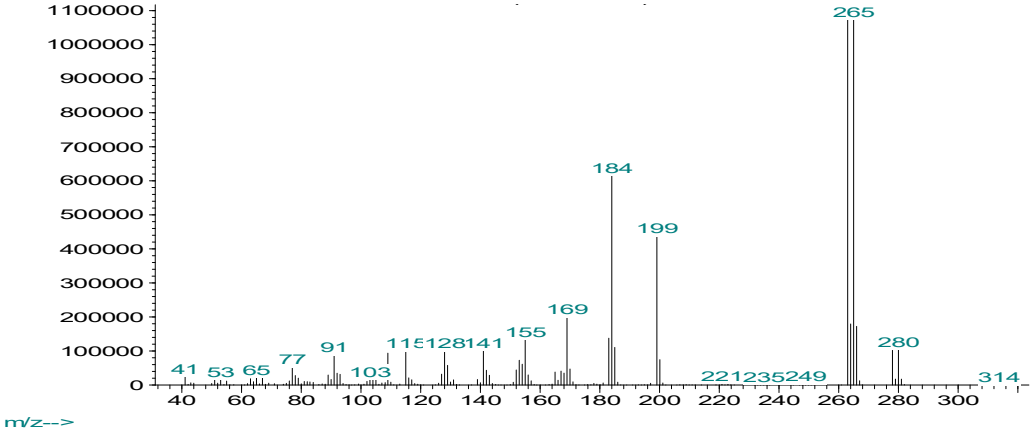

Figure 23. Mass spectrum (EIMS) of metabolite **3**.

In the ^{1}H NMR spectrum of metabolite **3** (Figure 24) obvious were:

- One aliphatic methyl on a non-protonated carbon at δ 1.38,
- Two olefinic methyls at δ 1.35 and 1.68,
- One singlet at δ 4.46 integrating for two protons and attributed to an aromatic halogenated methylene, and
- Two doublets at δ 7.18 and 7.28 integrating for two protons each and attributed to four aromatic protons.

Analysis of the NMR and MS data of **3** led to the molecular formula $C_{15}H_{19}Br$. Taking into account the four carbon-carbon double bonds as four of the six degrees of unsaturation, the molecular structure of **3** was determined as bicyclic.

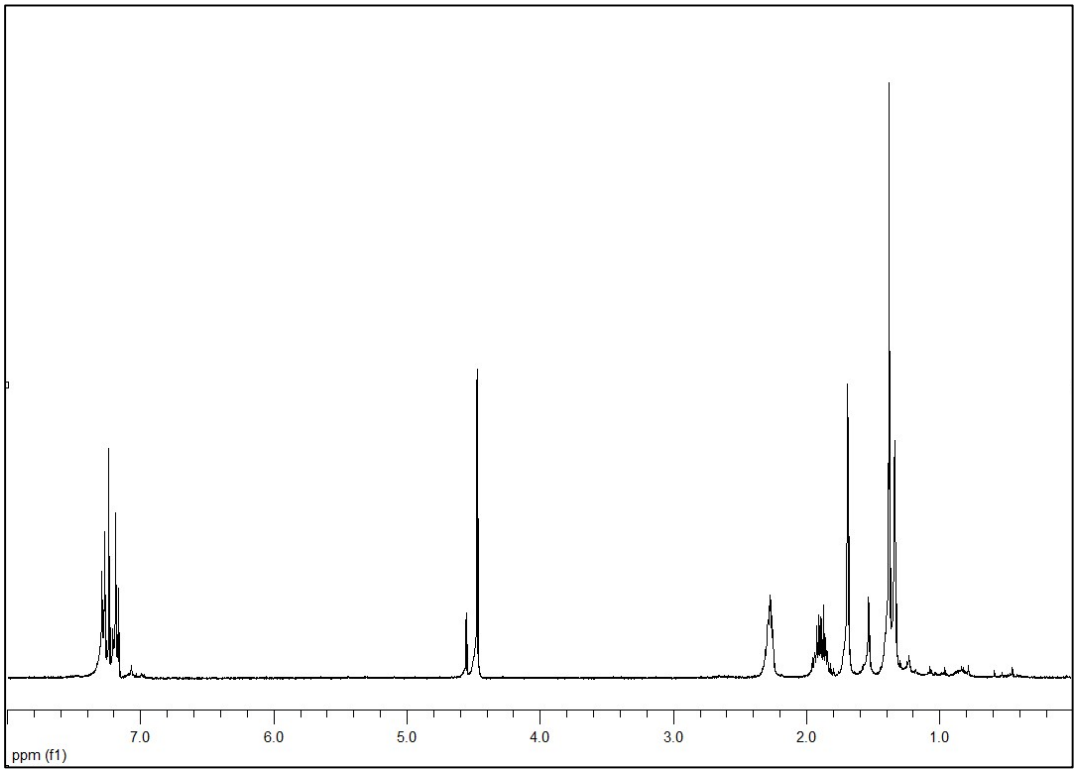

Figure 24. ^{1}H NMR spectrum of metabolite **3**.

The planar structure of metabolite **3** was determined on the basis of the homonuclear and heteronuclear correlations (Figure 25) observed in the HSQC-DEPT (Figure 26), HMBC (Figure 27) and COSY (Figure 28) spectra. In particular, the position of Me-14 on C-1 was evident from the HMBC correlations of Me-14 (δ_H 1.38) with C-1 (δ_C 53.8), C-2 (δ_C 136.4) and C-6 (δ_C 150.1), while the correlations of Me-12 (δ_H 1.37) with C-1, C-2 and C-3 (δ_C 132.9), as well as of Me-13 (δ_H 1.70) with C-2, C-3 and C-4 (δ_C 35.8) secured the position of Me-12 and Me-13 at C-2 and C-3, respectively. The presence of a 1,4-disubstituted benzene ring was indicated by the two doublets at δ 7.18 and 7.28 integrating for four aromatic methines. The position of the brominated methylene at C-15 was confirmed by the correlations of H_2-15 with C-8/C-10 (δ_C 128.8) and C-9 (δ_C 133.0).

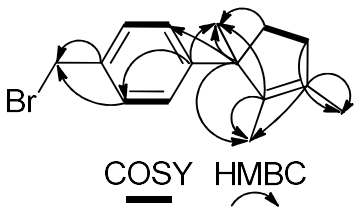

Figure 25. COSY and important HMBC correlations observed for metabolite **3**.

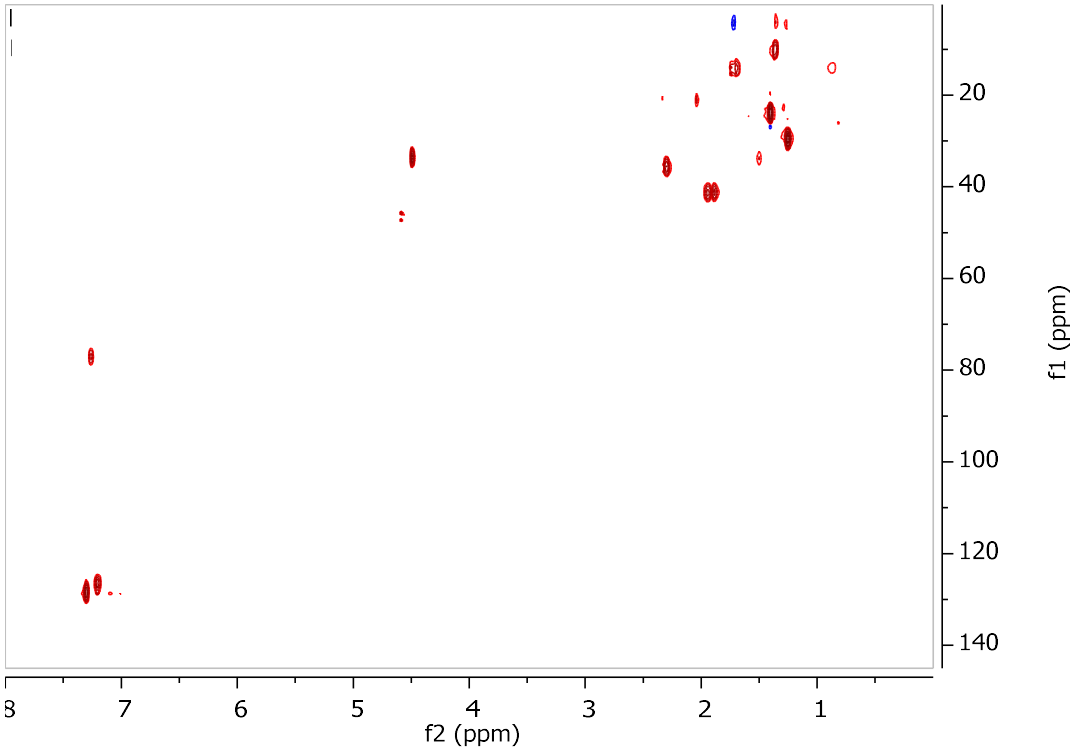

Figure 26. HSQC-DEPT spectrum of metabolite **3**.

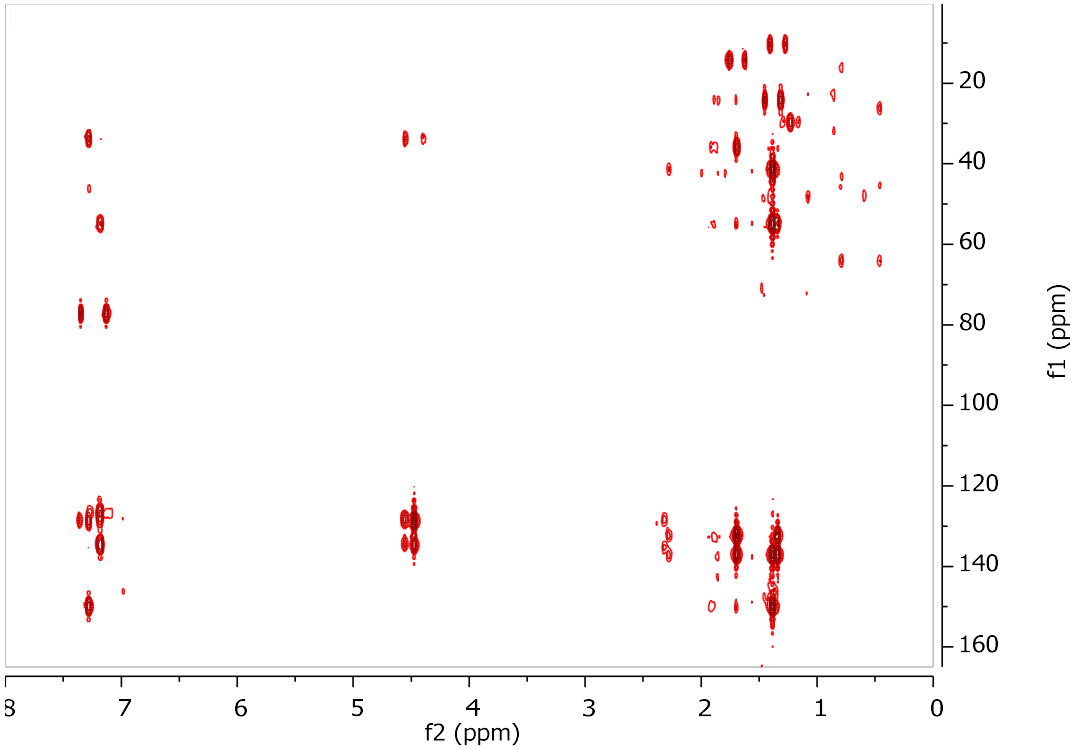

Figure 27. HMBC spectrum of metabolite **3**.

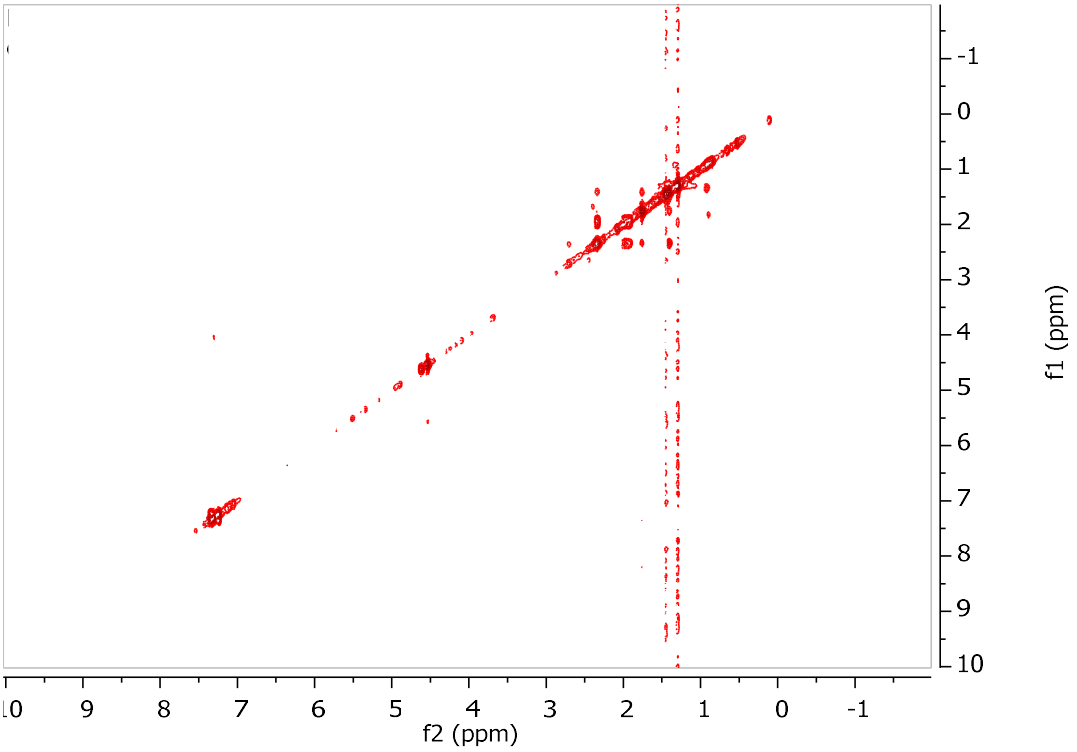

Figure 28. COSY spectrum of metabolite **3**.

Comparison of the spectroscopic and physical characteristics of metabolite **3** with those reported in the literature led to its identification as a new natural product, which was designated as 15-bromo-isolaurene. The NMR data of metabolite **3** are reported in Table 137.

Table 137. ^{1}H and ^{13}C NMR data of metabolite **3** in $CDCl_3$ (δ in ppm, J in Hz).

Position	δ_C	δ_H
1	53.8	-
2	136.4	-
3	132.9	-
4	35.2	2.27 (m)
5	41.5	1.91 (m), 1.87 (m)
6	150.2	-
7	126.3	7.18 (d, 8.2)
8	128.8	7.28 (d, 8.2)
9	133.0	-
10	128.8	7.28 (d, 8.2)
11	126.3	7.18 (d, 8.2)
12	10.3	1.38 (s)
13	14.0	1.70 (s)
14	24.0	1.35 (s)
15	34.0	4.46 (s)

3.1.4 Metabolite 4

Metabolite **4** (LMH20) was isolated after a series of chromatographic separations as a colorless oil (2.0 mg).

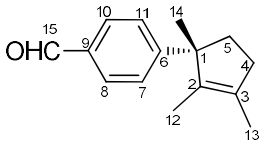

The mass spectrum of metabolite **4** (Figure 29) exhibited a molecular ion peak $[M]^+$ at *m/z* 214, as well as a fragment ion peak at *m/*z 199, corresponding to $[M\text{-}CH_3]^+$.

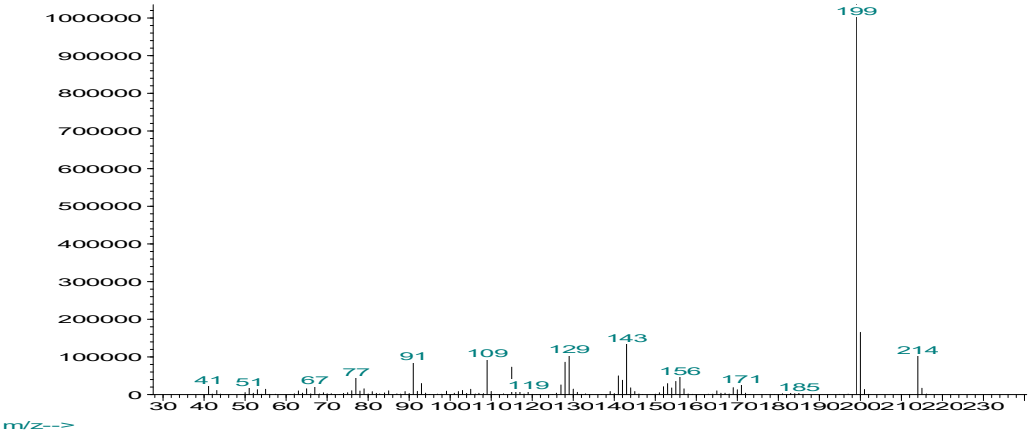

Figure 29. Mass spectrum (EIMS) of metabolite **4**.

In the ^{1}H NMR spectrum of metabolite **4** (Figure 30) obvious were:

- One aliphatic methyl on a non-protonated carbon at δ 1.34,
- Two olefinic methyls at δ 1.43 and 1.71,
- Two doublets at δ 7.38 and 7.77 integrating for two protons each and attributed to four aromatic protons, and
- One singlet at δ 9.95 integrating for one proton and attributed to an aldehyde proton.

Analysis of the NMR and MS data of **4** led to the molecular formula $C_{15}H_{18}O$. Taking into account the four carbon-carbon double bonds and the carbonyl moiety as five of the seven degrees of unsaturation, the molecular structure of **4** was determined as bicyclic.

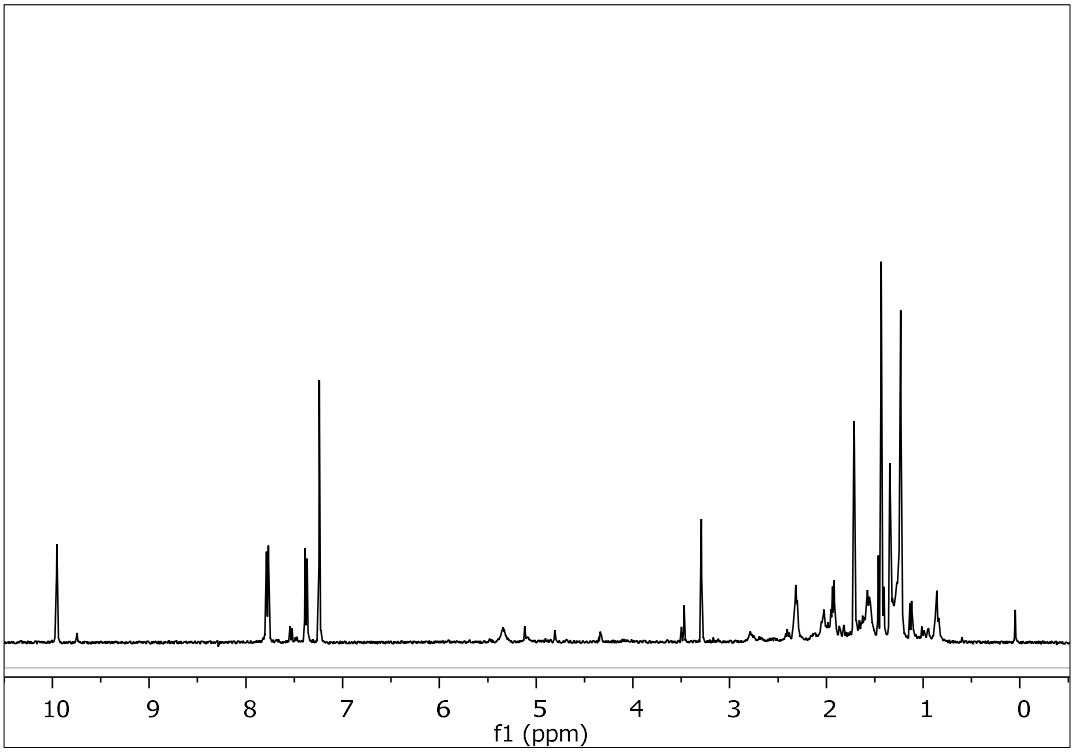

Figure 30. ^{1}H NMR spectrum of metabolite **4**.

Comparison of the spectroscopic and physical characteristics of metabolite **4** with those reported in the literature led to its identification as isolauraldehyde, previously isolated from the red alga *L. obtusa* (Alarif et al., 2012). The ^{1}H NMR data of metabolite **4** are reported in Table 138.

Table 138. ^{1}H NMR data of metabolite **4** in $CDCl_3$ (δ in ppm, J in Hz).

Position	$\delta_{H,exp}$	$\delta_{H,lit}$
4	2.33 (m), 2.30 (m)	2.34 (m), 2.30 (m)
5	1.94 (m), 1.91 (m)	1.95 (m), 1.88 (m)
7	7.38 (d, 8.3)	7.4 (d, 7.8)
8	7.77 (d, 8.3)	7.8 (d, 7.8)
10	7.77 (d, 8.3)	7.8 (d, 7.8)
11	7.38 (d, 8.3)	7.4 (d, 7.8)
12	1.43 (s)	1.45 (s)
13	1.71 (s)	1.72 (s)
14	1.34 (s)	1.36 (s)
15	9.95 (s)	9.98 (s)

3.1.5 Metabolite 5

Metabolite **5** (LMH18) was isolated after a series of chromatographic separations as a colorless oil (0.8 mg).

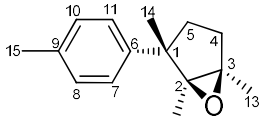

The mass spectrum of metabolite **5** (Figure 31) exhibited a molecular ion peak $[M]^+$ at *m/z* 216.

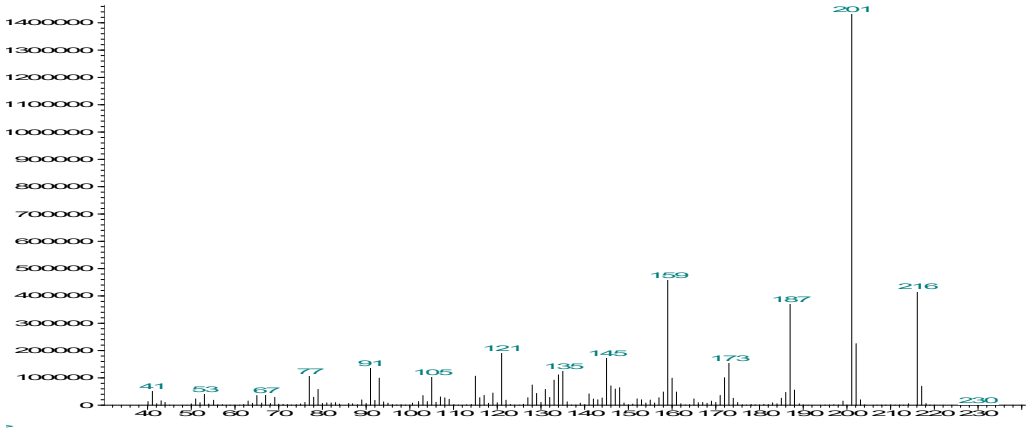

Figure 31. Mass spectrum (EIMS) of metabolite **5**.

In the ^{1}H NMR spectrum of metabolite **5** (Figure 32) obvious were:

- One aliphatic methyl on a non-protonated carbon at δ 1.45,
- Two methyls on non-protonated oxygenated carbons at δ 1.10 and 1.48,
- One aromatic methyl at δ 2.31, and
- Two doublets at δ 7.05 and 7.10 integrating for two protons each and attributed to four aromatic protons.

Analysis of the NMR and MS data of **5** led to the molecular formula $C_{15}H_{20}O$. Taking into account the three carbon-carbon double bonds as three of the six degrees of unsaturation, the molecular structure of **5** was determined as tricyclic.

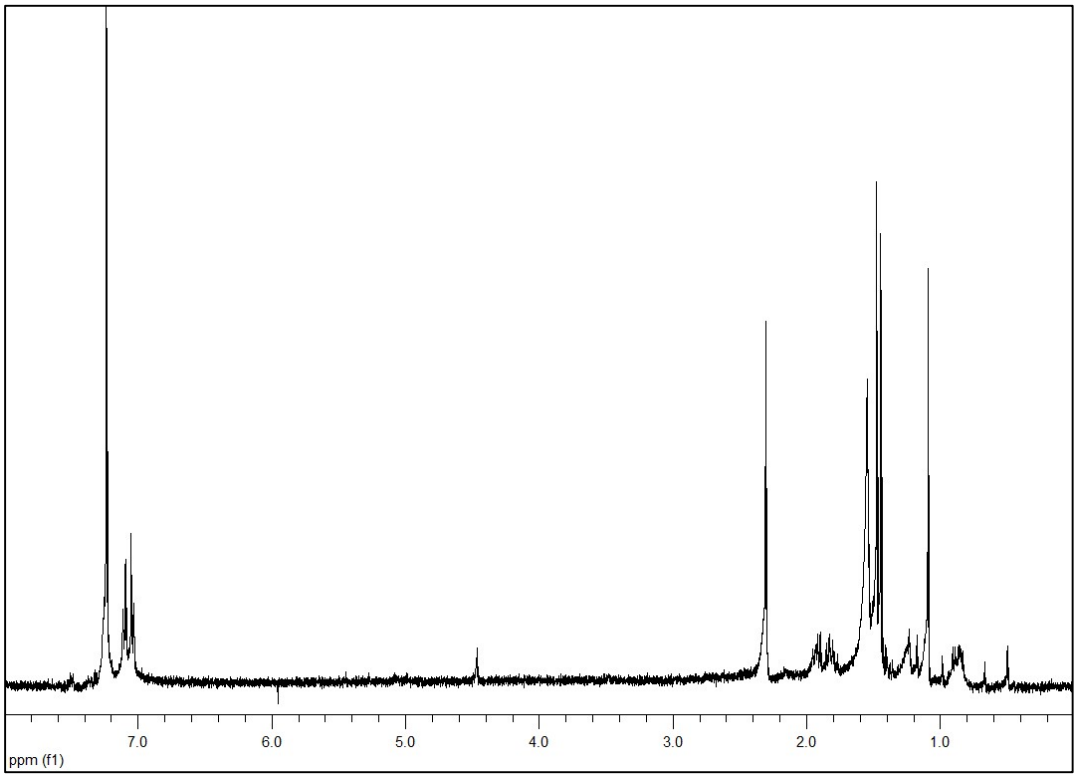

Figure 32. ^{1}H NMR spectrum of metabolite **5**.

The planar structure of metabolite **5** was determined on the basis of the homonuclear and heteronuclear correlations (Figure 33) observed in the HSQC-DEPT (Figure 34), HMBC (Figure 35) and COSY (Figure 36) spectra. In particular, the position of Me-14 on C-1 was evident from the HMBC correlations of Me-14 (δ_H 1.45) with C-1 (δ_C 48.3), C-2 (δ_C 72.6) and C-6 (δ_C 143.4), while the correlations of Me-12 (δ_H 1.10) with C-1, C-2 and C-3 (δ_C 70.3), as well as of Me-13 (δ_H 1.48) with C-2, C-3 and C-4 (δ_C 37.3) secured the position of Me-12 and Me-13 at C-2 and C-3, respectively. The presence of a 1,4-disubstituted benzene ring was indicated by the two doublets at δ 7.05 and 7.10 integrating for four aromatic methines.

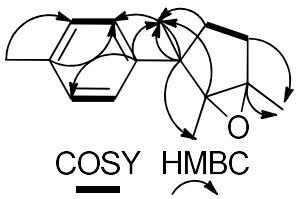

Figure 33. COSY and important HMBC correlations observed for metabolite **5**.

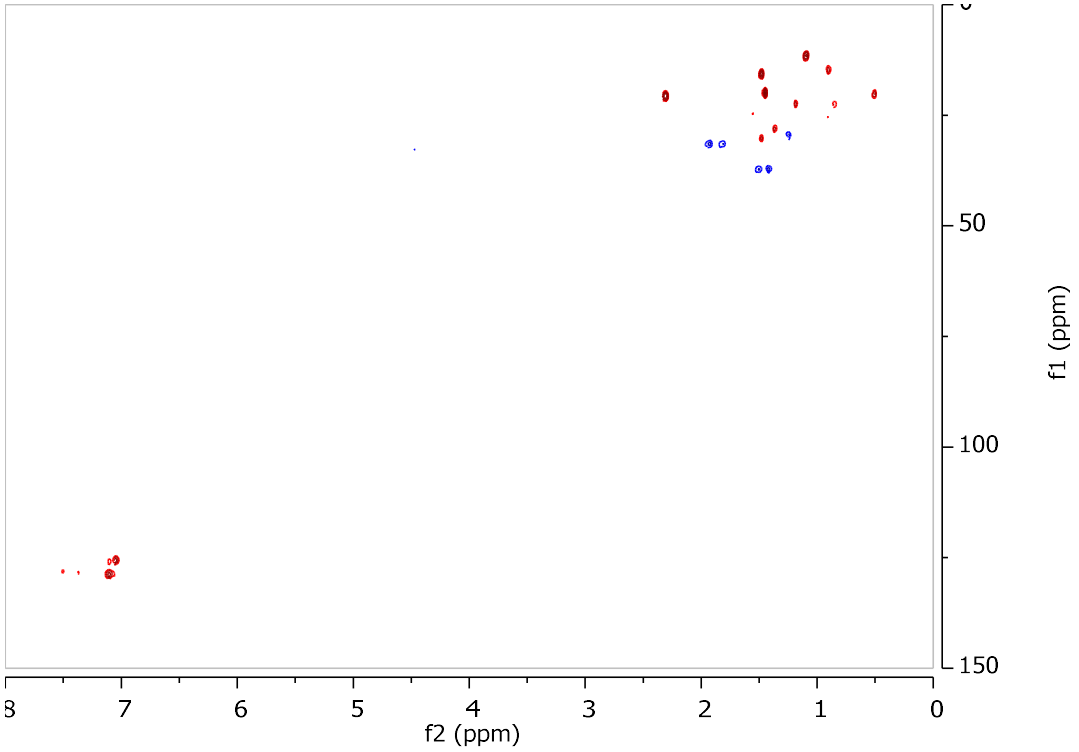

Figure 34. HSQC-DEPT spectrum of metabolite **5**.

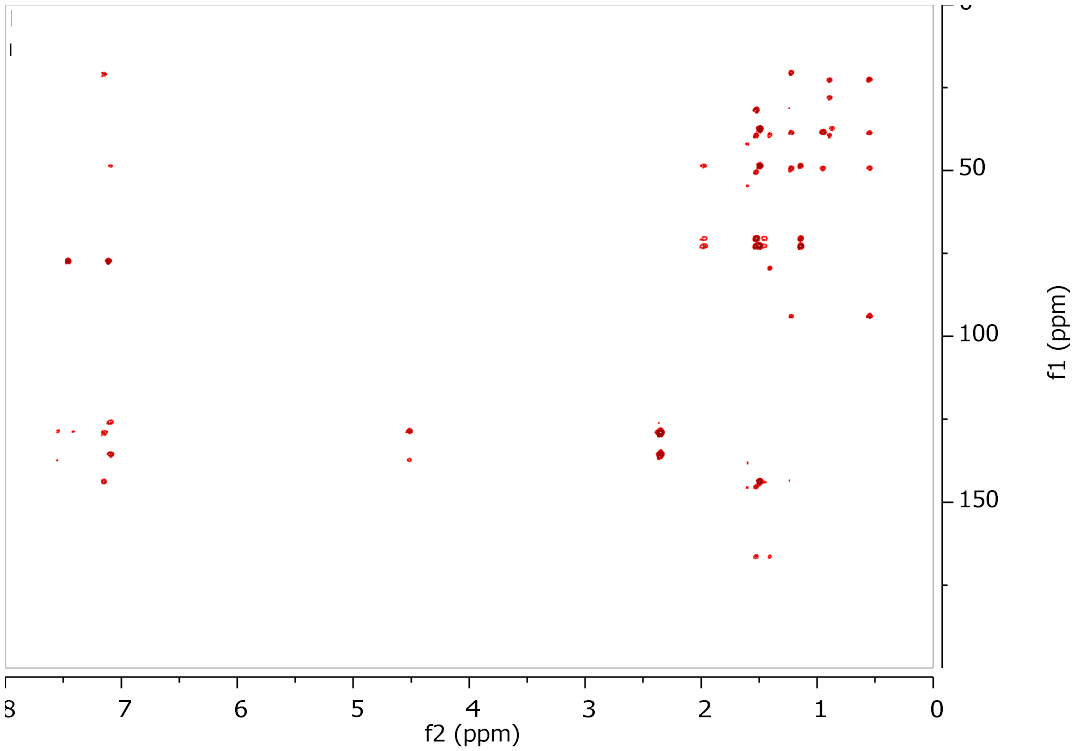

Figure 35. HMBC spectrum of metabolite **5**.

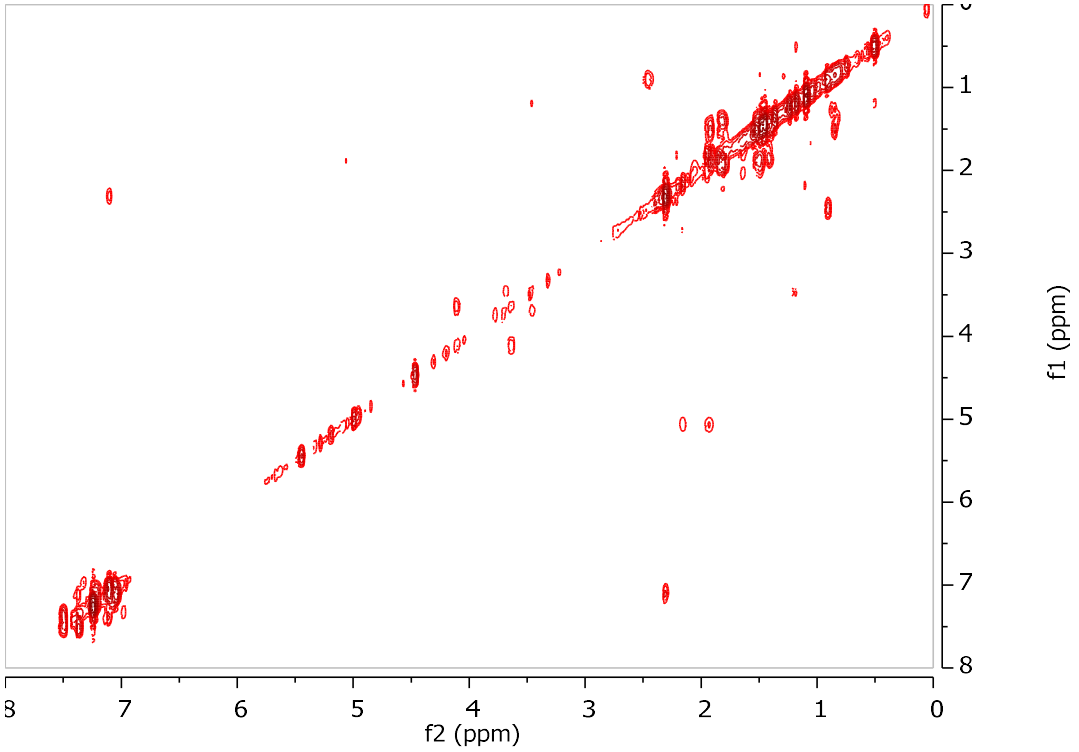

Figure 36. COSY spectrum of metabolite **5**.

Metabolite **5** was proven unstable and degraded prior to the acquisition of NOESY spectrum. Nevertheless, the high structural similarity of metabolite **5** with metabolite **6**, i.e. Me-12 (δ_H 1.10), Me-13 (δ_H 1.48), Me-14 (δ_H 1.45), C-2 (δ_C 72.6) and C-3 (δ_C 70.3) of metabolite **5** vs. Me-12 (δ_H 1.09), Me-13 (δ_H 1.49), Me-14 (δ_H 1.47), C-2 (δ_C 72.6) and C-3 (δ_C 70.4) of metabolite **6**, renders safe the assumption that both **5** and **6** share the same relative configuration at their stereogenic centers.

Comparison of the spectroscopic and physical characteristics of metabolite **5** with those reported in the literature led to its identification as a new natural product, which was designated as 2*S**,3*R**-epoxy-dihydro-isolaurene. The NMR data of metabolite **5** are reported in Table 139.

Table 139. ^{1}H and ^{13}C NMR data of metabolite **5** in $CDCl_3$ (δ in ppm, J in Hz)

Position	δ_C	δ_H
1	48.3	-
2	72.6	-
3	70.3	-
4	37.3	1.50 (m), 1.41 (m)
5	31.6	1.93 (m), 1.82 (m)
6	143.4	-
7	125.7	7.05 (d, 8.0)
8	129.1	7.10 (d, 8.0)
9	135.5	-
10	129.1	7.10 (d, 8.0)
11	125.7	7.05 (d, 8.0)
12	11.5	1.10 (s)
13	15.8	1.48 (s)
14	20.3	1.45 (s)
15	20.6	2.31 (s)

3.1.6 Metabolite 6

Metabolite **6** (LMH25) was isolated after a series of chromatographic separations as a colorless oil (1.5 mg).

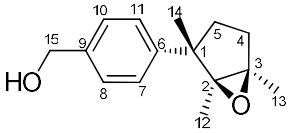

The mass spectrum of metabolite **6** (Figure 37) exhibited a molecular ion peak $[M]^+$ at *m/z* 232, as well as fragment ion peak at *m/z* 214 corresponding to $[M\text{-}H_2O]^+$.

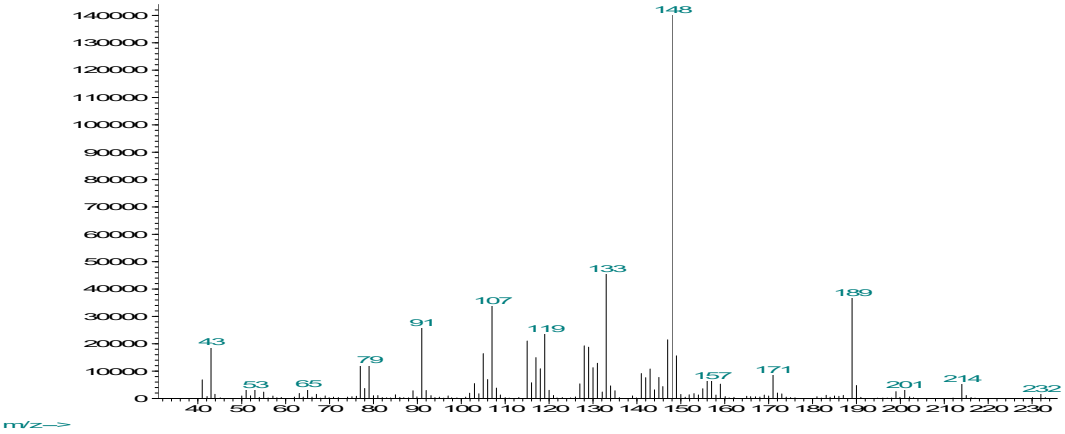

Figure 37. Mass spectrum (EIMS) of metabolite **6**.

In the ^1H NMR spectrum of metabolite **6** (Figure 38) obvious were:

- One aliphatic methyl on a non-protonated carbon at δ 1.09,
- Two methyls on non-protonated oxygenated carbons at δ 1.47 and 1.49,
- One broad singlet at δ 4.66 integrating for two protons and attributed to an aromatic hydroxymethylene, and
- Two doublets at δ 7.15 and 7.30 integrating for two protons each and attributed to four aromatic protons.

Analysis of the NMR and MS data of **6** led to the molecular formula $C_{15}H_{20}O_2$. Taking into account the three carbon-carbon double bonds as three of the six degrees of unsaturation, the molecular structure of **6** was determined as tricyclic.

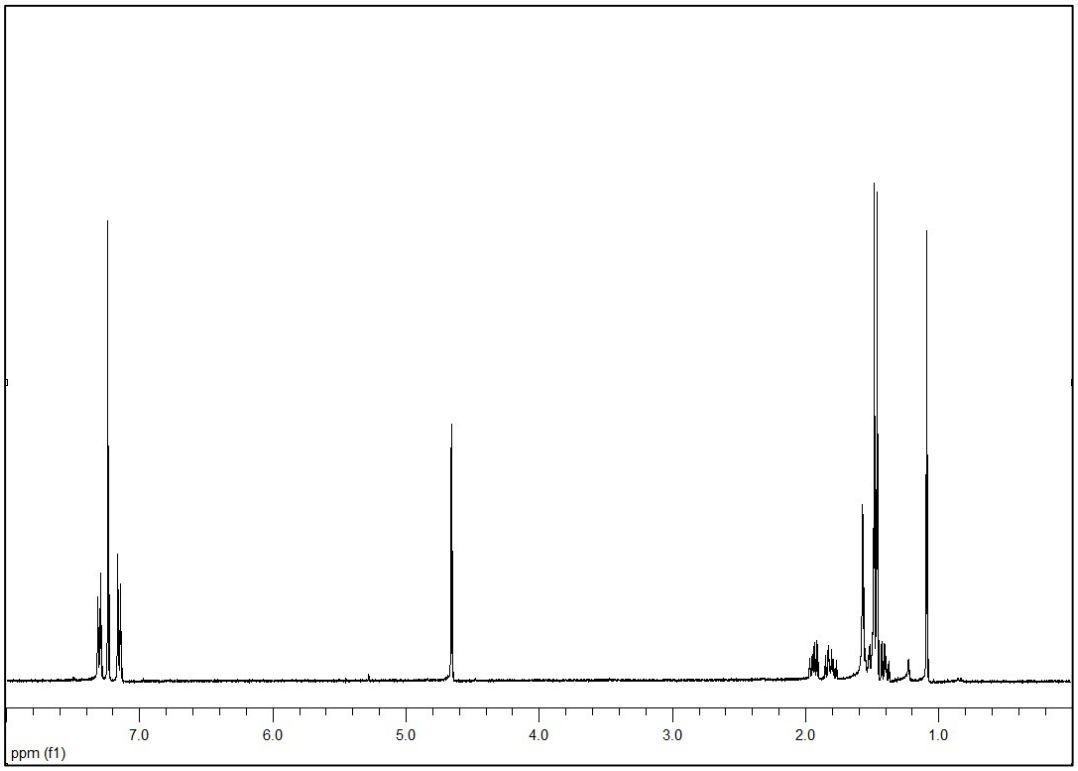

Figure 38. ^{1}H NMR spectrum of metabolite **6**.

The spectroscopic data of **6** were rather similar to those of metabolite **5**, with the main difference being the replacement of the methyl group at C-9 by a hydroxymethylene. Indeed, the planar structure of metabolite **6** was confirmed by the homonuclear and heteronuclear correlations (Figure 39) observed in the HSQC-DEPT (Figure 40), HMBC (Figure 41) and COSY (Figure 42) spectra.

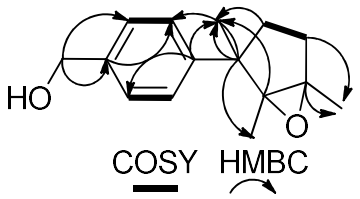

Figure 39. COSY and important HMBC correlations observed for metabolite **6**.

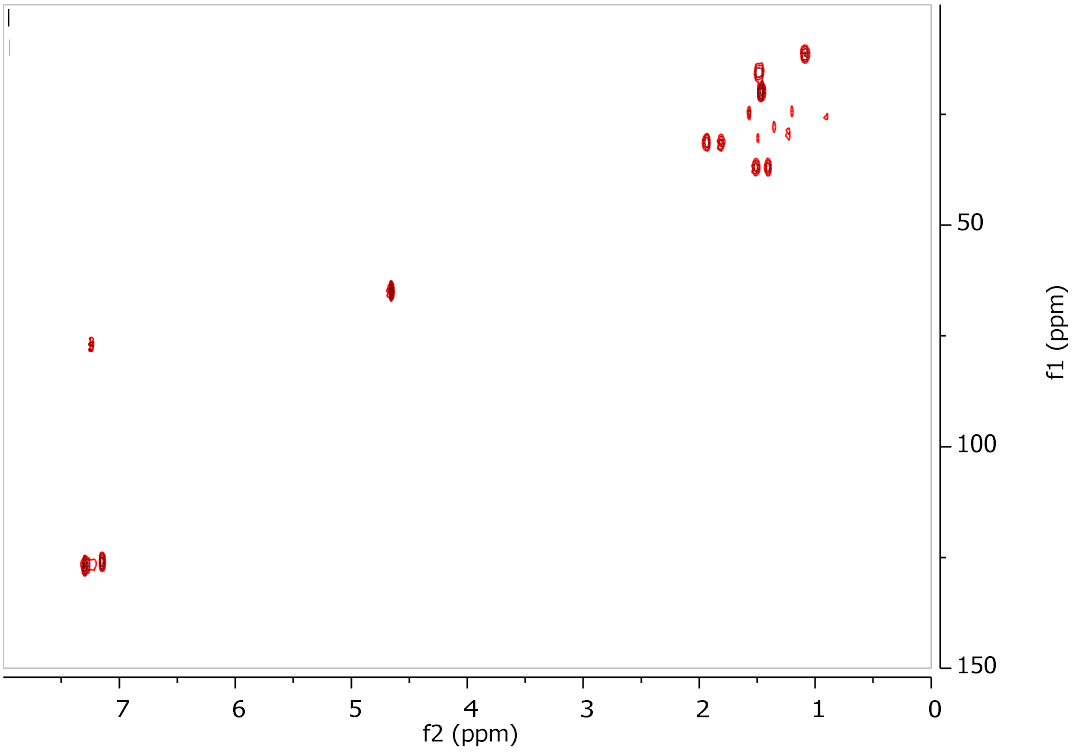

Figure 40. HSQC-DEPT spectrum of metabolite **6**.

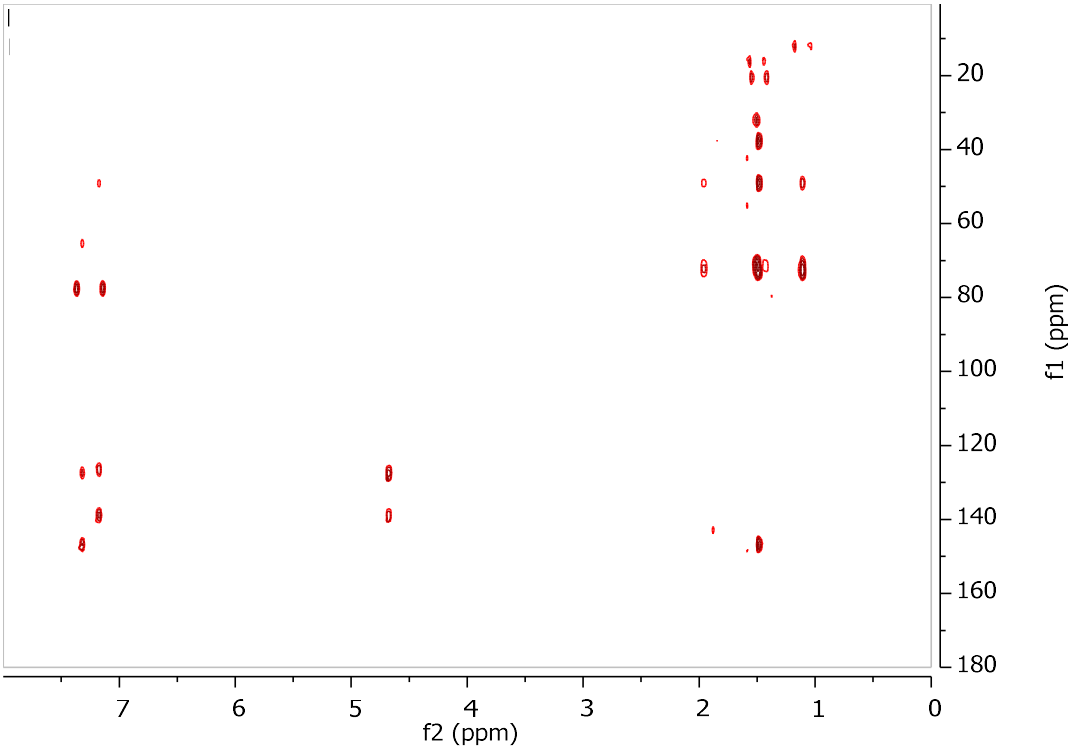

Figure 41. HMBC spectrum of metabolite **6**.

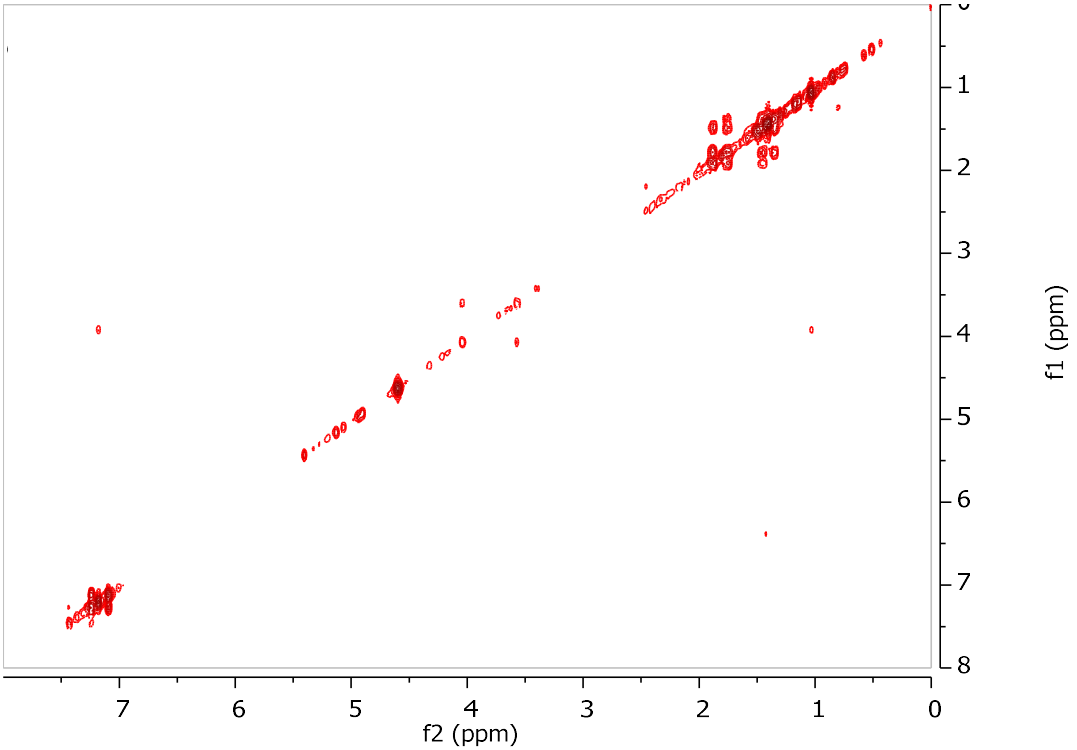

Figure 42. COSY spectrum of metabolite **6**.

The relative configuration of the asymmetric centers of metabolite **6** was determined on the basis of the correlations observed in the NOESY spectrum (Figure 43). Specifically, the strong NOE correlation between Me-12 and Me-13, in conjunction with the lack of NOE correlation between Me-12 or Me-13 and Me-14 suggested the opposite orientation of Me-14 in relation to Me-12 and Me-13.

Comparison of the spectroscopic and physical characteristics of metabolite **6** with those reported in the literature led to its identification as a new natural product, which was designated as 2*S**,3*R**-epoxy-15-hydroxy-dihydro-isolaurene. The NMR data of metabolite **6** are reported in Table 140 .

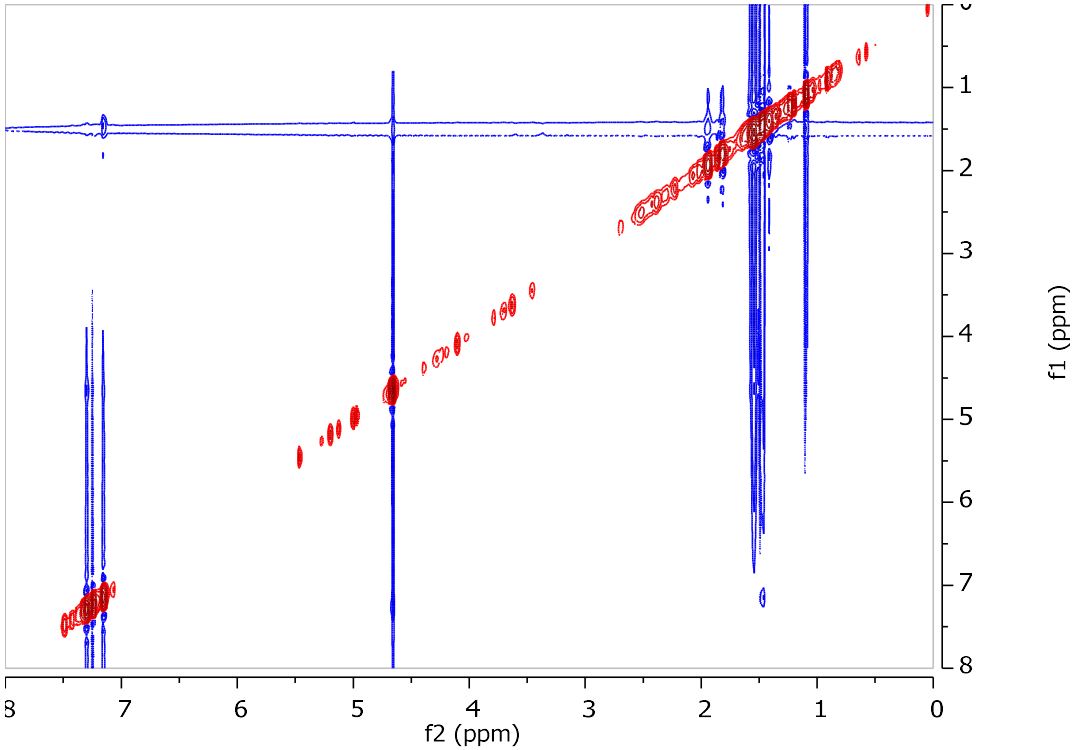

Figure 43. NOESY spectrum of metabolite **6**.

Table 140. ^{1}H and ^{13}C NMR data of metabolite **6** in $CDCl_3$ (δ in ppm, J in Hz)

Position	δ_C	δ_H
1	48.7	-
2	72.6	-
3	70.4	-
4	37.4	1.53 (m), 1.42 (m)
5	31.7	1.94 (m), 1.83 (m)
6	146.4	-
7	127.2	7.30 (d, 8.1)
8	126.1	7.15 (d, 8.1)
9	138.5	-
10	126.1	7.15 (d, 8.1)
11	127.2	7.30 (d, 8.1)
12	11.8	1.10 (s)
13	15.9	1.49 (s)
14	20.2	1.47 (s)
15	65.1	4.66 (brs)

3.1.7 Metabolite 7

Metabolite **7** (LMH24) was isolated after a series of chromatographic separations as a colorless oil (mg).

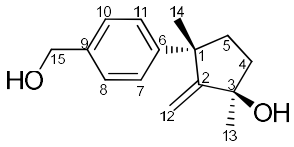

The mass spectrum of metabolite **7** (Figure 44) exhibited a molecular ion peak $[M]^+$ at *m/z* 232, as well as a fragment ion peak at *m/z* 214 corresponding to $[M\text{-}H_2O]^+$.

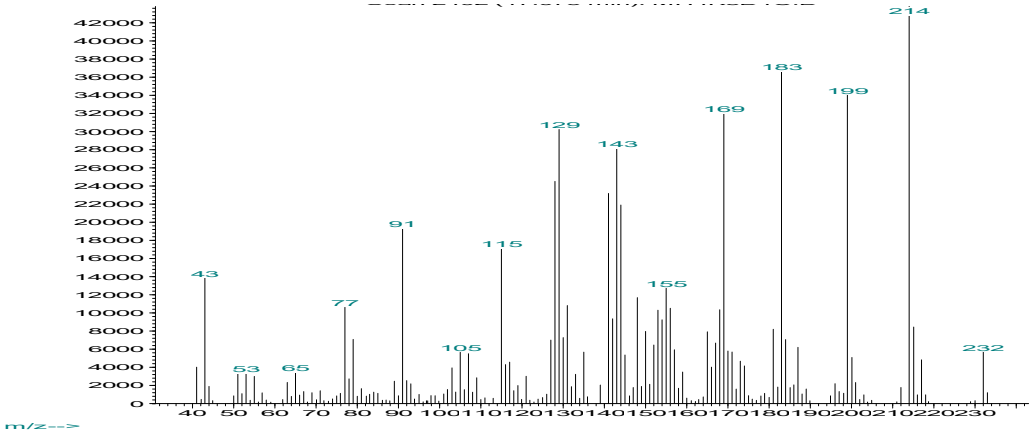

Figure 44. Mass spectrum (EIMS) of metabolite **7**.

In the ^{1}H NMR spectrum of metabolite **7** (Figure 45) obvious were:

- One aliphatic methyl on a non-protonated carbon at δ 1.49,
- One methyl on a non-protonated oxygenated carbon at δ 1.36,
- One singlet at δ 4.65 integrating for two protons and attributed to an aromatic hydroxymethylene,
- Two singlets at δ 5.00 and 5.47 integrating for one proton each and attributed to the protons of an exomethylene group, and
- Two doublets at δ 7.27 and 7.33 integrating for two protons each and attributed to four aromatic protons.

Analysis of the NMR and MS data of **7** led to the molecular formula $C_{15}H_{20}O_2$. Taking into account the four carbon-carbon double bonds as four of the six degrees of unsaturation, the molecular structure of **7** was determined as bicyclic.

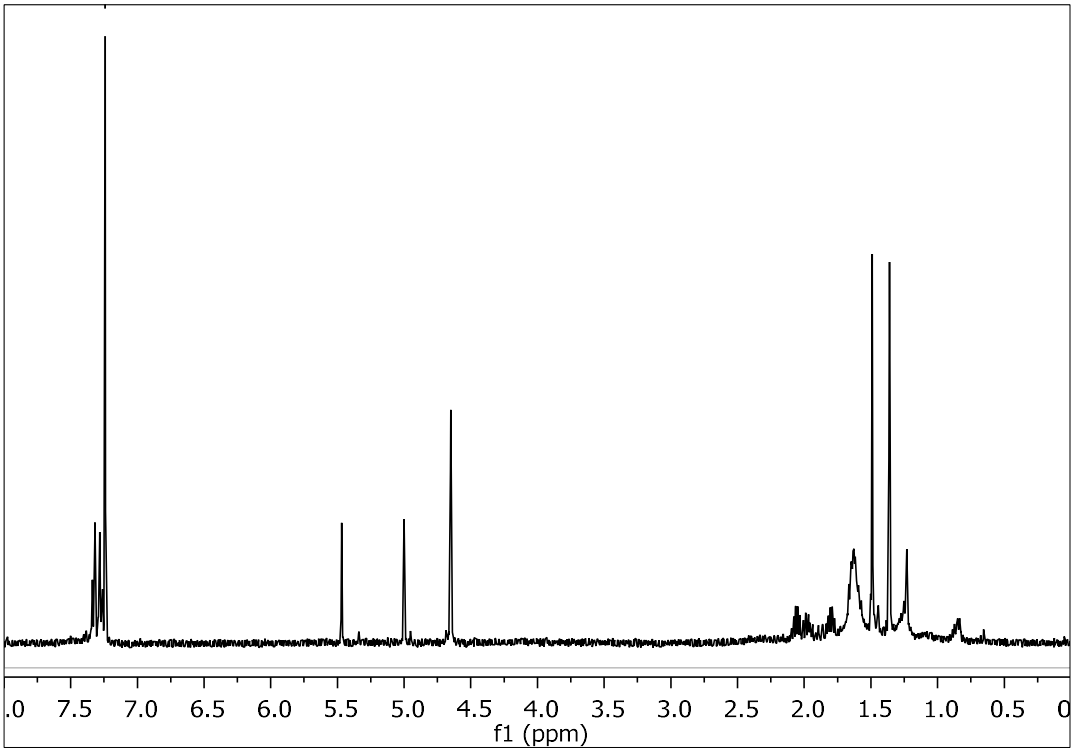

Figure 45. ^{1}H NMR of metabolite **7**.

Comparison of the spectroscopic and physical characteristics of metabolite **7** with those reported in the literature led to its identification as laur-2-ene-3,15-diol, previously isolated from the alga *L. obtusa* (Angawi et al., 2014). The ^{1}H NMR data of metabolite **7** are reported in Table 141.

Table 141. ^{1}H NMR data of metabolite **7** in $CDCl_3$ (δ in ppm, J in Hz).

Position	$\boldsymbol{\delta_{H,exp}}$	$\boldsymbol{\delta_{H,lit}}$
4	2.05 (m), 1.97 (m)	2.11 (ddd, 12.6, 6.6, 6.0), 2.03 (ddd, 13.2, 9.0, 1.8)
5	1.82 (m), 1.61 (m)	1.86 (ddd, 12.6, 6.6, 6.0), 1.65 (ddd, 13.2, 6.6, 1.8)
7	7.33 (d, 8.4)	7.37 (d, 8.4)
8	7.27 (d, 8.4)	7.31 (d, 8.4)
10	7.27 (d, 8.4)	7.31 (d, 8.4)
11	7.33 (d, 8.4)	7.37 (d, 8.4)
12	5.47 (s), 5.00 (s)	5.52 (s), 5.05 (s)
13	1.36 (s)	1.41 (brs)
14	1.49 (s)	1.54 (s)
15	4.65 (s)	4.69 (s)

3.1.8 Metabolite 8

Metabolite **8** (LMH19) was isolated after a series of chromatographic separations as a colorless oil (6.0 mg).

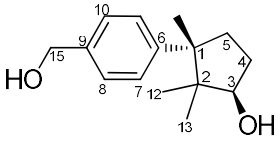

The mass spectrum of metabolite **8** (Figure 46) exhibited a fragment ion peak at *m/z* 216 corresponding to $[M\text{-}H_2O]^+$.

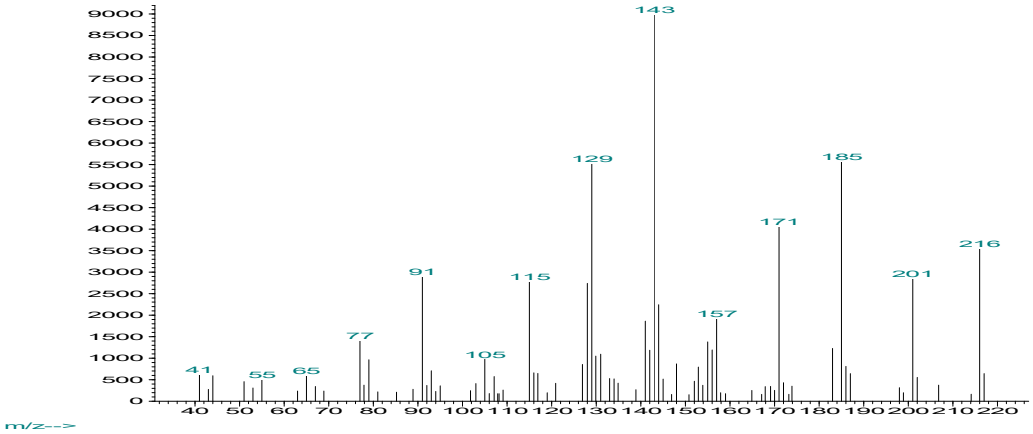

Figure 46. Mass spectrum (EIMS) of metabolite **8**.

In the ^{1}H NMR spectrum of metabolite **8** (Figure 47) obvious were:

- Three aliphatic methyls on non-protonated carbons at δ 0.60, 1.08 and 1.42,
- One oxygenated methine at δ 4.03,
- One singlet at δ 4.65 integrating for two protons and attributed to a hydroxymethylene group, and
- Two doublets at δ 7.20 and 7.27 integrating for two protons each and attributed to four aromatic protons.

Analysis of the NMR and MS data of **8** led to the molecular formula $C_{15}H_{22}O_2$. Taking into account the three carbon-carbon double bonds as three of the five degrees of unsaturation, the molecular structure of **8** was determined as bicyclic.

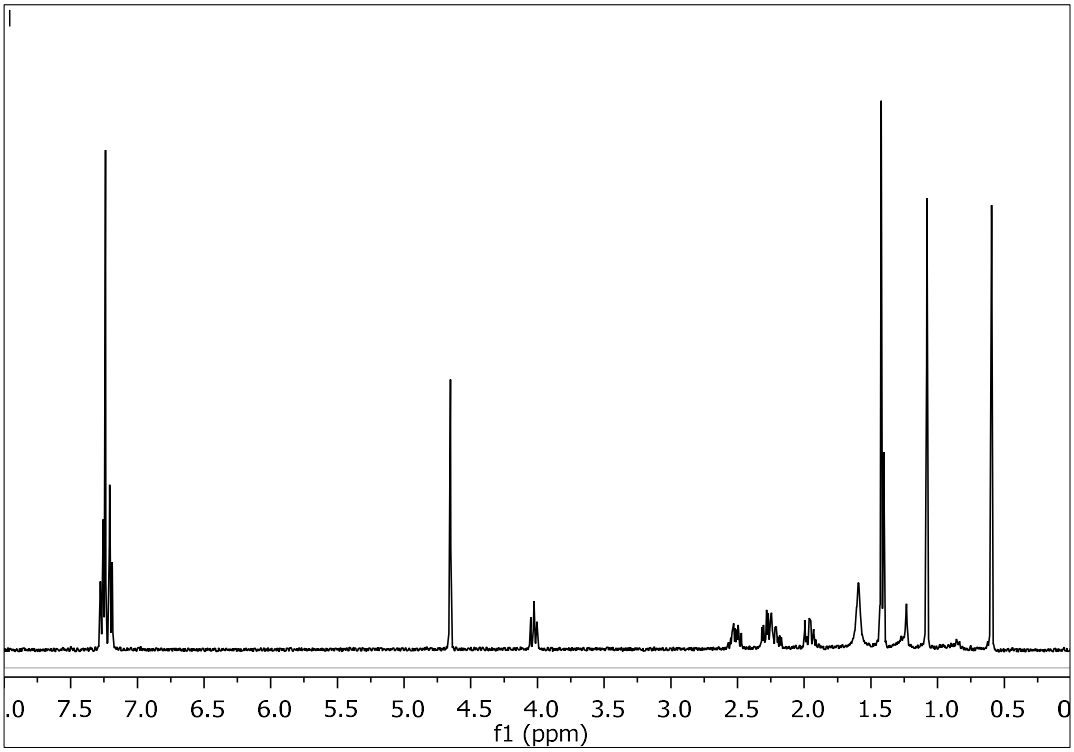

Figure 47. ^{1}H NMR of metabolite **8**.

Comparison of the spectroscopic and physical characteristics of metabolite **8** with those reported in the literature led to its identification as cuparene-3,15-diol, previously isolated from the red alga *L. obtusa* (Angawi et al., 2014). The ^{1}H NMR data of metabolite **8** are reported in Table 142.

Table 142. ^{1}H NMR data of metabolite **8** in $CDCl_3$ (δ in ppm, J in Hz).

Position	$\delta_{H,exp}$	$\delta_{H,lit}$
3	4.03 (t, 9.4)	4.08 (dd, 10.2, 9.0)
4	2.52 (m), 2.21 (m)	2.56 (dddd, 15.0, 9.6, 9.0, 5.4), 2.26 (dddd, 15.0, 10.2, 10.2, 4.8)
5	2.29 (m), 1.95 (m)	2.33 (ddd, 13.2, 9.6, 4.8), 2.01 (ddd, 13.2, 10.2, 5.4)
7	7.27 (d, 8.4)	7.30 (d, 8.4)
8	7.20 (d, 8.4)	7.24 (d, 8.4)
10	7.20 (d, 8.4)	7.24 (d, 8.4)
11	7.27 (d, 8.4)	7.30 (d, 8.4)
12	0.60 (s)	0.65 (s)
13	1.08 (s)	1.13 (s)
14	1.42 (s)	1.47 (s)
15	4.65 (s)	4.69 (s)

3.1.9 Metabolite 9

Metabolite **9** (LMH26) was isolated after a series of chromatographic separations as a colorless oil (0.8 mg).

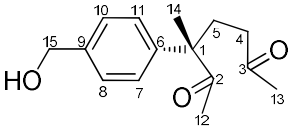

The mass spectrum of metabolite **9** (Figure 48) exhibited a fragment ion peak at *m/z* 230 corresponding to $[M\text{-}H_2O]^+$.

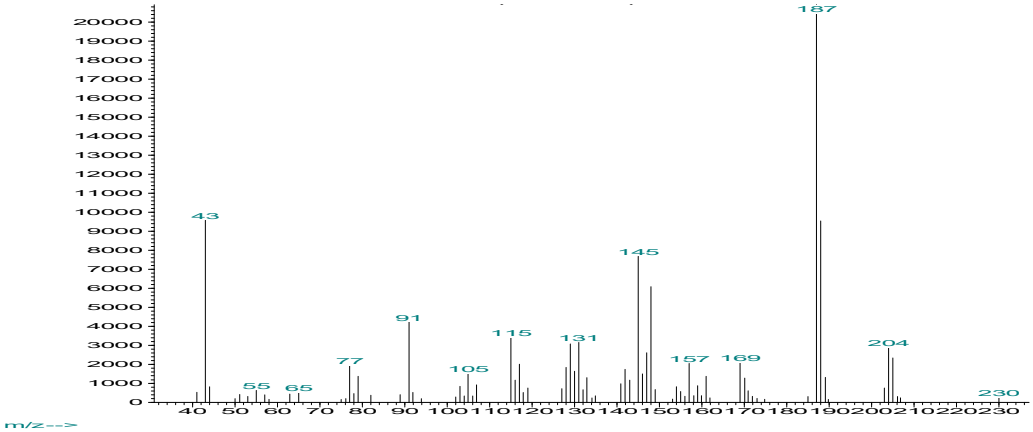

Figure 48. Mass spectrum (EIMS) of metabolite **9**.

In the ^{1}H NMR spectrum of metabolite **9** (Figure 49) obvious were:

- One aliphatic methyl on a non-protonated carbon at δ 1.45,
- Two deshielded methyls on non-protonated carbons at δ 1.90 and 2.07,
- One broad singlet at δ 4.69 integrating for two protons and attributed to an aromatic hydroxymethylene, and
- Two doublets at δ 7.20 and 7.34 integrating for two protons each and attributed to four aromatic protons.

Analysis of the NMR and MS data of **9** led to the molecular formula $C_{15}H_{20}O_3$. Taking into account the three carbon-carbon double bonds and the two carbonyl moieties as five of the six degrees of unsaturation, the molecular structure of **9** was determined as monocyclic.

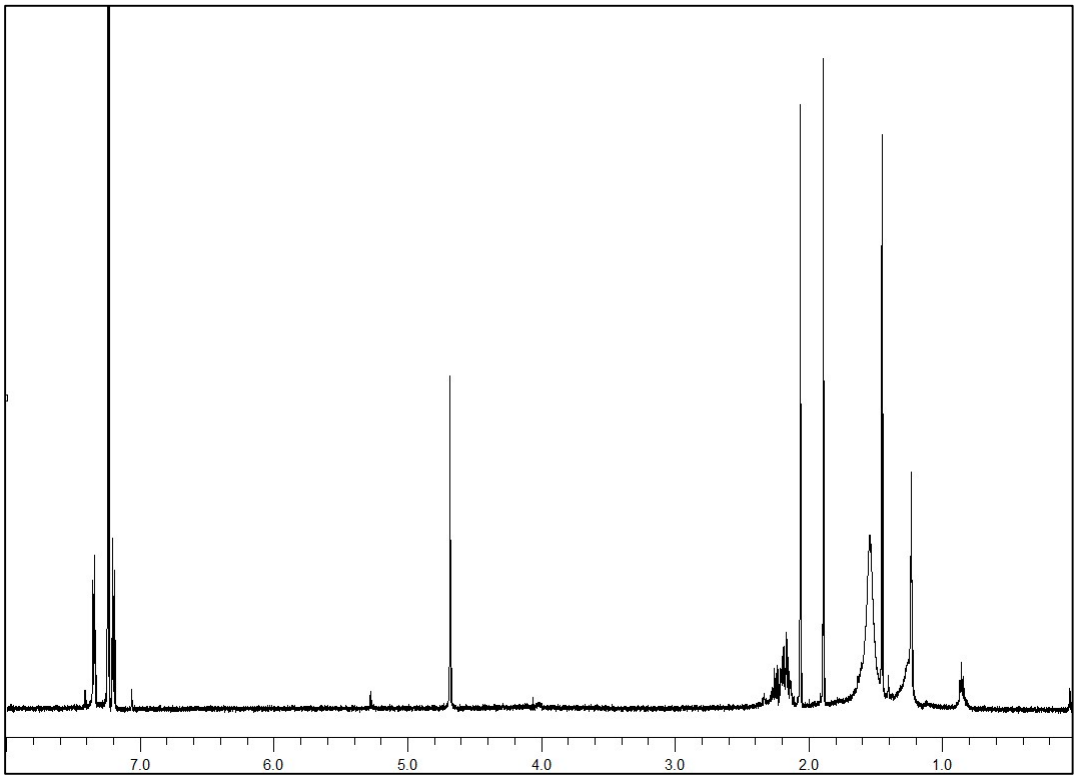

Figure 49. ^{1}H NMR spectrum of metabolite **9**.

The planar structure of metabolite **9** was determined on the basis of the homonuclear and heteronuclear correlations (Figure 50) observed in the HSQC-DEPT (Figure 51), HMBC (Figure 52) and COSY (Figure 53) spectra. In particular, the position of Me-14 (δ_H 1.45) was fixed at C-1 due to its correlations with C-1 (δ_C 54.8), C-2 (δ_C 210.0), C-5 (δ_C 31.2) and C-6 (δ_C 141.5) observed in the HMBC spectrum. In addition, the HMBC correlations of Me-12 (δ_H 1.90) with the carbonyl carbon C-2 (δ_C 210.0) and of Me-13 (δ_H 2.07) with the carbonyl carbon C-3 (δ_C 208.1) supported the cleavage of C-2/C-3 bond. The presence of the aromatic hydroxymethylene at position C-15 was verified by the HMBC correlations of H_2-15 with C-8/C-10 (δ_C 127.7) and C-9 (δ_C 139.2).

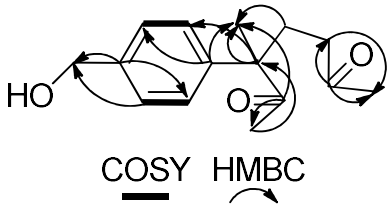

Figure 50. COSY and important HMBC correlations observed for metabolite **9**.

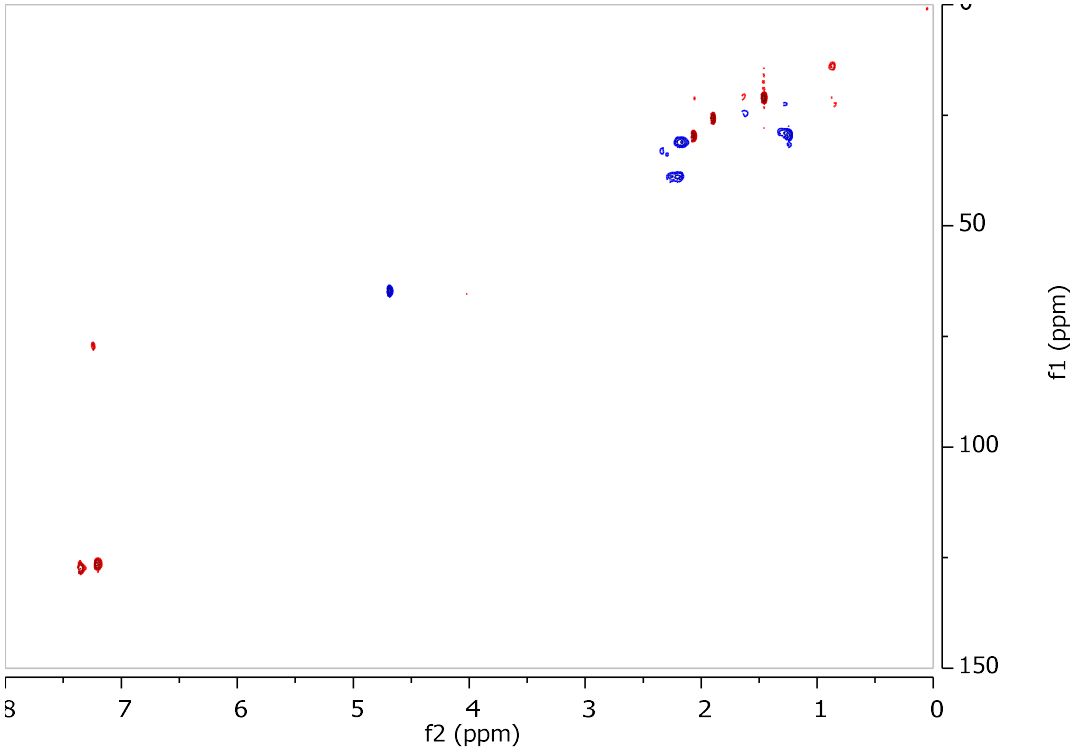

Figure 51. HSQC-DEPT spectrum of metabolite **9**.

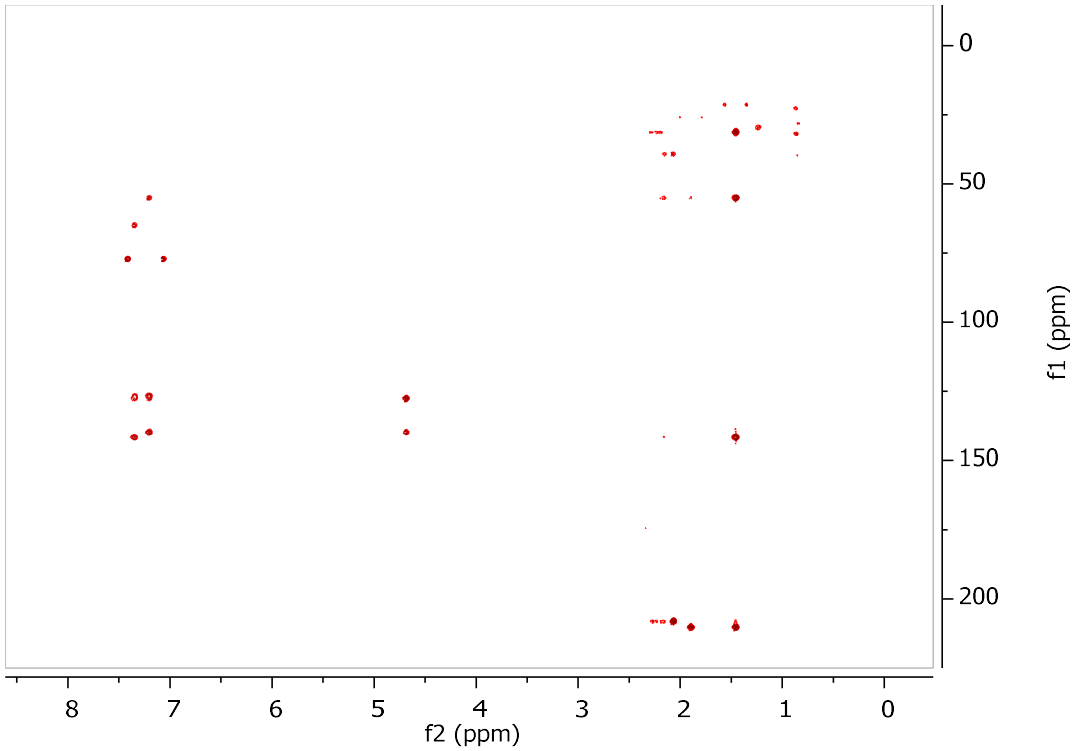

Figure 52. HMBC spectrum of metabolite **9**.

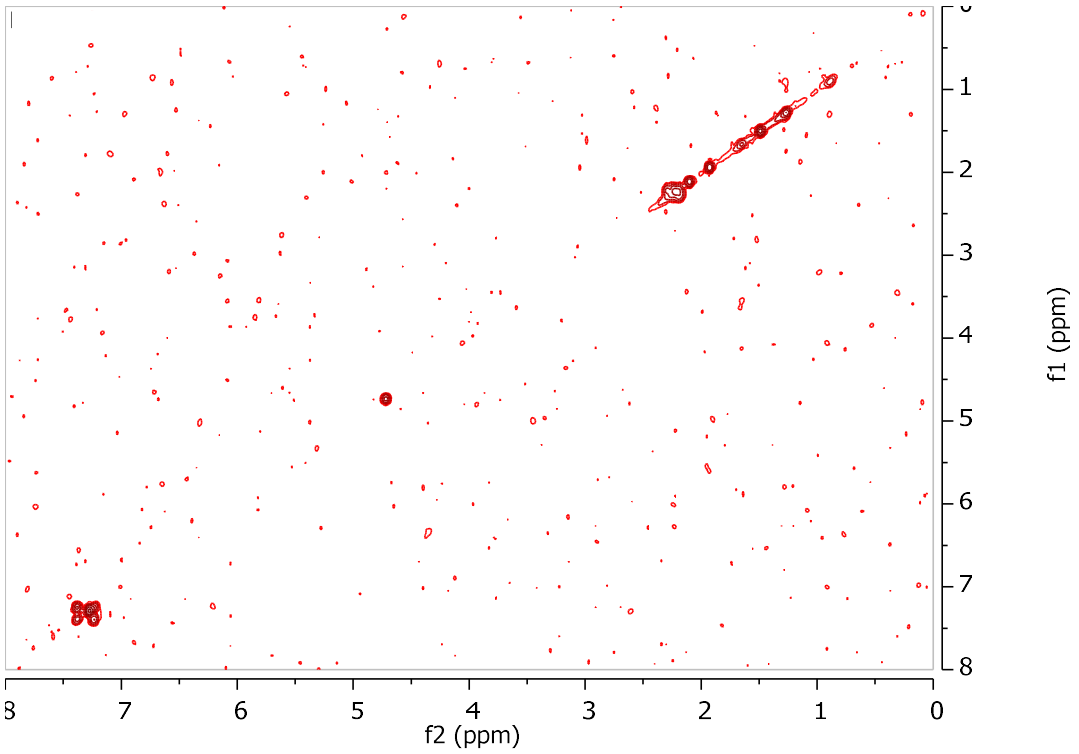

Figure 53. COSY spectrum of metabolite **9**.

Comparison of the spectroscopic and physical characteristics of metabolite **9** with those reported in the literature led to its identification as a new natural product. The NMR data of metabolite **9** are reported in Table 143.

Table 143. ^{1}H and ^{13C} NMR data of metabolite **9** in $CDCl_3$ (δ in ppm, J in Hz).

Position	δ_C	δ_H
1	54.8	-
2	210.0	-
3	208.1	-
4	38.8	2.24 (m), 2.18 (m)
5	31.2	2.18 (m), 2.14 (m)
6	141.5	-
7	126.5	7.20 (d, 8.1)
8	127.7	7.34 (d, 8.1)
9	139.2	-
10	127.7	7.34 (d, 8.1)
11	126.5	7.20 (d, 8.1)
12	25.7	1.90 (s)
13	29.8	2.07 (s)
14	21.3	1.45 (s)
15	64.8	4.69 (brs)

3.1.10 Metabolite 10

Metabolite **10** (LMH23) was isolated after a series of chromatographic separations as a colorless oil (1.0 mg).

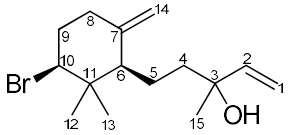

The mass spectrum of metabolite **10** (Figure 54) exhibited fragment ion peaks at *m/z* 282 and 284 in a 1:1 intensity corresponding to $[M\text{-}H_2O]^+$ and suggesting the presence of one bromine atom in the molecule.

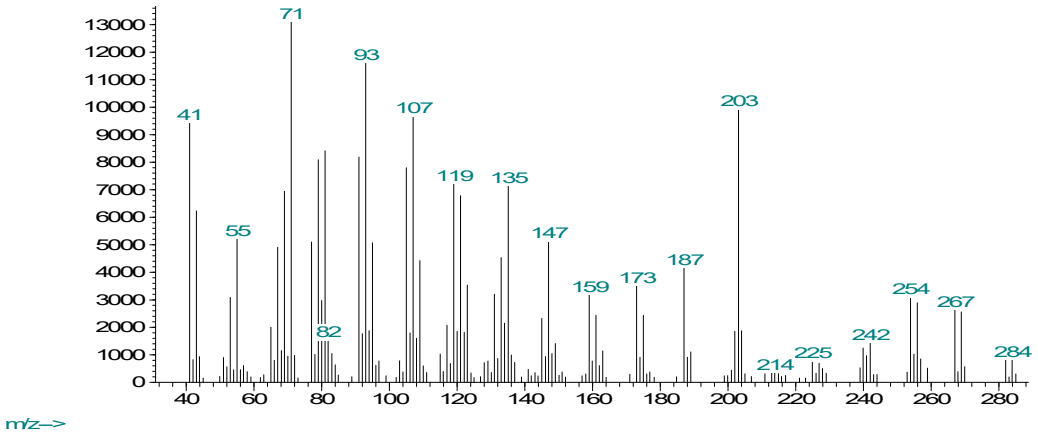

Figure 54. Mass spectrum (EIMS) of metabolite **10**.

In the ^{1}H NMR spectrum of metabolite **10** (Figure 55) obvious were:

- Three aliphatic methyls on non-protonated carbons at δ 0.81, 1.15 and 1.27,
- One doublet of doublets at δ 4.11 attributed to a halogenated methine,
- Two broad singlets at δ 4.63 and 4.89 integrating for one proton each and attributed to the protons of an exomethylene group
- Three doublets of doublets at δ 5.05, 5.20 and 5.89 integrating for one proton each and attributed to the olefinic protons of a monosubstituted double bond.

Analysis of the NMR and MS data of **10** led to the molecular formula $C_{15}H_{25}BrO$. Taking into account the two carbon-carbon double bonds as two of the three degrees of unsaturation, the molecular structure of **10** was determined as monocyclic.

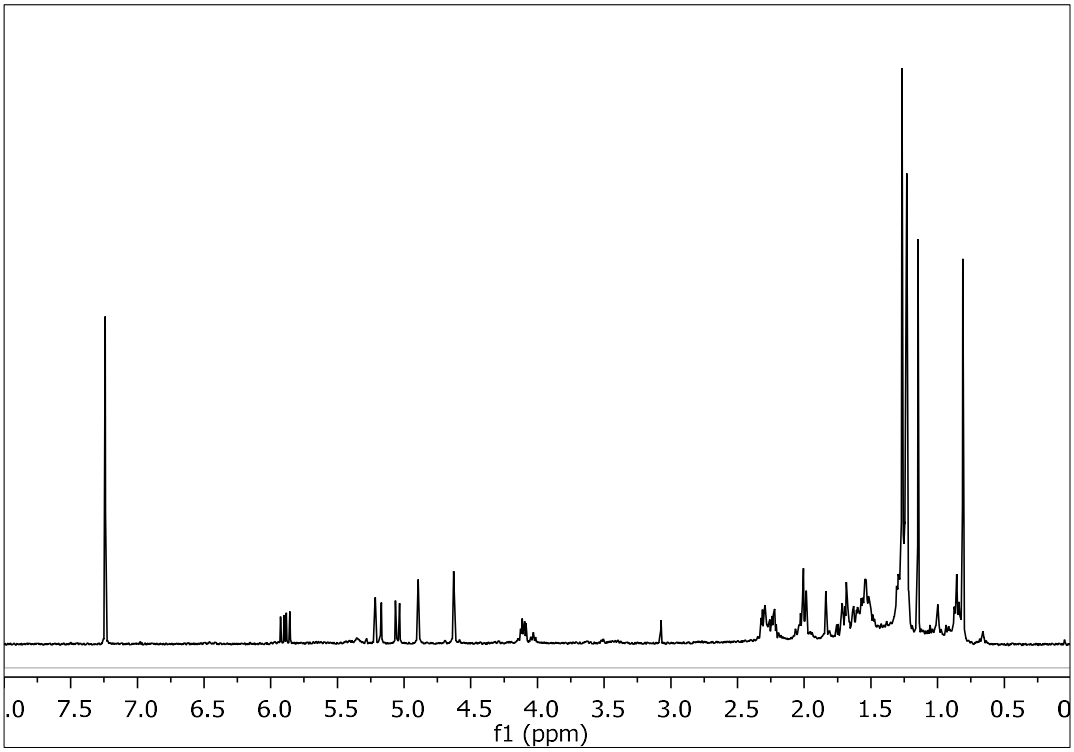

Figure 55. ^{1}H NMR spectrum of metabolite **10**.

Comparison of the spectroscopic and physical characteristics of metabolite **10** with those reported in the literature led to its identification as *β*-snyderol, previously isolated from the red alga *L. obtusa* (Topcu et al., 2003). The ^{1}H NMR data of metabolite **10** are reported in Table 144.

Table 144. ^{1}H NMR data of metabolite **10** in $CDCl_3$ (δ in ppm, J in Hz).

Position	$\delta_{H,exp}$	$\delta_{H,lit}$
1	5.20 (dd, 17.4, 1.1), 5.05 (dd, 10.8, 1.1)	5.22 (dd, 17.5, 1.0), 5.07 (dd, 11.0, 1.0)
2	5.89 (dd, 17.4, 10.8)	5.91 (dd, 17.4, 10.7)
4	1.76 (m), 1.60 (m)	1.78 (dd, 11.1, 4), 1.62 (dd, 11.5, 5.4)
5	1.51 (m), 1.30 (m)	1.51 (m), 1.30 (m)
6	1.71 (m)	1.71 (dd, 7.8, 7.8)
8	2.31 (m), 2.05 (m)	2.35 (dd, 7.6, 4.7), 2.08 (dd, 6.5, 5.9)
9	2.28 (m), 2.00 (m)	2.29 (dt, 5.8, 2.9), 2.03 (dt, 4.5, 2.9)
10	4.11 (dd, 11.6, 4.3)	4.12 (dd, 11.7, 4.5)
12	1.15 (s)	1.16 (s)
13	0.81 (s)	0.83 (s)
14	4.89 (brs), 4.63 (brs)	4.91 (brs), 4.65 (brs)
15	1.27 (s)	1.28 (s)

3.1.11 Metabolite 11

Metabolite **11** (LMH01) was isolated after a series of chromatographic separations as a colorless oil (76.6 mg).

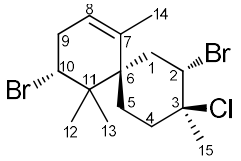

The mass spectrum of metabolite **11** (Figure 56) exhibited a molecular ion peak $[M]^+$ at *m/z* 396 and isotopic ion peaks at *m/z* 398, 400 and 402 at a relative intensity suggestive of the presence of one chlorine and two bromine atoms.

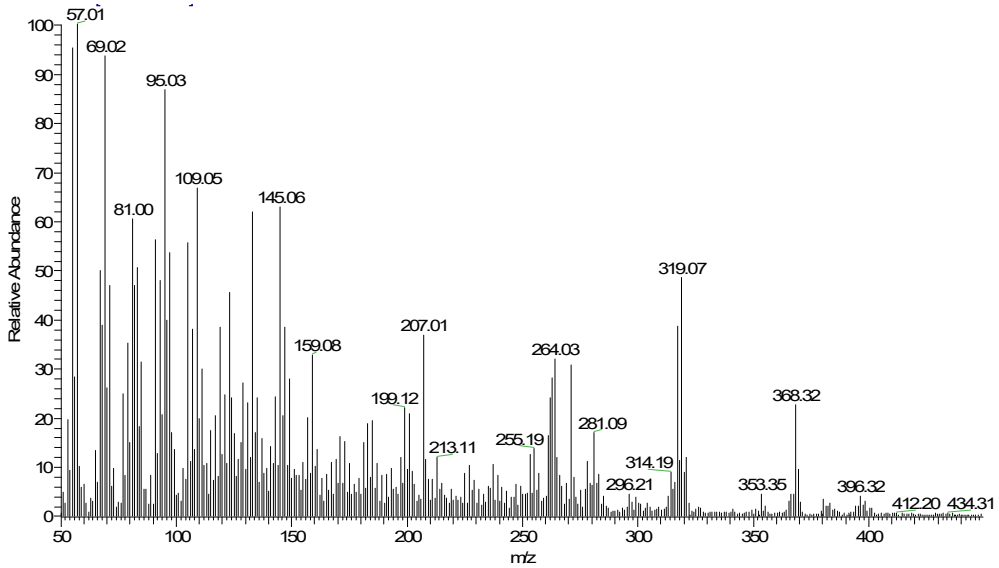

Figure 56. Mass spectrum (EIMS) of metabolite **11**.

In the ^{1}H NMR spectrum of metabolite **11** (Figure 57) obvious were:

- Two aliphatic methyls on non-protonated carbons at δ 0.91 and 1.19,
- One olefinic methyl at δ 1.66,
- One methyl on a non-protonated halogenated carbon at δ 1.96,
- Two doublets of doublets at δ 4.45 and 4.80 integrating for one proton each and attributed to two halogenated methines, and
- One broad singlet δ 5.21 integrating for one proton and attributed to an olefinic methine.

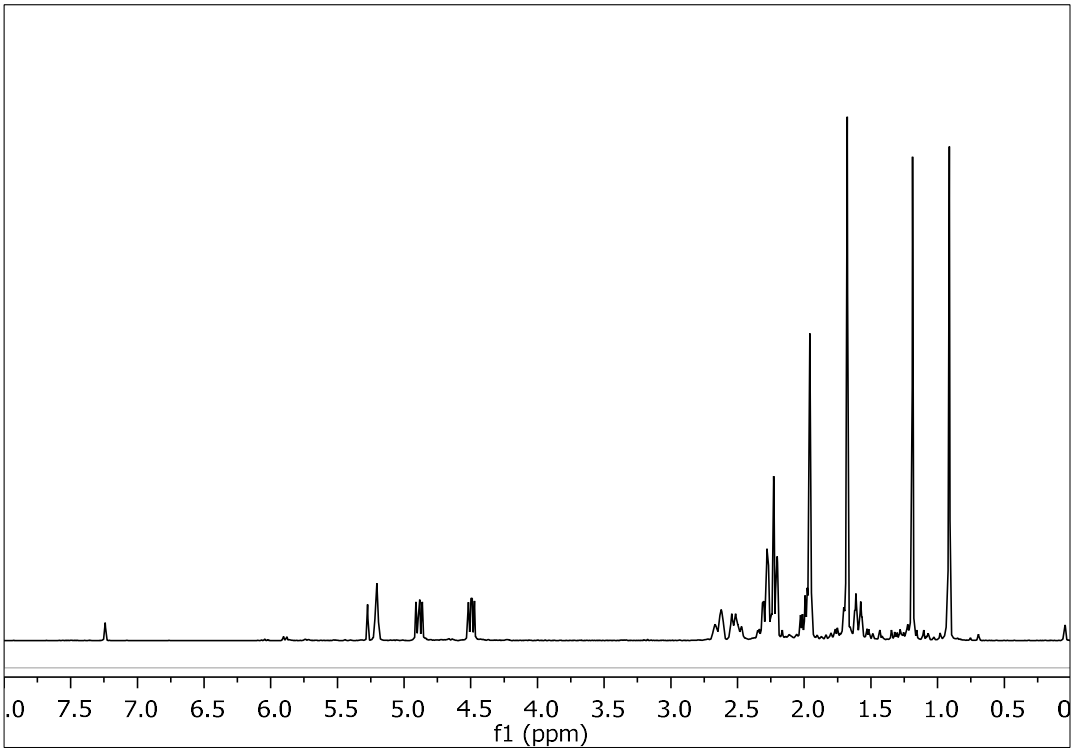

Figure 57. ^{1}H NMR spectrum of metabolite **11**.

Analysis of the NMR and MS data of **11** led to the molecular formula $C_{15}H_{23}Br_2Cl$. Taking into account the one carbon-carbon double bond as one of the three degrees of unsaturation, the molecular structure of **11** was determined as bicyclic.

Comparison of the spectroscopic and physical characteristics of metabolite **11** with those reported in the literature led to its identification as 2,10-dibromo-3-chloro-α-chamigrene, previously isolated from an alga of the genus *Laurencia* (Howard & Fenical, 1975). The ^{1}H NMR data of metabolite **11** are reported in Table 145.

Table 145. ^{1}H NMR data of metabolite **11** in $CDCl_3$ (δ in ppm, J in Hz).

Position	$\delta_{H,exp}$	$\delta_{H,lit}$
2	4.80 (dd, 10.6, 7.8)	4.75 (m)
8	5.21 (brs)	5.16 (brs)
10	4.45 (dd, 10.7, 6.9)	4.39 (m)
12	1.19 (s)	1.16 (s)
13	0.91 (s)	0.89 (s)
14	1.66 (s)	1.61 (s)
15	1.96 (s)	1.95s)

3.1.12 Metabolite 12

Metabolite **12** (LMH15) was isolated after a series of chromatographic separations as a colorless oil (0.7 mg).

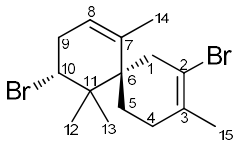

The mass spectrum of metabolite **12** (Figure 58) exhibited a molecular ion peak $[M]^+$ at *m/z* 360 with isotopic ion peaks at *m/z* 362 and 364 at a 1:2:1 intensity, characteristic for the presence of two bromine atoms, as well as fragment ion peaks at *m/z* 281 and 283 corresponding to $[M\text{-}Br]^+$.

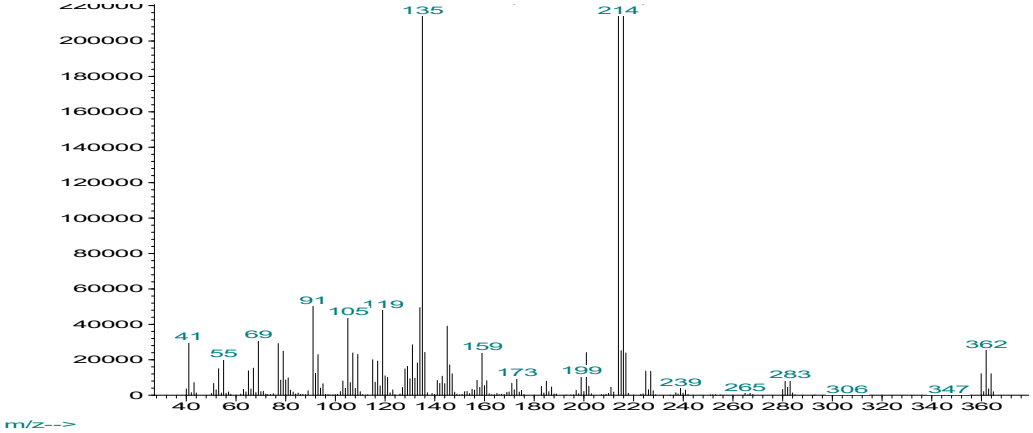

Figure 58. Mass spectrum (EIMS) of metabolite **12**.

In the ^{1}H NMR spectrum of metabolite **12** (Figure 59) obvious were:

- Two aliphatic methyls on non-protonated carbons at δ 0.92 and 1.11,
- Two olefinic methyls at δ 1.65 and 1.78,
- One doublet of doublets at δ 4.64 integrating for one proton and attributed to a halogenated methine, and
- One broad singlet δ 5.22 integrating for one proton and attributed to an olefinic methine.

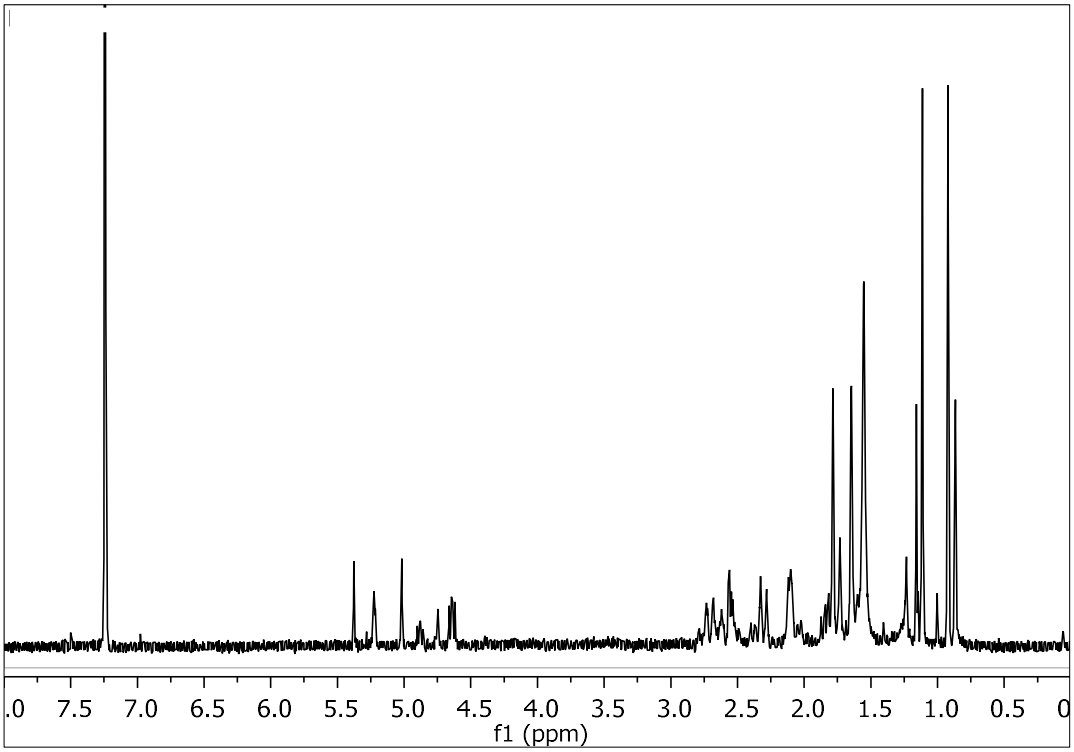

Figure 59. ^{1}H NMR spectrum of metabolite **12** in $CDCl_3$.

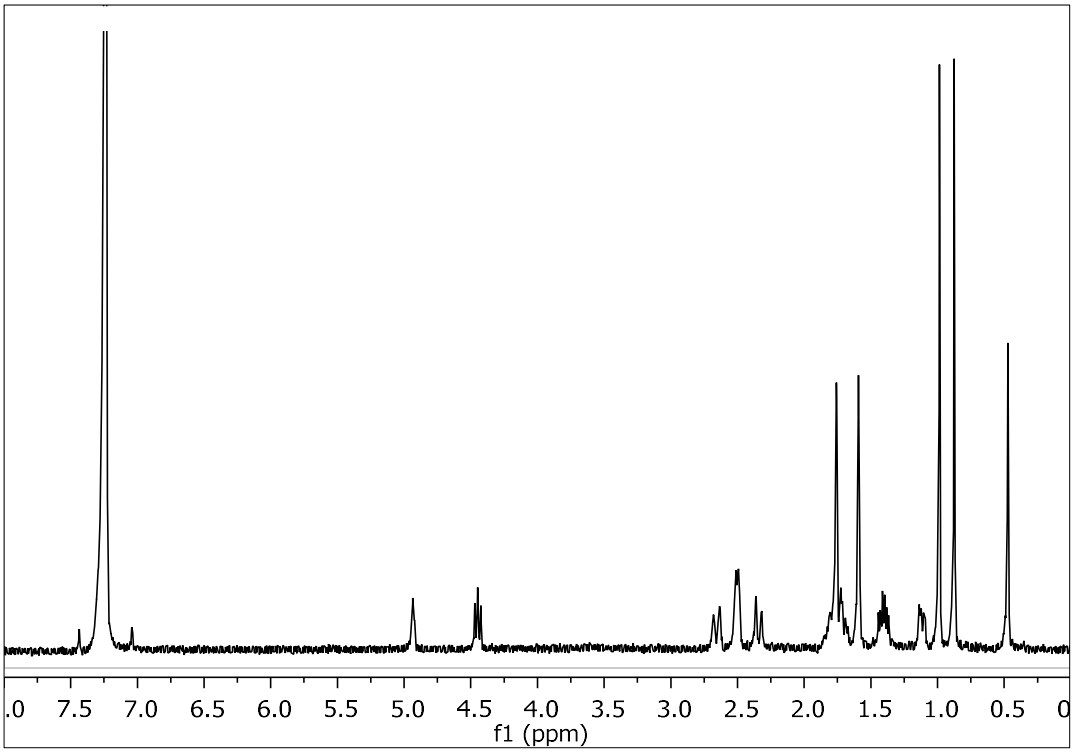

Figure 60. ^{1}H NMR spectrum of metabolite **12** in C_6D_6.

Analysis of the NMR and MS data of **12** led to the molecular formula $C_{15}H_{22}Br_2$. Taking into account the two carbon-carbon double bonds as two of the four degrees of unsaturation, the molecular structure of **12** was determined as bicyclic.

Comparison of the spectroscopic and physical characteristics of metabolite **12** with those reported in the literature led to its identification as laurecomin C, previously isolated from the alga *L. composita* (Li et al., 2012b). The ^{1}H NMR data of metabolite **12** are reported in Table 146.

Table 146. ^{1}H NMR data of metabolite **12** in $CDCl_3$ (δ in ppm, J in Hz).

Position	$\boldsymbol{\delta_{H,exp}}$	$\boldsymbol{\delta_{H,lit}}$
8	5.22 (brs)	5.25 (brs)
10	4.64 (dd, 10.7, 6.8)	4.66 (dd, 10.8, 6.8)
12	0.92 (s)	0.94 (s)
13	1.11 (s)	1.13 (s)
14	1.65 (brs)	1.67 (brs)
15	1.78 (brs)	1.81 (brs)

3.1.13 Metabolite 13

Metabolite **13** (LMH03) was isolated after a series of chromatographic separations as a colorless oil (2.0 mg).

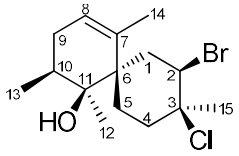

The mass spectrum of metabolite **13** (Figure 61) exhibited fragment ion peaks at *m/z* 298 and 300 at an 1:1 intensity suggesting the presence of a bromine atom and corresponding to $[M\text{-}Cl]^+$.

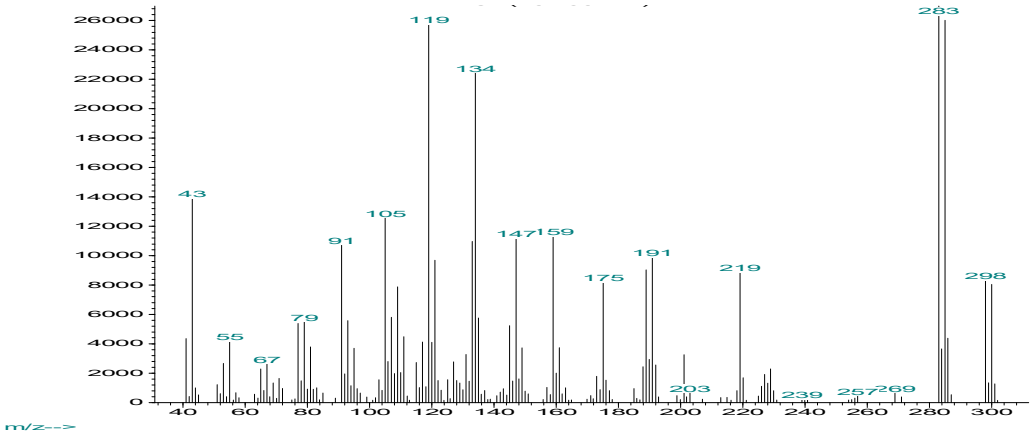

Figure 61. Mass spectrum (EIMS) of metabolite **13**.

In the ^{1}H NMR spectrum of metabolite **13** (Figure 62) obvious were:

- One aliphatic methyl on a tertiary carbon at δ 0.90,
- One aliphatic methyl on a non-protonated carbon at δ 0.93,
- One methyl on a non-protonated halogenated carbon at δ 1.72,
- One olefinic methyl at δ 1.90,
- One doublet of doublets at δ 4.68 integrating for one proton and attributed to a halogenated methine, and
- One broad singlet δ 5.21 integrating for one proton and attributed to an olefinic methine.

Analysis of the NMR and MS data of **13** led to the molecular formula $C_{15}H_{24}BrClO$. Taking into account the one carbon-carbon double bond as one of the three degrees of unsaturation, the molecular structure of **13** was determined as bicyclic.

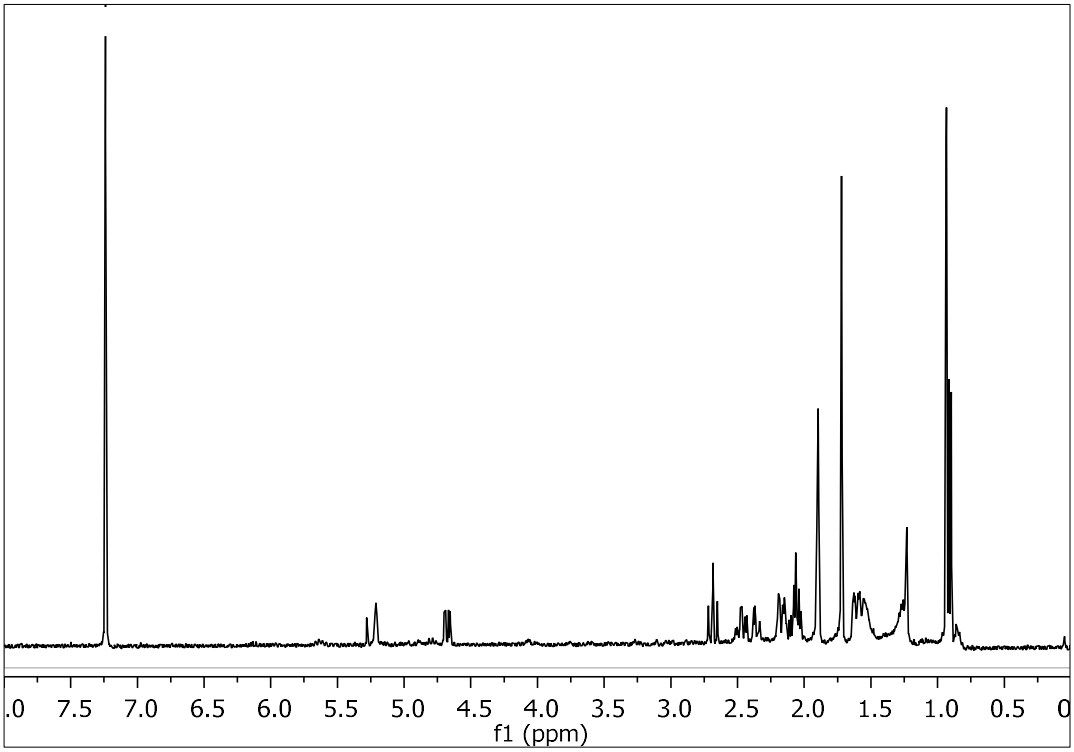

Figure 62. ^{1}H NMR spectrum of metabolite **13**.

Comparison of the spectroscopic and physical characteristics of metabolite **13** with those reported in the literature led to its identification as compositacin A, previously isolated from the red alga *L. composita* (Yu et al., 2017). The ^{1}H NMR data of metabolite **13** are reported in Table 147.

Table 147. ^{1}H NMR data of metabolite **13** in $CDCl_3$ (δ in ppm, J in Hz).

Position	$\delta_{H,exp}$	$\delta_{H,lit}$
1	2.68 (t, 13.6), 2.17 (ddd, 13.6, 5.3, 1.9)	2.70 (dd, 13.8, 13.2), 2.19 (ddd, 13.8, 5.4, 1.8)
2	4.68 (dd, 13.6, 5.3)	4.70 (dd, 13.2, 5.4)
4	2.49 (td, 14.3, 4.8), 2.38 (ddd, 14.3, 5.7, 2.4)	2.49 (ddd, 14.4, 14.2, 4.8), 2.38 (ddd, 14.4, 5.4, 2.4)
5	2.07 (m), 1.62 (m)	2.08 (ddd, 15.0, 14.2, 5.4), 1.63 (ddd, 15.0, 4.8, 2.4)
8	5.21 (brs)	5.23 (brs)
9	2.13 (m), 1.58 (m)	2.19 (m), 1.62 (m)
10	2.03 (m)	2.06 (m)
12	0.93 (s)	0.95 (s)
13	0.90 (d, 6.8)	0.93 (d, 6.6)
14	1.90 (brs)	1.92 (dd, 3.6, 1.8)
15	1.72 (s)	1.74 (s)

3.1.14 Metabolite 14

Metabolite **14** (LMH14) was isolated after a series of chromatographic separations as a colorless oil (2.1 mg).

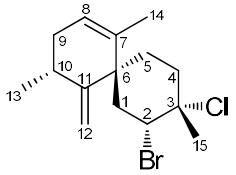

The mass spectrum of metabolite **14** (Figure 63) exhibited a molecular ion peak $[M]^+$ at *m/z* 316 with isotopic ion peaks at *m/z* 318 and 320 at an intensity suggestive of the presence of one bromine and one chlorine atom.

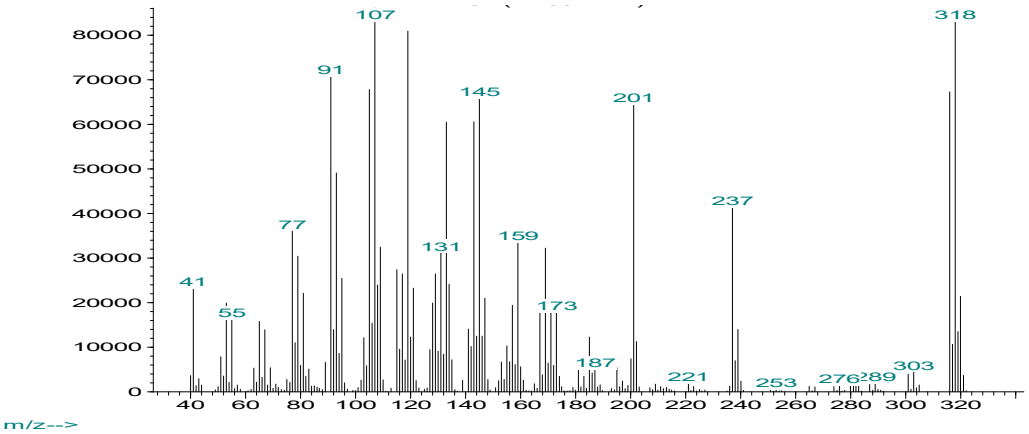

Figure 63. Mass spectrum (EIMS) of metabolite **14**.

In the ^{1}H NMR spectrum of metabolite **14** (Figure 64) obvious were:

- One aliphatic methyl on a tertiary carbon at δ 1.12,
- One olefinic methyl at δ 1.62,
- One methyl on non-protonated halogenated carbon at δ 1.65,
- One doublet of doublets at δ 4.16 integrating for one proton and attributed to a halogenated methine,
- Two broad singlets at δ 4.90 and 4.96 integrating for one proton each and attributed to the protons of an exomethylene, and
- One broad singlet at δ 5.22 integrating for one proton and attributed to an olefinic methine.

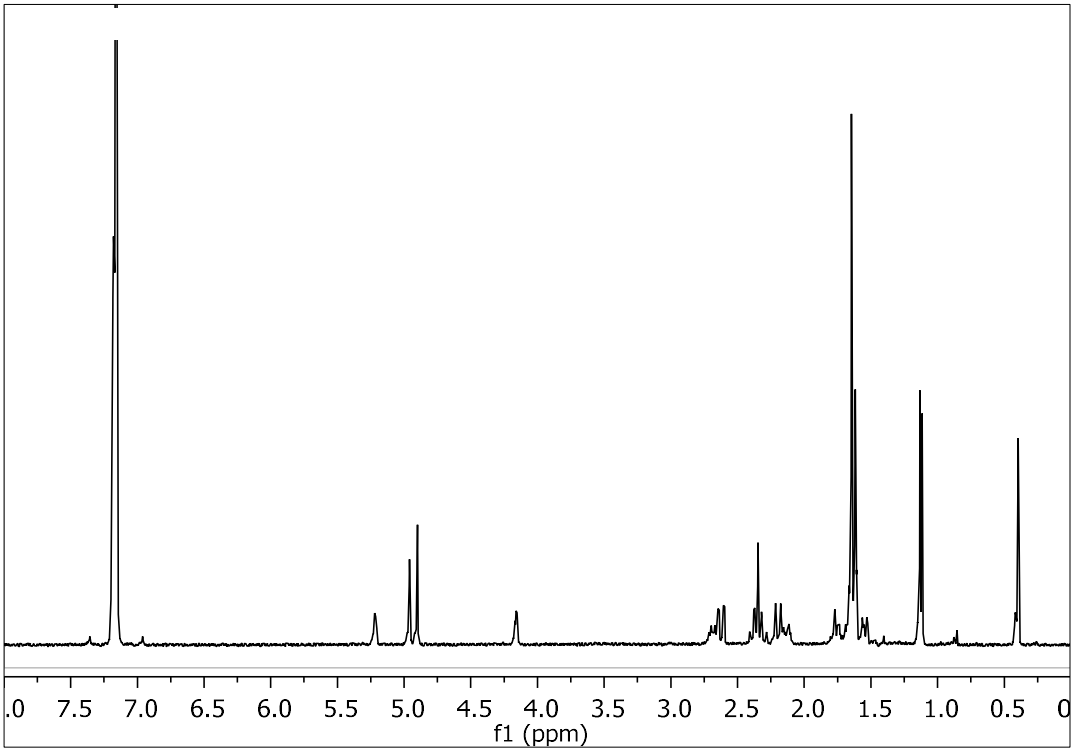

Figure 64. ^{1}H NMR spectrum of metabolite **14**.

Analysis of the NMR and MS data of **14** led to the molecular formula $C_{15}H_{22}BrCl$. Taking into account the two carbon-carbon double bonds as two of the four degrees of unsaturation, the molecular structure of **14** was determined as bicyclic.

Comparison of the spectroscopic and physical characteristics of metabolite **14** with those reported in the literature led to its identification as laurokamin A, previously isolated from the alga *L. okamurai* (Li et al., 2012a). The ^{1}H NMR data of metabolite **14** are reported in Table 148.

Table 148. ^{1}H NMR data of metabolite **14** in C_6D_6 and $CDCl_3$ (δ in ppm, J in Hz).

Position	$\boldsymbol{\delta}_{\mathbf{H,exp}}$ (in C_6D_6)	$\boldsymbol{\delta}_{\mathbf{H,lit}}$ (in $CDCl_3$)
2	4.16 (dd, 5.9, 2.9)	4.40 (dd, 5.4, 3.8)
8	5.22 (brs)	5.35 (brd, 3.6)
12	4.96 (brs), 4.90 (brs)	4.94 (s), 4.89 (s)
13	1.12 (d, 6.5)	1.13 (d, 6.6)
14	1.62 (brs)	1.72 (brs)
15	1.65 (s)	1.78 (s)

3.1.15 Metabolite 15

Metabolite **15** (LMH05) was isolated after a series of chromatographic separations as a colorless oil (8.8 mg).

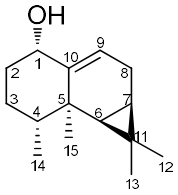

The mass spectrum of metabolite **15** (Figure 65) exhibited a molecular ion peak $[M]^+$ at *m/z* 220, as well as a fragment ion peak at *m/z* 205 corresponding to $[M\text{-}CH_3]^+$.

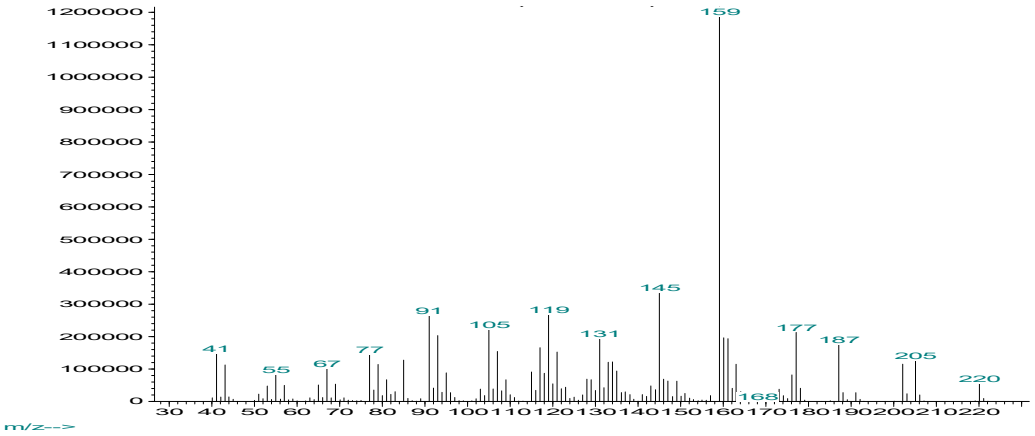

Figure 65. Mass spectrum (EIMS) of metabolite **15**.

In the ^{1}H NMR spectrum of metabolite **15** (Figure 66) obvious were:

- One aliphatic methyl on a tertiary carbon at δ 0.95,
- Three aliphatic methyls on non-protonated carbons at δ 0.99, 0.99 and 1.21,
- One triplet at δ 4.18 integrating for one proton and attributed to an oxygenated methine, and
- One multiplet at δ 5.45 integrating for one proton and attributed to an olefinic methine.

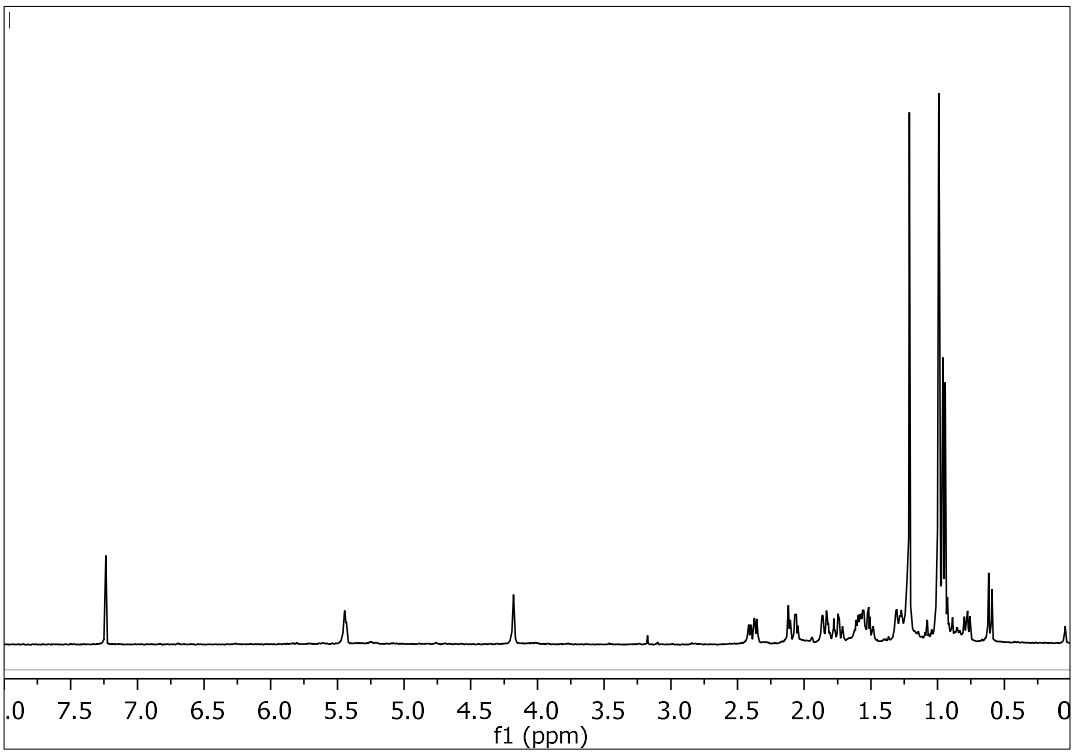

Figure 66. ^{1}H NMR spectrum of metabolite **15**.

Analysis of the NMR and MS data of **15** led to the molecular formula $C_{15}H_{24}O$. Taking into account the one carbon-carbon double bond as one of the four degrees of unsaturation, the molecular structure of **15** was determined as tricyclic.

Comparison of the spectroscopic and physical characteristics of metabolite **15** with those reported in the literature led to its identification as aristol-9(10)-en-1α-ol, previously isolated from the alga *L. similis* (Kamada & Vairappan, 2013) and synthetically prepared (Takeshita et al., 1980). The ^{1}H NMR data of metabolite **15** are reported in Table 149.

Table 149. ^{1}H NMR data of metabolite **15** in $CDCl_3$ and $(CD_3)_2SO$ (δ in ppm, J in Hz).

Position	$\delta_{H,exp}$ (in $CDCl_3$)	$\delta_{H,lit}$ (in $(CD_3)_2SO$)
1	4.18 (t, 2.7)	4.17 (m)
6	0.61 (d, 9.5)	
7	0.78 (dd, 9.5, 7.2)	
9	5.45 (m)	5.42 (m)
12	0.99 (s)	1.02 (s)
13	0.99 (s)	1.02 (s)
14	0.95 (d, 6.8)	1.0 (d, 7.0)
15	1.21 (s)	1.23 (s)

3.1.16 Metabolite 16

Metabolite **16** (LMH11) was isolated after a series of chromatographic separations as a colorless oil (1.5 mg).

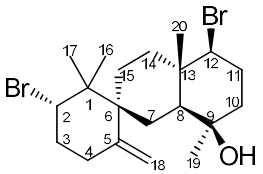

The mass spectrum of metabolite **16** (Figure 67) exhibited isotopic fragment ion peaks at *m/z* 428, 430 and 432 at an intensity suggestive of the presence of two bromine atoms in the molecule and corresponding to $[M\text{-}H_2O]^+$.

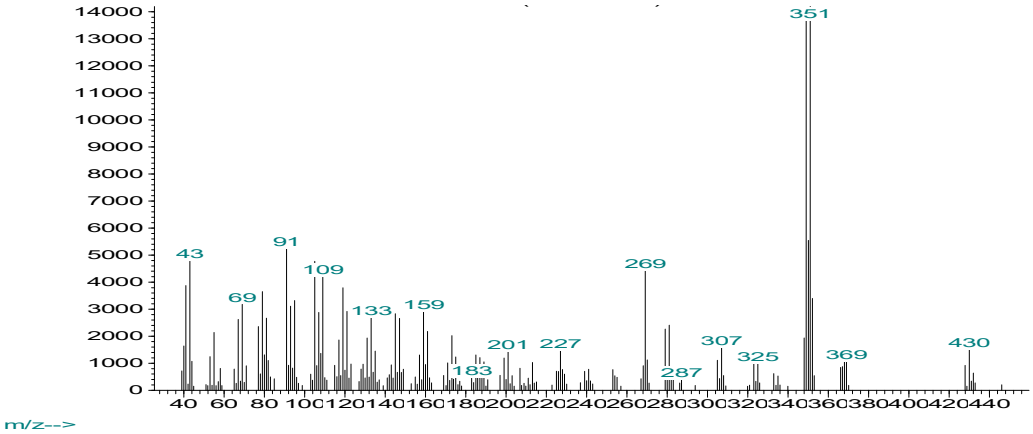

Figure 67. Mass spectrum (EIMS) of metabolite **16**.

In the ^{1}H NMR spectrum of metabolite **16** (Figure 68) obvious were:

- Four aliphatic methyls on non-protonated carbons at δ 0.94, 1.12, 1.18 and 1.19,
- Two doublets of doublets at δ 3.87 and 4.60 integrating for one proton each and attributed to two halogenated methines, and
- Two broad singlets at δ 4.87 and 5.11 integrating for one proton each and attributed to the protons of an exomethylene.

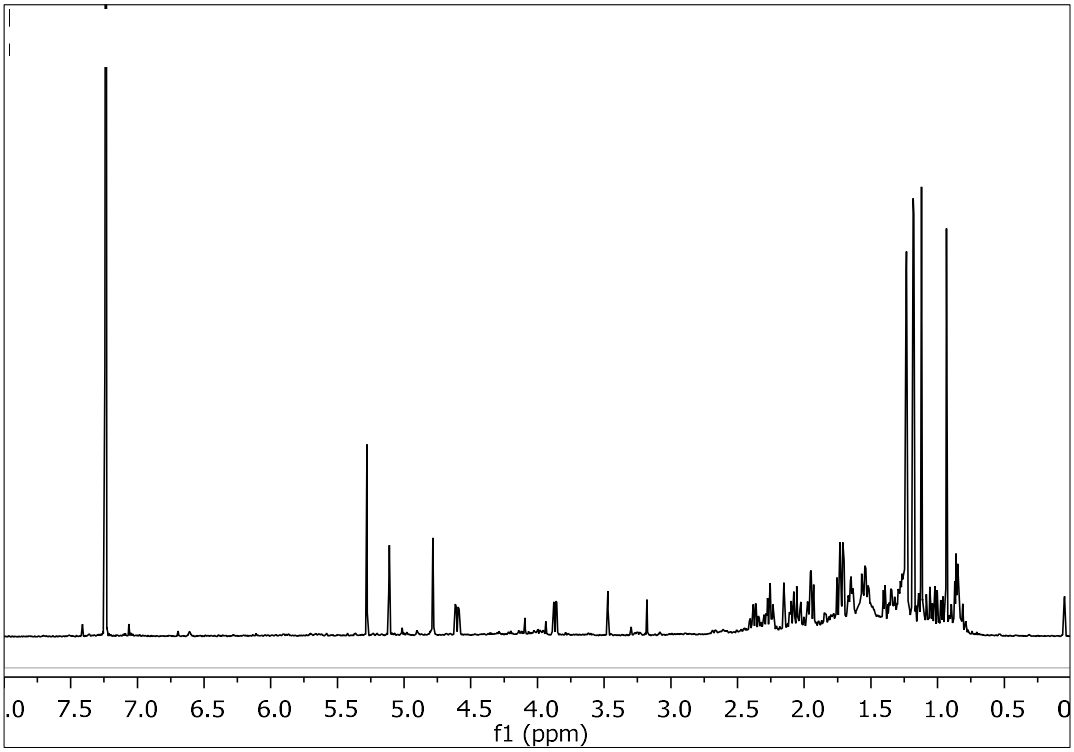

Figure 68. ^{1}H NMR spectrum of metabolite **16**.

Analysis of the NMR and MS data of **16** led to the molecular formula $C_{20}H_{32}Br_2O$. Taking into account the one carbon-carbon double bond as one of the four degrees of unsaturation, the molecular structure of **16** was determined as tricyclic.

The planar structure of metabolite **16** was determined on the basis of the homonuclear and heteronuclear correlations observed in the HSQC-DEPT (Figure 69), HMBC (Figure 70) and COSY (Figure 71) spectra.

Comparison of the spectroscopic and physical characteristics of metabolite **16** with those reported in the literature led to its identification as kahukuene B, previously isolated from the alga *L. majuscula* (Brennan et al., 1993). The ^{1}H NMR data of metabolite **16** are reported in Table 150.

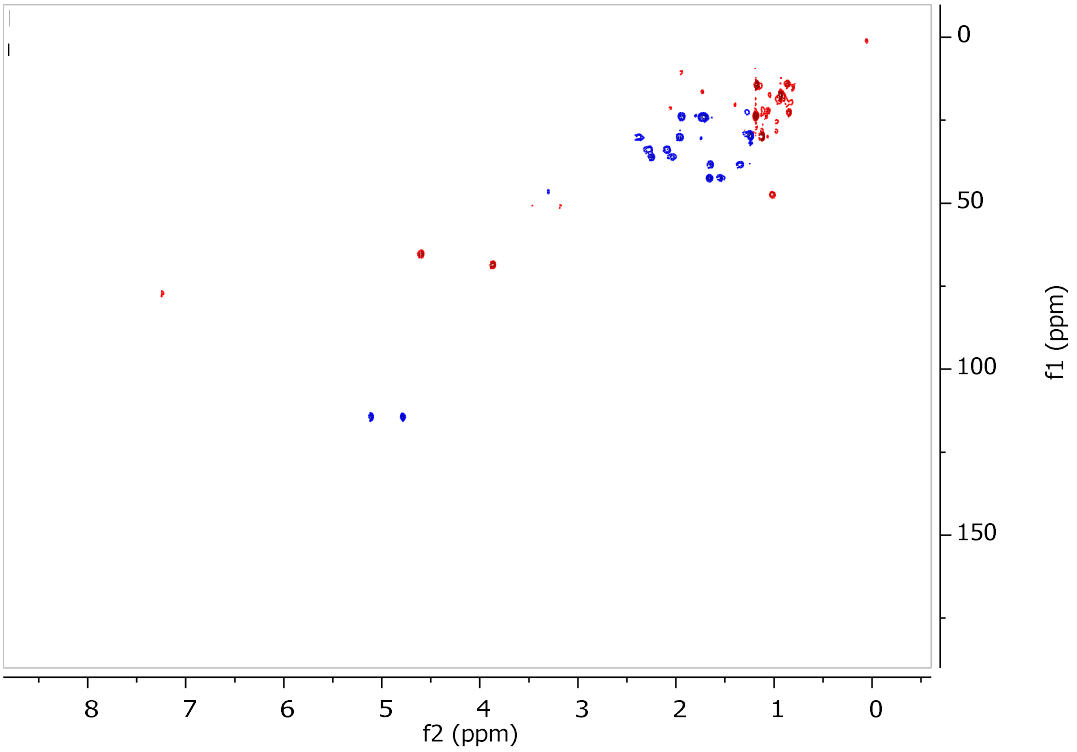

Figure 69. HSQC-DEPT spectrum of metabolite **16**.

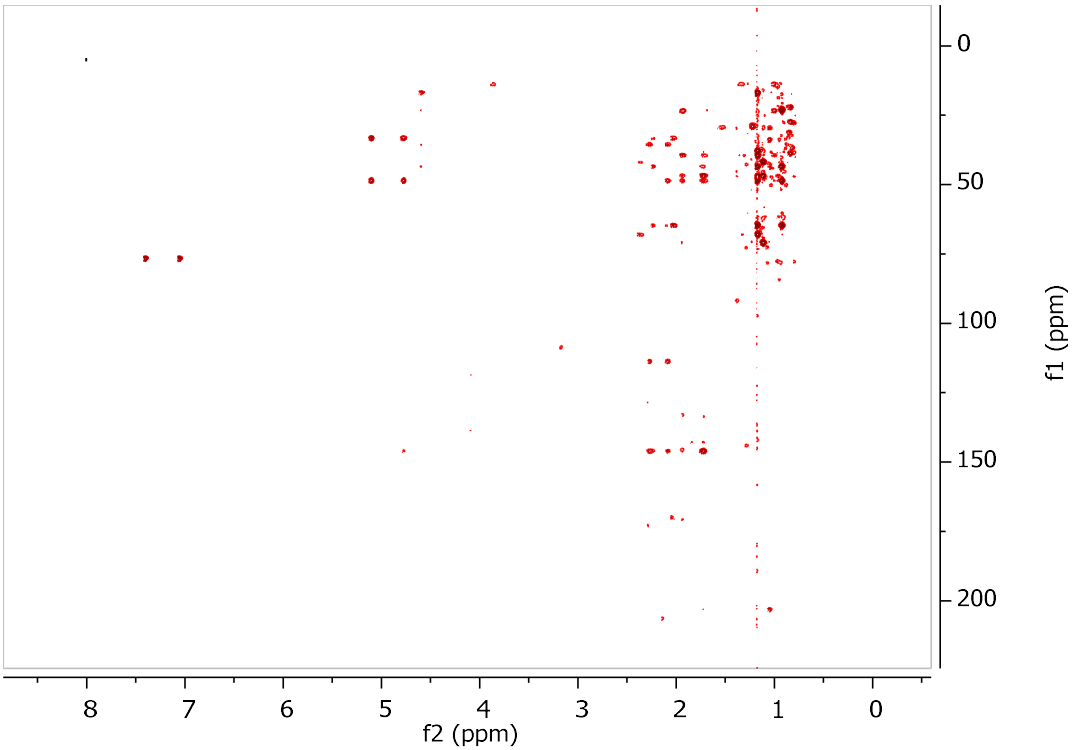

Figure 70. HMBC spectrum of metabolite **16**.

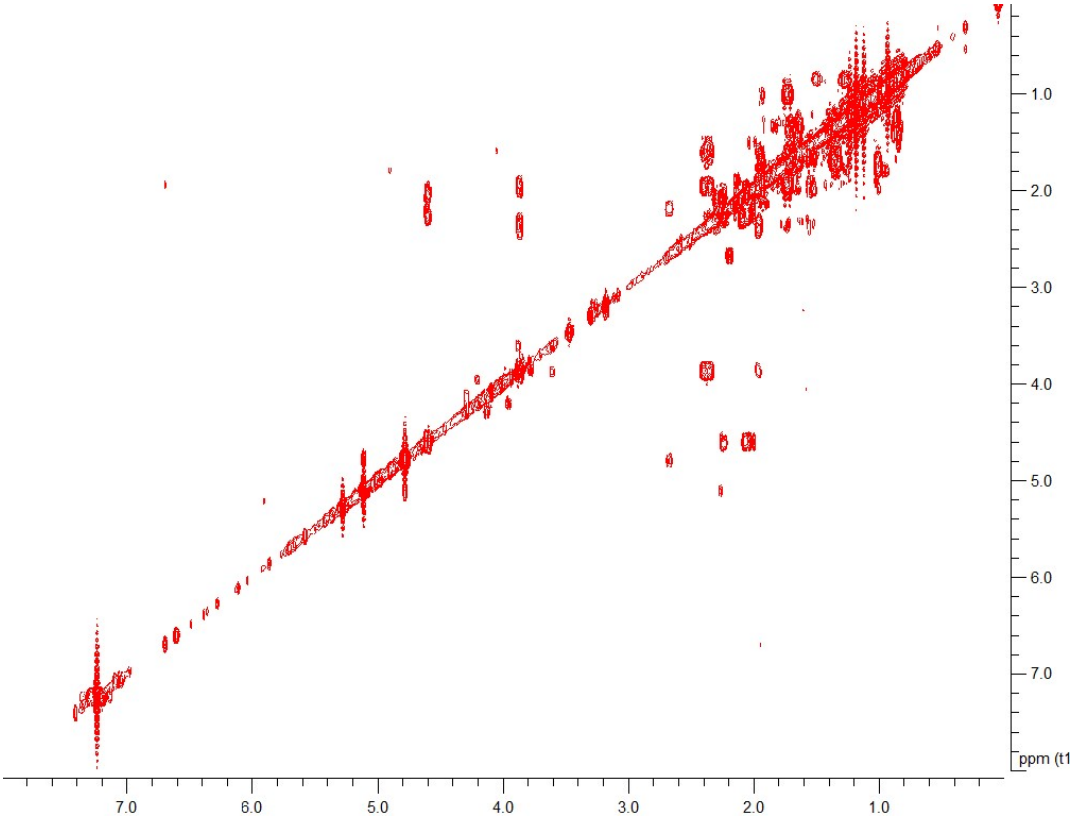

Figure 71. COSY spectrum of metabolite **16**.

Table 150. ^{1}H and ^{13}C NMR data of metabolite **16** in $CDCl_3$ and C_6D_6 (δ in ppm, J in Hz).

Position	$\delta_{C,exp}$	$\delta_{H,exp}$	$\delta_{C,lit}$	$\delta_{H,lit}$
	in $CDCl_3$		in C_6D_6	
1	44.1	-	44.2	-
2	65.2	4.60 (dd, 12.7, 4.5)	65.4	4.45 (dd, 14.7, 2.7)
3	35.8	2.24 (m), 2.03 (m)	36.5	2.04 (qd, 11.5, 6.8, 4.7, 2.7), 2.00 (qd, 14.7, 13.5, 11.5, 6.8)
4	33.7	2.27 (m), 2.08 (m)	33.9	1.98 (ddd, 13.5, 12.8, 6.8) 1.73 (ddd, 12.8, 6.0, 4.7)
5	146.7	-	147.1	-
6	48.7	-	49.2	-
7	24.1	1.94 (m), 1.71 (m)	24.0	1.59 (dd, 10.2, 1.11), 1.56 (dd, 13.3, 10.2)
8	47.4	1.01 (m)	47.5	0.68 (dd, 13.3, 1.1)
9	71.7	-	70.8	-
10	42.3	1.66 (m), 1.55 (m)	42.3	1.14 (ddd, 14.2, 4.3, 2.8), 0.91 (ddd, 14.2, 13.4, 4.5)
11	30.0	2.37 (m), 1.95 (m)	30.5	2.39 (qd, 13.4, 13.3, 12.7, 4.3), 1.80 (qd, 13.3, 4.5, 3.8, 2.8)
12	68.6	3.87 (dd, 12.7, 3.7)	68.8	3.63 (dd, 12.7, 3.8)
13	39.9	-	40.3	-
14	38.2	1.65 (m), 1.33 (m)	38.7	1.70 (ddd, 13.1, 4.2, 3.1) 1.23 (ddd, 14.6, 13.1, 3.5)
15	24.2	1.73 (m)	24.4	1.46 (ddd, 14.6, 12.5, 4.2), 1.42 (ddd, 12.5, 3.5, 3.1)
16	23.5	1.19 (s)	23.7	1.09 (s)
17	17.5	0.94 (s)	17.7	0.96 (s)
18	114.2	5.11 (brs), 4.78 (brs)	114.1	4.89 (brs), 4.59 (brs)
19	29.6	1.12 (s)	29.7	0.64 (s)
20	14.4	1.18 (s)	14.5	1.29 (s)

3.1.17 Metabolite 17

Metabolite **17** (LMH04) was isolated after a series of chromatographic separations as a colorless oil (3.6 mg).

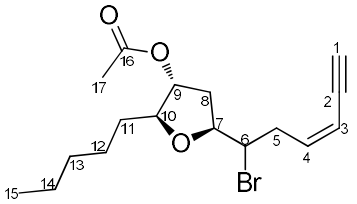

The mass spectrum of metabolite **17** (Figure 72) exhibited a molecular ion peak $[M]^+$ at *m/z* 356 with an isotopic ion peak at *m/z* 358 at an intensity of 1:1, suggesting the presence of a bromine atom in the molecule.

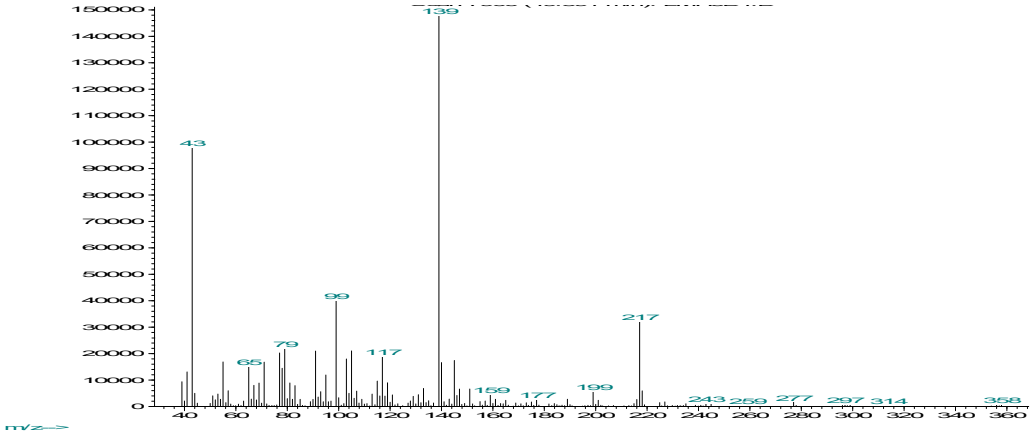

Figure 72. Mass spectrum (EIMS) of metabolite **17**.

In the ^{1}H NMR spectrum of metabolite **17** (Figure 73) obvious were:

- One aliphatic methyl on a secondary carbon at δ 0.87,
- One acetoxy methyl at δ 1.70,
- One acetylenic methine at δ 2.75,
- One doublet of triplets at δ 3.38 and three doublets of doublets of doublets at δ 3.69, 3.85 and 5.08 integrating for one proton each and attributed to four oxygenated or halogenated methines, and
- Two doublets at δ 5.35 and 5.85 integrating for one proton each and attributed to two olefinic methines.

Analysis of the NMR and MS data of **17** led to the molecular formula $C_{17}H_{25}BrO_3$. Taking into account the one carbon-carbon triple bond, the one carbon-carbon double bond and the carbonyl moiety as four of the five degrees of unsaturation, the molecular structure of **17** was determined as monocyclic.

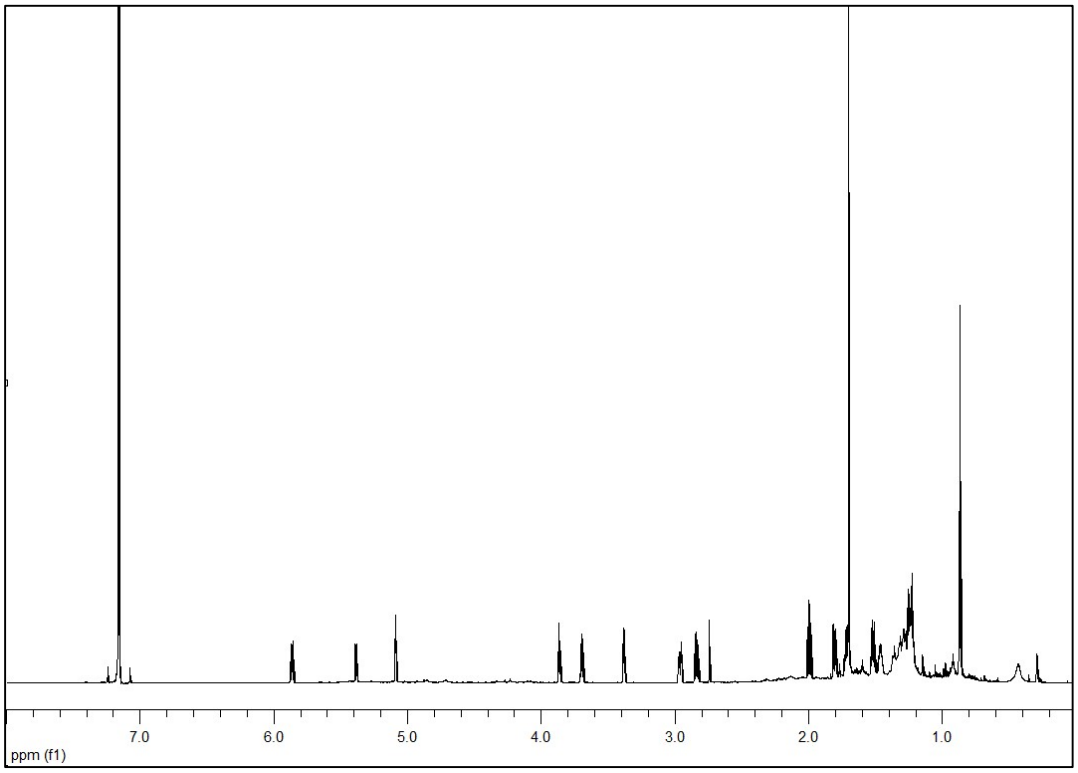

Figure 73. ^{1}H NMR spectrum of metabolite **17**.

The planar structure of metabolite **17** was determined on the basis of the homonuclear and heteronuclear correlations (Figure 74) observed in the HSQC-DEPT (Figure 75), HMBC (Figure 76) and COSY (Figure 77) spectra. In particular, the HSQC spectrum revealed correlations for two methyls, six methylenes and seven methines, among which one was halogenated and three were oxygenated. The COSY cross-peaks indicated the presence of a single spin system extending from H-1 to H_3-15, revealing the position of the bromine atom at C-6 and confirming the presence of an enyne functionality. The HMBC correlation of H-7 (δ_H 3.69) with C-10 (δ_C 81.8) indicated the formation of an ether bridge between C-7 and C-10. Moreover, the acetoxy group was placed at C-9 on the basis of the HMBC correlation between H-9 (δ_H 5.08) and the carbonyl carbon C-16 (δ_C 169.2).

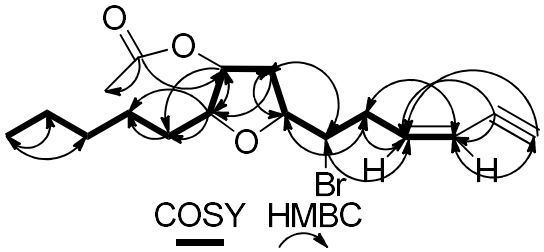

Figure 74. COSY and important HMBC correlations observed for metabolite **17**.

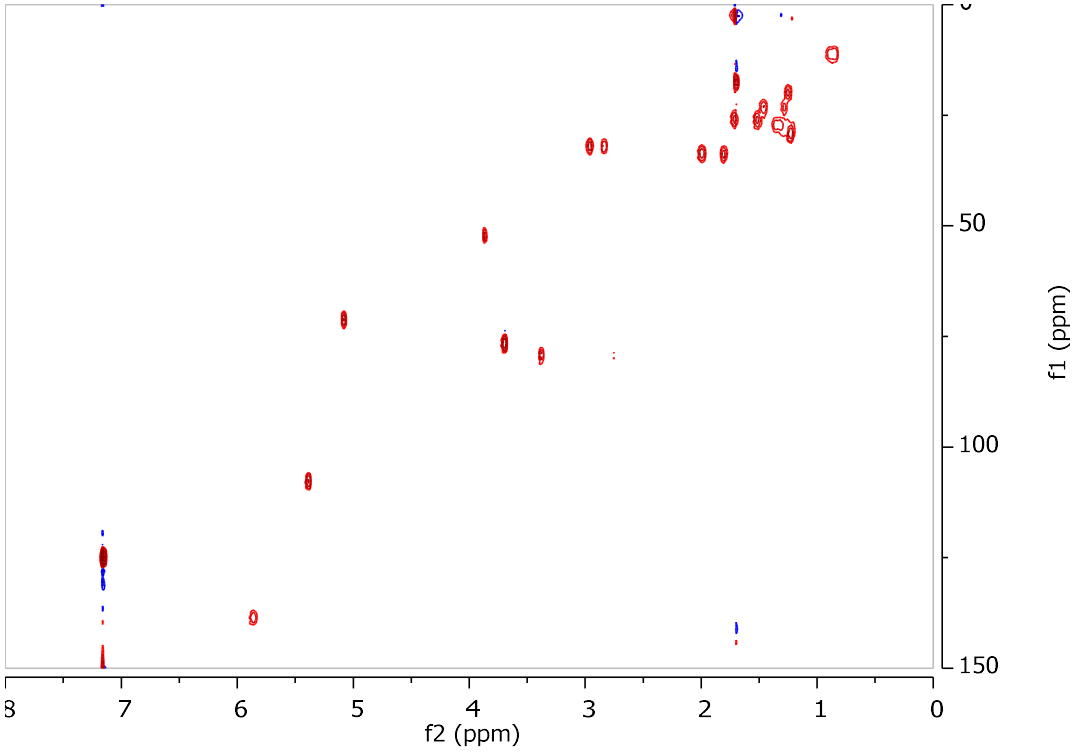

Figure 75. HSQC-DEPT spectrum of metabolite **17**.

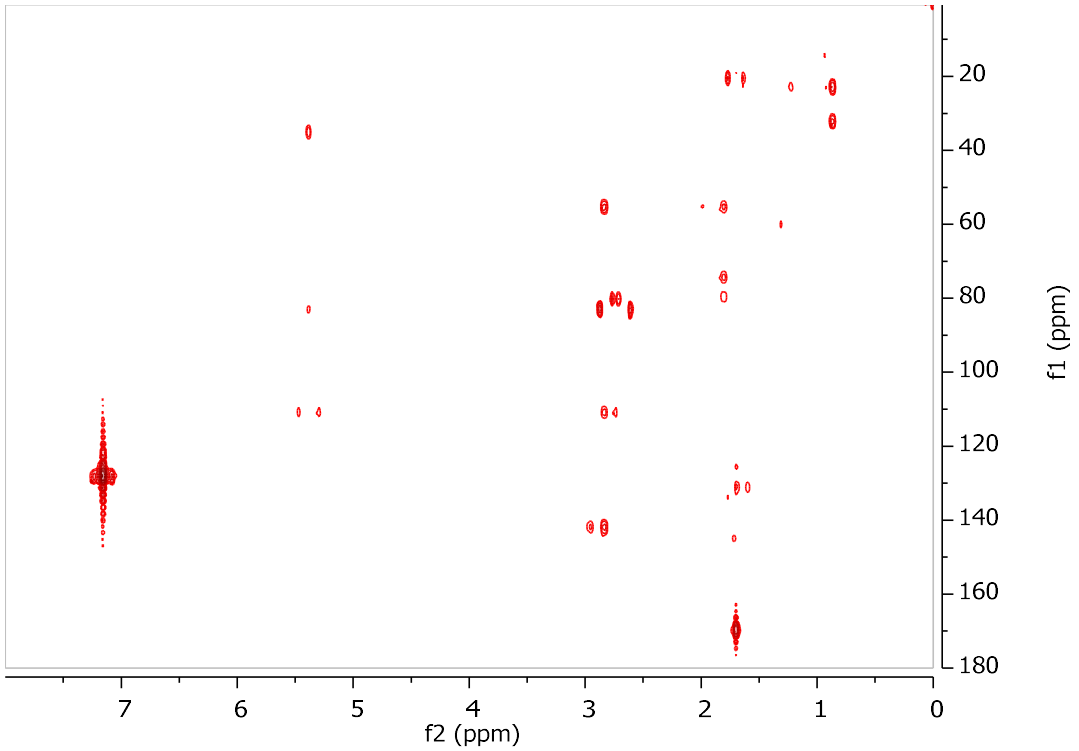

Figure 76. HMBC spectrum of metabolite **17**.

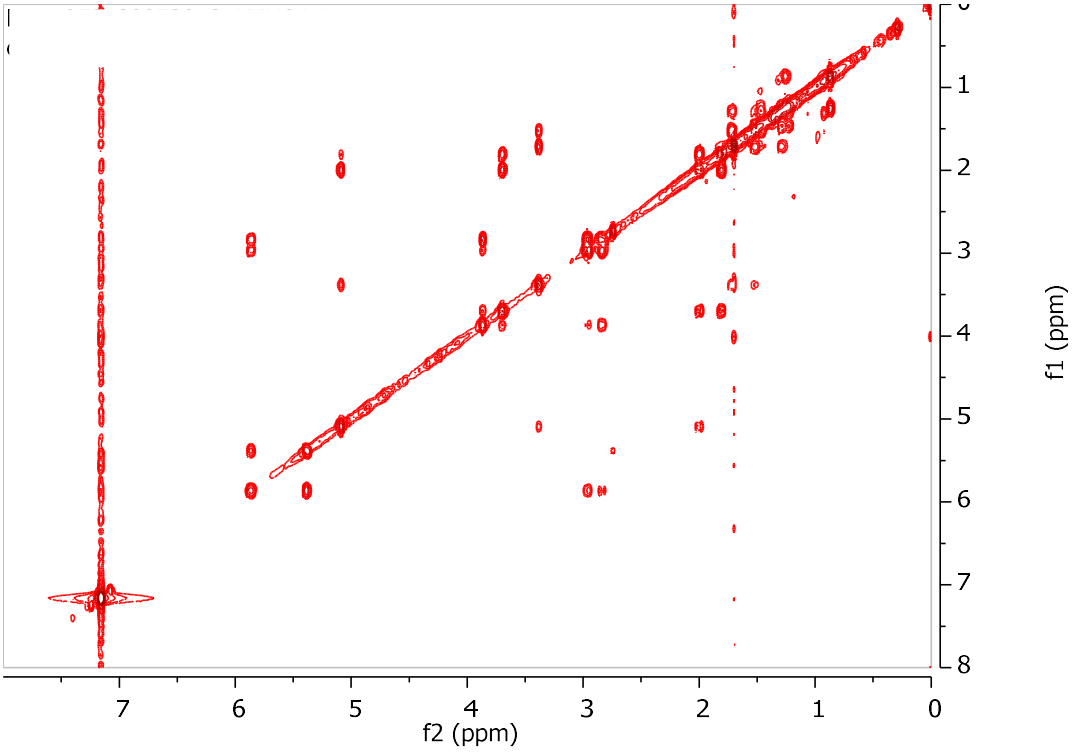

Figure 77. COSY spectrum of metabolite **17**.

The relative configuration of the asymmetric centers of metabolite **17** was determined on the basis of the correlations observed in the NOESY spectrum (Figure 78). Specifically, the strong NOE enhancement between H-7 and H-10 indicated their *cis* orientation, while the lack of NOE correlation between H-7 and H-9 indicated their *trans* orientation. The geometry of the carbon-carbon double bond of the -enyne moiety was determined as *Z* on the basis of the measured coupling constant between H-3 and H-4 (J = 10.6 Hz), as already indicated by the chemical shift of the acetylenic proton resonating at δ 2.75.

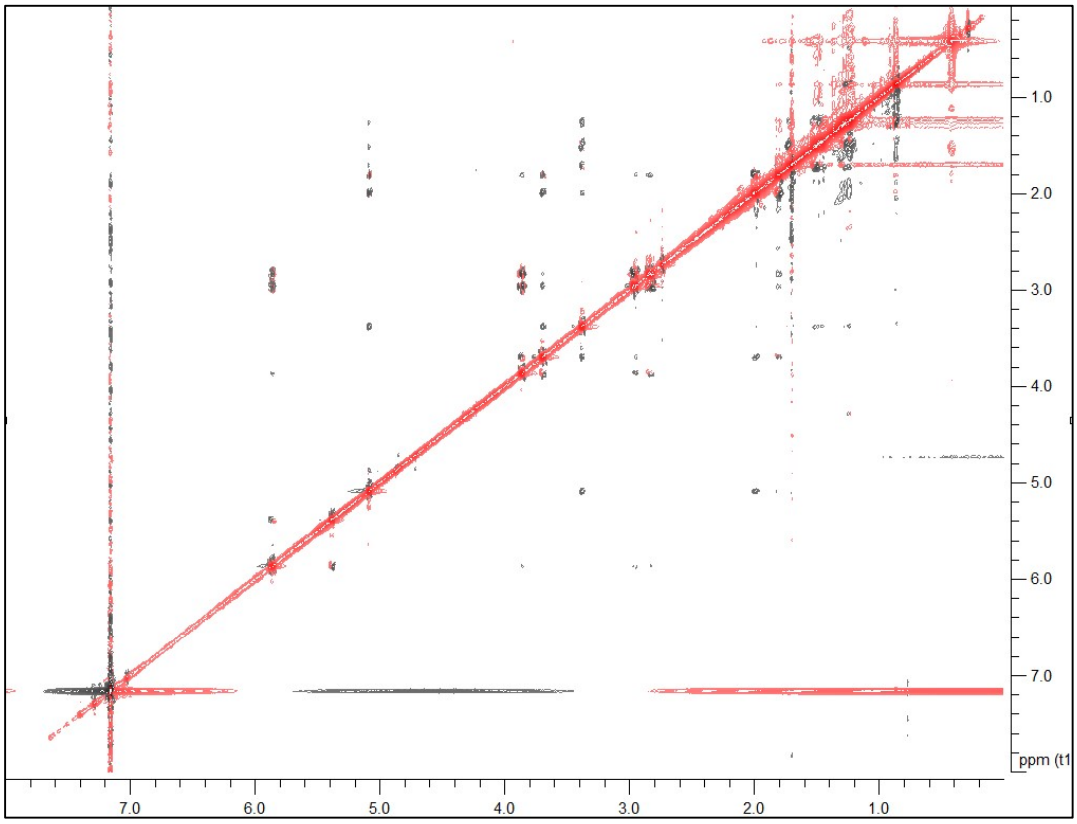

Figure 78. NOESY spectrum of metabolite **17**.

Comparison of the spectroscopic and physical characteristics of metabolite **17** with those reported in the literature led to its identification as a new natural product. The NMR data of metabolite **17** are reported in Table 151.

Table 151. ^{1}H and ^{13}C NMR data of metabolite **17** in C_6D_6 (δ in ppm, J in Hz).

Position	δ_C	δ_H
1	82.2	2.75 (d, 1.4)
2	79.7	-
3	110.3	5.38 (dd, 10.6, 1.4)
4	141.4	5.85 (dt, 10.6, 7.0)
5	34.7	2.95 (ddd, 15.7, 7.0, 4.5), 2.83 (ddd, 15.7, 9.2, 7.0)
6	54.5	3.85 (ddd, 9.2, 5.1, 4.5)
7	79.3	3.69 (ddd, 8.3, 7.0, 5.1)
8	36.3	1.99 (ddd, 14.5, 8.3, 6.5), 1.81 (ddd, 14.5, 7.0, 2.0)
9	73.4	5.08 (ddd, 6.5, 4.3, 2.0)
10	81.8	3.38 (dt, 8.7, 4.3)
11	28.7	1.72 (m), 1.52 (m)
12	25.7	1.47 (m), 1.29 (m)
13	31.8	1.25 (m)
14	22.2	1.26 (m)
15	13.6	0.87 (t, 7.1)
16	169.2	-
17	19.9	1.70 (s)

3.1.18 Metabolite 18

Metabolite **18** (LMH02) was isolated after a series of chromatographic separations as a colorless oil (30.0 mg).

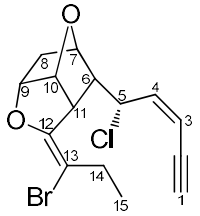

The mass spectrum of metabolite **18** (Figure 79) exhibited a molecular ion peak $[M]^+$ at *m/z* 342 with isotopic ion peaks at *m/z* 344 and 346 at a relative intensity characteristic for the presence of one bromine and one chlorine atom in the molecule.

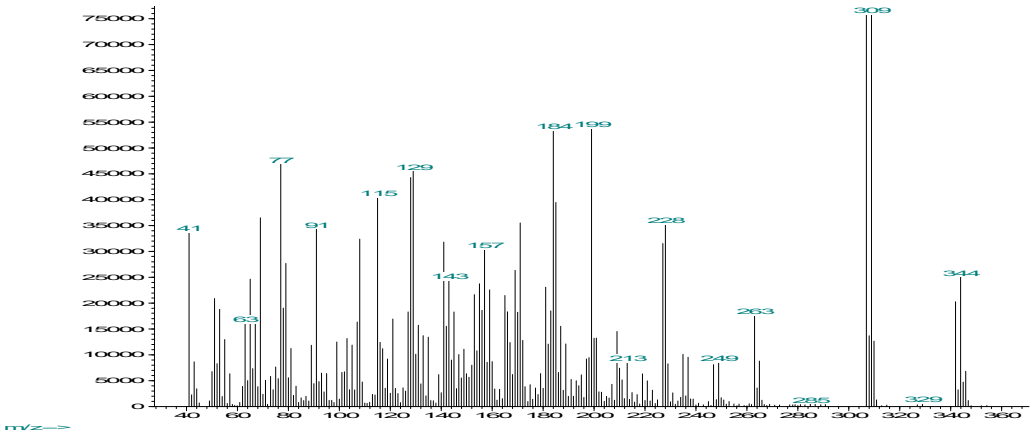

Figure 79. Mass spectrum (EIMS) of metabolite **18**.

In the ^{1}H NMR spectrum of metabolite **18** (Figure 80) obvious were:

- One aliphatic methyl on a secondary carbon at δ 1.02,
- One acetylenic methine at δ 2.68,
- Four signals at δ 4.10, 4.43, 4.53 and 4.91 integrating for one proton each and attributed to four oxygenated or halogenated methines, and
- Two signals at δ 5.20 and 5.59 integrating for one proton each and attributed to two olefinic methines.

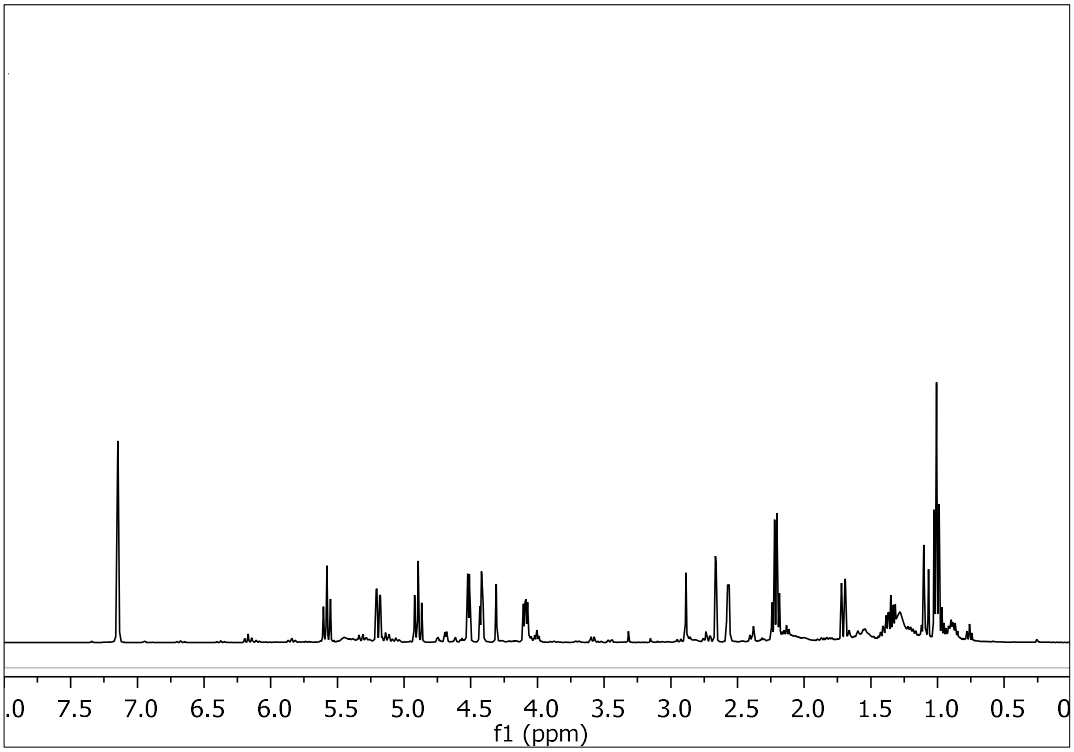

Figure 80. ^{1}H NMR spectrum of metabolite **18** in C_6D_6.

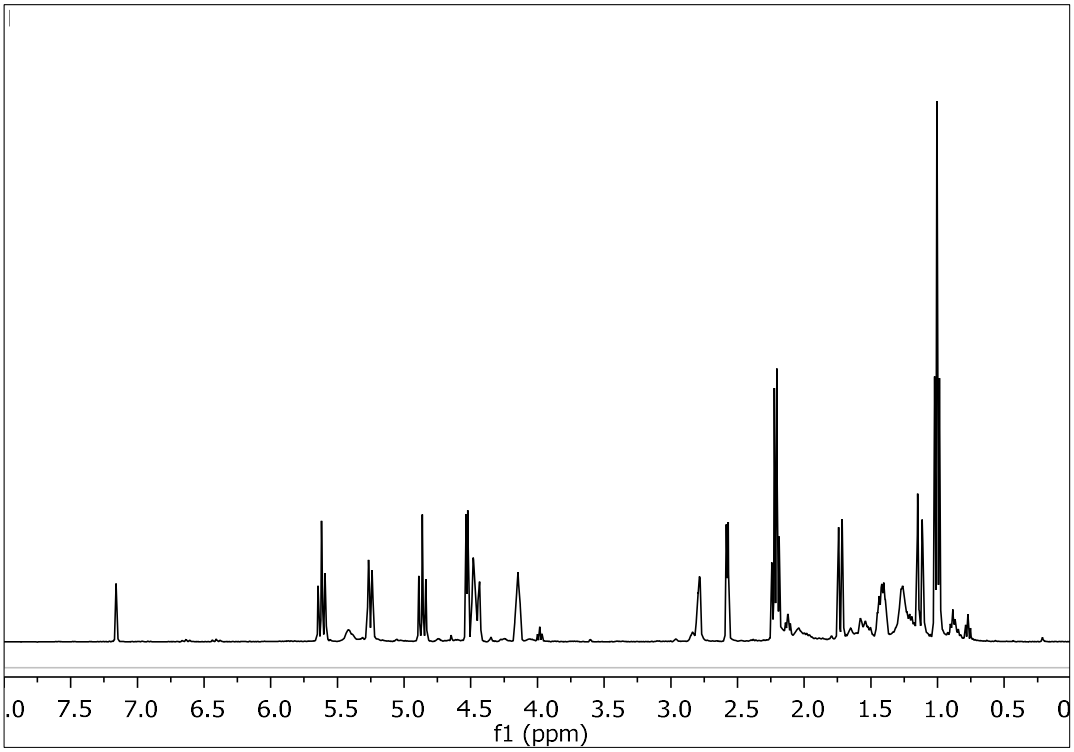

Figure 81. ^{1}H NMR spectrum of metabolite **18** in $CDCl_3$.

Analysis of the NMR and MS data of **18** led to the molecular formula $C_{15}H_{16}BrClO_2$. Taking into account the one carbon-carbon triple bond and the two carbon-carbon double bonds as four of the seven degrees of unsaturation, the molecular structure of **18** was determined as tricyclic.

Comparison of the spectroscopic and physical characteristics of metabolite **18** with those reported in the literature led to its identification as *cis*-maneonene-D, previously isolated from the red alga *L. obtusa* (Ayyad et al., 2011). The ^{1}H NMR data of metabolite **18** are reported in Table 152.

Table 152. ^{1}H and ^{13}C NMR data of metabolite **18** in C_6D_6 (δ in ppm, J in Hz).

Position	$\boldsymbol{\delta_{H,exp}}$	$\boldsymbol{\delta_{H,lit}}$
1	2.68 (d, 2.2)	2.63 (dd, 2.4, 1.2)
3	5.20 (dd, 10.5, 2.2)	5.19 (dd, 10.8, 2.4)
4	5.59 (t, 10.5)	5.59 (ddd, 10.8, 10.8, 1.2)
5	4.91 (t, 10.5)	4.92 (dd, 10.8, 10.8)
6	1.72 (d, 10.5)	1.72 (dd, 10.8, 1.8)
7	4.53 (d, 5.2)	4.53 (brd, 5.4)
8	1.34 (m), 1.10 (d, 13.2)	1.34 (ddd, 13.2, 7.8, 5.4), 1.08 (d, 13.2)
9	4.10 (dd, 7.6, 4.7)	4.08 (dd, 7.8, 4.8)
10	4.43 (m)	4.41 (dd, 4.8, 4.8)
11	2.58 (d, 5.0)	2.58 (brd, 4.8)
14	2.23 (q, 7.3)	2.23 (q, 7.2)
15	1.02 (t, 7.3)	1.03 (t, 7.2)

3.1.19 Metabolite 19

Metabolite **19** (LMH06) was isolated after a series of chromatographic separations as a colorless oil (7.6 mg).

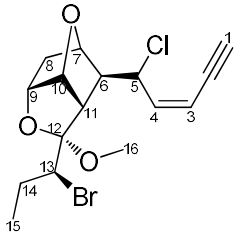

The mass spectrum of metabolite **19** (Figure 82) exhibited a fragment ion peak at *m/z* 343 and isotopic ion peaks at *m/z* 345 and 347 at a relative intensity characteristic for the presence of one bromine and one chlorine atom in the molecule and corresponding to $[M\text{-}OCH_3]^+$.

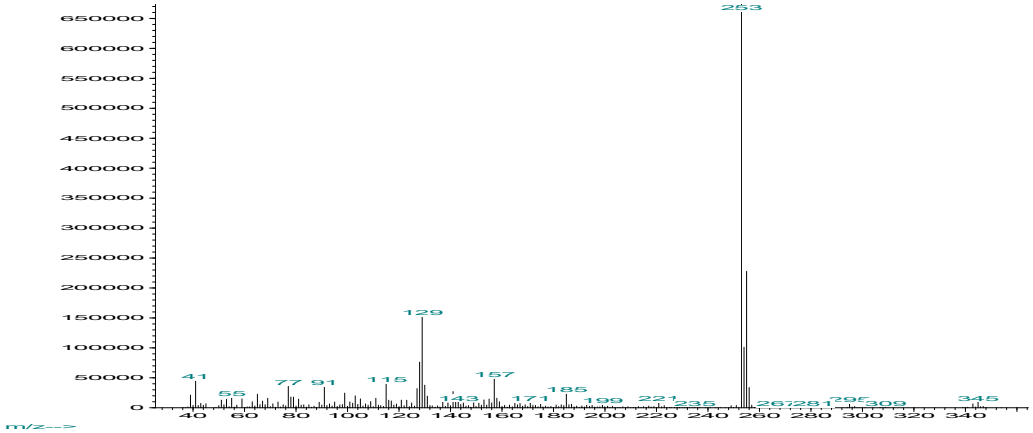

Figure 82. Mass spectrum (EIMS) of metabolite **19**.

In the ^{1}H NMR spectrum of metabolite **19** (Figure 83) obvious were:

- One aliphatic methyl on a secondary carbon at δ 1.06,
- One acetylenic methine at δ 3.24,
- One oxygenated methyl at δ 3.27,
- Five signals at δ 4.04, 4.40, 4.72, 4.80 and 5.30 integrating for one proton each and attributed to five oxygenated or halogenated methines, and
- Two signals at δ 5.60 and 5.90 integrating for one proton each and attributed to two olefinic methines.

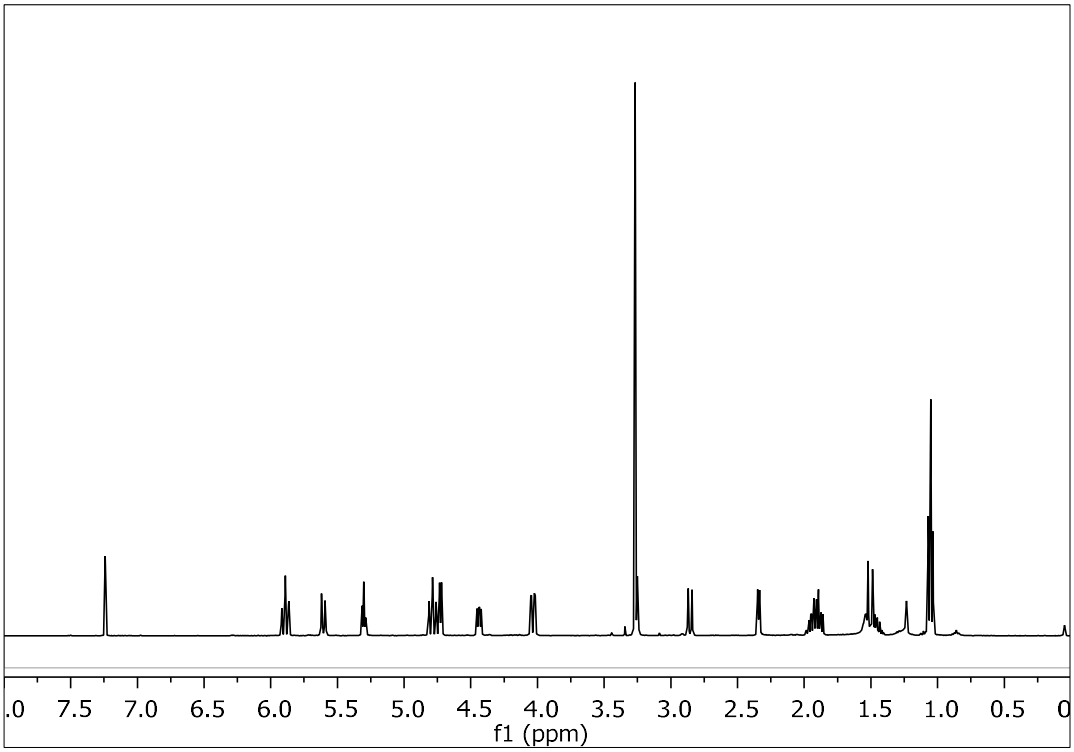

Figure 83. ^{1}H NMR spectrum of metabolite **19**.

Analysis of the NMR and MS data of **19** led to the molecular formula $C_{16}H_{20}BrClO_3$. Taking into account the one carbon-carbon triple bond and the one carbon-carbon double bond as three of the six degrees of unsaturation, the molecular structure of **19** was determined as tricyclic.

The planar structure of metabolite **19** was determined on the basis of the homonuclear and heteronuclear correlations (Figure 84) observed in the HSQC-DEPT (Figure 85), HMBC (Figure 86) and COSY (Figure 87) spectra. In particular, the correlations observed in the HSQC-DEPT spectrum revealed the presence of two methyls, two methylenes and ten methines. The COSY cross-peaks indicated the presence of an extended spin system ranging from H-1 to H-11, as well as that of short one from H-13 to H_3-15. The HMBC correlations of H-10 (δ_H 5.30) with C-7 (δ_C 77.5), as well as of H-9 (δ_H 4.40) with C-12 (δ_C 108.2), identified the formation of two ether bridges between C-7 and C-10 and C-9 and C-10, while the correlations of C-12 with H-6 (δ_H 2.87) and H-13 (δ_H 4.04) connected the two spin systems and indicated the formation of the tricyclic skeleton. In addition, the HMBC correlations of C-2 (δ_C 78.3) with H-3 (δ_H 5.60) and H-4 (δ_H 5.90), as well as of C-4 (δ_C 141.6) with H-1 (δ_H 3.24) confirmed the presence of the terminal enyne moiety, which is frequently encountered in C_{15} acetogenins (Takahashi et al., 1999). Moreover, the HMBC correlation of Me-16 (δ_H 3.27) with C-12 (δ_C 108.2) secured the position of the methoxy group at C-12.

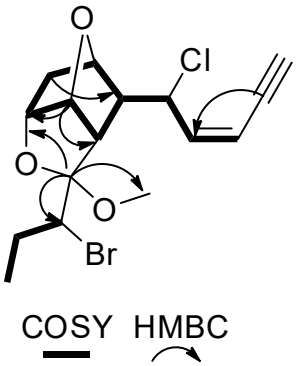

Figure 84. COSY and important HMBC correlations observed for metabolite **19**.

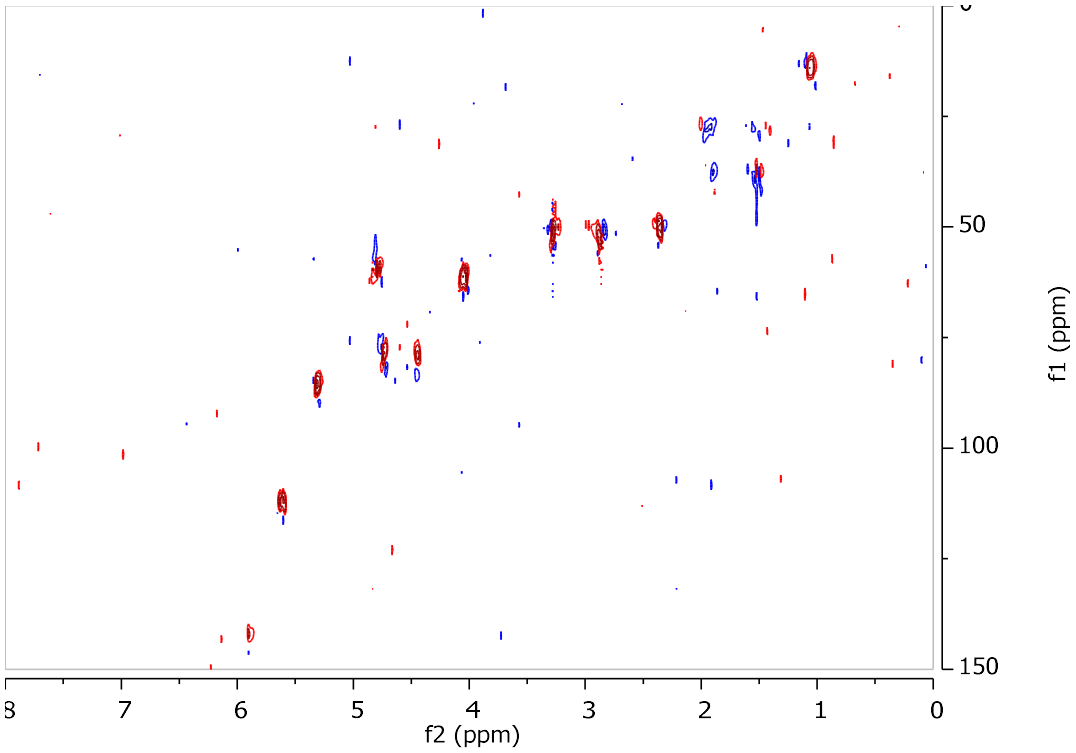

Figure 85. HSQC-DEPT spectrum of metabolite **19**.

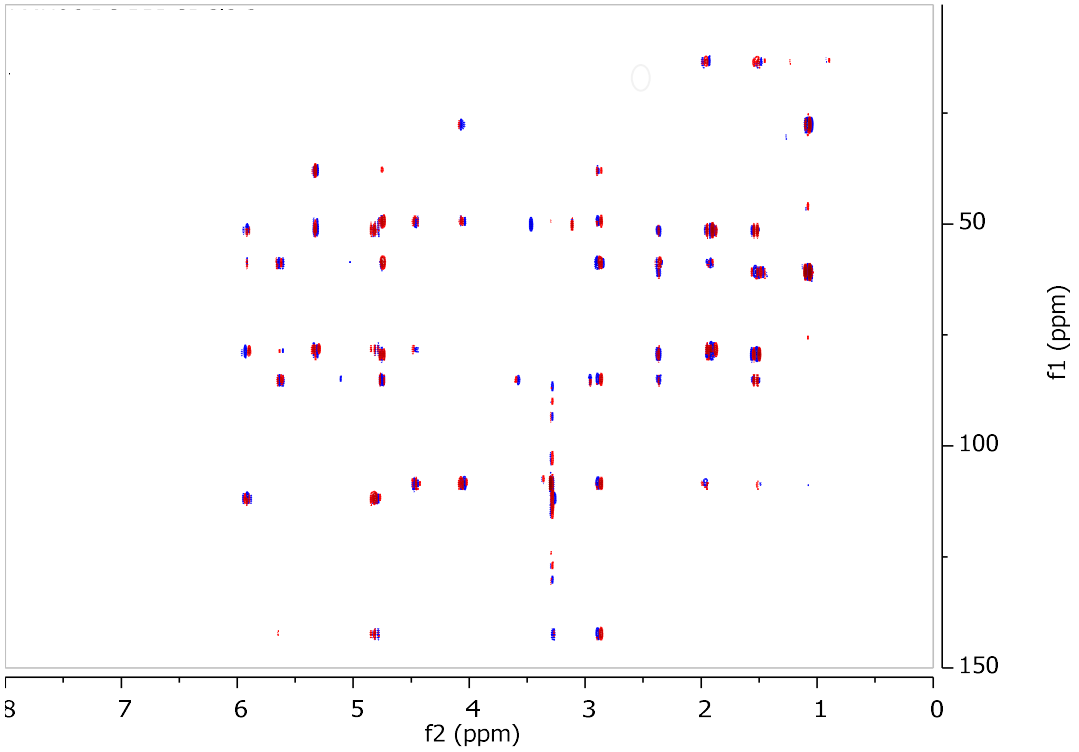

Figure 86. HMBC spectrum of metabolite **19**.

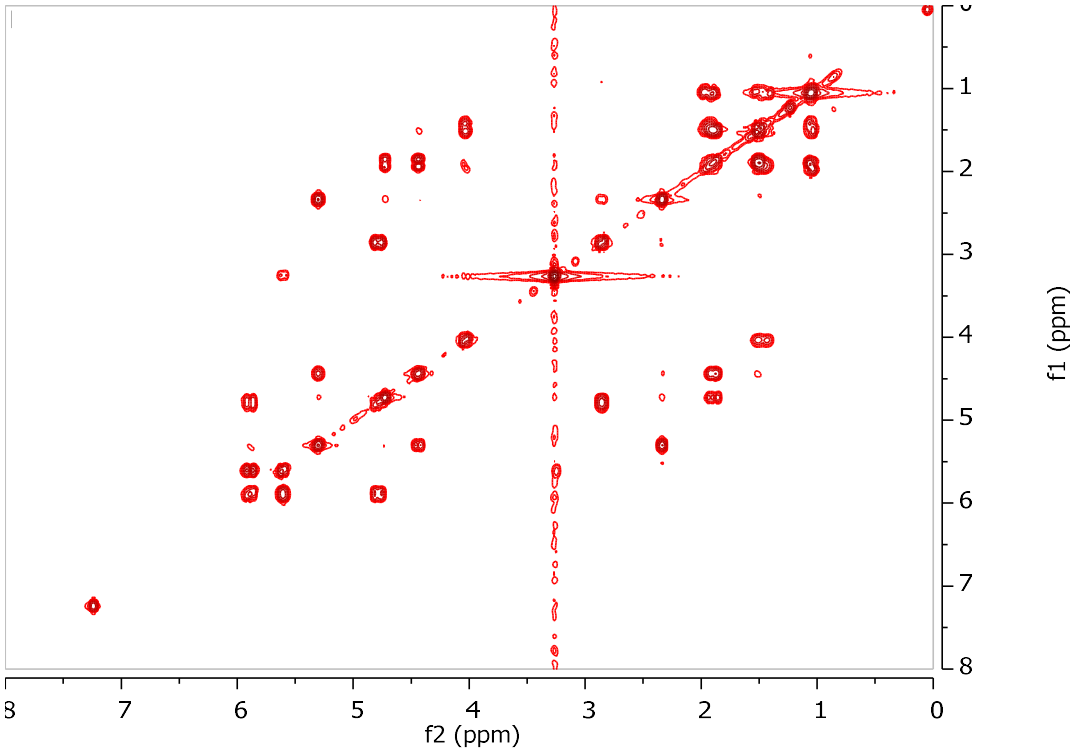

Figure 87. COSY spectrum of metabolite **19**.

The relative configuration of the asymmetric centers of metabolite **19** was determined on the basis of the correlations observed in the NOESY spectrum (Figure

88). Specifically, the NOE enhancements of H_3-16 with H-13 and of H-11 with H-14b (δ 1.48), as well as of H-11 with H-10 and of H-10 with H-9 secured the relative configuration at C-9, C-10, C-11, C-12 and C-13. Furthermore, the absence of coupling of H-6 with H-7 and/or H-11 in the COSY spectrum indicating an almost 90° dihedral angle between H-6–C-6–C-7–H-7, as well as between H-6–C-6–C-11–H-11, in conjunction with the NOE enhancement of H-5 with H-11 secured the relative configuration at C-6 (Figure 89).

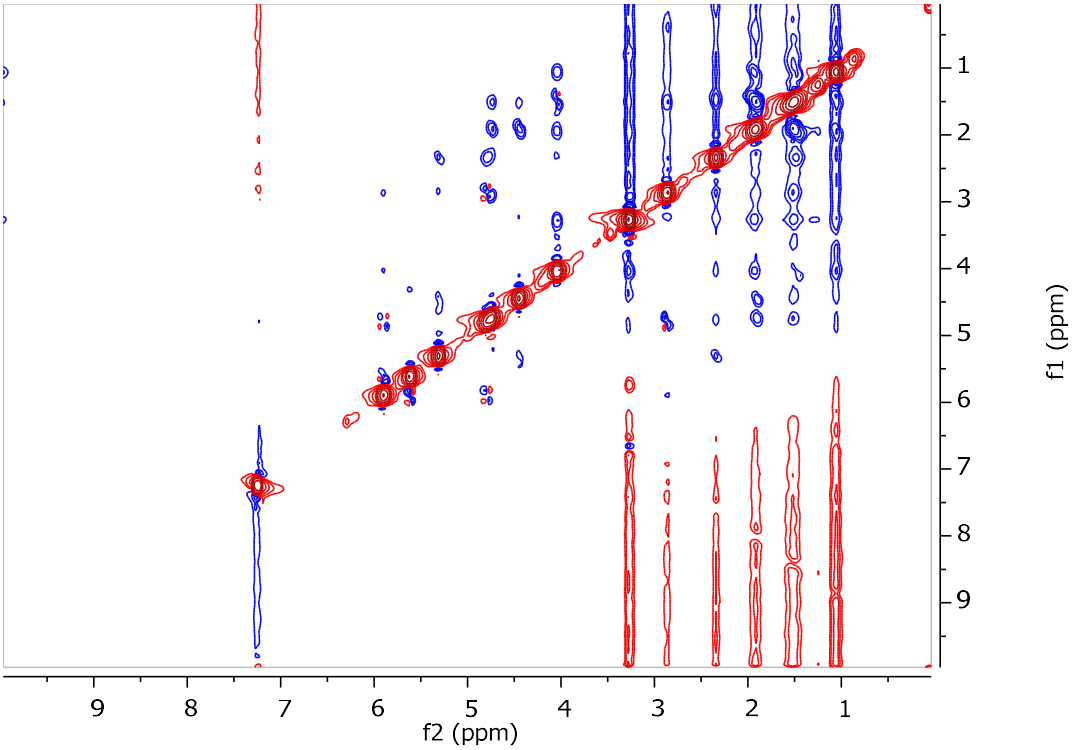

Figure 88. NOESY spectrum of metabolite **19**.

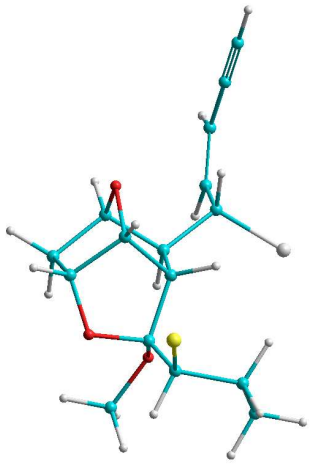

Figure 89. 3D structure of metabolite **19**.

Comparison of the spectroscopic and physical characteristics of metabolite **19** with those reported in the literature led to its identification as a new natural product. The NMR data of metabolite **19** are reported in Table 153.

Table 153. ^{1}H and ^{13}C NMR data of metabolite **19** in $CDCl_3$ (δ in ppm, J in Hz).

Position	δ_C	δ_H
1	78.0	3.24 (d, 2.3)
2	78.3	-
3	111.8	5.60 (dd, 10.6, 2.3)
4	141.6	5.90 (t, 10.6)
5	57.1	4.80 (t, 10.6)
6	52.3	2.87 (brd, 10.6)
7	77.5	4.72 (d, 5.2)
8	36.7	1.89-1.93 (m), 1.54 (m)
9	78.2	4.40 (dd, 8.2, 5.0)
10	84.9	5.30 (t, 5.0)
11	49.0	2.33 (d, 5.0)
12	108.2	-
13	60.7	4.04 (dd, 11.3, 2.1)
14	26.8	1.93 (m), 1.48 (m)
15	12.5	1.06 (t, 7.3)
16	48.7	3.27 (s)

3.1.20 Metabolite 20

Metabolite **20** (LMH07) was isolated after a series of chromatographic separations as a colorless oil (8.2 mg).

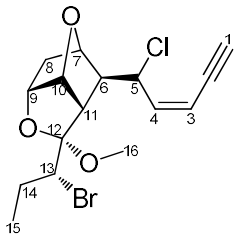

The mass spectrum of metabolite **20** (Figure 90) exhibited a fragment ion peak at *m/z* 343 and isotopic ion peaks at *m/z* 345 and 347 at a relative intensity characteristic for the presence of one bromine and one chlorine atom in the molecule and corresponding to $[M\text{-}OCH_3]^+$.

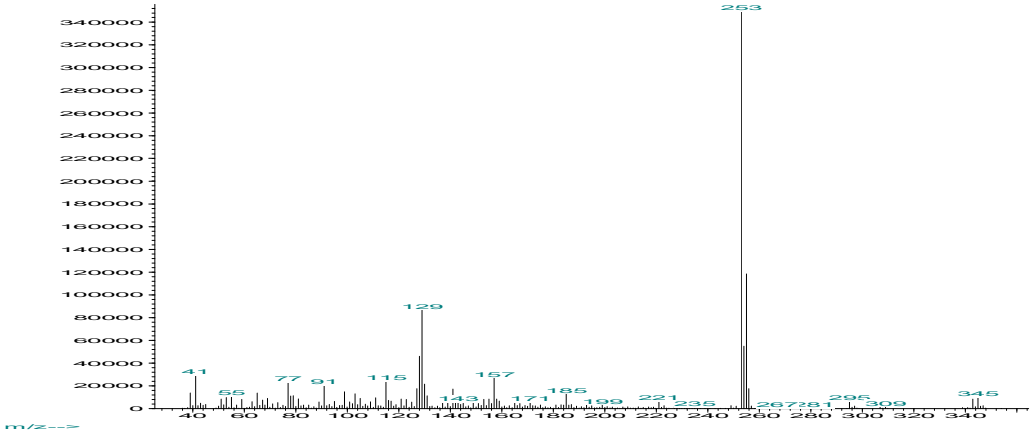

Figure 90. Mass spectrum (EIMS) of metabolite **20**.

In the ^1H NMR spectrum of metabolite **20** (Figure 91) obvious were:

- One aliphatic methyl on a secondary carbon at δ 1.08,
- One acetylenic methine at δ 3.22,
- One oxygenated methyl at δ 3.31,
- Five signals at δ 3.96, 4.41, 4.75, 4.80 and 4.88 integrating for one proton each and attributed to five oxygenated or halogenated methines, and
- Two signals at δ 5.62 and 5.99 integrating for one proton each and attributed to two olefinic methines.

Analysis of the NMR and MS data of **20** led to the molecular formula $C_{16}H_{20}BrClO_3$. Taking into account the one carbon-carbon triple bond and the one carbon-carbon double bond as three of the six degrees of unsaturation, the molecular structure of **20** was determined as tricyclic.

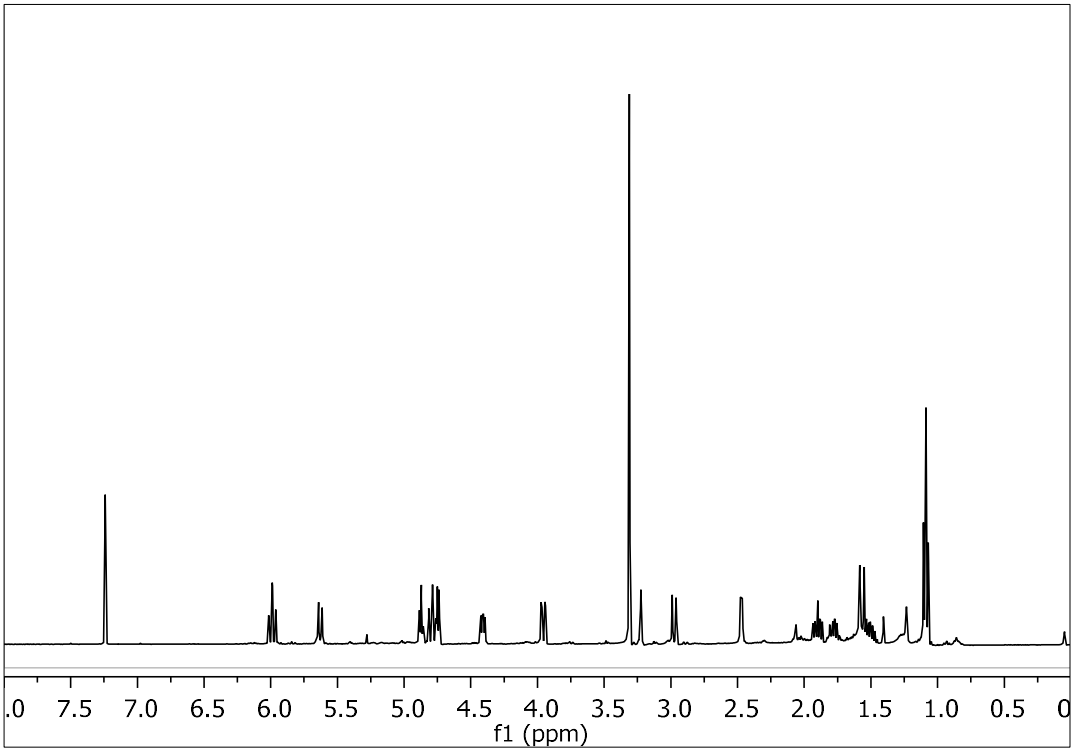

Figure 91. ^{1}H NMR spectrum of metabolite **20**.

The spectroscopic data of **20** were rather similar to those of metabolite **19**. Indeed, the planar structure of metabolite **20** was determined to be the same as that of **19** on the basis of the homonuclear and heteronuclear correlations (Figure 92) observed in the HSQC-DEPT (Figure 93), HMBC (Figure 94) and COSY (Figure 95) spectra.

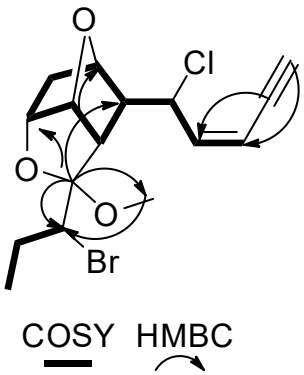

Figure 92. COSY and important HMBC correlations observed for metabolite **20**.

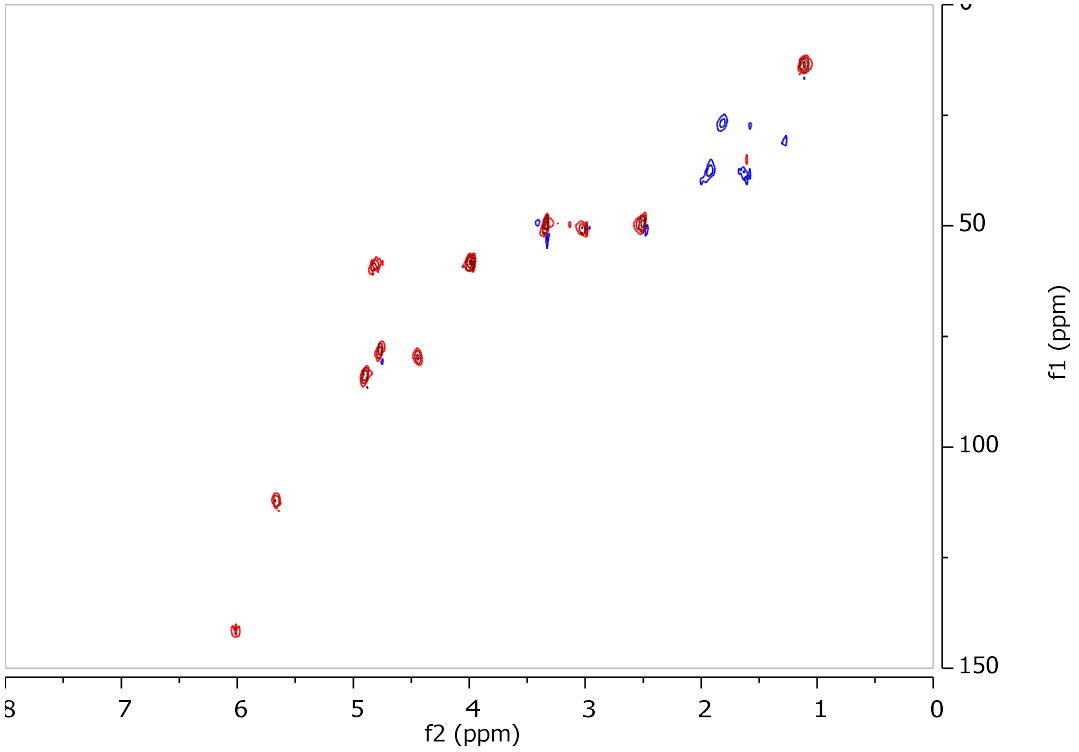

Figure 93. HSQC-DEPT spectrum of metabolite **20**.

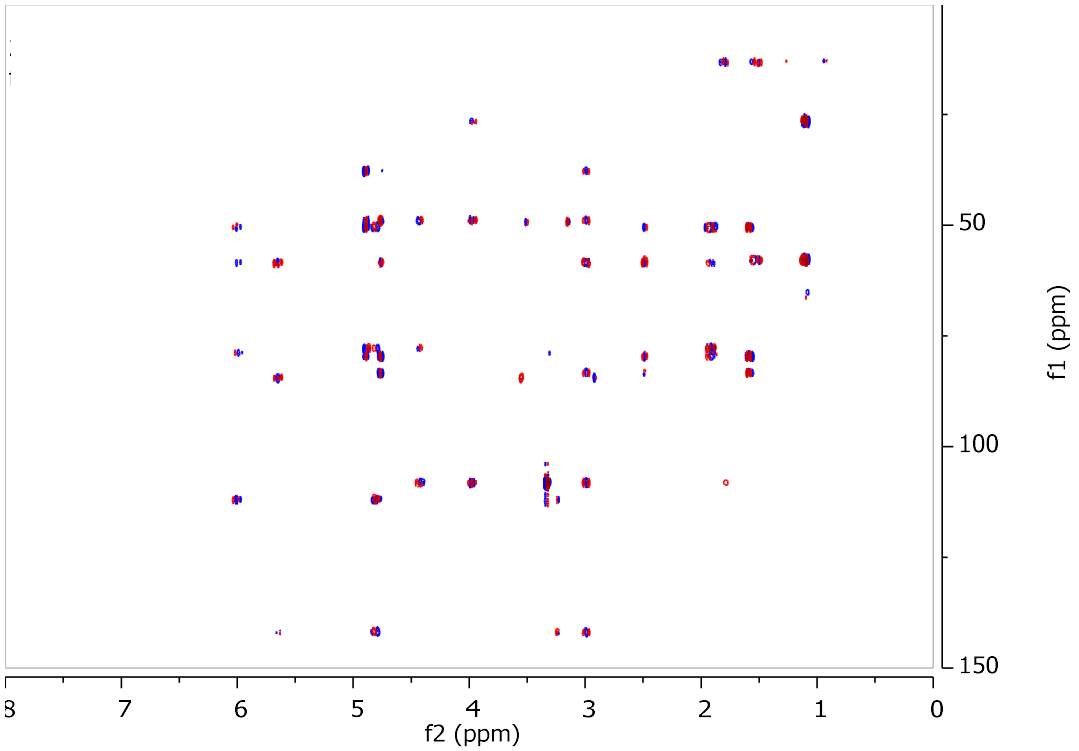

Figure 94. HMBC spectrum of metabolite **20**.

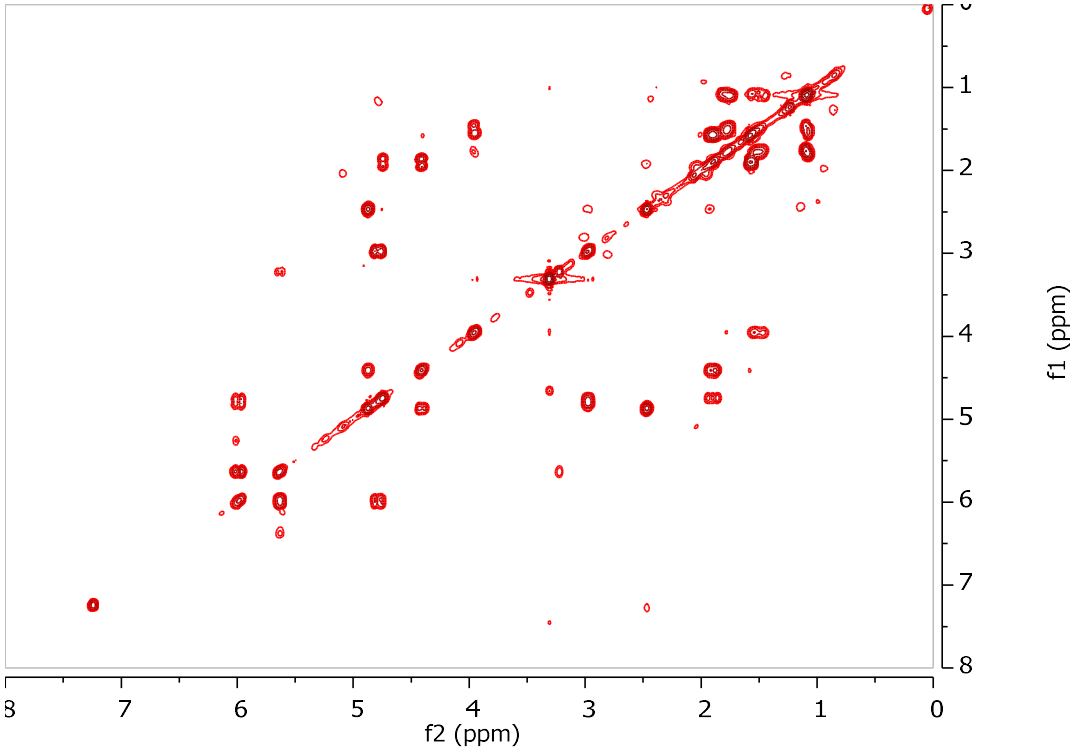

Figure 95. COSY spectrum of metabolite **20**.

The relative configuration of the asymmetric centers of metabolite **20** was determined on the basis of the correlations observed in the NOESY spectrum (Figure 96). Specifically, as in the case of **19**, the absence of coupling of H-6 with H-7 and/or H-11 in the COSY spectrum indicating an almost 90° dihedral angle between H-6–C-6–C-7–H-7, as well as between H-6–C-6–C-11–H-11, in conjunction with the NOE enhancement of H-5 with H-11 secured the relative configuration at C-6. The NOE enhancements of H_3-16 with H-13 and of H-11 with H-14b (δ 1.51), as well as of H-11 with H-10 and of H-10 with H-9 secured the relative configuration at C-9, C-10, C-11 and C-12. However, the fact that H-10 and H-13 were shielded (in comparison to compound **19**) suggested a change in the relative configuration of C-13.

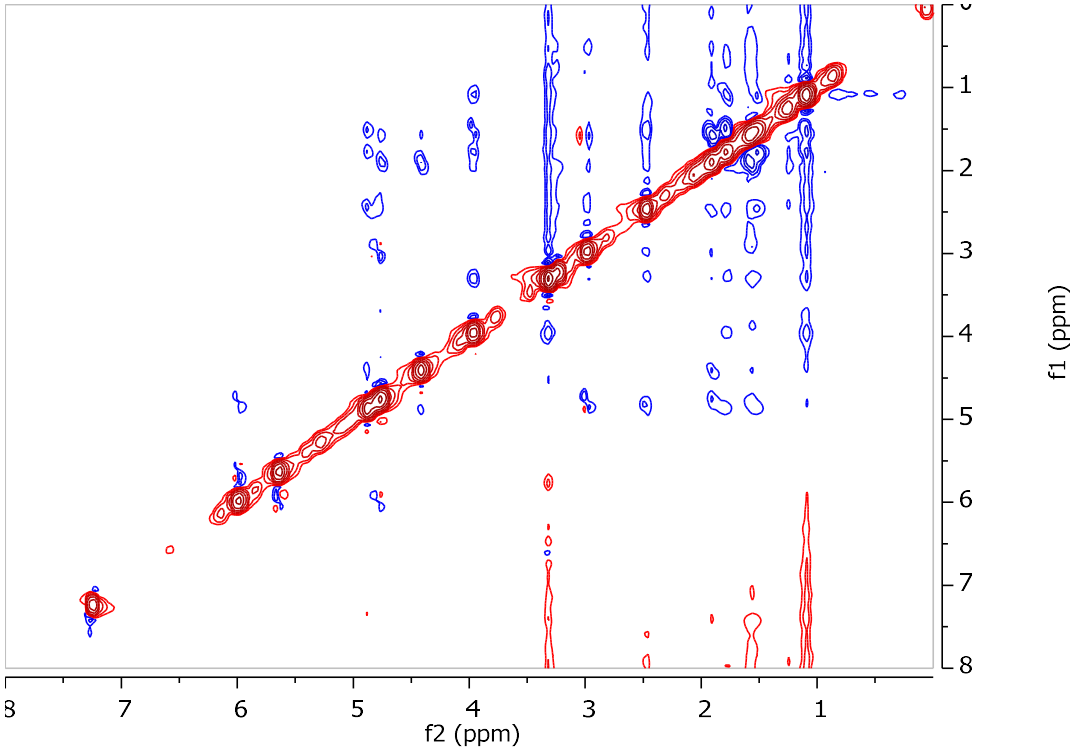

Figure 96. NOESY spectrum of metabolite **20**.

Comparison of the spectroscopic and physical characteristics of metabolite **20** with those reported in the literature led to its identification as a new natural product. The NMR data of metabolite **20** are reported in Table 154.

Table 154. ^{1}H and ^{13}C NMR data of metabolite **20** in $CDCl_3$ (δ in ppm, J in Hz)

Position	δ_C	δ_H
1	81.0	3.22 (d, 2.3)
2	79.0	-
3	111.8	5.62 (dd, 10.5, 2.3)
4	141.6	5.99 (t, 10.5)
5	58.5	4.80 (t, 10.5)
6	52.3	2.97 (brd, 10.5)
7	77.5	4.75 (d, 5.0)
8	37.4	1.89 (m), 1.58 (m)
9	78.2	4.41 (dd, 8.2, 5.0)
10	84.9	4.88 (t, 5.0)
11	49.0	2.44 (d, 5.0)
12	108.5	-
13	60.7	3.96 (dd, 11.5, 2.0)
14	26.7	1.79 (m), 1.51 (m)
15	13.1	1.08 (t, 7.2)
16	49.0	3.31 (s)

3.1.21 Metabolite 21

Metabolite **21** (LMH08) was isolated after a series of chromatographic separations as a colorless oil (19.5 mg).

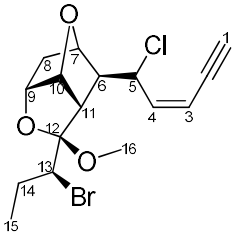

The mass spectrum of metabolite **21** (Figure 97) exhibited a fragment ion peak at *m/z* 343 and isotopic ion peaks at *m/z* 345 and 347 at a relative intensity characteristic for the presence of one bromine and one chlorine atom in the molecule and corresponding to $[M\text{-}OCH_3]^+$.

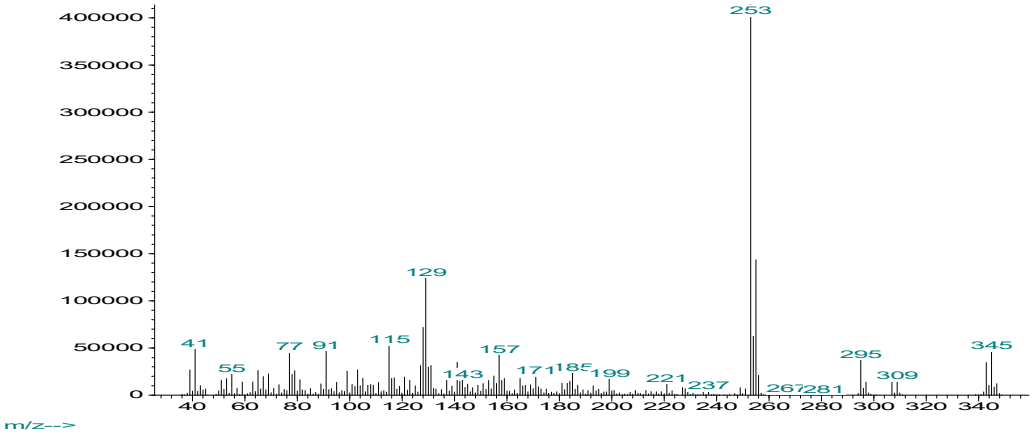

Figure 97. Mass spectrum (EIMS) of metabolite **21**.

In the ^{1}H NMR spectrum of metabolite **21** (Figure 98) obvious were:

- One aliphatic methyl on a secondary carbon at δ 1.05,
- One acetylenic methine at δ 3.21,
- One oxygenated methyl at δ 3.24,
- Five signals at δ 3.76, 4.52, 4.76, 4.82 and 5.16 integrating for one proton each and attributed to five oxygenated or halogenated methines, and
- Two signals at δ 5.63 and 6.18 integrating for one proton each and attributed to two olefinic methines.

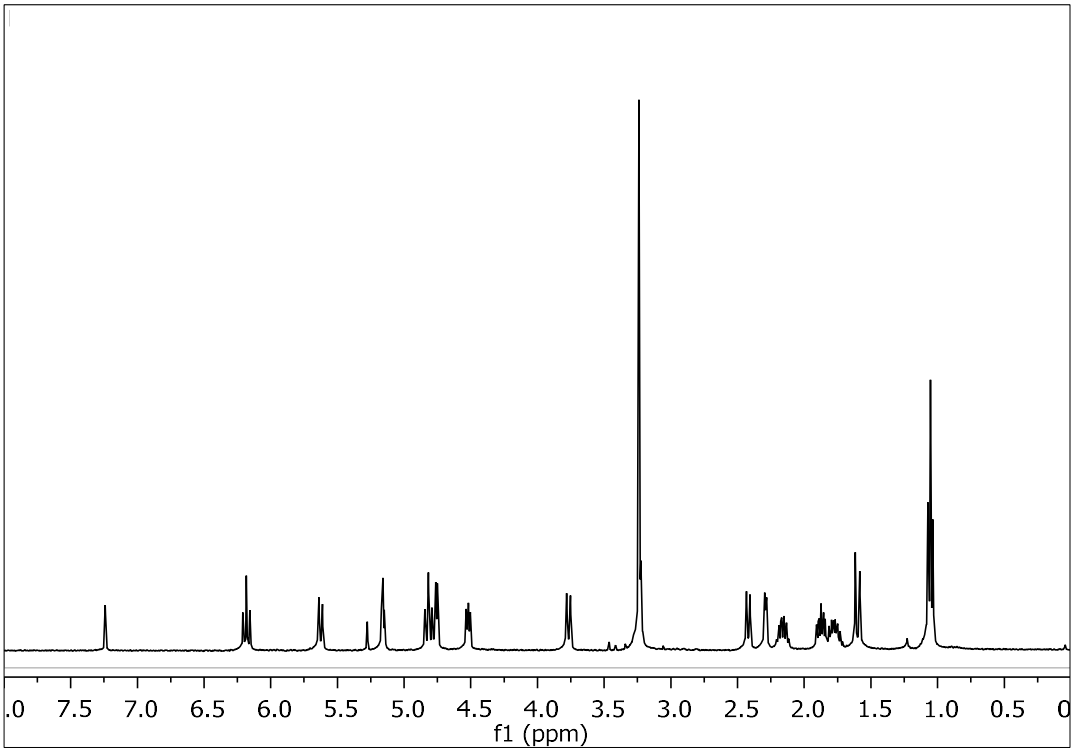

Figure 98. ^{1}H NMR spectrum of metabolite **21**.

Analysis of the NMR and MS data of **21** led to the molecular formula $C_{16}H_{20}BrClO_3$. Taking into account the one carbon-carbon triple bond and the one carbon-carbon double bond as three of the six degrees of unsaturation, the molecular structure of **21** was determined as tricyclic.

The spectroscopic data of **21** were rather similar to those of metabolites **19** and **20**. Indeed, the planar structure of metabolite **21** was determined to be the same as that of **19** and **20** on the basis of the homonuclear and heteronuclear correlations observed in the HSQC-DEPT (Figure 99) and COSY (Figure 100) spectra.

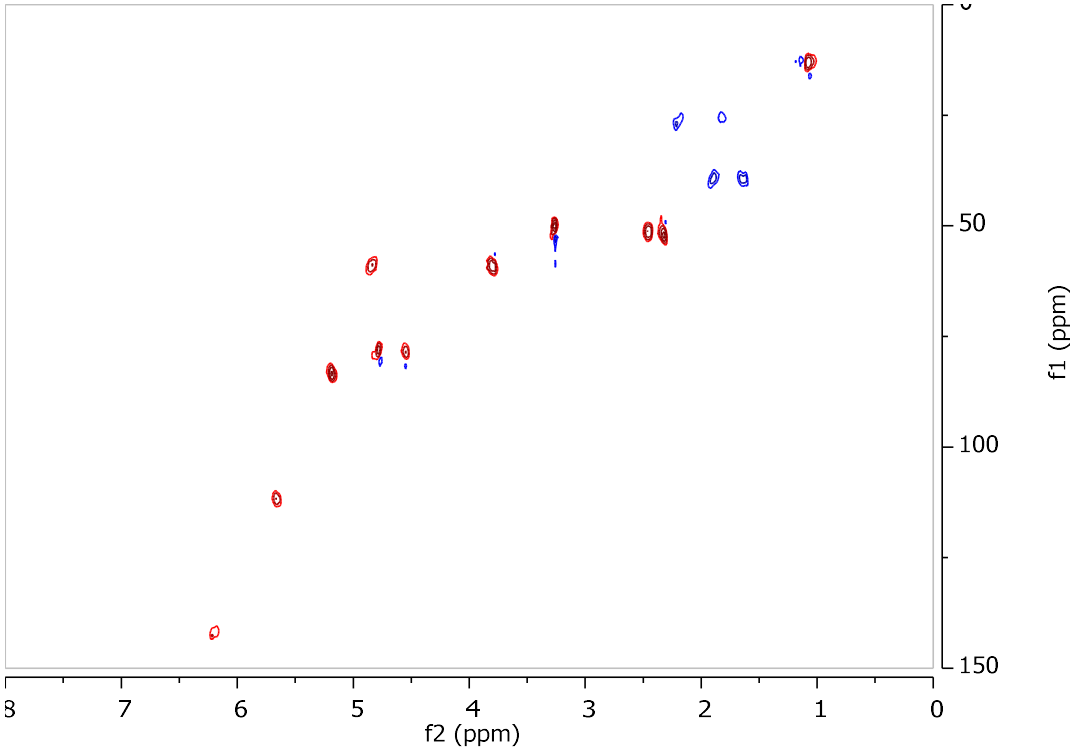

Figure 99. HSQC-DEPT spectrum of metabolite **21**.

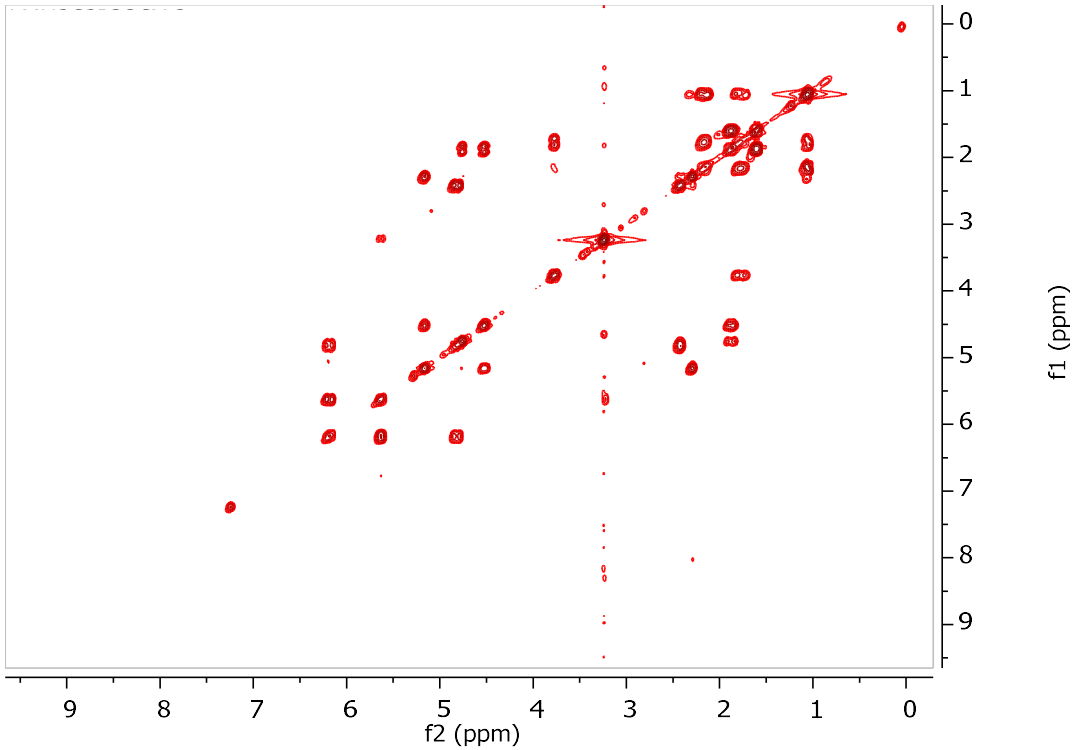

Figure 100. COSY spectrum of metabolite **21**.

The relative configuration of the asymmetric centers of metabolite **21** was determined on the basis of the correlations observed in the NOESY spectrum (Figure

101). Specifically, the absence of coupling of H-6 with H-7 and/or H-11 in the COSY spectrum indicating an almost 90° dihedral angle between H-6–C-6–C-7–H-7, as well as between H-6–C-6–C-11–H-11, in conjunction with the NOE enhancement of H-5 with H-11 secured the relative configuration at C-6. Furthermore, the NOE enhancements of H-11 with H-14b (δ 1.77), as well as of H-11 with H-10 and of H-10 with H-9, in combination with that of H-13 with H-6 secured the relative configuration at C-9, C-10 and C-11 and suggested the inversion of the relative configuration at C-12 (Figure 102).

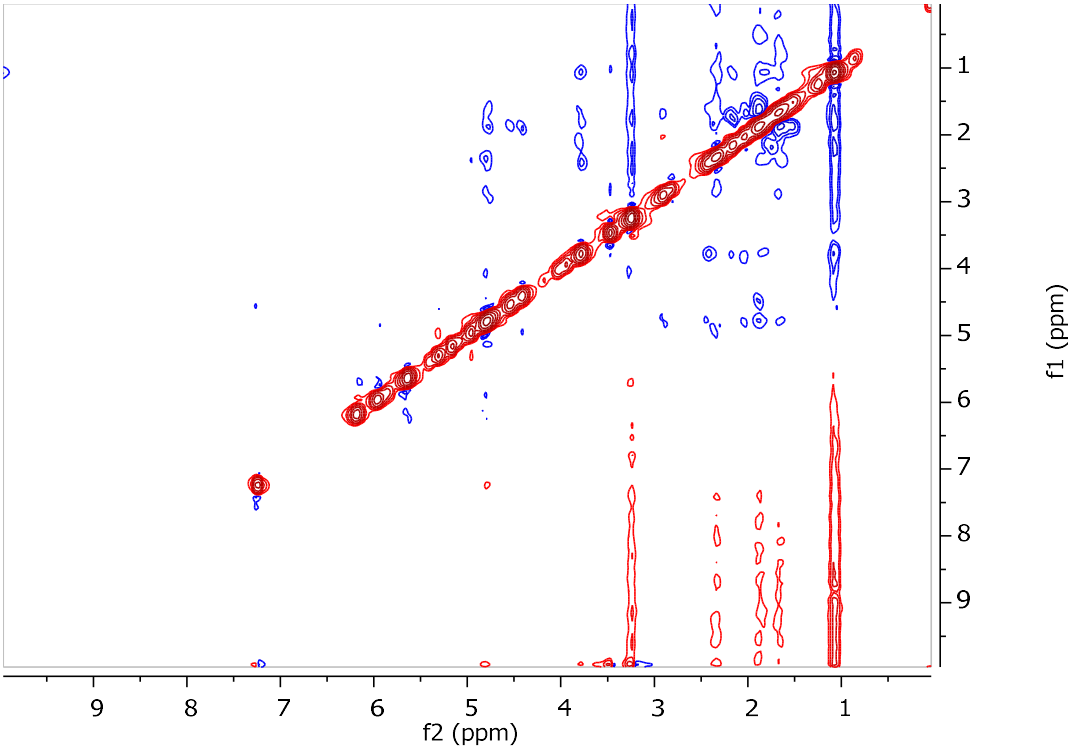

Figure 101. NOESY spectrum of metabolite **21**.

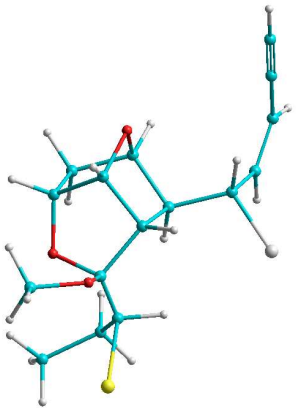

Figure 102. 3D structure of metabolite **21**.

Comparison of the spectroscopic and physical characteristics of metabolite **21** with those reported in the literature led to its identification as a new natural product. The NMR data of metabolite **21** are reported in Table 155.

Table 155. ^{1}H and ^{13}C NMR data of metabolite **21** in $CDCl_3$ (δ in ppm, J in Hz).

Position	δ_C	δ_H
1	n.d.	3.21 (d, 2.2)
2	79.0	-
3	111.5	5.63 (dd, 10.6, 2.2)
4	141.6	6.18 (t, 10.6)
5	59.1	4.82 (t, 10.6)
6	51.6	2.43 (dd, 10.6, 1.0)
7	78.5	4.76 (dd, 5.0, 5.0)
8	39.7	1.88 (ddd, 12.8, 7.3, 5.0), 1.60 (d, 12.8)
9	78.8	4.52 (dd, 7.3, 4.7)
10	83.3	5.16 (t, 4.7)
11	52.3	2.31 (d, 4.7)
12	108.2	-
13	59.4	3.76 (dd, 11.1, 2.0)
14	26.1	2.16 (m), 1.77 (m)
15	13.8	1.05 (t, 7.2)
16	50.3	3.24 (s)

n.d.: not determined

3.1.22 Metabolite 22

Metabolite **22** (LMH16) was isolated after a series of chromatographic separations as a colorless oil (3.8 mg).

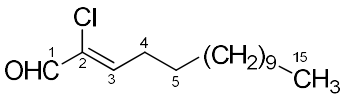

The mass spectrum of metabolite **22** (Figure 103) exhibited a fragment ion peak at *m/z* 223 corresponding to $[M\text{-}Cl]^+$.

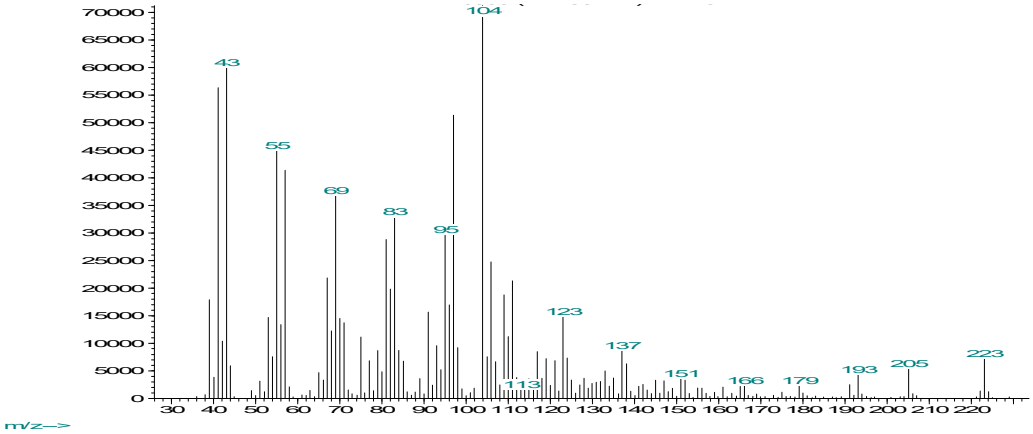

Figure 103. Mass spectrum (EIMS) of metabolite **22**.

In the ^1H NMR spectrum of metabolite **22** (Figure 104) obvious were:

- One aliphatic methyl on a secondary carbon at δ 0.85,
- One olefinic methine at 6.87, and,
- One singlet at δ 9.35 integrating for one proton and attributed to the proton of an aldehyde group.

Analysis of the NMR and MS data of **22** led to the molecular formula $C_{15}H_{27}ClO$. Taking into account the one carbon-carbon double bond and the carbonyl moiety as two of the two degrees of unsaturation, the molecular structure of **22** was determined as linear.

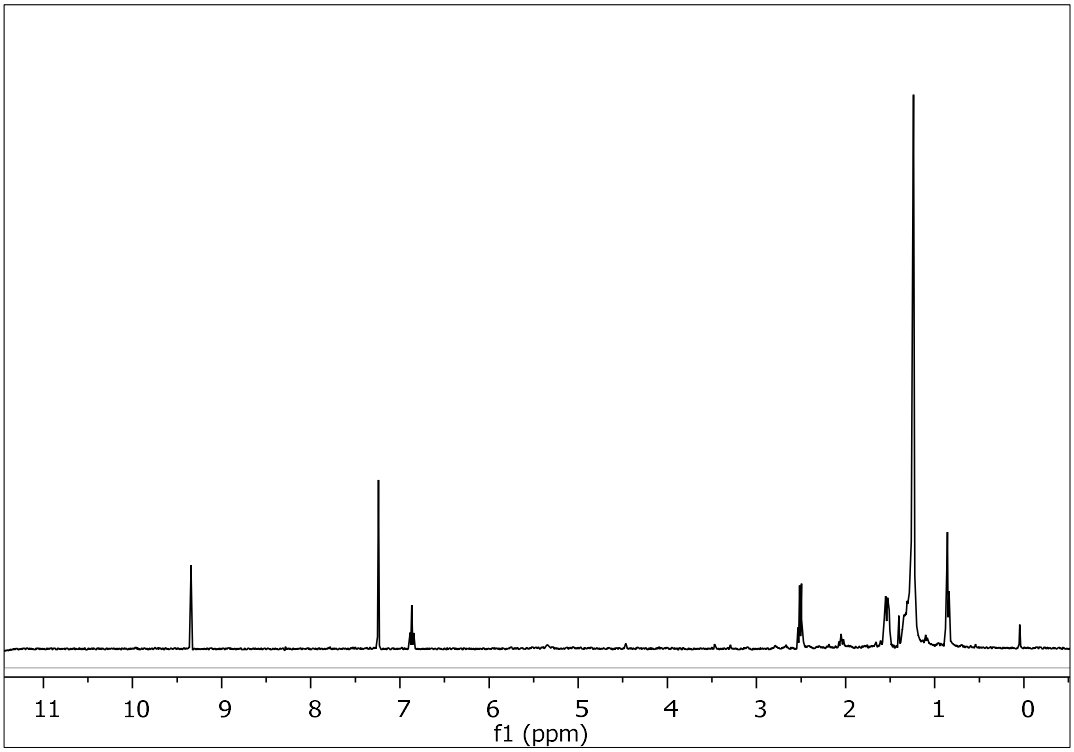

Figure 104. ^{1}H NMR spectrum of metabolite **22**.

Comparison of the spectroscopic and physical characteristics of metabolite **22** with those reported in the literature led to its identification as (2*Z*)-2-chloro-pentadec-2enal, previously isolated from the *Laurencia flexilis* (de Nys et al., 1993). The ^{1}H NMR data of metabolite **22** are reported in Table 156.

Table 156. ^{1}H NMR data of metabolite **22** in $CDCl_3$ (δ in ppm, *J* in Hz).

Position	$\delta_{H,exp}$	$\delta_{H,lit}$
1	9.35 (s)	9.36 (s)
3	6.87 (t, 7.3)	6.89 dd (7.2, 7.2)
4	2.52 (m), 2.45 (m)	2.52 ddd (7.2, 7.3, 7.3)
5	1.52 (m)	1.55 (m)
6~14	1.24 (m)	1.26 (brs)
15	0.85 (t, 6.7)	0.88 (m)

3.2 Identification and structure elucidation of isolated metabolites from the sponge *Lamellodysidea* sp.

3.2.1 Metabolite 23

Metabolite **23** (KR649-13) was isolated after a series of chromatographic separations as colorless crystals (15.6 mg).

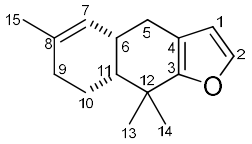

The mass spectrum of metabolite **23** (Figure 105) exhibited a molecular ion peak $[M]^+$ at *m/z* 216, as well as a fragment ion peak at *m/z* 201 corresponding to $[M\text{-}CH_3]^+$.

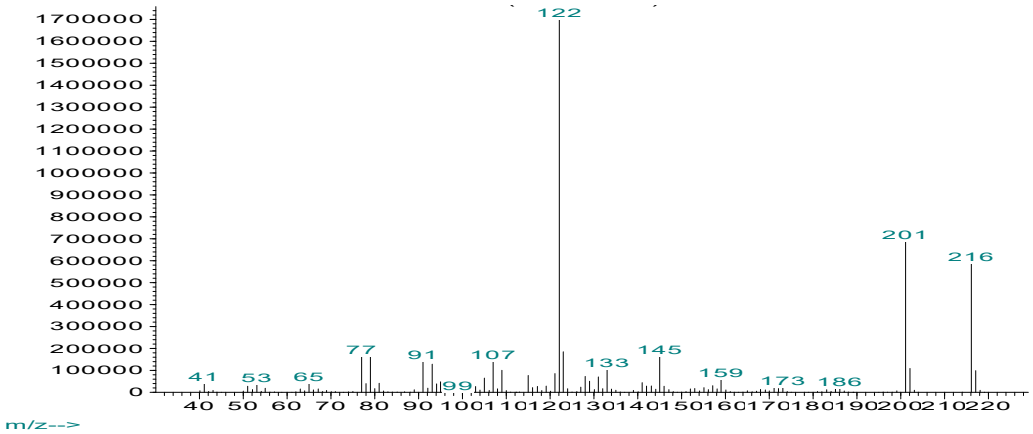

Figure 105. Mass spectrum (EIMS) of metabolite **23**.

In the ^{1}H NMR spectrum of metabolite **23** (Figure 106) obvious were:

- Two aliphatic methyls on non-protonated carbons at δ 1.23 and 1.25,
- One olefinic methyl at δ 1.65,
- One signal at δ 5.58 integrating for one proton and attributed to one olefinic methine, and
- Two broad doublets at δ 6.08 and 7.21 integrating for one proton each and attributed to the olefinic protons of a furan ring.

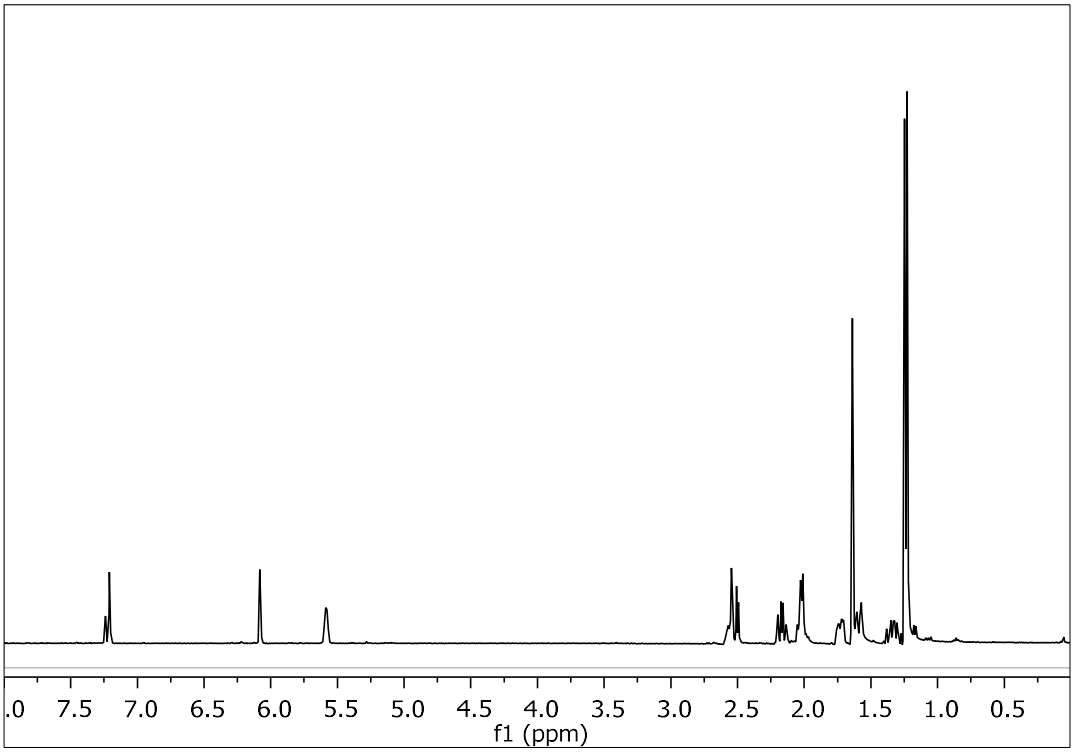

Figure 106. ^{1}H NMR spectrum of metabolite **23**.

Analysis of the NMR and MS data of **23** led to the molecular formula $C_{15}H_{20}O$. Taking into account the three carbon-carbon double bonds as the three of the six degrees of unsaturation, the molecular structure of **23** was determined as tricyclic.

Comparison of the spectroscopic and physical characteristics of metabolite **23** with those reported in the literature led to its identification as furodysin, previously isolated from the marine sponge *Dysidea* sp. (Kazlauskas et al., 1978). The ^{1}H NMR data of metabolite **23** are reported in Table 157.

Table 157. ^{1}H NMR data of metabolite **23** in $CDCl_3$ and CCl_4 (δ in ppm, J in Hz)

Position	$\boldsymbol{\delta}_{\mathbf{H,exp}}$ (in $CDCl_3$)	$\boldsymbol{\delta}_{\mathbf{H,lit}}$ (in CCl_4)
1	7.21 (brd, 1.8)	7.03 (d, 2)
2	6.08 (brd, 1.8)	5.90 (d, 2)
5	2.52 (m), 2.19 (m)	2.48 (dd, 17.0, 5.5), 2.1 (dd, 17.0, 12.0)
7	5.58 (brd, 5.8)	5.50 (brd, 6)
13	1.23 (s)	1.23 (s)
14	1.25 (s)	1.23 (s)
15	1.65 (s)	1.61 (s)

3.2.2 Metabolite 24

Metabolite **24** (KR649-12) was isolated after a series of chromatographic separations as colorless crystals (76 mg).

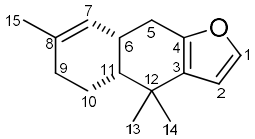

The mass spectrum of metabolite **24** (Figure 107) exhibited a molecular ion peak $[M]^+$ at *m/z* 216, as well as a fragment ion peak at *m/z* 201 corresponding to $[M\text{-}CH_3]^+$.

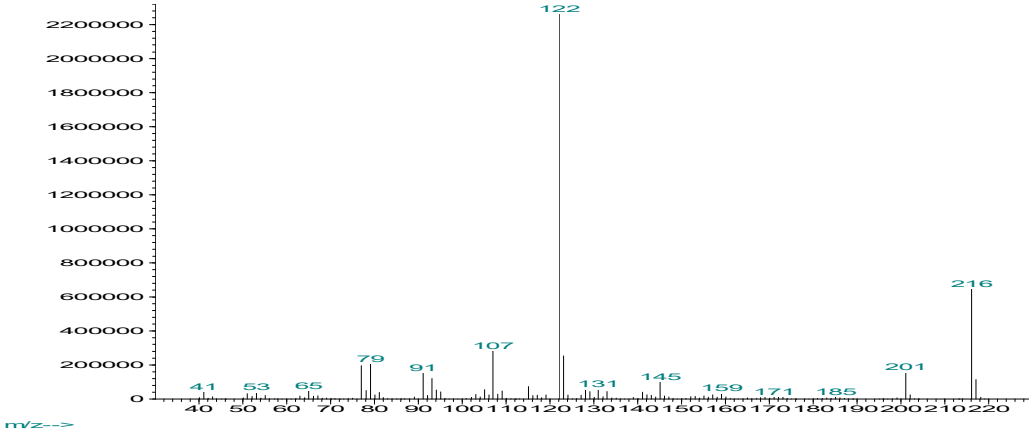

Figure 107. Mass spectrum (EIMS) of metabolite **24**.

In the ^{1}H NMR spectrum of metabolite **24** (Figure 108) obvious were:

- Two aliphatic methyls on non-protonated carbons at δ 1.17 and 1.19,
- One olefinic methyl at δ 1.65,
- One signal at δ 5.61 integrating for one proton and attributed to one olefinic methine, and
- Two broad singlets at δ 6.22 and 7.20 integrating for one proton each and attributed to the olefinic protons of a furan ring.

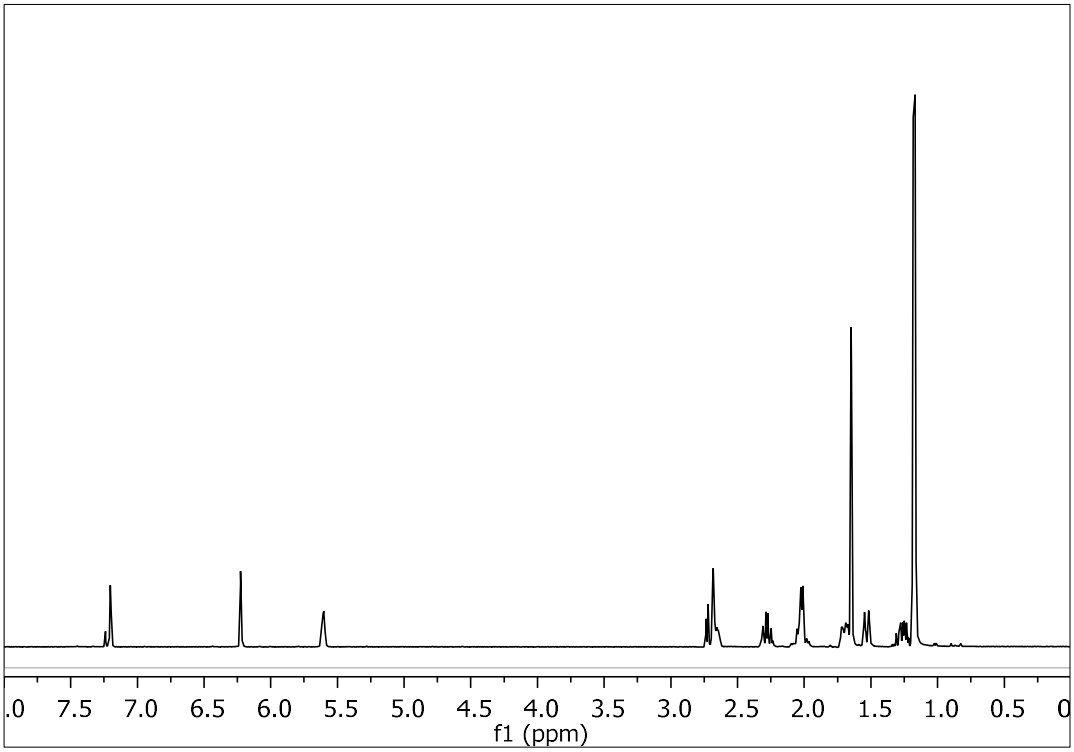

Figure 108. ^{1}H NMR spectrum of metabolite **24**.

Analysis of the NMR and MS data of **24** led to the molecular formula $C_{15}H_{20}O$. Taking into account the three carbon-carbon double bonds as three of the six degrees of unsaturation, the molecular structure of **24** was determined as tricyclic.

Comparison of the spectroscopic and physical characteristics of metabolite **24** with those reported in the literature led to its identification as furodysinin, previously isolated from the marine sponge *Dysidea* sp. (Kazlauskas et al., 1978). The ^{1}H NMR data of metabolite **24** are reported in Table 158.

Table 158. ^{1}H NMR data of metabolite **24** in $CDCl_3$ and CCl_4 (δ in ppm, J in Hz).

Position	$\boldsymbol{\delta}_{\mathbf{H,exp}}$ (in $CDCl_3$)	$\boldsymbol{\delta}_{\mathbf{H,lit}}$ (in CCl_4)
1	7.20 (brs)	6.98 (brs)
2	6.22 (brs)	6.01 (d, 2)
5	2.65 (m), 2.28 (m)	2.56 (m), 2.19 (dd, 17.5, 12.5)
6	2.70 (m)	2.64 (dd, 17.5, 5.5)
7	5.61 (brd, 3.6)	5.50 (brd, 6)
13	1.17 (s)	1.15 (s)
14	1.19 (s)	1.15 (s)
15	1.65 (s)	1.60 (s)

3.2.3 Metabolite 25

Metabolite **25** (KR649-23) was isolated after a series of chromatographic separations as a colorless oil (1.0 mg).

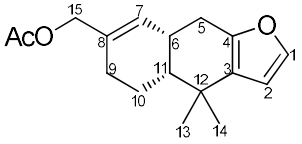

The mass spectrum of metabolite **25** (Figure 109) exhibited a molecular ion peak $[M]^+$ at *m/z* 274 and a fragment ion peak at *m/z* 214 corresponding to $[M\text{-AcOH}]^+$.

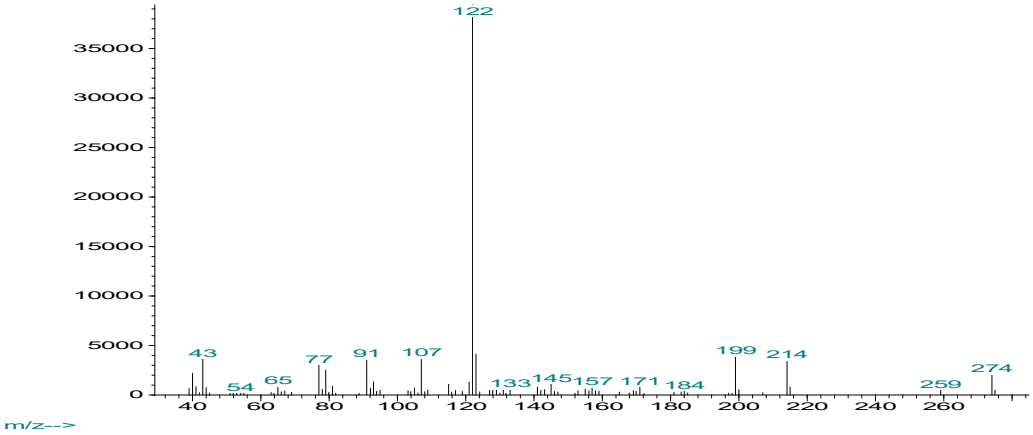

Figure 109. Mass spectrum (EIMS) of metabolite **25**.

In the ^{1}H NMR spectrum of metabolite **25** (Figure 110) obvious were:

- Two aliphatic methyls on non-protonated carbons at δ 1.17 and 1.19,
- One acetoxy methyl at δ 2.07,
- One broad singlet at δ 4.45 integrating for two protons and attributed to the protons of an oxygenated methylene,
- One signal at δ 5.94 integrating for one proton and attributed to one olefinic methine, and
- Two broad doublets at δ 6.22 and 7.21 integrating for one proton each and attributed to the olefinic protons of a furan ring.

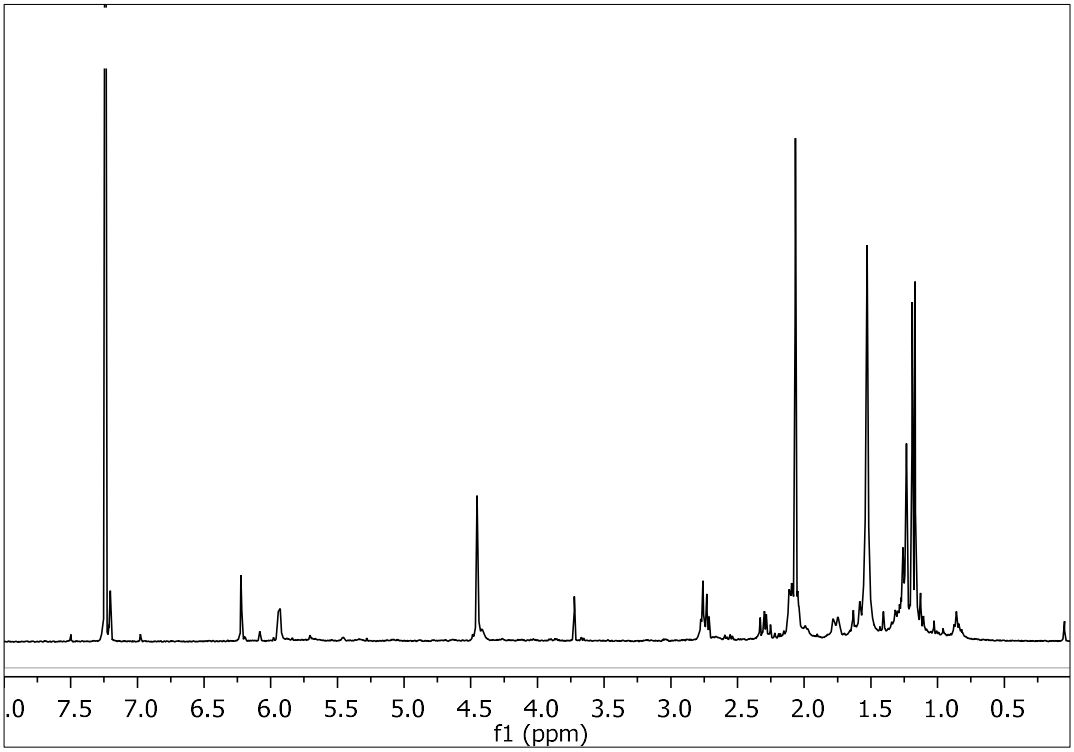

Figure 110. ^{1}H NMR spectrum of metabolite **25**.

Analysis of the NMR and MS data of **25** led to the molecular formula $C_{17}H_{22}O_3$. Taking into account the three carbon-carbon double bonds and the carbonyl moiety as four of the seven degrees of unsaturation, the molecular structure of **25** was determined as tricyclic.

The spectroscopic data of metabolite **25** revealed close similarity to those of **24**, with the striking difference observed for Me-15 where oxidation and subsequent acetylation had taken place. Indeed, the planar structure of metabolite **25** was verified on the basis of the homonuclear and heteronuclear correlations (Figure 111) observed in the HSQC-DEPT (Figure 112), HMBC (Figure 113) and COSY (Figure 114) spectra.

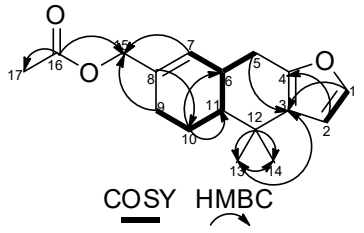

Figure 111. COSY and important HMBC correlations observed for metabolite **25**.

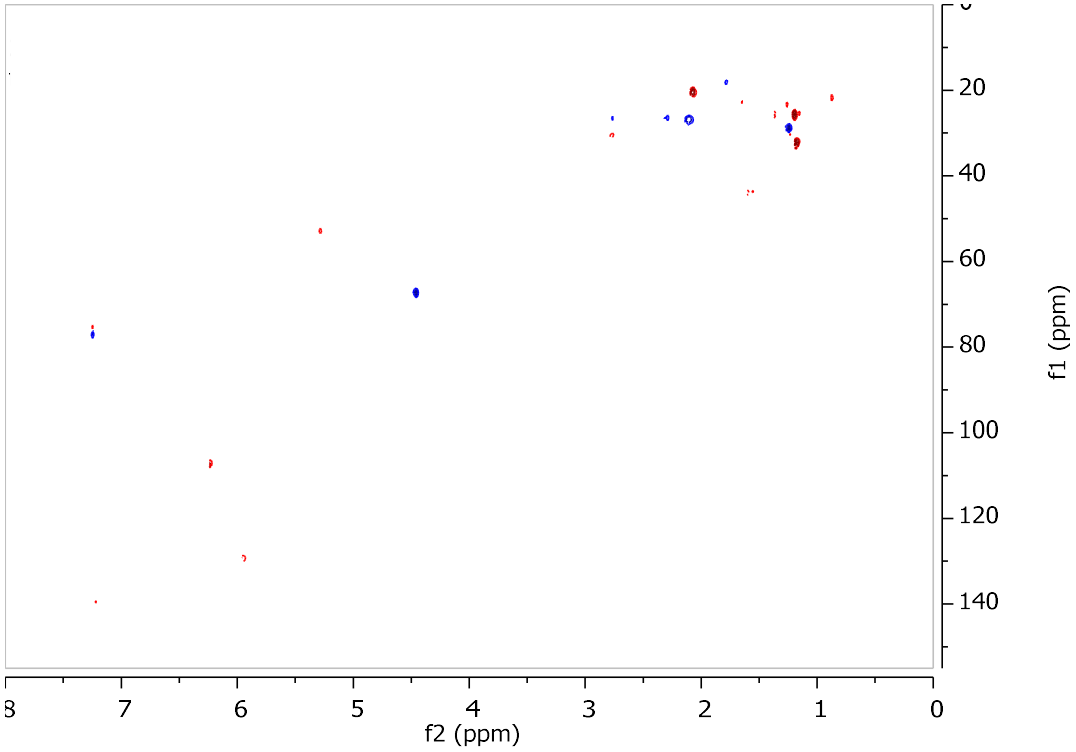

Figure 112. HSQC-DEPT spectrum of metabolite **25**.

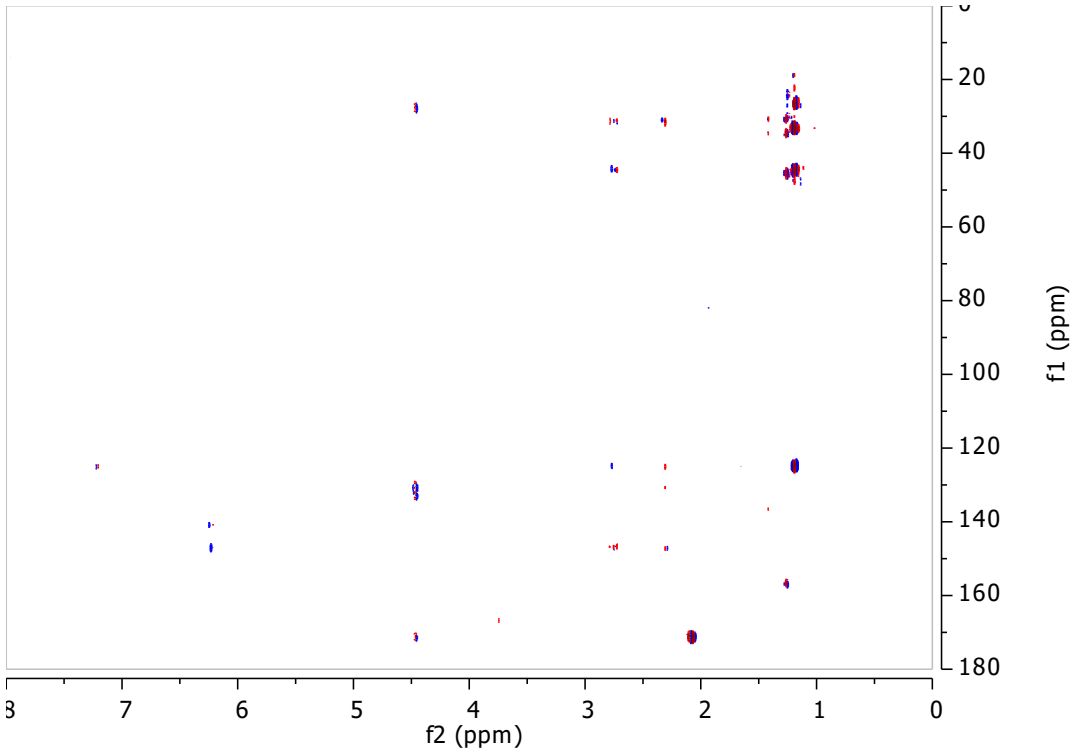

Figure 113. HMBC spectrum of metabolite **25**.

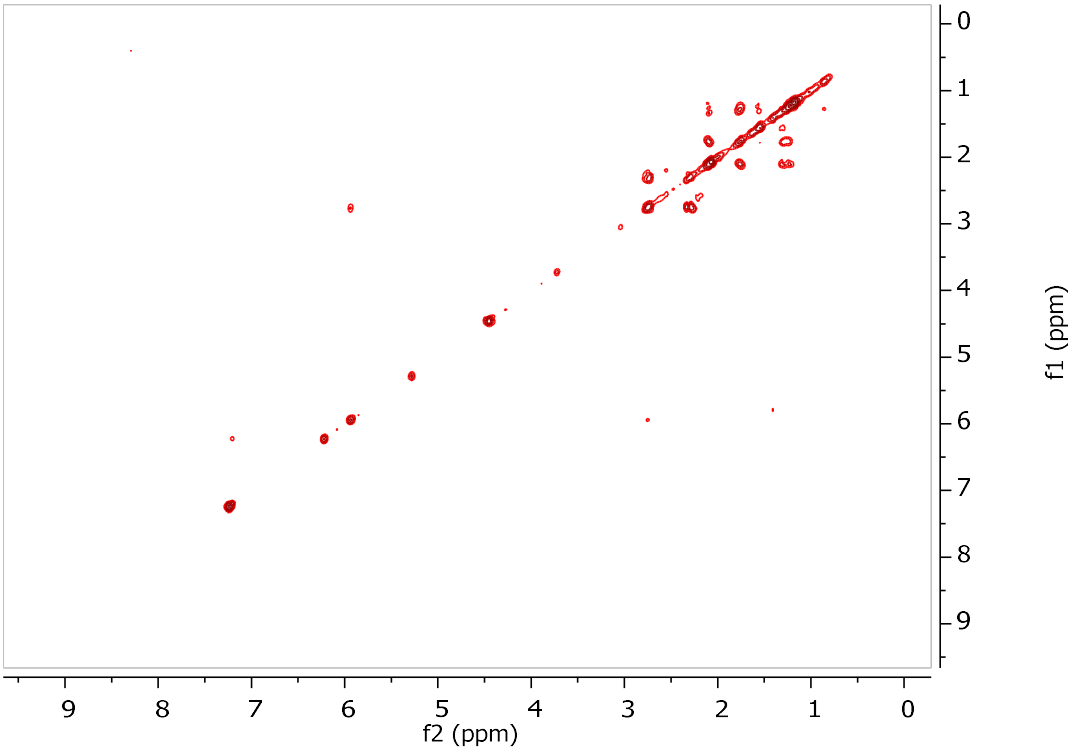

Figure 114. COSY spectrum of metabolite **25**.

The relative configuration of the asymmetric centers of metabolite **25** was determined on the basis of the correlations observed in the NOESY spectrum (Figure 115). Specifically, the NOE enhancement of H-6 with H-11 confirmed the *cis* fusion of the two cyclohexane rings.

Comparison of the spectroscopic and physical characteristics of metabolite **25**with those reported in the literature led to its identification as a new natural product, which was designated as 15-acetoxy-furodysinin. The NMR data of metabolite **25** are reported in Table 159.

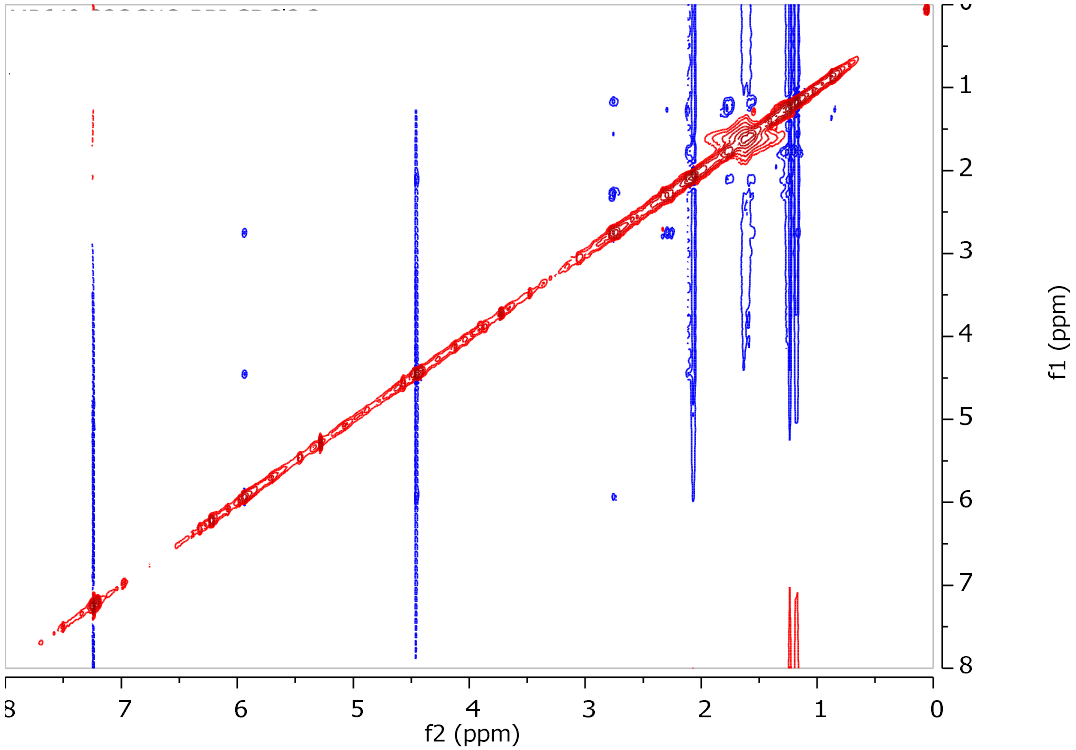

Figure 115. NOESY spectrum of metabolite **25**.

Table 159. ^{1}H and ^{13}C NMR data of metabolite **25** in $CDCl_3$ (δ in ppm, J in Hz).

Position	δ_C	δ_H
1	140.6	7.21 (d, 1.2)
2	108.0	6.22 (d, 1.8)
3	124.5	-
4	146.2	-
5	27.2	2.74 (m), 2.30 (dd, 18.1, 12.0)
6	31.1	2.75 (m)
7	130.2	5.94 (d, 5.4)
8	156.9	-
9	27.7	2.10 (m)
10	18,6	1.80 (m), 1.28 (m)
11	44.8	1.59 (m)
12	33.3	-
13	33.0	1.17 (s)
14	26.3	1.19 (s)
15	68.1	4.45 (brs)
16	171.1	-
17	21.3	2.07 (s)

3.2.4 Metabolite 26

Metabolite **26** (KR649-10) was isolated after a series of chromatographic separations as a colorless oil (24.0 mg).

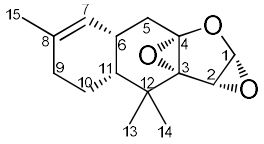

The mass spectrum of metabolite **26** (Figure 116) exhibited a molecular ion peak $[M]^+$ at *m/z* 248.

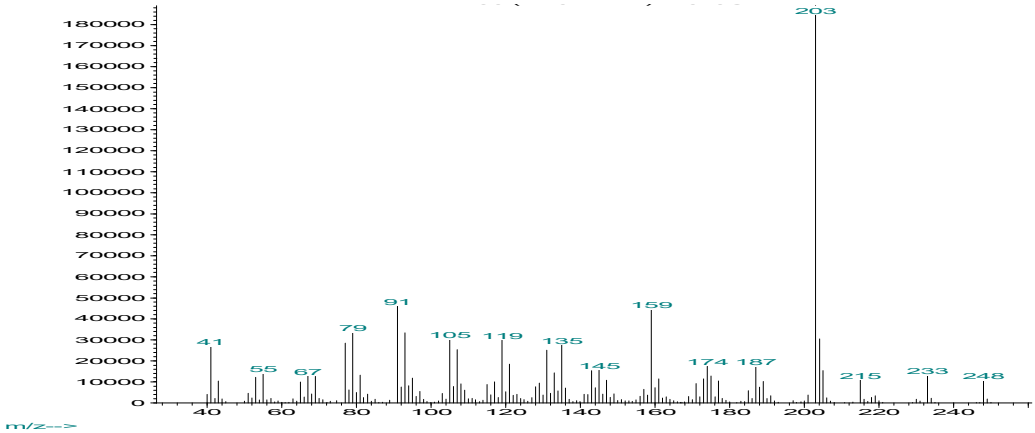

Figure 116. Mass spectrum (EIMS) of metabolite **26**.

In the ^{1}H NMR spectrum of metabolite **26** (Figure 117) obvious were:

- Two aliphatic methyls on non-protonated carbons at δ 1.13 and 1.18,
- One olefinic methyl at δ 1.65, and
- Three signals at δ 3.53, 5.32 and 5.46 integrating for one proton each and attributed to either oxygenated or olefinic methines.

Analysis of the NMR and MS data of **26** led to the molecular formula $C_{15}H_{20}O_3$. Taking into account the one carbon-carbon double bond as one of the six degrees of unsaturation, the molecular structure of **26** was determined as pentacyclic.

Comparison of the spectroscopic and physical characteristics of metabolite **26** with those reported in the literature led to its identification as furodysinin lactone (bis-epoxide), previously isolated from the marine nudibranch *Chromodoris funerea* (Carté et al., 1986). The ^{1}H NMR data of metabolite **26** are reported in Table 160.

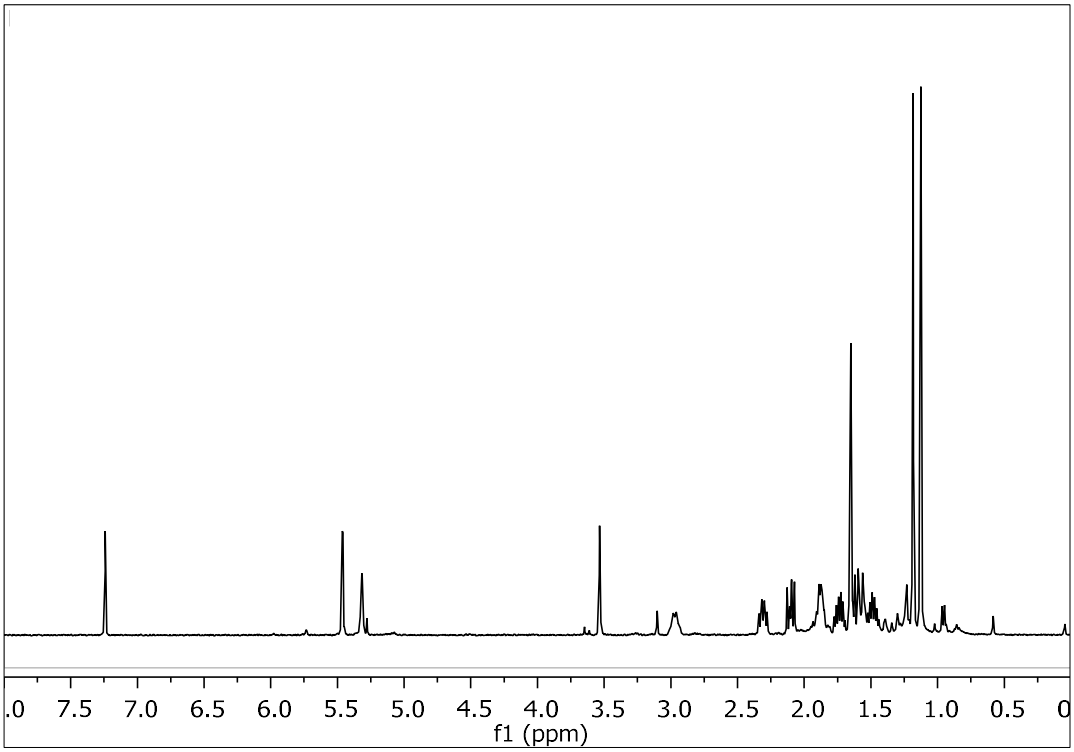

Figure 117. ^{1}H NMR spectrum of metabolite **26**.

Table 160. ^{1}H NMR data of metabolite **26** in $CDCl_3$ (δ in ppm, J in Hz).

Position	$\boldsymbol{\delta}_{\mathbf{H,exp}}$	$\boldsymbol{\delta}_{\mathbf{H,lit}}$
1	5.46 (d, 2.3)	5.48 (d, 1.0)
2	3.53 (d, 2.3)	3.55 (d, 1.0)
5	2.10 (dd, 13.3, 8.4), 1.59 (dd, 13.3, 10.0)	2.12 (dd, 13.8, 8.0), 1.58 (m)
6	2.97 (m)	2.99 (m)
7	5.32 (brs)	5.34 (brs)
9	1.88 (m)	
10	1.74 (ddd, 13.2, 12.7, 6.2), 1.48 (dt, 13.2, 6.5)	1.77 (m), 1.51 (m)
11	2.31 (m)	
13	1.13 (s)	1.15 (s)
14	1.18 (s)	1.21 (s)
15	1.65 (s)	1.67 (brs)

3.2.5 Metabolite 27

Metabolite **27** (KR649-21) was isolated after a series of chromatographic separations as a colorless oil (1.6 mg).

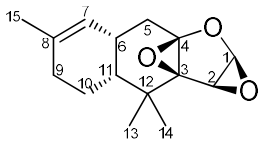

The mass spectrum of metabolite **27** (Figure 118) exhibited a molecular ion peak $[M]^+$ at *m/z* 248.

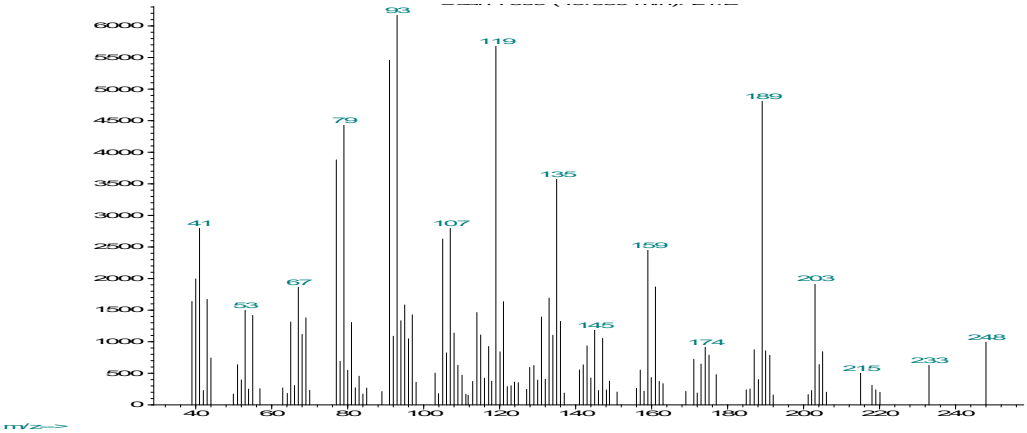

Figure 118. Mass spectrum (EIMS) of metabolite **27**.

In the ^{1}H NMR spectrum of metabolite **27** (Figure 119) obvious were:

- Two aliphatic methyls on non-protonated carbons at δ 1.02 and 1.15,
- One olefinic methyl at δ 1.65, and
- Three signals at δ 3.78, 5.38 and 5.56 integrating for one proton each and attributed to either oxygenated or olefinic methines.

Analysis of the NMR and MS data of **27** led to the molecular formula $C_{15}H_{20}O_3$. Taking into account the one carbon-carbon double bond as one of the six degrees of unsaturation, the molecular structure of **27** was determined as pentacyclic.

Comparison of the spectroscopic and physical characteristics of metabolite **27** with those reported in the literature led to its identification as furodysinin lactone (bis-epoxide), previously isolated from the marine nudibranch *Chromodoris funerea* (Carté et al., 1986). The ^{1}H NMR data of metabolite **27** are reported in Table 161.

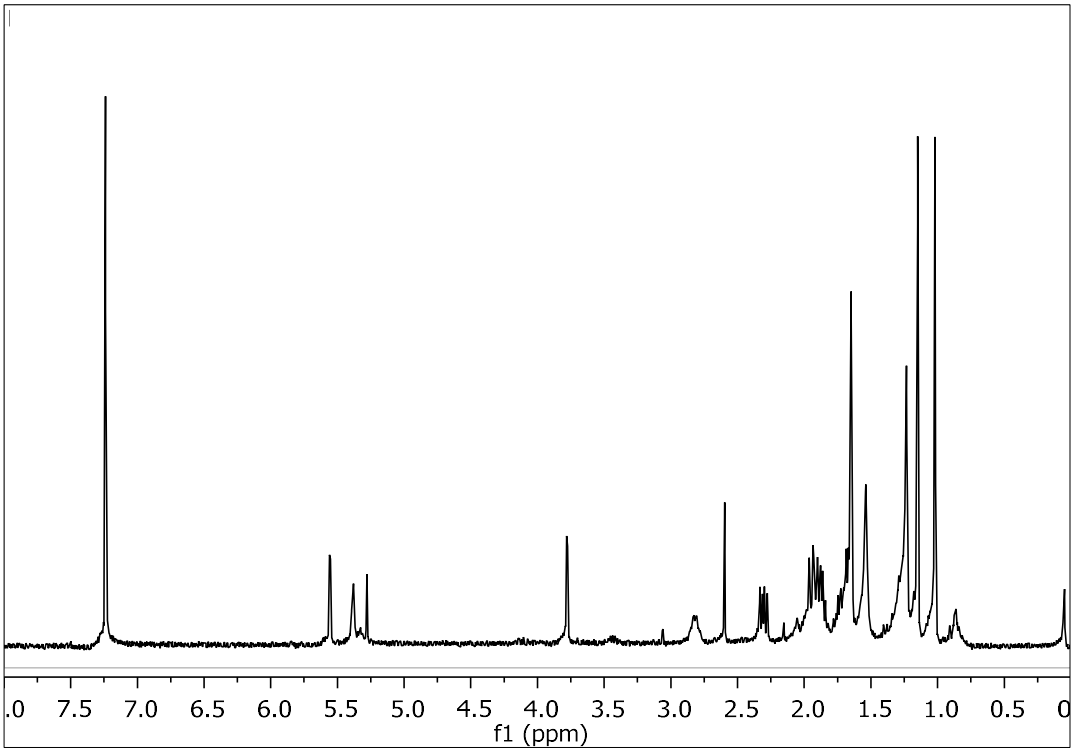

Figure 119. ^{1}H NMR spectrum of metabolite **27**.

Table 161. ^{1}H NMR data of metabolite **27** in $CDCl_3$ (δ in ppm, J in Hz).

Position	$\delta_{H,exp}$	$\delta_{H,lit}$
1	5.56 (d, 2.1)	5.58 (d, 1.0)
2	3.78 (d, 2.1)	3.80 (d, 1.0)
5	2.29 (m), 1.94 (m)	2.33 (m), 2.09 (m)
6	2.80 (m)	2.83 (m)
7	5.38 (brs)	5.41 (brs)
9	1.88 (m)	1.88 (m)
10	1.88 (m), 1.69 (m)	1.93 (m), 1.70 (m)
11	2.31 (m)	2.33 (m)
13	1.02 (s)	1.04 (s)
14	1.15 (s)	1.17 (s)
15	1.65 (s)	1.67 (brs)

3.2.6 Metabolite 28

Metabolite **28** (KR649-07) was isolated after a series of chromatographic separations as a colorless oil (9.2 mg).

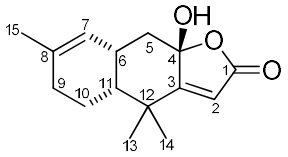

The mass spectrum of metabolite **28** (Figure 120) exhibited a fragment ion peak at *m/z* 230, corresponding to $[M\text{-}H_2O]^+$.

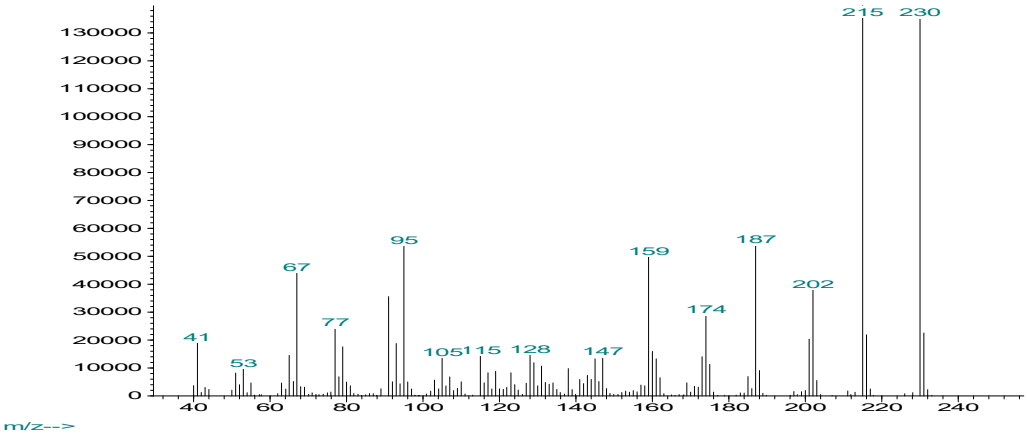

Figure 120. Mass spectrum (EIMS) of metabolite **28**.

In the ^{1}H NMR spectrum of metabolite **28** (Figure 121) obvious were:

- Two aliphatic methyls on non-protonated carbons at δ 1.21 and 1.39,
- One olefinic methyl at δ 1.60, and
- Two olefinic methines at δ 5.35 and 5.67.

Analysis of the NMR and MS data of **28** led to the molecular formula $C_{15}H_{20}O_3$. Taking into account the two carbon-carbon double bonds and the carbonyl moiety as three of the six degrees of unsaturation, the molecular structure of **28** was determined as tricyclic.

Comparison of the spectroscopic and physical characteristics of metabolite **28** with those reported in the literature led to its identification as furodysinin lactone, previously isolated from the marine sponge *Dysidea etheria* (Grode & Cardellina, 1984). The ^{1}H NMR data of metabolite **28** are reported in Table 162.

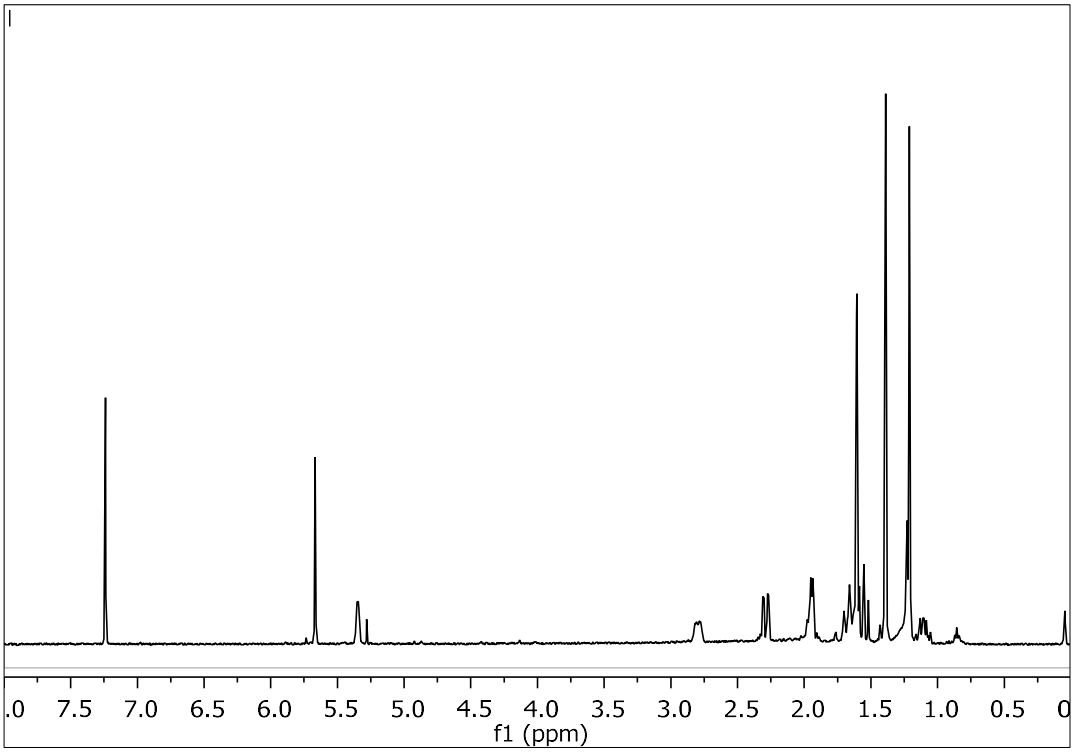

Figure 121. ^{1}H NMR spectrum of metabolite **28**.

Table 162. ^{1}H NMR data of metabolite **28** in $CDCl_3$ (δ in ppm, J in Hz).

Position	$\boldsymbol{\delta_{H,exp}}$	$\boldsymbol{\delta_{H,lit}}$
2	5.67 (brs)	5.67 (s)
5	2.29 (dd, 13.5, 3.7), 1.55 (t, 13.5)	2.28 (dd, 14.0, 3.8), 1.57 (dd, 14.0, 13.0)
6	2.80 (m)	2.80 (m)
7	5.35 (brd, 4.2)	5.36 (brdd, 5.7, 1.4)
9	1.94 (m)	1.96 (m)
10	1.69 (m), 1.10 (m)	1.70 (brddd, 12.6, 3.7, 3.1), 1.12 (brddd, 12.6, 12.6)
11	1.63 (m)	1.63 (m)
13	1.39 (s)	1.38 (s)
14	1.21 (s)	1.21 (s)
15	1.60 (s)	1.60 (brs)

3.2.7 Metabolite 29

Metabolite **29** (KR649-02) was isolated after a series of chromatographic separations as a colorless oil (52.4 mg).

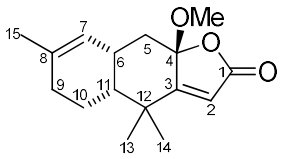

The mass spectrum of metabolite **29** (Figure 122) exhibited a molecular ion peak at *m/z* 262 and a fragment ion peak at *m/z* 230, corresponding to $[M\text{-}MeOH]^+$.

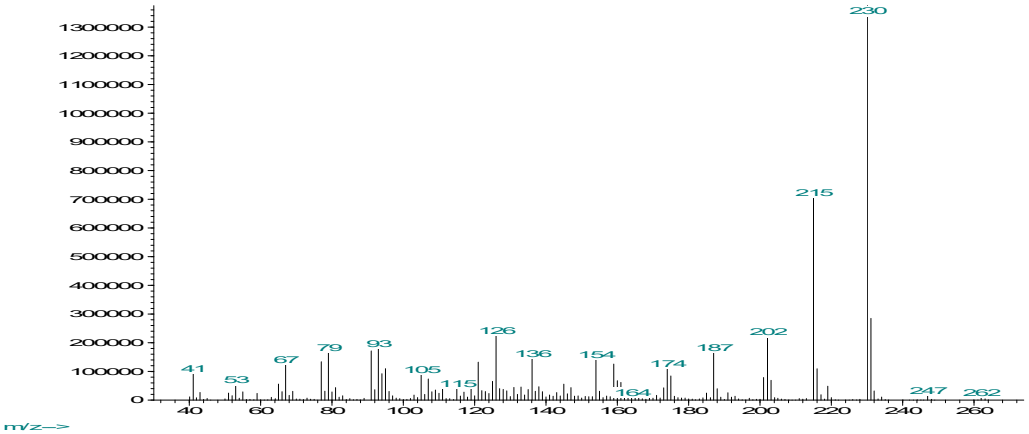

Figure 122. Mass spectrum (EIMS) of metabolite **29**.

In the ^{1}H NMR spectrum of metabolite **29** (Figure 123) obvious were:

- Two aliphatic methyls on non-protonated carbons at δ 1.21 and 1.34,
- One olefinic methyl at δ 1.59,
- One methyl of a methoxy group at δ 3.15, and
- Two olefinic methines at δ 5.33 and 5.79.

Analysis of the NMR and MS data of **29** led to the molecular formula $C_{16}H_{22}O_3$. Taking into account the two carbon-carbon double bonds and the carbonyl moiety as three of the six degrees of unsaturation, the molecular structure of **29** was determined as tricyclic.

Comparison of the spectroscopic and physical characteristics of metabolite **29** with those reported in the literature led to its identification as *O*-methyl-furodysinin lactone, previously isolated from the marine sponge *Dysidea arenaria* (Grode & Cardellina, 1984). The ^{1}H NMR data of metabolite **29** are reported in Table 163.

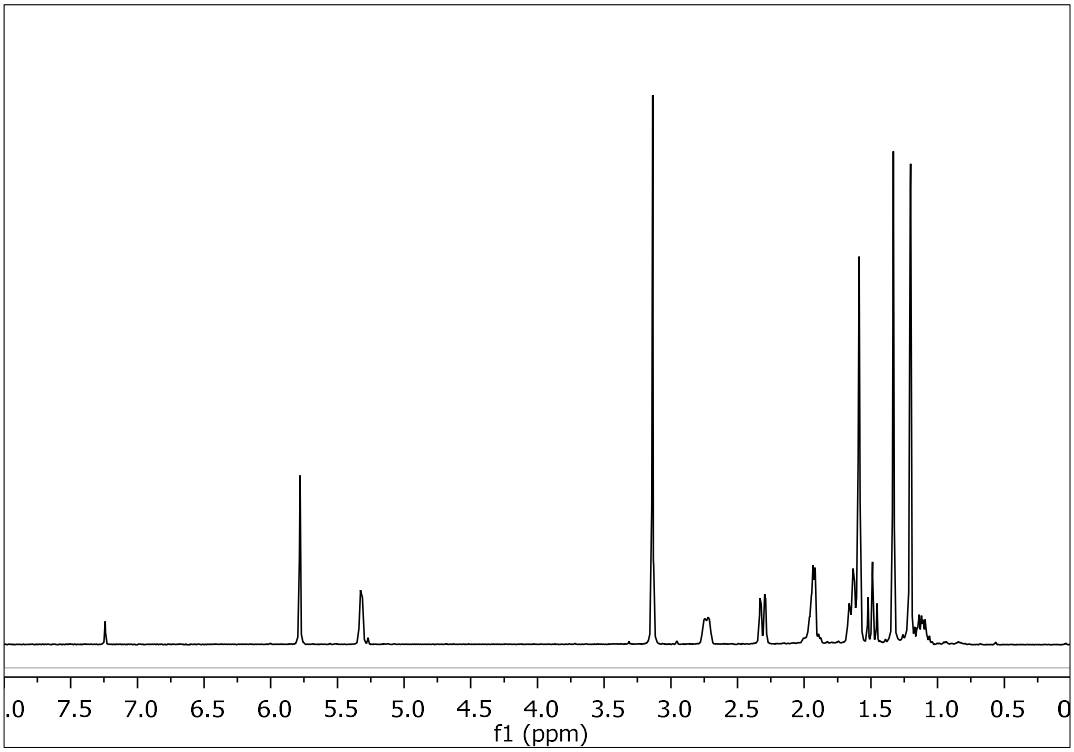

Figure 123. ^{1}H NMR spectrum of metabolite **29**.

Table 163. ^{1}H NMR data of metabolite **29** in $CDCl_3$ (δ in ppm, J in Hz).

Position	$\boldsymbol{\delta_{H,exp}}$	$\boldsymbol{\delta_{H,lit}}$
2	5.79 (brs)	5.78 (s)
5	2.32 (dd, 13.5, 3.8), 1.50 (t, 13.5)	2.30 (dd, 13.8, 4.0), 1.55 (dd, 14, 14)
6	2.74 (m)	2.70 (m)
7	5.33 (brd, 4.3)	5.30 (brdd, 5.7, 1.5)
9	1.94 (m)	1.96 (m)
10	1.65 (m), 1.12 (m)	1.69 (brddd, 12.6, 3.7, 3.1), 1.10 (brddd, 12.9, 12, 5.9)
13	1.34 (s)	1.31 (s)
14	1.21 (s)	1.20 (s)
15	1.59 (s)	1.59 (brs)
16	3.15 (s)	3.12 (s)

3.2.8 Metabolite 30

Metabolite **30** (KR649-20) was isolated after a series of chromatographic separations as a colorless oil (1.3 mg).

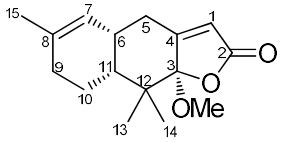

The mass spectrum of metabolite **30** (Figure 124) exhibited a molecular ion peak $[M]^+$ at *m/z* 262 and a fragment ion peak at *m/z* 230 corresponding to $[M\text{-}MeOH]^+$.

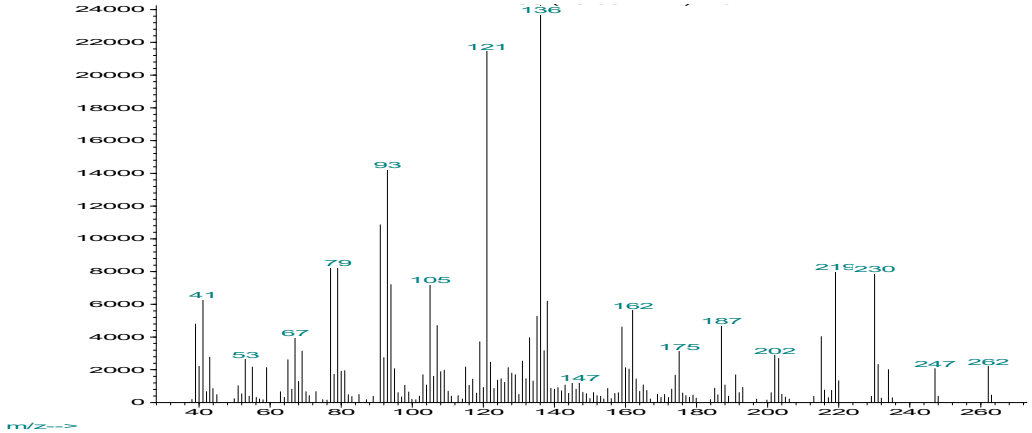

Figure 124. Mass spectrum (EIMS) of metabolite **30**.

In the ^1H NMR spectrum of metabolite **30** (Figure 125) obvious were:

- Two aliphatic methyls on non-protonated carbons at δ 0.91 and 1.18,
- One olefinic methyl δ 1.64,
- One methyl of a methoxy group at δ 3.06, and
- Two olefinic methines at δ 5.32 and 5.85.

Analysis of the NMR and MS data of **30** led to the molecular formula $C_{16}H_{22}O_3$. Taking into account the two carbon-carbon double bonds and the carbonyl moiety as three of the six degrees of unsaturation, the molecular structure of **30** was determined as tricyclic.

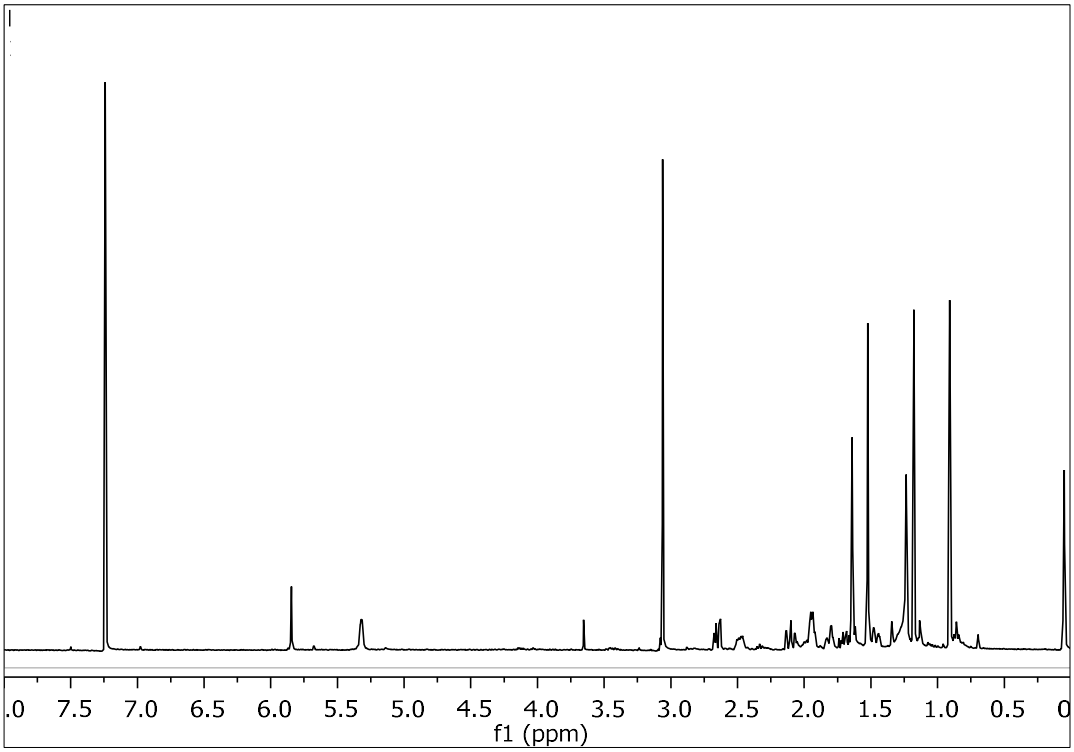

Figure 125. ^{1}H NMR spectrum of metabolite **30**.

The spectroscopic data of metabolite **30** were rather similar to those of **29**, suggesting the close resemblance of the two chemical structures. The planar structure of metabolite **30** was determined on the basis of the homonuclear and heteronuclear correlations (Figure 126) observed in the HSQC-DEPT (Figure 127), HMBC (Figure 128) and COSY (Figure 129) spectra. In particular, the HMBC correlations of the doubly oxygenated C-3 (δ_C 110.9) with H-1 (δ_H 5.85), H_3-13 (δ_H 1.18), H_3-14 (δ_H 0.91) and H_3-16 (δ_H 3.06) allowed for the identification of **30** as the oxygenated derivative of the rearranged furanosesquiterpene **23**.

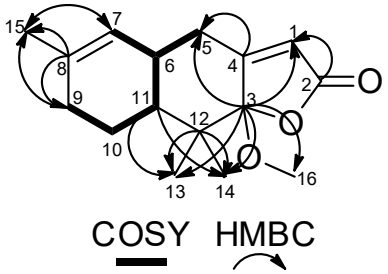

Figure 126. COSY and important HMBC correlations observed for metabolite **30**.

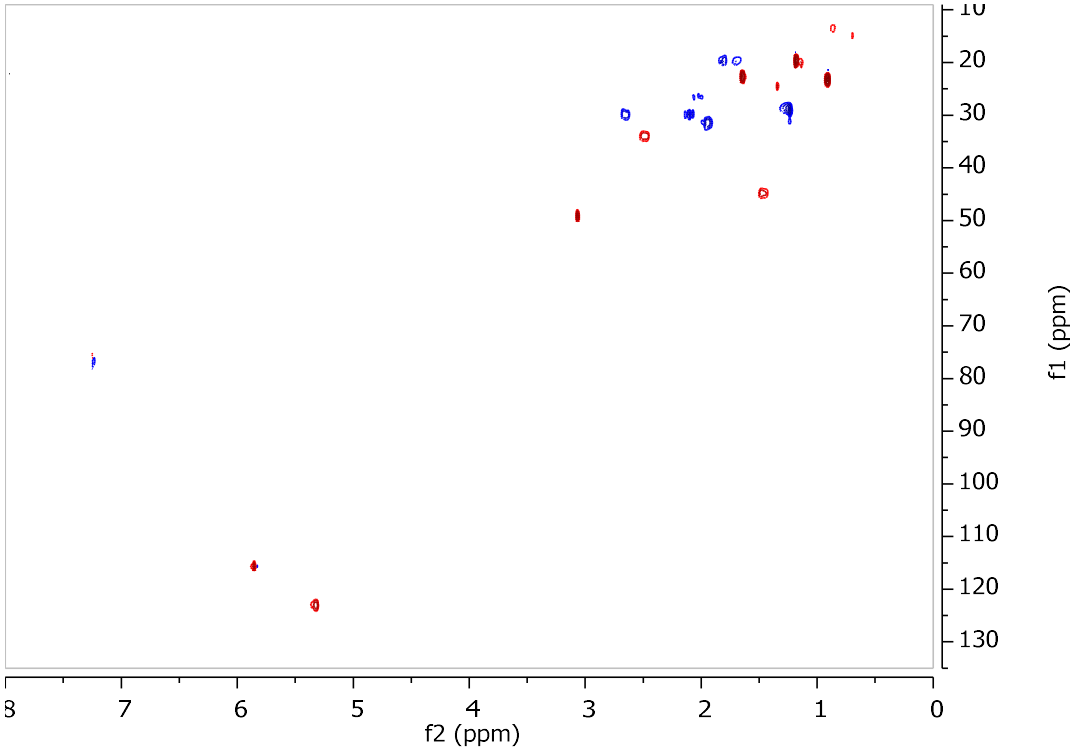

Figure 127. HSQC-DEPT spectrum of metabolite **30**.

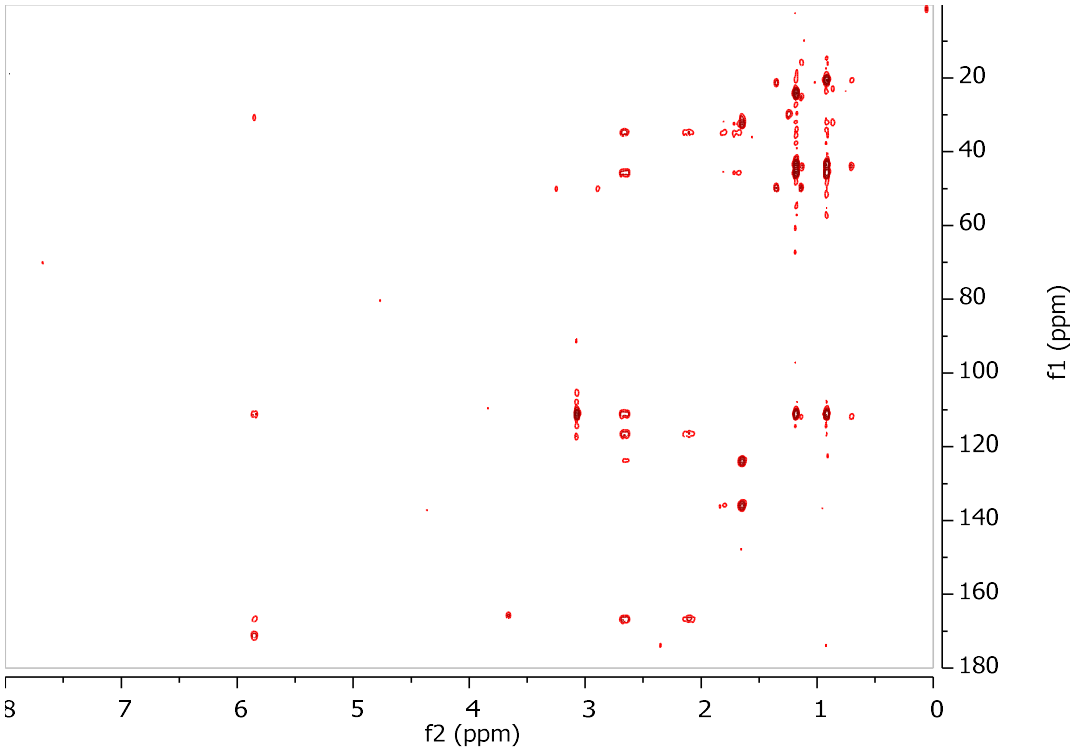

Figure 128. HMBC spectrum of metabolite **30**.

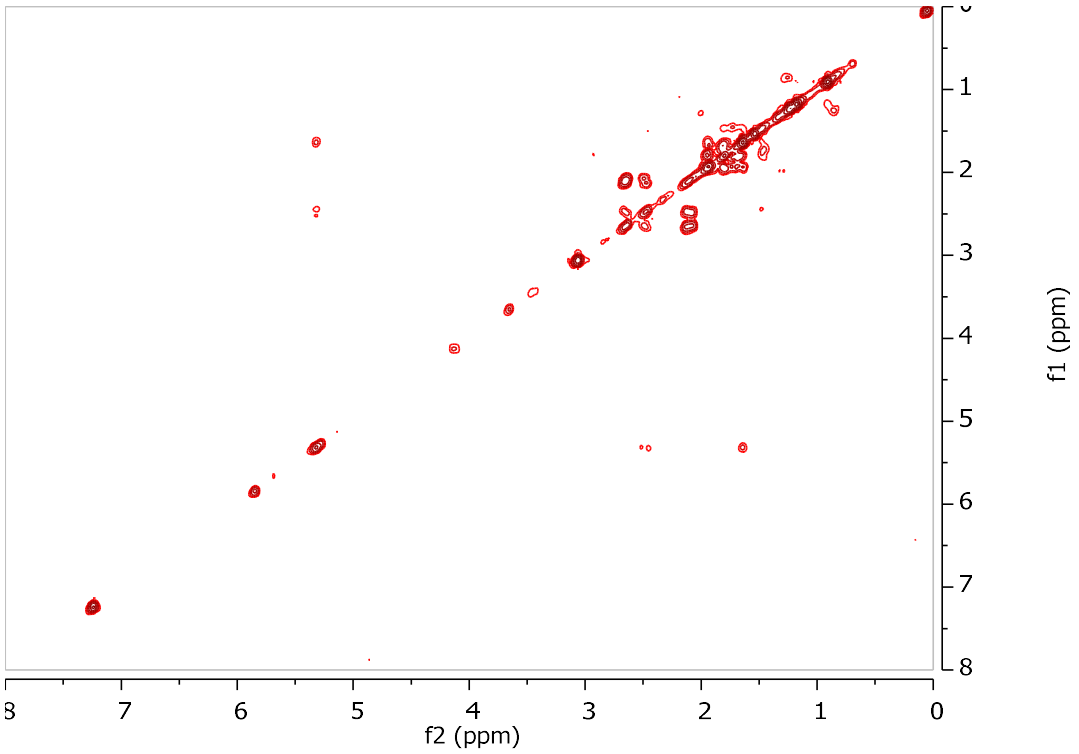

Figure 129. COSY spectrum of metabolite **30**.

The relative configuration of the asymmetric centers of metabolite **30** was determined on the basis of the correlations observed in the NOESY spectrum (Figure 130). Specifically, the NOE enhancements of H3-14 with H-6, of H-6 with H-11 and of H-11 with H3-14 indicated their cofacial orientation, while the NOE correlation of H3-13 with H3-16 suggested their orientation on the opposite side of the plane.

Comparison of the spectroscopic and physical characteristics of metabolite **30** with those reported in the literature led to its identification as a new natural product, which was designated as *O*-methyl-furodysin lactone. The NMR data of metabolite **30** are reported in Table 164.

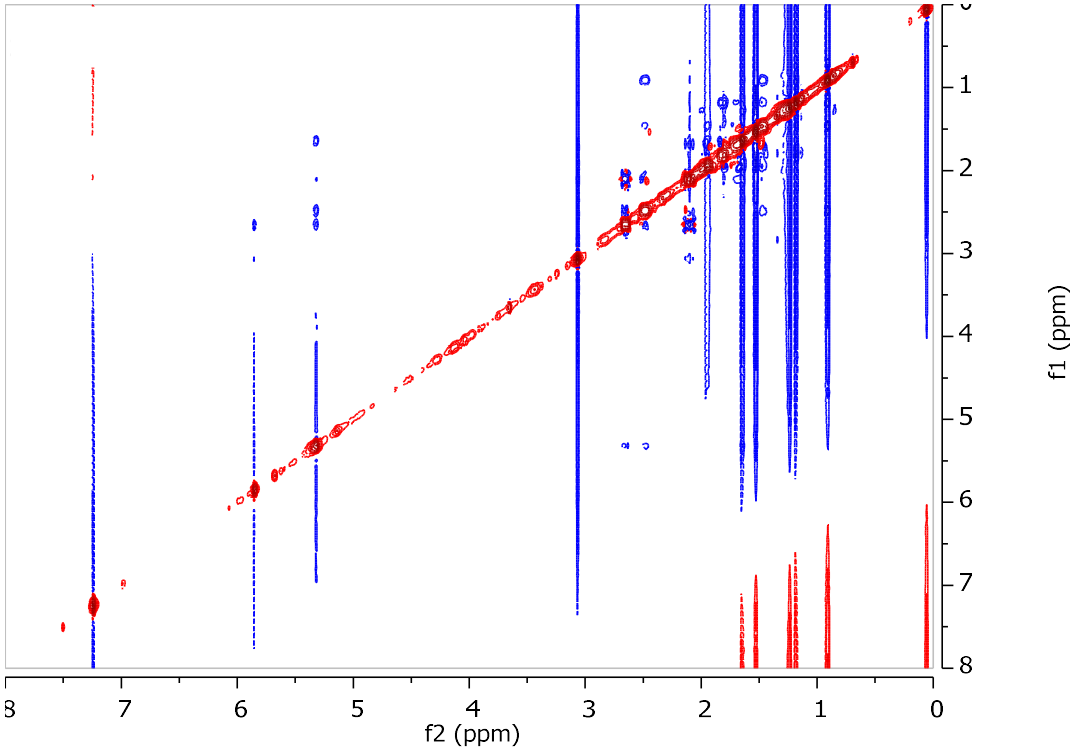

Figure 130. NOESY spectrum of metabolite **30**.

Table 164. ^{1}H and ^{13}C NMR data of metabolite **30** in $CDCl_3$ (δ in ppm, J in Hz).

Position	δ_C	δ_H
1	116.6	5.85 (d, 2.4)
2	171.4	-
3	110.9	-
4	166.5	-
5	30.6	2.65 (dd, 13.4, 4.2), 2.11 (m)
6	34.7	2.48 (m)
7	123.7	5.32 (d, 4.6)
8	135.9	-
9	32.2	1.94 (m)
10	20.3	1.80 (m), 1.71 (m)
11	45.6	1.45 (m)
12	43.1	-
13	20.3	1.18 (s)
14	23.7	0.91 (s)
15	23.1	1.64 (brs)
16	49.7	3.06 (s)

3.2.9 Metabolite 31

Metabolite **31** (KR649-19) was isolated after a series of chromatographic separations as a colorless oil (2.1 mg).

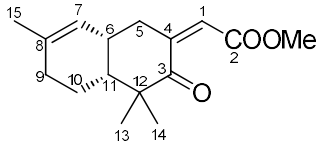

The mass spectrum of metabolite **31** (Figure 131) exhibited a molecular ion peak $[M]^+$ at *m/z* 262.

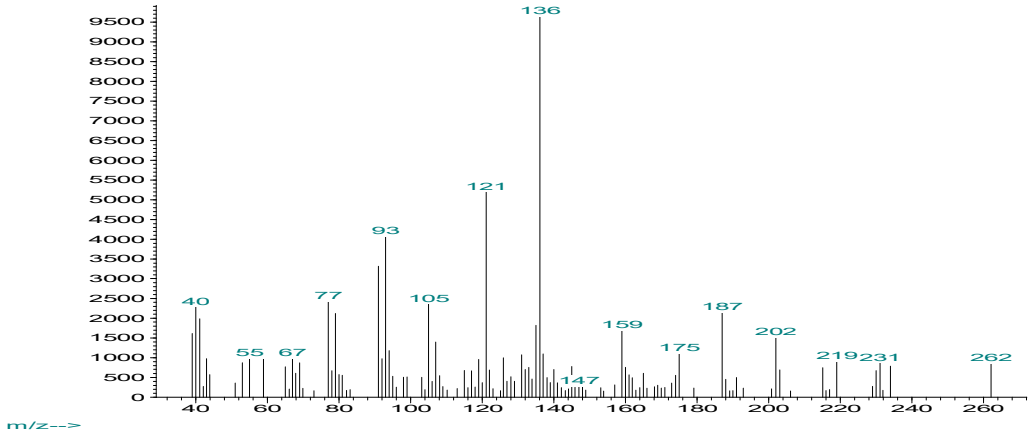

Figure 131. Mass spectrum (EIMS) of metabolite **31**.

In the ^{1}H NMR spectrum of metabolite **31** (Figure 132) obvious were:

- Two aliphatic methyls on non-protonated carbons at δ 1.13 and 1.34,
- One olefinic methyl δ 1.60,
- One methyl of an ester group at δ 3.65, and
- Two olefinic methines at δ 5.34 and 5.67.

Analysis of the NMR and MS data of **31** led to the molecular formula $C_{16}H_{22}O_3$. Taking into account the two carbon-carbon double bonds and the two carbonyl moieties as four of the six degrees of unsaturation, the molecular structure of **31** was determined as bicyclic.

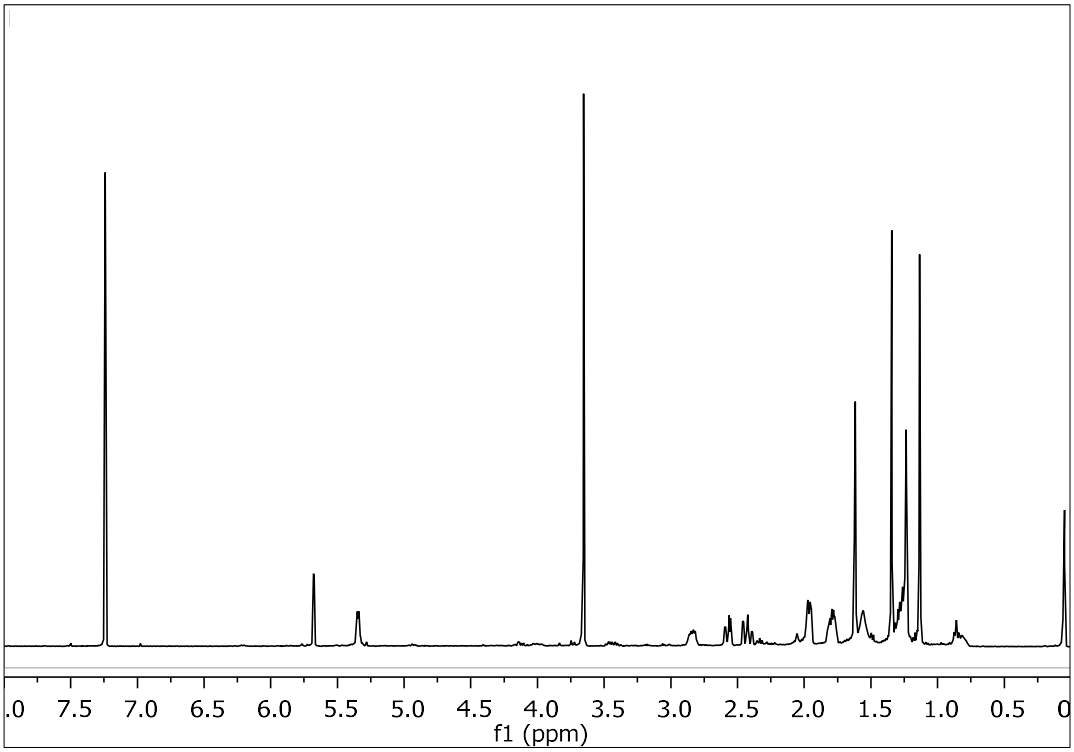

Figure 132. ^{1}H NMR spectrum of metabolite **31**.

Even though the spectroscopic data of metabolite **31** resembled those of **29** and **30**, the bicyclic structure, as dictated from the above-mentioned data, suggested the ring opening of the lactone ring. The planar structure of metabolite **31** was determined on the basis of the homonuclear and heteronuclear correlations (Figure 133) observed in the HSQC-DEPT (Figure 134), HMBC (Figure 135) and COSY (Figure 136) spectra. In particular, the HMBC correlations of C-2 (δ_C 165.4), C-3 (δ_C 209.4), C-4 (δ_C 155.9) and C-5 (δ_C 41.3) with H-1 (δ_H 5.67), as well as of C-2 with H_3-16 (δ_H 3.65) and of C-3 with H-11 (δ_H 1.80), H_3-13 (δ_H 1.34) and H_3-14 (δ_H 1.13) secured the assignment of the planar structure of compound **31**.

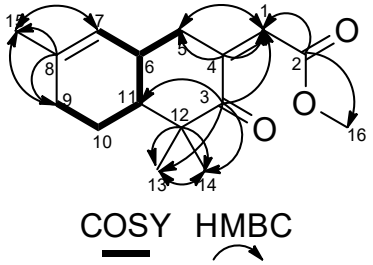

Figure 133. COSY and important HMBC correlations observed for metabolite **31**.

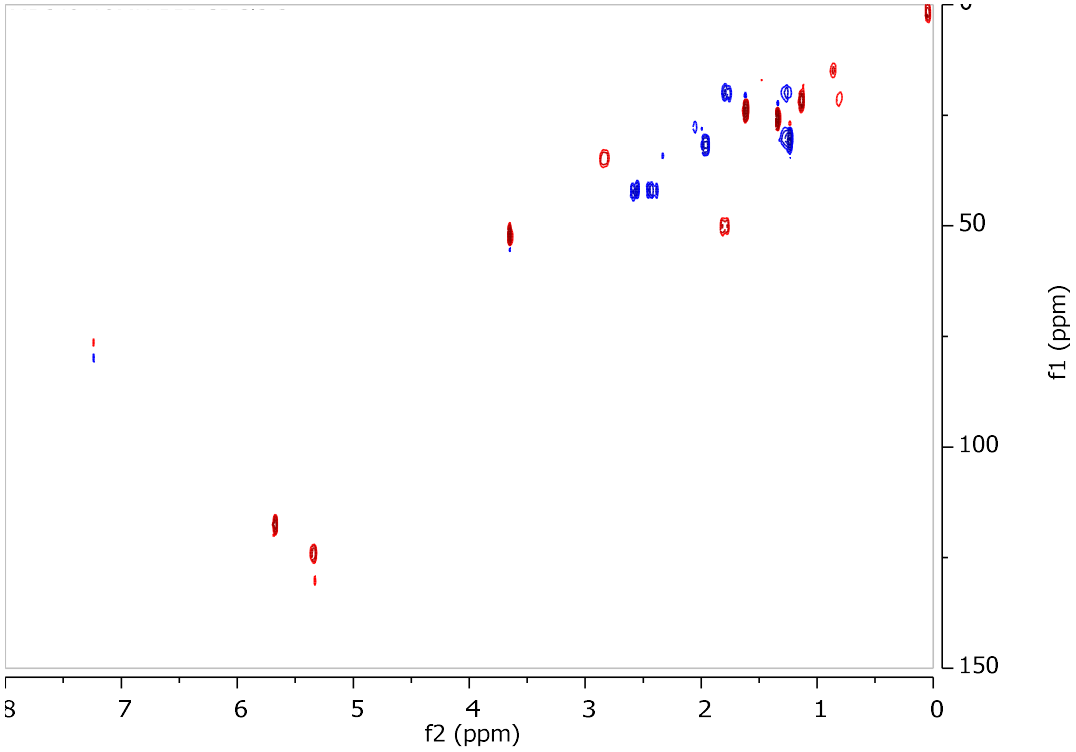

Figure 134. HSQC-DEPT spectrum of metabolite **31**.

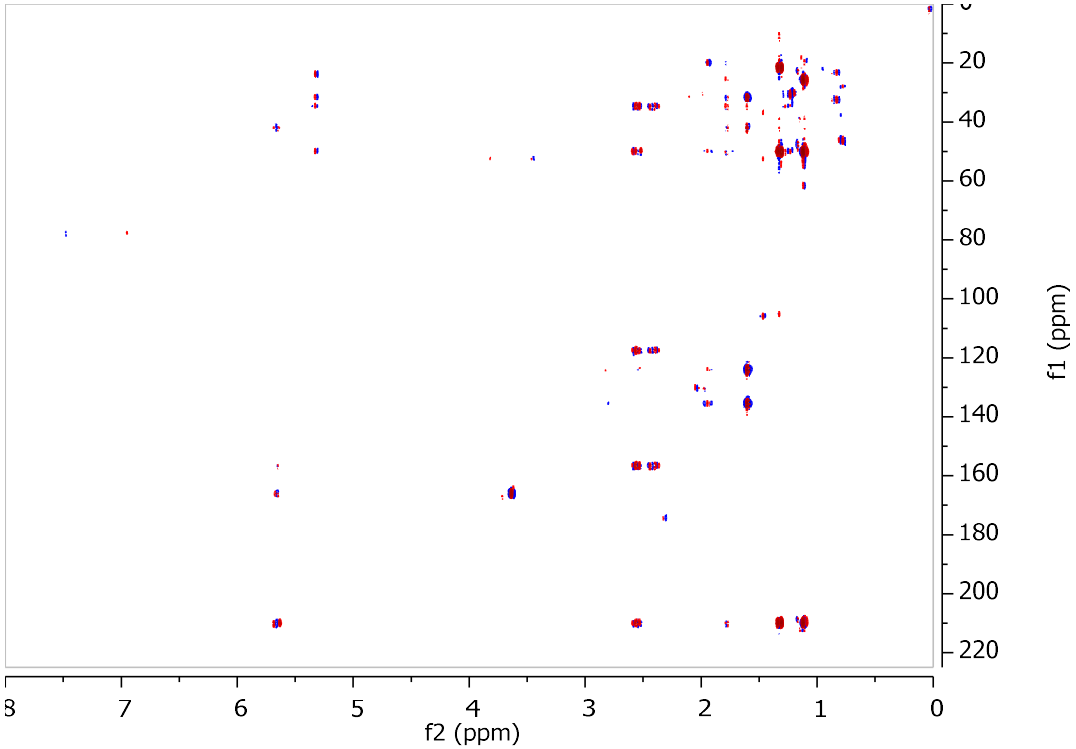

Figure 135. HMBC spectrum of metabolite **31**.

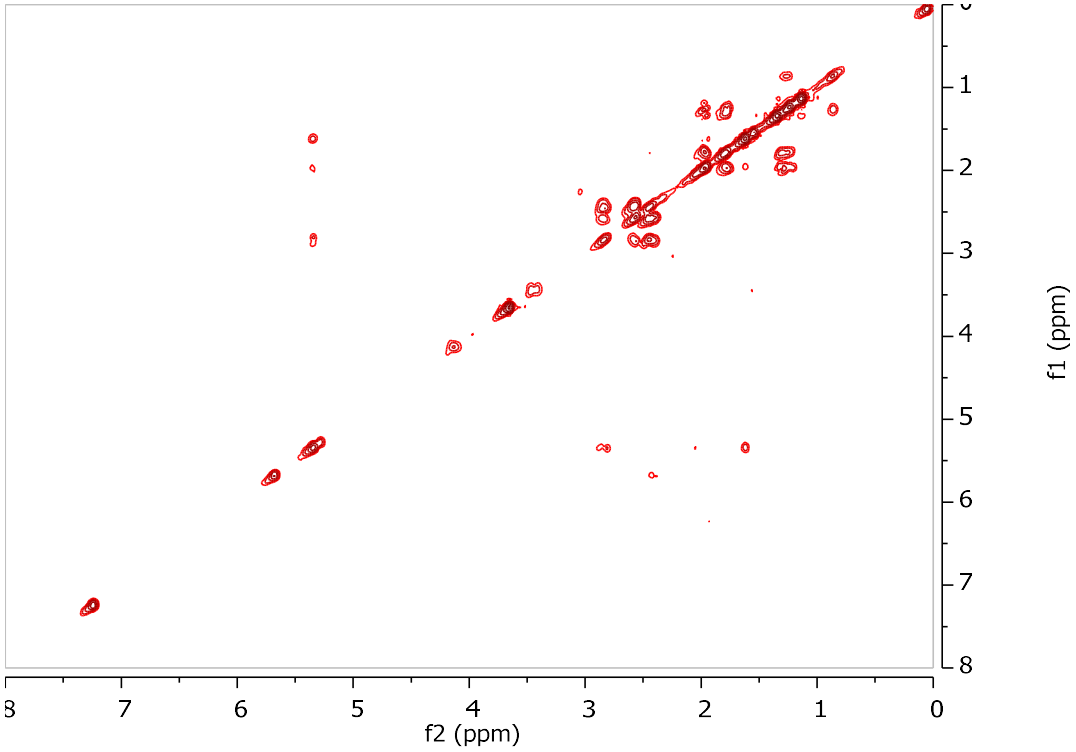

Figure 136. COSY spectrum of metabolite **31**.

The relative configuration of the asymmetric centers of metabolite **31** was suggested on the basis of biogenetic considerations, in comparison to the previously isolated compounds **22**-**30**.

Comparison of the spectroscopic and physical characteristics of metabolite **31** with those reported in the literature led to its identification as a new natural product, which was designated as; The NMR data of metabolite **31** are reported in Table 165.

Table 165. ^{1}H and ^{13}C NMR data of metabolite **31** in $CDCl_3$ (δ in ppm, J in Hz)

Position	δ_C	δ_H
1	117.0	5.67 (d, 2.3)
2	165.4	-
3	209.4	-
4	155.9	-
5	41.3	2.57 (dd, 14.5, 4.1), 2.42 (ddd, 14.5, 12.2, 2.3)
6	34.4	2.84 (m)
7	123.1	5.34 (d, 4.2)
8	134.7	-
9	31.4	1.99 (m)
10	19.2	1.79 (m), 1.28 (m)
11	49.1	1.80 (m)
12	50.0	-
13	25.2	1.34 (s)
14	20.9	1.13 (s)
15	23.9	1.60 (brs)
16	51.2	3.65 (s)

3.2.10 Metabolite 32

Metabolite **32** (KR649-29) was isolated after a series of chromatographic separations as a colorless oil (3.3 mg).

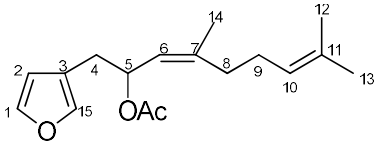

The mass spectrum of metabolite **32** (Figure 137) exhibited a fragment ion peak at *m/z* 216 corresponding to $[M\text{-}AcOH]^+$.

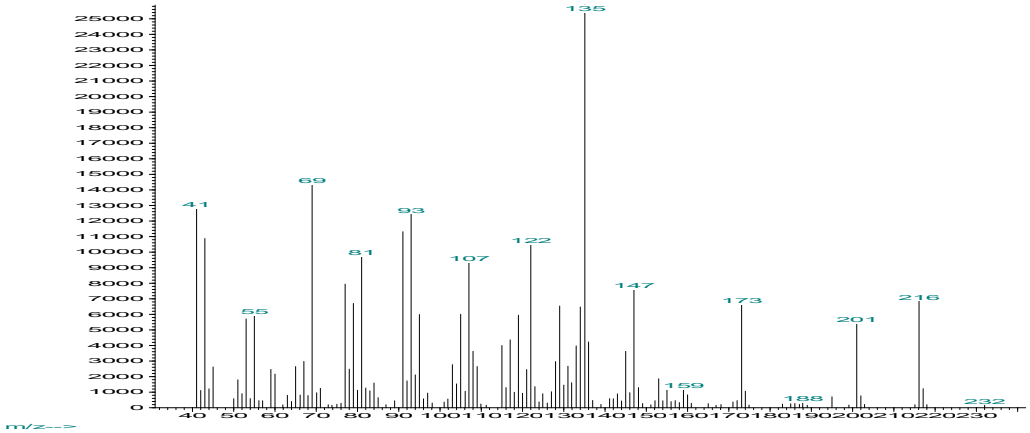

Figure 137. Mass spectrum (EIMS) of metabolite **32**.

In the ^{1}H NMR spectrum of metabolite **32** (Figure 138) obvious were:

- Three olefinic methyls at δ 1.57, 1.65 and 1.70,
- One methyl of an acetoxy group at δ 1.99,
- Three signals at δ 5.05, 5.13 and 5.61 integrating for one proton each and attributed to three oxygenated or olefinic protons, and
- Three olefinic methines at 6.26, 7.21 and 7.31 integrating for one proton each and attributed to the olefinic protons of a monosubstituted furan ring.

Analysis of the NMR and MS data of **32** led to the molecular formula $C_{17}H_{24}O_3$. Taking into account the four carbon-carbon double bonds and the carbonyl moiety as five of the six degrees of unsaturation, the molecular structure of **32** was determined as monocyclic.

Comparison of the spectroscopic and physical characteristic of metabolite **32** with those reported in the literature led to its identification as (5*R*,6*Z*)-dendrolasin-5-acetate, previously isolated from the marine nudibranch *Hypselodoris jacksoni* (Mudianta et al., 2013). The ^{1}H NMR data of metabolite **32** are reported in Table 166.

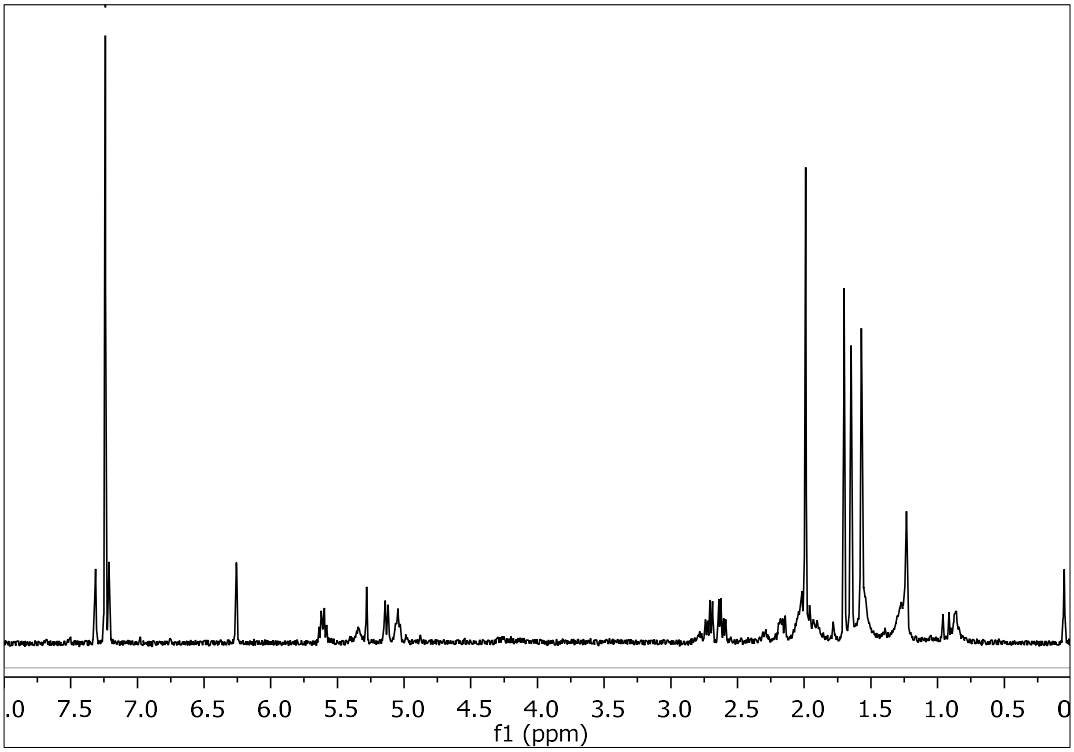

Figure 138. ^{1}H NMR spectrum of metabolite **32**.

Table 166. ^{1}H NMR data of metabolite **32** in $CDCl_3$ (δ in ppm, J in Hz).

Position	$\boldsymbol{\delta_{H,exp}}$	$\boldsymbol{\delta_{H,lit}}$
1	7.31 (brs)	7.33 (brs)
2	6.26 (brs)	6.27 (brs)
4	2.72 (dd, 14.4, 6.7), 2.61 (dd, 14.4, 5.9)	2.73 (dd, 14.5,6.7), 2.63 (dd, 14.5, 6.0)
5	5.61 (ddd, 9.4, 6.7, 5.9)	5.64 (bdt, 9.3, 6.4)
6	5.13 (d, 9.4)	5.15 (d, 9.3)
8	2.16 (m), 1.99 (m)	2.15 (m)
9	2.06 (m), 1.95 (m)	1.95 (m)
10	5.05 (brt, 6.7)	5.07 (brt, 6.9)
12	1.65 (s)	1.67 (s)
13	1.57 (s)	1.59 (s)
14	1.70 (s)	1.72 (s)
15	7.21 (brs)	7.23 (s)
OAc	1.99 (s)	2.01 (s)

3.2.11 Metabolite 33

Metabolite **33** (KR649-30) was isolated after a series of chromatographic separations as a colorless oil (2.4 mg).

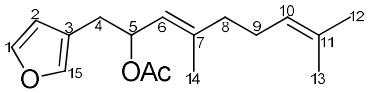

The mass spectrum of metabolite **33** (Figure 139) exhibited a fragment ion peak at *m/z* 216 corresponding to $[M\text{-}AcOH]^+$.

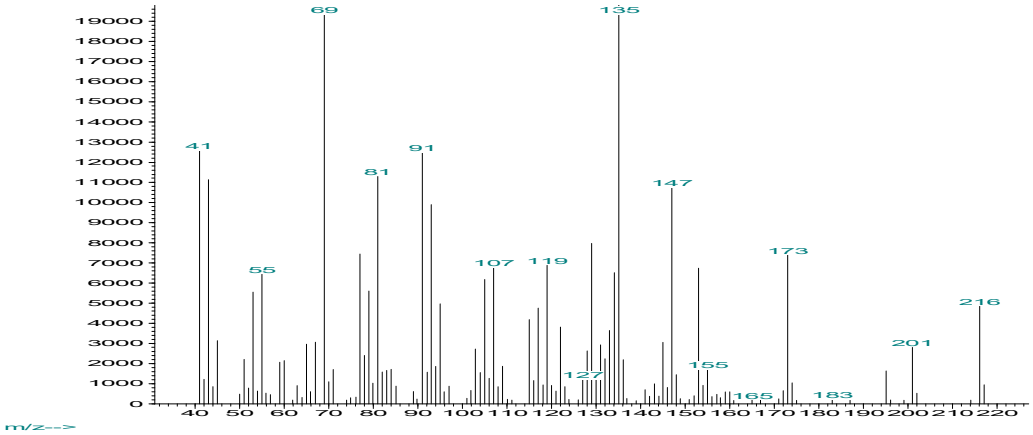

Figure 139. Mass spectrum (EIMS) of metabolite **33**.

In the ^{1}H NMR spectrum of metabolite **33** (Figure 140) obvious were:

- Three olefinic methyls at δ 1.57, 1.62 and 1.66,
- One methyl of an acetoxy group at δ 2.00,
- Three signals at δ 55.02, 5.11 and 5.60 integrating for one proton each and attributed to three oxygenated or olefinic protons, and
- Three olefinic methines at 6.26, 7.21 and 7.31 integrating for one proton each and attributed to the olefinic protons of a monosubstituted furan ring.

Analysis of the NMR and MS data of **33** led to the molecular formula $C_{17}H_{24}O_3$. Taking into account the four carbon-carbon double bonds and the carbonyl moiety as five of the six degrees of unsaturation, the molecular structure of **33** was determined as monocyclic.

Comparison of the spectroscopic and physical characteristics of metabolite **33** with those reported in the literature led to its identification as (6*E*)-dendrolasin-5-acetate, previously reported only synthetically (Tsubuki et al., 2009). The ^{1}H NMR data of metabolite **33** are reported in Table 167.

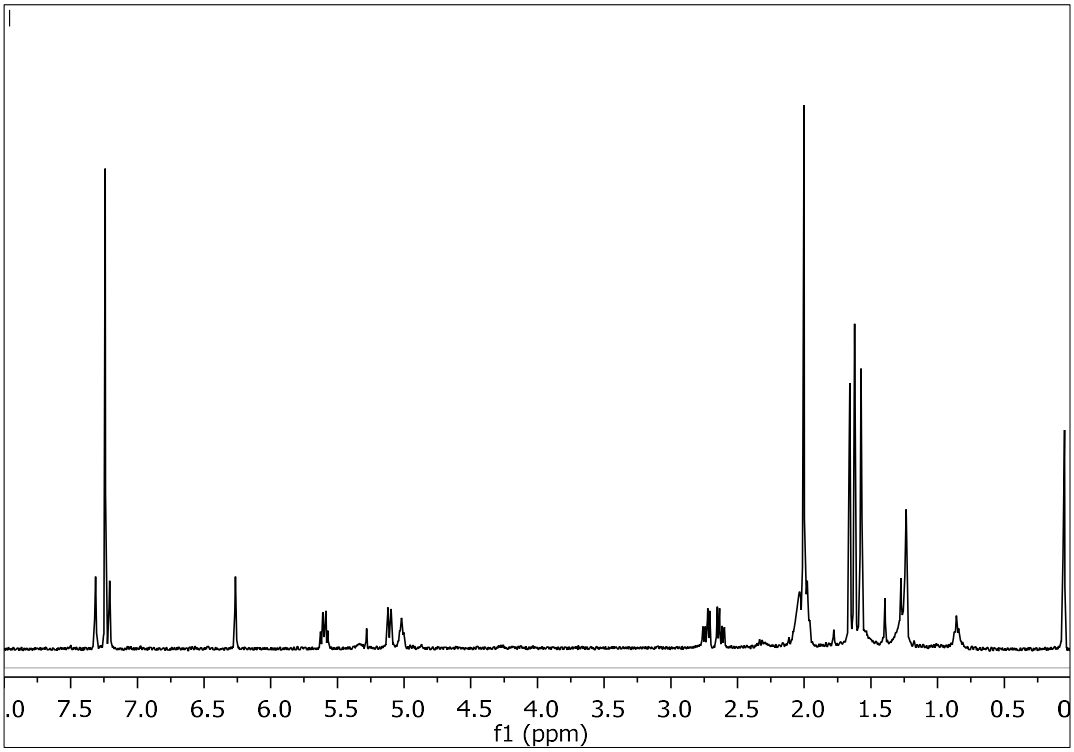

Figure 140. ^{1}H NMR spectrum of metabolite **33**.

Table 167. ^{1}H NMR data of metabolite **33** in $CDCl_3$ (δ in ppm, J in Hz).

Position	$\boldsymbol{\delta}_{\mathbf{H,exp}}$	$\boldsymbol{\delta}_{\mathbf{H,lit}}$
1	7.31 (brs)	7.33 (t, 1.8)
2	6.26 (brs)	6.28 (d, 1.2)
4	2.73 (dd, 14.4, 6.5), 2.62 (dd, 14.4, 6.5)	2.76 (dd, 14.7,6.7), 2.62 (dd, 14.7, 6.7)
5	5.60 (dt, 8.6, 6.5)	5.62 (dt, 9.1, 6.7)
6	5.11 (dd, 8.6, 1.0)	5.13 (dd, 9.1, 1.2)
8	2.16 (m), 1.99 (m)	2.16 (m)
9	2.06 (m), 1.95 (m)	1.95 (m)
10	5.02 (t, 6.2)	5.04 (brt, 6.7)
12	1.66 (s)	1.68 (s)
13	1.57 (s)	1.59 (s)
14	1.62 (s)	1.64 (s)
15	7.21 (brs)	7.23 (s)
OAc	2.00 (s)	2.01 (s)

3.3 Identification and structure elucidation of isolated metabolites from the soft coral *Sinularia polydactyla*

3.3.1 Metabolite 34

Metabolite **34** (SP31) was isolated after a series of chromatographic separations as a white amorphous solid (0.7 mg).

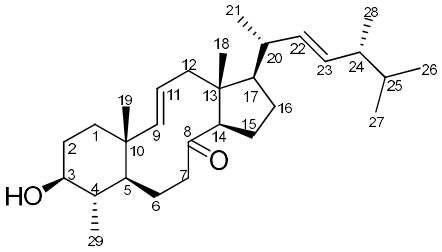

The high-resolution mass spectrum of the metabolite **34** (Figure 141) showed a pseudomolecular ion peak at *m/z* 429.3724 corresponding to $[M+H]^+$ (calcd. for $C_{29}H_{49}O_2$, 429.3727).

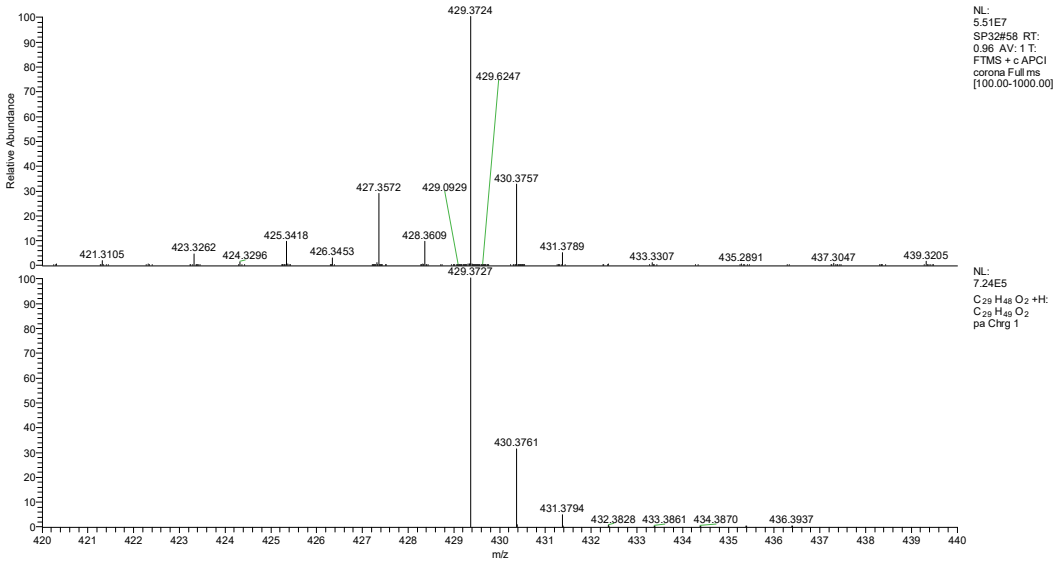

Figure 141. Mass spectrum (HR-APCIMS) of metabolite **34**.

In the ^{1}H NMR spectrum of metabolite **34** (Figure 142) obvious were:

- Two aliphatic methyls on non-protonated carbons at δ 0.94 and 1.08,
- Five aliphatic methyls on tertiary carbons at δ 0.80, 0.81, 0.89, 0.99 and 1.04,
- One oxygenated methine at δ 3.09, and
- Four olefinic methines at δ 5.15, 5.20, 5.28 and 5.41.

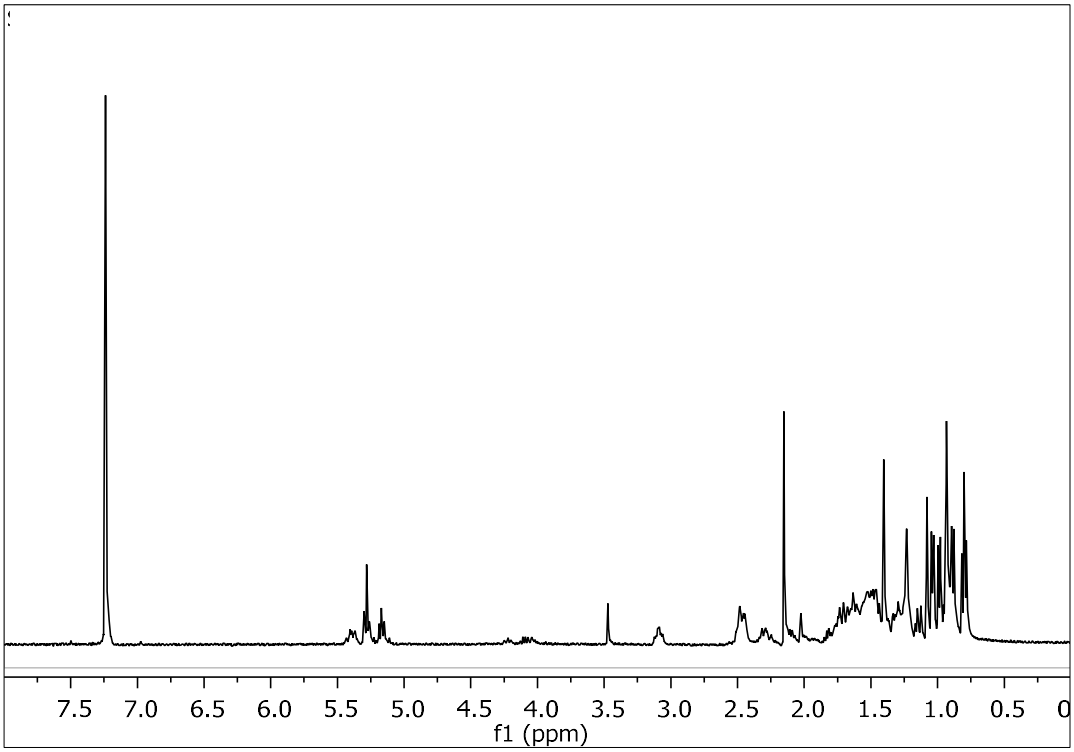

Figure 142. ^{1}H NMR spectrum of metabolite **34**.

Analysis of the NMR and MS data of **34** led to the molecular formula $C_{29}H_{48}O_2$. Taking into account the two carbon-carbon double bonds and the carbonyl moiety as three of the six degrees of unsaturation, the molecular structure of **34** was determined as tricyclic.

The planar structure of metabolite **34** was determined on the basis of the homonuclear and heteronuclear correlations (Figure 143) observed in the HSQC-DEPT (Figure 144), HMBC (Figure 145) and COSY (Figure 146) spectra. In particular, the ^{13}C NMR and HSQC-DEPT spectra revealed the presence of 29 carbon atoms, corresponding to seven methyls, seven methylenes, twelve methines, and three non-protonated carbon atoms. Among them, evident were one carbonyl resonating at δ_C 213.1, four olefinic carbons resonating at δ_C 127.6, 132.6, 135.2, and 142.0 and an oxygenated carbon resonating at δ_C 76.6. In the ^{1}H NMR spectrum evident were two methyls on non-protonated carbons (δ_H 0.94 and 1.08), five methyls on tertiary carbons (δ_H 0.80, 0.81, 0.89, 0.99, and 1.04), one oxygenated methine (δ_H 3.09), and four olefinic methines (δ_H 5.15, 5.20, 5.28, and 5.41). The spectroscopic features of metabolite **34**, in conjunction with the homonuclear and heteronuclear correlations observed in its HSQC, HMBC, and COSY spectra suggested that compound **34** possessed a 8-oxo-3-hydroxy-4-methyl-8,9-seco steroidal nucleus with a $\Delta^{9,11}$ and a C_9H_{17} unsaturated side chain with a 1,2-disubstituted double bond between C-22 and C-23. Specifically, the correlations observed in the COSY spectrum identified three distinct spin systems, namely (a) a spin system starting from H-1 to H_2-7, incorporating H_3-29 which was coupled to H-4, (b) a short spin system from H-9 to H_2-12 through H-11, and (c) an extended branched spin system from H-14 to H_3-26, including H_3-21, H_3-

27, and H_3-28 which were coupled to H-20, H-25, and H-24, respectively. The HMBC correlations of H_3-19 with C-1, C-5, C-9, and C-10 concluded the six-membered ring and positioned the first angular methyl on C-10, connecting at the same time spin systems (a) and (b). Additionally, the HMBC correlations of H_3-18 with C-12, C-13, C-14, and C-17 identified the five-membered ring and fixed the position of the second angular methyl on C-13, connecting spin systems (b) and (c). The HMBC correlations of H_2-6, H_2-7, and H-14 with the carbonyl carbon C-8 supported the cleavage of the C-8/C-9 bond, giving rise to the decalin ring and connecting spin systems (a) and (c).

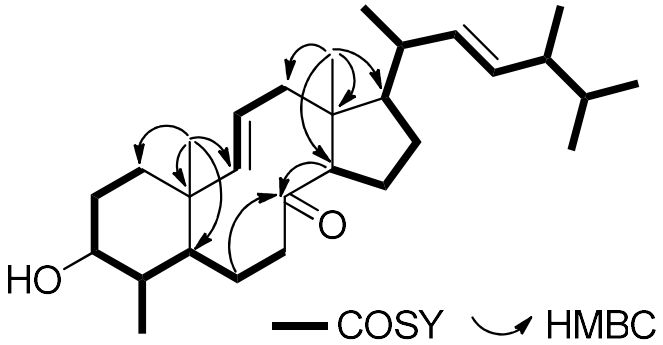

Figure 143. COSY and important HMBC correlations observed for metabolite **34**.

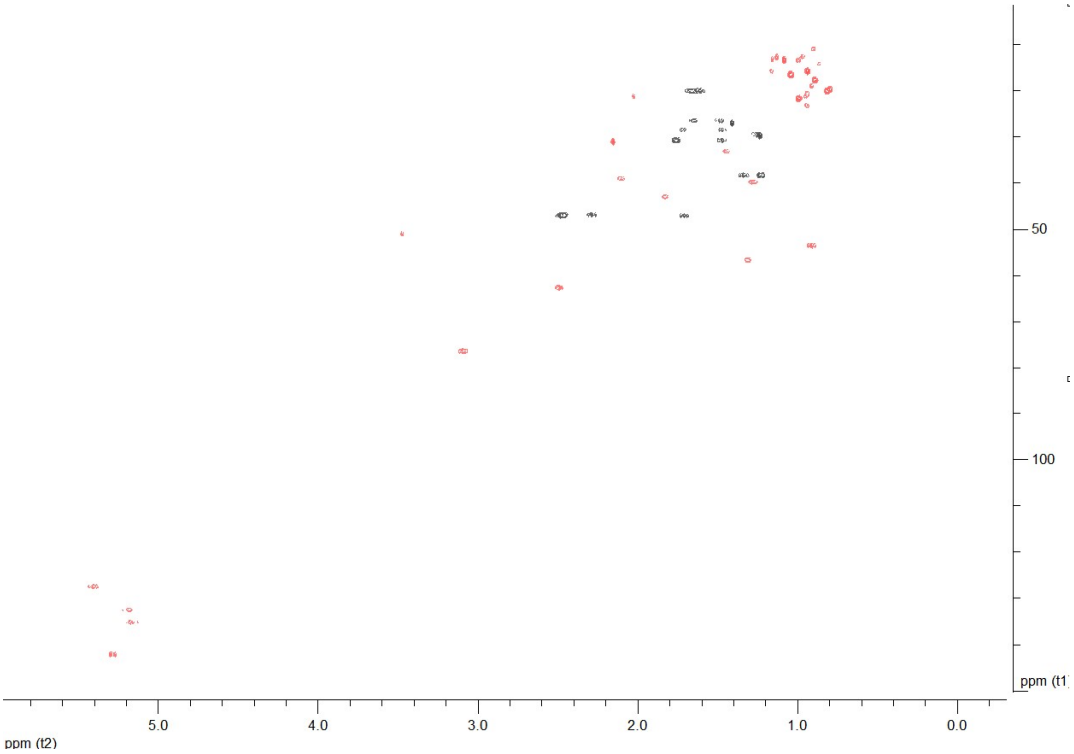

Figure 144. HSQC-DEPT spectrum of metabolite **34**.

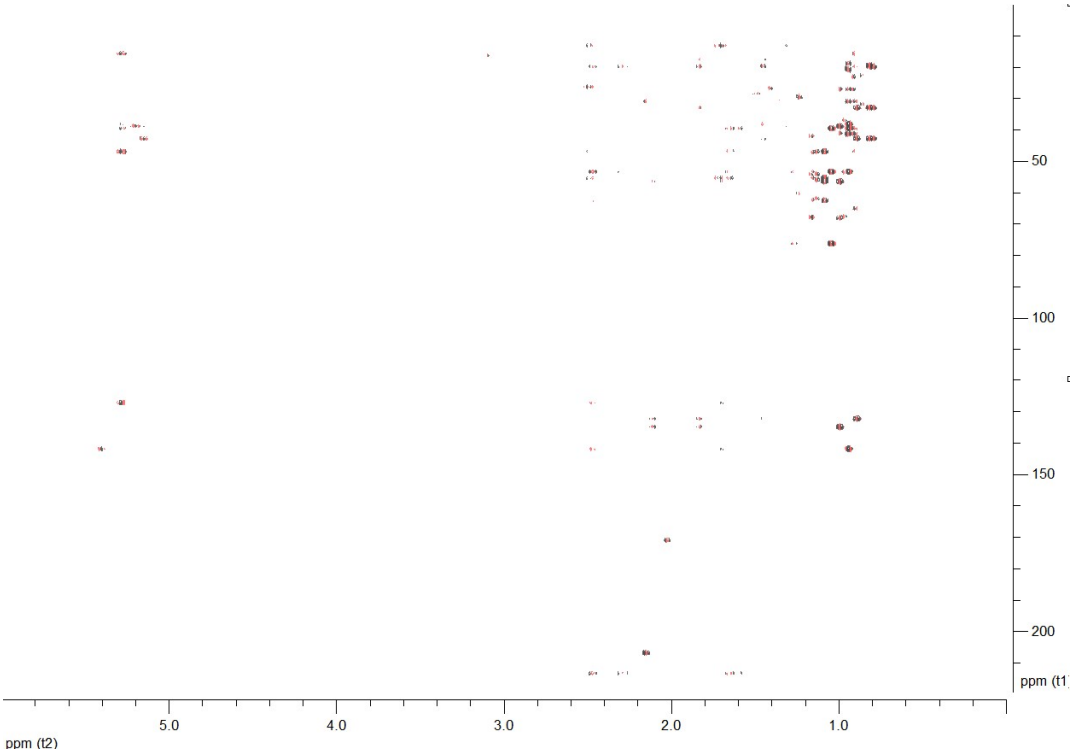

Figure 145. HMBC spectrum of metabolite **34**.

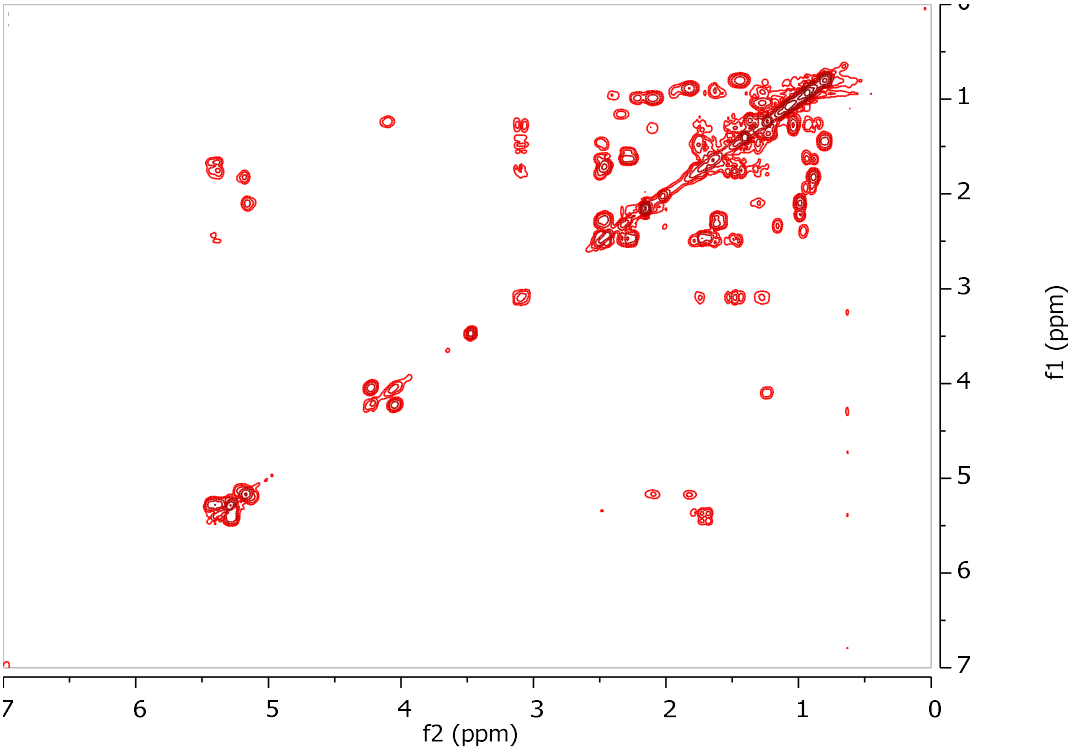

Figure 146. COSY spectrum of metabolite **34**.

The geometry of the two double bonds was determined as *E* in both cases on the basis of the measured coupling constants ($J_{9,11}$ = 15.3 Hz and $J_{22,23}$ = 15.2 Hz). The

enhancements of H-3/H-5, H-3/H_3-29, H-4/H_3-19, H-5/H-9, H-9/H-12α, H-9/H-14, H-11/H-12β, H-11/H_3-18, H-11/H_3-19, H-14/H-17, and H_3-18/H-20 observed in the NOESY spectrum of metabolite **34** (Figure 147) verified the *trans* fusion of the six-membered and the ten-membered rings, as well as the *trans* fusion of the latter with the five-membered ring and determined the relative configuration of the stereogenic centers. The *R* configuration at C-24 was proposed on the basis of the 0.3 ppm difference in the chemical shifts of C-26 and C-27 and the chemical shift of C-28 resonating at 17.6 ppm (Zovko Končić et al., 2016).

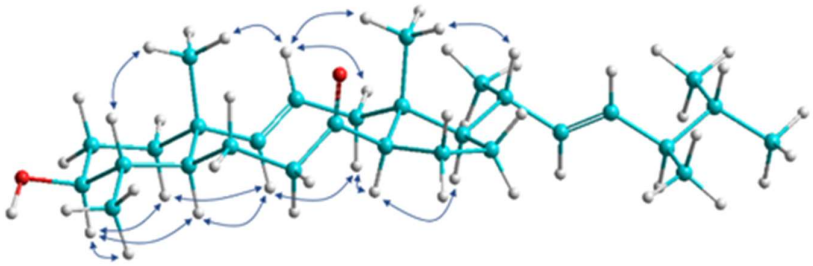

Figure 147. 3D structure and key NOESY cross-peaks for metabolite **34**.

Comparison of the spectroscopic and physical characteristics of metabolite **34** with those reported in the literature led to its identification as a new natural product, which was designated as (9*E*,22*E*,24*R*)-3*β*-hydroxy-4*α*,24-dimethyl-8,9-seco-5α-cholesta-9(11),22-dien-8-one. The NMR data of metabolite **34** are reported in Table 168.

Table 168. ^{1}H and ^{13}C NMR data of metabolite **34** in $CDCl_3$ (δ in ppm, J in Hz).

Position	δ_C	δ_H
1	38.5	1.33 (m), 1.22 (m)
2	30.7	1.76 (m), 1.48 (m)
3	76.6	3.09 td (10.1, 4.8)
4	39.8	1.27 (m)
5	53.5	0.91 (m)
6	20.0	1.66 (m), 1.60 (m)
7	47.1	2.29 (m), 1.75 (m)
8	213.1	-
9	142.0	5.28 (d, 15.3)
10	39.1	-
11	127.6	5.41 (ddd, 15.3, 11.1, 3.8)
12	46.8	2.47 (m), 1.70 (m)
13	55.2	-
14	62.7	2.49 (m)
15	26.6	1.64 (m), 1.48 (m)
16	28.4	1.70 (m), 1.47 (m)
17	56.7	1.31 (m)
18	13.5	1.08 (s)
19	15.8	0.94 (s)
20	39.1	2.10 (m)
21	21.7	0.99 (d, 6.8)
22	135.2	5.15 (dd, 15.2, 8.1)
23	132.6	5.20 (dd, 15.2, 7.3)
24	43.0	1.83 (m)
25	33.2	1.44 (m)
26	19.8	0.81 (d, 6.8)
27	20.1	0.80 (d, 6.8)
28	17.6	0.89 (d, 6.8)
29	16.4	1.03 (d, 6.1)

3.3.2 Metabolite 35

Metabolite **35** (SP30) was isolated after a series of chromatographic separations as a white amorphous solid (0.3 mg).

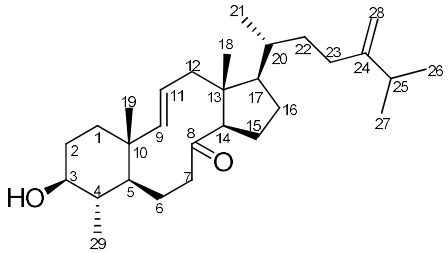

The high-resolution mass spectrum of the metabolite **35** (Figure 148) showed a pseudomolecular ion peak at *m/z* 429.3725 corresponding to $[M+H]^+$ (calcd. for $C_{29}H_{49}O_2$, 429.3727).

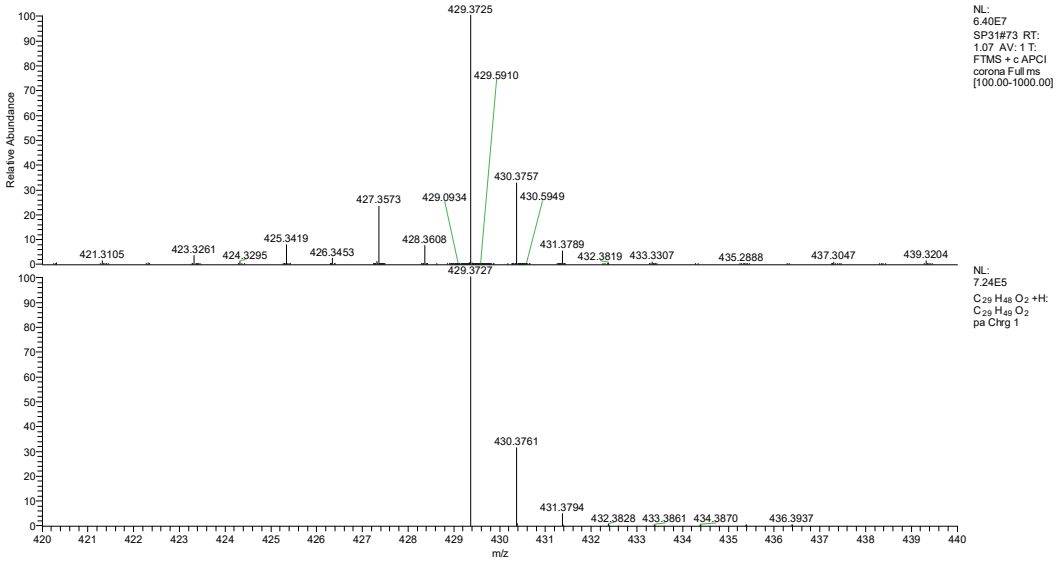

Figure 148. Mass spectrum (HR-APCIMS) of metabolite **35**.

In the ^{1}H NMR spectrum of metabolite **35** (Figure 149) obvious were:

- Two aliphatic methyls on non-protonated carbon at δ 0.94 and 1.09,
- Four aliphatic methyls on tertiary carbons at δ 0.93, 1.00, 1.01 and 1.04,
- One oxygenated methine at δ 3.10,
- Two broad singlets at δ 4.63 and 4.70 integrating for one proton each and attributed to the protons of an exomethylene group, and
- Two olefinic methines at δ 5.27 and 5.41.

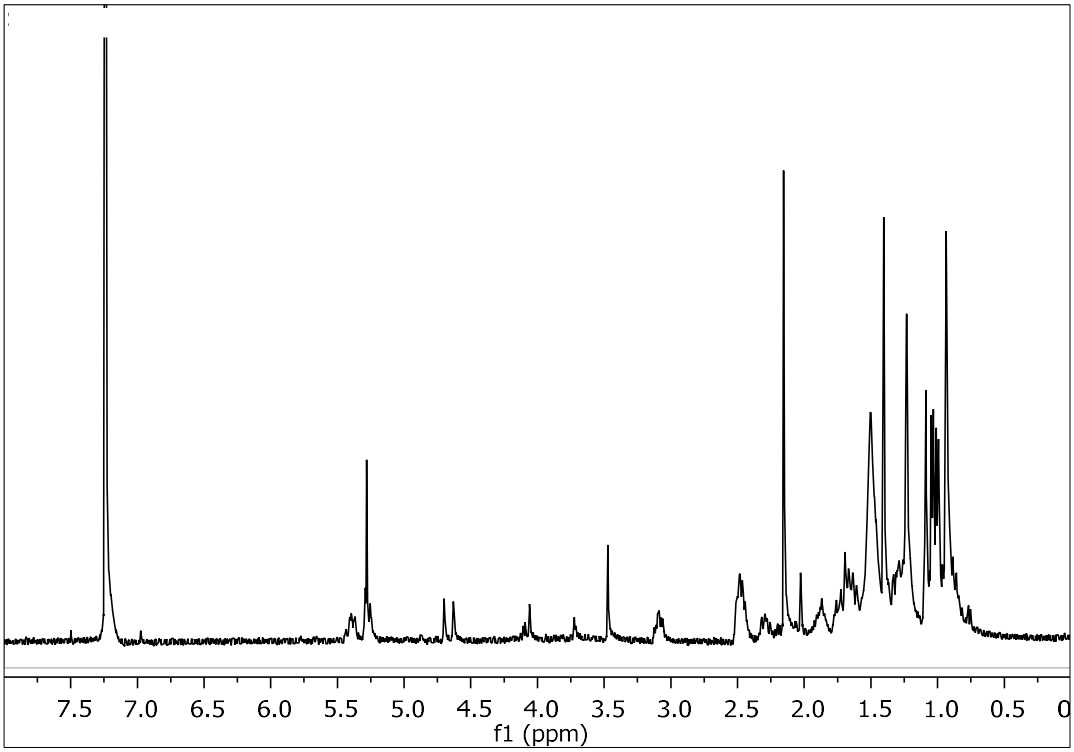

Figure 149. ^{1}H NMR spectrum of metabolite **35**.

Analysis of the NMR and MS data of **35** led to the molecular formula $C_{29}H_{48}O_2$. Taking into account the two carbon-carbon double bonds and the carbonyl moieties as three of the six degrees of unsaturation, the molecular structure of **35** was determined as tricyclic.

Metabolite **35** shared quite similar spectroscopic features with metabolite **34**. In particular, all signals attributed to the steroidal nucleus, with the most prominent being the signals of the two angular methyls H_3-18 and H_3-19 (δ_H 1.09 and 0.94, respectively), the methyl at C-4 (δ_H 1.04), the oxymethine H-3 (δ_H 3.10) and the two olefinic protons H-9 and H-11 (δ_H 5.27 and 5.41, respectively), were also evident in the ^{1}H NMR spectrum of **35**. The most significant difference observed was the replacement of the 1,2-disubstituted double bond in the side chain of metabolite **34** by a 1,1-disustituted double bond (δ_H 4.63 and 4.70) in the side chain of metabolite **35**. The correlations observed in the COSY spectrum of **35** (Figure 150) identified the relevant spin systems; however, metabolite **35** was proven unstable and degraded prior to the acquisition of heteronuclear NMR spectra. Nevertheless, the high structural similarity of metabolite **35** with metabolite **34** renders safe the proposed identification of metabolite **35** as (9*E*)-3*β*-hydroxy-4*α*,24-dimethyl-8,9-seco-5α-cholesta-9(11),24(28)-dien-8-one. Comparison of the spectroscopic and physical characteristics of metabolite **35** with those reported in the literature led to its identification as a new natural product. The NMR data of metabolite **35** are reported in Table 169.

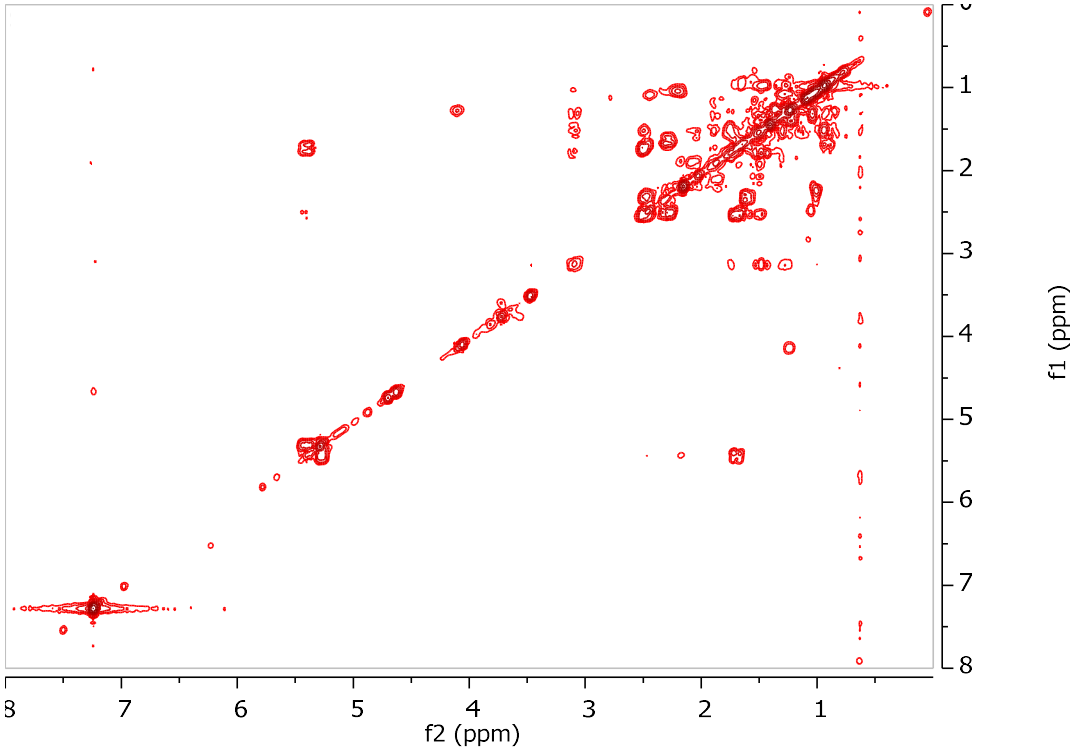

Figure 150. COSY spectrum of metabolite **35**.

Table 169. ^{1}H NMR data of metabolite **35** in $CDCl_3$ (δ in ppm, J in Hz)

Position	$\boldsymbol{\delta_H}$
1	1.36 (m), 1.24 (m)
2	1.76 (m), 1.49 (m)
3	3.10 (m)
4	1.28 (m)
5	0.92 (m)
6	1.66 (m), 1.62 (m)
7	2.48 (m), 2.24 (m)
9	5.27 (m)
11	5.41 (m)
12	2.50 (m), 1.72 (m)
14	2.50 (m)
15	1.64 (m), 1.50 (m)
16	1.73 (m), 1.49 (m)
17	1.28 (m)
18	1.09 (s)
19	0.94 (s)
20	2.11 (m)
21	0.93 (d, 6.1)
22	1.53 (m), 1.14 (m)
23	2.08 (m), 1.88 (m)
25	2.21 (m)
26	1.00 (d, 6.8)
27	1.01 (d, 6.9)
28	4.70 (brs), 4.63 (brs)
29	1.04 (d, 6.1)

3.3.3 Metabolite 36

Metabolite **36** (SP16) was isolated after a series of chromatographic separations as a colorless oil (11.3 mg).

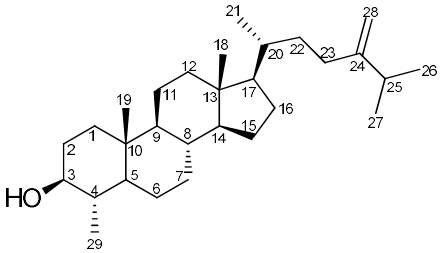

The mass spectrum of metabolite **36** (Figure 151) exhibited a molecular ion peak $[M]^+$ at *m/z* 414.

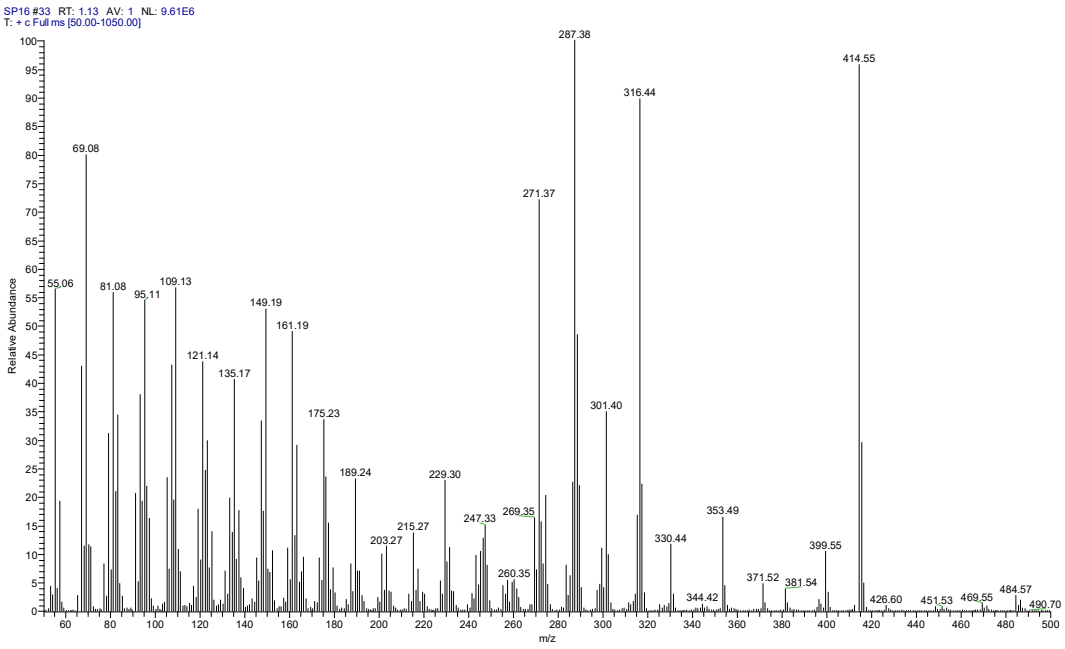

Figure 151. Mass spectrum (EIMS) of metabolite **36**.

In the ^{1}H NMR spectrum of metabolite **36** (Figure 152) obvious were:

- Two aliphatic methyls on non-protonated carbons at δ 0.63 and 0.80,
- Four aliphatic methyls on tertiary carbons at δ 0.91, 0.93, 1.00 and 1.00,
- One oxygenated methine at δ 3.08, and,
- Two broad singlets at δ 4.63 and 4.69 integrating for one proton each and attributed to the protons of an exomethylene group.

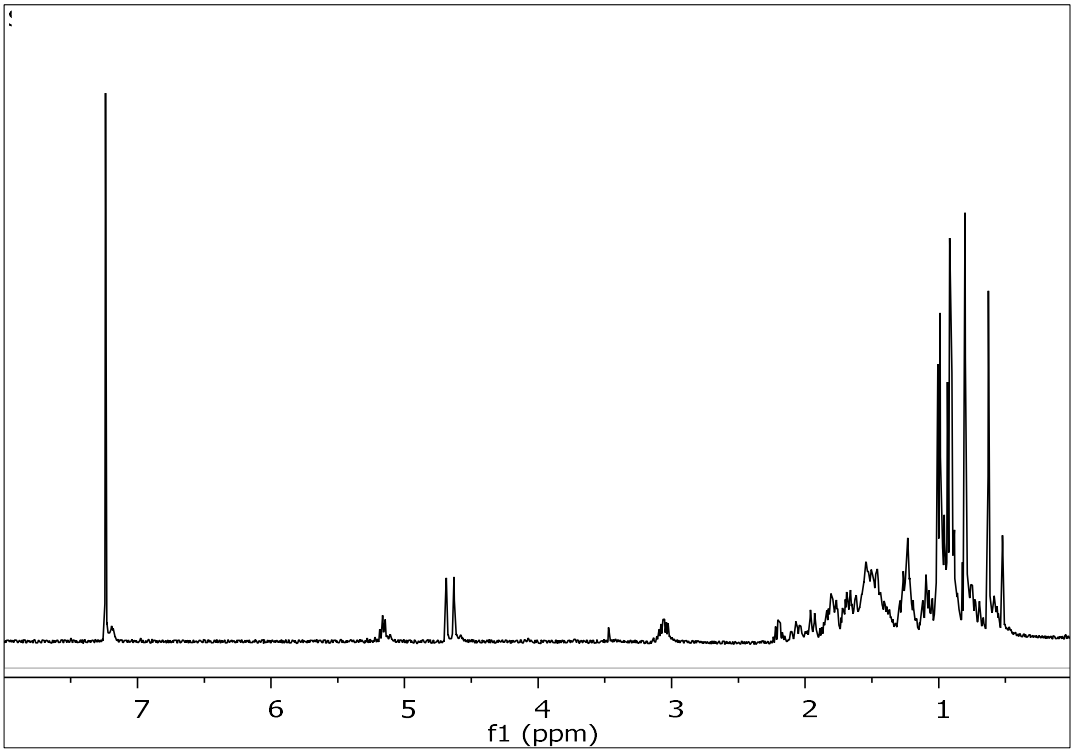

Figure 152. ^{1}H NMR spectrum of metabolite **36**.

Analysis of the NMR and MS data of **36** led to the molecular formula $C_{29}H_{50}O$. Taking into account the one carbon-carbon double bond as one of the five degrees of unsaturation, the molecular structure of **36** was determined as tetracyclic.

Comparison of the spectroscopic and physical characteristics of metabolite **36** with those reported in the literature led to its identification as 4*α*,24-dimethyl-5*α*-cholest-24(28)-en-3*β*-ol, previously isolated from the gorgonian *Briareum asbestinum* (Kokke et al., 1982). The ^{1}H NMR data of metabolite **36** are reported in Table 170.

Table 170. ^{1}H NMR data of metabolite **36** in $CDCl_3$ (δ in ppm, J in Hz)

Position	$\delta_{H,exp}$	$\delta_{H,lit}$
3	3.08 (m)	3.1 (m)
18	0.63 (s)	0.65 (s)
19	0.80 (s)	0.82 (s)
21	0.91 (d, 6.5)	0.93 (d, 6.2)
26	1.00 (d, 6.8)	1.02 (d, 6.9)
27	1.00 (d, 6.8)	1.02 (d, 7.0)
28	4.69 (brs), 4.63 (brs)	4.71 (s), 4.65 (s)
29	0.93 (d, 6.5)	0.95 (d, 6.2)

3.3.4 Metabolite 37

Metabolite **37** (SP15) was isolated after a series of chromatographic separations as a colorless oil (8.8 mg).

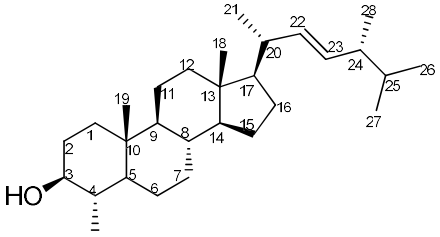

The high-resolution mass spectrum of the metabolite **37** (Figure 153) showed a molecular ion peak $[M]^+$ at *m/z* 414.

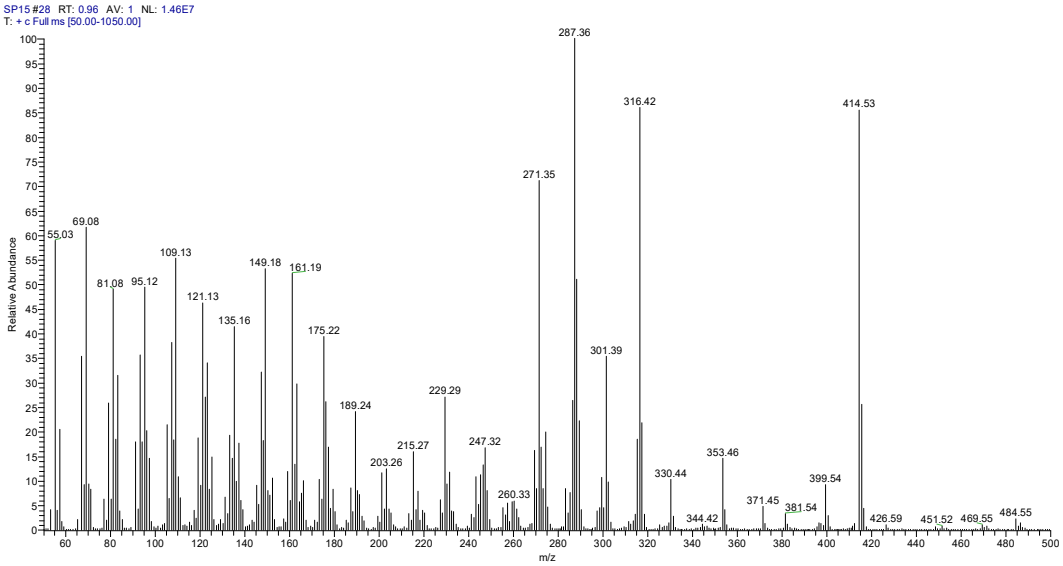

Figure 153. Mass spectrum (HR-ESIMS) of metabolite **37**.

In the ^{1}H NMR spectrum of metabolite **37** (Figure 154) obvious were:

- Two aliphatic methyls on non-protonated carbons at δ 0.64 and 0.80,
- Five aliphatic methyls on tertiary carbons at δ 0.79, 0.81, 0.88, 0.92 and 0.97,
- One oxygenated methine at δ 3.06, and,
- Two olefinic methines at δ 5.12 and 5.17.

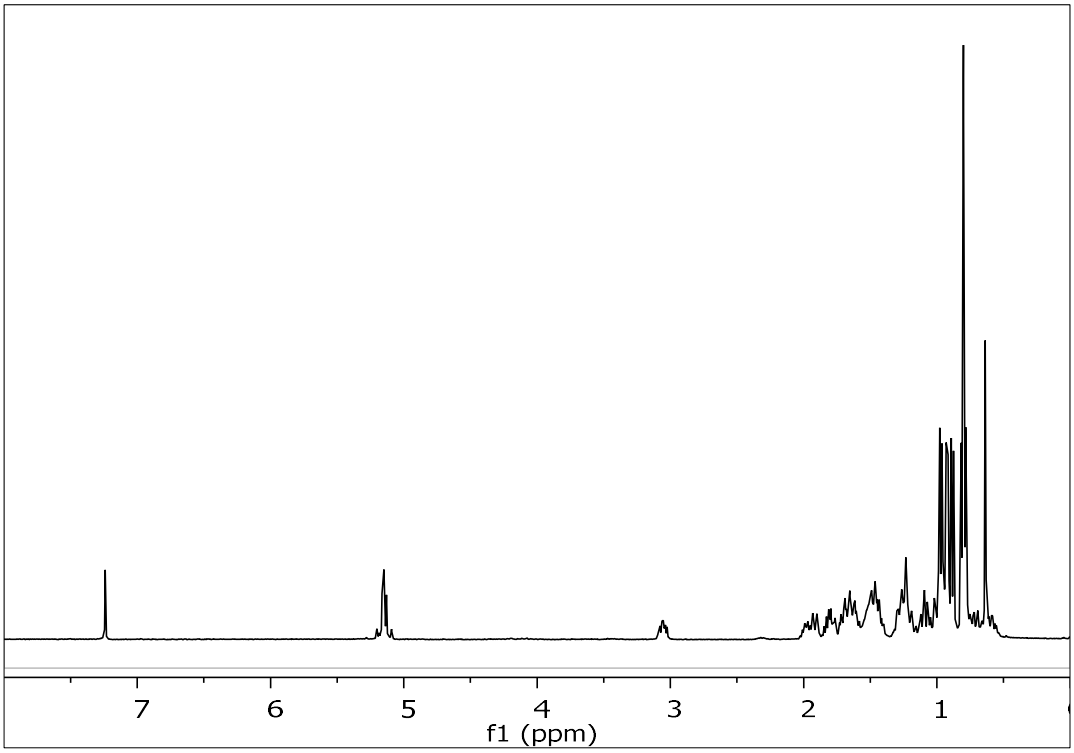

Figure 154. ^{1}H NMR spectrum of metabolite **37**.

Analysis of the NMR and MS data of **37** led to the molecular formula $C_{29}H_{50}O$. Taking into account the one carbon-carbon double bond as one of the five degrees of unsaturation, the molecular structure of **37** was determined as tetracyclic.

Comparison of the spectroscopic and physical characteristics of metabolite **37** with those reported in the literature led to its identification as (22*E*,24*R*)-4*α*,24-dimethyl-5*α*-cholest-22-en-3*β*-ol, previously isolated from the soft coral *Sarcophyton glaucum* (Kobayashi et al., 1982). The ^{1}H NMR data of metabolite **37** are reported in Table 171.

Table 171. ^{1}H and ^{13}C NMR data of metabolite **37** in $CDCl_3$ (δ in ppm, J in Hz).

Position	$\delta_{H,exp}$	$\delta_{H,lit}$
3	3.06 (td, 10.5, 4.9)	3.10 (m)
18	0.64 (s)	0.66 (s)
19	0.80 (s)	0.82 (s)
21	0.97 (d, 6.6)	0.99 (d, 6.6)
22	5.12 (dd, 15.1, 7.6)	5.15 (m)
23	5.17 (dd, 15.1, 7.0)	5.20 (m)
26	0.81 (d, 6.8)	0.83 (d, 6.6)
27	0.79 (d, 6.8)	0.82 (d, 6.4)
28	0.88 (d, 6.8)	0.91 (d, 6.8)
29	0.92 (d, 6.3)	0.94 (d, 6.8)

3.3.5 Metabolite 38

Metabolite **38** (SP13) was isolated after a series of chromatographic separations as a colorless oil (12.2 mg).

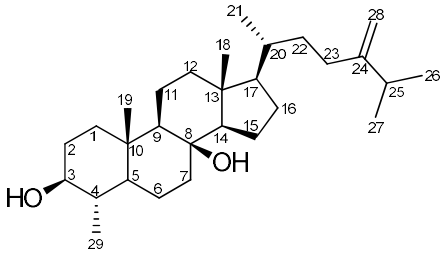

The mass spectrum of metabolite **38** (Figure 155) exhibited a fragment ion peak at *m/z* 412 corresponding to $[M\text{-}H_2O]^+$.

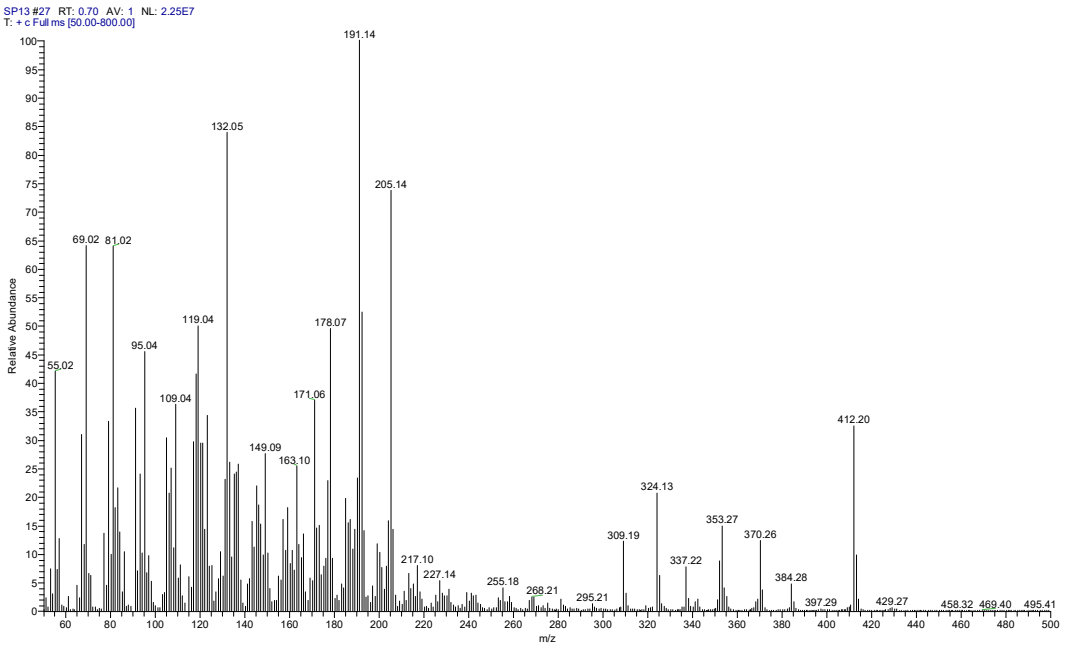

Figure 155. Mass spectrum (EIMS) of metabolite **38**.

In the ^{1}H NMR spectrum of metabolite **38** (Figure 156) obvious were:

- Two aliphatic methyls on non-protonated carbons at δ 0.90 and 0.96,
- Four aliphatic methyls on tertiary carbons at δ 0.87, 0.94, 0.99 and 1.00,
- One oxygenated methine at δ 3.01, and,
- Two broad singlets at δ 4.63 and 4.69 integrating for one proton each and attributed to the protons of an exomethylene group.

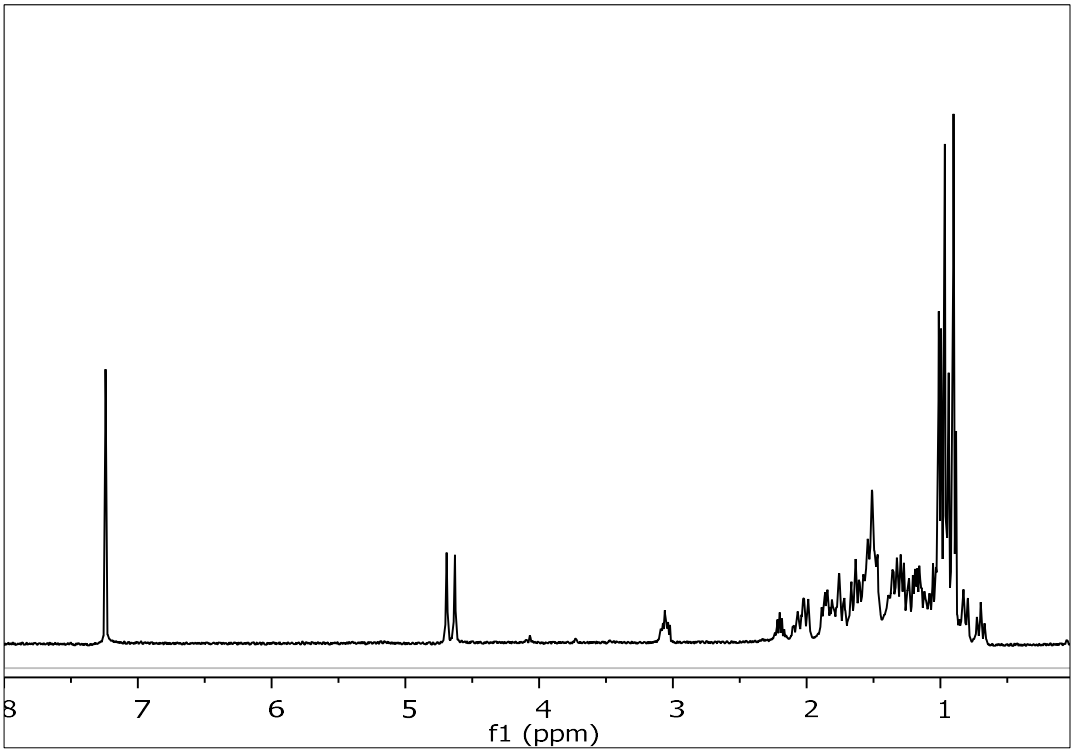

Figure 156. ^{1}H NMR spectrum of metabolite **38**.

Analysis of the NMR and MS data of **38** led to the molecular formula $C_{29}H_{50}O_2$. Taking into account the one carbon-carbon double bond as one of the five degrees of unsaturation, the molecular structure of **38** was determined as tetracyclic.

Comparison of the spectroscopic and physical characteristics of metabolite **38** with those reported in the literature led to its identification as 4*α*,24-dimethyl-5*α*-cholest-24(28)-en-3*β*,8*β*-diol, previously isolated from the soft coral *Nephthea chabroli* (Mehta et al., 1999). The ^{1}H NMR data of metabolite **38** are reported in Table 172.

Table 172. ^{1}H NMR data of metabolite **38** in $CDCl_3$ (δ in ppm, J in Hz).

Position	$\delta_{H,exp}$	$\delta_{H,lit}$
3	3.01 (m)	3.05 (dt, 9.0,4.5)
18	0.90 (s)	0.95 (s)
19	0.96 (s)	1.00 (s)
21	0.94 (d, 6.3)	0.90 (d, 6.5)
26	0.99 (d, 6.8)	1.03 (d, 7.5)
27	1.00 (d, 6.8)	1.03 (d, 7.5)
28	4.69 (brs), 4.63 (brs)	4.70 (brs), 4.62 (brs)
29	0.87 (d, 6.3)	0.89 (d, 6.5)

3.3.6 Metabolite 39

Metabolite **39** (SP14) was isolated after a series of chromatographic separations as a white amorphous solid (9.3 mg).

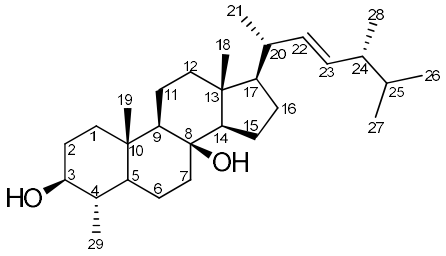

The high-resolution mass spectrum of the metabolite **39** (Figure 157) showed a pseudomolecular ion peak at *m/z* 413.3773 corresponding to $[M\text{-}H_2O+H]^+$ (calcd. for $C_{29}H_{49}O$, 413.3778).

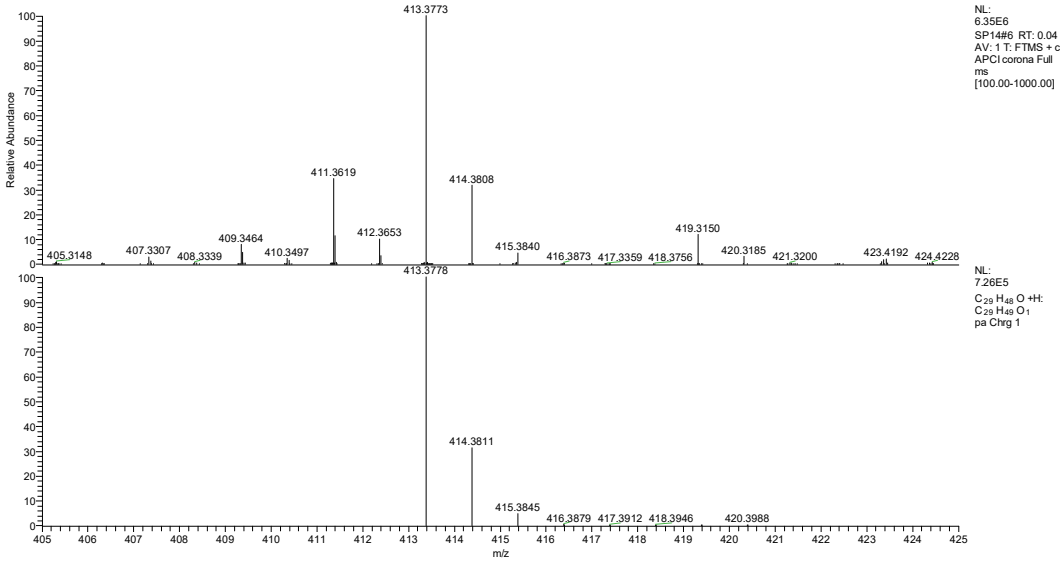

Figure 157. Mass spectrum (HR-APCIMS) of metabolite **39**.

In the ^{1}H NMR spectrum of metabolite **39** (Figure 158) obvious were:

- Two aliphatic methyls on non-protonated carbons at δ 0.92 and 0.97,
- Five aliphatic methyls on tertiary carbons at δ 0.79, 0.81, 0.88, 0.94 and 0.95,
- One oxygenated methine at δ 3.04, and
- Two olefinic methines at δ 5.09 and 5.16.

Analysis of the NMR and MS data of **39** led to the molecular formula $C_{29}H_{50}O_2$. Taking into account the one carbon-carbon double bond as one of the five degrees of unsaturation, the molecular structure of **39** was determined as tetracyclic.

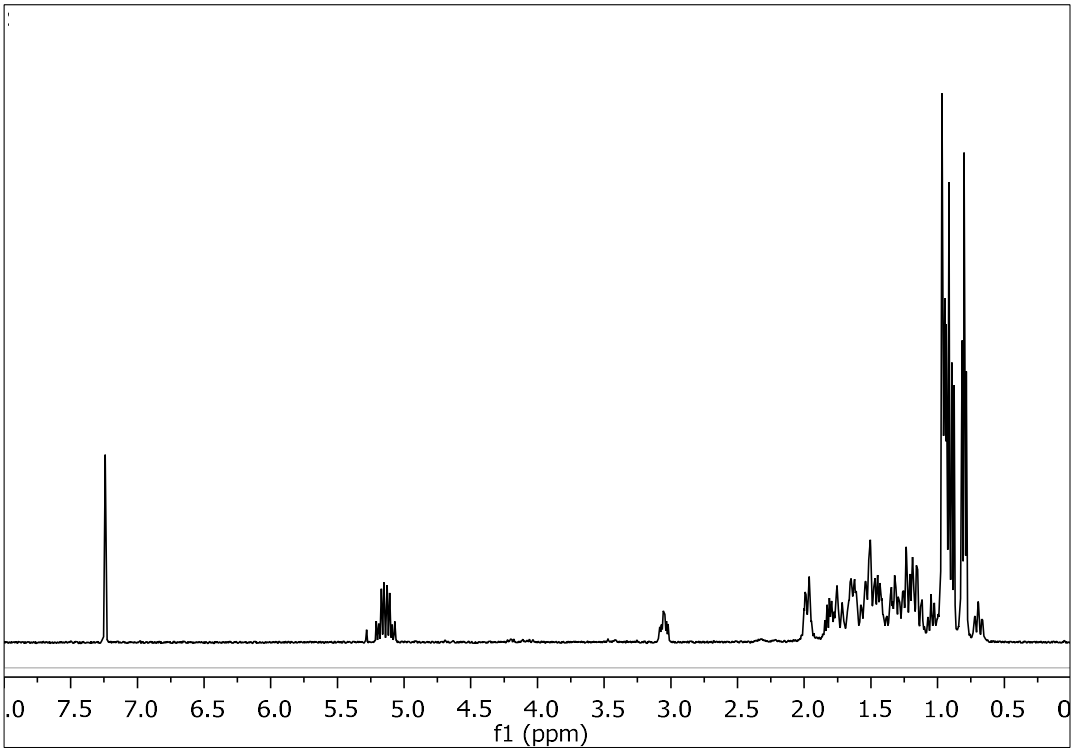

Figure 158. ^{1}H NMR spectrum of metabolite **39**.

The planar structure of metabolite **39** was determined on the basis of the homonuclear and heteronuclear correlations (Figure 159) observed in the HSQC-DEPT (Figure 160), HMBC (Figure 161) and COSY (Figure 162) spectra. In particular, the presence of the two angular methyls at δ_H 0.92 and 0.97, the doublet methyl at δ_H 0.95, the oxygenated methine at δ_H 3.04 and the quaternary oxygenated carbon at δ_C 73.6, in conjunction with the correlations observed in the HMBC and COSY spectra, verified the 3,8-dihydroxy-4-methyl steroidal nucleus. The side chain of compound **6** included four doublet methyls ($\delta_{H/C}$ 0.79/20.2, 0.81/19.9, 0.88/18.0, and 0.95/16.0) and two olefinic methines ($\delta_{H/C}$ 5.09/135.7 and 5.16/131.8) that was assigned on the basis of the COSY and HMBC correlations.

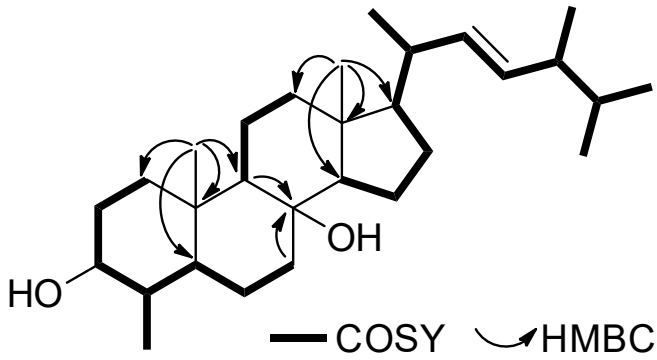

Figure 159. COSY and important HMBC correlations observed for metabolite **39**.

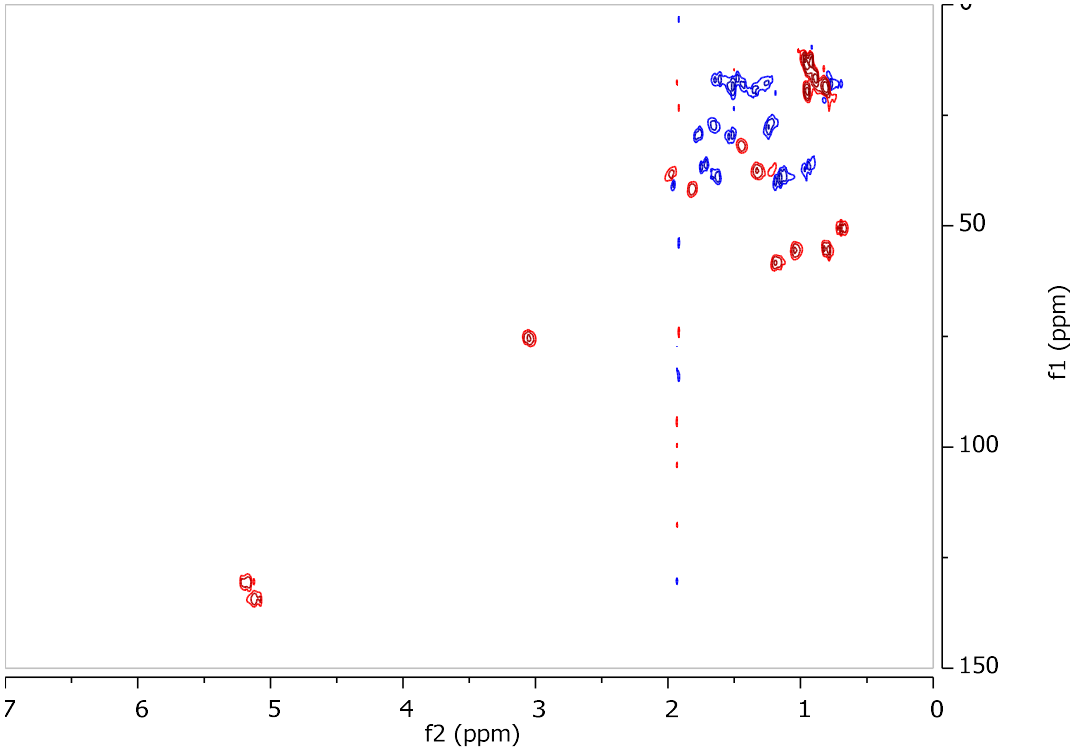

Figure 160. HSQC-DEPT spectrum of metabolite **39**.

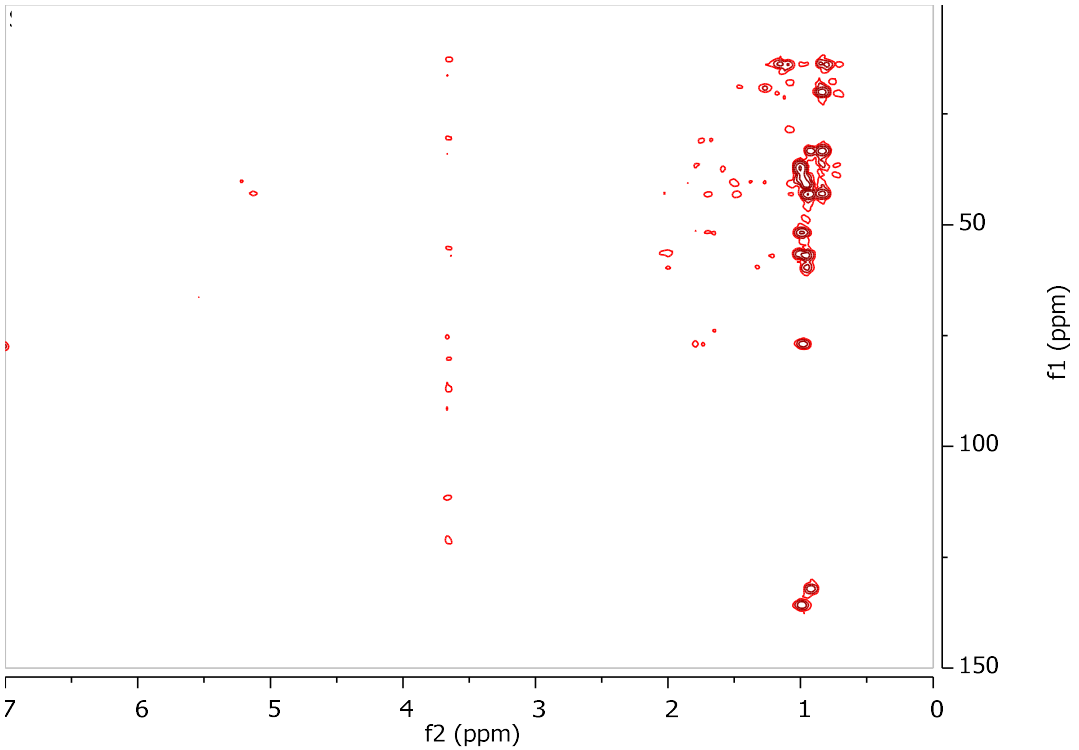

Figure 161. HMBC spectrum of metabolite **39**.

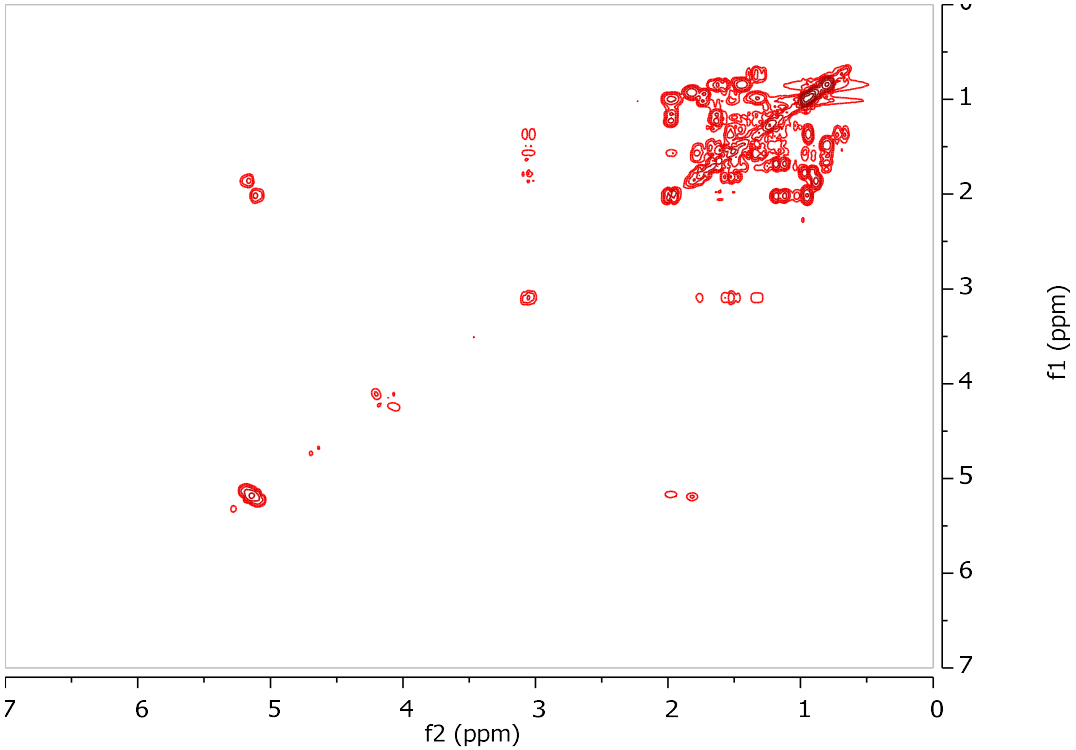

Figure 162. COSY spectrum of metabolite **39**.

The *E* geometry of the Δ^{22} double bond was supported by the large coupling constant of H-22/H-23 (J = 15.3 Hz). The enhancements of H-3/H-5, H-3/H_3-29, H-4/H_3-19, H-5/H-9, H-5/H_3-29, H-9/H-12α, H-9/H-14, H-12β/H_3-18, and H_3-18/H-20 observed in the NOESY spectrum (Figure 163) verified the *trans* fusion of rings A/B, B/C, and C/D and suggested the axial orientation of the hydroxy group at C-8. The configuration at C-24 was proposed as *R* due to the fact that the difference in the chemical shifts of C-26 and C-27 was 0.3 ppm and that C-28 resonated at 18.0 ppm (Zovko Končić et al., 2016).

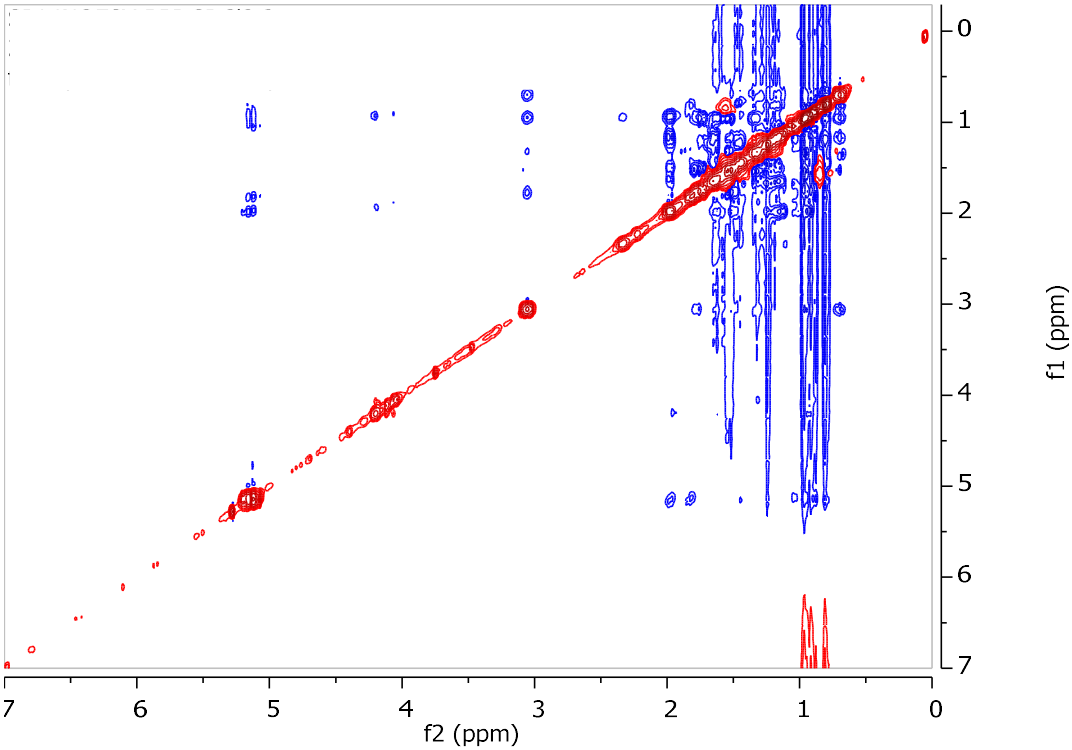

Figure 163. NOESY spectrum of metabolite **39**.

Comparison of the spectroscopic and physical characteristics of metabolite **39** with those reported in the literature led to its identification as a new natural product, which was designated as (22*E*,24*R*)-4*α*,24-dimethyl-5*α*-cholest-22-en-3*β*,8*β*-diol. The NMR data of metabolite **39** are reported in Table 173.

Table 173. ^{1}H and ^{13}C NMR data of metabolite **39** in $CDCl_3$ (δ in ppm, J in Hz).

Position	δ_C	δ_H
1	37.7	1.72 (m), 0.93 (m)
2	30.9	1.77 (m), 1.52 (m)
3	76.8	3.04 (td, 10.2, 4.9)
4	39.0	1.31 (m)
5	51.9	0.68 (td, 12.4, 2.9)
6	20.5	1.50 (m), 1.33 (m)
7	40.1	1.63 (m), 1.13 (m)
8	73.6	-
9	56.6	0.80 (m)
10	36.9	-
11	18.3	1.62 (m), 1.49 (m)
12	41.6	1.95 (m), 1.16 (m)
13	43.0	-
14	59.7	1.18 (m)
15	19.0	1.45 (m), 1.23 (m)
16	28.3	1.64 (m), 1.23 (m)
17	57.1	1.03 (m)
18	14.0	0.92 (s)
19	13.8	0.97 (s)
20	39.6	1.96 (m)
21	21.3	0.94 (d, 6.4)
22	135.7	5.09 (dd, 15.2, 8.2)
23	131.8	5.16 (dd, 15.2, 7.4)
24	43.2	1.80 (m)
25	33.8	1.42 (m)
26	19.9	0.81 (d, 6.8)
27	20.2	0.79 (d, 6.8)
28	18.0	0.88 (d, 6.8)
29	16.0	0.95 (d, 6.8)

3.3.7 Metabolite 40

Metabolite **40** (SP21) was isolated after a series of chromatographic separations as a colorless oil (7.6 mg).

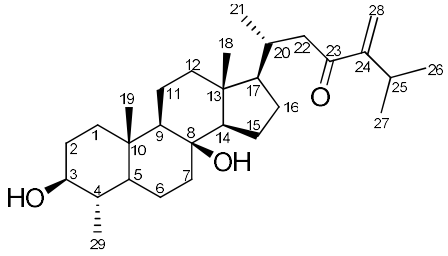

The mass spectrum of metabolite **40** (Figure 164) exhibited a molecular ion peak $[M]^+$ at *m/z* 444, as well as a fragment ion peak at *m/z* 426 corresponding to $[M\text{-}H_2O]^+$.

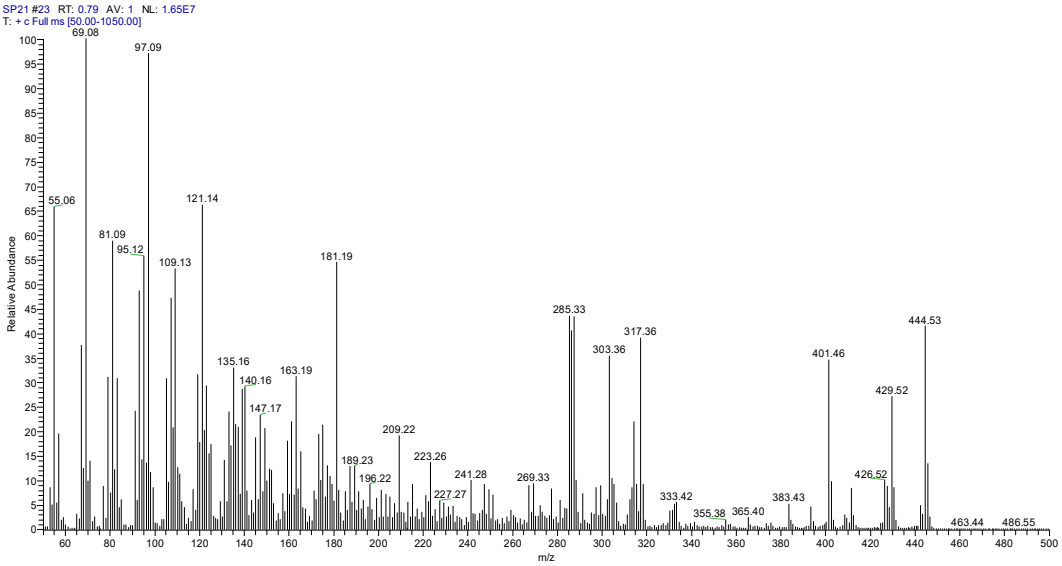

Figure 164. Mass spectrum (EIMS) of metabolite **40**.

In the ^{1}H NMR spectrum of metabolite **40** (Figure 165) obvious were:

- Two aliphatic methyls on non-protonated carbons at δ 0.94 and 0.96,
- Four aliphatic methyls on tertiary carbons at δ 0.85, 0.94, 0.98 and 1.00,
- One oxygenated methine at δ 3.05, and,
- Two broad singlets at δ 5.63 and 5.88 integrating for one proton each and attributed to the protons of an exomethylene group.

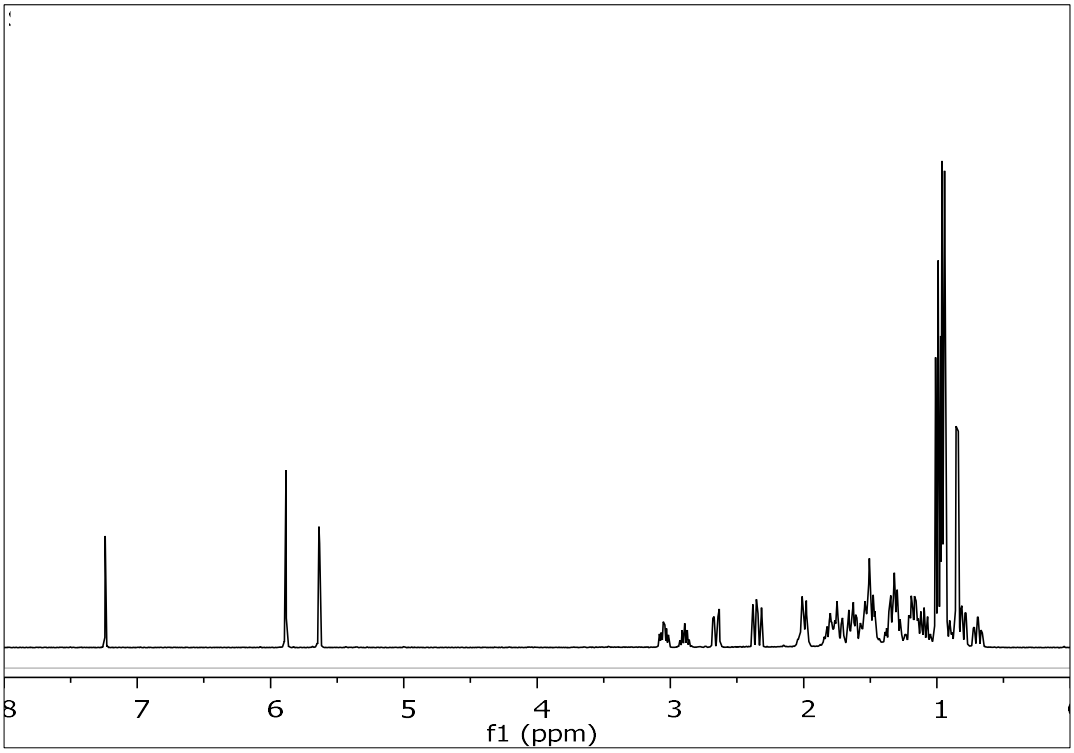

Figure 165. ^{1}H NMR spectrum of metabolite **40**.

Analysis of the NMR and MS data of **40** led to the molecular formula $C_{29}H_{48}O_3$. Taking into account the one carbon-carbon double bond and the carbonyl moiety as two of the six degrees of unsaturation, the molecular structure of **40** was determined as tetracyclic.

Comparison of the spectroscopic and physical characteristics of metabolite **40** with those reported in the literature led to its identification as 23-oxo-4*α*,24-dimethyl-5*α*-cholest-24(28)-en-3*β*,8*β*-diol, previously isolated from the soft coral *Litophyton viridis* (Bortolotto et al., 1977). The ^{1}H NMR data of metabolite **40** are reported in Table 174.

Table 174. ^{1}H and ^{13}C NMR data of metabolite **40** in $CDCl_3$ (δ in ppm, J in Hz).

Position	$\delta_{C,exp}$	$\delta_{H,exp}$
1	38.1	1.73 (m), 0.94 (m)
2	31.3	1.78 (m), 1.54 (m)
3	76.9	3.05 (m)
4	39.7	1.33 (m)
5	57.2	0.81 (m)
6	19.0	1.62 (m), 1.59 (m)
7	40.3	1.64 (m), 1.18 (m)
8	73.6	-
9	57.8	1.08 (m)
10	n.d.	-
11	18.7	1.51 (m), 1.31 (m)
12	41.6	2.0 (m), 1.98 (m)
13	n.d.	-
14	59.4	0.68 (m)
15	20.0	1.51 (m), 1.37 (m)
16	28.4	1.82 (m), 1.28 (m)
17	59.4	1.15 (dd, 4.9, 3.0)
18	13.8	0.94 (s)
19	14.8	0.96 (s)
20	33.5	2.00 (m)
21	20.0	0.85 (d, 6.5)
22	46.2	2.66 (dd, 15.5, 3.2), 2.34 (dd, 15.5, 10.0)
23	203.0	-
24	155.20	-
25	28.7	2.91 (m)
26	22.9	1.00 (d, 7.1)
27	22.9	0.98 (d, 7.1)
28	121.2	5.88 (brs), 5.63 (brs)
29	16.7	0.94 (d, 6.3)

3.3.8 Metabolite 41

Metabolite **41 (**SP20) was isolated after a series of chromatographic separations as a white amorphous solid (0.5 mg).

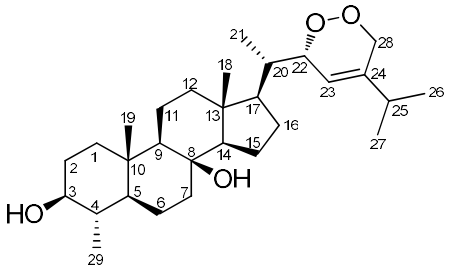

The high-resolution mass spectrum of the metabolite **41** (Figure 166) showed a pseudomolecular ion peak at *m/z* 459.3475 corresponding to $[M-H]^-$ (calcd. for $C_{29}H_{47}O_4$, 459.3480).

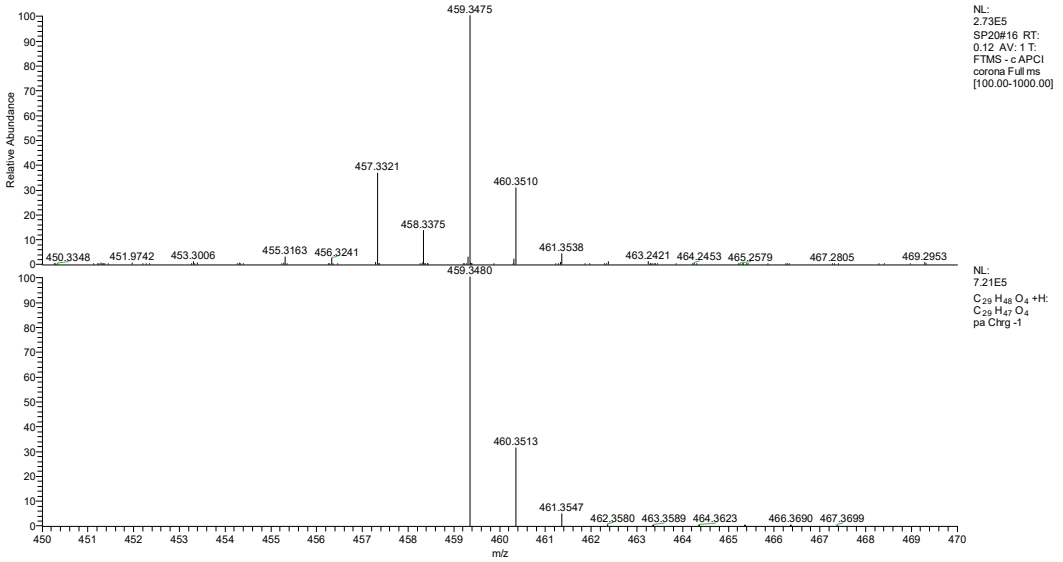

Figure 166. Mass spectrum (HR-APCIMS) of metabolite **41**.

In the ^{1}H NMR spectrum of metabolite **41** (Figure 167) obvious were:

- Two aliphatic methyls on non-protonated carbons at δ 0.89 and 0.96,
- Four aliphatic methyls on tertiary carbons at δ 0.83, 0.95, 1.05 and 1.05,
- Two oxygenated methines at δ 3.06 and 4.72,
- Two doublets at δ 4.20 and 4.62 integrating for one proton each and attributed to the protons of an oxygenated methylene, and,
- One olefinic methine at δ 5.36.

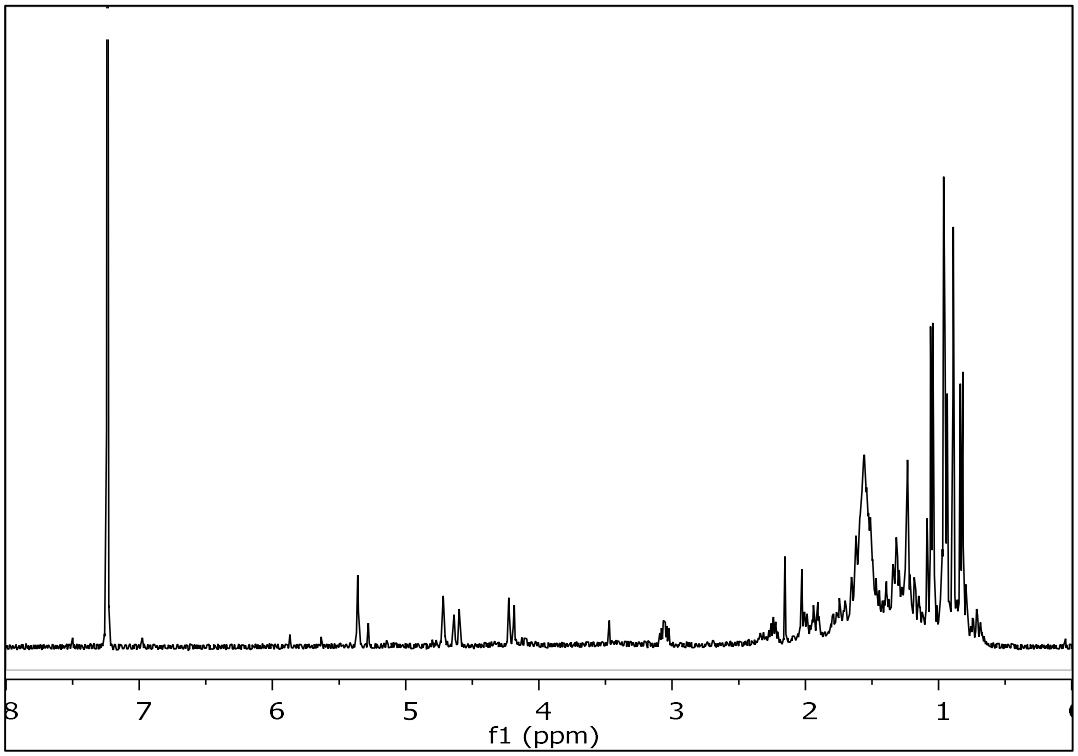

Figure 167. ^{1}H NMR spectrum of metabolite **41**.

Analysis of the NMR and MS data of **41** led to the molecular formula $C_{29}H_{48}O_4$. Taking into account the one carbon-carbon double bond as one of the six degrees of unsaturation, the molecular structure of **41** was determined as pentacyclic.

The high degree of similarity of the spectroscopic data of metabolite **41** with those of **38**–**40** indicated the same 3,8-dihydroxy-4-methyl steroidal nucleus. Taking into account that the steroidal nucleus of **41** accounts for four of the six degrees of unsaturation and the presence of one double bond on the side chain, the latter should also contain an additional ring. The ^{1}H and ^{13}C NMR signals corresponding to the side chain of compound **41** included three doublet methyls ($\delta_{H/C}$ 0.95/14.9, 1.05/21.0, and 1.05/21.0), one oxygenated methine ($\delta_{H/C}$ 4.72/79.9), one oxygenated methylene ($\delta_{H/C}$ 4.20, 4.62/70.6), one olefinic methine ($\delta_{H/C}$ 5.36/119.4), and one non-protonated olefinic carbon (δ_C 142.0). The COSY cross-peaks of H-20/H_3-21, H-20/H-22, H-22/H-23, H-25/H_3-26, and H-25/H_3-27, in combination with the HMBC correlations of H_3-21 with C-17, C-20, and C-22, of H-23, H-25, H_3-26, and H_3-27 with C-24 and of H_2-28 with C-23, C-24, and C-25 verified the side chain. The planar structure of metabolite **41** was determined on the basis of the homonuclear and heteronuclear correlations (Figure 168) observed in the HSQC-DEPT (Figure 169), HMBC (Figure 170) and COSY (Figure 171) spectra.

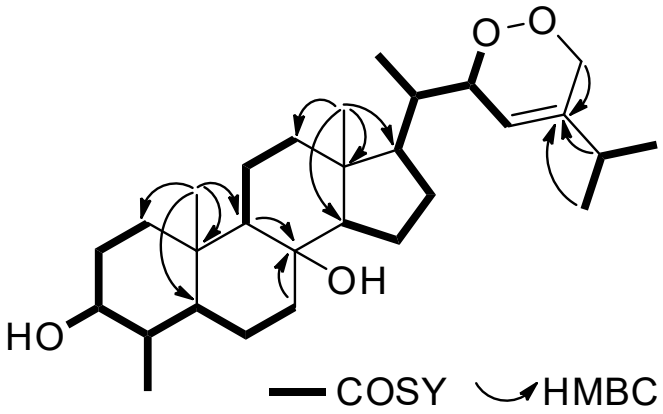

Figure 168. COSY and important HMBC correlations observed for metabolite **41**.

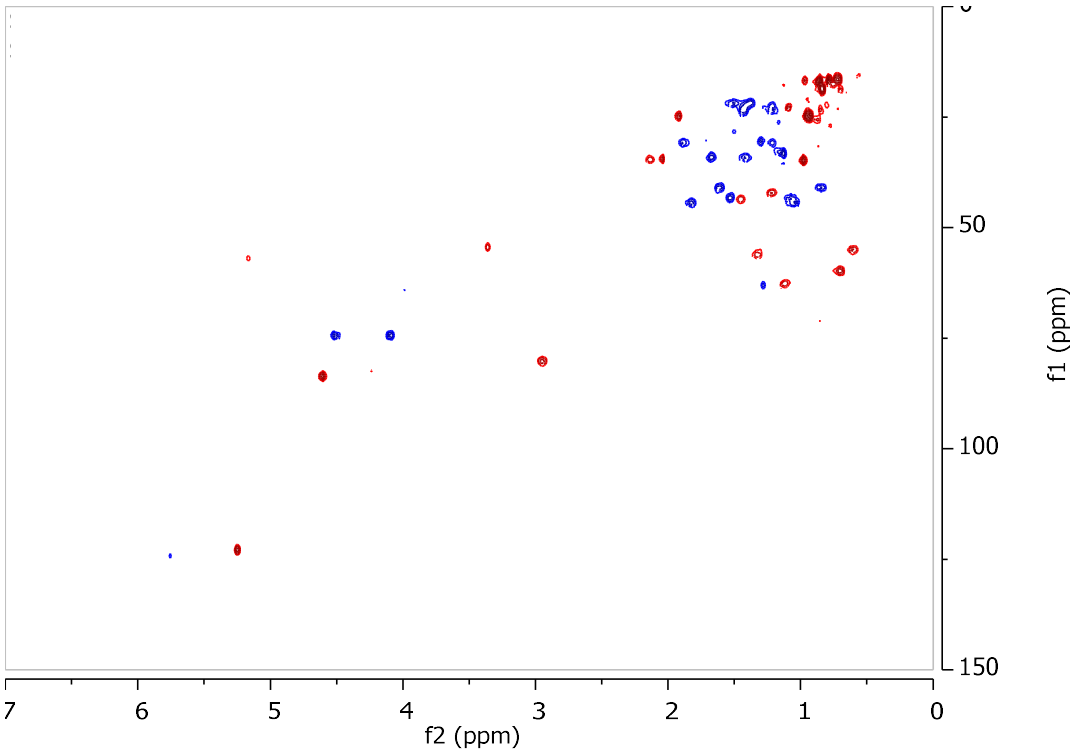

Figure 169. HSQC-DEPT spectrum of metabolite **41**.

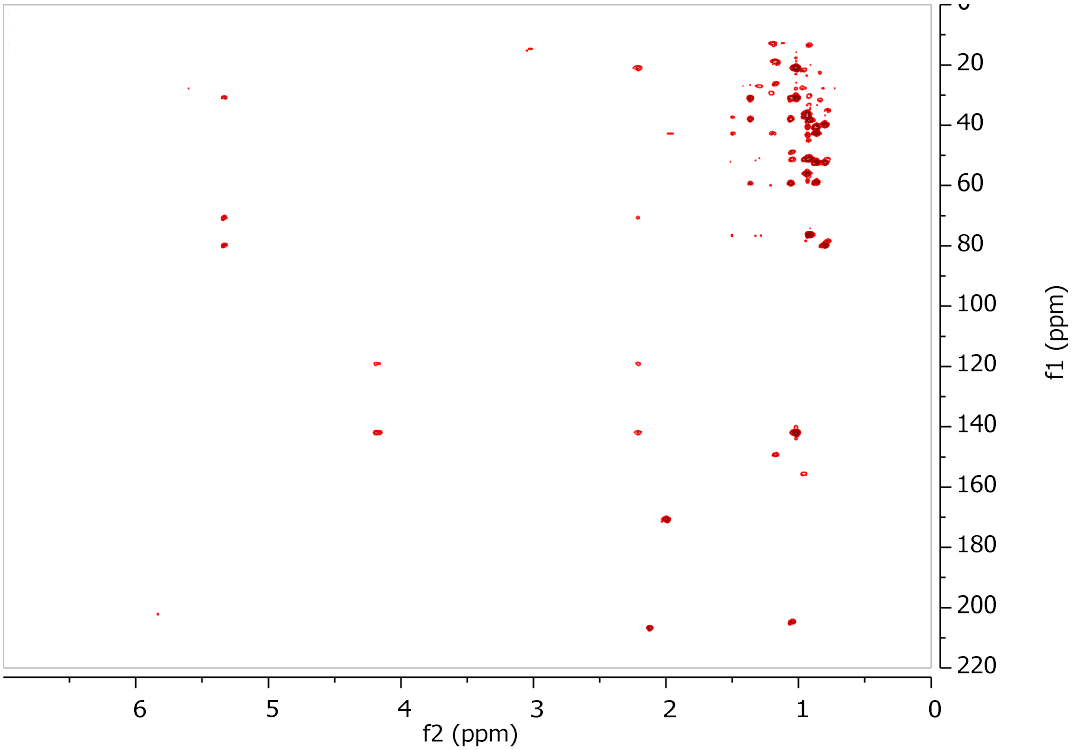

Figure 170. HMBC spectrum of metabolite **41**.

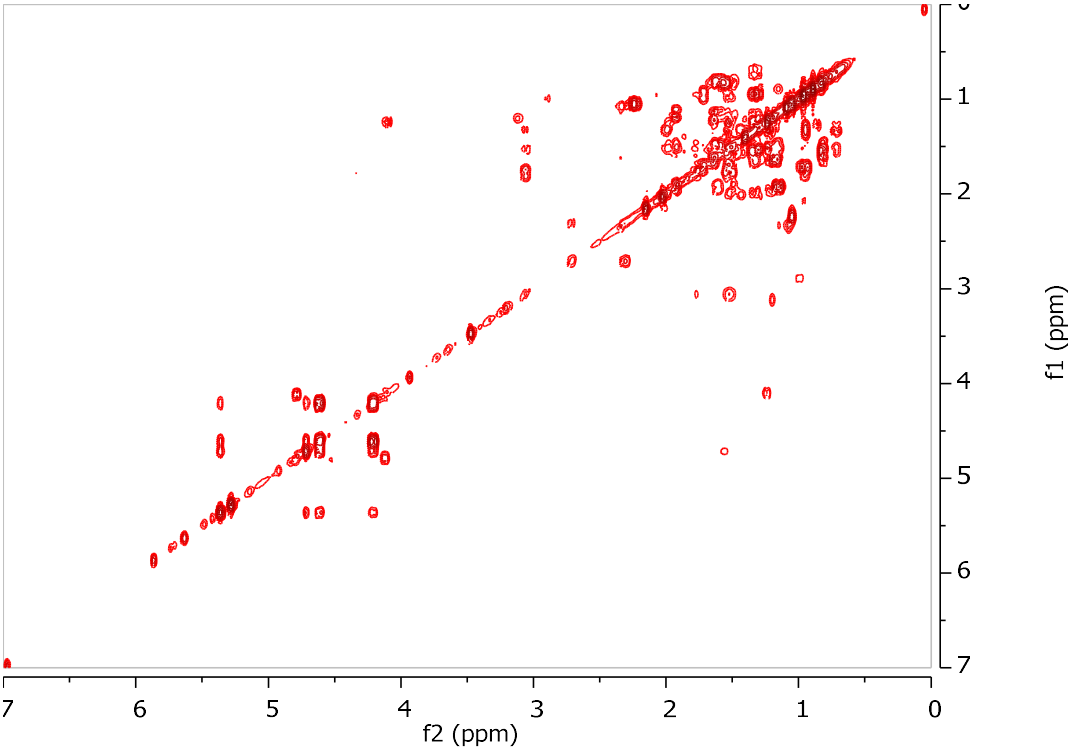

Figure 171. COSY spectrum of metabolite **41**.

The relative configuration of the asymmetric centers of metabolite **41** was determined on the basis of the correlations observed in the NOESY spectrum (Figure

172). In accordance with the literature, H-22 was assigned to be on the opposite side of H_3-21, as also suggested by the chemical shift of C-23 which resonated at 119.4 ppm. Instead, when H-22 and H_3-21 are co-planar, C-23 is shielded, resonating at 115-116 ppm (Yu et al., 2006).

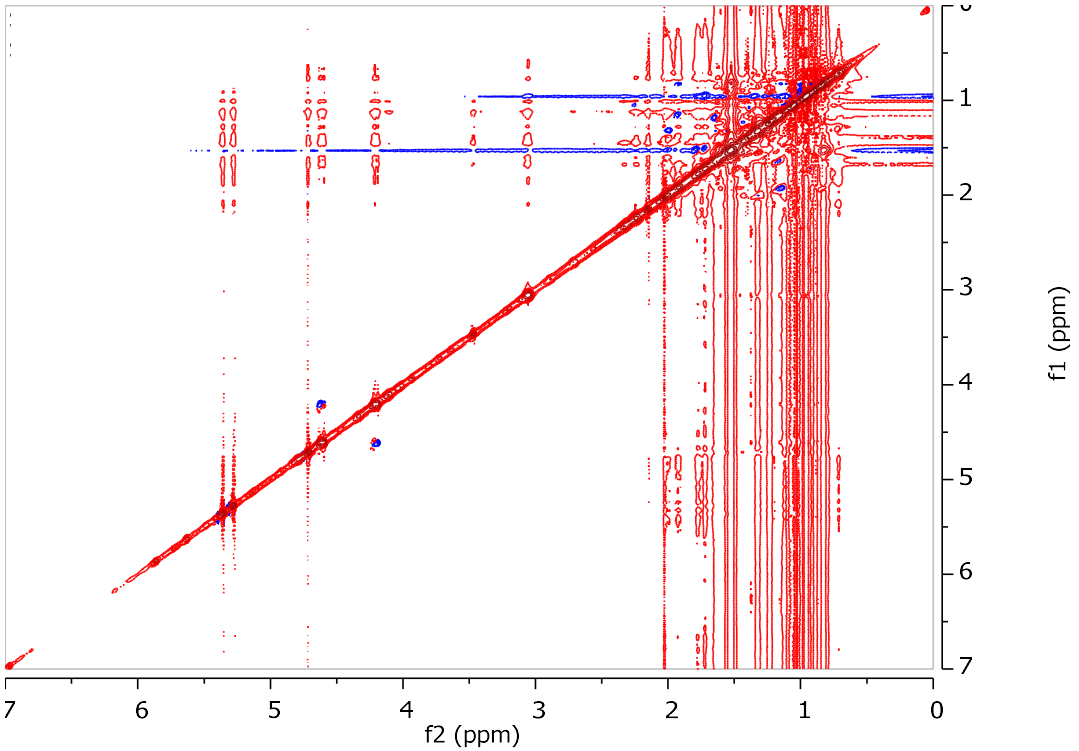

Figure 172. NOESY spectrum of metabolite **41**.

Comparison of the spectroscopic and physical characteristics of metabolite **41** with those reported in the literature led to its identification as a new natural product, which was designated as (23*E*)-22*α*,28-Epidioxy-4*α*,24-dimethyl-5*α*-cholest-23-en-3*β*,8*β*-diol. The NMR data of metabolite **41** are reported in Table 175.

Table 175. ^{1}H and ^{13}C NMR data of metabolite **41** in $CDCl_3$ (δ in ppm, J in Hz)

Position	δ_C	δ_H
1	37.2	1.72 (m), 0.96 (m)
2	30.3	1.78 (m), 1.52 (m)
3	76.4	3.06 (td, 10.5, 5.2)
4	38.5	1.33 (m)
5	51.2	0.71 (td, 12.2, 2.2)
6	19.8	1.53 (m), 1.33 (m)
7	39.6	1.64 (m), 1.19 (m)
8	73.5	-
9	56.0	0.81 (m)
10	36.3	-
11	18.1	1.62 (m), 1.48 (m)
12	40.5	1.93 (m), 1.17 (m)
13	42.7	-
14	59.0	1.23 (m)
15	18.7	1.53 (m), 1.33 (m)
16	27.0	1.99 (m), 1.31 (m)
17	52.4	1.43 (m)
18	12.8	0.89 (s)
19	13.2	0.96 (s)
20	39.8	1.56 (m)
21	12.8	0.83 (d, 6.9)
22	79.9	4.72 (brs)
23	119.4	5.36 (brs)
24	142.0	-
25	30.8	2.24 (septet, 6.9)
26	21.0	1.05 (d, 6.9)
27	21.0	1.05 (d, 6.9)
28	70.6	4.62 (d, 15.7), 4.20 (d, 15.7)
29	14.9	0.95 (d, 6.4)

3.3.9 Metabolite 42

Metabolite **42** (SP09) was isolated after a series of chromatographic separations as a colorless oil (8.7 mg).

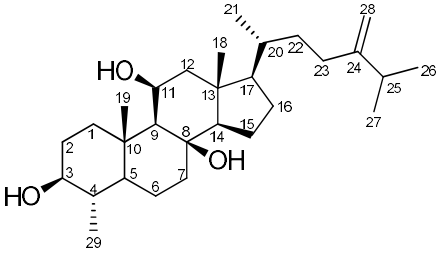

The mass spectrum of metabolite **42** (Figure 173) exhibited a molecular ion peak $[M]^+$ at *m/z* 446.

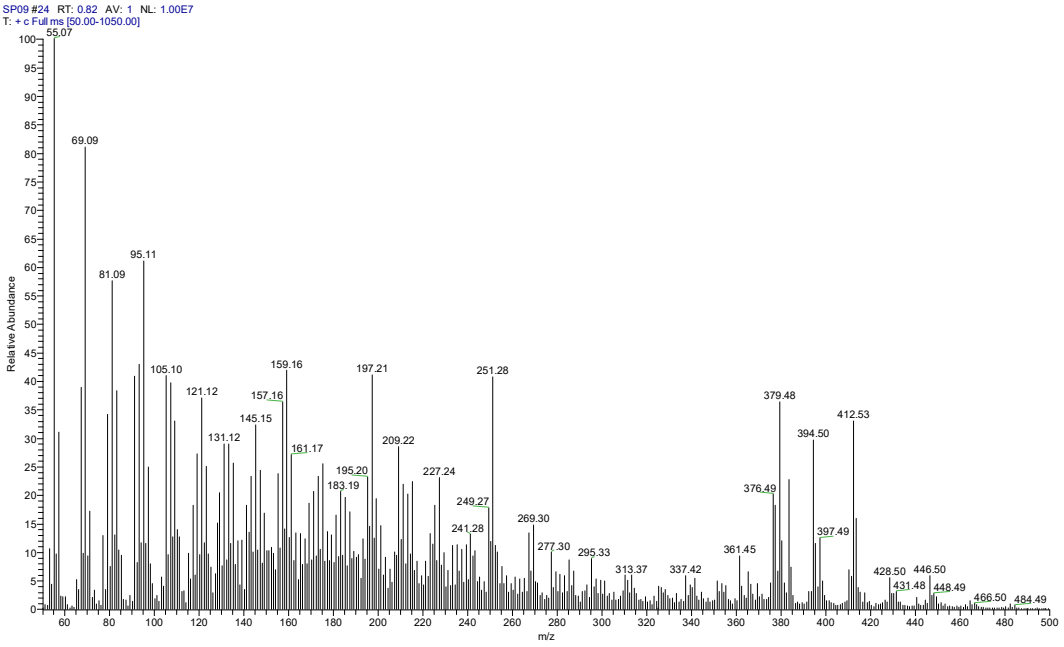

Figure 173. Mass spectrum (EIMS) of metabolite **42**.

In the ^{1}H NMR spectrum of metabolite **42** (Figure 174) obvious were:

- Two aliphatic methyls on non-protonated carbons at δ 1.10 and 1.33,
- Four aliphatic methyls on tertiary carbons at δ 0.91, 0.96, 0.99 and 1.00,
- Two oxygenated methines at δ 3.04 and 4.43, and
- Two broad singlets at δ 4.63 and 4.69 integrating for one proton each and attributed to the protons of an exomethylene group.

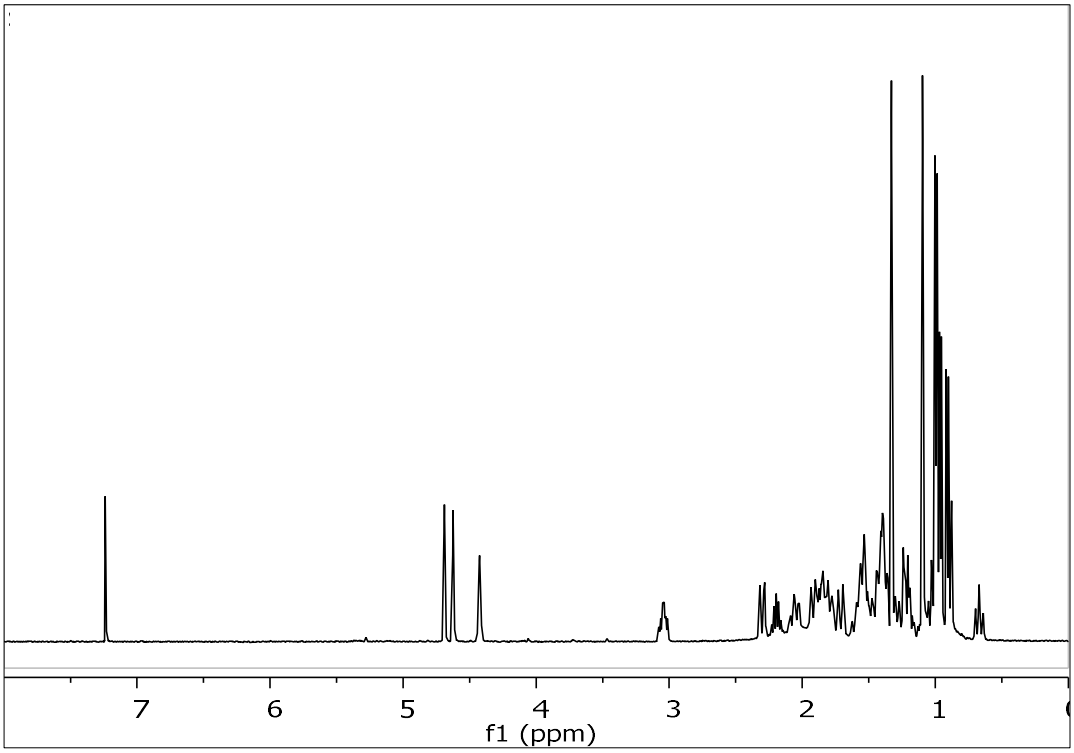

Figure 174. ^{1}H NMR spectrum of metabolite **42**.

Analysis of the NMR and MS data of **42** led to the molecular formula $C_{29}H_{50}O_3$. Taking into account the one carbon-carbon double bond as one of the five degrees of unsaturation, the molecular structure of **42** was determined as tetracyclic.

Comparison of the spectroscopic and physical characteristics of metabolite **42** with those reported in the literature led to its identification as nebrosteroid M (4*α*,24-dimethyl-5*α*-cholest-24(28)-en-3*β*,8*β*,11*β*-triol), previously isolated from the soft coral *N. chabroli* (Cheng et al., 2009). The ^{1}H NMR data of metabolite **42** are reported in Table 176.

Table 176. ^{1}H and ^{13}C NMR data of metabolite **42** in $CDCl_3$ (δ in ppm, J in Hz).

Position	$\delta_{H,exp}$	$\delta_{H,lit}$
1	1.92 (m), 1.02 (m)	1.92 (m), 1.0 (m)
2	1.77 (m), 1.61 (m)	1.79 (m), 1.61 (m)
3	3.04 (td, 11.0, 4.0)	3.07 (td, 10.4, 5.2)
4	1.41 (m)	1.42 (m)
5	0.68 (m)	0.71 (m)
6	1.54 (m), 1.15 (m)	1.53 (m), 1.14 (m)
7	1.73 (m), 1.20 (m)	1.72 (m), 1.19 (m)
9	0.90 (m)	0.90 (m)
11	4.43 (brs)	4.45 (brs)
12	2.32 (m), 1.39 (m)	2.32 (m), 1.38 (m)
14	1.23 (m)	1.23 (m)
15	1.56 (m), 1.47 (m)	1.57 (m), 1.48 (m)
16	1.84 (m), 1.27 (m)	1.85 (m), 1.29 (m)
17	1.05 (m)	1.05 (m)
18	1.10 (s)	1.12 (s)
19	1.33 (s)	1.35 (s)
20	1.44 (m)	1.44 (m)
21	0.91 (d, 6.5)	0.93 (d, 6.4)
22	1.51 (m), 1.09 (m)	1.50 (m), 1.09 (m)
23	2.06 (m), 1.87 (m)	2.09 (m), 1.89 (m)
25	2.20 (m)	2.22 (heptet, 6.8)
26	0.99 (d, 6.8)	1.02 (d, 6.8)
27	1.00 (d, 6.8)	1.02 (d, 6.8)
28	4.69 (brs), 4.63 (brs)	4.72 (s), 4.65 (s)
29	0.96 (d, 6.3)	0.99 (d, 6.4)
11-OH	2.52 (s)	-

3.3.10 Metabolite 43

Metabolite **43** (SP23) was isolated after a series of chromatographic separations as a white amorphous solid (16.9 mg).

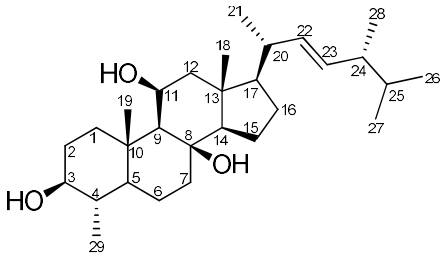

The mass spectrum of metabolite **43** (Figure 175) exhibited a molecular ion peak $[M]^+$ at *m/z* 446, as well as a fragment ion peak at *m/z* 428 corresponding to $[M\text{-}H_2O]^+$.

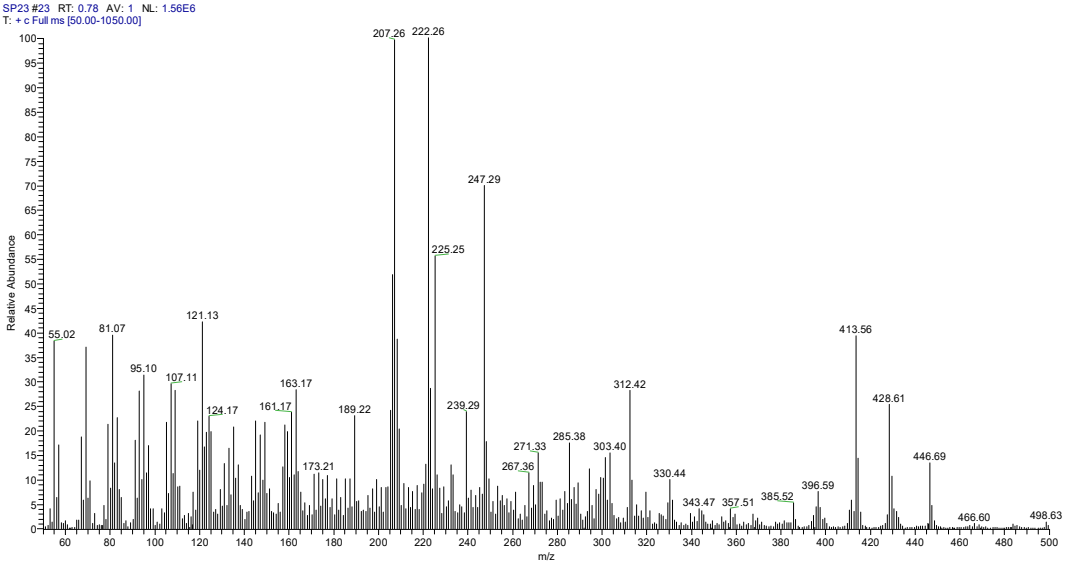

Figure 175. Mass spectrum (EIMS) of metabolite **43**.

In the ^{1}H NMR spectrum of metabolite **43** (Figure 176) obvious were:

- Two aliphatic methyls on non-protonated carbons at δ 1.11 and 1.33,
- Five aliphatic methyls on tertiary carbons at δ 0.79, 0.80, 0.86, 0.96 and 0.98,
- Two oxygenated methines at δ 3.05 and 4.43, and,
- Two olefinic methines at δ 5.09 and 5.19.

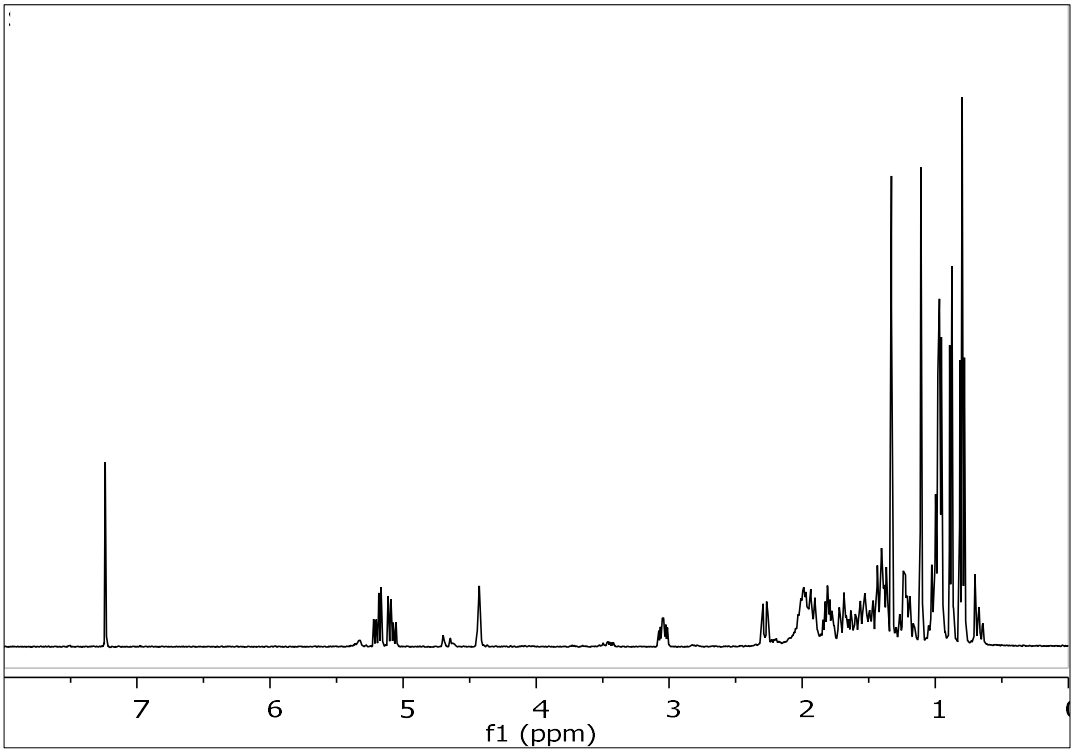

Figure 176. ^{1}H NMR spectrum of metabolite **43**.

Analysis of the NMR and MS data of **43** led to the molecular formula $C_{29}H_{50}O_3$. Taking into account the one carbon-carbon double bond as one of the five degrees of unsaturation, the molecular structure of **43** was determined as tetracyclic.

Comparison of the spectroscopic and physical characteristics of metabolite **43** with those reported in the literature led to its identification as (22*E*,24*R*)-4*α*,24-dimethyl-5*α*-cholest-22-en-3*β*,8*β*,11*β*-triol, previously isolated from the soft coral *Litophyton mollis* (Zovko Končić et al., 2016). The ^{1}H NMR data of metabolite **43** are reported in Table 177.

Table 177. ^{1}H NMR data of metabolite **43** in $CDCl_3$ (δ in ppm, J in Hz).

Position	$\delta_{H,exp}$	$\delta_{H,lit}$
1	1.91 (m), 0.99 (m)	1.91 (m), 1.00 (m)
2	1.79 (m), 1.60 (m)	1.79 (m), 1.59 (m)
3	3.05 (dt, 11.1, 11.2,5.1)	3.04 (td, 107, 4.9)
4	1.42 (m)	1.40 (m)
5	0.68 (m)	0.68 (td, 11.6, 2.6)
6	1.51 (m), 1.42 (m)	1.50 (m), 1.41 (m)
7	1.72 (m), 1.20 (m)	1.70 (m), 1.22 (m)
9	0.88 (m)	0.88 (m)
11	4.43 (brs)	4.43 (brs)
12	2.28 (dd, 14.0, 2.8), 1.39 (m)	2.28 (dd, 13.9, 3.0), 1.39 (m)
14	1.23 (m)	1.23 (m)
15	1.54 (m), 1.43 (m)	1.54 (m), 1.43 (m)
16	1.66 (m), 1.27 (m)	1.67 (m), 1.26 (m)
17	1.03 (m)	1.03 (m)
18	1.11 (s)	1.10 (s)
19	1.33 (s)	1.33 (s)
20	2.01 (m)	2.00 (m)
21	0.96 (d, 6.5)	0.97 (d, 6.5)
22	5.09 (dd, 15.3, 8.3)	5.08 (dd, 15.2, 8.3)
23	5.19 (dd, 15.3, 7.6)	5.19 (dd, 15.2, 7.7)
24	1.81 (m)	1.82 (m)
25	1.44 (m)	1.44 (m)
26	0.79 (d, 6.7)	0.79 (d, 6.6)
27	0.80 (d, 6.6)	0.81 (d, 6.6)
28	0.86 (d, 6.8)	0.88 (d, 6.8)
29	0.98 (d, 6.1)	0.96 (d, 6.1)
11-OH	-	2.46 (d, 6.1)

3.3.11 Metabolite 44

Metabolite **44** (SP26) was isolated after a series of chromatographic separations as a colorless oil (4 mg).

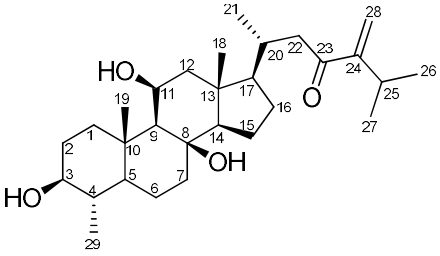

The mass spectrum of metabolite **44** (Figure 177) exhibited a molecular ion peak $[M]^+$ at *m/z* 460, as well as a fragment ion peak at *m/z* 442 corresponding to $[M\text{-}H_2O]^+$.

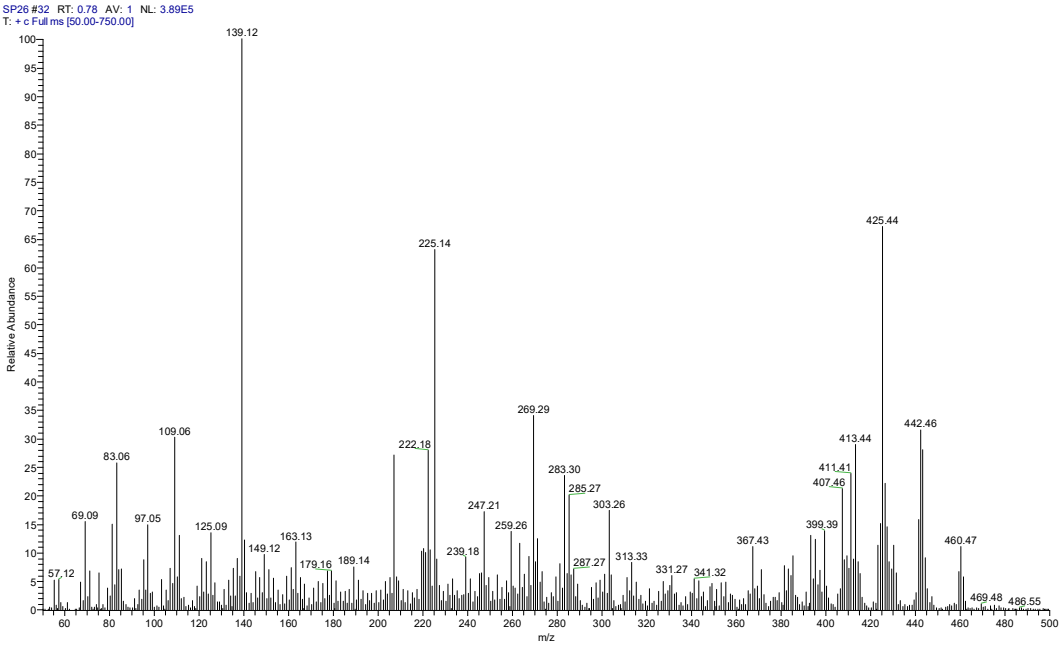

Figure 177. Mass spectrum (EIMS) of metabolite **44**.

In the ^{1}H NMR spectrum of metabolite **44** (Figure 178) obvious were:

- Two aliphatic methyls on non-protonated carbons at δ 1.14 and 1.33,
- Four aliphatic methyls on tertiary carbons at δ 0.87, 0.96, 0.99 and 1.00,
- Two oxygenated methines at δ 3.05 and 4.44, and
- Two broad singlets at δ 5.64 and 5.87 integrating for one proton each and attributed to the protons of an exomethylene group.

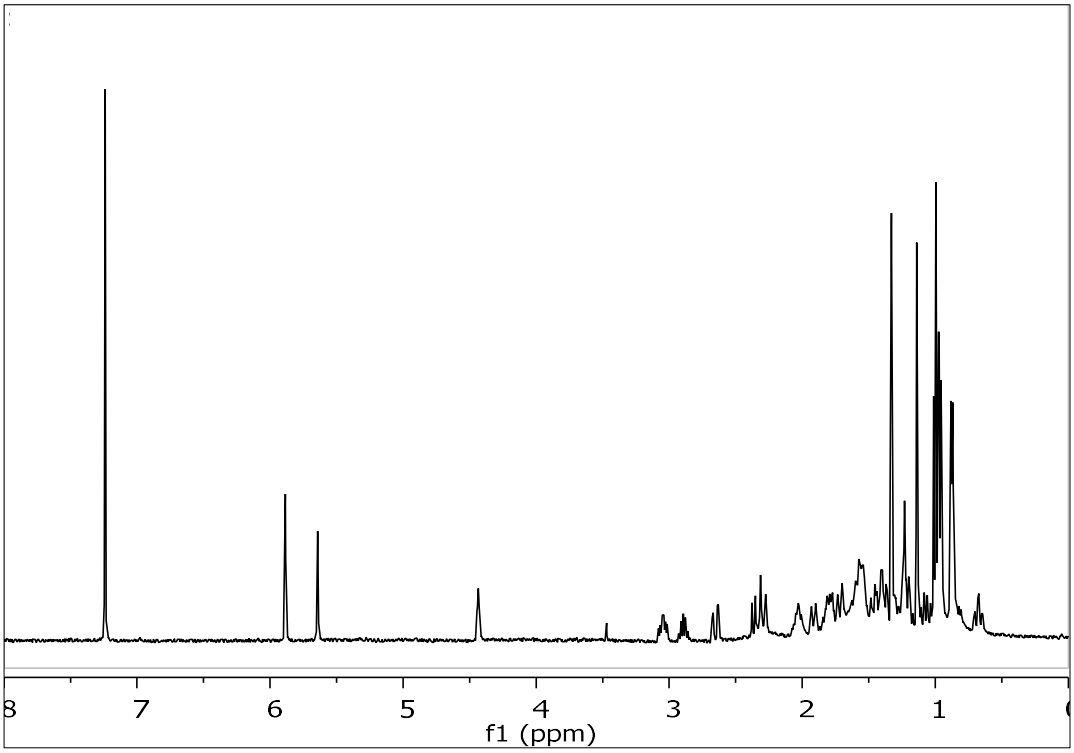

Figure 178. ^{1}H NMR spectrum of metabolite **44**.

Analysis of the NMR and MS data of **44** led to the molecular formula $C_{29}H_{48}O_4$. Taking into account the one carbon-carbon double bond and the carbonyl moiety as two of the six degrees of unsaturation, the molecular structure of **44** was determined as tetracyclic.

Comparison of the spectroscopic and physical characteristics of metabolite **44** with those reported in the literature led to its identification as nebrosteroid A (23-oxo-4α,24-dimethyl-5α-cholest-24(28)-en-3β,8β,11β-triol), previously isolated from the soft coral *N. chabroli* (Huang et al., 2008). The ^{1}H NMR data of metabolite **44** are reported in Table 178.

Table 178. ^{1}H NMR data of metabolite **44** in $CDCl_3$ (δ in ppm, J in Hz)

Position	$\delta_{H,exp}$	$\delta_{H,lit}$
1	1.93 (m), 1.03 (m)	1.92 (m), 1.02 (m)
2	1.77 (m), 1.66 (ddd, 5.8, 3.1, 1.3)	1.77 (m), 1.66 (m)
3	3.05 (td, 11.0, 11.0, 5.8)	3.05 (td, 10.4, 5.6)
4	1.41 (m)	1.41 (m)
5	0.68 (td, 12.4, 12.1, 2.4)	0.68 (td, 11.1, 2.4)
6	1.57 (m), 1.47 (m)	1.57 (m), 1.47 (m)
7	1.72 (m), 1.21 (m)	1.71 (m), 1.21 (m)
9	0.88 (m)	0.88 (m)
11	4.44 (brs)	4.45 (brs)
12	2.29 (m), 1.38 (m)	2.29 (m), 1.39 (m)
14	1.25 (m)	1.24 (m)
15	1.57 (m), 0.88 (m)	1.57 (m), 0.88 (m)
16	1.81 (m), 1.32 (m)	1.81 (m), 1.32 (m)
17	1.07 (m)	1.08 (m)
18	1.14 (s)	1.15 (s)
19	1.33 (s)	1.34 (s)
20	2.04 (m)	2.04 (m)
21	0.87 (d, 6.2)	0.88 (d, 6.6)
22	2.65 (dd, 15.5, 3.1), 2.36 (m)	2.67 (dd, 16.6, 2.7), 2.35 (m)
25	2.88 (m)	2.89 (septet, 6.6)
26	0.99 (d, 7.2)	1.01 (d, 6.6)
27	1.00 (d, 7.2)	1.03 (d, 6.6)
28	5.87 (brs), 5.64 (brs)	5.91 (s), 5.67 (s)
29	0.96 (d, 6.4)	0.97 (d, 6.6)
11-OH	2.31 (s)	-

3.3.12 Metabolite 45

Metabolite **45** (SP27) was isolated after a series of chromatographic separations as a white amorphous solid (2.2 mg).

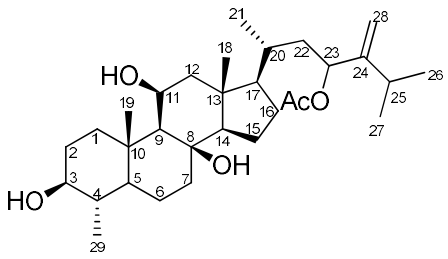

The mass spectrum of metabolite **45** (Figure 179) exhibited a fragment ion peak at *m/z* 444 corresponding to $[M\text{-}AcOH]^+$.

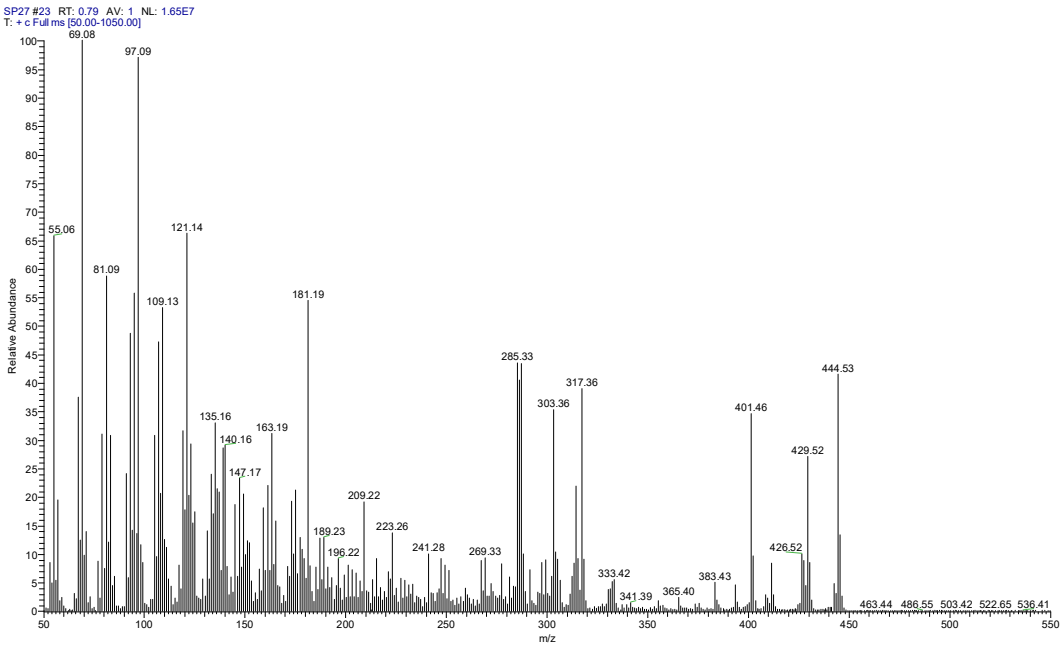

Figure 179. Mass spectrum (EIMS) of metabolite **45**.

In the ^{1}H NMR spectrum of metabolite **45** (Figure 180) obvious were:

- Two aliphatic methyls on non-protonated carbons at δ 1.07 and 1.33,
- Four aliphatic methyls on tertiary carbons at δ 0.95, 0.96, 1.03 and 1.07,
- One methyl of an acetoxy group at δ 2.01,
- Three oxygenated methines at δ 3.05, 4.43 and 5.25, and
- Two broad singlets at δ 4.96 and 5.01 integrating for one proton each and attributed to the protons of an exomethylene group.

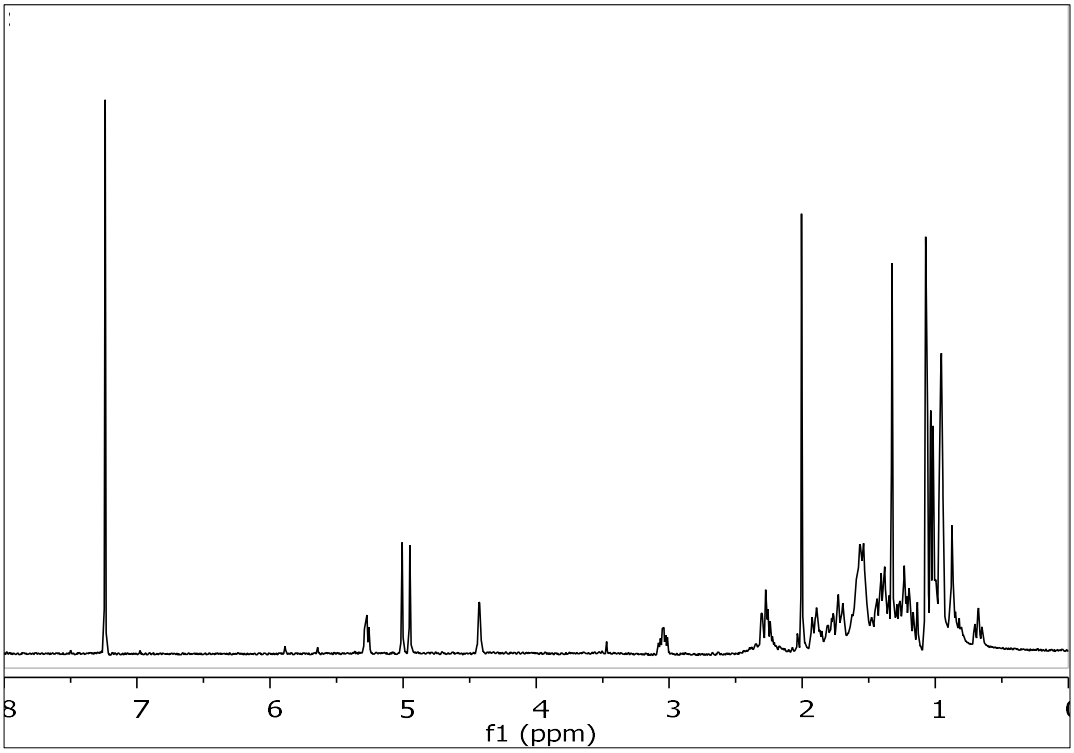

Figure 180. ^{1}H NMR spectrum of metabolite **45**.

Analysis of the NMR and MS data of **45** led to the molecular formula $C_{31}H_{52}O_5$. Taking into account the one carbon-carbon double bond and the carbonyl moiety as two of the six degrees of unsaturation, the molecular structure of **45** was determined as tetracyclic.

Comparison of the spectroscopic and physical characteristics of metabolite **45** with those reported in the literature led to its identification as 23ξ-acetoxy-4α,24-dimethyl-5α-cholest-24(28)-en-3β,8β,11β-triol, previously isolated from the soft coral *L. mollis* (Zovko Končić et al., 2016). The ^{1}H NMR data of metabolite **45** are reported in Table 179.

Table 179. ^{1}H NMR data of metabolite **45** in $CDCl_3$ (δ in ppm, J in Hz).

Position	$\delta_{H,exp}$	$\delta_{H,lit}$
1	1.90 (m), 1.0 (m)	1.89 (m), 0.99 (m)
2	1.80 (m), 1.58 (m)	1.79 (m), 1.58 (m)
3	3.05 (ddd, 11.3, 10.8, 3.6)	3.05 (td, 10.9, 5.0)
4	1.41 (ddd, 5.8, 3.1, 2.2)	1.40 (m)
5	0.69 (td, 11.5, 2.3)	0.67 (td, 11.7, 2.7)
6	1.49 (m), 1.41 (ddd, 5.8, 3.1, 2.2)	1.49 (m), 1.40 (m)
7	1.7 (m), 1.21 (m)	1.71 (m), 1.20 (m)
9	0.85 (m)	0.86 (m)
11	4.43 (brs)	4.42 (brs)
12	2.26 (m), 1.38 (m)	2.29 (dd, 14.0, 3.0), 1.37 (m)
14	1.18 (m)	1.18 (m)
15	1.54 (m), 1.44 (m)	1.54 (m), 1.44 (m)
16	1.86 (m), 1.24 (m)	1.86 (m), 1.25 (m)
17	1.01 (m)	1.01 (m)
18	1.07 (s)	1.07 (s)
19	1.33 (s)	1.32 (s)
20	1.36 (m)	1.36 (m)
21	0.95 (d, 5.6)	0.95 (d, 6.2)
22	1.73 (m), 1.29 (m)	1.74 (m), 1.29 (m)
23	5.25 (m)	5.27 (dd, 7.5, 6.2)
25	2.24 (m)	2.24 (m)
26	1.03 (d, 6.8)	1.03 (d, 6.6)
27	1.07 (d, 5.5)	1.07 (d, 6.6)
28	5.01 (brs), 4.96 (brs)	5.01 (brs), 4.95 (brs)
29	0.96 (d, 6.0)	0.96 (d, 6.2)
OAc	2.01 (s)	2.01 (s)
11-OH	2.3 (d, 7.1)	2.39 (d, 5.9)

3.3.13 Metabolite 46

Metabolite **46** (SP25) was isolated after a series of chromatographic separations as a white amorphous solid (1.3 mg).

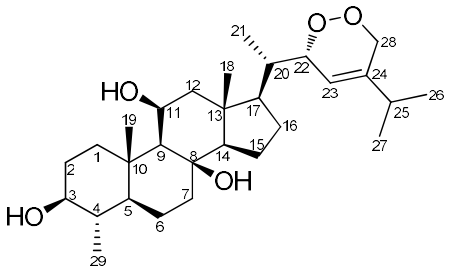

The high-resolution mass spectrum of the metabolite **46** (Figure 181) showed a pseudomolecular ion peak at *m/z* 475.3424 corresponding to $[M-H]^-$ (calcd. for $C_{29}H_{47}O_5$, 475.3429).

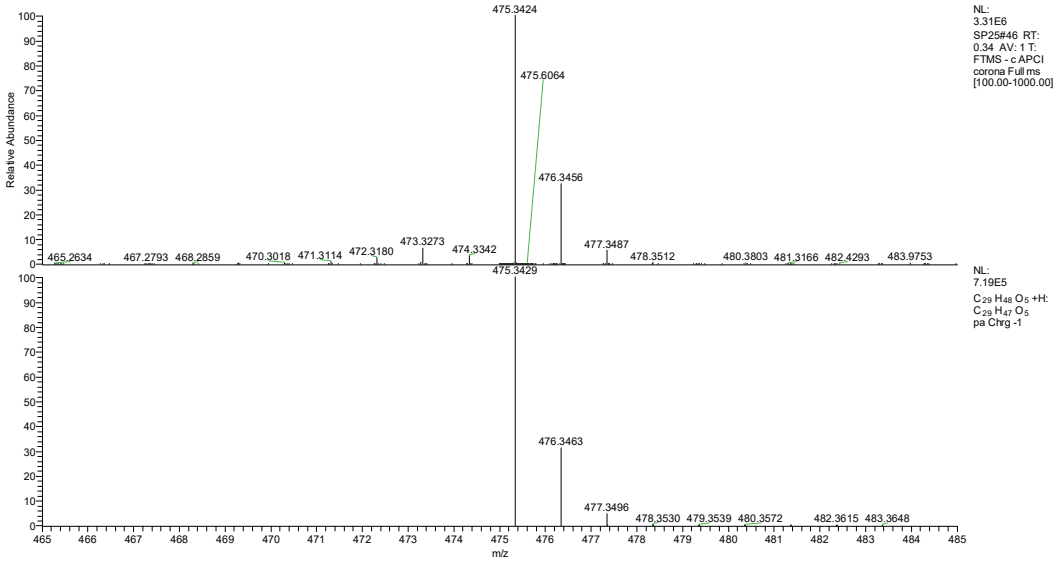

Figure 181. Mass spectrum (HR-APCIMS) of metabolite **46**.

In the ^{1}H NMR spectrum of metabolite **46** (Figure 182) obvious were:

- Two aliphatic methyls on non-protonated carbons at δ 1.09 and 1.33,
- Four aliphatic methyls on tertiary carbons at δ 0.85, 0.96, 1.05 and 1.06,
- Three oxygenated methines at δ 3.05, 4.43 and 4.70,
- Two doublets at δ 4.21 and 4.59 integrating for one proton each and attributed to the protons of an oxygenated methylene, and,
- One olefinic methine at δ 5.36.

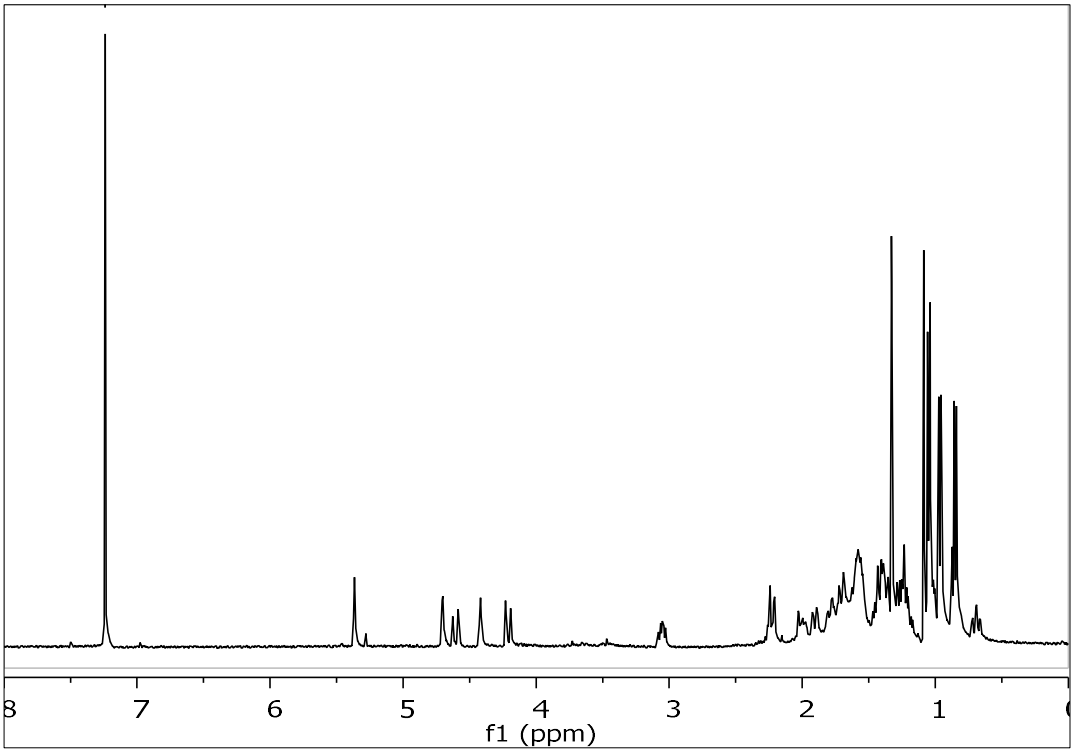

Figure 182. ^{1}H NMR spectrum of metabolite **46**.

Analysis of the NMR and MS data of **46** led to the molecular formula $C_{29}H_{48}O_5$. Taking into account the one carbon-carbon double bond as one of the six degrees of unsaturation, the molecular structure of **46** was determined as pentacyclic.

The spectroscopic data of metabolite **46** related to the steroidal nucleus displayed high similarity with those of **42**–**45**, suggesting a 3,8,11-trihydroxy-4-methyl steroidal nucleus. Additionally, the NMR data concerning the side chain of compound **46** were rather similar to those of **41**. Indeed, the planar structure of metabolite **46** was determined on the basis of the homonuclear and heteronuclear correlations (Figure 183) observed in the HSQC-DEPT (Figure 184), HMBC (Figure 185) and COSY (Figure 186) spectra.

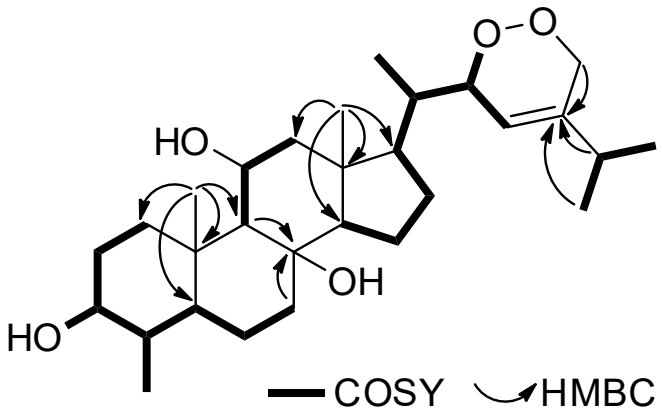

Figure 183. COSY and important HMBC correlations observed for metabolite **46**.

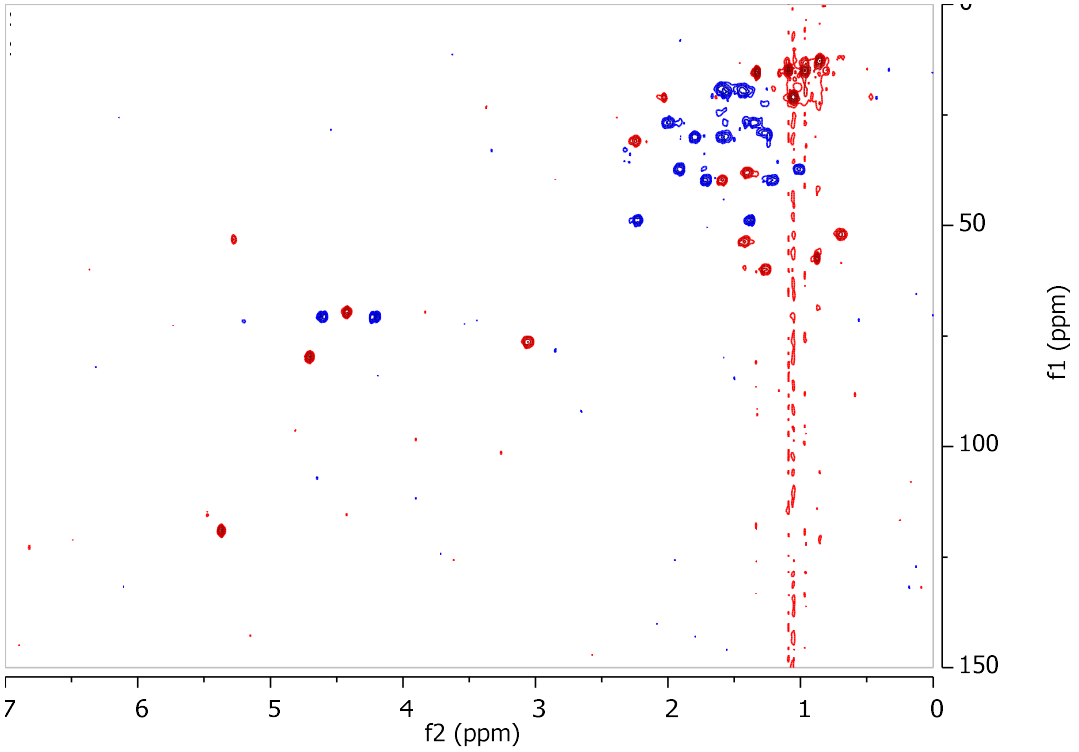

Figure 184. HSQC-DEPT spectrum of metabolite **46**.

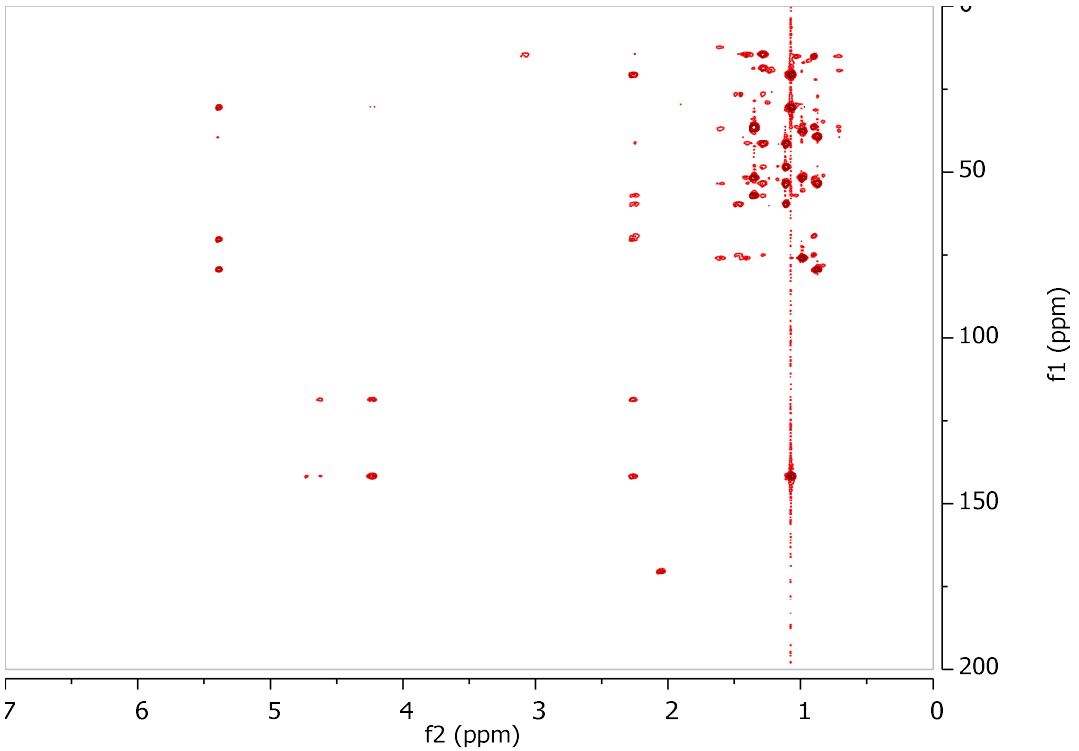

Figure 185. HMBC spectrum of metabolite **46**.

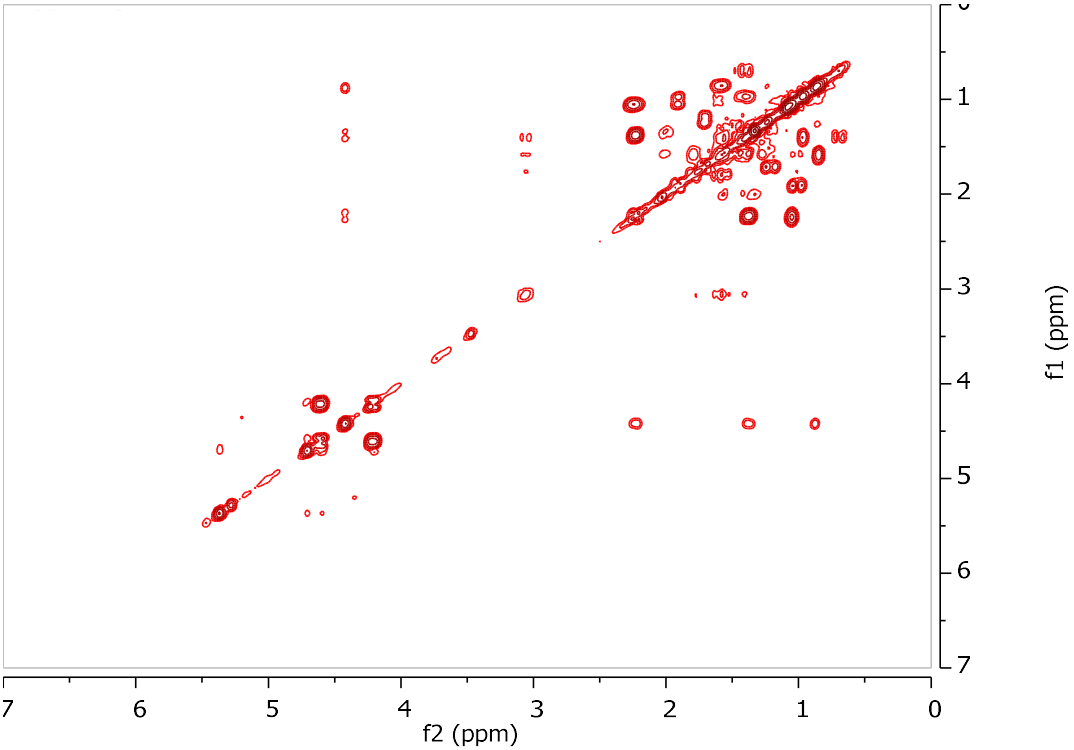

Figure 186. COSY spectrum of metabolite **46**.

The relative configuration of the asymmetric centers of metabolite **46** was determined on the basis of the correlations observed in the NOESY spectrum (Figure 187). As in the case of **41**, H-22 was assigned to be on the opposite side of H_3-21, as also suggested by the chemical shift of C-23 which resonated at 119.2 ppm. Instead, when H-22 and H_3-21 are co-planar, C-23 is shielded, resonating at 115-116 ppm (Yu et al., 2006).

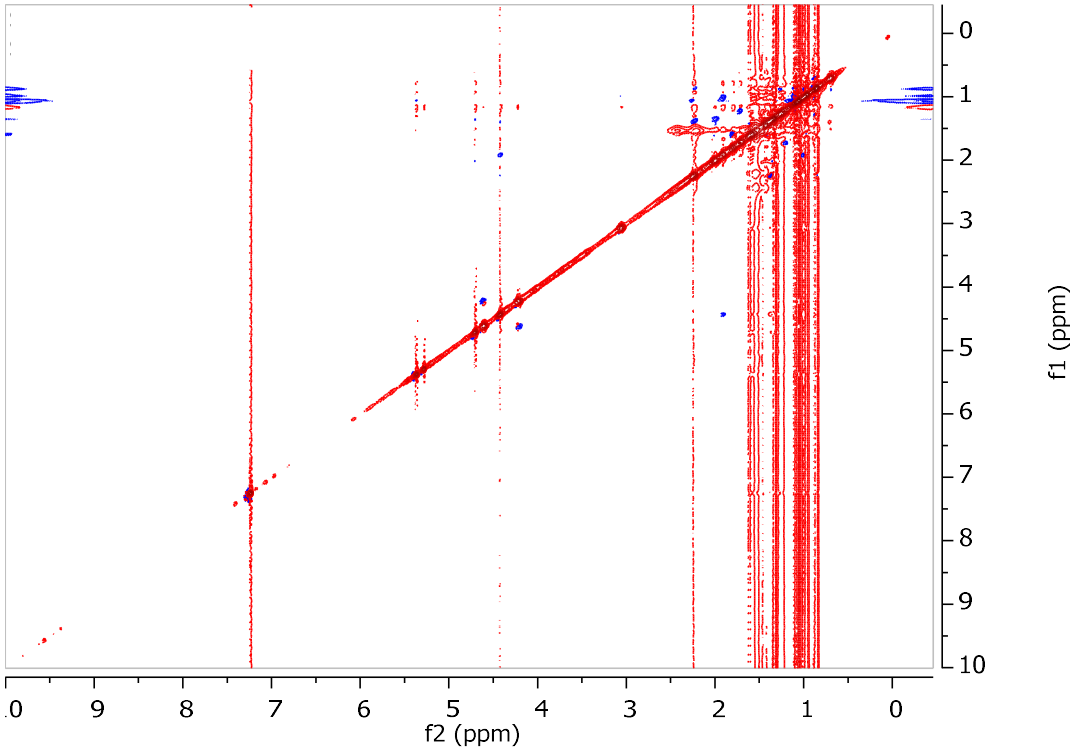

Figure 187. NOESY spectrum of metabolite **46**.

Comparison of the spectroscopic and physical characteristics of metabolite **46** with those reported in the literature led to its identification as a new natural product, which was designated as (23*E*)-22*α*,28-epidioxy-4*α*,24-dimethyl-5*α*-cholest-23-en-3*β*,8*β*,11*β*-triol. The NMR data of metabolite **46** are reported in Table 180.

Table 180. ^{1}H and ^{13}C NMR data of metabolite **46** in $CDCl_3$ (δ in ppm, J in Hz).

Position	δ_C	δ_H
1	37.5	1.91 (m), 1.00 (m)
2	30.2	1.79 (m), 1.58 (m)
3	76.5	3.05 (td, 10.8, 5.0)
4	38.2	1.41 (m)
5	52.3	0.69 (td, 11.9, 2.2)
6	20.0	1.56 (m), 1.39 (m)
7	39.9	1.71 (m), 1.22 (m)
8	75.3	-
9	57.6	0.88 (m)
10	36.8	-
11	69.8	4.43 (brd, 1.9)
12	49.0	2.23 (m), 1.37 (m)
13	41.8	-
14	60.2	1.27 (m)
15	19.2	1.60 (m), 1.46 (m)
16	26.9	2.00 (m), 1.35 (m)
17	53.9	1.43 (m)
18	15.0	1.09 (s)
19	15.6	1.33 (s)
20	40.0	1.59 (m)
21	12.9	0.85 (d, 7.0)
22	79.7	4.70 (brs)
23	119.2	5.36 (brs)
24	142.0	-
25	31.1	2.24 (septet, 6.9)
26	21.1	1.05 (d, 6.9)
27	21.1	1.06 (d, 6.9)
28	70.8	4.59 (d, 15.7), 4.21 (d, 15.7)
29	15.2	0.96 (d, 6.4)

3.3.14 Metabolite 47

Metabolite **47** (SP28) was isolated after a series of chromatographic separations as a white amorphous solid (1.1 mg).

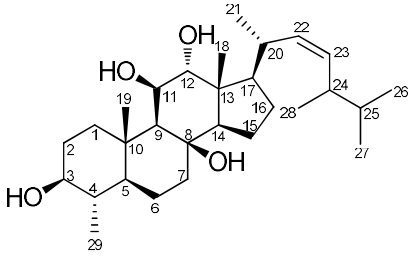

The mass spectrum of metabolite **47** (Figure 188) exhibited a fragment ion peak at *m/z* 426 corresponding to $[M\text{-}2H_2O]^+$.

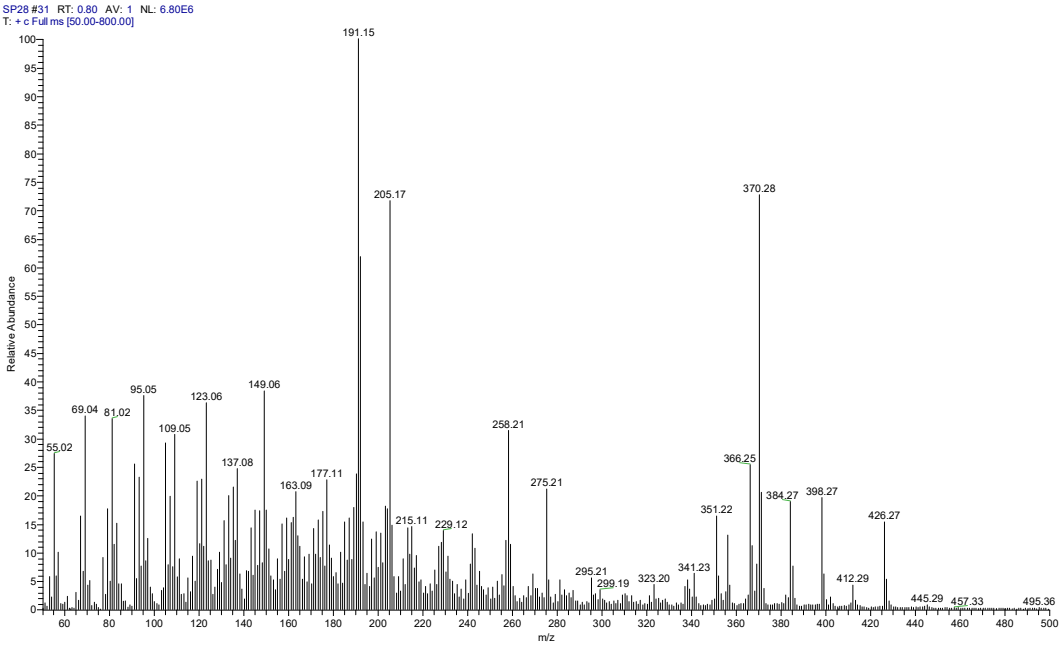

Figure 188. Mass spectrum (EIMS) of metabolite **47**.

In the ^{1}H NMR spectrum of metabolite **47** (Figure 189) obvious were:

- Two aliphatic methyls on non-protonated carbons at δ 1.00 and 1.34,
- Five aliphatic methyls on tertiary carbons at δ 0.80, 0.81, 0.90, 0.97 and 1.12,
- Three oxygenated methines at δ 3.05, 3.22 and 4.21, and
- Two olefinic methines at δ 5.19 and 5.20.

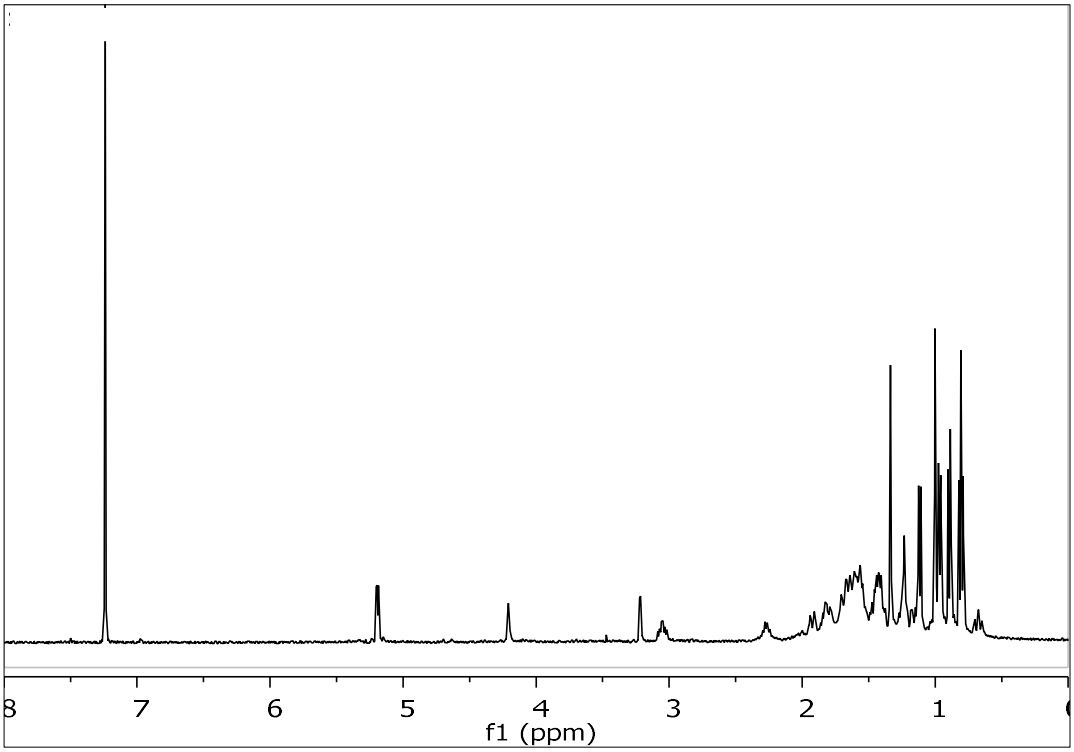

Figure 189. ^{1}H NMR spectrum of metabolite **47**.

Analysis of the NMR and MS data of **47** led to the molecular formula $C_{29}H_{50}O_4$. Taking into account the one carbon-carbon double bond as one of the five degrees of unsaturation, the molecular structure of **47** was determined as tetracyclic.

Comparison of the spectroscopic and physical characteristics of metabolite **47** with those reported in the literature led to its identification as (22Z)-4*α*,24*ξ*-dimethyl-5*α*-cholest-22-en-3*β*,8*β*,11*β*,12*α*-tetraol, previously isolated from the soft coral *L. mollis* (Zovko Končić et al., 2016). The ^{1}H NMR data of metabolite **47** are reported in Table 181.

Table 181. ^{1}H NMR data of metabolite **47** in $CDCl_3$ (δ in ppm, J in Hz)

Position	$\delta_{H,exp}$	$\delta_{H,lit}$
1	1.93 (m), 1.04 (m)	1.95 (m), 1.00 (m)
2	1.80 (m), 1.59 (m)	1.82 (m), 1.60 (m)
3	3.05 (td, 10.7, 4.8)	3.05 (m)
4	1.40 (m)	1.40 (m)
5	0.66 (m)	0.67 (td, 11.5, 2.7)
6	1.42 (m), 1.37 (m)	1.43 (m), 1.39 (m)
7	1.70 (m), 1.19 (m)	1.70 (m), 1.17 (m)
9	0.86 (m)	0.88 (m)
11	4.21 (m)	4.21 (m)
12	3.22 (dd, 8.5, 3.8)	3.22 (dd, 8.4, 3.4)
14	1.15 (m)	1.14 (m)
15	1.57 (m), 1.44 (m)	1.57 (m), 1.44 (m)
16	1.62 (m), 1.41 (m)	1.62 (m), 1.41 (m)
17	1.23 (m)	1.23 (m)
18	1.00 (s)	1.00 (s)
19	1.34 (s)	1.34 (s)
20	2.27 (m)	2.28 (m)
21	1.12 (d, 6.7)	1.12 (d, 6.7)
22	5.19 (m)	5.18 (m)
23	5.20 (m)	5.20 (m)
24	1.85 (m)	1.84 (m)
25	1.45 (m)	1.45 (m)
26	0.80 (d, 6.5)	0.80 (d, 6.6)
27	0.81 (d, 6.5)	0.81 (d, 6.6)
28	0.90 (d, 6.9)	0.90 (d, 6.8)
29	0.97 (d, 6.3)	0.97 (d, 6.3)
11-OH	-	2.68 (d, 8.4)
12-OH	-	3.02 (d, 6.9)

3.3.15 Metabolite 48

Metabolite **48** (SP05) was isolated after a series of chromatographic separations as a white amorphous solid (9.4 mg).

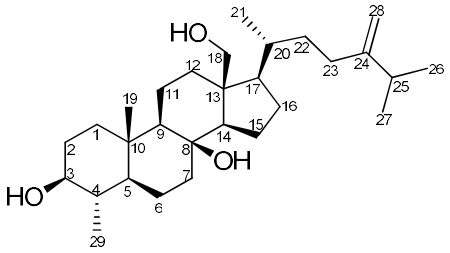

The mass spectrum of metabolite **48** (Figure 190) exhibited a molecular ion peak $[M]^+$ at *m/z* 446.

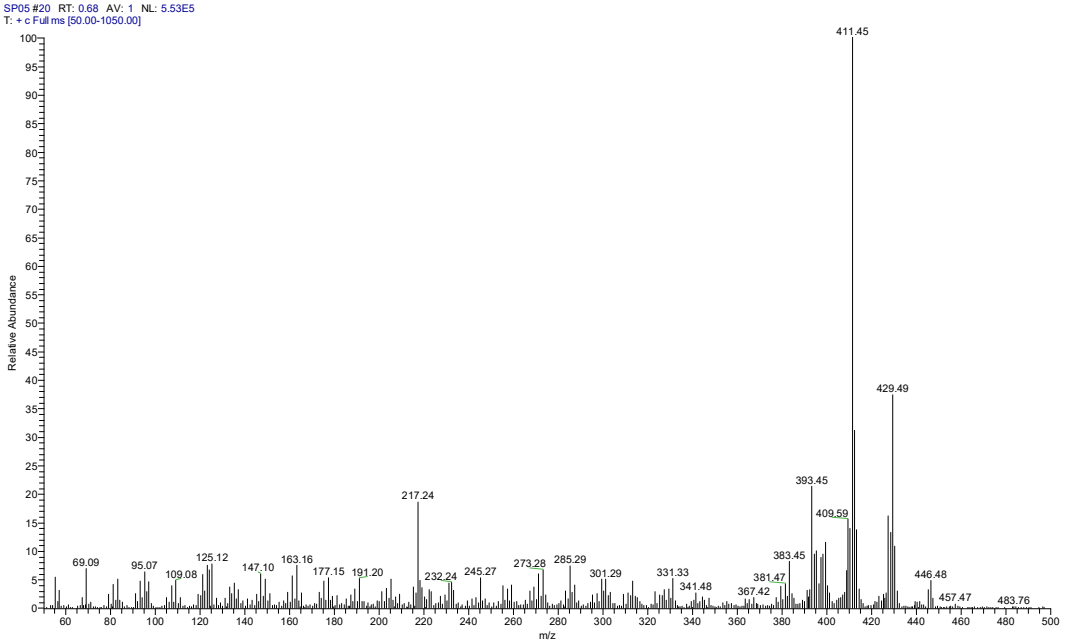

Figure 190. Mass spectrum (EIMS) of metabolite **48**.

In the ^{1}H NMR spectrum of metabolite **48** (Figure 191) obvious were:

- One aliphatic methyl on a non-protonated carbon at δ 0.96,
- Four aliphatic methyls on tertiary carbons at δ 0.94, 0.95, 0.99 and 0.99,
- Two doublets at δ 3.62 and 3.70 integrating for one proton each and attributed to the protons of a hydroxy methylene,
- One oxygenated methine at δ 3.06, and
- Two broad singlets at δ 4.62 and 4.69 integrating for one proton each and attributed to the protons of an exomethylene group.

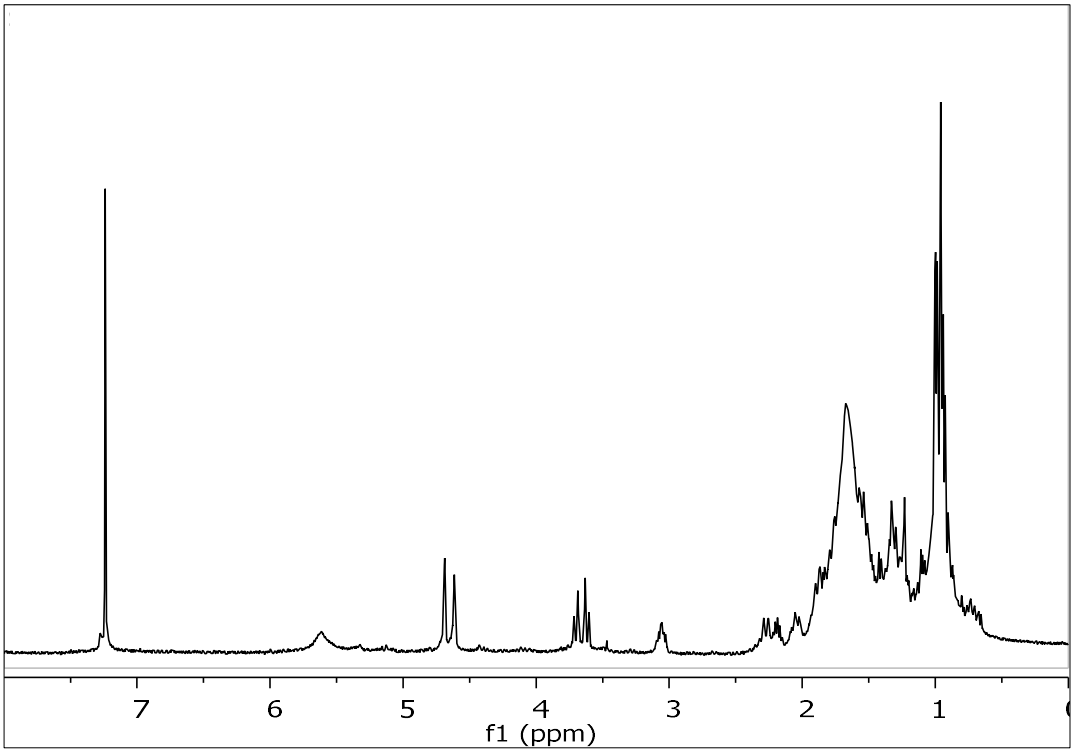

Figure 191. ^{1}H NMR spectrum of metabolite **48**.

Analysis of the NMR and MS data of **48** led to the molecular formula $C_{29}H_{50}O_3$. Taking into account the one carbon-carbon double bond as one of the five degrees of unsaturation, the molecular structure of **48** was determined as tetracyclic.

Comparison of the spectroscopic and physical characteristics of metabolite **48** with those reported in the literature led to its identification as 4*α*,24-dimethyl-5*α*-cholest-24(28)-en-3*β*,8*β*,18-triol, previously isolated from the soft coral *L. mollis* (Zovko Končić et al., 2016). The ^{1}H NMR data of metabolite **48** are reported in Table 182.

Table 182. ^{1}H NMR data of metabolite **48** in $CDCl_3$ (δ in ppm, J in Hz)

Position	$\delta_{H,exp}$	$\delta_{H,lit}$
1	1.71 (m), 0.94 (m)	1.71 (m), 0.94 (m)
2	1.76 (m), 1.51 (m)	1.76 (m), 1.51 (m)
3	3.06 (td, 10.5, 10.5, 4.9)	3.06 (td, 10.2, 5.2)
4	1.35 (m)	1.35 (m)
5	0.73 (m)	0.74 (m)
6	1.49 (m), 1.30 (m)	1.49 (m), 1.31 (m)
7	1.73 (m), 1.24 (m)	1.73 (m), 1.24 (m)
9	0.87 (m)	0.88 (m)
11	1.91 (m), 1.30 (m)	1.89 (m), 1.31 (m)
12	2.27 (m), 1.20 (m)	2.27 (ddd, 13.1, 3.6, 2.5), 1.21 (m)
14	1.41 (m)	1.41 (m)
15	1.56 (m)	1.56 (m)
16	1.88 (m)	1.88 (m), 1.28 (m)
17	1.11 (m)	1.11 (m)
18	3.70 (d, 11.6), 3.62 (d, 11.6)	3.71 (d, 11.8), 3.62 (d, 11.8)
19	0.96 (s)	0.96 (s)
20	1.34 (m)	1.34 (m)
21	0.95 (d, 6.3)	0.96 (d, 6.5)
22	1.52 (m), 1.07 (m)	1.52 (m), 1.07 (m)
23	2.05 (m)	2.05 (m)
25	2.17 (m)	2.19 (m)
26	0.99 (d, 6.8)	0.99 (d, 6.8)
27	0.99 (d, 6.8)	1.00 (d, 6.8)
28	4.69 (brs), 4.62 (brs)	4.69 (brs), 4.62 (brs)
29	0.94 (d, 6.3)	0.94 (d, 6.5)

3.3.16 Metabolite 49

Metabolite **49 (**SP24) was isolated after a series of chromatographic separations as a white amorphous solid (3.5 mg).

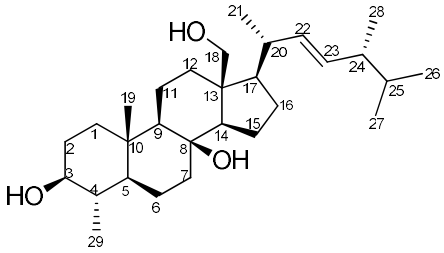

The mass spectrum of metabolite **49** (Figure 192) exhibited a molecular ion peak $[M]^+$ at *m/z* 446.

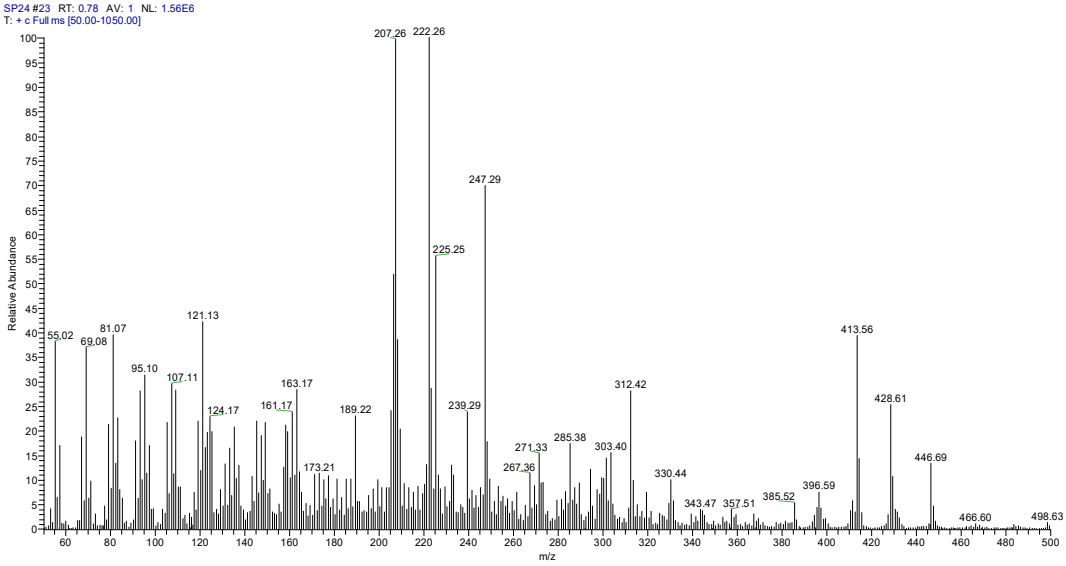

Figure 192. Mass spectrum (EIMS) of metabolite **49**.

In the ^{1}H NMR spectrum of metabolite **49** (Figure 193) obvious were:

- One aliphatic methyl on a non-protonated carbon at δ 0.96,
- Five aliphatic methyls on tertiary carbons at δ 0.78, 0.80, 0.88, 0.95 and 0.99,
- Two doublets at δ 3.64 and 3.74 integrating for one proton each and attributed to the protons of a hydroxy methylene,
- One oxygenated methine at δ 3.06, and
- Two olefinic methines at δ 5.04 and 5.19.

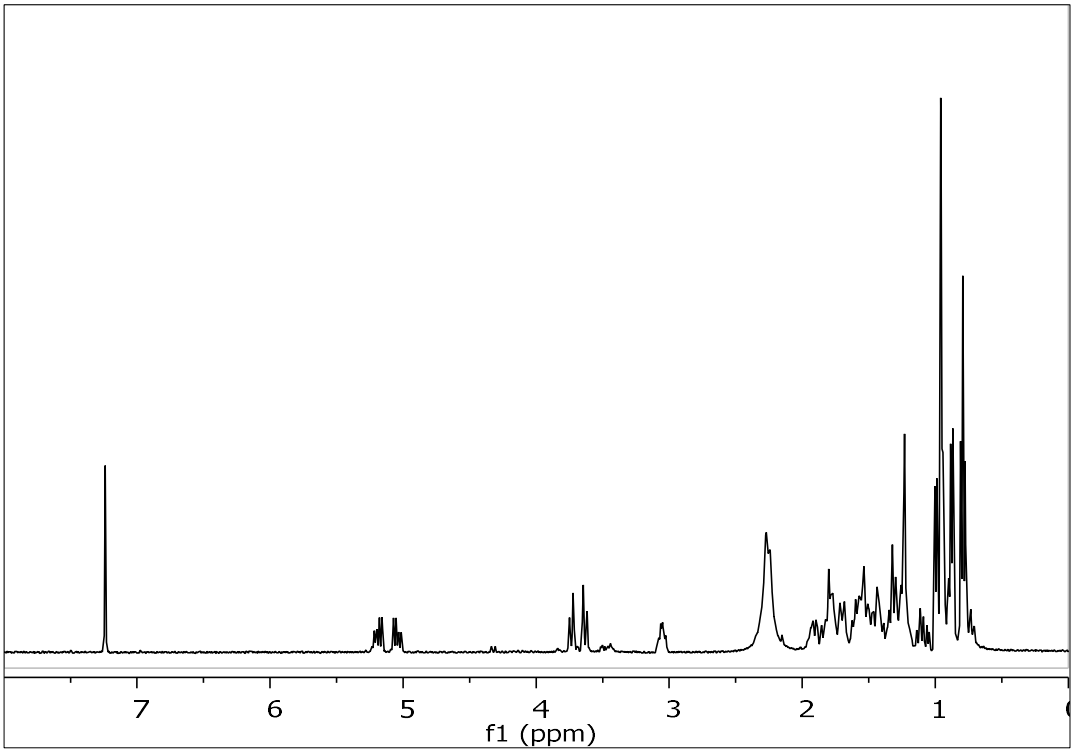

Figure 193. ^{1}H NMR spectrum of metabolite **49**.

Analysis of the NMR and MS data of **49** led to the molecular formula $C_{29}H_{50}O_3$. Taking into account the one carbon-carbon double bond as one of the five degrees of unsaturation, the molecular structure of **49** was determined as tetracyclic.

Comparison of the spectroscopic and physical characteristics of metabolite **49** with those reported in the literature led to its identification as (22*E*,24*R*)-4*α*,24-dimethyl-5*α*-cholest-22-en-3*β*,8*β*,18-triol, previously isolated from the soft coral *L. mollis* (Zovko Končić et al., 2016). The ^{1}H NMR data of metabolite **49** are reported in Table 183.

Table 183. ^{1}H NMR data of metabolite **49** in $CDCl_3$ (δ in ppm, J in Hz).

Position	$\delta_{H,exp}$	$\delta_{H,lit}$
1	1.72 (m), 0.96 (m)	1.70 (m), 0.93 (m)
2	1.78 (m), 1.54 (m)	1.78 (m), 1.53 (m)
3	3.06 (td, 10.2, 10.2, 4.6)	3.06 (td, 10.7, 5.0)
4	1.34 (m)	1.34 (m)
5	0.74 (m)	0.74 (m)
6	1.48 (m), 1.32 (m)	1.48 (m), 1.32 (m)
7	1.74 (m), 1.30 (m)	1.74 (m), 1.30 (m)
9	0.90 (m)	0.88 (m)
11	1.88 (m), 1.33 (m)	1.88 (m), 1.31 (m)
12	2.25 (m), 1.25 (m)	2.25 (ddd, 12.7, 3.3, 2.5), 1.24 (m)
14	1.42 (m)	1.41 (m)
15	1.60 (m)	1.60 (m)
16	1.71 (m), 1.24 (m)	1.70 (m), 1.26 (m)
17	1.11 (m)	1.09 (m)
18	3.74 (d, 11.5), 3.64 (d, 11.5)	3.72 (d, 11.6), 3.62 (d, 11.6)
19	0.96 (s)	0.96 (s)
20	1.95 (m)	1.94 (m)
21	0.99 (d, 6.5)	0.99 (d, 6.6)
22	5.04 (dd, 15.3, 7.7)	5.05 (dd, 15.2, 7.7)
23	5.19 (dd, 15.3, 7.7)	5.19 (dd, 15.2, 7.7)
24	1.82 (m)	1.81 (m)
25	1.46 (m)	1.45 (m)
26	0.80 (d, 6.6)	0.80 (d, 6.7)
27	0.78 (d, 6.7)	0.78 (d, 6.7)
28	0.88 (d, 6.7)	0.88 (d, 6.8)
29	0.95 (d, 6.2)	0.94 (d, 6.2)

3.3.17 Metabolite 50

Metabolite **50** (SP02) was isolated after a series of chromatographic separations as a colorless oil (232.9 mg).

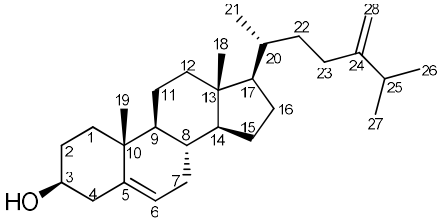

The mass spectrum of metabolite **50** (Figure 194) exhibited a molecular ion peak $[M]^+$ at *m/z* 398.

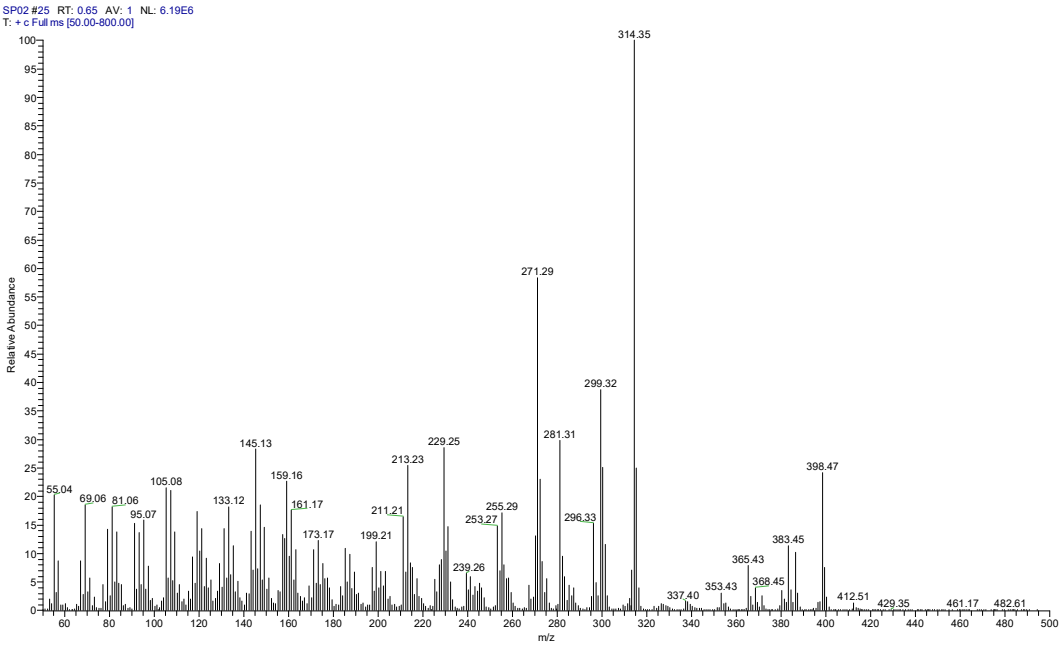

Figure 194. Mass spectrum (EIMS) of metabolite **50**.

In the ^{1}H NMR spectrum of metabolite **50** (Figure 195) obvious were:

- Two aliphatic methyls on non-protonated carbons at δ 0.65 and 0.97,
- Three aliphatic methyls on tertiary carbons at δ 0.92, 0.99 and 1.00,
- One oxygenated methine at δ 3.50,
- Two broad singlets at δ 4.63 and 4.69 integrating for one proton each and attributed to the protons of an exomethylene group, and
- One olefinic methine at δ 5.32.

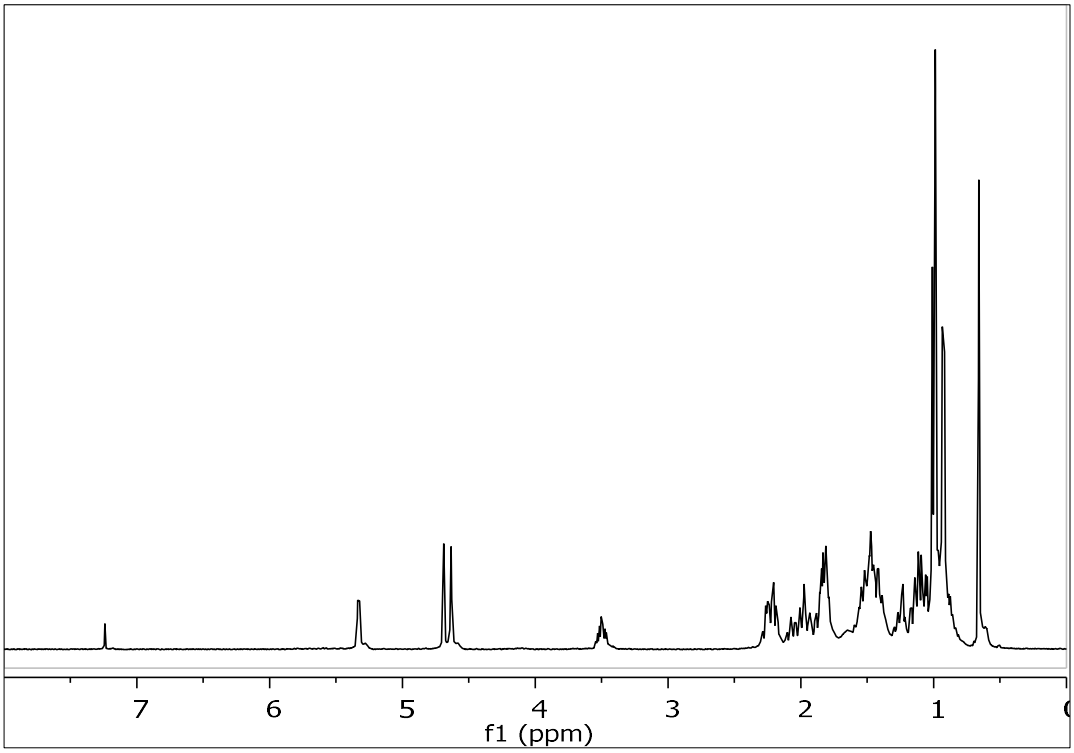

Figure 195. ^{1}H NMR spectrum of metabolite **50**.

Analysis of the NMR and MS data of **50** led to the molecular formula $C_{28}H_{46}O$. Taking into account the two carbon-carbon double bonds as two of the six degrees of unsaturation, the molecular structure of **50** was determined as tetracyclic.

Comparison of the spectroscopic and physical characteristics of metabolite **50** with those reported in the literature led to its identification as 24-methyl-cholesta-5,24(28)-dien-3-*β*-ol, previously isolated from the sponge *Haliclona simulans* (Viegelmann et al., 2014). The ^{1}H NMR data of metabolite **50** are reported in Table 184.

Table 184. ^{1}H NMR data of metabolite **50** in $CDCl_3$ (δ in ppm, J in Hz).

Position	$\delta_{H,exp}$	$\delta_{H,lit}$
3	3.50 (m)	3.52 (td, 11.0, 5.3)
6	5.32 (m)	5.34 (d, 5.7)
7	1.97 (m)	1.95 (m)
18	0.65 (s)	0.67 (s)
19	0.97 (s)	0.99 (s)
21	0.92 (d, 6.5)	0.93 (d, 6.7)
26	0.99 (d, 6.8)	1.02 (d, 2.3)
27	1.00 (d, 6.8)	1.02 (d, 2.3)
28	4.69 (brs), 4.63 (brs)	4.70 (s), 4.64 (s)

3.3.18 Metabolite 51

Metabolite **51** (SP04) was isolated after a series of chromatographic separations as a colorless oil (11.9 mg).

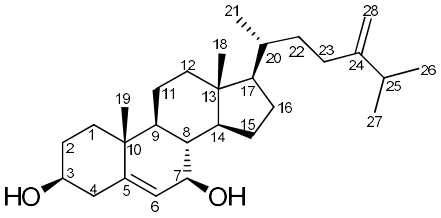

The mass spectrum of metabolite **51** (Figure 196) exhibited a molecular ion peak $[M]^+$ at *m/z* 414.

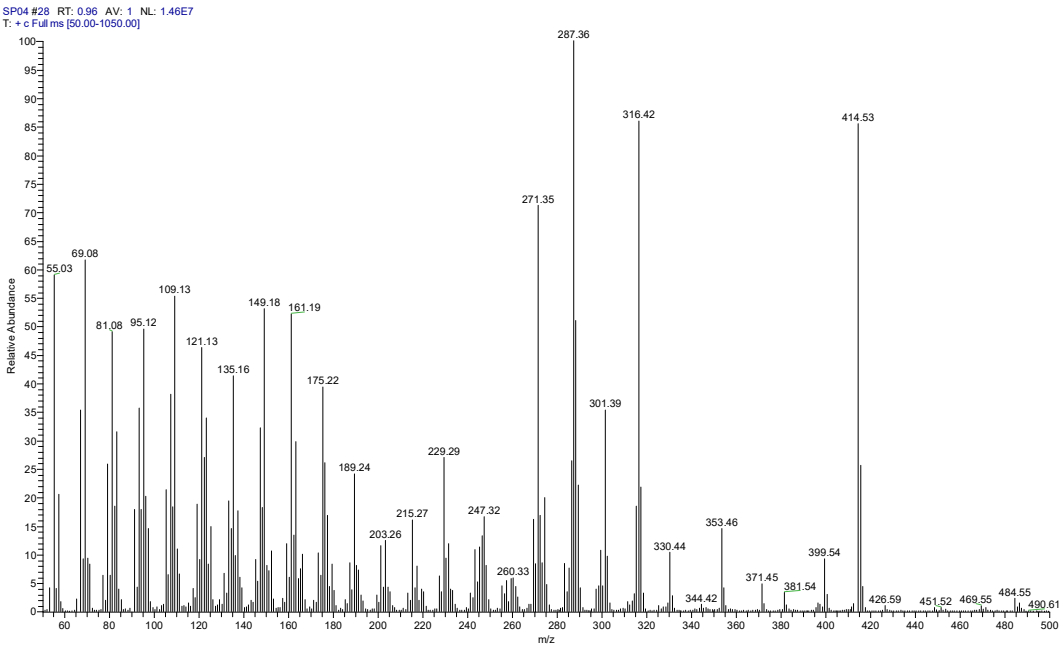

Figure 196. Mass spectrum (EIMS) of metabolite **51**.

In the ^{1}H NMR spectrum of metabolite **51** (Figure 197) obvious were:

- Two aliphatic methyls on non-protonated carbons at δ 0.67 and 1.03,
- Three aliphatic methyls on tertiary carbons at δ 0.93, 1.01 and 1.03,
- Two oxygenated methines at δ 3.53 and 3.83,
- Two broad singlets at δ 4.63 and 4.69 integrating for one proton each and attributed to the protons of an exomethylene group, and
- One olefinic methine at δ 5.27.

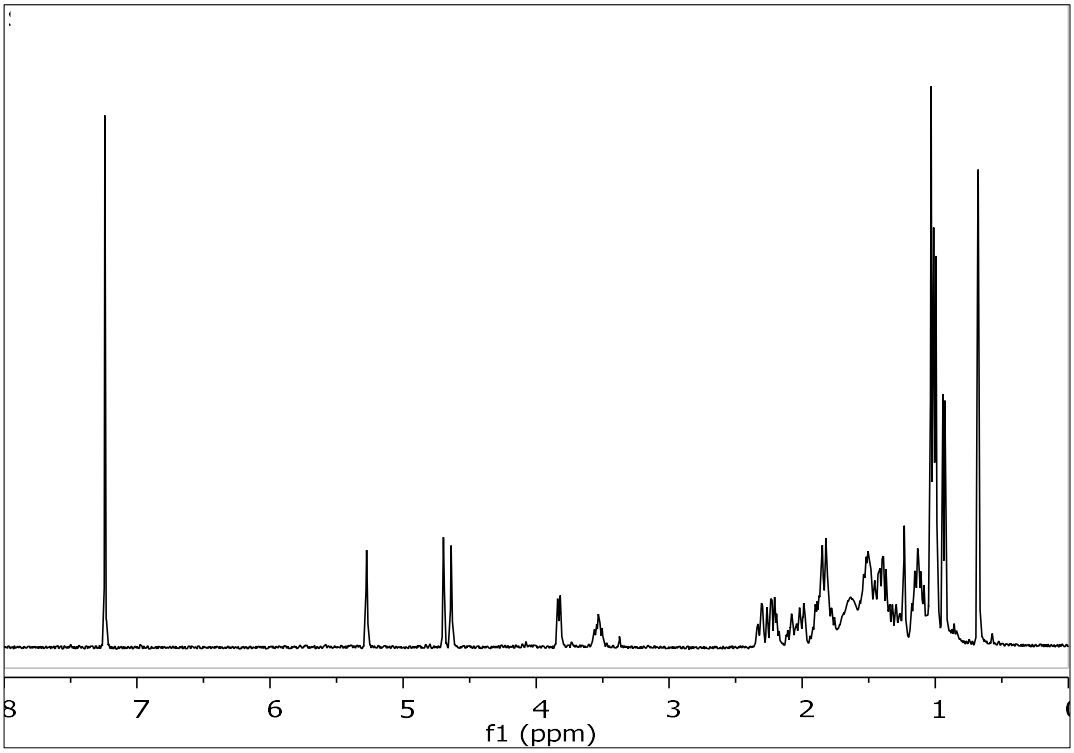

Figure 197. ^{1}H NMR spectrum of metabolite **51**.

Analysis of the NMR and MS data of **51** led to the molecular formula $C_{28}H_{46}O_2$. Taking into account the two carbon-carbon double bonds as two of the six degrees of unsaturation, the molecular structure of **51** was determined as tetracyclic.

Comparison of the spectroscopic and physical characteristics of metabolite **51** with those reported in the literature led to its identification as 24-methyl-cholesta-5,24(28)-dien-3*β*,7*β*-diol, previously isolated from the sponge *Stelodoryx chlorophylla* (de Riccardis et al., 1993). The ^{1}H NMR data of metabolite **51** are reported in Table 185.

Table 185. ^{1}H NMR data of metabolite **51** in $CDCl_3$ (δ in ppm, J in Hz).

Position	$\delta_{H,exp}$	$\delta_{H,lit}$
3	3.53 (m)	3.56 (m)
6	5.27 (t, 1.8)	5.30 (t, 1.5)
7	3.83 (m)	3.86 (td, 7.8)
18	0.67 (s)	0.70 (s)
19	1.03 (s)	1.06 (s)
21	0.93 (d, 6.6)	0.96 (d, 7.0)
26	1.01 (d, 6.8)	1.04 (d, 6.8)
27	1.03 (d, 6.8)	1.06 (d, 6.8)
28	4.69 (brs), 4.63 (brs)	4.71 (brs), 4.66 (brs)

3.3.19 Metabolite 52

Metabolite **52** (SP03) was isolated after a series of chromatographic separations as a colorless oil (42.3 mg).

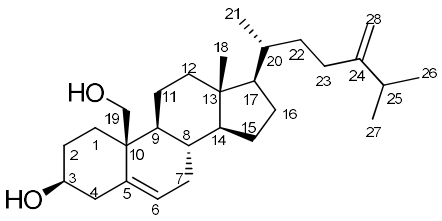

The mass spectrum of metabolite **52** (Figure 198) exhibited a molecular ion peak $[M]^+$ at *m/z* 414.

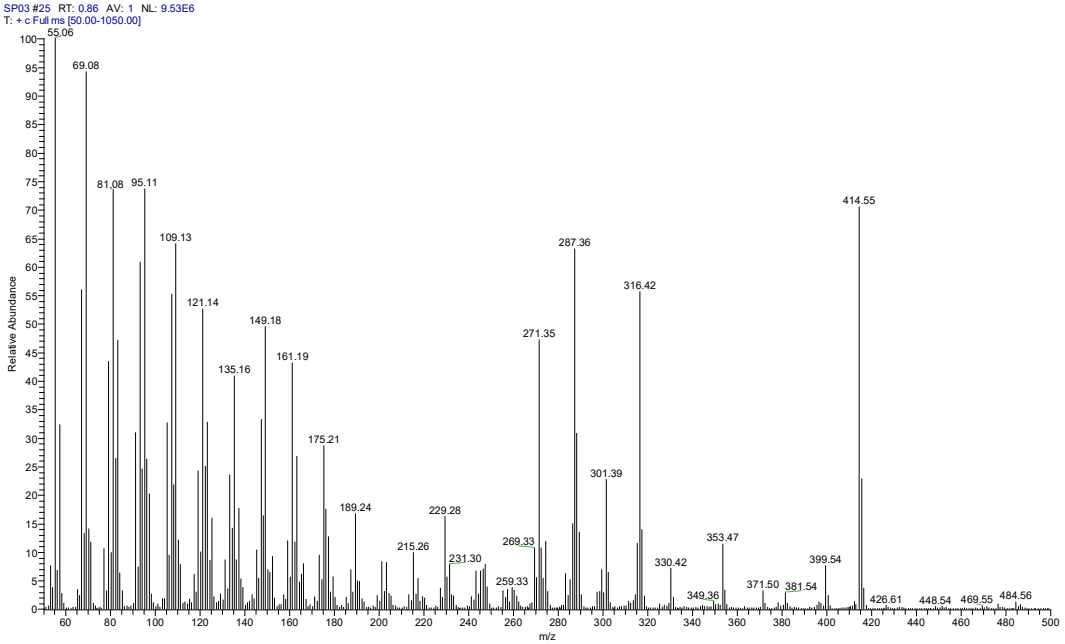

Figure 198. Mass spectrum (EIMS) of metabolite **52**.

In the ^{1}H NMR spectrum of metabolite **52** (Figure 199) obvious were:

- One aliphatic methyl on a non-protonated carbon at δ 0.71,
- Three aliphatic methyls on tertiary carbons at δ 0.92, 0.99 and 1.01,
- Two doublets at δ 3.58 and 3.80 integrating for one proton each and attributed to the protons of a hydroxymethylene,
- One oxygenated methine at δ 3.57,
- Two broad singlets at δ 4.63 and 4.69 integrating for one proton each and attributed to the protons of an exomethylene group, and
- One olefinic methine at δ 5.73.

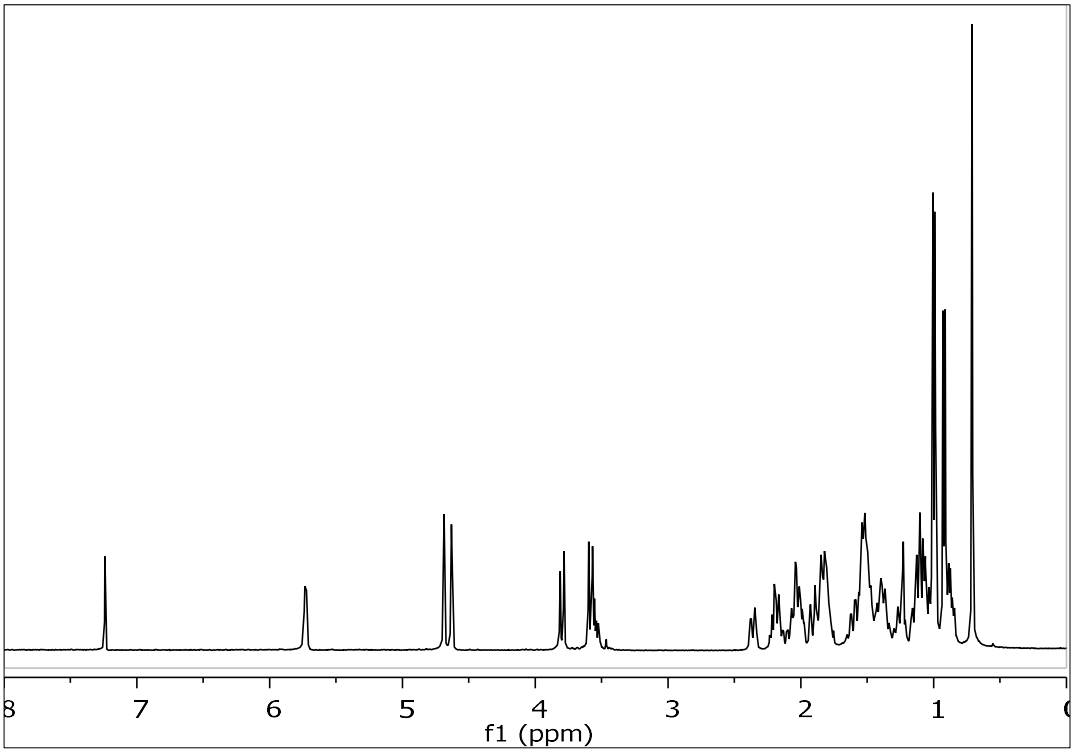

Figure 199. ^{1}H NMR spectrum of metabolite **52**.

Analysis of the NMR and MS data of **52** led to the molecular formula $C_{28}H_{46}O_2$. Taking into account the two carbon-carbon double bonds as two of the six degrees of unsaturation, the molecular structure of **52** was determined as tetracyclic.

Comparison of the spectroscopic and physical characteristics of metabolite **52** with those reported in the literature led to its identification as 24-methyl-cholesta-5,24(28)-dien-3*β*,19-diol, previously isolated from the soft coral *L. viridis* (Iguchi et al., 1989). The ^{1}H NMR data of metabolite **52** are reported in Table 186.

Table 186. ^{1}H NMR data of metabolite **52** in $CDCl_3$ (δ in ppm, J in Hz).

Position	$\delta_{H,exp}$	$\delta_{H,lit}$
3	3.57 (m)	3.59 (d, 11.2)
6	5.73 (m)	5.75 (brd, 4.0)
18	0.71 (s)	0.73 (s)
19	3.80 (d, 11.4), 3.58 (d, 11.4)	3.8 (d, 11.2), 3.56 (m)
21	0.92 (d, 6.5)	0.94 (d, 6.6)
26	1.01 (d, 6.8)	1.02 (d, 6.6)
27	0.99 (d, 6.8)	1.02 (d, 6.6)
28	4.69 (brs), 4.63 (brs)	4.70 (brs), 4.65 (brs)

3.3.20 Metabolite 53

Metabolite **53** (SP29) was isolated after a series of chromatographic separations as a white amorphous solid (2.0 mg).

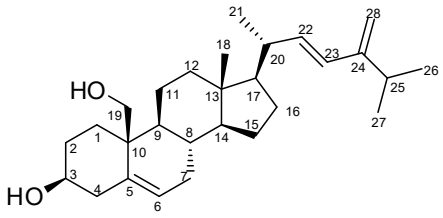

The high-resolution mass spectrum of the metabolite **53** (Figure 200) showed a pseudomolecular ion peak at *m/z* 411.3271 corresponding to $[M-H]^-$ (calcd. for $C_{28}H_{43}O_2$, 411.3269).

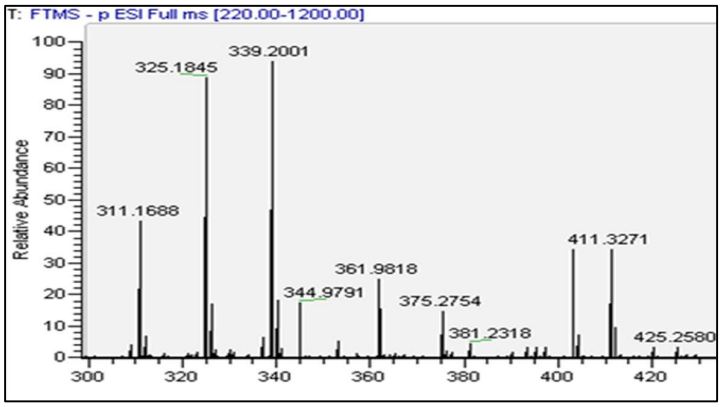

Figure 200. Mass spectrum (HR-ESIMS) of metabolite **53**.

In the ^{1}H NMR spectrum of metabolite **53** (Figure 201) obvious were:

- One aliphatic methyl on a non-protonated carbon at δ 0.75,
- Three aliphatic methyls on tertiary carbons at δ 1.03, 1.04 and 1.06,
- Two doublets at δ 3.59 and 3.81 integrating for one proton each and attributed to the protons of a hydroxymethylene,
- One oxygenated methine at δ 3.56,
- Two broad singlets at δ 4.79 and 4.83 integrating for one proton each and attributed to the protons of an exomethylene group,
- Three olefinic methines at δ 5.56, 5.73 and 5.92.

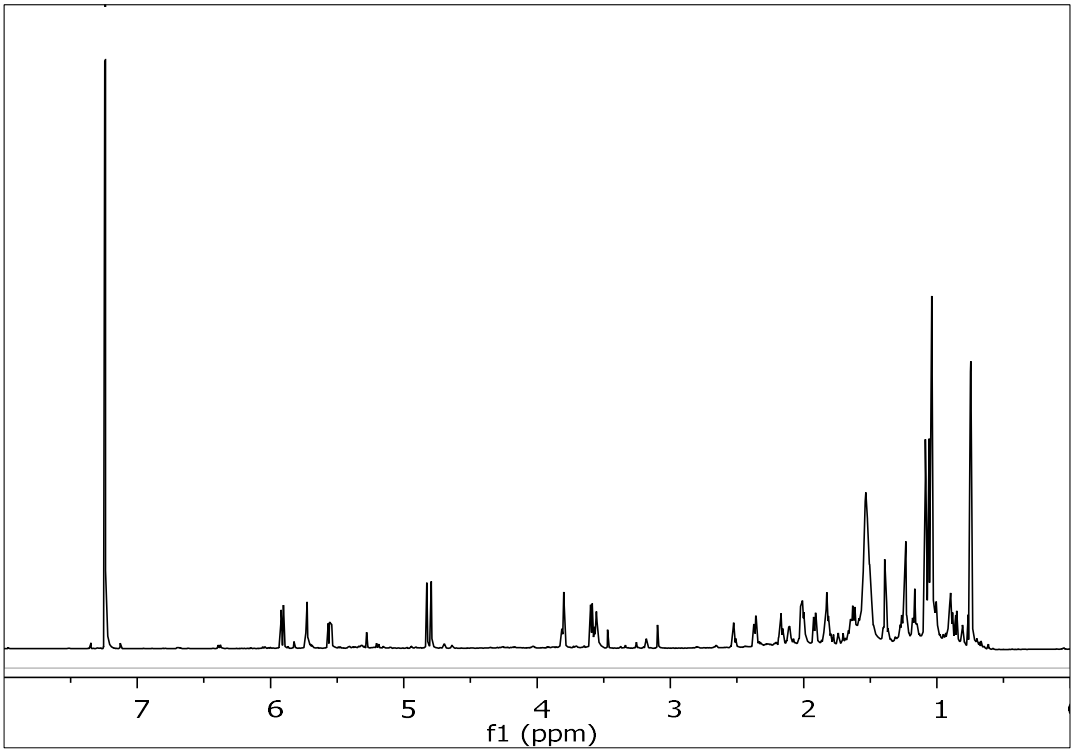

Figure 201. ^{1}H NMR spectrum of metabolite **53**.

Analysis of the NMR and MS data of **53** led to the molecular formula $C_{28}H_{44}O_2$. Taking into account the three carbon-carbon double bonds as three of the seven degrees of unsaturation, the molecular structure of **53** was determined as tetracyclic.

The spectroscopic data of **53** closely resembled those of the co-occurring **52**, with the main difference being the presence of an additional 1,2-disubstituted double bond in the side chain of **53**. The planar structure of metabolite **53** was determined on the basis of the homonuclear and heteronuclear correlations (Figure 202) observed in the HSQC-DEPT (Figure 203), HMBC (Figure 204) and COSY (Figure 205) spectra.

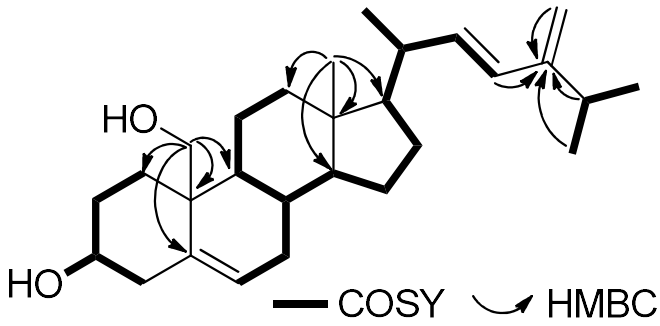

Figure 202. COSY and important HMBC correlations observed for metabolite **53**.

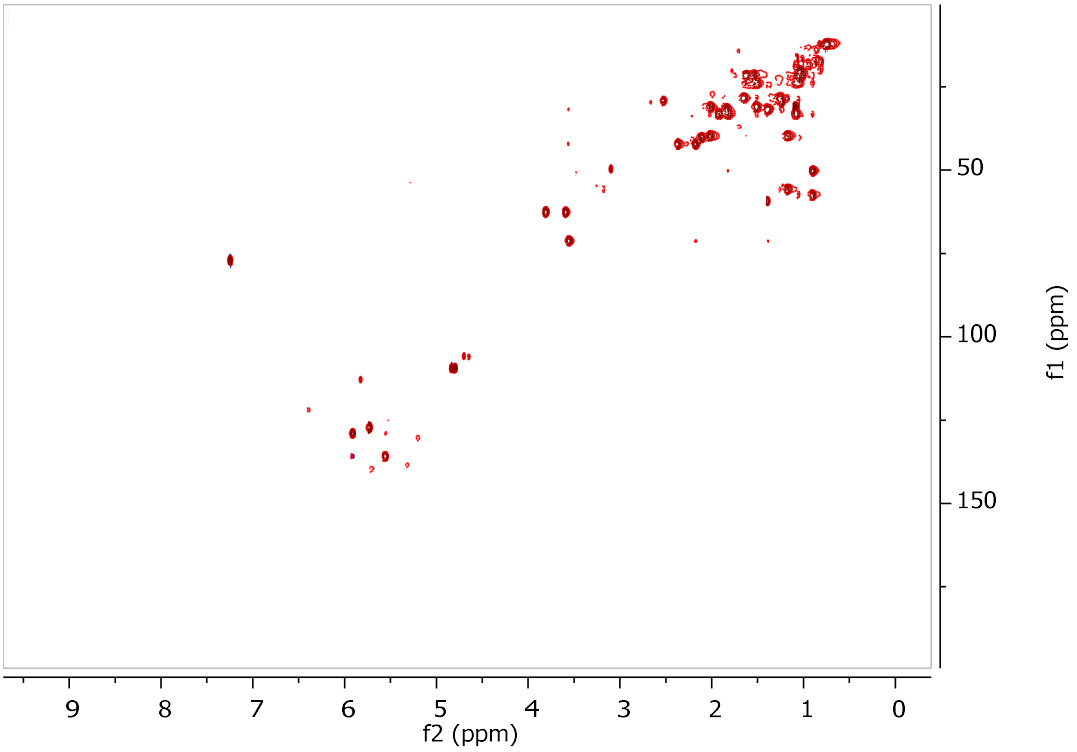

Figure 203. HSQC-DEPT spectrum of metabolite **53**.

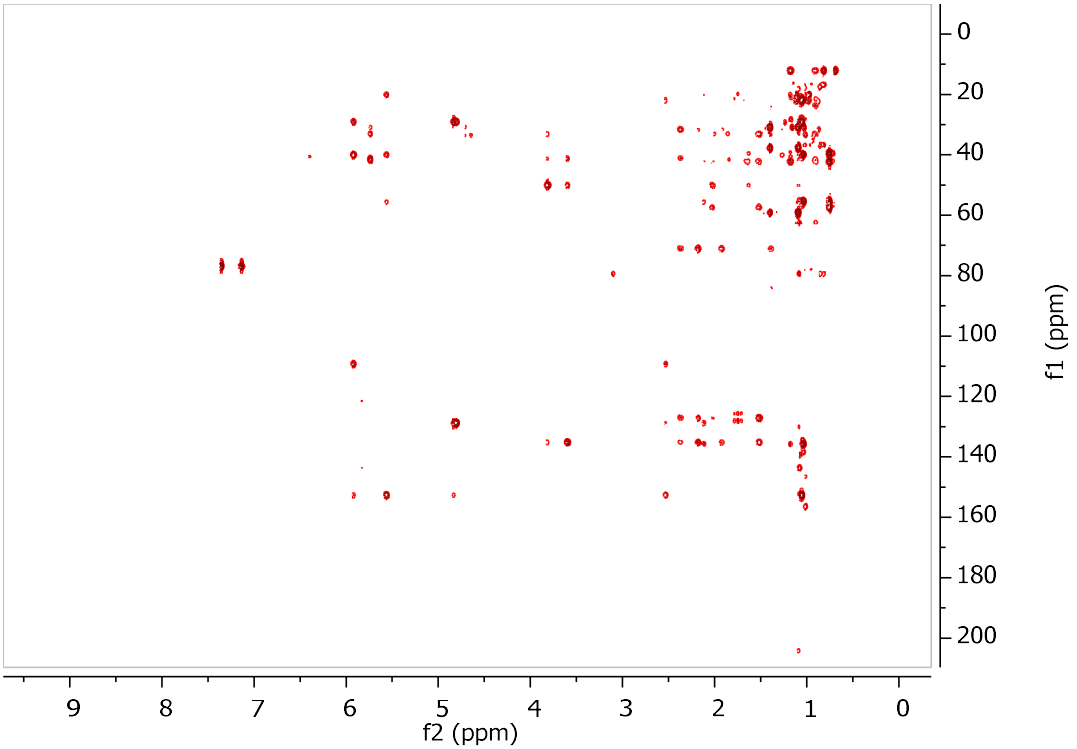

Figure 204. HMBC spectrum of metabolite **53**.

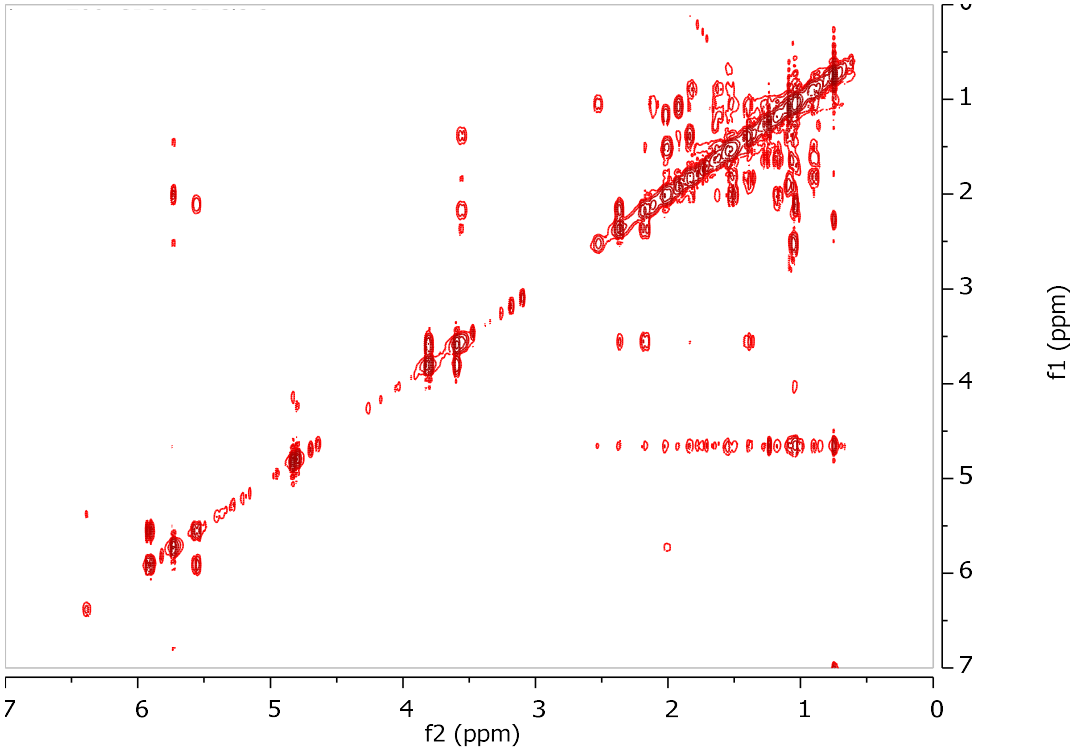

Figure 205. COSY spectrum of metabolite **53**.

The relative configuration of the asymmetric centers of metabolite **53** was determined on the basis of the correlations observed in the NOESY spectrum (Figure 206), in accordance to that of metabolite **52**. The *E* geometry of the Δ^{22} double bond was assigned on the basis of the measured coupling constant between H-22 with H-23 (J = 15.7 Hz).

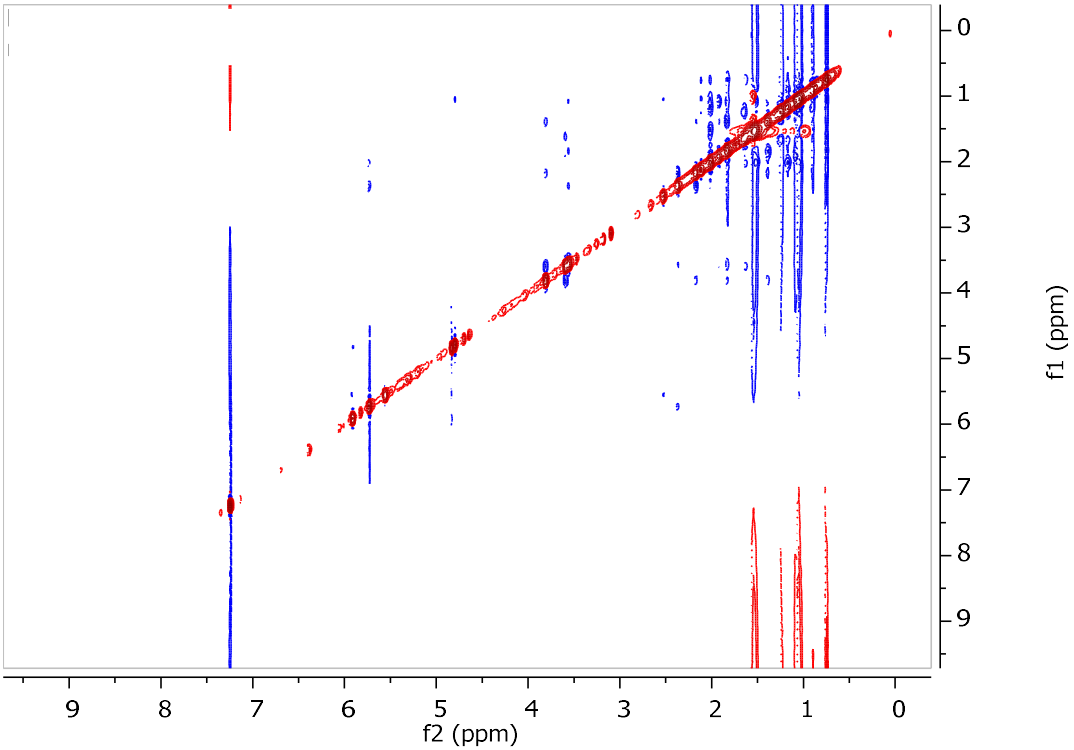

Figure 206. NOESY spectrum of metabolite **53**.

Comparison of the spectroscopic and physical characteristics of metabolite **53** with those reported in the literature led to its identification as a new natural product, which was designated as (22*E*)-24-methyl-cholesta-5,22,24(28)-trien-3β,19-diol. The NMR data of metabolite **53** are reported in Table 187.

Table 187. ^{1}H and ^{13}C NMR data of metabolite **53** in $CDCl_3$ (δ in ppm, J in Hz).

Position	δ_C	δ_H
1	32.9	1.91 (m), 1.08 (m)
2	31.7	1.84 (m), 1.40 (m)
3	70.8	3.56 (m)
4	41.9	2.37 (m), 2.18 (m)
5	134.9	-
6	126.8	5.73 (m)
7	30.8	2.01 (m), 1.51 (m)
8	33.4	1.82 (m)
9	49.9	0.89 (m)
10	41.0	-
11	21.4	1.62 (m), 1.53 (m)
12	39.6	2.01 (m), 1.17 (m)
13	42.3	-
14	57.5	0.90 (m)
15	24.1	1.50 (m), 1.05 (m)
16	28.1	1.64 (m), 1.26 (m)
17	55.4	1.18 (m)
18	12.0	0.75 (s)
19	62.3	3.81 (d, 11.5), 3.59 (d, 11.5)
20	39.9	2.11 (m)
21	20.2	1.03 (d, 6.5)
22	135.4	5.56 (dd, 15.7, 8.7)
23	128.8	5.92 (d, 15.7)
24	153.0	-
25	28.8	2.53 (septet, 6.8)
26	21.7	1.06 (d, 6.8)
27	22.1	1.04 (d, 6.8)
28	109.0	4.83 (brs), 4.79 (brs)

3.3.21 Metabolite 54

Metabolite **54** (SP19) was isolated after a series of chromatographic separations as a colorless oil (2.3 mg).

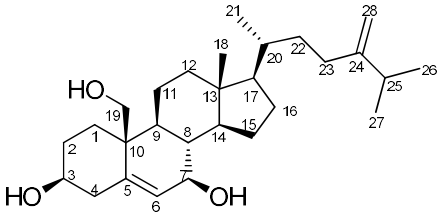

The mass spectrum of metabolite **54** (Figure 207) exhibited a fragment ion peak at *m/z* 412 corresponding to $[M\text{-}H_2O]^+$.

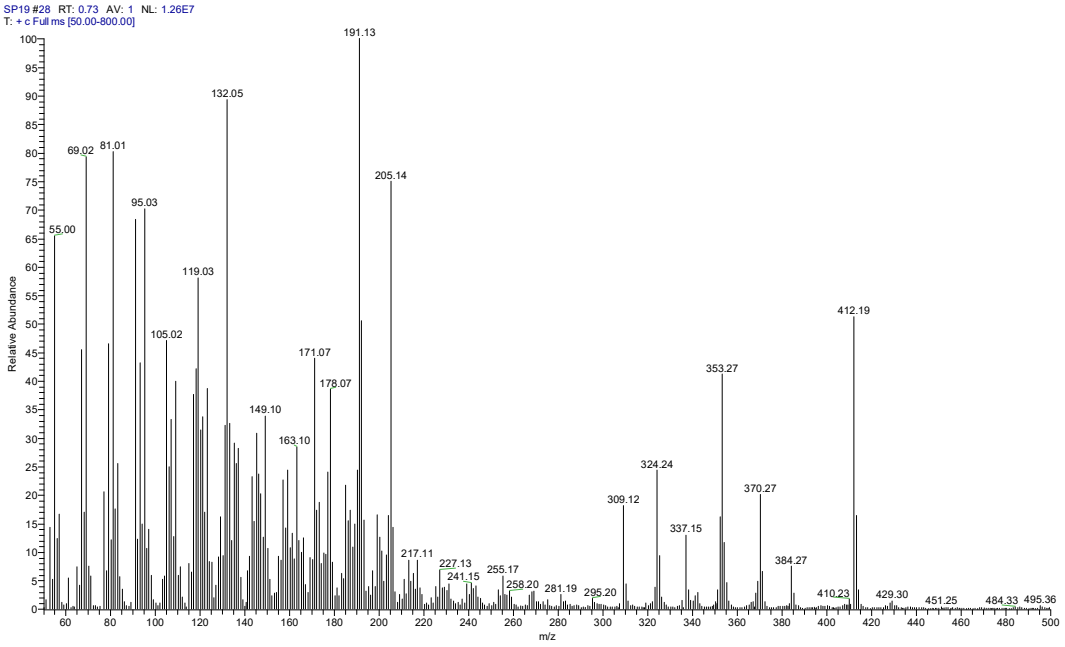

Figure 207. Mass spectrum (EIMS) of metabolite **54**.

In the ^{1}H NMR spectrum of metabolite **54** (Figure 208) obvious were:

- One aliphatic methyl on a non-protonated carbon at δ 0.73,
- Three aliphatic methyls on tertiary carbons at δ 0.93, 0.99 and 1.01,
- Two doublets at δ 3.61 and 3.81 integrating for one proton each and attributed to the protons of a hydroxymethylene,
- Two oxygenated methines at δ 3.56 and 3.84,
- Two broad singlets at δ 4.63 and 4.69 integrating for one proton each and attributed to the protons of an exomethylene group, and
- One olefinic methine at δ 5.64.

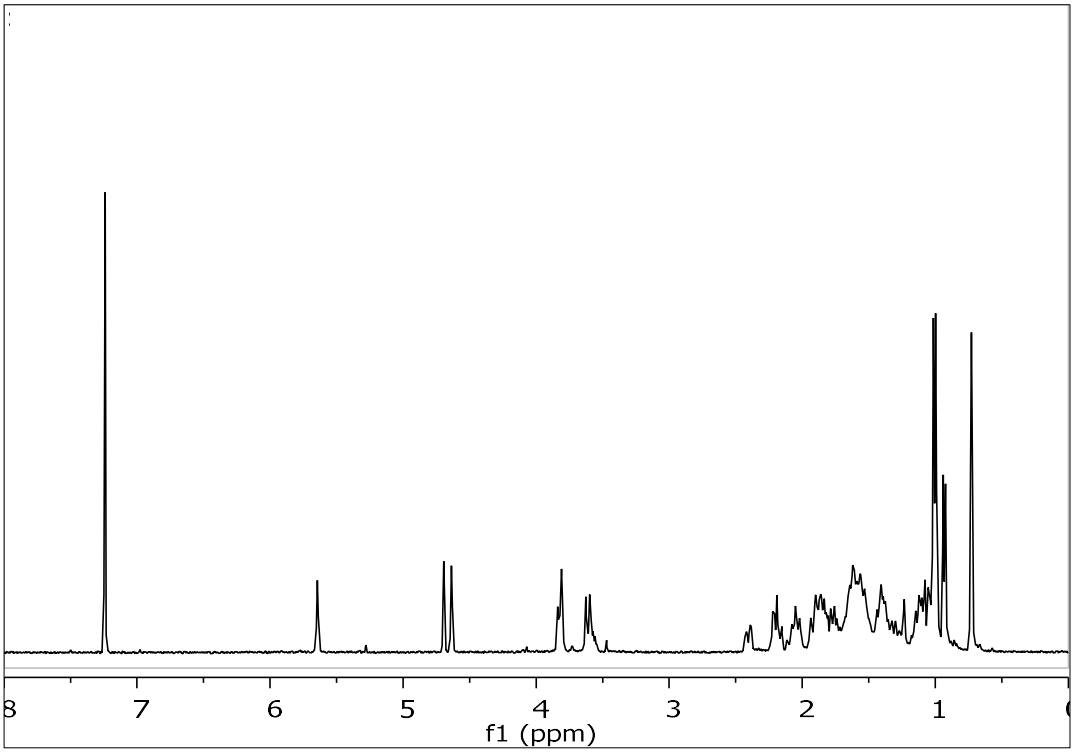

Figure 208. ^{1}H NMR spectrum of metabolite **54**.

Analysis of the NMR and MS data of **54** led to the molecular formula $C_{28}H_{46}O_3$. Taking into account the two carbon-carbon double bonds as two of the six degrees of unsaturation, the molecular structure of **54** was determined as tetracyclic.

Comparison of the spectroscopic and physical characteristics of metabolite **54** with those reported in the literature led to its identification as 24-methyl-cholesta-5,24(28)-dien-3*β*,7*β*,19-triol, previously isolated from the soft coral *Nephthea erecta* (Cheng et al., 2007). The ^{1}H NMR data of metabolite **54** are reported in Table 188.

Table 188. ^{1}H NMR data of metabolite **54** in $CDCl_3$ and CD_3OD (δ in ppm, J in Hz).

Position	$\delta_{H,exp}$ (in $CDCl_3$)	$\delta_{H,lit}$ (in CD_3OD)
3	3.56 (m)	3.53 (m)
6	5.64 (s)	5.79 (d, 4.5)
7	3.84 (m)	3.79 (t, 4.5)
18	0.73 (s)	0.77 (s)
19	3.81 (d, 11.5), 3.61 (d, 11.5)	3.87 (d, 11.5), 3.58 (d, 11.5)
21	0.93 (d, 6.5)	0.98 (d, 6.5)
26	1.01 (d, 6.8)	1.02 (d, 6.5)
27	0.99 (d, 6.8)	1.03 (d, 6.5)
28	4.69 (brs), 4.63 (brs)	4.69 (s), 4.65 (s)

3.3.22 Metabolite 55

Metabolite **55** (SP01) was isolated after a series of chromatographic separations as a colorless oil (155.4 mg).

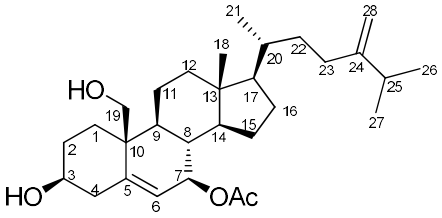

The mass spectrum of metabolite **55** (Figure 209) exhibited a fragment ion peak at *m/z* 412 corresponding to $[M\text{-}AcOH]^+$.

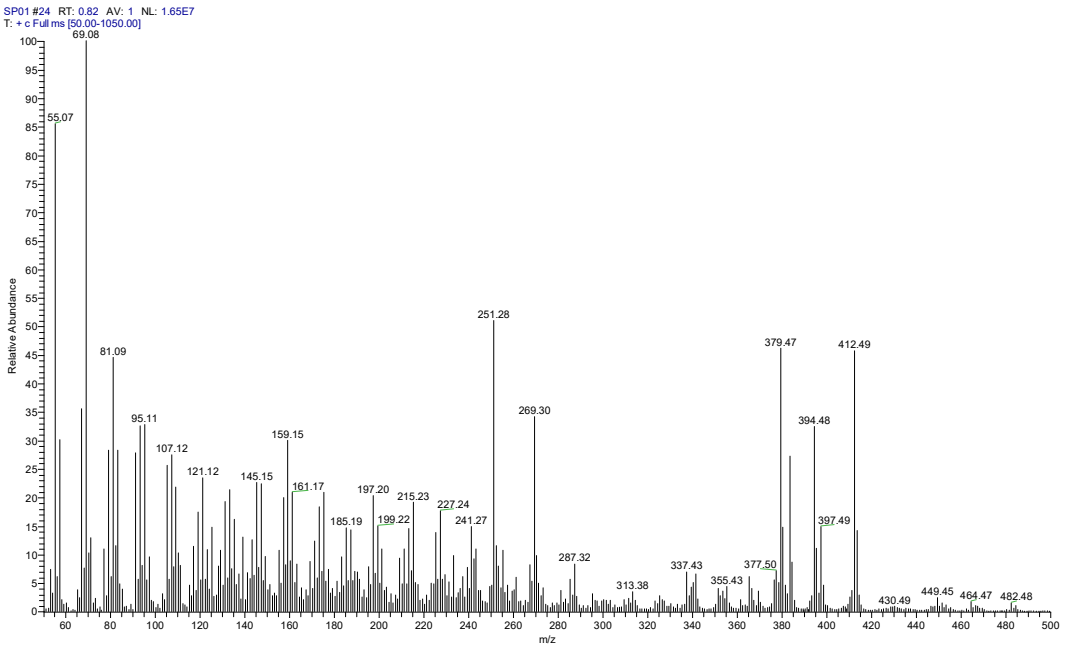

Figure 209. Mass spectrum (EIMS) of metabolite **55**.

In the ^{1}H NMR spectrum of metabolite **55** (Figure 210) obvious were:

- One aliphatic methyl on a non-protonated carbon at δ 0.73,
- Three aliphatic methyls on tertiary carbons at δ 0.93, 0.99 and 1.00,
- One methyl of an acetoxy group at δ 2.01,
- Two doublets at δ 3.64 and 3.86 integrating for one proton each and attributed to the protons of a hydroxymethylene,
- Two oxygenated methines at δ 3.57 and 4.95,
- Two broad singlets at δ 4.63 and 4.69 integrating for one proton each and attributed to the protons of an exomethylene group, and
- One olefinic methine at δ 5.56.

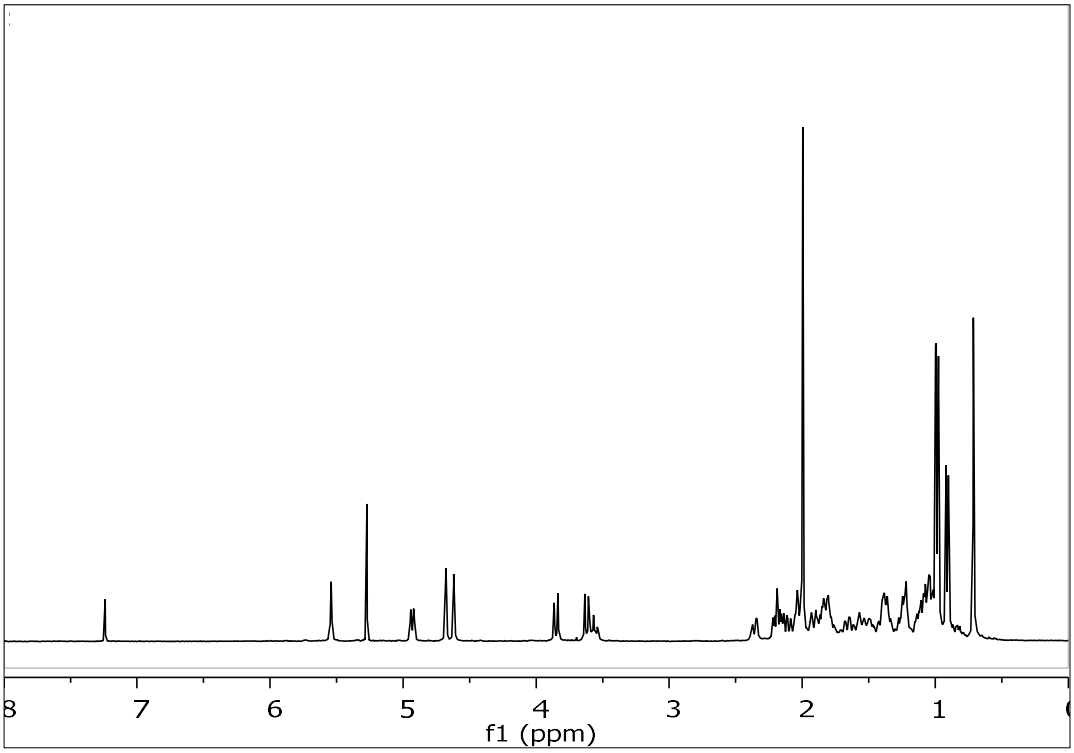

Figure 210. ^{1}H NMR spectrum of metabolite **55**.

Analysis of the NMR and MS data of **55** led to the molecular formula $C_{30}H_{48}O_4$. Taking into account the two carbon-carbon double bonds and the carbonyl moiety as three of the seven degrees of unsaturation, the molecular structure of **55** was determined as tetracyclic.

Comparison of the spectroscopic and physical characteristics of metabolite **55** with those reported in the literature led to its identification as 7*β*-acetoxy-24-methyl-cholesta-5,24(28)-dien-3*β*,19-diol, previously isolated from the soft coral *Litophyton arboretum* (Ellithey et al., 2013). The ^{1}H NMR data of metabolite **55** are reported in Table 189.

Table 189. ^{1}H NMR data of metabolite **55** in $CDCl_3$ (δ in ppm, J in Hz).

Position	$\delta_{H,exp}$	$\delta_{H,lit}$
3	3.57 (m)	3.59 (tt, 11.2, 4.7)
6	5.56 (s)	5.56 (t, 2)
7	4.95 (d, 8.6)	4.95 (d, 8.6)
18	0.73 (s)	0.73 (s)
19	3.86 (d, 11.5), 3.64 (d, 11.5)	3.86 (d, 11.5), 3.64 (d, 11.5)
21	0.93 (d, 6.5)	0.93 (d, 6.8)
26	1.00 (d, 6.8)	1.01 (d, 6.8)
27	0.99 (d, 6.8)	1.00 (d, 6.8)
28	4.69 (brs), 4.63 (brs)	4.70 (t, 1.3), 4.64 (dd, 1.3, 1.7)
OAc	2.01 (s)	2.01 (s)

3.3.23 Metabolite 56

Metabolite **56** (SP06) was isolated after a series of chromatographic separations as a colorless oil (1.6 mg).

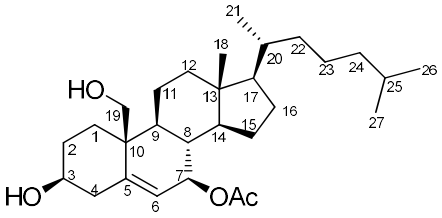

The mass spectrum of metabolite **56** (Figure 211) exhibited a molecular ion peak $[M]^+$ at *m/z* 460.

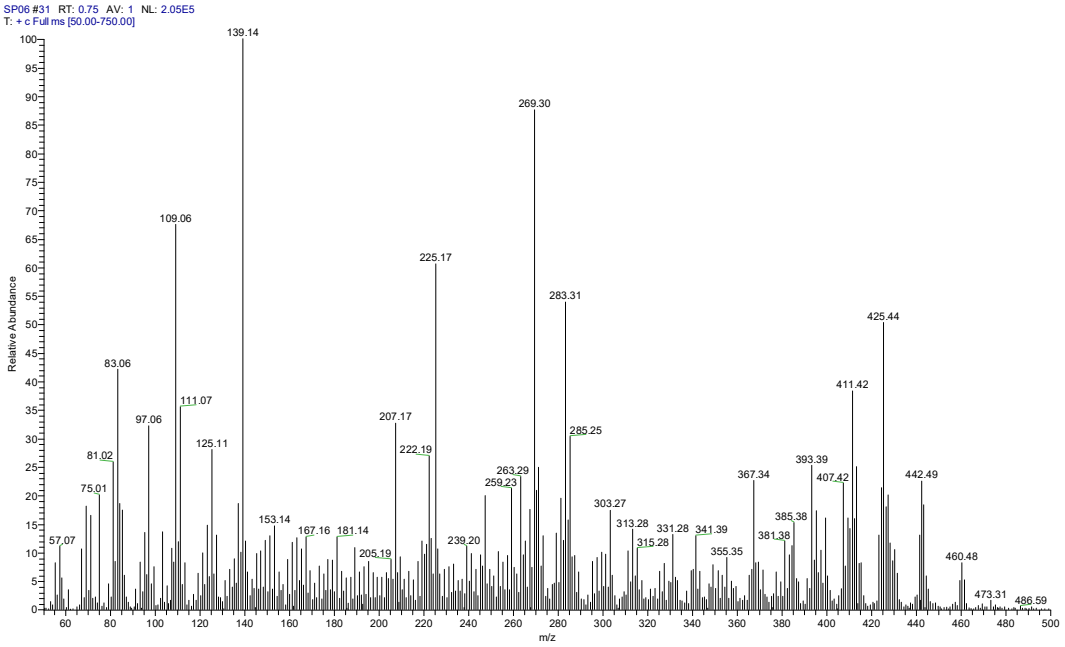

Figure 211. Mass spectrum (EIMS) of metabolite **56**.

In the ^{1}H NMR spectrum of metabolite **56** (Figure 212) obvious were:

- One aliphatic methyl on a non-protonated carbon at δ 0.74,
- Three aliphatic methyls on tertiary carbons at δ 0.84, 0.84 and 0.89,
- One methyl of an acetoxy group at δ 2.01,
- Two doublets at δ 3.64 and 3.86 integrating for one proton each and attributed to the protons of a hydroxymethylene,
- Two oxygenated methines at δ 3.58 and 4.94, and
- One olefinic methine at δ 5.56.

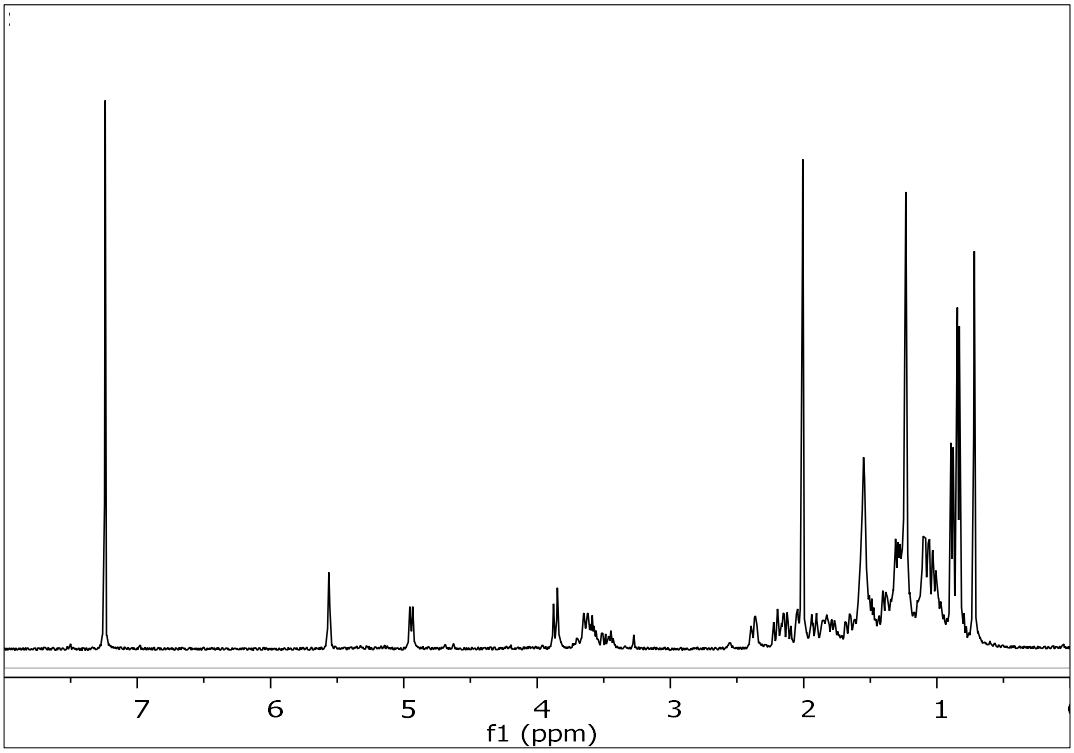

Figure 212. ^{1}H NMR spectrum of metabolite **56**.

Analysis of the NMR and MS data of **56** led to the molecular formula $C_{29}H_{48}O_4$. Taking into account the one carbon-carbon double bond and the carbonyl moiety as two of the six degrees of unsaturation, the molecular structure of **56** was determined as tetracyclic.

Comparison of the spectroscopic and physical characteristics of metabolite **56** with those reported in the literature led to its identification as 7*β*-acetoxy-cholest-5-en-3*β*,19-diol, previously isolated from the soft coral *N. erecta* (Cheng et al., 2007). The ^{1}H NMR data of metabolite **56** are reported in Table 190.

Table 190. ^{1}H NMR data of metabolite **56** in $CDCl_3$ (δ in ppm, J in Hz).

Position	$\delta_{H,exp}$	$\delta_{H,lit}$
1	1.06 (d, 4.1), 1.92 (m)	1.06 (m), 1.92 (m)
2	1.84 (m), 1.38 (m)	1.84 (m), 1.38 (m)
3	3.58 (m)	3.60 (m)
4	2.38 (ddd, 13.4, 4.6, 2.1), 2.21 (m)	2.38 (m), 2.21 (m)
6	5.56 (s)	5.58 (brs)
7	4.94 (d, 8.6)	4.96 (brd, 8.6)
8	2.15 (m)	2.14 (m)
9	1.09 (m)	1.08 (m)
11	1.67 (m), 1.58 (m)	1.66 (m), 1.58 (m)
12	1.29 (m), 2.07 (m)	1.27 (m), 2.07 (m)
14	1.02 (m)	1.02 (m)
15	1.31 (m), 1.10 (m)	1.31 (m), 1.09 (m)
16	1.41 (m), 1.26 (m)	1.40 (m), 1.26 (m)
17	1.03 (m)	1.03 (m)
18	0.74 (s)	0.72 (s)
19	3.86 (d, 11.5), 3.64 (d, 11.5)	3.89 (d, 11.5), 3.66 (d, 11.5)
20	1.34 (m)	1.34 (m)
21	0.89 (d, 6.5)	0.91 (d, 6.4)
22	1.03 (m)	1.03 (m)
23	1.76 (m), 1.23 (m)	1.79 (m), 1.23 (m)
24	1.14 (m)	1.13 (m)
25	1.50 (m)	1.50 (m)
26	0.84 (d, 6.6)	0.86 (d, 6.6)
27	0.84 (d, 6.6)	0.86 (d, 6.6)
OAc	2.01 (s)	2.01 (s)

3.3.24 Metabolite 57

Metabolite **57** (SP07) was isolated after a series of chromatographic separations as a colorless oil (6.9 mg).

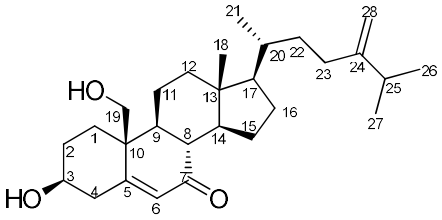

The mass spectrum of metabolite **57** (Figure 213) exhibited a molecular ion peak $[M]^+$ at *m/z* 428.

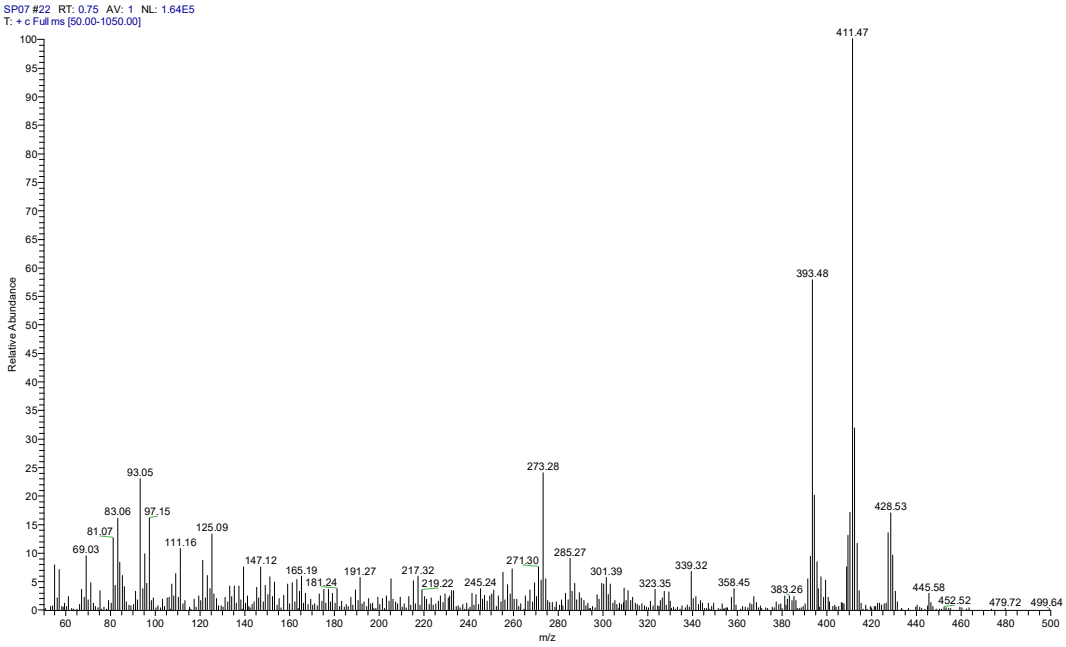

Figure 213. Mass spectrum (EIMS) of metabolite **57**.

In the ^{1}H NMR spectrum of metabolite **57** (Figure 214) obvious were:

- One aliphatic methyl on a non-protonated carbon at δ 0.71,
- Three aliphatic methyls on tertiary carbons at δ 0.93, 1.00 and 1.00,
- Two doublets at δ 3.64 and 4.01 integrating for one proton each and attributed to the protons of a hydroxymethylene,
- One oxygenated methine at δ 3.70,
- Two broad singlets at δ 4.63 and 4.69 integrating for one proton each and attributed to the protons of an exomethylene group, and
- One olefinic methine at δ 5.90.

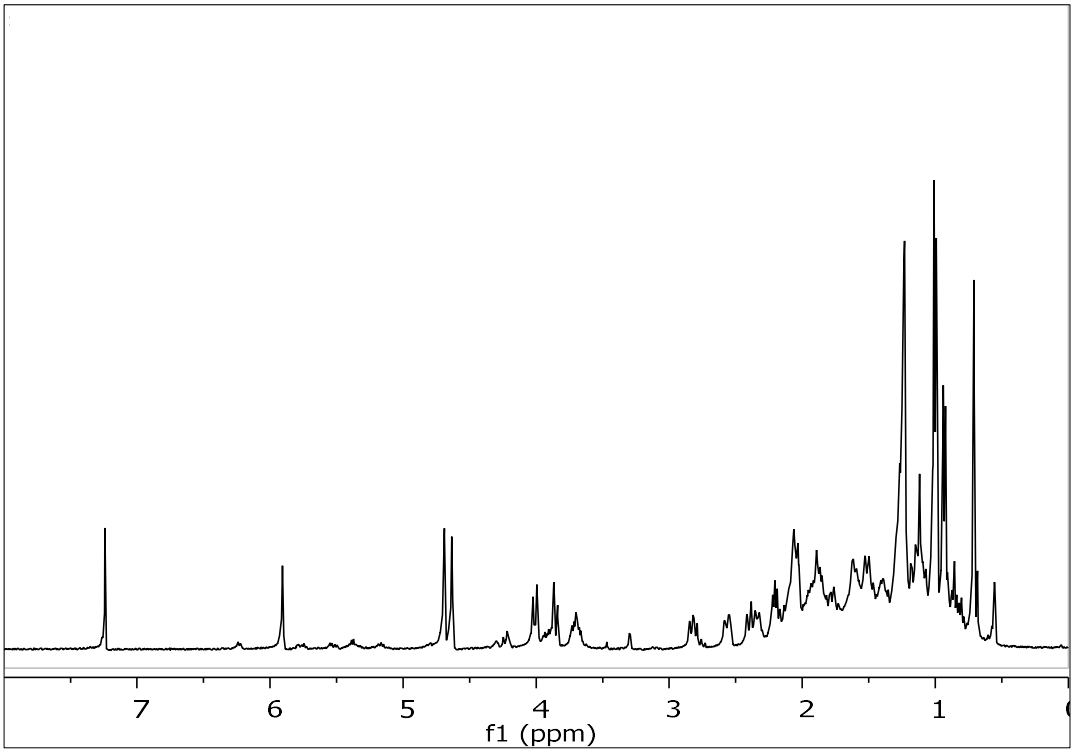

Figure 214. ^{1}H NMR spectrum of metabolite **57**.

Analysis of the NMR and MS data of **57** led to the molecular formula $C_{28}H_{44}O_3$. Taking into account the two carbon-carbon double bonds and the carbonyl moiety as three of the seven degrees of unsaturation, the molecular structure of **57** was determined as tetracyclic.

Comparison of the spectroscopic and physical characteristics of metabolite **57** with those reported in the literature led to its identification as 7-oxo-24-methyl-cholesta-5,24(28)-diene-3*β*,19-diol, previously isolated from the soft coral *N. erecta* (Duh et al., 1998). The NMR data of metabolite **57** are reported in Table 191.

Table 191. ^{1}H and ^{13}C NMR data of metabolite **57** in $CDCl_3$ and CD_3OD (δ in ppm, J in Hz)

Position	$\boldsymbol{\delta_{C,exp}}$	$\boldsymbol{\delta_{H,exp}}$	$\boldsymbol{\delta_{C,lit}}$	$\boldsymbol{\delta_{H,lit}}$
	(in $CDCl_3$)	(in $CDCl_3$)	(in $CDCl_3$)	(in CD_3OD)
1	33.1		33.1	
2	31.6		31.6	
3	70.4	3.70 (m)	70.4	3.73 (m)
4	42.1		42.1	
5	160.0		160.0	
6	129.5	5.90 (s)	129.6	5.93 (s)
7	202.7	-	202.6	-
8	46.9		49.6	
9	50.3		50.3	
10	43.2	-	43.2	-
11	21.9		21.9	
12	39.2		39.2	
13	43.5	-	43.5	-
14	51.3		51.3	
15	26.2		26.1	
16	28.6		28.6	
17	54.7		54.7	
18	12.3	0.71 (s)	12.3	0.73 (s)
19	63.8	4.01 (d, 11.4), 3.64 (d, 11.4)	63.8	4.03 (d, 11.7), 4.03 (d, 11.7)
20	35.7		35.7	
21	18.9	0.93 (d, 6.4)	18.9	0.95 (d, 6.6)
22	34.7		34.7	
23	31.0		31.0	
24	156.8		156.8	
25	33.8		33.8	
26	21.9	1.00 (d, 6.8)	21.9	1.02 (d, 6.6)
27	22.0	1.00 (d, 6.8)	22.0	1.03 (d, 6.9)
28	106.0	4.69 (brs), 4.63 (brs)	106.0	4.71 (brs), 4.66 (brs)

3.3.25 Metabolite 58

Metabolite **58** (SP17) was isolated after a series of chromatographic separations as a colorless oil (6.1 mg).

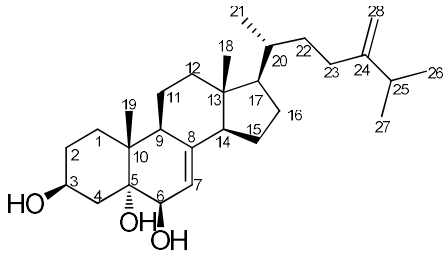

The mass spectrum of metabolite **58** (Figure 215) exhibited fragment ion peaks at *m/z* 412 and 394 corresponding to $[M\text{-}H_2O]^+$ and $[M\text{-}2H_2O]^+$, respectively.

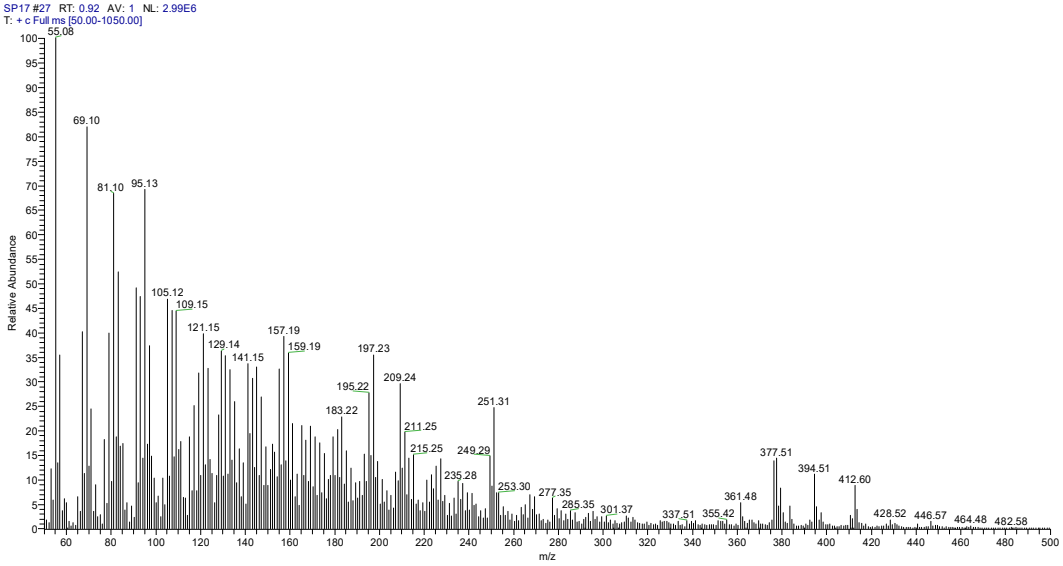

Figure 215. Mass spectrum (EIMS) of metabolite **58**.

In the ^{1}H NMR spectrum of metabolite **58** (Figure 216) obvious were:

- Two aliphatic methyls on non-protonated carbons at δ 0.64 and 1.07,
- Three aliphatic methyls on tertiary carbons at δ 0.99, 1.04 and 1.05,
- Two oxygenated methines at δ 3.55 and 3.97,
- Two broad singlets at δ 4.66 and 4.72 integrating for one proton each and attributed to the protons of an exomethylene group, and
- One olefinic methine at δ 5.27.

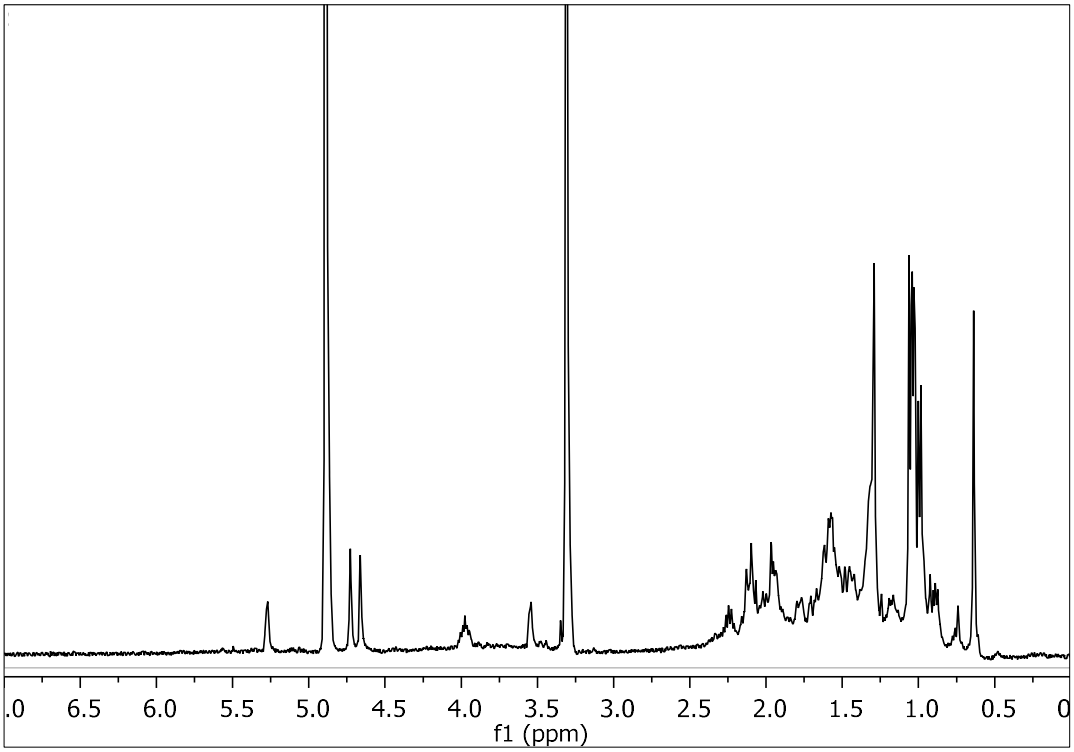

Figure 216. ^{1}H NMR spectrum of metabolite **58** in CD_3OD.

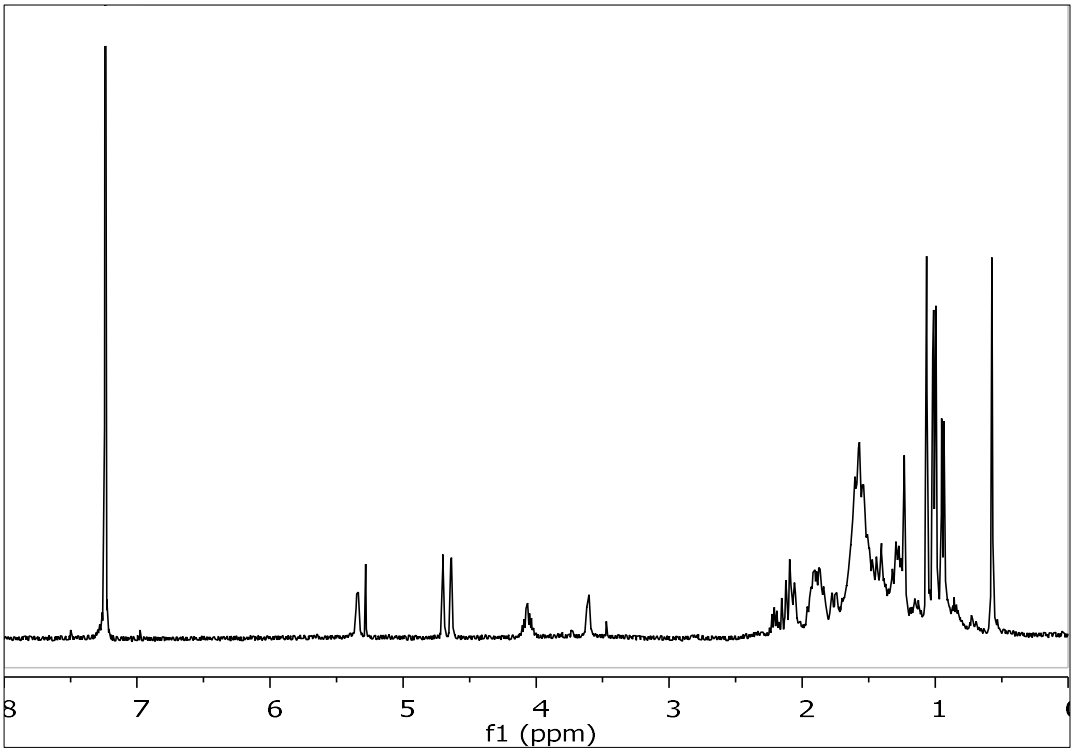

Figure 217. ^{1}H NMR spectrum of metabolite **58** in $CDCl_3$.

Analysis of the NMR and MS data of **58** led to the molecular formula $C_{28}H_{46}O_3$. Taking into account the two carbon-carbon double bonds as two of the six degrees of unsaturation, the molecular structure of **58** was determined as tetracyclic.

Comparison of the spectroscopic and physical characteristics of metabolite **58** with those reported in the literature led to its identification as 24-methyl-cholesta-7,24(28)-dien-3*β*,5*α*,6*β*-triol, previously isolated from the marine scallop *Patinopecten yessoensis* (Iorizzi et al., 1988). The ^{1}H NMR data of metabolite **58** are reported in Table 192.

Table 192. ^{1}H NMR data of metabolite **58** in CD_3OD (δ in ppm, J in Hz)

Position	$\delta_{H,exp}$	$\delta_{H,lit}$
3	3.97 (m)	4.01 (m)
6	3.55 (d, 4.0)	3.57 (brd, 4.0)
7	5.27 (d, 4.8)	5.30 (m)
18	0.64 (s)	0.67 (s)
19	1.07 (s)	1.09 (s)
21	0.99 (d, 6.5)	1.02 (d, 6.8)
26	1.04 (d, 6.8)	1.06 (d, 6.8)
27	1.05 (d, 6.8)	1.07 (d, 6.8)
28	4.72 (brs), 4.66 (brs)	4.76 (brs), 4.68 (brs)

3.3.26 Metabolite 59

Metabolite **59** (SP08) was isolated after a series of chromatographic separations as a colorless oil (2.0 mg).

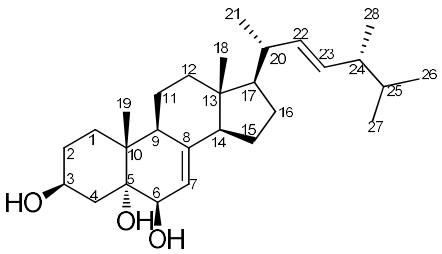

The mass spectrum of metabolite **59** (Figure 218) exhibited fragment ion peaks at *m/z* 412 and 394 corresponding to $[M\text{-}H_2O]^+$ and $[M\text{-}2H_2O]^+$, respectively.

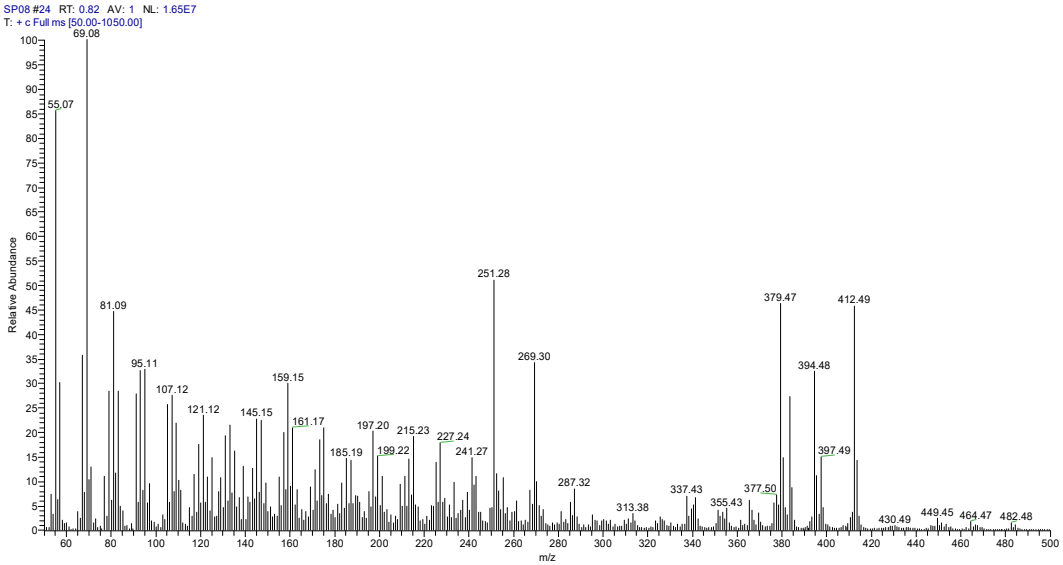

Figure 218. Mass spectrum (EIMS) of metabolite **59**.

In the ^{1}H NMR spectrum of metabolite **59** (Figure 219) obvious were:

- Two aliphatic methyls on non-protonated carbons at δ 0.65 and 1.06,
- Four aliphatic methyls on tertiary carbons at δ 0.84, 0.87, 0.95 and 1.01,
- Two oxygenated methines at δ 3.55 and 4.06,
- One multiplet at δ 5.25-5.30 integrating for three protons and attributed to three olefinic methines.

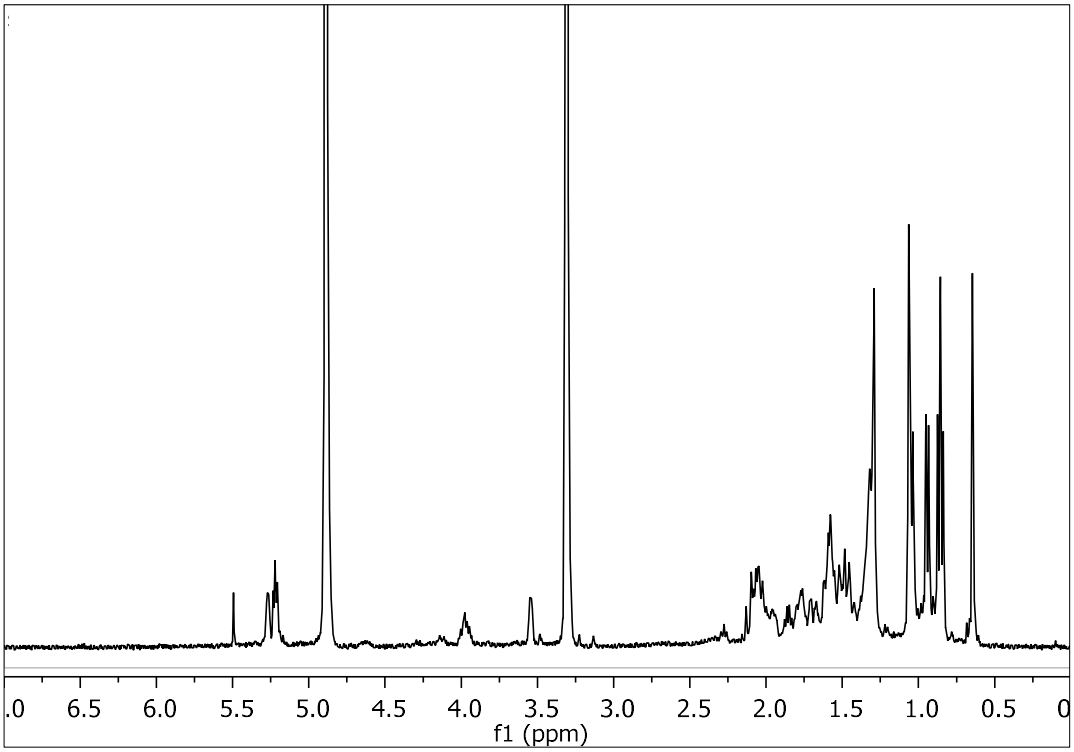

Figure 219. ^{1}H NMR spectrum of metabolite **59** in CD_3OD.

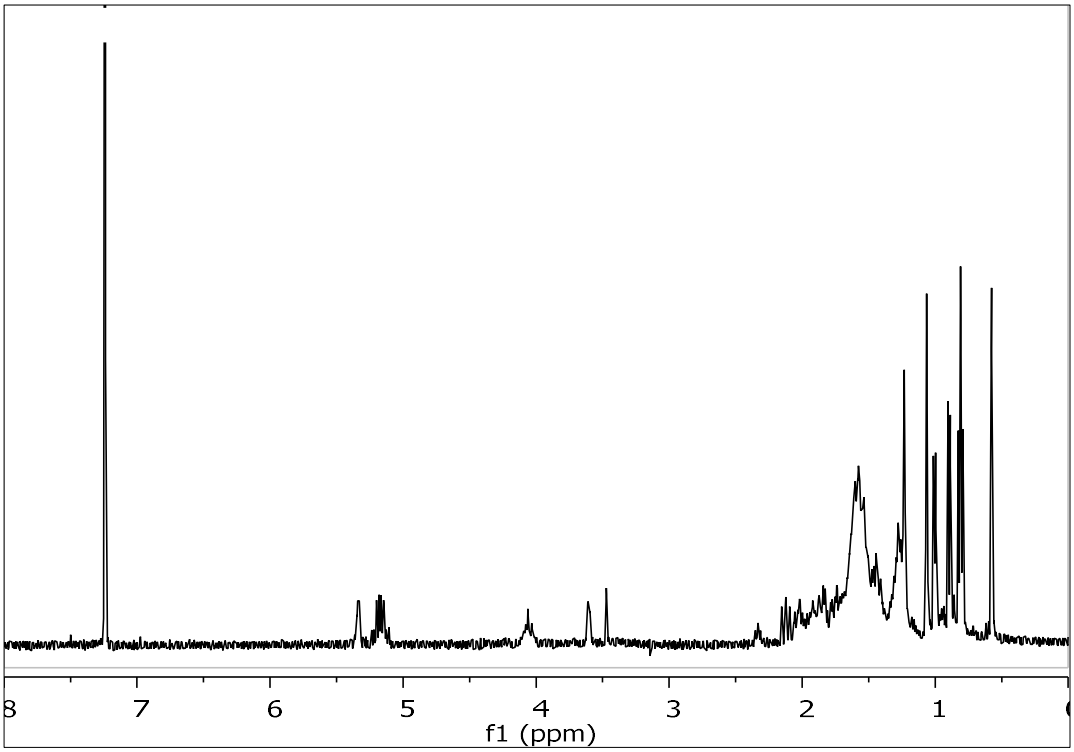

Figure 220. ^{1}H NMR spectrum of metabolite **59** in $CDCl_3$.

Analysis of the NMR and MS data of **59** led to the molecular formula $C_{28}H_{46}O_3$. Taking into account the two carbon-carbon double bonds as two of the six degrees of unsaturation, the molecular structure of **59** was determined as tetracyclic.

Comparison of the spectroscopic and physical characteristics of metabolite **59** with those reported in the literature led to its identification as (22*E*,24*R*)-24-methyl-cholesta-7,22-dien-3*β*,5*α*,6*β*-triol, previously isolated from the marine scallop *P. yessoensis* (Iorizzi et al., 1988). The ^{1}H NMR data of metabolite **59** are reported in Table 193.

Table 193. ^{1}H NMR data of metabolite **59** in CD_3OD (δ in ppm, J in Hz).

Position	$\delta_{H,exp}$	$\delta_{H,lit}$
3	4.06 (m)	4.01 (m)
6	3.55 (d, 4.1)	3.57 (brd, 4.0)
7	5.25-5.30 (m)	5.30 (m)
18	0.65 (s)	0.68 (s)
19	1.06 (s)	1.09 (s)
21	1.01 (d, 6.7)	1.07 (d, 7.0)
22	5.25-5.30 (m)	5.23 (m)
23	5.25-5.30 (m)	5.23 (m)
26	0.84 (d, 6.5)	0.86 (d, 7.0)
27	0.87 (d, 6.5)	0.90 (d, 6.5)
28	0.95 (d, 6.8)	0.96 (d, 7.0)

3.4 Evaluation of the biological activity of isolated compounds

Compounds **36**–**40**, **42**–**45**, **47**–**53** and **55**–**59**, which were isolated in sufficient amounts, were evaluated *in vitro* in human tumor and non-cancerous cell lines for a number of biological activities, including cytotoxicity, anti-inflammatory, anti-angiogenic, and neuroprotective activity, as well as for their effect on androgen receptor (AR)-regulated transcription.

Initially, the cytotoxic activity of metabolites **36**–**40**, **42**–**45**, **47**–**53** and **55**–**59** was evaluated in human cancer and normal cells after 72 h of treatment. Human cervical cancer (HeLa), human breast adenocarcinoma (MCF7) cell lines and human normal fibroblasts (BJ) were used for the screening. Among the tested compounds, **55** and **56** strongly reduced the viability of cancer cells in the low micromolar range (Table 194), compounds **42-45**, **49-49**, **51** and **57** showed moderate cytotoxic activity, while the remaining ten steroids were proven inactive. Most of the compounds with activity against cancer cells also showed cytotoxicity towards normal cells (BJ), except for compounds **44**, **45**, **47**, **48** and **51**. Compared to cisplatin, these compounds exhibit a wide therapeutic window because of the absence of cytotoxicity on normal human fibroblasts. Moreover, metabolite **55** was proven more active against the HeLa cell line than the reference standard cisplatin.

Table 194. Cytotoxicity (IC_{50}; μM) of compounds **36**–**40**, **42**–**45**, **47**–**53** and **55**–**59** against human cancer cell lines and fibroblasts after 72 h of treatment.
Cisplatin was used as a positive control.

Compound	HeLa	MCF7	BJ
36	>50	>50	>50
37	>50	>50	>50
38	>50	>50	>50
39	>50	>50	>50
40	>50	>50	>50
42	25.9 ± 4.9	36.4 ± 5.7	18.3 ± 4.0
43	32.9 ± 6.8	32.7 ± 1.3	4.1 ± 1.9
44	18.8 ± 6.4	21.7 ± 1.4	>50
45	15.7 ± 2.0	25.3 ± 6.5	>50
47	>50	29.1 ± 5.0	>50
48	19.0 ± 4.3	18.9 ± 0.1	>50
49	32.9 ± 5.2	33.8 ± 1.0	23.2 ± 1.4
50	>50	>50	>50
51	22.6 ± 0.4	28.6 ± 5.3	>50
52	>50	>50	>50
53	>50	>50	>50
55	7.5 ± 0.1	8.9 ± 0.0	14.8 ± 5.8
56	12.0 ± 1.7	11.2 ± 0.5	14.5 ± 3.9
57	21.4 ± 2.0	31.7 ± 0.3	45.9 ± 2.8
58	>50	>50	>50
59	>50	>50	>50
cisplatin	11.4 ± 3.8	7.7 ± 1.7	6.9 ± 0.9

Subsequently, we examined whether the isolated steroids could influence angiogenesis or inflammation *in vitro*. Compounds **36**–**40**, **42**–**45**, **47**–**53** and **55**–**59** and 2-methoxy-estradiol, which is known as an anti-angiogenic drug for the treatment of tumors and was used herein as positive control (Sattler et al., 2003) were tested in the migration scratch and the tube formation assays using human umbilical vein endothelial cells (HUVEC). Only non-cytotoxic concentrations in HUVECs were used for the scratch assay. Metabolites **44**, **45**, **55** and **56** partially inhibited HUVEC migration at 20 µM after 20 h of treatment (Figure 221), while in the tube formation assay, where HUVECs may form tube-like structures, no activity was observed for the tested compounds (data not shown). Thus, all tested steroids showed either little or no antiangiogenic activity.

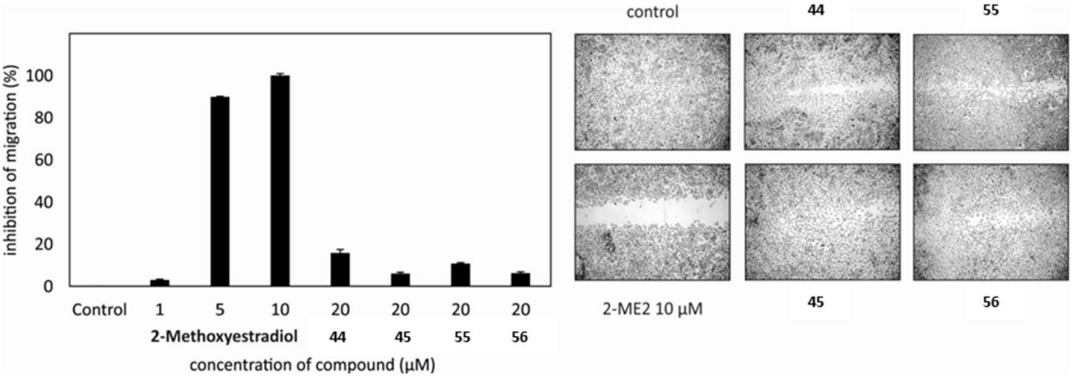

Figure 221. Compounds **44**, **45**, **55** and **56** inhibited migration of HUVECs after 20 h of treatment at 20 µM.
2-Methoxy-estradiol was used as a positive control. The experiment was repeated three times in triplicates.

The anti-inflammatory properties of metabolites **36**–**40**, **42**–**45**, **47**–**53** and **55**–**59** were determined by measuring the levels of endothelial leukocyte adhesion molecule-1 (ELAM/E-selectin), which is a key molecular marker in the initiation of inflammation, expressed on the cell surface. Cell adhesion molecules (ICAM-1, VCAM-1, E-selectin) are significantly increased on the vascular endothelium activated by pro-inflammatory mediators (tumor necrosis factor *α*, TNF*α*) as a crucial step for the extravasation of leukocytes into inflamed tissue (Trepels et al., 2006). TNF*α* stimulates NFκB (nuclear factor kappa-light-chain-enhancer of activated B cells) and thus E-selectin (CD62E, ELAM). Endothelial cells were pre-treated for 30 min with the tested compounds and then activated with TNF*α* for 4 h. Curcumin, which inhibits activation of NF-κB and thus inhibits expression and activity of the COX-2 gene induced by TNF*α* (F. Zhang et al., 1999), was used as a positive control, decreasing ELAM production to 25% at 10 µM. None of the tested compounds decreased the levels of ELAM (Figure 222).

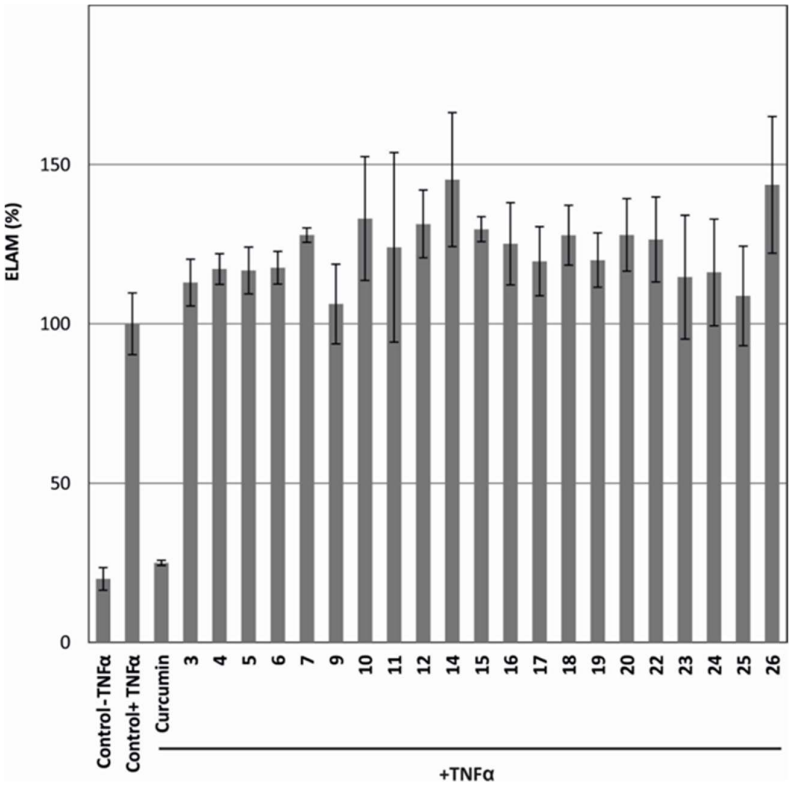

Figure 222. Compounds **36**–**40**, **42**–**45**, **47**–**53** and **55**–**59** did not affect the relative amount of E-selectin on the cell surface of endothelial cells.
Cells were pretreated with 10 μM compounds for 30 min and subsequently stimulated with 10 ng/ml TNFα for 4 h. Data are means ± SDs (*n* = 3).

It has been previously observed that several steroids with bulky or long side chains, such as galeterone derivatives or cholestanes, can also inhibit AR (Jorda et al., 2019; Rárová et al., 2018). Therefore, we further analyzed the influence of the isolated steroids on AR-mediated transcription. Compounds **36**–**40**, **42**–**45**, **47**–**53** and **55**–**59** in six different concentrations were evaluated on the reporter cell line 22Rv1-ARE14 for 24 h. Galeterone and enzalutamide, which were used as positive controls, showed a strong dose-dependent reduction of AR-regulated transcription (22 % and 20% inhibition at 10 μM, respectively). Compounds **44**, **45**, **49** and **53** showed clearly reduced luciferase activity in a dose-dependent manner, already at submicromolar concentrations (Figure 223). The strongest inhibition of AR was displayed by compound **44** at 10 μM. Surprisingly, steroids **43**, **49** and **53** showed increased inhibition of AR (or decreased the luciferase activity) with decreasing concentrations. All other steroids tested inhibited AR by no more than 20% (data not shown).

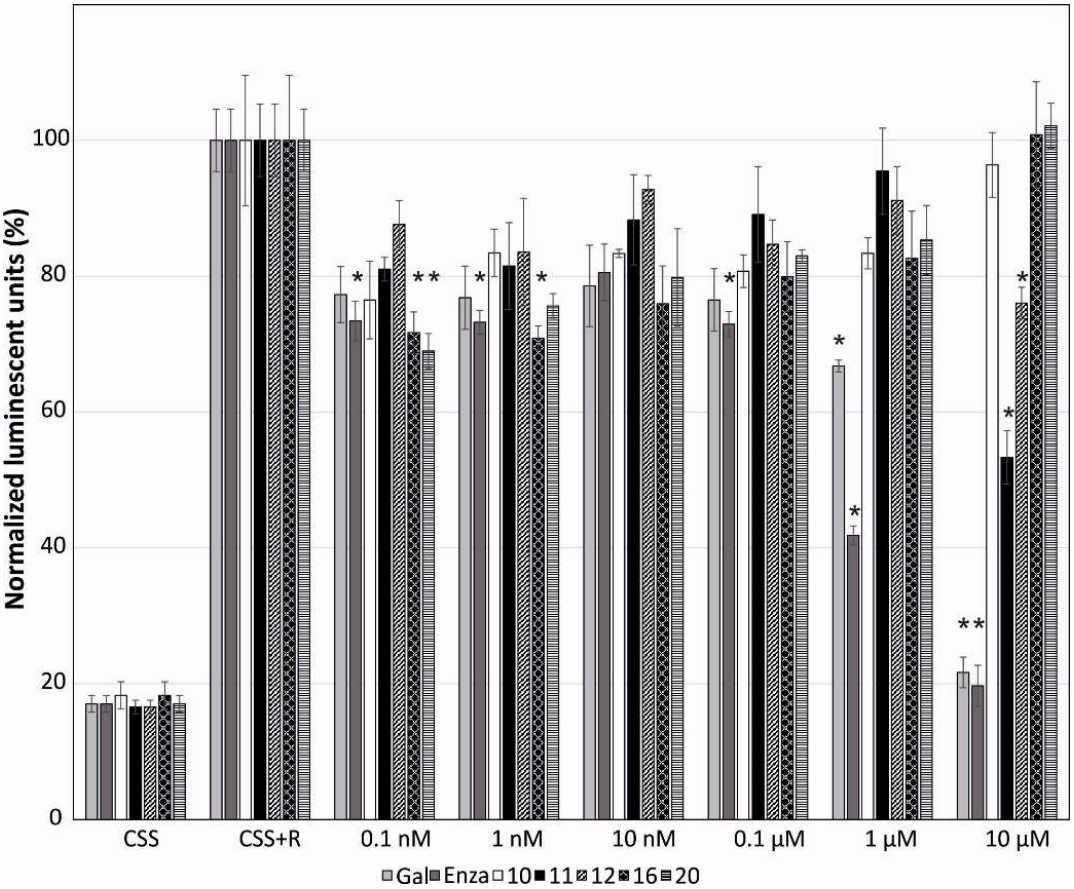

Figure 223. The influence of compounds **43**, **44**, **45**, **49** and **53** on the androgen receptor-mediated transcription in the 22Rv1-ARE14 reporter cell line.

Control cells were grown in charcoal-stripped serum medium (CSS). Cells were stimulated with either 1 nM methyltrienolone R1881 (R) or with the tested compounds in six different concentrations for 24 h in CSS. The luciferase activity was measured in the cell lysate. Enzalutamide (Enza) and galeterone (Gal) were used as positive controls. The experiment was repeated three times in triplicates. Bars with asterisk (*) are significantly different from the control (CSS+R) based on Tukey's multiple comparison test ($P \leq 0.05$).

Since anti-androgens have shown neuroprotective effects in the *in vivo* model of Huntington's disease (Guzman et al., 2014), selected compounds that showed cytotoxic activity and moderate activity in the migration scratch assay were tested for their cytotoxicity on differentiated human SH-SY5Y cells (neuron-like cells). Specifically, based on the combined results obtained for compounds **36–40, 42–45, 47–53** and **55–59** in the cytotoxicity assay, the anti-inflammatory activity assay, the migration scratch assay, and the tube formation assay in HUVECs, as well as in the reporter assay with AR, compounds **44** and **56** were selected as the two most active compounds that were subsequently evaluated for their neuroprotective activity. As shown in Figure 224 (A), compounds **44** and **56**, as well as *N*-acetylcystein (NAC) that was used as a positive control, did not show cytotoxic, but rather stimulatory activity. In order to evaluate the potential neuroprotective effect of the compounds, neuroblastoma cell line SH-SY5Y was differentiated for 48 h and further exposed to 20 mM 3-nitropropionic acid (3-NPA) as an agent mimicking Huntington's disease *in vitro* (Colle et al., 2016). 3-NPA

was used alone or in co-treatment with the tested compounds at concentrations of 0.1–10 µM. As shown in Figure 224 (B), 3-NPA caused dramatic (approx. 70%) decrease in cell viability determined by the Calcein AM assay. The positive control (NAC) showed partial (cell viability 77.9 ± 8.99 % at 100 µM) or almost complete (cell viability 90.2 ± 5.28 % at 1000 µM) protection of cells from the negative effect of 3-NPA. Compounds **44** and **56** showed significant protective effects at 10 µM (cell viability 64.4 ± 6.02% for **44** and 62.5 ± 3.95% for **56**), comparable to 100 µM of the positive control NAC. Being encouraged by the promising results, we further analysed the protective effects of **44** and **56** using an orthogonal method (propidium iodide (PI) assay) to verify their activity. In general, PI as a positively charged dye is associated with an increase of cell damage or death, since it penetrates cells with cell disrupted membranes (Dengler et al., 1995). Within the 3-NPA model, its toxic effect was considered as 100% of the PI signal and thus reduction of cell death was determined. As shown in Figure 224 (C), compounds **44** and **56** significantly reduced cell death (maximal effect at 10 µM) in a manner similar to NAC (100 µM, 77.2 ± 9.53%; 1000 µM, 62.1 ± 4.19%), thus confirming the protective effects of **44** and **56** observed in the viability assay.

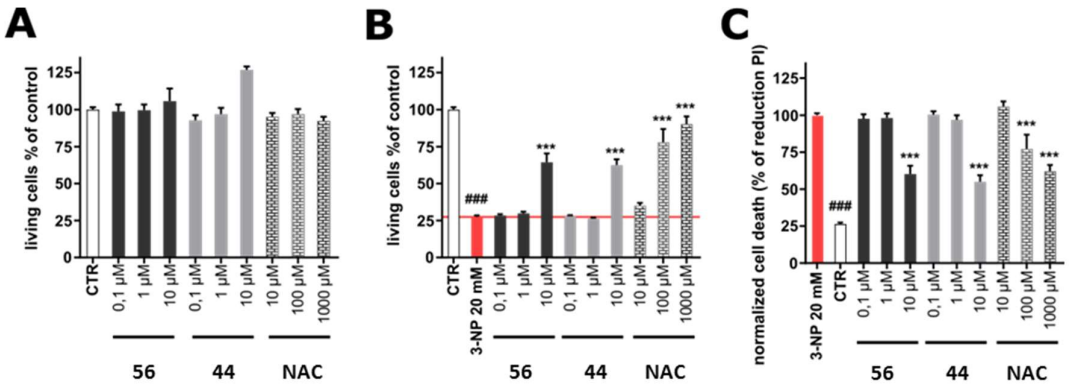

Figure 224. (A) Cytotoxicity of compounds **44** and **56** in human neuron-like SH-SY5Y cells after 48 h of treatment. (B) Neuroprotective activity of compounds **44** and **56** in the 3-nitropropionic acid (3-NPA)-induced model of Huntington's disease on human neuron-like SH-S. (C) Cell death of neuron-like SH-SY5Y induced by 3-NPA and the protective effect of compounds **44** and **56** after 48 h.
All results are presented as mean ± standard error of the mean (SEM) from at least three independent experiments in triplicates. *N*-acetylcysteine (NAC) was used as a positive control. *** *P* compared with vehicle with 20 mM 3-NPA, ### *P* compared with vehicle without 20 mM 3-NPA.

CONCLUSIONS

The aim of the present PhD thesis was the chemical investigation of marine organisms collected from the Red Sea towards the isolation of new secondary metabolites with bioactivity. After a preliminary screening of the chemical profiles of the organic extracts of a number of marine organisms from the Red Sea, the organic extracts of the red alga *Laurencia majuscula*, the marine sponge *Lamellodysidea* sp. and the soft coral *Sinularia polydactyla* were selected for in depth phytochemical study.

The organic extracts of these three marine organisms were subjected to a long series of chromatographic separations to allow for the isolation of 64 secondary metabolites, among which 59 (**1–59**) have been structurally characterized using extensive spectroscopic analyses and comparison with literature data, when available. In total, 18 new natural products have been isolated and characterized. In particular:

- Twenty-two secondary metabolites (**1-22**) were isolated and identified on the basis of their spectroscopic characteristics from the red alga *L. majuscula* collected from Hurghada, Egypt. These included seven laurane sesquiterpenes (**1-7**), one cuparane sesquiterpene (**8**), one seco-laurane derivative (**9**), one snyderane derivative (**10**), two chamigranes (**11** and **12**) and two rearranged chamigranes (**13** and **14**), one aristolane sesquiterpene (**15**), one tricyclic diterpene (**16**), one five-membered C_{15} acetogenin (**17**), four tricyclic C_{15} acetogenins of the maneonene type (**18-21**) and a chlorinated fatty acid derivative (**22**). Compounds **2**, **3**, **5**, **6**, **9**, **17** and **19-21** are new natural products.

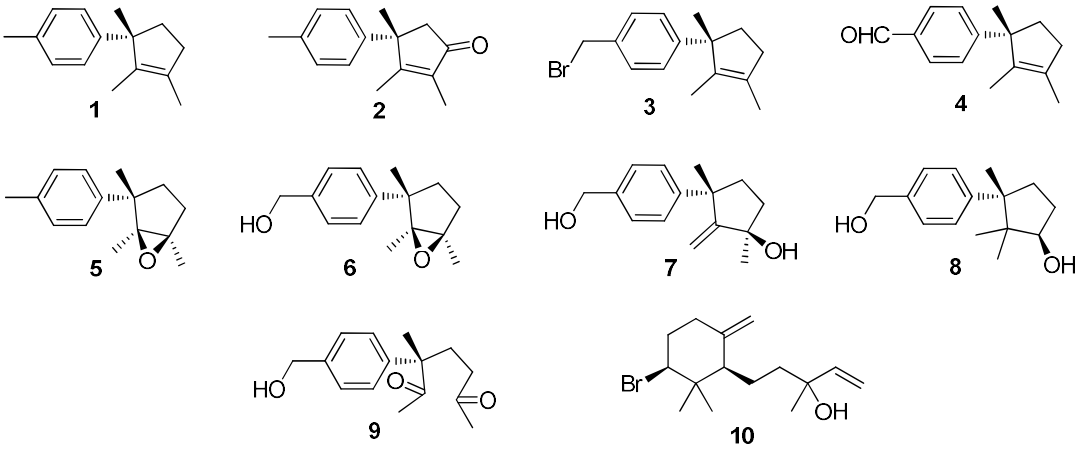

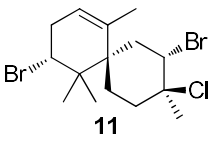

11

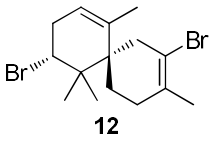

12

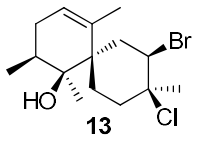

13

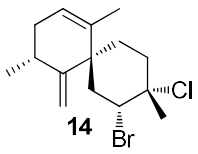

14

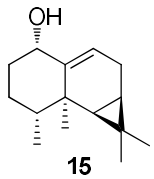

15

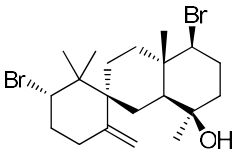

16

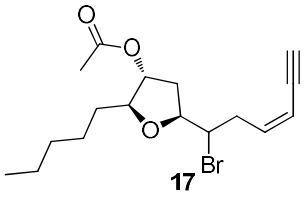

17

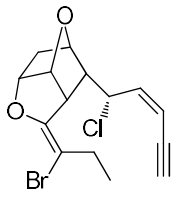

18

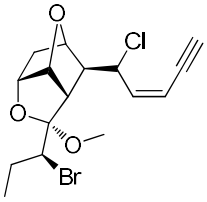

19

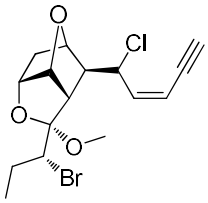

20

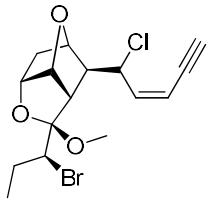

21

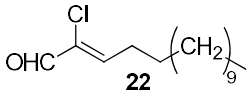

22

- From the marine sponge *Lamellodysidea* sp. collected from KAEC lagoon near Thuwal in Saudi Arabia, 11 sesquiterpenes (**23**-**31**), mostly containing furan or γ-lactone in their structures, were isolated, three of which are new natural products (**25**, **30** and **31**) and one (**33**) is reported for the first time from a natural source.

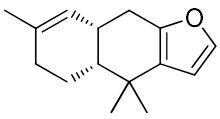

23

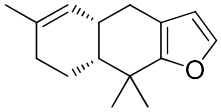

24

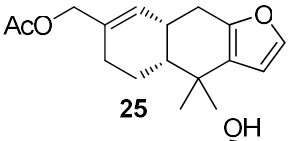

25

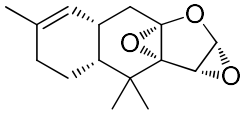

26

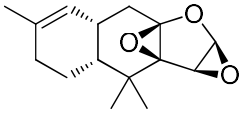

27

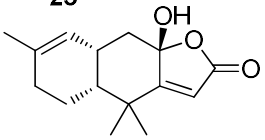

28

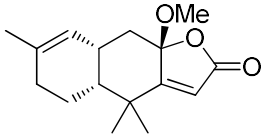

29

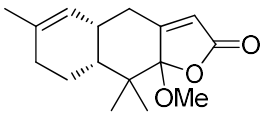

30

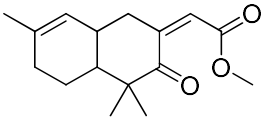

31

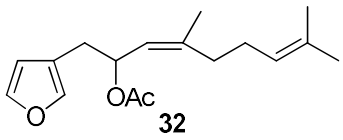

32

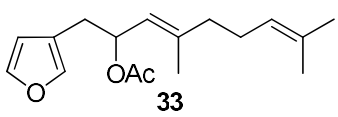

33

- Twenty six steroids (**34-59**) have been isolated and structurally characterized from the soft coral *S. polydactyla* collected from Hurghada, Egypt, including 15 4*α*-methylated derivatives. Compounds **34**, **35**, **39**, **41**, **46** and **53** are new natural products. Among them, metabolites **34** and **35** feature the rare 4-methyl-8,9-seco-cholastane steroidal nucleus.

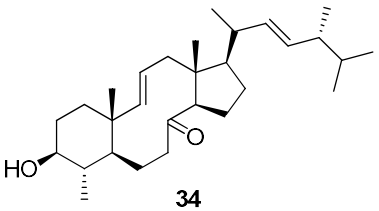

34

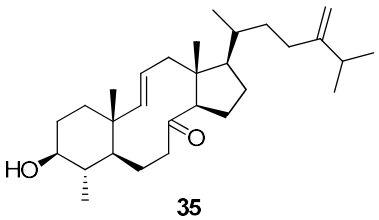

35

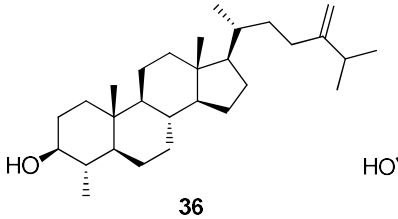

36

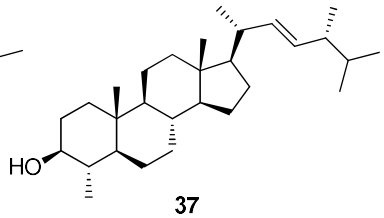

37

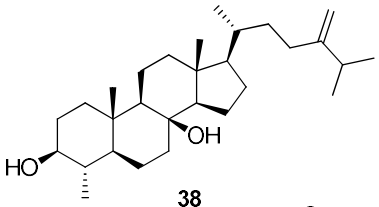

38

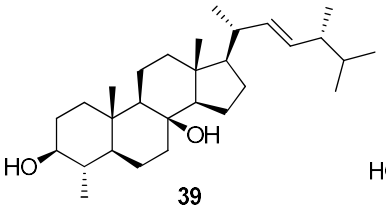

39

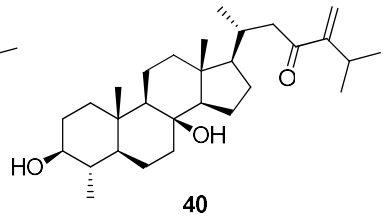

40

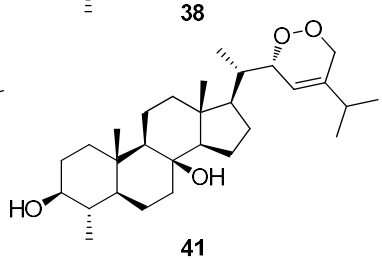

41

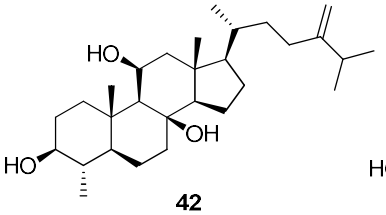

42

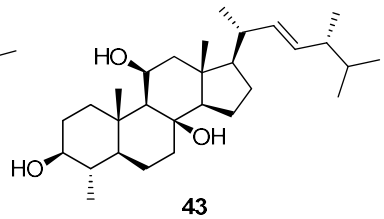

43

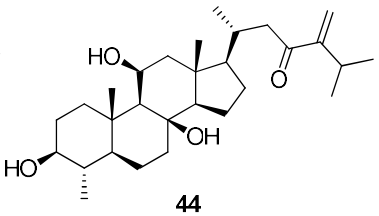

44

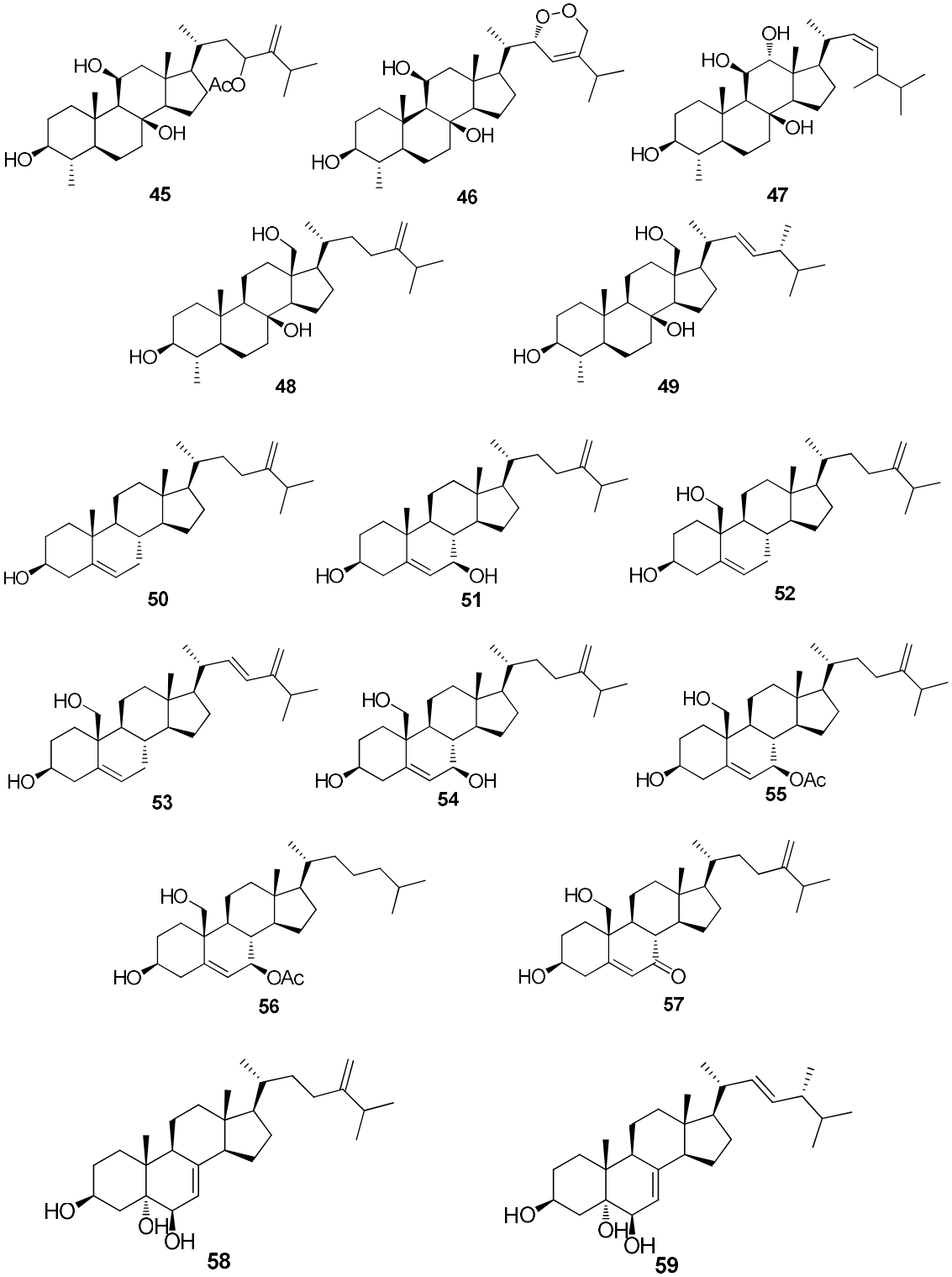

Evaluation of cytotoxic, anti-inflammatory, anti-angiogenic, and neuroprotective activity of metabolites **36**–**40**, **42**–**45**, **47**–**53** and **55**–**59** that were isolated in adequate quantities revealed significant cytotoxicity in the low micromolar range against the HeLa and MCF7 cancer cell lines for compounds **55** and **56**, while compounds **44**, **45**,

55, and **56** inhibited the migration of endothelial cells at 20 μM. Most of the compounds with activity against cancer cells also showed cytotoxicity toward normal cells (BJ), except for compounds **44**, **45**, **47**, **48**, and **51**. Compared to cisplatin, these compounds have therefore a broad therapeutic window due to low or zero cytotoxicity on normal human fibroblasts. Moreover, metabolite **55** was more active against HeLa cells than cisplatin used as positive control. Furthermore, the effect of the isolated metabolites on AR-regulated transcription was evaluated in vitro in human tumor and non-cancerous cells, with compound **44** exhibiting the strongest inhibition of AR at 10 μM. It is worth-noting that metabolites **43**, **49**, and **53** displayed increased inhibition of AR with decreasing concentrations. In addition, compounds **44** and **56** showed neuroprotective activity on neuron-like SH-SY5Y cells.

REFERENCES

Abdel-Mageed, W. M., Ebel, R., Valeriote, F. A., & Jaspars, M. (2010). Laurefurenynes A-F, new cyclic ether acetogenins from a marine red alga, *Laurencia* sp. *Tetrahedron*, *66*(15), 2855–2862. https://doi.org/10.1016/j.tet.2010.02.041

Ahmed, A. F., Kuo, Y. H., Dai, C. F., & Sheu, J. H. (2005). Oxygenated terpenoids from a formosan soft coral *Sinularia gibberosa*. *Journal of Natural Products*, *68*(8), 1208–1212. https://doi.org/10.1021/np050114u

Ahmed, A. F., Tai, S. H., Wen, Z. H., Su, J. H., Wu, Y. C., Hu, W. P., & Sheu, J. H. (2008). A C-3 methylated isocembranoid and 10-oxocembranoids from a formosan soft coral, *Sinularia grandilobata*. *Journal of Natural Products*, *71*(6), 946–951. https://doi.org/10.1021/np7007335

Ahmed, A. F., Tai, S. H., Wu, Y. C., & Sheu, J. H. (2007). Sinugrandisterols A-D, trihydroxysteroids from the soft coral *Sinularia grandilobata*. *Steroids*, *72*(4), 368–374. https://doi.org/10.1016/j.steroids.2007.01.001

Ahmed, S., Ibrahim, A., & Arafa, A. S. (2013). Anti-H5N1 virus metabolites from the Red Sea soft coral, *Sinularia candidula*. *Tetrahedron Letters*, *54*(19), 2377–2381. https://doi.org/10.1016/j.tetlet.2013.02.088

Alarif, W. M, Al-Lihaibi, S. S., Ayyad, S. E. N., Abdel-Rhaman, M. H., & Badria, F. A. (2012). Laurene-type sesquiterpenes from the Red Sea red alga *Laurencia obtusa* as potential antitumor-antimicrobial agents. *European Journal of Medicinal Chemistry*, *55*, 462–466. https://doi.org/10.1016/j.ejmech.2012.06.060

Alarif, W. M., Al-Lihaibi, S. S., Bawakid, N. O., Abdel-Lateff, A., & Al-malky, H. S. (2019). Rare acetogenins with anti-inflammatory effect from the red alga *Laurencia obtusa*. *Molecules*, *24*(3). https://doi.org/10.3390/molecules24030476

Amico, V., Caccamese, S., Neri, P., Russo, G., & Foti, M. (1991). Brasilane-type sesquiterpenoids from the mediterranean red alga *Laurencia obtusa*. *Phytochemistry*, *30*(6), 1921–1927. https://doi.org/10.1016/0031-9422(91)85041-W

Angawi, R. F., Alarif, W. M., Hamza, R. I., Badria, F. A., & Ayyad, S.-E. N. (2014). New cytotoxic laurene-, cuparene-, and laurokamurene-type sesquiterpenes from the red alga *Laurencia obtusa*. *Helvetica Chimica Acta*, *97*(10), 1388–1395. https://doi.org/10.1002/hlca.201300464

Anjaneyulu, A. S. R., & Sagar, K. S. (1996). Flexibilolide and dihydroflexibilolide, the first trihydroxy-cembranolide lactones from the soft coral *Sinularia flexibilis* of the Indian Ocean. *Natural Product Letters*, *9*(2), 127–135. https://doi.org/10.1080/10575639608044936

Arepalli, S. K., Sridhar, V., Rao, J. V., Kennady, P. K., & Venkateswarlu, Y. (2009). Furano-sesquiterpene from soft coral, *Sinularia kavarittiensis*: Induces apoptosis via the mitochondrial-mediated caspase-dependent pathway in THP-1, leukemia cell line. *Apoptosis*, *14*(5), 729–740. https://doi.org/10.1007/s10495-009-0332-z

Aydoğmuş, Z., Imre, S., Ersoy, L., & Wray, V. (2004). Halogenated secondary metabolites from *Laurencia obtusa*. *Natural Product Research*, *18*(1), 43–49.

https://doi.org/10.1080/1057563031000122086

Ayyad, S. E. N., Al-Footy, K. O., Alarif, W. M., Sobahi, T. R., Bassaif, S. A., Makki, M. S., Asiri, A. M., Al Halawani, A. Y., Badria, A. F., & Badria, F. A. A. R. (2011). Bioactive C15 acetogenins from the red alga *Laurencia obtusa*. *Chemical and Pharmaceutical Bulletin*, *59*(10), 1294–1298. https://doi.org/10.1248/cpb.59.1294

Bartonkova, I., Novotna, A., & Dvorak, Z. (2015). Novel stably transfected human reporter cell line AIZ-AR as a tool for an assessment of human androgen receptor transcriptional activity. *PLoS ONE*, *10*(3). https://doi.org/10.1371/journal.pone.0121316

Blunt, J. W., Copp, B. R., Keyzers, R. A., Munro, M. H. G., & Prinsep, M. R. (2015). Marine natural products. *Natural Product Reports*, *32*(2), 116–211. https://doi.org/10.1039/c4np00144c

Bortolotto, M., Braekman, J. C., Daloze, D., Tursch, B., & Karlsson, R. (1977). Chemical studies of marine invertebrates. XXIX (1) (1) For part XXVIII see J.C. Braekhan, D. Daloze, R. Schubert, M. Albericci, B. Tursch, Tetrahedron, in press. 4*α*-methyl-3*β*,8*β*-dihydroxy-5*α*-ergost-24(28)-en-23-one, a novel polyoxygenated sterol from the . *Steroids*, *30*(2), 159–164. https://doi.org/10.1016/0039-128X(77)90077-0

Bowden, B. F., Coll, J. C., Mitchell, S. J., & Kazlauskas, R. (1981). Studies of australian soft corals. XXIV Two cembranoid diterpenes from the soft coral *Sinularia facile*. *Australian Journal of Chemistry*, *34*(7), 1551–1556. https://doi.org/10.1071/CH9811551

Braekman, J. C., Daloze, D., Tursch, B., Hull, S. E., Declercq, J. P., Germain, G., & Van Meerssche, M. (1980). Chemical studies of marine invertebrates. XXXVIII. Δ9(15)-africanene, a new sesquiterpene hydrocarbon from *Sinularia polydactyla* (Coelenterata, Octocorallia, Alcyonaceae). *Experientia*, *36*(8), 893. https://doi.org/10.1007/BF01953776

Brennan, M. R., Kim, I. K., & Erickson, K. L. (1993). Kahukuenes, new diterpenoids from the marine alga *Laurencia majuscula*. *Journal of Natural Products*, *56*(1), 76–84. https://doi.org/10.1021/np50091a011

Brouwer, N., Liu, Q., Harrington, D., Kohen, J., Vemulpad, S., Jamie, J., Randall, M., & Randall, D. (2005). An ethnopharmacological study of medicinal plants in New South Wales. *Molecules*, *10*(10), 1252–1262. https://doi.org/10.3390/10101252

Carroll, A. R., Buchanan, M. S., Edser, A., Hyde, E., Simpson, M., & Quinn, R. J. (2004). Dysinosins B-D, inhibitors of factor VIIa and thrombin from the Australian sponge *Lamellodysidea chlorea*. *Journal of Natural Products*, *67*(8), 1291–1294. https://doi.org/10.1021/np049968p

Carté, B., Kernan, M. R., Barrabee, E. B., Faulkner, D. J., Matsumoto, G. K., & Clardy, J. (1986). Metabolites of the nudibranch chromodoris funerea and the singlet oxygen oxidation products of furodysin and furodysinin. *Journal of Organic Chemistry*, *51*(18), 3528–3532. https://doi.org/10.1021/jo00368a025

Cassano, V., De Paula, J., Fujii, M., Da Gama, B., & Teixeira, V. (2008). Sesquiterpenes from the introduced red seaweed *Laurencia caduciramulosa*

(Rhodomelaceae, Ceramiales). *Biochemical Systematics and Ecology*, *36*, 223–226. https://doi.org/10.1016/j.bse.2007.07.005

Chao, C. H., Wu, C. Y., Huang, C. Y., Wang, H. C., Dai, C. F., Wu, Y. C., & Sheu, J. H. (2016). Cubitanoids and cembranoids from the soft coral *Sinularia nanolobata*. *Marine Drugs*, *14*(8). https://doi.org/10.3390/md14080150

Chen, J. Y., Huang, C. Y., Lin, Y. S., Hwang, T. L., Wang, W. L., Chiou, S. F., & Sheu, J. H. (2016). Halogenated sesquiterpenoids from the Red Alga *Laurencia tristicha* collected in Taiwan. *Journal of Natural Products*, *79*(9), 2315–2323. https://doi.org/10.1021/acs.jnatprod.6b00452

Chen, W., Li, Y., & Guo, Y. (2012). Terpenoids of *Sinularia* soft corals: chemistry and bioactivity. *Acta Pharmaceutica Sinica B*, *2*(3), 227–237. https://doi.org/10.1016/j.apsb.2012.04.004

Chen, W. T., Li, J., Wang, J. R., Li, X. W., & Guo, Y. W. (2015). Structural diversity of terpenoids in the soft coral *Sinularia flexibilis*, evidenced by a collection from the South China Sea. *RSC Advances*, *5*(30), 23973–23980. https://doi.org/10.1039/c5ra01151e

Cheng, S. Y., Dai, C. F., & Duh, C. Y. (2007). New 4-methylated and 19-oxygenated steroids from the formosan soft coral *Nephthea erecta*. *Steroids*, *72*(8), 653–659. https://doi.org/10.1016/j.steroids.2007.05.001

Cheng, S. Y., Huang, K. J., Wang, S. K., Wen, Z. H., Chen, P. W., & Duh, C. Y. (2010). Antiviral and anti-inflammatory metabolites from the soft coral *Sinularia capillosa*. *Journal of Natural Products*, *73*(4), 771–775. https://doi.org/10.1021/np9008078

Cheng, S. Y., Huang, Y. C., Wen, Z. H., Hsu, C. H., Wang, S. K., Dai, C. F., & Duh, C. Y. (2009). New 19-oxygenated and 4-methylated steroids from the Formosan soft coral *Nephthea chabroli*. *Steroids*, *74*(6), 543–547. https://doi.org/10.1016/j.steroids.2009.02.004

Cheung, Y. T., Lau, W. K. W., Yu, M. S., Lai, C. S. W., Yeung, S. C., So, K. F., & Chang, R. C. C. (2009). Effects of all-trans-retinoic acid on human SH-SY5Y neuroblastoma as in vitro model in neurotoxicity research. *NeuroToxicology*, *30*(1), 127–135. https://doi.org/10.1016/j.neuro.2008.11.001

Chu, M. J., Tang, X. L., Han, X., Li, T., Luo, X. C., Jiang, M. M., Van Ofwegen, L., Luo, L. Z., Zhang, G., Li, P. L., & Li, G. Q. (2018). Metabolites from the Paracel Islands soft coral *Sinularia cf. molesta*. *Marine Drugs*, *16*(12). https://doi.org/10.3390/md16120517

Coll, J. C., Mitchell, S. J., & Stokie, G. J. (1977). Studies of Australian soft corals. v - a novel furano-sesquiterpene acid from the soft coral *Sinularia gonatodes* (Kolonko). *Tetrahedron Letters*, *18*(18), 1539–1542. https://doi.org/10.1016/S0040-4039(01)93097-7

Coll, J. C., & Wright, A. D. (1989). Tropical marine algae. IV: Novel metabolites from the red alga *Laurencia implicate* (rhodophyta, rhodophyceae, ceramiales, rhodomelaceae). *Australian Journal of Chemistry*, *42*(10), 1685–1693. https://doi.org/10.1071/CH9891685

Colle, D., Santos, D. B., Hartwig, J. M., Godoi, M., Engel, D. F., de Bem, A. F., Braga,

A. L., & Farina, M. (2016). Succinobucol, a lipid-lowering drug, protects against 3-nitropropionic acid-induced mitochondrial dysfunction and oxidative stress in SH-SY5Y cells via upregulation of glutathione levels and glutamate cysteine ligase activity. *Molecular Neurobiology*, *53*(2), 1280–1295. https://doi.org/10.1007/s12035-014-9086-x

da Silva Machado, F. L., Pacienza-Lima, W., Rossi-Bergmann, B., De Souza Gestinari, L. M., Fujii, M. T., Campos De Paula, J., Costa, S. S., Lopes, N. P., Kaiser, C. R., & Soares, A. R. (2011). Antileishmanial sesquiterpenes from the Brazilian red alga *Laurencia dendroidea*. *Planta Medica*, *77*(7), 733–735. https://doi.org/10.1055/s-0030-1250526

da Silva Machado, F. L., Ventura, T. L. B., De Souza Gestinari, L. M., Cassano, V., Resende, J. A. L. C., Kaiser, C. R., Lasunskaia, E. B., Muzitano, M. F., & Soares, A. R. (2014). Sesquiterpenes from the Brazilian red alga *Laurencia dendroidea* J. Agardh. *Molecules*, *19*(3), 3181–3192. https://doi.org/10.3390/molecules19033181

Darley, M. (1982). Algal Biology: A Physiological Approach (Basic microbiology). In *Wilkinson JF (ser ed) Basic microbiology* (p. 168). Blackwell Science Inc.

de Nys, R., König, G. M., Wright, A. D., & Sticher, O. (1993). Two metabolites from the red alga *Laurencia flexilis*. *Phytochemistry*, *34*(3), 725–728. https://doi.org/10.1016/0031-9422(93)85347-T

de Riccardis, F., Minale, L., Iorizzi, M., Debitus, C., & Lévi, C. (1993). Marine sterols. side-chain-oxygenated sterols, possibly of abiotic origin, from the new caledonian sponge *Stelodoryx chlorophylla*. *Journal of Natural Products*, *56*(2), 282–287. https://doi.org/10.1021/np50092a016

Dengler, W. A., Schulte, J., Berger, D. P., Mertelsmann, R., & Fiebig, H. H. (1995). Development of a propidium iodide fluorescence assay for proliferation and cytotoxicity assays. *Anti-Cancer Drugs*, *6*(4), 522–532. https://doi.org/10.1097/00001813-199508000-00005

Duh, C. Y., Wang, S. K., Chu, M. J., & Sheu, J. H. (1998). Cytotoxic sterols from the soft coral *Nephthea erecta*. *Journal of Natural Products*, *61*(8), 1022–1024. https://doi.org/10.1021/np9800497

Dwane, S., Durack, E., & Kiely, P. A. (2013). Optimising parameters for the differentiation of SH-SY5Y cells to study cell adhesion and cell migration. *BMC Research Notes*, *6*(1). https://doi.org/10.1186/1756-0500-6-366

Dziwornu, G. A., Caira, M. R., De La Mare, J. A., Edkins, A. L., Bolton, J. J., Beukes, D. R., Sunassee, S. N., & Newman, D. J. (2017). Isolation, characterization and antiproliferative activity of new metabolites from the South African endemic red algal species *Laurencia alfredensis*. *Molecules*, *22*(4). https://doi.org/10.3390/molecules22040513

El-Demerdash, A., Atanasov, A. G., Horbanczuk, O. K., Tammam, M. A., Abdel-Mogib, M., Hooper, J. N. A., Sekeroglu, N., Al-Mourabit, A., & Kijjoa, A. (2019). Chemical diversity and biological activities of marine sponges of the genus *Suberea*: A systematic review. *Marine Drugs*, *17*(2). https://doi.org/10.3390/md17020115

El-Demerdash, A., Tammam, M. A., Atanasov, A. G., Hooper, J. N. A. A., Al-

Mourabit, A., & Kijjoa, A. (2018). Chemistry and biological activities of the marine sponges of the genera *Mycale* (Arenochalina), *Biemna* and *Clathria*. *Marine Drugs*, *16*(6). https://doi.org/10.3390/md16060214

Ellithey, M. S., Lall, N., Hussein, A. A., & Meyer, D. (2013). Cytotoxic, cytostatic and HIV-1 PR inhibitory activities of the soft coral *Litophyton arboreum*. *Marine Drugs*, *11*(12), 4917–4936. https://doi.org/10.3390/md11124917

Esselin, H., Tomi, F., Bighelli, A., & Sutour, S. (2018). New metabolites isolated from a *laurencia obtusa* population collected in corsica. *Molecules*, *23*(4). https://doi.org/10.3390/molecules23040720

Fernández, J. J., Souto, M. L., Gil, L. V, & Norte, M. (2005). Isolation of naturally occurring dactylomelane metabolites as *Laurencia constituents*. *Tetrahedron*, *61*(37), 8910–8915. https://doi.org/10.1016/j.tet.2005.07.024

Ghandourah, M., Alarif, W., & Bawakid, N. (2019). New bioactive C $_{15}$ acetogenins from the red alga *Laurencia obtusa*. *Pharmacognosy Magazine*, *15*(61), 199. https://doi.org/10.4103/pm.pm_298_18

Goud, T., Reddy, N., Krishnaiah, P., & Venkateswarlu, Y. (2002). Spathulenol: A rare sesquiterpene from soft coral *Sinularia kavarattiensis. Biochemical Systematics and Ecology*, *30*, 493–495. https://doi.org/10.1016/S0305-1978(01)00094-1

Grace, K. J. S., Zavortink, D., & Jacobs, R. S. (1994). Inactivation of bee venom phospholipase A2 by a sesquiterpene furanoic acid marine natural product. *Biochemical Pharmacology*, *47*(8), 1427–1434. https://doi.org/10.1016/0006-2952(94)90343-3

Grode, S. H., & Cardellina, J. H. (1984). Sesquiterpenes from the sponge *Dysidea etheria* and the nudibranch *Hypselodoris zebra*. *Journal of Natural Products*, *47*(1), 76–83. https://doi.org/10.1021/np50031a009

Guella, G., & Pietra, F. (1991). Rogiolenyne A, B, and C: The first branched marine C15 acetogenins. Isolation from the red seaweed *Laurencia microcladia* or the *sponge Spongia zimocca* of II Rogiolo. *Helvetica Chimica Acta*, *74*(1), 47–54. https://doi.org/10.1002/hlca.19910740107

Guella, G., Pietra, F., & Marchetti, F. (1997). Rogioldiol A, a new obtusane diterpene, and rogiolal, a degraded derivative, of the red seaweed *Laurencia microcladia* from II rogiolo along the coast of tuscany: A synergism in structural elucidation. *Helvetica Chimica Acta*, *80*(3), 684–694. https://doi.org/10.1002/hlca.19970800306

Guiry, M. D., & Guiry, G. M. (2015). *AlgaeBase.* World-wide electronic publication.National University of Ireland, Galway. https://www.algaebase.org

Gutiérrez-Cepeda, A., Fernández, J. J., Norte, M., López-Rodríguez, M., Brito, I., Muller, C. D., & Souto, M. L. (2016). Additional insights into the obtusallene family: components of *Laurencia marilzae*. *Journal of Natural Products*, *79*(4), 1184–1188. https://doi.org/10.1021/acs.jnatprod.5b01080

Guzman, D., Bratoeff, E., Riveros, A., Brizuela, N., Mejia, G., Garcia, E., Olguin, H., & Cruz, E. (2014). Effect of two antiandrogens as protectors of prostate and brain in a huntington´s animal model. *Anti-Cancer Agents in Medicinal Chemistry*, *14*(9), 1293–1301. https://doi.org/10.2174/1871520614666141010094847

Hall, J. G., & Reiss, J. A. (1986). Elatenyne—a pyrano[3,2-b]pyranyl vinyl acetylene from the red alga *Laurencia elata*. *Australian Journal of Chemistry*, *39*, 1401–1409. https://doi.org/10.1071/CH9861401

Hammer, D. A. T., Ryan, P. D., Hammer, Ø., & Harper, D. A. T. (2001). Past: paleontological statistics software package for education and data analysis. *Palaeontologia Electronica*, *4*(1), 178. http://palaeo-electronica.orghttp//palaeo-electronica.org/2001_1/past/issue1_01.htm.

Hanif, N., Tanaka, J., Setiawan, A., Trianto, A., de Voogd, N., Murni, A., Tanaka, C., & Higa, T. (2007). Polybrominated diphenyl ethers from the indonesian sponge *Lamellodysidea herbacea*. *Journal of Natural Products*, *70*, 432–435. https://doi.org/10.1021/np0605081

Harizani, M., Ioannou, E., & Roussis, V. (2016). The *Laurencia* Paradox: an endless source of chemodiversity. *Progress in the Chemistry of Organic Natural Products*, *102*, 91–252. https://doi.org/10.1007/978-3-319-33172-0_2

Harper, J. T., & Garbary, D. J. (1997). Marine algae of northern senegal: The flora and its biogeography. *Botanica Marina*, *40*(2), 129–138. https://doi.org/10.1515/botm.1997.40.1-6.129

Hegazy, M.-E., Mohamed, T., Elshamy, A., Al-Hammady, M., Ohta, S., & Paré, P. (2016). Casbane diterpenes from Red Sea coral *Sinularia polydactyla*. *Molecules*, *21*(3), 308. https://doi.org/10.3390/molecules21030308

Howard, B. M., & Fenical, W. (1975). Structures and chemistry of two new halogen-containing chamigrene derivatives from *Laurencia*. *Tetrahedron Letters*, *16*(21), 1687–1690. https://doi.org/10.1016/S0040-4039(00)72233-7

Huang, Y. C., Wen, Z. H., Wang, S. K., Hsu, C. H., & Duh, C. Y. (2008). New anti-inflammatory 4-methylated steroids from the Formosan soft coral *Nephthea chabroli*. *Steroids*, *73*(11), 1181–1186. https://doi.org/10.1016/j.steroids.2008.05.007

Huong, N. T., Ngoc, N. T., Thanh, N. Van, Dang, N. H., Cuong, N. X., Nam, N. H., Thung, D. C., The, H. Van, Tuan, V. S., Kiem, P. Van, & Minh, C. Van. (2018). Eudesmane and aromadendrane sesquiterpenoids from the Vietnamese soft coral *Sinularia erecta*. *Natural Product Research*, *32*(15), 1798–1802. https://doi.org/10.1080/14786419.2017.1402326

Iguchi, K., Saitoh, S., & Yamada, Y. (1989). Novel 19-oxygenated sterols from the Okinawan soft coral *Litophyton viridis*. *Chemical & pharmaceutical bulletin*, *37*(9), 2553–2554. https://doi.org/10.1248/cpb.37.2553

Iliopoulou, D., Mihopoulos, N., Vagias, C., Papazafiri, P., & Roussis, V. (2003). Novel cytotoxic brominated diterpenes from the red alga *Laurencia obtusa*. *Journal of Organic Chemistry*, *68*(20), 7667–7674. https://doi.org/10.1021/jo0342323

Iorizzi, M., Minale, L., Riccio, R., Lee, J. S., & Yasumoto, T. (1988). Polar steroids from the marine scallop *Patinopecten yessoensis*. *Journal of Natural Products*, *51*(6), 1098–1103. https://doi.org/10.1021/np50060a008

Ji, N.-Y., Li, X.-M., Cui, C.-M., & Wang, B.-G. (2007a). Terpenes and Polybromoindoles from the Marine Red Alga *Laurencia decumbens* (Rhodomelaceae). *Helvetica Chimica Acta*, *90*(9), 1731–1736.

https://doi.org/10.1002/hlca.200790181

Ji, N. Y., Li, X. M., Ding, L. P., & Wang, B. G. (2016). Halogenated eudesmane derivatives and other terpenes from the marine red alga *Laurencia pinnata* and their chemotaxonomic significance. *Biochemical Systematics and Ecology*, *64*, 1–5. https://doi.org/10.1016/j.bse.2015.11.010

Ji, N. Y., Li, X. M., Li, K., & Wang, B. G. (2007b). Laurendecumallenes A-B and laurendecumenynes A-B, halogenated nonterpenoid C15-acetogenins from the marine red alga *Laurencia decumbens*. *Journal of Natural Products*, *70*(9), 1499–1502. https://doi.org/10.1021/np0701172

Ji, N. Y., Li, X. M., & Wang, B. G. (2008). Halogenated terpenes and a C(15)-acetogenin from the marine red alga *Laurencia saitoi*. *Molecules (Basel, Switzerland)*, *13*(11), 2894–2899. https://doi.org/10.3390/molecules13112894

Jorda, R., Řezníčková, E., Kiełczewska, U., Maj, J., Morzycki, J. W., Siergiejczyk, L., Bazgier, V., Berka, K., Rárová, L., & Wojtkielewicz, A. (2019). Synthesis of novel galeterone derivatives and evaluation of their in vitro activity against prostate cancer cell lines. *European Journal of Medicinal Chemistry*, *179*, 483–492. https://doi.org/10.1016/j.ejmech.2019.06.040

Kamada, T., & Vairappan, C. (2013). New Bioactive Secondary Metabolites from Bornean Red Alga, *Laurencia similis* (Ceramiales). *Natural Product Communications*, *8*, 287–288. https://doi.org/10.1177/1934578X1300800302

Kamel, H., & Slattery, M. (2005). Terpenoids of *Sinularia*.: Chemistry and Biomedical Applications. *Pharmaceutical Biology*, *43*. https://doi.org/10.1080/13880200590928852

Kapojos, M. M., Abdjul, D. B., Yamazaki, H., Kirikoshi, R., Takahashi, O., Rotinsulu, H., Wewengkang, D. S., Sumilat, D. A., Ukai, K., & Namikoshi, M. (2018). Protein tyrosine phosphatase 1B inhibitory polybromobiphenyl ethers and monocyclofarnesol-type sesquiterpenes from the Indonesian marine sponge *Lamellodysidea cf. herbacea*. *Phytochemistry Letters*, *24*, 10–14. https://doi.org/10.1016/j.phytol.2017.11.016

Kazlauskas, R., Murphy, P., & Wells, R. (1978). Two sesquiterpene furans with new carboxylic ring systems and related thiol acetates from a species of the sponge genus *Dysidea*. *Tetrahedron Letters*, *19*(49), 4951–4954.

Kennedy, D. J., Selby, I. A., Cowe, H. J., Cox, P. J., & Thomson, R. H. (1984). Bromoallenes from the alga *Laurencia microcladia*. *Journal of the Chemical Society, Chemical Communications*, *3*, 153–155. https://doi.org/10.1039/C39840000153

Kimura, J., Kamada, N., & Tsujimoto, Y. (1999). Fourteen chamigrane derivatives from a red alga, *Laurencia nidifica*. *Bulletin of the Chemical Society of Japan*, *72*(2), 289–292. https://doi.org/10.1246/bcsj.72.289

Kladi, M., Vagias, C., Papazafiri, P., Brogi, S., Tafi, A., & Roussis, V. (2009). Tetrahydrofuran acetogenins from *Laurencia glandulifera*. *Journal of Natural Products*, *72*(2), 190–193. https://doi.org/10.1021/np800481w

Kladi, M., Xenaki, H., Vagias, C., Papazafiri, P., & Roussis, V. (2006). New cytotoxic sesquiterpenes from the red algae *Laurencia obtusa* and Laurencia microcladia.

Tetrahedron, *62*(1), 182–189. https://doi.org/10.1016/j.tet.2005.09.113

Kobayashi, M., Ishizaka, T., & Mitsuhashi, H. (1982). Marine Sterols X. minor constituents of the sterols of the soft coral *Sarcophyton glaucum*. *Steroids*, *40*(2), 209–221. https://doi.org/10.1016/0039-128X(82)90034-4

Kokke, W. C. M. C., Bohlin, L., Fenical, W., & Djerassi, C. (1982). Novel dinoflagellate 4α-methylated sterols from four caribbean gorgonians. *Phytochemistry*, *21*(4), 881–887. https://doi.org/10.1016/0031-9422(82)80085-X

Kokkotou, K., Ioannou, E., Nomikou, M., Pitterl, F., Vonaparti, A., Siapi, E., Zervou, M., & Roussis, V. (2014). An integrated approach using UHPLC-PDA-HRMS and 2D HSQC NMR for the metabolic profiling of the red alga *Laurencia*: Dereplication and tracing of natural products dedicated to the memory of Professor Constantinos Vagias. *Phytochemistry*, *108*, 208–219. https://doi.org/10.1016/j.phytochem.2014.10.007

Kong, D. X., Jiang, Y. Y., & Zhang, H. Y. (2010). Marine natural products as sources of novel scaffolds: Achievement and concern. *Drug Discovery Today*, *15*(21–22), 884–886. https://doi.org/10.1016/j.drudis.2010.09.002

Kuniyoshi, M., Marma, M. S., Higa, T., Bernardinelli, G., & Jefford, C. W. (2000). 3-bromobarekoxide, an unusual diterpene from *Laurencia luzonensis*. *Chemical Communications*, *13*, 1155–1156. https://doi.org/10.1039/b002530p

Lei, L. F., Chen, M. F., Wang, T., He, X. X., Liu, B. X., Deng, Y., Chen, X. J., Li, Y. T., Guan, S. Y., Yao, J. H., Li, W., Ye, W. C., Zhang, D. M., & Zhang, C. X. (2014). Novel cytotoxic nine-membered macrocyclic polysulfur cembranoid lactones from the soft coral *Sinularia* sp. *Tetrahedron*, *70*(38), 6851–6858. https://doi.org/10.1016/j.tet.2014.07.042

Lhullier, C., Falkenberg, M., Ioannou, E., Quesada, A., Papazafiri, P., Horta, P. A., Schenkel, E. P., Vagias, C., & Roussis, V. (2010). Cytotoxic halogenated metabolites from the Brazilian red alga *Laurencia catarinensis*. *Journal of Natural Products*, *73*(1), 27–32. https://doi.org/10.1021/np900627r

Li, C. S., Li, X. M., Cui, C. M., & Wang, B. G. (2010). Brominated metabolites from the marine red alga *Laurencia similis*. *Zeitschrift Fur Naturforschung - Section B Journal of Chemical Sciences*, *65*(1), 87–89. https://doi.org/10.1515/znb-2010-0115

Li, M. C., Sun, W. S., Cheng, W., Liu, D., Liang, H., Zhang, Q. Y., & Lin, W. H. (2016). Four new minor brominated indole related alkaloids with antibacterial activities from *Laurencia similis*. *Bioorganic and Medicinal Chemistry Letters*, *26*(15), 3590–3593. https://doi.org/10.1016/j.bmcl.2016.06.015

Li, S. W., Chen, W. T., Yao, L. G., & Guo, Y. W. (2018). Two new cytotoxic steroids from the Chinese soft coral *Sinularia* sp. *Steroids*, *136*, 17–21. https://doi.org/10.1016/j.steroids.2018.05.009

Li, X.-D., Ding, W., Miao, F.-P., & Ji, N.-Y. (2012a). Halogenated chamigrane sesquiterpenes from *Laurencia okamurae*. *Magnetic Resonance in Chemistry*, *50*(2), 174–177. https://doi.org/10.1002/mrc.2870

Li, X. D., Miao, F. P., Li, K., & Ji, N. Y. (2012c). Sesquiterpenes and acetogenins from the marine red alga *Laurencia okamurai*. *Fitoterapia*, *83*(3), 518–522.

https://doi.org/10.1016/j.fitote.2011.12.018
Li, X. D., Miao, F. P., Yin, X. L., Liu, J. L., & Ji, N. Y. (2012b). Sesquiterpenes from the marine red alga *Laurencia composita*. *Fitoterapia*, *83*(7), 1191–1195. https://doi.org/10.1016/j.fitote.2012.07.001
Li, X. L., He, W. F., Li, J., Lan, L. F., Li, X. W., & Guo, Y. W. (2015). New laurane-type sesquiterpenoids from the Chinese red alga *Laurencia okamurai* Yamada. *Journal of Asian Natural Products Research*, *17*(12), 1146–1152. https://doi.org/10.1080/10286020.2015.1102135
Liang, Y., Li, X. M., Cui, C. M., Li, C. S., Sun, H., & Wang, B. G. (2012). Sesquiterpene and acetogenin derivatives from the marine red alga *Laurencia okamurai*. *Marine Drugs*, *10*(12), 2817–2825. https://doi.org/10.3390/md10122817
Lyakhova, E. G., Kalinovsky, A. I., Dmitrenok, A. S., Kolesnikova, S. A., Fedorov, S. N., Vaskovsky, V. E., & Stonik, V. A. (2006). Structures and absolute stereochemistry of nipponallene and neonipponallene, new brominated allenes from the red alga *Laurencia nipponica*. *Tetrahedron Letters*, *47*(37), 6549–6552. https://doi.org/10.1016/j.tetlet.2006.07.015
Lyakhova, E. G., Kalinovsky, A. I., Kolesnikova, S. A., Vaskovsky, V. E., & Stonik, V. A. (2004). Halogenated diterpenoids from the red alga *Laurencia nipponica*. *Phytochemistry*, *65*(18), 2527–2532. https://doi.org/10.1016/j.phytochem.2004.07.005
Makhanu, D.S., Yokoyama, M., Miono, T., Maesato, T., Maedomari, M., Wisespongpand, P., Kuniyoshi, M. (2006). New sesquiterpenes from the Okinawan red alga *Laurencia luzonensis*. *Bull Fac Sci Univ Ryukuyus*, *81*, 115.
Majeed, A., Chaudhry, Z., & Muhammad, Z. (2012). Allelopathic assessment of fresh aqueous extracts of *Chenopodium Album* L. for growth and yield of wheat (*Triticum aestivum* L.). *Pakistan Journal of Botany*, *44*, 165–167.
Manríquez, C. P., Souto, M. L., Gavín, J. A., Norte, M., & Fernández, J. J. (2001). Several new squalene-derived triterpenes from *Laurencia*. *Tetrahedron*, *57*(15), 3117–3123. https://doi.org/10.1016/S0040-4020(01)00169-7
Mao, S.-C., & Guo, Y.-W. (2005). Cuparene-derived sesquiterpenes from the Chinese red alga *Laurencia okamurai* Yamada. *Helvetica Chimica Acta*, *88*, 1034–1039. https://doi.org/10.1002/hlca.200590074
MarinLit. A database of the marine natural products literature. Available online: http://pubs.rsc.org/marinlit/ (accessed on 30 September 2020).
Masuda, M., Kawaguchi, S., & Abe, T. (2002). Additional analysis of chemical diversity of the red algal genus *Laurencia* (Rhodomelaceae) from Japan. *Phycological Research*, *50*(2), 135–144. https://doi.org/10.1046/j.1440-1835.2002.00267.x
McDermid, J. (1988). *Laurencia* (Rhodophyta, Rhodomelaceae). In I. A. Abbott, J. N. Norris, & L. A. Abbott (Eds.), *Taxonomy of economic seaweeds : with reference to some Pacific and Caribbean species*. California Sea Grant College Program, La Jolla, CA. https://escholarship.org/uc/item/6xm1n104
Medina-Franco, J. L. (2019). New approaches for the discovery of pharmacologically-active natural compounds. *Biomolecules*, *9*(3), 115.

https://doi.org/10.3390/biom9030115

Mehta, G., Venkateswarlu, Y., Rao, M. R., & Uma, R. (1999). A novel 4*α*-methyl sterol from the soft coral *Nephthea chabroli*. *Journal of Chemical Research - Part S*, *10*, 628–629. https://doi.org/10.1039/a904057i

Mohammed, K. A., Hossain, C. F., Zhang, L., Bruick, R. K., Zhou, Y. D., & Nagle, D. G. (2004). Laurenditerpenol, A New diterpene from the tropical marine alga *Laurencia intricata* that potently inhibits HIF-1 mediated hypoxic signaling in breast tumor cells. *Journal of Natural Products*, *67*(12), 2002–2007. https://doi.org/10.1021/np049753f

Montaser, R., & Luesch, H. (2011). Marine natural products: A New wave of drugs? *Future Medicinal Chemistry*, *3*(12), 1475–1489. https://doi.org/10.4155/fmc.11.118

Morrogh-Bernard, H. C., Foitová, I., Yeen, Z., Wilkin, P., De Martin, R., Rárová, L., Doležal, K., Nurcahyo, W., & Olšanský, M. (2017). Self-medication by orang-utans (*Pongo pygmaeus*) using bioactive properties of *Dracaena Cantleyi*. *Scientific Reports*, *7*(1). https://doi.org/10.1038/s41598-017-16621-w

Mudianta, W., Challinor, V., Winters, A., Cheney, K., Voss, J., & Garson, M. (2013). Synthesis and determination of the absolute configuration of (-)-(5*R*,6*Z*)-dendrolasin-5-acetate from the nudibranch *Hypselodoris jacksoni*. *Beilstein Journal of Organic Chemistry*, *9*, 2925–2933. https://doi.org/10.3762/bjoc.9.329

Nam, K., & Choi, H. (2000). A detailed morphological study of the type species of *Osmundea* (Rhodomelaceae, Rhodophyta). *Botanica Marina - BOT MAR*, *43*, 291–297. https://doi.org/10.1515/BOT.2000.031

Newman, D. J., & Cragg, G. M. (2016). Natural products as sources of new drugs from 1981 to 2014. *Journal of Natural Products*, *79*(3), 629–661. https://doi.org/10.1021/acs.jnatprod.5b01055

Ngoc, N. T., Huong, P. T. M., Thanh, N. Van, Cuong, N. X., Nam, N. H., Thung, D. C., Kiem, P. Van, & Minh, C. Van. (2017). Sesquiterpene constituents from the soft coral *Sinularia nanolobata*. *Natural Product Research*, *31*(15), 1799–1804. https://doi.org/10.1080/14786419.2017.1292508

Oguri, Y., Watanabe, M., Ishikawa, T., Kamada, T., Vairappan, C. S., Matsuura, H., Kaneko, K., Ishii, T., Suzuki, M., Yoshimura, E., Nogata, Y., & Okino, T. (2017). New marine antifouling compounds from the red alga *Laurencia* sp. *Marine Drugs*, *15*(9). https://doi.org/10.3390/md15090267

Ojika, M., Islam, M. K., Shintani, T., Zhang, Y., Okamoto, T., & Sakagami, Y. (2003). Three new cytotoxic acylspermidines from the soft coral, *Sinularia* sp. *Bioscience, Biotechnology and Biochemistry*, *67*(6), 1410–1412. https://doi.org/10.1271/bbb.67.1410

Patridge, E., Gareiss, P., Kinch, M. S., & Hoyer, D. (2016). An analysis of FDA-approved drugs: Natural products and their derivatives. *Drug Discovery Today*, *21*(2), 204–207. https://doi.org/10.1016/j.drudis.2015.01.009

Perdikaris, S., Mangoni, A., Grauso, L., Papazafiri, P., Roussis, V., & Ioannou, E. (2019). Vagiallene, a rearranged C 15 acetogenin from *Laurencia obtusa*. *Organic Letters*, *21*(9), 3183–3186. https://doi.org/10.1021/acs.orglett.9b00897

Putra, M. Y., Bavestrello, G., Cerrano, C., Renga, B., D'Amore, C., Fiorucci, S., Fattorusso, E., & Taglialatela-Scafati, O. (2012). Polyhydroxylated sterols from the Indonesian soft coral *Sinularia* sp. and their effect on farnesoid X-activated receptor. *Steroids*, *77*(5), 433–440. https://doi.org/10.1016/j.steroids.2011.12.026

Qin, J., Su, H., Zhang, Y., Gao, J., Zhu, L., Wu, X., Pan, H., & Li, X. (2010). Highly brominated metabolites from marine red alga *Laurencia similis* inhibit protein tyrosine phosphatase 1B. *Bioorganic and Medicinal Chemistry Letters*, *20*(23), 7152–7154. https://doi.org/10.1016/j.bmcl.2010.08.144

Rahelivao, M. P., Gruner, M., Andriamanantoanina, H., Andriamihaja, B., Bauer, I., & Knölker, H. J. (2015). Red algae (Rhodophyta) from the coast of Madagascar: Preliminary bioactivity studies and isolation of natural products. *Marine Drugs*, *13*(7), 4197–4216. https://doi.org/10.3390/md13074197

Ramesh, P., & Venkateswarlu, Y. (1999). Novel steroid constituents of the soft coral *Sinularia dissecta*. *Steroids*, *64*(11), 785–789. https://doi.org/10.1016/S0039-128X(99)00069-0

Rárová, L., Sedlák, D., Oklestkova, J., Steigerová, J., Liebl, J., Zahler, S., Bartůněk, P., Kolář, Z., Kohout, L., Kvasnica, M., & Strnad, M. (2018). The novel brassinosteroid analog BR4848 inhibits angiogenesis in human endothelial cells and induces apoptosis in human cancer cells in vitro. *Journal of Steroid Biochemistry and Molecular Biology*, *178*, 263–271. https://doi.org/10.1016/j.jsbmb.2018.01.005

Rárová, L., Steigerová, J., Kvasnica, M., Bartůněk, P., Křížová, K., Chodounská, H., Kolář, Z., Sedlák, D., Oklestkova, J., & Strnad, M. (2016). Structure activity relationship studies on cytotoxicity and the effects on steroid receptors of AB-functionalized cholestanes. *Journal of Steroid Biochemistry and Molecular Biology*, *159*, 154–169. https://doi.org/10.1016/j.jsbmb.2016.03.017

Reddy, B. S. G., Rao, V. D., Rao, B. C., Dhananjaya, N., Kuttan, R., & Babu, T. D. (1999). Isolation and structural determination of new sphingolipids and pharmacological activity of Africanene and other metabolites from *Sinularia leptoclados*. *Chemical and Pharmaceutical Bulletin*, *47*(9), 1214–1220. https://doi.org/10.1248/cpb.47.1214

Sattler, M., Quinnan, L. R., Pride, Y. B., Gramlich, J. L., Chu, S. C., Even, G. C., Kraeft, S. K., Chen, L. B., & Salgia, R. (2003). 2-Methoxyestradiol alters cell motility, migration, and adhesion. *Blood*, *102*(1), 289–296. https://doi.org/10.1182/blood-2002-03-0729

Sauleau, P., & Bourguet-Kondracki, M.-L. L. (2005). Novel polyhydroxysterols from the Red Sea marine sponge *Lamellodysidea herbacea*. *Steroids*, *70*(14), 954–959. https://doi.org/10.1016/j.steroids.2005.07.004

Sauleau, P., Retailleau, P., Vacelet, J., & Bourguet-Kondracki, M.-L. (2005). New polychlorinated pyrrolidinones from the Red Sea marine sponge *Lamellodysidea herbacea*. *Tetrahedron*, *61*(4), 955–963. https://doi.org/https://doi.org/10.1016/j.tet.2004.11.011

Serio, D., Cormaci, M., & Furnari, G. (1999). *Osmundea maggsiana* sp. nov. (Ceramiales, Rhodophyta) from the Mediterranean Sea. *Phycologia*, *38*(4), 277–

282. https://doi.org/10.2216/i0031-8884-38-4-277.1

Shen, S., Zhu, H., Chen, D., Liu, D., Ofwegen, L. Van, Proksch, P., & Lin, W. (2012). Pavidolides A-E, new cembranoids from the soft coral *Sinularia pavida*. *Tetrahedron Letters*, *53*(43), 5759–5762. https://doi.org/10.1016/j.tetlet.2012.08.049

Stone, W. L., Qui, M., & Smith, M. (2003). Lipopolysaccharide enhances the cytotoxicity of 2-chloroethyl ethyl sulfide. *BMC Cell Biology*, *4*. https://doi.org/10.1186/1471-2121-4-1

Su, H., Yuan, Z.-H., Li, J., Guo, S.-J., Deng, L.-P., Han, L.-J., Zhu, X.-B., & Shi, D.-Y. (2009a). Sesquiterpenes from the Marine Red Alga *Laurencia saitoi*. *Helvetica Chimica Acta*, *92*(7), 1291–1297. https://doi.org/10.1002/hlca.200800437

Su, H., Yuan, Z. H., Li, J., Guo, S. J., Deng, L. P., Han, L. J., Zhu, X. Bin, & Shi, D. Y. (2009b). Two new bromoindoles from red alga *Laurencia similis*. *Chinese Chemical Letters*, *20*(4), 456–458. https://doi.org/10.1016/j.cclet.2008.12.016

Su, J., Yang, R., Kuang, Y., & Zeng, L. (2000). A new cembranolide from the soft coral *Sinularia capillosa*. *Journal of Natural Products*, *63*(11), 1543–1545. https://doi.org/10.1021/np0000264

Sun, H., Liu, F., Feng, M. R., Peng, Q., Liao, X. J., Liu, T. T., Zhang, J., & Xu, S. H. (2016). Isolation of a new cytotoxic polyhydroxysterol from the South China Sea soft coral *Sinularia* sp. *Natural Product Research*, *30*(24), 2819–2824. https://doi.org/10.1080/14786419.2016.1166495

Sun, J., Shi, D., Ma, M., Li, S., Wang, S., Han, L., Yang, Y., Fan, X., Shi, J., & He, L. (2005). Sesquiterpenes from the red alga *Laurencia tristicha*. *Journal of Natural Products*, *68*(6), 915–919. https://doi.org/10.1021/np050096g

Sun, W.-S., Su, S., Zhu, R.-X., Tu, G.-Z., Cheng, W., Liang, H., Guo, X.-Y., Zhao, Y.-Y., & Zhang, Q.-Y. (2013). A pair of unprecedented spiro-trisindole enantiomers fused through a five-member ring from *Laurencia similis*. *Tetrahedron Letters*, *54*, 3617–3620. https://doi.org/10.1016/j.tetlet.2013.04.111

Suzuki, M, Segawa, M., Kikuchi, H., Suzuki, T., & Kurosawa, E. (1985). (5S,7R,10R)-Selin-4(14)-en5α-ol, a sesquiterpene alcohol from the red alga *Laurencia nipponica*. *Phytochemistry*, *24*(2011).

Suzuki, M., & Kurosawa, E. (1979). Halogenated and Non-halogenated Aromatic Sesquiterpenes from the Red Algae *Laurencia okamurai* Yamada. *Bulletin of the Chemical Society of Japan*, *52*(11), 3352–3354. https://doi.org/10.1246/bcsj.52.3352

Takahashi, H., Takahashi, Y., Suzuki, M., Abe, T., & Masuda, M. (2010). Neoirietriol. *Acta Crystallographica Section E*, *E66*(o1795). https://doi.org/10.1107/S1600536810022336

Takahashi, Y., Suzuki, M., Abe, T., & Masuda, M. (1999). Japonenynes, halogenated C15 acetogenins from *Laurencia japonensis*. *Phytochemistry*, *50*(5), 799–803. https://doi.org/10.1016/S0031-9422(98)00616-5

Takeshita, H., Mori, A., & Nakamura, S. (1984). Synthetic Photochemistry. Xxviii. A Photochemical C5-Homologation Of 4-Isopropenyltoluene with methyl 2,4-dioxopentanoate to isolaurene and a formal synthesis of cuparene. *Bulletin of the*

Chemical Society of Japan, *57*(11), 3152–3155. https://doi.org/10.1246/bcsj.57.3152

Takeshita, H., Shimooda, I., & Hatsui, T. (1980). Synthetic Photochemistry. XXL. The Sensitized Photooxygenation of Calarene. A facile hock cleavage of an allylhydroperoxide and structure revision for aristolenols. *Bulletin of the Chemical Society of Japan*, *53*(12), 3721–3722. https://doi.org/10.1246/bcsj.53.3721

Topcu, G., Aydogmus, Z., Imre, S., Gören, A. C., Pezzuto, J. M., Clement, J. A., & Kingston, D. G. I. (2003). Brominated sesquiterpenes from the red alga *Laurencia obtusa*. *Journal of Natural Products*, *66*(11), 1505–1508. https://doi.org/10.1021/np030176p

Torii, M., Kato, H., Hitora, Y., Angkouw, E. D., Mangindaan, R. E. P., De Voogd, N. J., & Tsukamoto, S. (2017). Lamellodysidines A and B, sesquiterpenes isolated from the marine sponge *Lamellodysidea herbacea*. *Journal of Natural Products*, *80*(9), 2536–2541. https://doi.org/10.1021/acs.jnatprod.7b00610

Tran, H. H. T., Nguyen Viet, P., Nguyen Van, T., Tran, H. T., Nguyen Xuan, C., Nguyen Hoai, N., Do Cong, T., Phan Van, K., & Chau Van, M. (2017). Cytotoxic steroid derivatives from the Vietnamese soft coral *Sinularia brassica*. *Journal of Asian Natural Products Research*, *19*(12), 1183–1190. https://doi.org/10.1080/10286020.2017.1307192

Trepels, T., Zeiher, A. M., & Fichtlscherer, S. (2006). The endothelium and inflammation. *Endothelium: Journal of Endothelial Cell Research*, *13*(6), 423–429. https://doi.org/10.1080/10623320601061862

Tsubuki, M., Honda, T., Okita, H., Kaneko, K., & Shigihara, A. (2009). Wittig rearrangement of 3-furylmethyl ethers: facile synthesis of 3-methyl-2-furylmethanols and 3-furylethanols. *Heterocycles*, *77*. https://doi.org/10.3987/COM-08-S(F)40

Umezawa, T., Oguri, Y., Matsuura, H., Yamazaki, S., Suzuki, M., Yoshimura, E., Furuta, T., Nogata, Y., Serisawa, Y., Matsuyama-Serisawa, K., Abe, T., Matsuda, F., Suzuki, M., & Okino, T. (2014). Omaezallene from red alga *Laurencia* sp.: Structure elucidation, total synthesis, and antifouling activity. *Angewandte Chemie - International Edition*, *53*(15), 3909–3912. https://doi.org/10.1002/anie.201311175

Vairappan, C. S., Zanil, I. I., & Kamada, T. (2014). Structural diversity and geographical distribution of halogenated secondary metabolites in red algae, *Laurencia nangii* Masuda (Rhodomelaceae, Ceramiales), in the coastal waters of North Borneo Island. *Journal of Applied Phycology*, *26*(2), 1189–1198. https://doi.org/10.1007/s10811-013-0161-x

Veeresham, C. (2012). Natural products derived from plants as a source of drugs. *Journal of Advanced Pharmaceutical Technology and Research*, *3*(4), 200–201. https://doi.org/10.4103/2231-4040.104709

Verseveldt, J. (1980). A revision of the genus *Sinularia* May (Octocorallia, Alcyonacea). *Zoologische Verhandelingen*, *179*(1), 1–128.

Viegelmann, C., Parker, J., Ooi, T., Clements, C., Abbott, G., Young, L., Kennedy, J., Dobson, A. D. W., & Edrada-Ebel, R. A. (2014). Isolation and identification of

antitrypanosomal and antimycobacterial active steroids from the sponge *Haliclona simulans*. *Marine Drugs*, *12*(5), 2937–2952. https://doi.org/10.3390/md12052937

Wright, A. D., Goclik, E., & König, G. M. (2003). Three new sesquiterpenes from the red alga *Laurencia perforata*. *Journal of Natural Products*, *66*(3), 435–437. https://doi.org/10.1021/np020274v

Wu, Q., Li, X. W., Li, H., Yao, L. G., Tang, W., Miao, Z. H., Wang, H., & Guo, Y. W. (2019). Bioactive polyoxygenated cembranoids from a novel Hainan chemotype of the soft coral *Sinularia flexibilis*. *Bioorganic and Medicinal Chemistry Letters*, *29*(2), 185–188. https://doi.org/10.1016/j.bmcl.2018.12.004

Yang, X.-X., Su, Y.-Z., Tan, J., Cai, C.-E., & Jia, R. (2018). A new dimeric sesquiterpene and other related derivatives from the marine red alga *Laurencia okamurai*. *Biochemical Systematics and Ecology*, *79*, 57–59. https://doi.org/10.1016/j.bse.2018.05.003

Ye, F., Zhu, Z. D., Chen, J. S., Li, J., Gu, Y. C., Zhu, W. L., Li, X. W., & Guo, Y. W. (2017). Xishacorenes A-C, diterpenes with bicyclo[3.3.1]nonane nucleus from the Xisha soft coral *Sinularia polydactyla*. *Organic Letters*, *19*(16), 4183–4186. https://doi.org/10.1021/acs.orglett.7b01716

Yoneshigue-Valentin, Y., Fujii, M. T., & Gurgel, C. F. D. (2003). Osmundea lata (M. Howe & W.R. Taylor) comb. nov. (Ceramiales, Rhodophyta) from the Brazilian south-eastern continental shelf. *Phycologia*, *42*(3), 301–307. https://doi.org/10.2216/i0031-8884-42-3-301.1

Yu, S., Deng, Z., van Ofwegen, L., Proksch, P., & Lin, W. (2006). 5,8-Epidioxysterols and related derivatives from a Chinese Soft Coral *Sinularia flexibilis*. *Steroids*, *71*(11–12), 955–959. https://doi.org/10.1016/j.steroids.2006.07.002

Yu, X. Q., He, W. F., Liu, D. Q., Feng, M. T., Fang, Y., Wang, B., Feng, L. H., Guo, Y. W., & Mao, S. C. (2014). A seco-laurane sesquiterpene and related laurane derivatives from the red alga *Laurencia okamurai* Yamada. *Phytochemistry*, *103*, 162–170. https://doi.org/10.1016/j.phytochem.2014.03.021

Yu, X. Q., Jiang, C. S., Zhang, Y., Sun, P., Kurtán, T., Mándi, A., Li, X. L., Yao, L. G., Liu, A. H., Wang, B., Guo, Y. W., & Mao, S. C. (2017). Compositacins A–K: Bioactive chamigrane-type halosesquiterpenoids from the red alga *Laurencia composita* Yamada. *Phytochemistry*, *136*, 81–93. https://doi.org/10.1016/j.phytochem.2017.01.007

Zhang, C.-X., Zhu, C.-C., Yan, S.-J., Li, J., Su, J.-Y., Liang, Y.-J., Yang, X.-P., Zheng, K.-C., & Zeng, L.-M. (2008). Two new sesquiterpenoids from the soft coral *Sinularia polydactyla* (Ehreberg). *Journal of Asian Natural Products Research*, *10*(3–4), 307–311. https://doi.org/10.1080/10286020701833503

Zhang, C. X., Yan, S. J., Zhang, G. W., Lu, W. G., Su, J. Y., Zeng, L. M., Gu, L. Q., Yang, X. P., & Lian, Y. J. (2005). Cytotoxic diterpenoids from the soft coral *Sinularia microclavata*. *Journal of Natural Products*, *68*(7), 1087–1089. https://doi.org/10.1021/np058006v

Zhang, F., Altorki, N. K., Mestre, J. R., Subbaramaiah, K., & Dannenberg, A. J. (1999). Curcumin inhibits cyclooxygenase-2 transcription in bile acid- and phorbol ester-treated human gastrointestinal epithelial cells. *Carcinogenesis*, *20*(3), 445–451.

https://doi.org/10.1093/carcin/20.3.445
Zhang, N. X., Tang, X. L., Van Ofwegen, L., Xue, L., Song, W. J., Li, P. L., & Li, G. Q. (2015). Cyclopentenone derivatives and polyhydroxylated steroids from the soft coral *Sinularia acuta*. *Chemistry and Biodiversity*, *12*(2), 273–283. https://doi.org/10.1002/cbdv.201400044
Zhao, C., Xu, J. J., Wang, J., Li, S. Y., Qiao, W., & Tang, S. A. (2018). Five new cembrane diterpenoids from the South China Sea soft coral *Sinularia flexibilis*. *Phytochemistry Letters*, *25*, 180–183. https://doi.org/10.1016/j.phytol.2018.04.012
Zovko Končić, M., Ioannou, E., Sawadogo, W. R., Abdel-Razik, A. F., Vagias, C., Diederich, M., & Roussis, V. (2016). 4*α*-Methylated steroids with cytotoxic activity from the soft coral *Litophyton mollis*. *Steroids*, *115*, 130–135. https://doi.org/10.1016/j.steroids.2016.08.017